STEM CELL THERAPIES FOR THE TREATMENT OF ENTERIC NEUROPATHY ASSOCIATED WITH INFLAMMATORY BOWEL DISEASE

Ainsley Maree Robinson

This thesis is submitted in total fulfilment of the requirements for the degree of Doctor of Philosophy

Principal Supervisor: Associate Professor Kulmira Nurgali
Co-Supervisor: Dr Samy Sakkal

College of Health and Biomedicine
Victoria University, Melbourne, Australia
May 2019

ABSTRACT

Although not associated with mortality, symptoms, complications and the relapsing nature of inflammatory bowel disease (IBD) severely impact patient's quality of life. Current treatments are coupled with side effects and loss of patient response. Damage to the enteric neurons is consistently associated with intestinal inflammation and considered to underlie the generation of symptoms. Therefore, the enteric neurons are a potential target for novel IBD therapies. Mesenchymal stem cells (MSCs) exhibit anti-inflammatory, immunomodulating, and neuroprotective effects and are demonstrated to participate in tissue regeneration and repair in many pathological conditions. Hence, they are a viable option for the treatment of enteric neuropathy associated with IBD. The studies in this thesis aim to investigate the effects of MSC therapy in averting enteric neuropathy in acute and chronic models of IBD. The results of our studies demonstrated that MSC and conditioned medium attenuated inflammation and averted enteric neuropathy and colonic dysmotility in an acute model of IBD. The effects of MSC treatment are dose-dependent and occur as early as 24h post treatment. We characterized changes to colonic innervation, motility, transit time, microbiota and metabolome in the *Winnie* mouse model of spontaneously occurring chronic colitis. Our results demonstrated that the *Winnie* mouse is highly representative of human IBD. The mechanisms underlying colonic dysmotility in *Winnie* mice were due to inhibition of neuromuscular transmission and smooth muscle responses. We found that multiple high dose MSC treatments induce anti-inflammatory and neurotrophic effects in mice with chronic colitis. Single dose and multiple low dose MSC administrations were ineffective in this model. Overall, we have established the capacity of MSC treatments to attenuate inflammation and enteric neuropathy in acute and chronic models of IBD. These findings are both novel and highly relevant for clinical translation and future investigations of MSC therapy for the treatment of IBD.

DECLARATION

I, Ainsley Maree Robinson, declare that the PhD thesis entitled “Stem cell therapies for the treatment of enteric neuropathy associated with inflammatory bowel disease” is no more than 100,000 words in length including quotes and exclusive of tables, figures, appendices, bibliography, references and footnotes. This thesis contains no material that has been submitted previously, in whole or in part, for the award of any other academic degree or diploma. Except where otherwise indicated, this thesis is my own work.

Ainsley Robinson

DECLARATION OF CONTRIBUTION TO WORK

Under my direction, the following people have made the stated contributions to this work:

Chapter 1

Assistance in preparing the manuscript for this chapter was provided by K Nurgali.

Chapter 2

Technical assistance with MSC-based treatments, immunohistochemistry and histology was provided by V Jovanovska and S Miller. S Sakkal and A Park performed MSC culture, characterization and validation. N Payne and S Miller contributed to MSC experiments. Assistance in preparing the manuscript for this chapter was provided by S Sakkal, SE Carbone, JC Bornstein, C Bernard, R Boyd, and K Nurgali.

Chapter 3

Technical assistance with MSC treatments was provided by S Miller. S Miller performed MSC culture. Assistance in preparing the manuscript for this chapter was provided by S Sakkal, R Boyd and K Nurgali.

Chapter 4

Technical assistance with immunohistochemical and histological studies was provided by V Jovanovska and AA Rahman. SE Carbone performed intracellular electrophysiology experiments. AA Rahman performed force contraction experiments. S Randall-Demllo contributed to motility experiments. Assistance in preparing the manuscript for this chapter was provided by R Eri, JC Bornstein, and K Nurgali.

Chapter 5

SV Gondalia performed the bioinformatics analysis. A Karpe performed the metabolome profiling. Assistance in preparing the manuscript for this chapter was provided by EA Palombo and K Nurgali.

Chapter 6

Technical assistance with MSC treatments and immunohistochemistry was provided by S Miller and R Stavely. MSC culture was performed by S Miller. Assistance in preparing the manuscript for this chapter was provided by K Nurgali.

Chapter 7

Technical assistance with MSC treatments and immunohistochemistry was provided by S Miller and R Stavely. MSC culture was performed by R Stavely and S Miller. Assistance in preparing the manuscript for this chapter was provided by K Nurgali.

Chapter 8

Assistance in preparing the manuscript for this chapter was provided by K Nurgali.

PUBLICATIONS

PUBLICATIONS FROM THIS THESIS

PUBLISHED ORIGINAL RESEARCH PAPERS

Robinson, A. M., Rahman, A. A., Carbone, S. E., Randall-Demllo, S., Filippone, R., Bornstein, J. C., Eri, R. & Nurgali, K. 2017. Alterations of colonic function in the *Winnie* mouse model of spontaneous chronic colitis. *Am J Physiol Gastrointest Liver Physiol,* 312, G85-102.

Robinson, A. M., Rahman, A. A., Miller, S., Stavely. R., Sakkal, S. & Nurgali, K. 2017. The neuroprotective effects of human bone marrow mesenchymal stem cells are dose-dependent in TNBS colitis. *Stem Cell Res Ther,* 8, 87.

Robinson, A. M., Gondalia, S. V., Karpe, A. V., Eri, R., Beale, D. J., Morrison, P. D., Palombo, E. A. & Nurgali, K. 2016. Fecal microbiota and metabolome in a mouse model of spontaneous chronic colitis: Relevance to human inflammatory bowel disease. *Inflamm Bowel Dis,* 22, 2627-87.

Rahman, A. A., **Robinson, A. M.**, Jovanovska, V., Eri, E. & Nurgali, K. 2015. Alterations in the distal colon innervation in *Winnie* mouse model of spontaneous chronic colitis. *Cell Tissue Res,* 362, 497-512.

Robinson, A. M., Miller, S., Payne, N., Boyd, R., Sakkal, S. & Nurgali, K. 2015. Neuroprotective potential of mesenchymal stem cell-based therapy in acute stages of TNBS-induced colitis in guinea-pigs. *PLoS One,* 10, e0139023.

Robinson, A. M., Sakkal, S., Park, A., Jovanovska, V., Payne, N., Carbone, S. E., Miller, S., Bornstein, J. C., Bernard, C., Boyd, R. & Nurgali, K. 2014. Mesenchymal stem cells and conditioned medium avert enteric neuropathy and colon dysfunction in guinea-pig TNBS-induced colitis. *Am J Physiol Gastrointest Liver Physiol,* 307, G1115-29.

PUBLISHED REFEREED ABSTRACTS

Robinson, A. M., Sakkal, S., Park, A., Jovanovska, V., Payne, N., Bernard, C., Boyd, R., Nurgali, K. 2013. Anti-inflammatory and neuroprotective effects of human bone marrow-derived mesenchymal stem cells in the guinea-pig model of TNBS-induced colitis. *Neurogastroenterology and Motility*, 25 Suppl 1, 1-48.

Robinson, A. M., Miller, S., Sakkal, S., Park, A., Jovanovska, V., Payne, N., Carbone, S. E., Bornstein, J. C., Bernard, C., Boyd, R., Nurgali, K. 2014. Mesenchymal stem cells and conditioned medium avert inflammation-induced enteric neuropathy. *Neurogastroenterology and Motility*, 26 Suppl 1, 1-82.

ORIGINAL RESEARCH PAPERS IN PREPARATION FOR SUBMISSION

Robinson, A. M., Miller, S., Stavely, R., Nurgali, K. 2019. A single dose of mesenchymal stem cell treatment does not exert beneficial effects on enteric neuropathy in the *Winnie* mouse model of spontaneously occurring colitis.

Robinson, A. M., Stavely, R., Miller, S., Nurgali, K. 2019. Multiple high dose mesenchymal stem cell treatments avert inflammation and enteric nerve fiber damage in the *Winnie* mouse model of spontaneously occurring colitis.

OTHER PUBLICATIONS

PUBLISHED ORIGINAL RESEARCH PAPERS

Filippone, R. T., **Robinson, A. M.**, Jovanovska, V., Stavely, R., Apostolopoulos, V., Bornstein, J. C., Nurgali, K. 2018. Targeting eotaxin-1 and CCR3 receptor alleviates enteric neuropathy and colonic dysfunction in TNBS-induced colitis in guinea pigs. *Neurogastroenterol Motil*, e13391.

Timpani CA, Trewin AJ, Stojanovska V, **Robinson A**, Goodman CA, Nurgali K, Betik AC, Stepto N, Hayes A, McConell GK, Rybalka E. 2017. Attempting to compensate for reduced neuronal nitric oxide synthase protein with nitrate supplementation cannot overcome metabolic dysfunction but rather has detrimental effects in dystrophin-deficient mdx muscle. *Neurotherapeutics*, 14, 429-46.

McQuade, R. M., Carbone, S. E., Stojanovska, V., Rahman, A. A., Gwynne, R. M., **Robinson, A. M.**, Goodman, C. A., Bornstein, J. C., Nurgali, K. 2016. Role of oxidative stress in oxaliplatin-induced enteric neuropathy and colonic dysmotility in mice. *Br J Pharmacol*, 16, 3502-21.

Rahman, A. A*., **Robinson, A. M*.**, Brookes, S. J. H., Eri, R., Nurgali, K. 2016. Rectal prolapse in *Winnie* mice with spontaneous chronic colitis: changes in intrinsic and extrinsic innervation of the rectum. *Cell Tissue Res*, 366, 285-99.

Robinson, A. M., Stojanovska, V., Rahman, A. A., McQuade, R. M., Senior, P. V., Nurgali K. Effects of oxaliplatin treatment on the enteric glial cells and neurons in the mouse ileum. *J Histochem Cytochem*. 64, 530-45.

Stavely, R*., **Robinson, A. M*.**, Miller, S., Boyd, R., Sakkal, S., Nurgali, K. 2015. Allogeneic guinea pig mesenchymal stem cells ameliorate neurological changes in experimental colitis. *Stem Cell Res Ther*, 6, 263.

Stavely, R*., **Robinson, A. M*.**, Miller, S., Boyd, R., Sakkal, S., Nurgali, K. 2015. Human adult stem cells derived from adipose tissue and bone marrow attenuate enteric neuropathy in the guinea-pig model of acute colitis. *Stem Cell Res Ther*, 6, 244.

*Contributed equally to the work.

PUBLISHED REFEREED ABSTRACTS

Rahman, A. A., **Robinson, A. M.**, Eri, R., Nurgali, K. 2016. Understanding mechanisms of rectal prolapse in the mouse model of spontaneous chronic colitis: damage to the muscles and nerves. *Neurogastroenterology and Motility*, 28 Suppl 1, 1-116.

MEDIA RELEASES

Allogeneic guinea pig mesenchymal stem cells ameliorate neurological changes in experimental colitis, *Mesenchymal Cell News: Vol 8.00, January 5, 2016.* http://www.mesenchymalcellnews.com/issue/volume-8-00-jan-5/

PRESENTATIONS

INVITED ORAL PRESENTATIONS

Stavely, R., **Robinson, A. M.**, Fraser, S., Apostolopoulos, V., Sakkal, S., Nurgali, K. 2018. Enteric neuropathy associated with chronic intestinal inflammation: Benefits of mesenchymal stem cell therapy as an anti-inflammatory and neuroprotective treatment. *Australian Gastroenterology Week*, Brisbane, Australia.

Stavely, R., **Robinson, A. M.**, Miller, S., Sakkal, S., Nurgali, K. 2016. Mesenchymal Stem Cells Derived from Bone Marrow and Adipose Tissue: Comparison in a Model of Intestinal Neuropathy, *The University of Texas at El Paso (UTEP) – Victoria University Health Research Symposium*, Melbourne, Australia.

Robinson, A. M., Sakkal, S., Park, A., Jovanovska, V., Payne, N., Bernard, C., Boyd, R., Nurgali, K. 2013. Human bone marrow mesenchymal stem cells as an anti-inflammatory and neuroprotective treatment in the guinea-pig model of TNBS-colitis. *Victoria University Biomedical and Lifestyle Diseases (BioLED) Research Seminar*, Melbourne, Australia.

Robinson, A. M., Sakkal, S., Park, A., Jovanovska, V., Payne, N., Bernard, C., Boyd, R., Nurgali, K. 2013. Anti-inflammatory and neuroprotective effects of human bone marrow mesenchymal stem cells in the guinea-pig model of TNBS-colitis. *The University of Texas at El Paso (UTEP) – Victoria University Health Research Symposium*, Melbourne, Australia.

ORAL PRESENTATIONS SELECTED FROM ABSTRACT

Stavely, R., **Robinson, A. M.**, Fraser, S., Apostolopoulos, V., Sakkal, S., Nurgali, K. 2018. Therapeutic mechanisms of mesenchymal stem cell therapy in chronic

colitis. *Little Brain Big Brain, Federation of Neurogastroenterology and Motility (FNM) Meeting,* Kleve, Germany.

Stavely, R., **Robinson, A. M.**, Filippone, R., Rahman, A. A., Eri, R., Sakkal, S., Nurgali, K. 2018. Mesenchymal stem cell treatment for colitis-associated enteric neuropathy. *Development of the Enteric Nervous System: Cells, Signals, Genes and Therapy, ENS Development Meeting*, Boston, USA.

Stavely, R., **Robinson, A. M.**, Rahman, A. A., Stojanovska, V., Sakkal, S., Bertrand, P., Nurgali, K. 2017. Mesenchymal stem cell therapy prevents the hypersecretion of mucosa derived serotonin associated with the onset and progression of chronic colitis by reducing enterochromaffin cell hyperplasia. *Victoria University, College of Health and Biomedicine Postgraduate Research Conference*, Melbourne, Australia.

Stavely, R., **Robinson, A. M.**, Rahman, A. A., Stojanovska, V., Sakkal, S., Bertrand, P., Nurgali, K. 2016. Characterisation of serotonin release in mice with spontaneous chronic colitis after mesenchymal stem cell therapy, *Victoria University Immunology Summit*, Melbourne, Australia.

Robinson, A. M., Miller, S. Sakkal, S., Nurgali, K. 2015. Mesenchymal stem cell-based treatments for enteric neuropathy associated with colitis. *Australasian Neurogastroenterology and Motility Association (ANGMA) Meeting*, Adelaide, Australia.

Robinson, A. M., Sakkal, S., Jovanovska, V., Park, A., Carbone, S. E., Boyd, R., Bernard, C., Nurgali, K. 2015. Bone marrow mesenchymal stem cells and conditioned medium prevent enteric neuropathy associated with inflammatory bowel disease. *Australian Society for Medical Research (ASMR) Victorian Student Research Symposium*, Melbourne, Australia.

Miller, S., **Robinson, A. M.**, Stavely, R., Eri, E., Sakkal, S., Nurgali, K. 2015. Mesenchymal stem cells attenuate enteric neuropathy in acute and chronic models of colitis. *Australian Society for Medical Research (ASMR) Victorian Student Research Symposium*, Melbourne, Australia.

Miller, S., **Robinson, A. M.**, Stavely, R., Eri, E., Sakkal, S., Nurgali, K. 2015. Mesenchymal stem cells attenuate enteric neuropathy in acute and chronic models of colitis. *Bugs, Bowels and Beyond: Innovations in Digestive Health and Disease Research, Australian Society for Medical Research (ASMR) National Scientific Conference*, Adelaide, Australia.

Miller, S., **Robinson, A. M.**, Sakkal, S., Park, A., Jovanovska, V., Payne, N., Carbone, S. E., Bernard, C., Boyd, R., Nurgali, K. 2014. Treatment of TNBS-colitis with bone marrow mesenchymal stem cells and conditioned medium can prevent enteric neuropathy in guinea-pigs. *Australasian Neuroscience Society (ANS) Meeting*, Adelaide, Australia.

Robinson, A. M., Sakkal, S., Park, A., Jovanovska, V., Payne, N., Bernard, C., Boyd, R., Nurgali, K. 2013. Anti-inflammatory and neuroprotective effects of human bone marrow mesenchymal stem cells in the guinea-pig model of TNBS-colitis. *American Neurogastroenterology and Motility (ANGM) Meeting*, Los Angeles, USA.

POSTER PRESENTATIONS

Stavely, R., **Robinson, A. M.**, Fraser, S., Apostolopoulos, V., Sakkal, S., Nurgali, K. 2018. Mesenchymal stem cell therapy in chronic colitis: Potential therapeutic mechanisms in alleviating oxidative stress and enteric neuropathy. *Federation of Neurogastroenterology and Motility (FNM) Meeting*, Amsterdam, Netherlands.

Stavely, R., **Robinson, A. M.**, Rahman, A. A., Fraser, S., Apostolopoulos, V., Sakkal, S., Nurgali, K. 2018. Enteric neuropathy associated with intestinal inflammation: Effects and potential mechanisms of mesenchymal stem cell therapy. *International Society for Stem Cell Therapy (ISSCT) Meeting*, Melbourne, Australia.

Stavely, R., **Robinson, A. M.**, Sakkal, S., Nurgali, K. 2018. Neurogenic mechanisms of mesenchymal stem cell therapy in chronic colitis. *Australian Society for Medical Research (ASMR) Victorian Student Research Symposium*, Melbourne, Australia.

Stavely, R., **Robinson, A. M.**, Filippone, R., Rahman, A. A., Eri, R., Sakkal, S., Nurgali, K. 2017. Mesenchymal stem cell treatment for enteric neuropathy associated with colitis. *International Society of Autonomic Neuroscience (ISAN) Congress*, Nagoya, Japan.

Stavely, R., **Robinson, A. M.**, Rahman, A. A., Stojanovska, V., Sakkal, S., Bertrand, P., Nurgali, K. 2017. Characterisation of serotonin release in mice with spontaneous chronic colitis after mesenchymal stem cell therapy, *Australasian Neurogastroenterology and Motility Association (ANGMA) Meeting*, Melbourne, Australia.

Stavely, R., **Robinson, A. M.**, Rahman, A. A., Stojanovska, V., Sakkal, S., Bertrand, P., Nurgali, K. 2017. Characterisation of serotonin release in mice with spontaneous chronic colitis after mesenchymal stem cell therapy, *Australian Society for Medical Research (ASMR) Victorian Student Research Symposium*, Melbourne, Australia.

Stavely, R., **Robinson, A. M.**, Miller, S., Sakkal, S., Nurgali, K. 2015. Efficacy of bone marrow and adipose tissue-derived allogeneic and xenogeneic mesenchymal stem cells for the treatment of intestinal inflammation, *Australian Society for Medical Research (ASMR) Victorian Student Research Symposium*, Melbourne, Australia.

Robinson, A. M., Miller, S., Sakkal, S., Park, A., Jovanovska, V., Payne, N., Carbone, S. E., Bornstein, J. C., Bernard, C., Boyd, R., Nurgali, K. 2014. Mesenchymal stem cells and conditioned medium avert inflammation-induced enteric neuropathy. *Federation of Neurogastroenterology and Motility (FNM) Meeting*, Guangzhou, China.

ACKNOWLEDGEMENTS

I am extremely grateful to the many people that assisted, guided and supported me during my PhD. Without you, completion of this thesis would not have been possible.

Firstly, I would like to thank my supervisor, **Associate Professor Kulmira Nurgali**. Your focus, dedication and knowledge inspired me to achieve so much more than I considered imaginable and I cannot possibly put into the words the entirety of my gratitude to you. I have learnt so much from you and whole heartedly appreciate everything you have done for me.

Many thanks to **Valentina Jovanovska** who taught me so many practical skills in the lab. You never doubted my abilities and were always willing to help when needed. I really enjoyed my time in the lab with you, the laughs we had always made the days better and brighter. To **Dr Ahmed Rahman** and **Dr Simona Carbone**, thank you for your knowledge, assistance and time during my PhD. Your support and contributions to my studies were invaluable.

A big thank you to the MSC team. To **Rhian Stavely**, I loved working with you – you are always a pleasure to be around, your intellect and ability to think outside the box was always valuable to our projects. To **Sarah Miller**, I thank you for your assistance and support through the good times and the bad and for all the laughs we shared.

I would also like to thank all other KN lab members, **Rhiannon**, **Elizabeth**, **Vanesa**, **Rachel**, **Elif**, and **Monica**, as well as people from other labs at WCHRE, **Suh**, **Cara, Alan,** and **Varsha** for all the help, guidance and support. Without the laughter and the friendships, completion of this PhD would have been much more difficult.

To **Camille**, your support, encouragement and positivity has been amazing – I am extremely grateful for your patience and keeping my head above the water

when I feel like giving up – now we can concentrate on you and me and making the life we want! To my family, **Mum** and **Dad**, **Elissa** and **John**, **Steven** and **Nat**, thank you for being there, understanding and supporting me throughout the years. You have all contributed to the completion of my PhD in many ways. To **Corinne**, thank you for your support and encouragement at the beginning of my studies. To **Justine**, my longest friend, thank you for taking my mind off things and always being there to talk to. To **Sy**, **Marvel**, **Norm** and **Peaches**, thank you for helping me escape the stress with pats and walks. To **Vamp** and **Jaspa**, thank you for your moral support while sitting on my feet or trying to walk on my keyboard!

While it has been a bumpy road at times, I have gained many new skills and much knowledge during my PhD which will be invaluable for my post thesis life. There are many more people that I haven't mentioned who have played a part in the completion of this thesis. I thank you all and acknowledge all your contributions.

TABLE OF CONTENTS

LIST OF FIGURES

LIST OF TABLES

CHAPTER SIX

CHAPTER SEVEN

APPENDICES

LIST OF ABBREVIATIONS

5-HT	serotonin
ACh	acetylcholine
AH	afterhyperpolarization
ALS	amyotrophic lateral sclerosis
AP	action potential
ATP	adenosine 5′-triphosphate
AVI	audio video interleaved
BCAAs	branched-chain amino acids
BDNF	brain-derived neurotrophic factor
BM	bone marrow
BMP	bone morphogenetic protein
CCR	chemokine receptor
CD	Crohn’s disease
CFU-F	colony-forming unit fibroblast
CGRP	calcitonin gene-related peptide
ChAT	choline acetyltransferase
CHOs	carbohydrates
CM	conditioned medium
CMMC	colonic migrating motor complex
CNS	central nervous system

COX	cyclooxygenase
CTT	colonic transit time
DAPI	4′-6-diamidino-2-phenylindole
DC	dendritic cell
DModX	distance between X modal plane
DMSO	dimethyl sulfoxide
DNBS	2,4-dinitrobenzenesulfonic acid
DPX	distrene plasticizer xylene
DSS	dextran sodium sulfate
EDTA	ethylenediaminetetraacetic acid
EGC	enteric glial cell
EJP	excitatory junction potential
ELISA	enzyme-linked immunosorbent assay
ENS	enteric nervous system
EPSP	excitatory postsynaptic potential
FACS	fluorescence activated cell sorting
FBS	fetal bovine serum
FC	fold change
fEJP	fast exciatory junction potential
fIJP	fast inhibitory junction potential
FITC	fluorescein isothiocyanate
GC	gas chromatograph

GC-MS	chromatography-mass spectrometry
GDNF	glial cell line-derived neurotrophic factor
GI	gastrointestinal
GMP	guanosine monophosphate
GPX	glutathione peroxidase
H&E	hematoxylin and eosin
HD	high dose
HGF	hepatocyte growth factor
HLA	human leukocyte antigen
IBD	inflammatory bowel disease
ICC	interstitial cells of Cajal
IEC-6	intestinal epithelial cell 6
IFN	interferon
IGF	insulin-like growth factor
IJP	inhibitory junction potential
IL	interleukin
IR	immunoreactive
IP	intraperitoneally
IPAN	intrinsic primary afferent neuron
IPSP	inhibitory postsynaptic potential
ISCT	International Society for Cellular Therapy
IV	intravenously

Lcn	lipocalin
LD	low dose
LMMP	longitudinal muscle-myenteric plexus
L-NNA	Nω-nitro-l-arginine
MEM	minimum essential medium
MHC	major histocompatibility class
MIP	macrophage inflammatory protein
MMC	migrating motor complex
MS	mass spectrometry
MSC	mesenchymal stem cell
nAChR	nicotinic acetylcholine receptor
NDS	normal donkey serum
NGF	nerve growth factor
NHP	non-human primate
nNOS	neuronal nitric oxide synthase
NO	nitric oxide
NT	neurotrophin
NF-κB	nuclear factor kappa B
OCT	optimum cutting temperature
OCTT	orocecal intestine transit time
OTUs	operational taxonomic units
PAI	plasminogen activator inhibitor

PBS	phosphate buffered solution
PCA	principal component analysis
PCoA	principal coordinate analysis
PCR	polymerase chain reaction
PDGF	platelet-derived growth factor
PE	phycoerythrin
PGP	protein gene product
PLS-DA	partial least square-discriminant analysis
QoL	quality of life
RGB	red, green, and blue
RMP	resting membrane potential
RT-PCR	reverse transcriptase-polymerase chain reaction
S	synaptic
SCFAs	short chain fatty acids
sEJP	slow excitatory junction potential
SEM	standard error of the mean
sIJP	slow inhibitory junction potential
SMA	smooth muscle actin
SNP	sodium nitroprusside
TGF	transforming growth factor
Th	T-helper
TH	tyrosine hydroxylase

TIMP	tissue inhibitor of metalloproteinases
TNBS	2,4,6-trinitrobenzene sulfonic acid
TNF	tumor necrosis factor
T. spiralis	Trichinella spiralis
TSG	tumor necrosis factor-stimulated gene
UC	ulcerative colitis
UCM	unconditioned medium
VAChT	vesicular acetylcholine transporter
VEGF	vascular endothelial growth factor
VIP	vasoactive intestinal polypeptide

CHAPTER ONE: OVERVIEW

1.1 Inflammatory Bowel Disease

Inflammatory bowel disease (IBD) is a broad term describing a group of disorders characterized by chronic, relapsing, and remitting activation of immune-mediated inflammation within the gastrointestinal (GI) tract (Fakhoury et al. 2014; Wallace et al. 2014; Zhang and Li 2014). The two major subtypes of IBD are Crohn's disease (CD) and ulcerative colitis (UC). Despite substantial overlapping of clinical and pathologic features, including GI disturbances, damage to the enteric nervous system (ENS) and altered immunity, CD and UC can be differentiated by the disease localization within the GI tract, type of histopathological changes in the intestinal wall, and complications from the disease (Fig. 1.1) (Matricon et al. 2010). In general, the inflammatory reaction in UC is initiated in the rectal mucosa, affecting the rectum only or extending proximally to involve part of or the entire colon (Conrad et al. 2014). CD may affect any part of the GI tract from the mouth to the anus but is most commonly localized to the terminal ileum and colon (Mulder et al. 2014). UC is defined by a continuous inflammation of the mucosa and submucosa only, whereas in CD, inflammation is discontinuous and transmural, affecting all layers of the bowel wall (Tontini et al. 2015). Both types of inflammation are related to changes in the structure and function of the ENS, which may play a role in the generation of symptoms (Lakhan and Kirchgessner 2010).

1.1.1 Symptoms and complications

IBD symptoms are often variable depending on the location, extent, and severity of disease involvement (Feuerstein and Cheifetz 2017). Visible blood and mucus in stools, rectal bleeding and urgency, chronic diarrhea with nocturnal defecation, abdominal pain and cramps, nausea, vomiting and, occasionally, severe constipation are commonly reported GI symptoms in IBD patients (Tontini et al. 2015; Dignass et al. 2012). Furthermore, systemic symptoms, such as weight loss, fever, and fatigue, occur frequently in both UC and CD (Wallace et al. 2014; Panaccione 2013; Dignass et al. 2012). The duration and severity of IBD has a

direct relationship with the burden of complications presenting locally within the gut or systematically (Tontini et al. 2015; Vatn 2009).

GI complications are especially prevalent in CD and include abscesses, linear clefts, fistulas, and strictures, which can lead to intestinal obstruction (Panaccione 2013; Khor et al. 2011; Lichtenstein et al. 2009). Because UC inflammation only involves the superficial layers of the bowel wall, crypt abscesses rather than fistulas are predominant (Hendrickson et al. 2002). Other GI complications that may arise from UC include perforation of the bowel, rectal hemorrhage, and toxic megacolon (Panaccione 2013). Systemic complications of IBD include malnutrition, osteoporosis, malignancy, kidney stones, venous thromboembolism, and metabolic bone disease (Vavricka et al. 2015; Huang et al. 2013). In addition, both CD and UC are associated with an increased risk of colorectal cancer, attributable to chronic inflammation (Kim and Chang 2014; Rubin et al. 2012).

Figure 1.1 Differences between UC and CD. Schematic diagram presenting the differences between UC and CD including localization of inflammation, pattern of inflammation, symptoms and GI complications.

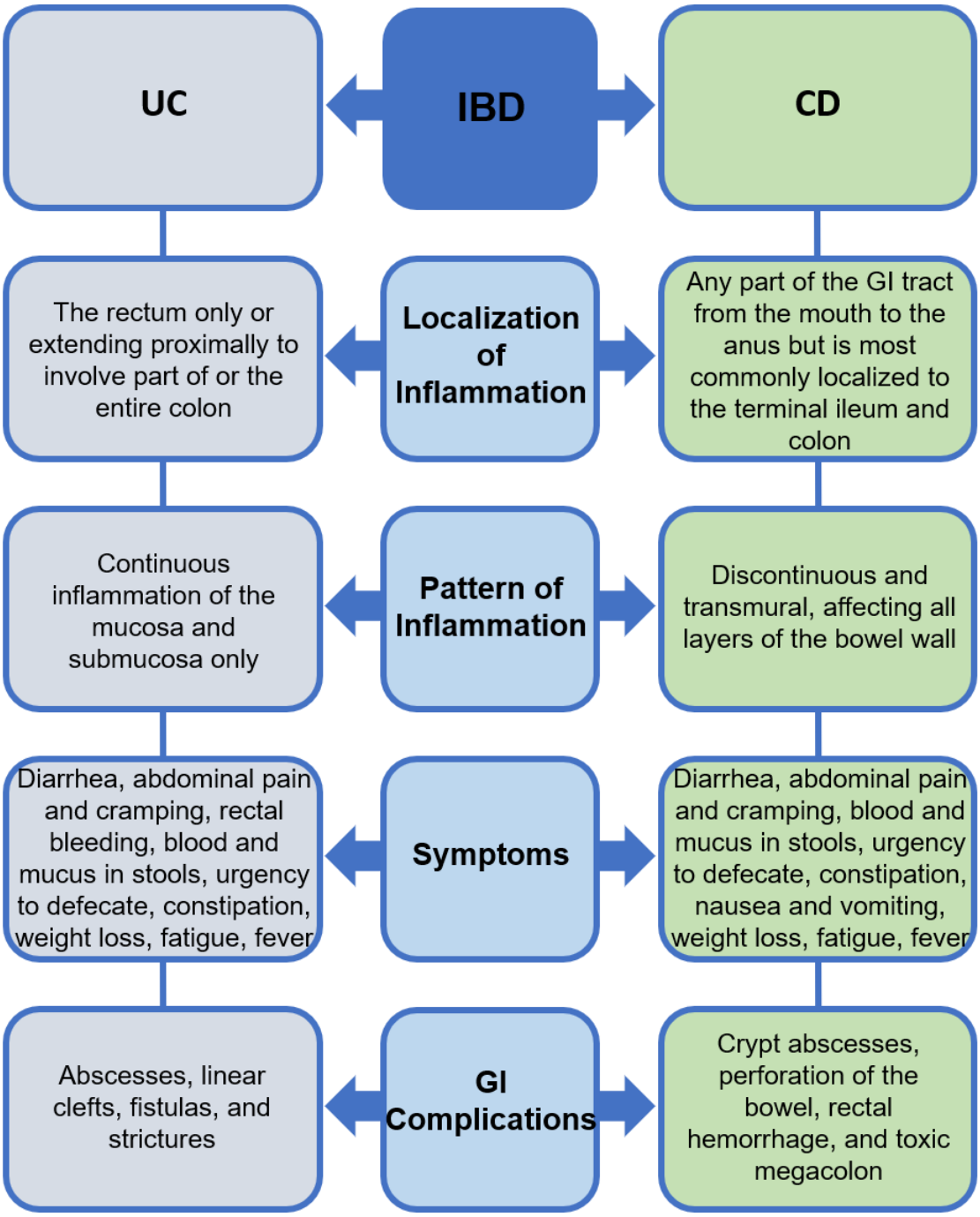
UC
IBD
CD
The rectum only or extending proximally to involve part of or the entire colon
Localization of Inflammation
Any part of the GI tract from the mouth to the anus but is most commonly localized to the terminal ileum and colon
Continuous inflammation of the mucosa and submucosa only
Pattern of Inflammation
Discontinuous and transmural, affecting all layers of the bowel wall
Diarrhea, abdominal pain and cramping, rectal bleeding, blood and mucus in stools, urgency to defecate, constipation, weight loss, fatigue, fever
Symptoms
Diarrhea, abdominal pain and cramping, blood and mucus in stools, urgency to defecate, constipation, nausea and vomiting, weight loss, fatigue, fever
Abscesses, linear clefts, fistulas, and strictures
GI Complications
Crypt abscesses, perforation of the bowel, rectal hemorrhage, and toxic megacolon

1.1.2 Age of onset

The peak age of onset for CD is 20-30 years and 30-40 years for UC (Cosnes et al. 2011). Some studies describe a second smaller peak of IBD onset between the ages of 60-80 years (Takahashi et al. 2014; Vind et al. 2006). However, bimodal distribution of IBD incidence is controversial, as other studies do not support these findings (Petritsch et al. 2013; Lakatos et al. 2011; Loftus et al. 2007). In general, CD patients are 5-10 years younger than UC patients at the age of diagnosis (Duricova et al. 2014). Approximately 10-15% of IBD patients receive their diagnosis at >60 years, while 5-25% of IBD cases onset during childhood or adolescence; 20% of CD patients and 12% of UC patients are diagnosed at <20 years (Ruel et al. 2014; Kappelman et al. 2013). CD is more commonly reported as pediatric-onset, whereas a higher number of UC diagnoses are made in adult-onset and elderly-onset age groups (Charpentier et al. 2014; Kariyawasam et al. 2013; Van Limbergen et al. 2008). Furthermore, there are gender differences corresponding to the age of IBD onset (Ruel et al. 2014). The incidence of pediatric CD, as well as adult-onset and elderly-onset UC is higher in males, while adult-onset and elderly-onset CD is more prevalent in females (Charpentier et al. 2014; Gupta et al. 2012). The male:female ratio is equal in pediatric-onset UC (Charpentier et al. 2014; Ruel et al. 2014).

1.1.3 Quality of life

The manifestation of IBD is associated with significant impairment of a patient's perception, body image, and quality of life (QoL), especially when the disease is active (Kalafateli et al. 2013; Umanskiy and Fichera 2010). Disease severity has a strong relationship to QoL; a greater disease severity corresponds to a lower QoL (Habibi et al. 2017; Gray et al. 2011). When the severity of IBD increases, symptoms, as well as the likelihood of complications, intensify which may heighten levels of emotional stress (Habibi et al. 2017; Keeton et al. 2015). Psychological stress, reduced well-being, anxiety and depression have all been reported to contribute to a lower QoL in IBD patients (Bannaga and Selinger 2015; Sajadinejad et al. 2012; Romberg-Camps et al. 2010). Furthermore, a

greater severity of disease is correlated to sleep difficulties and higher fatigue levels which are independently correlated with lower QoL (Romberg-Camps et al. 2010; Graff et al. 2006). IBD patients report high rates of sick leave and reduced work productivity, affecting QoL and hindering career and employment status (De Boer et al. 2016; Lonnfors et al. 2014). Other factors that promote a reduced QoL for IBD patients include worrying about availability of accessible toilets, inability to participate in leisure or social activities, and the impact on, or lack of, relationships with friends, work colleagues, family, and intimate partners (Kim et al. 2017; Becker et al. 2015b; Lonnfors et al. 2014). In addition, female gender, older age, lower education, and socioeconomic status may be associated with a lower QoL for IBD patients (Huppertz-Hauss et al. 2015; Sajadinejad et al. 2012).

1.1.4 Epidemiology

The incidence and prevalence of IBD steadily increased in westernized countries, including Europe, North America, Australia, and New Zealand in the latter part of the twentieth century (Kaplan and Ng 2017; Ng et al. 2017; Ananthakrishnan 2015; Molodecky et al. 2012). Conversely, IBD was relatively rare in developing countries at this time and therefore, was traditionally considered to be a condition that primarily affected the westernized world. However, from the beginning of the twenty first century, IBD emerged as a global disease due to an increased incidence in developing countries, such as the Middle East, South America, Asia, and Africa (Kaplan 2015; Park et al. 2014b). The increased incidence in developing countries has been attributed to rapid population growth, urbanization, industrialization, and westernization of culture (Kaplan and Ng 2017; Zwi and Mills 1995). In westernized countries, the trend for IBD incidence seems to have stabilized in the adult-onset and elderly-onset populations, but not for the pediatric-onset patients (Gasparetto and Guariso 2013). However, although not accelerating at the same rate as in the past, the incidence of IBD in the western world is still higher than in developing regions (Table 1.1) (Kaplan and Ng 2017; Ng et al. 2017; M'Koma 2013; Molodecky et al. 2012; Wilson et al. 2010; Gearry et al. 2006). Varying risk factors and differences in access to health-care may influence variation in IBD incidence between regions (Kaplan and Ng

2017; Kaplan 2015). North America, Europe, Australia, and New Zealand report the highest annual prevalence of IBD (Table 1.1) (Ng et al. 2017; M'Koma 2013; Wilson et al. 2010; Gearry et al. 2006). Prevalence remains lower in developing countries, however it is estimated to rise because of the increasing incidence in these countries (Ng et al. 2017; M'Koma 2013; Wilson et al. 2010; Gearry et al. 2006). Overall, despite the easing of the incidence rates in some regions, the prevalence of IBD continues to increase substantially worldwide and both the incidence and prevalence of IBD are expected to steadily climb in future years (Kaplan 2015; Molodecky et al. 2012).

Table 1.1 Incidence and prevalence of CD and UC*

	Incidence (per 100,000 person-years)		**Prevalence (per 100,000 persons)**	
	CD	**UC**	**CD**	**UC**
North America	20.2	19.2	319	249
Europe	12.7	24.3	322	505
Australia	17.4	11.2	197	196
New Zealand	16.5	7.6	155	145
Asia/Middle East	5.0	6.3	68	168
South America	3.5	6.8	41	44
Africa	5.9	3.3	19	11

*Kaplan and Ng 2017; Ng et al. 2017; M'Koma et al. 2013; Molodecky et al. 2012; Wilson et al. 2010; Gearry et al. 2006

1.1.5 Economic impact

The economic impact of CD and UC will increase exponentially in the next decades, corresponding to worldwide increases in the prevalence and incidence of IBD. Considerable direct and indirect costs of IBD are inflicted on patients, as well as economies and health-care systems already struggling to provide efficient care and access. Approximately 2.5-3 million people in Europe, 1 million in the

USA, 200,000 in Canada and 85,000 in Australia are estimated to have IBD, with direct health-care costs of €4.6-5.6 billion, US$6 billion, CDN$1.2 billion, and $AUD 3.2 billion, respectively (Crohn's & Colitis Australia 2017; Burisch et al. 2013; Kappelman et al. 2013; Rocchi et al. 2012). In westernized countries, hospitalization is the largest component contributing to the direct medical costs of IBD (Petryszyn and Witczak 2016). Surgery, ambulatory care, and pharmaceuticals are other major contributors to direct health-care-related costs of IBD (Kaplan 2015). These costs are greater for CD patients than for UC patients, and patients with active disease than those in remission, which may be a result of a higher proportion of in-patient hospital admissions (Jackson et al. 2017). The indirect costs of IBD include the value of lost earnings due to excess sick leave, short-term disability, and reduced work productivity, as well as loss of leisure time (Kaplan 2015; Holko et al. 2016). While the direct costs of IBD inflict a severe financial burden to both the patient and the economy, the indirect costs of the disease substantially impact on a patient's QoL.

1.1.6 Etiology

The exact etiology of IBD is unknown, however a combination of genetic susceptibility, environmental factors, gut microbiota, and the immune/inflammatory response are considered to be involved (Kim and Cheon 2017; Fiocchi 2015).

Technological advances in DNA analysis and sequencing have enhanced our understanding of the genetic contributions to IBD (Zhang and Li 2014; Gaya et al. 2006). The identification and confirmation of 163 IBD-associated gene loci, 30 CD specific, 23 UC specific, and 110 associated with both CD and UC, have confirmed that gene variants are implicated in IBD pathogenesis (Jostins et al. 2012). Furthermore, it has been demonstrated that the likelihood of developing UC or CD increases in direct proportion to the number of risk alleles carried (Wang et al. 2013c). While these findings demonstrate that genetic influences are significant constituents of IBD pathogenesis, the explainable susceptibility loci and genetic risk factors represent only 20-25% of the heritability for IBD (13.6%

for CD and 7.5% for UC) (Ellinghaus et al. 2015; Liu et al. 2015a; Uhlig 2013). Thus, genetic associations and heterogeneity alone fail to explain the etiology of IBD.

Changing epidemiology and global increases in the frequency of IBD strongly support the role of environmental factors in the disease pathogenesis (Shouval and Rufo 2017). Causative factors associated with changes in lifestyle and environmental conditions in westernized countries over the last century, and in developing countries over the past 20-30 years, has led to the concept that industrialization and a westernized lifestyle are involved in the onset and course of IBD. These findings have also contributed to the 'hygiene hypothesis' which suggests that improved sanitation, hygiene, and lack of exposure to enteric pathogens may result in inappropriate chronic immunological response following exposure to new antigens (Rogler et al. 2016). Other environmental risk factors for IBD that have been associated with the urbanization of societies include changes in diet, antibiotic use, and pollution (Ng et al. 2013). Furthermore, smoking, food additives, stress, and psychosocial factors have all been investigated and confirmed as potential triggers for IBD onset and relapse (Zhang and Li 2014; Molodecky and Kaplan 2010; Ardizzone and Porro 2002).

Previous studies have demonstrated an overall reduction in the biodiversity and stability of intestinal microbiota in IBD patients compared to healthy individuals (Sha et al. 2013; Nemoto et al. 2012), confirming the crucial role of microbial agents in the pathogenesis of the disease. Further evidence is provided by aversion of inflammation under germ-free conditions in experimental models of colitis (Rath 2002; Sellon et al. 1998), improvement of disease activity with fecal stream diversion in IBD patients (Villanacci et al. 2007; Fichera et al. 2005), and induction or maintenance of remission with the use of probiotics and antibiotics (Perencevich and Burakoff 2006; Kruis et al. 2004; Sartor 2004). In addition, the majority of reported IBD susceptibility genes are correlated with host-microbiome interactions and mucosal barrier function (Jostins et al. 2012). While there is clear evidence depicting the association between dysbiosis and IBD pathogenesis, it

is still unknown whether alterations to the intestinal microbiota are a causative or consequential of inflammation in IBD (Becker et al. 2015a).

It is considered that the induction and persistence of chronic inflammation in IBD is primarily due to excessive or uncontrolled activation of the adaptive immune system, either through enhanced levels of pro-inflammatory cytokines compelled by the T-helper (Th) subsets or by ineffective anti-inflammatory regulatory T-cells (Rogler et al. 2018; Wallace et al. 2014). In the inflamed mucosa of CD patients, Th1-associated pro-inflammatory cytokines (tumor necrosis factor (TNF)-α, interferon (IFN)-γ, interleukin (IL)-12), as well as Th17-associated cytokines (IL-17A, IL-21, IL-23) are significantly increased, whereas some inhibitory cytokines (transforming growth factor (TGF)-β, IL-10, IL-25, IL-33, and IL-37) are markedly reduced. Increases in Th-2-related pro-inflammatory cytokines, such as IL-4 and IL-13 are exhibited in inflamed tissues from UC patients (Liu et al. 2012; Ordas et al. 2012; 2011; 2009a). The pro-inflammatory cytokines augmented in CD and UC are powerful stimulators of T-cell and macrophage proliferation, chemokine expression, adhesion molecule expression, and secretion of other pro-inflammatory cytokines which have multiple pathogenic effects on the components of both the adaptive and the innate immune system (Geremia et al. 2014; Xu et al. 2014). In addition, mucosal innate immune responses, such as epithelial barrier integrity, innate microbial sensing, autophagy and unfolded protein response, are involved in the onset of intestinal inflammation in IBD (Geremia et al. 2014).

Many studies have described a correlation between intestinal inflammation and damage to the structure and function of the ENS (Moynes et al. 2014; Winston et al. 2013; Hoffman et al. 2011; Nurgali et al. 2011; Linden et al. 2005; Sharkey and Kroese 2001). It is generally considered that ENS abnormalities occur secondary to the inflammatory reaction in IBD (Geboes and Collins 1998). However, ENS anomalies also occur in non-inflamed areas of the intestine, leading to suggestions that changes to the ENS may precede inflammation and play a pathogenic role in IBD (Villanacci et al. 2008).

1.1.7 Treatment

Since the etiology of IBD is complex and only partially understood, therapies are directed at controlling symptoms rather than curing the disease. Overall, the main goals of treatment are 1) to induce clinical remission and improve QoL in patients with acute symptoms of IBD, 2) to maintain remission once it is attained, and 3) prevention of complications of both the disease and the treatment (Sandborn et al. 2014; Kornbluth and Sachar 2010; Lichtenstein et al. 2009). Treatment strategies correspond to disease severity, location, and phenotype and involve a range of pharmacological agents as a first step followed by surgical intervention if necessitated (Raad et al. 2016; Bodger 2011; Loftus 2011). Pharmacological approaches for treatment of IBD are based on medications exerting a direct or indirect effect on the inflammatory cascade (Lissner and Siegmund 2013; Scribano and Prantera 2013; Vermeire et al. 2013). These medications generally fall into five categories, including aminosalicylates, corticosteroids, immunomodulators, antibiotics, and biological therapies (Triantafillidis et al. 2011).

It is widely acknowledged that the anti-inflammatory agents, aminosalicylates, are effective for the induction and maintenance of remission in mild-moderate UC (Gisbert et al. 2011; Williams et al. 2011). However, approximately 50% of UC patients treated with this drug require escalation of therapy (Peyrin-Biroulet and Lemann 2011). The efficacy of aminosalicylates in CD patients, particularly those with small intestine disease, is controversial (Dignass et al. 2010; Lim and Hanauer 2010). Overall, aminosalicylates are well tolerated and safe (Williams et al. 2011). Side effects are minor, but may include headache, nausea, vomiting, abdominal pain and diarrhea (Lim and Hanauer 2010). Rare but severe side effects include pleuritis, myocarditis, pancreatitis, and cholestatic hepatitis (Williams et al. 2011).

Corticosteroids are well-established potent, non-selective systemic anti-inflammatory agents efficacious in rapidly resolving the symptoms of acutely active IBD (Waljee et al. 2016; Murphy et al. 2009). However, while

corticosteroids are effective at inducing remission, they are not useful for maintenance therapy as they are ineffective in preventing relapse (Martinez-Montiel et al. 2015). A proportion of IBD patients fail to respond to corticosteroid treatment or are unable to withdraw from treatment without relapse (Irving et al. 2007). Furthermore, despite the demonstrated efficacy of this medication in the short-term, the long-term use of corticosteroids is associated with many adverse effects including weight gain, acne, facial hair, hypertension, diabetes, loss of bone mass, venous thromboembolism, poor wound healing, and increased risk of infections (Waljee et al. 2016; Vecchi Brumatti et al. 2014).

In general, immunomodulators are prescribed to IBD patients who are unresponsive to aminosalicylates and corticosteroids, or to those who experience relapse upon steroid withdrawal (Kondamudi et al. 2013). Effective for both the induction and maintenance of remission in CD and UC, immunomodulators also provide modest steroid-sparing effects in active and quiescent disease (Thomas and Lodhia 2014; Feldman et al. 2007; Aberra and Lichtenstein 2005). These medications have a delayed onset of action and their maximal effects are generally observed after several months (Chande et al. 2013). Consequently, immunomodulators are mostly used to maintain clinical remission rather than for induction of remission in active disease (Feldman et al. 2007). While the clinical benefit of immunomodulators is clear, concerns remain regarding severe side effects and drug-induced toxicity, such as allergic reactions, pancreatitis, myelosuppression, bone marrow suppression, infections, hepatoxicity and malignancy (Van Dieren et al. 2007; Aberra and Lichtenstein 2005; Gearry et al. 2004). Approximately 15-30% of IBD patients discontinue treatment due to the significant side effect profile of these drugs (Gisbert et al. 2011; Takatsu et al. 2009; Lees et al. 2008).

There is an established role for antibiotic therapy in treating bacterial overgrowth and septic complications of IBD, such as abscesses, fistulae, and postoperative wound infections (Pithadia and Jain 2011; Isaacs and Sartor 2004; Sartor 2004). However, the role of antibiotic therapy in treating the primary disease process of IBD remains controversial; some studies demonstrate modest effects of

antibiotics in inducing and maintaining remission in IBD, while others report no benefits of the treatment (Nitzan et al. 2016; Su et al. 2015). Despite conflicting literature, antibiotics are commonly prescribed for the treatment of IBD (Su et al. 2015; Khan et al. 2011; Prantera et al. 2012; Wang et al. 2012b). Long term treatment with antibiotics might decrease recurrence rate, though it is frequently associated with side effects and intolerance to treatment. Side effects associated with prolonged courses of antibiotic treatment include GI disturbances, peripheral neuropathy, tendon rupture, and photosensitivity, which often lead to a discontinuation of treatment, *Clostridium dificile* infection, and increased antibiotic resistance (Nitzan et al. 2016; 2013; Sarna et al. 2013).

Biological therapies, monoclonal antibodies which target TNF-α, integrins or IL-12/23, are frequently recommended when IBD patients do not respond, lose response, or are intolerant to conventional treatments (Park and Jeen 2015; Kornbluth and Sachar 2010; Panaccione and Ghosh 2010; Lichtenstein et al. 2009). Many studies report beneficial effects of biologic therapy in IBD in inducing and maintaining remission, reducing steroid dependence, decreasing hospitalizations and need for surgical intervention, and potential prevention of complications (Park and Jeen 2015; Mandel et al. 2014; Schreiber 2011; Panaccione and Ghosh 2010; Lichtenstein et al. 2009; Colombel et al. 2007). Nonetheless, a loss of response to biologic therapy will occur in approximately 30% of patients over time, whereas some patients do not respond at all (Chan and Ng 2017; Yanai and Hanauer 2011). The use of biologics in IBD is limited due to the high cost of the treatment and uncertainty about long-term safety (Park and Bass 2011; D'Haens 2007). Significant adverse effects, such as infection, malignancy, hypersensitivity reactions and skin lesions, demyelinization and neurological events, lymphoma, and tuberculosis are associated with biological therapies, validating safety concerns (de Silva et al. 2010; Stallmach et al. 2010; D'Haens 2007).

Although conventional treatments are the first step for IBD therapy, medications do not elicit a response in approximately 20-40% of patients (Park and Jeen 2015; Hilsden 2002). Hence, without the means to modify the disease course and

prevent potential complications, operative management is often required. Correspondingly, failure of medical management remains the most common indication for surgery in IBD (Cohen et al. 2005). A total proctocolectomy with end ileostomy or ileal pouch anal anastomosis is necessitated in 25-35% of UC patients (Regueiro et al. 2016; Sandborn et al. 2009; Hwang and Varma 2008). Approximately 70-90% of CD patients will require a surgical intervention, such as resection of the diseased segment, intestinal bypass, ileostomy, and stricturoplasty, over the course of their disease (Vermeire et al. 2012; Gardiner and Dasari 2007). However, surgery is not curative and disease recurrence often occurs within 3-6 months after the initial intervention, necessitating repeated surgeries in the majority of patients (Buisson et al. 2012).

Overall, IBD therapies are mostly effective in providing symptom relief and improving patient QoL in the short-term. However, loss of patient response, severe side effects, and cost associated with conventional therapies, as well as high rates of disease recurrence following surgery indicates the need for novel treatments.

1.1.8 Experimental models

Advancing our understanding of the underlying mechanisms of IBD is imperative to develop effective prevention and treatment strategies. Although immunohistological and *in vitro* studies using human tissue have enhanced comprehension of IBD pathogenesis, most of the progress made in recent years has stemmed from experimental models of intestinal inflammation (Jiminez et al. 2015). Animal models mimic fundamental clinical, histological, and immunological findings in IBD and although no single model can exactly reproduce the complexity of human IBD, each model provides valuable insights into aspects of the disease (Kiesler et al. 2015). It is unquestionable that studies using tissue samples from IBD patients would provide the most reliable data; however, there are complexities involved in attaining human tissue for research, such as accessibility and isolation of tissue, small sample sizes, genetic variability, and ethical concerns (Jiminez et al. 2015). Hence, comparative whole

animal models are necessary to provide information representative of GI inflammation in humans and essential to furthering our understanding of the pathogenesis of IBD under *in vivo* conditions.

A range of animals have been utilized to investigate intestinal inflammation. Rodents are commonly used in IBD research due to similar immune responses, genes and intestinal epithelium as humans (Waterston et al. 2002; Lin and Hackam 2011). Pigs are advantageous to study the mechanisms underlying gut inflammation as the anatomy and function, as well as the immunity and microbiome, of the pig intestine is comparable to humans (Walters et al. 2012). Non-human primates (NHPs) are deemed the elite animal model for IBD research due to overwhelming similarities to human intestinal physiology, function, immunology, and microbiome (Jiminez et al. 2015). However, use of NHPs in research encounters several hurdles, including ethical considerations, high costs, and the potential risks of carrying highly virulent zoonotic agents (Coors et al. 2010). Nematodes, *Drosophila*, zebrafish, cats and dogs are amongst other animals utilized in studies of intestinal inflammation (Lin and Hackam 2011; Cerquetella et al. 2010; Lam et al. 2004).

More than 60 experimental models have been established to study IBD, including chemically-induced, bacterial-induced, genetically engineered, spontaneous, transgenic, and cell transfer models (Mizoguchi 2012). Chemically-induced animal models are commonly selected to study intestinal inflammation because they are reproducible, relatively easy to develop, accessible, inexpensive, and generate a rapid and robust inflammation (Cominelli et al. 2017; Jiminez et al. 2015; Randhawa et al. 2014). Dextran sodium sulphate (DSS) or 2,4,6-trinitrobenzene sulfonic acid (TNBS) are most frequently used to initiate inflammation, and acetic acid, oxazolone, and azoxymethane to a lesser extent (Jiminez et al. 2015). All of these models induce acute inflammation, however some chemicals, such as DSS and TNBS have the potential to incite both acute and chronic inflammatory responses by varying the concentration and duration of chemical administration (Mizoguchi 2012; Wirtz et al. 2007). Furthermore, whether the induced inflammation is acute or chronic can also be manipulated by

administering a combination of chemical inducers of inflammation (Sussman et al. 2012). The successful and reproducible induction of chemically-induced colitis is variable and depends on the molecular weight, concentration, manufacturer, and batch of the chemical, as well as the species, gender, genetic background, and microorganisms present in the intestine of the animal (Motavallian-Naeini et al. 2012; Perse and Cerar 2012; Nell et al. 2010).

Subacute and chronic colitis are induced in cell transfer animal models via the disruption of T-cell homeostasis (Kiesler et al. 2015; Yoshida et al. 2001). These models most commonly involve the adoptive transfer of naive CD4+ T-cells into syngeneic immunodeficient (severe combined immunodeficient or recombination-activating gene$^{-/-}$) recipient mice (Kiesler et al. 2015; Song-Zhao and Maloy 2014). Cell transfer models are useful for providing insight into immunologic factors that contribute to IBD pathogenesis, as well as cellular and molecular pathways that mediate intestinal inflammation *in vivo* (Song-Zhao and Maloy 2014; Wirtz and Neurath 2000). While adoptive transfer models are important for identifying pathogenic circuits, lymphopenic immunodeficient hosts are prone to infection and may have irregularities in lymphoid architecture (Song-Zhao and Maloy 2014). Furthermore, the severity and location of colitis ensuing from the cell transfer may fluctuate depending on the strain of donor and recipient mice (Ostanin et al. 2009; Powrie 1995).

Genetic knock-out and transgenic models of IBD develop acute and chronic active colitis by a genetically engineered deletion or overexpression of certain molecules, respectively (Mizoguchi 2012). These models are valuable for understanding the functional role of a specific gene product in contributing to, or protecting against, intestinal inflammation, however they have diminished pathogenic relevance as they do not fully represent the underlying mechanisms of the disease (Cominelli et al. 2017). Spontaneous models of IBD include animals that spontaneously develop mucosal inflammation or in which a genetic modification generates an inappropriate mucosal immune response (Borm and Bouma 2004). The recently developed *Winnie* mouse model of spontaneously occurring chronic colitis is quickly gaining recognition as an experimental model

that is highly representative of human IBD. In *Winnie* mice, a point mutation in the *Muc2* mucin gene causes a primary intestinal epithelial defect which alters the mucus layers of the gut, increases intestinal permeability, and amplifies susceptibility to luminal antigens leading to chronic intestinal inflammation (Eri et al. 2011; Heazlewood et al. 2008). Since intestinal inflammation occurs without any evident exogenous influences, similar to human IBD, this model and other spontaneous models of IBD are extremely appealing for studying intestinal inflammation (Goyal et al. 2014).

Congenic IBD models are generated through crossbreeding of mice with various genetic backgrounds, producing a spontaneous multifactorial disease with increased pathogenic relevance to the human condition (Cominelli et al. 2017). However, the genetic defects that contribute to intestinal inflammation is this model are largely unknown due to the crossbreeding (Valatas et al. 2013).

1.2 Neural control of the gastrointestinal tract

1.2.1 Structure and function of the gastrointestinal tract

The digestive system comprises the organs of the GI tract and its accessory structures. The GI tract is essentially a long continuous tube that starts at the mouth and proceeds to the esophagus, stomach, small intestine, and large intestine before terminating at the anus. Accessory structures include the tongue, teeth, gallbladder, salivary glands, liver, and pancreas, which support the GI tract in its primary functions: digestion and absorption of nutrients, secretion and reabsorption of fluid, and the expulsion of redundant or harmful substances (Johnson and Said 2012). These functions are facilitated by the unique architecture of the GI tract: 1) extensive infolding provides a large surface area for maximal absorption and secretion and 2) the gut wall is regularly arranged into four distinct layers from the esophagus to the anus, enabling generation of organized motor patterns for coordinated movement along the GI tract (Rao and Wang 2011). From the lumen outwards, the layers of the gut wall include the mucosa, submucosa, muscularis, and the serosa. The mucosa is a mucus membrane comprised of three layers: 1) an epithelial layer in direct contact with the luminal contents, 2) the lamina propria which consists of subepithelial connective tissue and lymph nodes, and 3) the muscularis mucosae, a thin layer of smooth muscle responsible for generating local movements. The submucosa, consisting of dense connective tissue, blood vessels, lymphatic vessels, and neural tissue, connects the overlying mucosa to the underlying muscularis. An inner layer of circular smooth muscle and an outer layer of longitudinal smooth muscle form the muscularis which is responsible for peristaltic contractile activity and mechanical digestion by segmentation. The outermost layer is the serosa, a serous membrane that provides protection from the spread of inflammatory and malignant processes (Sayegh and Washington 2012; Rao and Wang 2011).

1.2.2 Innervation of the gastrointestinal tract

The GI tract is innervated both extrinsically and intrinsically (Phillips and Powley 2007). Extrinsically, the GI tract is innervated by the parasympathetic and sympathetic nervous systems. The vagus and pelvic nerves provide the parasympathetic innervation to the GI tract; the vagus nerve innervates the esophagus, stomach, gallbladder, pancreas, small intestine, cecum, and proximal colon, while the pelvic nerves innervate the distal colon and anorectal region. All parts of the GI tract receive sympathetic innervation from the prevertebral ganglia. Parasympathetic and sympathetic afferent fibers send sensory information to the CNS, which drives reflexes to alter secretory and motor functions in the gut accordingly. Intrinsically, the gut is innervated by the ENS (Grundy and Brookes 2012). Complete enteric reflex circuits comprised of sensory neurons, interneurons and motor neurons in the small intestine and colon enable the ENS to control motility, secretion and local blood flow without input from the CNS. Overall, proper neuronal regulation of GI function and homeostasis involves assimilated communication between the central nervous system (CNS) and the ENS, between the ENS and the sympathetic ganglia, and within the ENS itself (Furness 2012).

1.2.3 Organization of the enteric nervous system (ENS)

The ENS is an intricate neural network composed of thousands of ganglia, interganglionic nerve fibers, and nerve fibers projecting to effector systems, such as smooth muscle cells, mucosal epithelium, immune cells and blood vessels (Furness 2012; Hansen 2003). The ganglia of the ENS comprise enteric neurons and enteric glial cells (EGCs) and are arranged into two interconnected plexuses embedded within the gut wall: the myenteric and submucosal plexuses.

The myenteric plexus, also known as Auerbach’s plexus, is located between the circular and longitudinal smooth muscle layers of the GI tract. Ganglia are arranged with quasi-regular spacing around the entire circumference of the gut from the upper esophagus to the internal anal sphincter. There are some variations in the structure of ganglia between species and gut regions, however

this is unlikely to have functional significance (Furness 2012). Approximately two thirds of enteric neurons are myenteric neurons, which are generally involved in the regulation of intestinal motility. The axons of myenteric neurons largely distend into interganglionic connectives that run longitudinally between ganglia and then to their target cell.

The submucosal plexus, or Meissner's plexus, is located between the circular muscle and mucosal epithelium of the small and large intestines. Submucosal ganglia tend to be smaller than myenteric ganglia, connected to other submucosal ganglia by interganglionic connectives. Submucosal neurons control secretion, mucosal function, blood flow and barrier function (Furness 2012).

1.2.4 Classification of enteric neurons

The human ENS contains a total of 400-600 million neurons, similar to the number of neurons in the spinal cord and more than in the sympathetic and parasympathetic ganglia (Furness 2012). The density of neurons is higher in the myenteric plexus compared to the submucosal plexus (Wood et al. 1999). Approximately 20 different types of enteric neurons have been identified, categorized according to their morphological, electrophysiological, neurochemical, or functional properties (Furness 2012; Hansen 2003).

1.2.4.1 Morphology

Morphologically, neurons can be classified as Dogiel types I-VII and giant neurons (Hansen 2003). Enteric neurons are most commonly classified morphologically as either Dogiel type I or Dogiel type II. Dogiel type I neurons have a relatively small cell body with many stubby lamellar dendrites and a single long axon. Dogiel type II neurons have large smooth cell bodies and several elongated, tapering, filamentous axons. The processes of type II neurons typically run circumferentially out of the ganglia of origin and branch extensively in surrounding myenteric ganglia (Costa and Brookes 2008; Brookes et al. 1995; Wattchow et al. 1995; Bornstein et al. 1991).

1.2.4.2 Electrical behavior

Enteric neurons may be differentiated by their electrical behavior as either afterhyperpolarization (AH)-type or synaptic (S)-type neurons. Following the discharge of an action potential (AP), AH-type neurons demonstrate long-lasting (>4sec) and substantial (often ≤15mV) AH potentials which limit AP firing. S-type neurons can be distinguished from AH-type neurons by lower resting membrane potentials, greater excitability, a monophasic AP and an absent AH potential (Bornstein 2006; Nurgali et al. 2004). AH-type neurons generally have a Dogiel type II morphology, whereas S-type neurons are typically classified as Dogiel type I (Hansen 2003; Brookes et al. 1995).

1.2.4.3 Neurochemical coding

Neurochemicals expressed by neurons has been used as a tool to classify enteric neurons (Furness 2000). Acetylcholine (ACh) is the major neurotransmitter in the ENS, however more than 30 other neurotransmitters have been identified in the ENS (de Jonge 2013; Serio et al. 2011). Each type of enteric neuron contains a fixed combination of neurotransmitters, transmitter-related enzymes, neuropeptides, neuromodulators and proteins that define its chemical coding. Many of these neurochemicals are functionally important themselves. Although many characteristics of the enteric neurons are analogous along the GI tract, some differences in neurochemical coding have been demonstrated to differ between intestinal regions and between species (Furness et al. 2004; Anlauf et al. 2003; Sang and Young 1998; Timmermans et al. 1997). Chemical coding is not random; the neurochemistry of enteric neurons correlates to its ‘type’. Furthermore, the neurochemical identity of an enteric neuron influences its functional properties (Uyttebroek et al. 2010; Hansen 2003; Furness 2000).

1.2.4.4 Functions

Functionally, enteric neurons are generally divided into three classes: sensory or intrinsic primary afferent neurons (IPANs), interneurons and motor neurons. In general, the ratio of sensory neurons, interneurons, and motor neurons in the GI tract is 2:1:1 (Hansen 2003).

Most IPANs are classified as AH/Dogiel type II neurons, comprising 30% and 14% of the neurons in the myenteric plexus and submucosal plexus, respectively (Reddy 2010). The long dendritic processes of IPANs ramify extensively, projecting orally and anally to connect with interneurons, motor neurons, and other sensory neurons within the ENS. IPANs also relay information to enteric intestinofugal neurons whose processes distend to the sympathetic prevertebral ganglia and pelvic ganglia (Yoo and Mazmanian 2017; Furness 2012; Ren and Bertrand 2008). IPANs may be activated directly by chemical (short chain fatty acids, HCl, bile acids) and mechanical (distortion of the mucosal villi, tension in the gut wall) stimulation or indirectly by serotonin (5-HT) or purines released by enterochromaffin cells. Activated IPANs then release neurotransmitters, calcitonin gene related peptide (CGRP) and substance P to initiate the appropriate action via reflex regulation of functions (Galligan 2009; Hansen 2003).

Interneurons extend either orally (ascending) or anally (descending) from their cell body located within the myenteric plexus (Ren and Bertrand 2008). The total number of ascending neurons is small (5%) and classified morphologically as Dogiel type I. Ascending interneurons contain ACh/choline acetyltransferase (ChAT) and tachykinins and appear to be involved in local motility reflexes (Furness 2012; Reddy 2010; Bornstein et al. 2004). These neurons receive fast synaptic inputs from other ascending interneurons, fast nicotinic and slow synaptic inputs from IPANs and synapse with excitatory motor neurons via fast nicotinic and non-cholinergic slow synaptic inputs. Most descending interneurons are Dogiel type II interneurons which project to both myenteric and submucous ganglia. The neurochemical coding of descending interneurons is complex and includes ACh/ChAT, nitric oxide (NO)/nitric oxide synthase (NOS), vasoactive intestinal polypeptide (VIP), 5-HT, and somatostatin (Hansen 2003). Descending interneurons are implicated in local motility and secretomotor reflexes with ACh, tachykinins, 5-HT, and purines mediating fast or slow synaptic transmission (Hansen 2003; Brehmer et al. 1999; Costa and Brookes 2008).

Enteric motor neurons are Dogiel type I and classified as muscle motor neurons, secretomotor neurons, and secretomotor/vasodilator neurons (Furness 2012). Muscle motor neurons are either excitatory or inhibitory, innervating the longitudinal and circular muscles, as well as the muscularis mucosae to stimulate smooth muscle contraction or relaxation. The chemical coding of excitatory neurons includes ACh and tachykinins, which are synthesized by ChAT, for predominantly muscarinic cholinergic and tachykinergic transmission. Excitatory muscle motor neurons receive mostly fast nicotinic synaptic input from IPANs and cholinergic ascending interneurons. Inhibitory muscle motor neurons elicit relaxation of GI smooth muscle mediated primarily by NO/NOS, as well as VIP and purines (Durnin et al. 2013; Rivera et al. 2011). These neurons receive fast nicotinic and non-cholinergic inputs from IPANs and descending interneurons. The secretomotor and secretomotor/vasodilator neurons are generally located in the submucosal plexus and regulate exocrine fluid secretions and blood flow in the GI tract. These cholinergic and non-cholinergic neurons release ACh or VIP after receiving fast or slow synaptic inputs from IPANs (Christofi 2008; Costa et al. 2000).

1.2.5 Enteric glial cells (EGCs)

Enteric neurons are supported by EGCs, the ENS counterparts of CNS astrocytes, capable of modulating neuronal function (Hoff et al. 2008). EGCs are morphologically small cells, characteristically possessing long laminar processes which envelope groups of enteric neuronal cell bodies and axon bundles and extending their processes into the intestinal mucosa (Hoff et al. 2008; Ruhl 2005). EGCs release a wide array of factors necessary for the development, survival and differentiation of neurons and have been traditionally contemplated as a mechanical support for enteric neurons (Laranjeira and Pachnis 2009). However, it is now known that EGCs have additional roles, including acting as modulators for the homeostasis of enteric neurons, involvement in enteric neurotransmission, and antigen-presenting cellular activity (Van Landeghem et al. 2009; Bassotti et al. 2007; Ruhl 2005). Furthermore, it is thought that EGCs may play a role in GI motor activity.

1.2.6 Signal transmission in the ENS

In the ENS, neurons communicate directly with other enteric neurons, as well as with the smooth muscle cells in the gut wall via chemical neurotransmission to ensure proper function of the GI tract. Neuron to neuron transmission may be labelled synaptic, while junctional transmission describes neuron to smooth muscle cell communication. Electrical impulses are relayed across a synapse/junction by chemical neurotransmitters released from nerve terminals. Neurotransmitters bind to specific receptors on the target cell which produce changes in the membrane potential: postsynaptic or junction potentials. These potentials propagate passively and may result from either depolarization or hyperpolarization. The effector cells may show only excitatory, inhibitory or both excitatory and inhibitory potentials (Goyal and Chaudhury 2013).

1.2.6.1 Synaptic potentials

Studies involving intracellular electrophysiological recordings have revealed distinctive synaptic and receptor properties in different classes of neurons and regions of the ENS; the vast majority of investigations have focused on the myenteric and submucosal plexuses of the guinea-pig intestine (Monro et al. 2008; 2004; Galligan and North 2004). Fundamental mechanisms for chemically induced synaptic transmission in the ENS are consistent with elsewhere in the nervous system (Hansen 2003). Primary synaptic events in the ENS include presynaptic facilitation and inhibition, excitatory postsynaptic potentials (EPSPs), and inhibitory postsynaptic potentials (IPSPs). ENS neurons may express signal transduction mechanisms for both slow and fast synaptic neurotransmission. Fast synaptic potentials are generally EPSPs, whereas slow synaptic potentials may be either EPSPs or IPSPs (Wood 2011).

Synaptic transmission may be enhanced by presynaptic facilitation or suppressed by presynaptic inhibition. Presynaptic facilitation is evidenced by an increase in amplitude of fast EPSPs at nicotinic synapses where it reflects enhanced release of ACh via nicotinic and 5-HT_4 receptors (Galligan et al. 2003; Schneider and Galligan 2000). Muscarinic receptors, 5-HT_{1A} receptors, galanin, and adenosine

receptors (A1) have been demonstrated as mediators for presynaptic inhibition (Gwynne and Bornstein 2007b).

Fast EPSPs are rapidly activating depolarizing responses of the postsynapatic membrane, lasting for ~30ms and <50ms and representing the major form of communication between enteric neurons (Gwynne and Bornstein 2007b; Galligan 2002). Fast EPSPs can be recorded in 70% of all myenteric neurons and 90% of all submucosal neurons; they are uncommon in AH-type neurons, but are present in almost all S-type neurons (Gwynne and Bornstein 2007b). Furthermore, they may be the sole mechanism of transmission between vagal efferents and enteric neurons (Wood 2011). The main mediator of fast EPSPs is ACh acting through nicotinic receptors (nAChR), but they can also be generated by adenosine 5′-triphosphate (ATP) acting at P2X receptors and by 5-HT acting at 5-HT_3 receptors (Ren and Bertrand 2008; Galligan and North 2004; Galligan et al. 2000). Fast EPSPs mediated by nAChR are involved in the relay of sensory information at every functionally defined synapse within the ascending excitatory pathway; an important component underlying of gut motility (Gwynne and Bornstein 2007b).

Slow EPSPs are characterized by slowly activating membrane depolarization which lasts for several seconds to minutes and even hours following termination of the stimulus (Gwynne and Bornstein 2007b; Wood and Kirchgessner 2004). There are differing types of slow EPSPs in the ENS associated with distinct time courses, pharmacology, and intracellular transduction mechanisms (Gwynne and Bornstein 2007b). Electrical stimulation applied to the myenteric and submucosal ganglia or interganglionic fiber tracts evokes slow EPSPs in AH/Dogiel type II and S/Dogiel type I enteric neurons. In AH/Dogiel type II neurons, slow EPSPs may be mediated by 5-HT acting at 5-HT_7 receptors, tachykinins acting at neurokinin (NK)-1 and NK3 receptors, and ACh acting at M1 muscarinic receptors (Monro et al. 2005; Johnson and Bornstein 2004; Alex et al. 2001; North et al. 1985). In S/Dogiel type I neurons, slow EPSPs are mediated by ATP acting at $P2Y_1$ receptors, tachykinins acting at NK1 receptors, and ACh acting at muscarinic receptors (Monro et al. 2004; Hu et al. 2003; Alex et al. 2002; North and Tokimasa 1982). Slow EPSPs mediated by $P2Y_1$ receptors are essential to

transmission in the descending inhibitory reflex pathway (Gwynne and Bornstein 2007b).

IPSPs are hyperpolarizing synaptic potentials that activate slowly and continue for several seconds after termination of the stimulation in both myenteric and submucosal neurons (Wood 2011). In the submucosal plexus, IPSPs predominantly occur in VIP-containing noncholinergic secretomotor neurons by adrenaline acting at α2-noradrenergic receptors, somatostatin acting at SST_1 and SST_2 receptors, and 5-HT acting at $5\text{-}HT_{1A}$ receptors (Foong et al. 2010; Shen and Surprenant 1993; North and Surprenant 1985). There are limited data regarding the transmitters mediating IPSPs in myenteric neurons; IPSPs are normally concealed by slow EPSPs (Bornstein 2008). However, since IPSPs are blocked by a $5\text{-}HT_{1A}$ receptor antagonist, it is suggested they may be mediated by 5-HT acting on $5\text{-}HT_{1A}$ receptors (Johnson and Bornstein 2004).

1.2.6.2 Junction potentials

Electrical potentials in smooth muscle cells in response to motor nerve stimulation are called junction potentials. Junctional transmissions are defined as ‘close’ or ‘wide’ based on the distance between the release site on the prejunctional nerve terminal and the postjunctional receptors on the target cell (Goyal and Chaudhury 2013). Close junctional transmission is associated with fast junction potentials, whereas wide junctional transmission is associated with slow junctional potentials. Most smooth muscles demonstrate both fast and slow junction potentials which are generally mediated by different types of receptors.

In close/fast junctional transmission, the distance between the prejunctional release site on the nerve terminal and the postjunctional receptor on the smooth muscle cell is typically 10-20nm (Goyal and Chaudhury 2013). Fast junction potentials last for 250ms-2.5sec (~1sec) and may be depolarizing (fast excitatory junction potential (fEJP)) or hyperpolarizing (fast inhibitory junction potential (fIJP)). fEJPs in the gut are mediated by both ACh acting on muscarinic M3 receptors and ATP acting on P2X receptors, while fIJPs are purinergic and

mediated by ATP or related purines acting on $P2Y_1$ receptors (Gallego et al. 2012; Zhang and Paterson 2005; Maggi et al. 1997).

The wide/slow junctional transmission is characterized by >100nm->2000nm of junctional space between the axon varicosities and smooth muscle cell postjunctional receptor (Goyal and Chaudhury 2013). Slow junctional potentials generally last seconds to minutes and may be depolarizing (slow excitatory junction potential (sEJP)) or hyperpolarizing (slow inhibitory junctional potential (sIJP)). sEJPs are mediated by NK acting on its metabotropic receptors, whereas sIJPs are mediated by NO acting via the guanylate cyclase/3'5' cyclic guanosine monophosphate pathway (Furness 2006; Van Geldre and Lefebvre 2004).

1.2.7 Neural regulation of gastrointestinal motility function

Normal motility function in the gut involves complex interactions between the enteric reflex circuits and myogenic mechanisms (smooth muscle cells and interstitial cells of Cajal (ICC)), as well as input from extrinsic sources including parasympathetic and sympathetic nerves, hormones and inflammatory mediators (Huizinga and Lammers 2009; Sanders 2008). Expression of various motor patterns is generally not the consequence of independent actions of different control systems but rather, depending on specific stimuli, of varying domination of one or more of the control activities. The different control systems of motility are unique but interconnected. The small and large intestines contain complete reflex circuits within the ENS, showing a significant degree of autonomy in the absence of extrinsic input. In contrast, the esophagus and stomach are much more dependent on extrinsic neural inputs and the ENS has little influence on peristaltic activity in these regions of the GI tract (Browning and Travagli 2014; Furness et al. 2014). The circular and longitudinal smooth muscle layers within the gut wall are direct effectors for propulsive and mixing movements throughout the entire GI tract. ICC are the intestinal pacemaker cells responsible for rhythmic propagation of circular muscle contractions (Huizinga et al. 2014).

The two main components of gut motility are mixing and propulsion of digesta along the GI tract. The intensity of mixing movements and the rates of propulsion

vary between organs; mixing movements intensify while propulsion rates slow as the digesta is transported distally towards the anus. In any segment of the GI tract, the spatiotemporal characteristics of smooth muscle contractions determine the efficacy of propulsion and mixing movements. The spatial characteristics of gut contractions include direction of propagation, distance of propagation, and velocity of propagation, whereas the temporal characteristics of gut contractions include frequency, amplitude, and duration. Based on these spatiotemporal characteristics, the main intestinal motor patterns observed in several species are peristaltic contractions, segmenting contractions and migrating motor complexes (MMCs) (Sarna 2010; Gonzalez and Sarna 2001). The motility functions of these contractions are markedly different and vary in fed and fasted states. Furthermore, the composition of contractions varies among gut organs depending on their specific requirements of motility function (Sarna 2010; Bornstein et al. 2002; Gonzalez and Sarna 2001).

1.2.7.1 Peristaltic contractions

Gut peristaltic contractions are anally directed propagating motor patterns involving fractional or complete occlusion of the lumen (Huizinga and Lammers 2009). It was originally considered that a neurally mediated polysynaptic reflex, the peristaltic reflex, was predominantly responsible for peristaltic contractions. The peristaltic reflex is initiated by a bolus causing distension of the intestinal wall, which activates IPANs. Sensory input is then relayed to motor neurons by ascending excitatory and descending inhibitory pathways, leading to contraction oral to the bolus and relaxation anal to the bolus (Huizinga and Lammers 2009). However, while the peristaltic reflex has been demonstrated convincingly and its pathways well established, peristaltic motor activity is not always evoked by the presence of a bolus, luminal stretch does not necessarily initiate the reflex, and contractions have been observed to propagate away from the stimulus in both oral and anal directions (Costa et al. 2000; Spencer et al. 1999). Although there is clearly a role for neural mediation in peristalsis, the peristaltic reflex alone cannot account for variations in propulsive motor activity. It is now proposed that peristalsis occurs due to the coordinated activities of the enteric neurons and the

ICC. ICC generate and propagate slow waves, spontaneous periodic depolarizations of smooth muscle cells which instigate short cycles of high and low excitability in the circular smooth muscle cells. During periods of high excitability, stimulation from muscle distension, excitatory neurotransmission, or inhibition of inhibitory neurotransmission elevates smooth muscle cell depolarization above threshold to evoke contraction (Rychter et al. 2014; Sarna 2010). Although distention can cause peristaltic activity without excitatory neural input, the ENS generally stipulates the force of contraction (Huizinga and Lammers 2009). In addition to the aforementioned mechanisms, peristaltic activity may also be driven by pattern generators in the CNS (Huizinga and Lammers 2009).

1.2.7.2 Segmenting contractions

Segmenting contractions are stationary rhythmic contractions of the circular smooth muscle that alternate with relaxations to repeatedly divide and re-divide a mass of intestinal content (Gwynne and Bornstein 2007a; Bornstein et al. 2002). These motor patterns are specialized for mixing and absorption functions and comprise more than 90% of the small intestine contractile activity during digestion (Bornstein 2008). The mechanisms underlying the initiation of segmentation motor patterns is not completely understood, however *in vitro* studies involving isolated guinea-pig small intestine have shown that segmentation can be evoked by intraluminal content including fatty acids and amino acids (Gwynne et al. 2004a; 2004b). *In vitro* studies have demonstrated abolishment of segmentation when the activity of the ENS is obstructed, as well as conversion of stationary contractions to propagating contractions when IJPs are blocked (Gwynne and Bornstein 2007a; Gwynne et al. 2004b). These results suggest that segmenting contractions are result of coordinated activity generated within the ENS independent of myogenic regulation. However, an *in vitro* study in the isolated mouse small intestine reported that segmentation can occur after total nerve blockade, proposing that interacting myogenic electrical activities underlie the segmentation motor pattern (Huizinga et al. 2014). While the data is conflicting, the critical importance of the segmentation motor pattern makes it unlikely that

there is only one single mechanism underlying it. Therefore, alike peristalsis, it is probable that segmentation is a result of the ENS working in concert with myogenic ICC pacemaker activities (Huizinga and Chen 2014).

1.2.7.3 Migrating motor complexes

MMCs are spontaneously occurring cyclical contractions of the smooth muscle layers in the stomach, small intestine or colon that can propagate over large regions of the gut (Spencer et al. 2003). Three distinct phases occur in a normal MMC cycle: 1) a period of quiescence, 2) a period of irregular contractions that increase in magnitude over 20–30% of the complex, 3) a period of very strong rhythmic contractions that propagate slowly along the intestine (Bornstein 2008). In humans and other species that feed intermittently, MMCs occur in the stomach and small intestine during the fasted state. However, in animals that feed constantly, such as guinea-pigs, rats and mice, MMCs can occur in the fed state (Deloose et al. 2012; Kunze and Furness 1999). Colonic MMCs (CMMCs) occur independently of MMCs in the small intestine in both fed and fasted states (Heredia et al. 2010). CMMCs are defined as contractions that migrate relatively slowing over >50% of the colon length in studies investigating motility in the isolated colon *in vitro* (Roberts et al. 2008b; 2007; Fida et al. 1997). Although most CMMCs propagate in a largely oral-to-anal (antegrade) direction, they can also propagate orally, in a retrograde fashion (Spencer and Bywater 2002; Bush et al. 2000; Fida et al. 1997). Previous studies have provided significant evidence to suggest that MMCs are neural in origin; CMMCs do not occur in aganglionic regions of colon and neuronal blockade with hexamethonium or tetrodotoxin abolishes MMC activity (Spencer et al. 2007; 1998; Fida et al. 1997). Furthermore, the occurrence of CMMCs in the isolated colon indicates that their initiation is independent of the CNS (Spencer et al. 2005). ACh release from excitatory motor neurons mediates the rapid component of the MMC, while the release of NO and ATP from inhibitory motor neurons appears primarily to be involved in maintaining quiescence between MMCs (Brierley et al. 2001).

1.2.8 Inflammation-induced changes to the ENS

Evidence from studies involving both animal models of colitis and biopsies from IBD patients demonstrate that inflammation, even if mild, is associated with ENS abnormalities (Nurgali et al. 2011; 2009; 2007; Villanacci et al. 2008; De Giorgio et al. 2002; Sanovic et al. 1999). These inflammation-induced changes to the ENS are well known to affect gut function. Furthermore, ENS damage and alterations to gut function persist long after acute intestinal inflammation is resolved, playing a role in the generation of IBD associated symptoms (Mawe 2015; Krauter et al. 2007b; Linden et al. 2005).

Intestinal inflammation has been consistently associated with decreases in the number of enteric neurons that does not appear restricted to specific neuronal populations. A 61% decrease in the number of enteric neurons was reported in colon tissues from UC patients (Bernardini et al. 2012). In consistency with these findings, significant neuronal loss has been demonstrated in several experimental models of colitis; the number of myenteric neurons is decreased by up to 33% in guinea-pigs and rats with TNBS-induced colitis and ileitis and up to 50% in rats and mice with DNBS-induced colitis (Nurgali et al. 2011; Sarnelli et al. 2009; Boyer et al. 2005; Lin et al. 2005; Linden et al. 2005; Poli et al. 2001; Sanovic et al. 1999). Furthermore, inflammation-induced neuronal loss is long-lasting, persisting for at least 56 days after the resolution of inflammation in the guinea-pig colon (Linden et al. 2005). While most studies describe neuronal loss, some studies diverge, reporting an increase or no change to the total number of enteric neurons to be associated with intestinal inflammation (Winston et al. 2013; Villanacci et al. 2008; Neunlist et al. 2003; Davis et al. 1955; Storsteen et al. 1953). Increased neuronal cell numbers in patients with CD may be due to parenteral nutrition which is used in most patients before surgery (bowel resection) (Villanacci et al. 2008). The region of the intestine analyzed, severity of inflammation, type of marker used to identify neurons, experimental model or disease type, age of patient, and method of quantification are among multiple factors that may contribute to controversial results (Winston et al. 2013; Bernardini et al. 2012).

Changes to ganglia, nerve fibers and EGCs have also be associated with intestinal inflammation. Hypertrophy and/or hyperplasia of ENS ganglia, extrinsic and intrinsic nerve bundles, and EGCs has been demonstrated in CD and UC (Vasina et al. 2006; Geboes and Collins 1998). Furthermore, nerve trunk hypertrophy is related to the extent of inflammatory infiltrate, suggesting that the presence of myenteric and submucosal plexitis may be predictive of IBD evolution and recurrence (Sokol et al. 2009; Ferrante et al. 2006; Vasina et al. 2006). Nerve fiber degeneration and necrosis evidenced by enlarged empty axons comprising large membrane-bound vacuoles, swollen mitochondria, and concentrated neurofibrils accompanies IBD in both inflamed and non-inflamed areas (Dvorak et al. 1993; Demir et al. 2013). A substantial loss of myenteric EGCs has been reported in GI inflammatory disorders, but it is unclear whether this precedes or follows neuronal loss (De Giorgio et al. 2012; Bassotti et al. 2006).

Based on the significant changes to the structure of the ENS observed in tissues from IBD patients and experimental models of colitis, it is not surprising that these alterations are accompanied by substantial changes in ENS function. Intestinal inflammation induces several changes in the intrinsic motor circuits of the gut, including neuronal hyperexcitability, increased synaptic facilitation, and decreased descending inhibitory neuromuscular transmission (Roberts et al. 2013; Strong et al. 2010; Nurgali et al. 2009; Krauter et al. 2007a; Lomax et al. 2005; Linden et al. 2003). Hyperexcitability of AH neurons induced by colitis have been well documented during and after the resolution of inflammation (Krauter et al. 2007b; Lomax et al. 2007a; 2005; Nurgali et al. 2007; Linden et al. 2003). Reductions in AHP due to elevated levels of prostaglandin E2 or reduced intracellular Ca^{2+} signaling may underlie neuronal hyperexcitability associated with gut inflammation (Mawe et al. 2009; Lomax et al. 2006; 2005; Linden et al. 2004). Increased synaptic facilitation in the inflamed gut is demonstrated by an augmented amplitude of evoked fast EPSPs in S-type neurons, most likely due to alterations in neurotransmitters that contribute to fast EPSPs (Lomax et al. 2005; Linden et al. 2003). An oxidative stress-stimulated decrease in purines released from inhibitory motor neurons causes a reduction in the purinergic component of the IJP in preparations of the inflamed colon from animals with

TNBS-induced colitis (Strong et al. 2010). Disruptions in the descending inhibitory pathway can affect propulsive motility by decreasing the extent of relaxation in the receiving segment during peristalsis (Mawe 2015). Altogether, the aforementioned changes in intrinsic motor circuitry contribute to alterations in intestinal motility, which underlie the symptoms of IBD, such as diarrhea and constipation (Mawe 2015).

The detrimental effects on the structure and function of the ENS during and following the resolution of inflammation have been well documented, suggesting a role for ENS damage in mechanisms underlying the pathogenesis of IBD. Together with the global increases in the epidemiology of IBD, impact on the economy and patient QoL, and the lack of adequate treatment options, the enteric neurons are a discernable target for potential IBD therapies.

1.3 Mesenchymal stem cells (MSCs)

Mesenchymal stem cells (MSCs) are a subset of stromal stem cells that play a major role in tissue regeneration, repair, and homeostasis due to their capacity for self-renewal, differentiation, immune modulation, and paracrine effects (Liu et al. 2009b; Barry and Murphy 2004; Pittenger et al. 1999). In response to signals, endogenous MSCs mobilize and migrate to injured or inflamed tissue where they exert their reparative effects (Rennert et al. 2012). However, most adult tissue is unable to regenerate following injury despite this endogenous MSC recruitment, suggesting that these mechanisms are easily overwhelmed. Additionally, reservoirs of MSCs can be depleted by degenerative disease, physiological aberrations, or age (Marquez-Curtis and Janowska-Wieczorek 2013). Therapies involving transplantation of exogenous MSCs imitate and augment the natural healing response by enhancing activation of the endogenous MSC pool as well as increasing the total number of MSCs available to promote tissue repair (Fong et al. 2011; Semont et al. 2013). In this way, several studies have demonstrated enhanced endogenous neurogenesis in experimental models of neurodegeneration following administration of exogenous MSCs (Oh et al. 2015; Park et al. 2012; Cova et al. 2010).

MSCs are multipotent cells that can be isolated from a range of non-embryonic tissues, including bone marrow (BM), adipose tissue, skeletal muscle, synovial membranes, umbilical cord, and placenta (Shi et al. 2012; Garcia-Bosch et al. 2010; Barry and Murphy 2004). Most commonly isolated from the BM, MSCs only represent a minute fraction (0.001-0.01%) of the total BM population of nucleated cells, however their adherent nature enables them to be sequestered and rapidly expanded for a number of passages without substantial modification of their major properties (Sotiropoulou et al. 2006). Although BM-MSCs and MSCs isolated from other adult tissues demonstrate many shared properties, they exhibit differences in morphology, phenotype, and aptitude for differentiation and proliferation (Liu et al. 2009b). Thus, MSC populations residing in different tissues are considered biologically heterogeneous; possibly a function of their tissue

microenvironment (Paul and Anisimov 2013; Hegyi et al. 2010; da Silva Meirelles et al. 2006).

Studies investigating the biological features and therapeutic prospective of MSCs have employed various methods of cell isolation, expansion, and characterization, which has generated many ambiguities and inconsistencies between reports (Gao et al. 2016). To address this issue, the International Society for Cellular Therapy (ISCT) proposed a set of standards to define MSCs for laboratory and clinical considerations (Dominici et al. 2006). For a population of cells to qualify as MSCs, the minimal requirements of three criteria must be met, including 1) adhere to tissue culture plastic, 2) expression of markers CD105, CD73, and CD90 must be ≥95%, while they must lack expression of CD34, CD45, CD14 or CD11b, CD79α or CD19, and HLA-DR in culture, and 3) capacity to differentiate into osteoblasts, adipocytes, and chondroblasts under standard *in vitro* differentiating conditions (Karp and Teo 2009; Dominici et al. 2006).

The therapeutic potential of MSCs has recently gained significance for promoting regenerative repair and providing a defense against pathological disease processes (Patel et al. 2013). MSCs possess an array of biological attributes that influence their capacity to exert therapeutic effects, including proficiency in homing to areas of tissue damage (Liu et al. 2009b; Ortiz et al. 2003), potential for differentiation into multiple cell types (Barry and Murphy 2004; Pittenger et al. 1999), and ability to release biological molecules with significant anti-proliferative, anti-inflammatory, anti-apoptotic, immunomodulating and neuroprotective properties (Ren et al. 2012a; Shi et al. 2012; Wang et al. 2012a). Furthermore, MSCs have low immunogenicity, able to evade the host's immune response due to lacking major histocompatibility class (MHC)-II and other costimulatory molecules required for immune cell stimulation (Ryan et al. 2005).

Many studies have confirmed the ability of MSCs to migrate to sites of tissue damage and inflammation, irrespective of the tissue or the pathologic condition (Wang et al. 2012a; Spaeth et al. 2008; Liu et al. 2007; Ortiz et al. 2003). Injured or inflamed tissues release chemokines, cytokines, and growth factors into the circulation which serve as chemoattractants for MSCs. Chemoattractants are

recognized by a wide variety of receptors expressed by MSCs, providing directional migration to the site of injury (De Becker and Riet 2016; Kang et al. 2012). Studies have revealed that MSC migration is dependent on certain chemokine-receptor interactions, such as stromal cell-derived factor-1/C-X-C chemokine receptor-4 (Son et al. 2006; Nakamizo et al. 2005), hepatocyte growth factor (HGF)/c-Met (Forte et al. 2006), vascular endothelial growth factor (VEGF)/VEGF receptor (Ball et al. 2007), platelet-derived growth factor (PDGF)/PDGF receptor (Nakamizo et al. 2005; Fiedler et al. 2002), and monocyte chemoattractant protein-1/C-C chemokine receptor-2 (Dwyer et al. 2007), amongst others. The migratory capacity of MSCs may also be influenced by a number of factors, including the age and passage number of cells, culturing conditions, and the mode of delivery (Ullah et al. 2015). Upon reaching the injury site, MSCs coordinate and interact with various types of stromal and inflammatory cells in order to participate in damage repair and regeneration processes (Zachar et al. 2016).

MSCs are multipotent progenitor cells with multilineage potential to differentiate into cell types of mesodermal origin, such as adipocytes, osteocytes, and chondrocytes *in vivo* and *in vitro* (Ullah et al. 2015; Kim and Cho 2013; Liu et al. 2009b; Barry and Murphy 2004; Pittenger et al. 1999). Some studies suggest that the differentiation potential of MSCs is not limited to mesenchymal derivatives, demonstrating that MSCs can also differentiate into cells of ectodermal (neurocytes) and endodermal lineages (hepatocytes) under appropriate cell culturing conditions or stimulation by specific endogenous or exogenous bioactive factors (An et al. 2014; Hang et al. 2014; Bae et al. 2011b; Datta et al. 2011; Naghdi et al. 2009). However, there is some doubt regarding the functional capacities of MSCs differentiated into cells other than conventional mesodermal lineages (Phinney and Prockop 2007). The original hypothesis underlying the therapeutic effects of MSCs was based on MSC differentiation to repair and replace damaged cells (Bussolati 2011). However, long-term survival and differentiation of transplanted MSCs is infrequently observed *in vivo* (Abouelkheir et al. 2016; Noiseux et al. 2006). Therefore, it is likely that the beneficial effects of MSC therapy are due to the paracrine actions of MSCs rather than their

differentiation capacity. MSCs act in a paracrine manner by releasing a widespread secretome of bioactive factors which can alleviate inflammation, influence immune interaction, encourage cell survival and matrix remodeling, and establish an environment favorable for regeneration by endogenous cells (Ranganath et al. 2012; Karp and Teo 2009).

MSCs possess diverse immunomodulatory abilities and are capable of influencing both innate and adaptive immunity. At the injury site, MSCs require activation by pro-inflammatory cytokines, such as IFN-γ, TNF-α and IL-1β, to exert these immunomodulatory effects (Ren et al. 2008; Krampera et al. 2006). Activated MSCs secrete a wide variety of immunosuppressive soluble factors including indoleamine 2,3-dioxygenase, prostaglandin E2, TNF-α stimulated protein/gene-6, NO, TGF-β1, human leukocyte antigen-G5, hemoxygenase-1, leukocyte inhibitory factor, IL-6, IL-8, and IL-10 (Zachar et al. 2016; de Witte et al. 2015; English 2013; Melief et al. 2013). These factors, amongst others, enable MSCs to interact with components of innate and adaptive immunity leading to polarization of pro-inflammatory M1 macrophages to the anti-inflammatory M2 phenotype, generation of T-regulatory cells and tolerogenic dendritic cells (DCs), promotion of Th1-Th2 switch, inhibition of mast cell and Th17 differentiation, B lymphocyte activation, natural killer cell cytotoxicity, and T-cell proliferation, as well as induction of T-cell apoptosis (Li et al. 2014; Ge et al. 2010; Ghannam et al. 2010; Nemeth et al. 2009; Ren et al. 2008; Corcione et al. 2006). MSCs have also been shown to impede the differentiation, maturation, and activation of DCs, hindering antigen-presenting functions and reducing their pro-inflammatory potential (Djouad et al. 2007; Jiang et al. 2005). In addition to immunomodulation via the release of soluble mediators, MSCs also exert immunosuppressive effects by cell-cell interaction. Inflammation induces upregulation of adhesion molecules, such as intercellular adhesion molecule-1 and vascular cell adhesion molecule-1, on the surface of MSCs, attracting and anchoring T-cells and inducing their apoptosis (Ren et al. 2011; 2008). Furthermore, MSCs may attach themselves to Th17 cells facilitating them to adopt a regulatory phenotype (Ghannam et al. 2010).

MSCs derived from various adult tissue sources have demonstrated an immense capacity for neurological regenerative therapy, promoting functional recovery and nerve fiber regeneration in animal models of spinal cord injury, stroke, and neurodegenerative diseases including Parkinson's disease, amyotrophic lateral sclerosis (ALS), Huntington's disease, Alzheimer's disease, and multiple sclerosis (Table 1.2) (Song et al. 2013; Al Jumah and Abumaree 2012; Park et al. 2008; Zhao et al. 2007; Shen et al. 2006). Furthermore, transplantation of MSCs is often reported to be associated with other positive effects in these models, both at histological and behavioral levels, as well as improved survival rates (Lo Furno et al. 2018; Volkman and Offen 2017). Several mechanisms by which MSCs exert their neuroprotective and neuroregenerative effects in damaged neural tissue have been proposed, including production and secretion of neurotrophic factors, induction of neurogenesis, modulation of inflammation, and prevention of misfolded protein aggregation (Table 1.2). Secretion of neurotrophic factors, such as glial cell-derived neurotrophic factor (GDNF), brain-derived neurotrophic factor (BDNF), nerve growth factor (NGF), and neurotrophin (NT)-3 has been implicated in nerve fiber regeneration and increased neuron survival both *in vitro* and *in vivo* (Oliveira et al. 2013; Kim et al. 2009; Park et al. 2008; Kurozumi et al. 2005). Additionally, certain soluble factors released by MSCs display neurogenic effects on neural stem/progenitor cells (Croft and Przyborski 2009; Wang et al. 2009b).

The release of soluble factors, such as anti-inflammatory cytokines, growth factors, and neuro-regulatory molecules into culture medium by MSCs may provide all the vital elements for tissue repair. Hence, MSC conditioned medium (CM) could consequently reiterate the positive effects of stem cell therapy for tissue repair (Ranganath et al. 2012; Burdon et al. 2011; Ribeiro et al. 2011; Salgado et al. 2010a). Several studies have demonstrated the therapeutic potential of the MSC secretome and/or CM on nervous system injury and degeneration, including facilitation of nerve regeneration, inhibition of apoptosis, and support of neuron survival (Yang et al. 2009; Isele et al. 2007; Neuhuber et al. 2005).

Table 1.2 MSCs in experimental models of neurodegeneration and neuronal injury

Disease	Suggested mechanism	Clinical improvement
Spinal cord injury (Chung et al. 2016; Tang et al. 2016; Ribeiro et al. 2015; Dadon-Nachum et al. 2011)	• Neurotrophic factor secretion • Modulation of inflammation • Immunomodulation	• Improved motor functions • Axonal regeneration • Reduced neuromuscular degeneration
Parkinson's disease (Park et al. 2016; 2014a; 2012; Cova et al. 2010; Glavaski-Joksimovic et al. 2010; Sadan et al. 2009; Dezawa et al. 2004)	• Neurotrophic factor secretion • Enhanced endogenous neurogenesis • Modulation of inflammation • Immunomodulation • Induced α-synuclein clearance	• Enhanced dopaminergic neurons survival • Dopamine fibers rejuvenation • Reduced dopamine depletion • Enhanced striatal regeneration
Alzheimer's disease (Oh et al. 2015; Shin et al. 2014; Kim et al. 2012; Lee et al. 2010)	• Neurotrophic factor secretion • Reduced Aβ and p-tau deposition • Immunomodulation • Induced Aβ clearance • Enhanced endogenous neurogenesis	• Improved learning • Improved memory performance • Reduced memory decline • Increased hippocampal neuronal survival
Stroke (Chung et al. 2015; Wang et al. 2013a; Bao et al. 2011; Kim et al. 2008)	• Neurotrophic factor secretion • Enhanced endogenous neurogenesis • MSC neuronal differentiation • Modulation of inflammation • Immunomodulation • Reduced endothelial vasculature damage	• Improved motor recovery • Reduced ischemic core • Functional recovery in neurological severity score • Reduced infarct volume • Enhanced neuronal survival

Table 1.2 MSCs in experimental models of neurodegeneration and neuronal injury (continued)

Disease	Suggested mechanism	Clinical improvement
Multiple sclerosis (Bravo et al. 2016; Shalaby et al. 2016; Fisher-Shoval et al. 2012; Payne et al. 2013b; 2012b; Gordon et al. 2010; Bai et al. 2009; Constantin et al. 2009; Zhang et al. 2006)	• Neurotrophic factor secretion • NGF mediated axonal protection • Immunomodulation • Enhanced oligodendrogenesis • Modulation of inflammation	• Deceleration in disease progression • Reduced disease severity • Reduced neuronal loss • Reduced axonal loss • Decreased white matter lesions • Decreased demyelination
Amyotrophic lateral sclerosis (ALS) (Krakora et al. 2013; Vercelli et al. 2008; Zhao et al. 2007)	• Neurotrophic factor secretion • Immunomodulation	• Sustained survival of motor neurons • Improved motor functions • Delayed disease onset • Prolonged lifespan • Sprouting and reinnervation of fibers
Huntington's disease (Pollock et al. 2016; Sadan et al. 2012)	• Neurotrophic factor secretion • Enhanced endogenous neurogenesis	• Reduced striatal atrophy • Enhanced neuron survival

The release of soluble factors, such as anti-inflammatory cytokines, growth factors, and neuro-regulatory molecules into culture medium by MSCs may provide all the vital elements for tissue repair. Hence, MSC conditioned medium (CM) could consequently reiterate the positive effects of stem cell therapy for tissue repair (Ranganath et al. 2012; Burdon et al. 2011; Ribeiro et al. 2011; Salgado et al. 2010a). Several studies have demonstrated the therapeutic potential of the MSC secretome and/or CM on nervous system injury and

degeneration, including facilitation of nerve regeneration, inhibition of apoptosis, and support of neuron survival (Yang et al. 2009; Isele et al. 2007; Neuhuber et al. 2005).

1.3.1 MSC therapy in inflammatory bowel disease

The unique properties of MSCs are appealing for use in the treatment of IBD. The efficacy of MSC therapy on histopathological changes to the gut wall and alterations in the immune response associated with IBD has been studied in various animal models of IBD, including DSS and TNBS-induced colitis (Liu et al. 2014; Castelo-Branco et al. 2012; Liang et al. 2011; Gonzalez-Rey et al. 2009; Ando et al. 2008; Hayashi et al. 2008; Tanaka et al. 2008). MSCs administered systemically (intravenously or intraperitoneally) and locally were shown to migrate and engraft in the wall of the intestine at the site of inflammation; the number of engrafted MSCs influenced by the degree of inflammation (Chen et al. 2013b; Fawzy et al. 2013; Castelo-Branco et al. 2012; Ando et al. 2008; Tanaka et al. 2008). In both DSS and TNBS-induced colitis, the attenuation of disease activity following MSC treatment is regularly demonstrated (Castelo-Branco et al. 2012; Hayashi et al. 2008). Macroscopically, MSCs reduce inflammation-induced shortening of the colon, rectal bleeding and weight loss, while improving stool consistency (Chen et al. 2013b; He et al. 2012; Tanaka et al. 2008). Histological analyses show MSCs accelerate the repair of the intestinal architecture, reducing ulceration, restoring goblet cell loss and epithelial cell lining, disseminating fibrosis and repairing distorted crypt structures (Chen et al. 2013b; Fawzy et al. 2013; He et al. 2012; Liang et al. 2011; Hayashi et al. 2008; Tanaka et al. 2008).

Healing of the intestinal surface epithelium is regulated by a complex network of highly divergent structurally distinct regulatory peptides, growth factors, angiogenic factors, and trophic factors which are expressed from various cell populations within the mucosa of the intestinal tract (Dignass 2001). During *in vitro* culture, MSCs have been shown to secrete significant amounts of such factors, including HGF, VEGF, TGF-β1, and adiponectin (Watanabe et al. 2014; Ando et al. 2008; Zvonic et al. 2007; Rehman et al. 2004). TGF-β1 and VEGF

are known to play significant roles in GI wound healing and thus, are considered to contribute to the repair of injured tissue in experimental colitis (Watanabe et al. 2014; Hayashi et al. 2008). A potent promoter of epithelial cell proliferation and migration, HGF facilitates repair of the epithelial cell lining and inhibits apoptosis of epithelial cells (Kanbe et al. 2006; Oh et al. 2005). Adiponectin exerts anti-inflammatory actions on a number of cell types and has been shown to provide an enhancing effect on the remodeling of damaged colonic tissue (Ouchi and Walsh 2007; Nishihara et al. 2006; Yamamoto et al. 2005).

MSCs have been demonstrated to exhibit remarkable immunomodulatory effects in experimental models of colitis. During intestinal inflammation, MSCs down-regulate pro-inflammatory signaling and up-regulate anti-inflammatory signaling by inhibiting the proliferation and function of innate and adaptive immune cells, as well as promoting the expansion of T-regulatory cells (Selmani et al. 2008; Uccelli et al. 2008; Aggarwal and Pittenger 2005). In TNBS colitis, various studies have demonstrated that MSCs significantly inhibit the production of Th1-cytokines such as IL-2, IL-12, TNF-α, IFN-γ and the Th1-specific transcription factor, T-bet, suggesting that MSCs can alter the inflammatory process by down-regulating Th1-driven autoimmune and inflammatory responses (Chen et al. 2013b; Liang et al. 2011; Gonzalez et al. 2009). Evidence also suggests that reductions in IL-23 and Th17 cytokines in MSC-treated animals may play a role in the amelioration of TNBS-induced colitis (Chen et al. 2013b; Liang et al. 2011). Thus, the mechanisms underlying attenuation of intestinal inflammation by MSC therapy may be via suppressive effects on the IL-23/Th17 axis and Th1-type immune responses, at least in TNBS-induced colitis.

Currently, two forms of MSC therapy have been investigated in clinical trials: systemic infusions of MSCs in CD and UC and local application of MSCs in perianal fistulizing CD. Local application of BM and adipose tissue MSCs from autologous (MSCs obtained from the patient's own body) and allogeneic (MSCs obtained from a donor) sources have shown promising results in the healing of perianal fistulas (Cho et al. 2013; de la Portilla et al. 2013; Lee et al. 2013a; Ciccocioppo et al. 2011; Garcia-Olmo et al. 2009; 2005). Complete healing of

fistulas was reported to occur within 8 weeks post treatment and can be maintained for up 24 months (Cho et al. 2015; Lee et al. 2013a; Ciccocioppo et al. 2011; Garcia-Olmo et al. 2009). Furthermore, lack of adverse events established that the use of MSCs in fistulizing CD is safe. In refractory luminal CD, the systemic administration of autologous and allogeneic BM-MSCs has been shown to be safe and feasible, reducing disease activity and inducing clinical remission (Forbes et al. 2014; Duijvestein et al. 2010). Systemic administration of umbilical cord-derived MSCs were associated with improved clinical response, including attenuation of ulceration and mucosal inflammation, without adverse effect in UC (Hu et al. 2016). Overall, these studies demonstrate that MSC therapy is safe and efficacious for the treatment of clinical symptoms associated with IBD.

1.4 Summary

IBD, comprised of CD and UC, is a complex disorder of the GI tract characterized by chronic relapsing inflammation. While there are many similarities between CD and UC, they differ in the location of the disease in the GI tract, the depth of inflammation within the gut wall, and the complications arising from the disease process. The symptoms of IBD are extensive, varying from mild to severe depending on disease activity. IBD patients commonly experience both GI and systemic symptoms which may lead to complications as the duration of the disease progresses. Although IBD is not associated with mortality, it causes considerable morbidity, inflicting substantial impact on the patient's QoL. The etiology of IBD is unknown but considered to be multifactorial, thus treatments are aimed at controlling IBD symptoms and improving patient QoL rather than addressing the disease pathogenesis. However, many patients experience side effects, lose response or do not respond at all to conventional treatments. IBD is an established global disease; the incidence and prevalence of IBD is continually increasing and expected to increase further over the next decade worldwide. Hence, novel therapies for the treatment of IBD are imperative.

Studies have consistently demonstrated the detrimental effects of intestinal inflammation on the ENS. Substantial neuronal loss, degeneration of nerve fibers, and alterations to EGCs have been reported in experimental models and in tissues from IBD patients. It is not surprising that inflammation-induced changes to the structure of the ENS alter the functional properties of enteric neurons and subsequently, modify gut function. Neuronal hyperexcitability and alterations to normal synaptic and junctional transmission associated with intestinal inflammation affect changes in GI motility. Hence, inflammatory effects on the structure and function of enteric neurons may underlie the generation of IBD symptoms, such as diarrhea and constipation. Overall, evidence from previous studies suggest that the enteric neurons are a viable target for novel treatments of IBD.

MSCs present an attractive option for the treatment of IBD. MSCs have been shown to play a major role in tissue repair and regeneration by migrating to the injury site and releasing a wide variety of biological factors with anti-inflammatory, immunomodulating, and neuroprotective effects. The therapeutic effect of MSC administration has been demonstrated in a variety of diseases, including inflammatory, autoimmune, and neurodegenerative diseases. MSC therapy provides anti-inflammatory and immunomodulating effects in experimental models of colitis and is deemed safe and feasible in IBD clinical trials. Given that MSC treatment has shown promising results in neurological disease and IBD, it is plausible that MSC therapy may be effective in attenuating enteric neuropathy associated with intestinal inflammation.

CHAPTER TWO: HUMAN BONE MARROW MESENCHYMAL STEM CELL-BASED THERAPY AVERTS ENTERIC NEUROPATHY AND COLON DYSFUNCTION IN THE ACUTE MODEL OF TNBS-INDUCED COLITIS IN GUINEA-PIGS

The material presented in this chapter is published and has been reproduced here with the permission of the publishers with minor alterations:

Robinson, A. M., Sakkal, S., Park, A., Jovanovska, V., Payne, N., Carbone, S. E., Miller, S., Bornstein, J. C., Bernard, C., Boyd, R., Nurgali, K. 2014. Mesenchymal stem cells and conditioned medium avert enteric neuropathy and colon dysfunction in guinea-pig TNBS-induced colitis. *Am J Physiol Gastrointest Liver Physiol,* 307, G1115-29.

Robinson, A. M., Miller, S., Payne, N., Boyd, R., Sakkal, S., Nurgali, K. 2015. Neuroprotective potential of mesenchymal stem cell-based therapy in acute stages of TNBS-induced colitis in guinea-pigs. *PLoS One,* 10, e0139023.

2.1 Summary

Background: Damage to the enteric nervous system (ENS) associated with intestinal inflammation may underlie persistent alterations to gut functions, suggesting that enteric neurons are viable targets for novel therapies. The therapeutic benefits of mesenchymal stem cells (MSCs), such as homing ability, multipotent differentiation capacity and secretion of soluble bioactive factors which exert neuroprotective, anti-inflammatory and immunomodulatory properties, have been attributed to attenuation of autoimmune, inflammatory and neurodegenerative disorders. In culture, MSCs release soluble bioactive factors promoting neuronal survival and suppressing inflammation suggesting that MSC-conditioned medium (CM) provides essential factors to repair damaged tissues. We aimed to investigate 1) whether MSC and CM treatments administered by enema avert enteric neuropathy and motility dysfunction associated with 2,4,6-trinitrobenzene-sulfonic acid (TNBS)-induced inflammation in the guinea-pig colon and 2) the earliest time point at which these effects may occur. **Methods:** Guinea-pigs were randomly assigned to experimental groups and received a single application of TNBS (30mg/kg) followed by 1×10^6 human bone marrow-derived MSCs, 300µL CM, or 300µL unconditioned medium 3h later. Colon tissues were collected 6h, 24h, 3 days and 7 days after administration of TNBS. Effects on body weight, gross morphological damage, immune cell infiltration, myenteric neurons and motility were evaluated. Reverse transcriptase-polymerase chain reaction, flow cytometry and an antibody array kit were used to identify neurotrophic and neuroprotective factors released by MSCs. **Results:** MSC and CM treatments prevented inflammation-associated weight loss, accelerated repair of colonic architecture and regeneration of nerve fibers, reduced infiltration of leukocytes into the colon wall and the myenteric plexus, averted myenteric neuronal loss, as well as changes in neuronal subpopulations, and alleviated inflammation-induced colonic dysmotility. The neuroprotective effects of MSC and CM treatments were observed as early as 24h after induction of inflammation even though the inflammatory reaction at the level of the myenteric ganglia had not completely subsided. A substantial number of

neurotrophic and neuroprotective factors released by MSCs were identified in their secretome. **Conclusions:** These results provide strong evidence that both MSC and CM treatments can effectively prevent damage to the ENS and alleviate gut dysfunction caused by TNBS-induced colitis. MSC-based therapies applied at the acute stages of TNBS-induced colitis start exerting their neuroprotective effects towards enteric neurons by 24h post treatment and maintain these effects for at least 7 days. The neuroprotective efficacy of MSC-based therapies can be exerted independently to their anti-inflammatory effects.

2.2 Introduction

Inflammatory bowel disease (IBD) includes two major pathological conditions, Crohn's disease (CD) and ulcerative colitis (UC), characterized by chronic relapsing inflammation within the gastrointestinal (GI) tract (Baumgart and Sandborn 2007). CD exhibits a transmural inflammation that may affect any part of the GI tract, whereas in UC, inflammation is confined to the colorectal mucosa (Swenson and Theise 2010). Inflammation, mucosal ulceration, and modification of colonic architecture associate with symptoms, such as abdominal pain and cramping, chronic diarrhea, nausea/vomiting, constipation, fatigue, poor appetite, weight loss, and malnutrition (Farrell and Savage 2012; Abraham and Cho 2009; Lanzoni et al. 2008; Baumgart and Sandborn 2007; Sands 2007). Furthermore, IBD sufferers may encounter complications such as fistulas, abscesses, and stenosis (CD), or rectal bleeding and abdominal bloating (UC) (Boirivant and Cossu 2012; Bernstein et al. 2010; Lanzoni et al. 2008). The incidence and prevalence of IBD is increasing in western countries, and although not particularly associated with mortality, this disorder inflicts a severe impact on patient quality of life (Wilson et al. 2010).

The exact etiology of IBD remains unknown, although environmental factors, the immune system, the microbiome and damage to the enteric nervous system (ENS) have been shown to influence its pathophysiology (Sharkey and Savidge 2014; Abraham and Cho 2009; Baumgart and Carding 2007). The ENS intrinsically innervates the GI tract and is responsible for monitoring and coordinating all aspects of gut function, including intestinal barrier function, secretion, visceral sensation, blood flow and gut motility (Furness 2012; Ohlsson et al. 2007; Boyer et al. 2005). It is now recognized that persistent GI inflammation and immune activation affects incessant structural changes to enteric neurons, such as neuronal loss and nerve fiber degeneration (Ohlsson et al. 2007; Boyer et al. 2005; Linden et al. 2005; De Giorgio et al. 2002; Sanovic et al. 1999), as well as ENS functional changes, including hyperexcitability of enteric neurons and alterations in neurotransmission (Nurgali et al. 2011; 2009; 2007; Linden et al. 2003). Furthermore, colonic inflammation affects changes in the

neurochemical coding of myenteric neurons such as choline acetyltransferase (ChAT) and neuronal nitric oxide synthase (nNOS) neurons, causing disruption of GI functions and altered intestinal motility (Winston et al. 2013; Neunlist et al. 2003; De Giorgio et al. 2002; Poli et al. 2001). Structural and functional changes in the ENS leading to alterations of intestinal functions can persist long after the resolution of acute intestinal inflammation (Krauter et al. 2007b; Lomax et al. 2007a). Infiltration of immune cells to the level of the myenteric and submucosal plexuses (plexitis) of the gut wall can be predictive of IBD recurrence (Sokol et al. 2009; Ferrante et al. 2006). Thus, damage to and changes within the ENS may be prognostic of disease progression, play a role in the generation of IBD symptoms and recurrence, and underlie gut dysfunction (Villanacci et al. 2008). This suggests that protection of enteric neurons may decrease disease severity.

Currently, IBD treatments are focused towards suppressing inflammation with lifelong medications, such as anti-inflammatories (e.g. 5-aminosalicylates), antibiotics, immunomodulators (e.g. azathioprine), corticosteroids and biologic agents (e.g. tumor necrosis factor (TNF)-α antagonists) (Chaudhari et al. 2014; Shepela 2008). While acting to combat acute inflammation and prolong remission, certain medications, particularly corticosteroids and immunosuppressants, can be very toxic and inflict severe adverse effects (Triantafillidis et al. 2011; Stallmach et al. 2010; Scribano 2008). Biological therapies produce fewer side effects, but many patients fail to respond to these treatments, rendering them ineffective over time (Boirivant and Cossu 2012; Stallmach et al. 2010). Overall, the severity of side effects, together with a diminished patient response, limits the efficiency of current therapies for IBD. A high percentage of IBD patients will require surgical intervention, such as bowel resection or stricturoplasty, and ~40% will need repeated surgeries and/or removal of the entire colon (Chaudhari et al. 2014; Lewis and Maron 2010; Lukas 2008; Sands 2007). Novel treatments for intestinal inflammation currently being investigated include the manipulation of gut microbiota and cellular therapies (Jin et al. 2014; Garcia-Olmo et al. 2009; 2005).

In recent years, mesenchymal stem cells (MSCs) have demonstrated significant potential for clinical use in a variety of inflammatory, autoimmune and nervous system diseases because of their differentiation potential and ability to advance tissue repair via the release of biologically active molecules (Galindo et al. 2011; da Silva Meirelles et al. 2009; Kassis et al. 2008; Zheng et al. 2008). MSCs play a major role in tissue regeneration, repair, and homeostasis with capacity for self-renewal and differentiation into multiple lineages, as well as cells of neuronal and glial lineage when cultured under particular experimental conditions (De Luca et al. 2013; Bae et al. 2011a; Zeng et al. 2011; Barry and Murphy 2004). These multipotent cells can be derived from many adult tissues, including bone marrow (BM), adipose tissue, umbilical cord, and placenta (Shi et al. 2012; Pittenger et al. 1999). Most commonly derived from the BM, MSCs only represent a fraction (0.001–0.01%) of the total population of BM nucleated cells; however, their adherent nature enables them to be isolated and rapidly expanded for a number of passages under appropriate cell culturing conditions (Garcia-Bosch et al. 2010; Barry and Murphy 2004). Potential advantages of MSCs for cellular therapy include: ease of isolation, *in vitro* expansion capacity, low immunogenicity, receptiveness to *in vitro* genetic modification, and a safe and feasible profile for transplantation into humans (Cohen 2013; Burdon et al. 2011).

Numerous studies, under an array of pathological conditions, have established the capacity of MSCs to migrate to sites of tissue damage and inflammation where they participate in mechanisms of regeneration, regardless of the tissue (Wang et al. 2012a; Karp and Teo 2009; Spaeth et al. 2008; Liu et al. 2007; Ortiz et al. 2003). Although not completely understood, it is considered that MSCs may exert therapeutic effects acting in a paracrine manner to release biologically active molecules, such as cytokines, growth factors, and neuroregulators, with anti-inflammatory, anti-apoptotic, and neuroprotective effects (Payne et al. 2013b; Molendijk et al. 2012; Ren et al. 2012a; Scheibe et al. 2012; Shi et al. 2012; Wang et al. 2012a). In addition, MSCs have been recognized to have immunomodulatory properties, including the capacity to evade allogeneic rejection, inhibit dendritic cell differentiation and T cell proliferation, regulate the functions of regulatory T cells and modulate natural killer cell activity (Zhao et al.

2016; Haddad and Saldanha-Araujo 2014; Ramasamy et al. 2007; Spaggiari et al. 2006; Aggarwal and Pittenger 2005; Ryan et al. 2005). MSCs demonstrate neuroprotective properties via anti-proliferative, anti-inflammatory, and anti-apoptotic influences on neurons within the central nervous system (CNS) (Payne et al. 2013b; Al Jumah and Abumaree 2012; Scheibe et al. 2012; Slavin et al. 2008; Suzuki et al. 2008). These neuroprotective and immunomodulatory MSC qualities imply a therapeutic potential of these cells in attaining neural repair and protection. Furthermore, soluble factors secreted by MSCs into the culture medium during *in vitro* expansion has demonstrated therapeutic potential in various pathologies and may provide all the vital elements for tissue repair (Ranganath et al. 2012; Burdon et al. 2011; Salgado et al. 2010a).

MSCs have been proposed for the treatment of IBD (Swenson and Theise 2010; Lanzoni et al. 2008). Clinical trials have demonstrated administration of MSCs as a safe and feasible treatment option for complex perianal fistulas associated with CD (Ciccocioppo et al. 2011; Duijvestein et al. 2010). In experimental models of colitis, it has been confirmed that MSCs administered intraperitoneally (IP), intravenously (IV), or directly into the colonic wall migrate to sites of inflammation and exert their anti-inflammatory actions for the restoration of epithelial barrier integrity and repair of damaged tissue (Castelo-Branco et al. 2012; He et al. 2012; Gonzalez-Rey et al. 2009; Yabana et al. 2009; Hayashi et al. 2008; Tanaka et al. 2008). However, the potential of MSCs to avert enteric neural dysfunction resulting from inflammation is unknown.

Despite advances in the prospect of MSCs for the treatment of IBD and numerous nervous system disorders, no studies have evaluated the capacity of MSCs and conditioned medium (CM) to attenuate enteric neuropathy associated with IBD. Considerable evidence implicating persistent ENS damage in the generation of IBD symptoms together with the demonstrated therapeutic abilities of MSCs in nervous system disorders indicate that the study of MSCs for the treatment of enteric neuropathy associated with IBD is warranted. Accordingly, we have investigated the therapeutic potential of enema-applied MSCs and CM for the treatment of enteric neuropathy in the guinea-pig model of 2,4,6-trinitrobenzene-

sulfonic acid (TNBS)-induced colitis. Previous studies in animal models of multiple sclerosis, spinal cord injury, myocardial infarction, glaucoma and kidney injury reported that therapeutic effects of MSCs occur as early as several hours to several days after administration (Torres-Espin et al. 2013b; Semedo et al. 2009; Hu et al. 2007; Jiang et al. 2006; Zhang et al. 2005). Furthermore, MSCs have been shown to exert neuroprotective, anti-inflammatory and immunomodulatory effects in experimental traumatic brain injury 2-3 days post administration (Nichols et al. 2013; Zhao et al. 2012). These studies suggest that long-term engraftment of MSCs is not required for their efficacy. Hence, we have chosen time points from 6h up to 7 days post induction of inflammation to evaluate the time frame required to observe the potential of a MSC-stimulated therapeutic effect. Human BM-derived MSCs have been most studied and can uniquely evade immune rejection when administered to other species (Ryan et al. 2005; Tse et al. 2003); therefore, they were used in this study.

2.3 Materials and methods

2.3.1 Animals

Male and female Hartley guinea-pigs (140-280g; *n*=122) were obtained from South Australian Health and Medical Research Institute (SAHMRI, Adelaide, SA, Australia) and housed in a temperature-controlled environment with 12h day/night cycles. Animals were randomly assigned to experimental groups and had free access to food and water. All procedures used throughout this study were conducted according to the Australian National Health and Medical Research Council guidelines and approved by the Victoria University Animal Experimentation Ethics Committee. All efforts were made to minimize animal suffering.

2.3.2 Mesenchymal stem cell (MSC) culture

Human BM-MSC cell lines BM-7025, BM-7081, and BM-5077 (Tulane University, New Orleans, LA, USA) were cultured in accordance with MSC culturing procedures previously described (Payne et al. 2013b). Briefly, 60 cells/cm^2 were cultured in complete culture medium; 20mL α-minimum essential medium (MEM) supplemented 16.5% MSC qualified fetal bovine serum (FBS; validated by Life Technologies and is tested to successfully support the differentiation and culture of human MSCs according to International Society for Cellular Therapy (ISCT) guidelines), 100U/mL penicillin/streptomycin, and 100X GlutaMAX (all purchased from Gibco®, Life Technologies, Mulgrave, VIC, Australia) at 37°C. Medium was replenished every 48-72h for 10-14 days until the cells were 70-85% confluent (maximum). MSCs were rinsed in 5mL sterile 0.1M phosphate buffered solution (PBS) prior to incubation with 3mL trypsin/ethylenediaminetetraacetic acid (EDTA) solution (TrypLE Select; Gibco®, Life Technologies) for 3min at 37°C to detach cells. Enzymatic activity was neutralized by 8mL of stop solution (α-MEM + 5% FBS) and MSCs were collected and centrifuged at 450*g* for 5min at room temperature. Cells were then resuspended in fresh culture medium and counted using a light microscope. CM was aspirated following a minimum of 48h

incubation with MSCs and used for *in vivo* experiments. Unconditioned medium (UCM) is the culture medium described above, but not exposed to MSCs.

2.3.3 MSC characterization

Passage 4 human BM-MSC cell lines were characterized for their expression of surface antigens, differentiation potential, and colony forming ability as previously described (Payne et al. 2013b). All tests confirmed that MSCs used in this study met criteria for defining *in vitro* MSC cultures proposed by the ISCT (Dominici et al. 2006). Phenotypic analysis of MSCs was performed by flow cytometry. MSCs were labeled with anti-human CD34-phycoerythrin, CD45-PerCPCy5.5, CD29-Alexa Fluor 488, CD44-brilliant violet 421, CD73-brilliant violet 421, and CD90-Alexa Fluor 647 antibodies (BioLegend, San Diego, CA, USA). Peripheral blood mononuclear cells were employed as controls. Osteogenic and adipogenic differentiation potential of MSCs was revealed by 1% Alizarin Red S or 0.3% Oil Red O (Sigma-Aldrich, Castle Hill, NSW, Australia) labeling as previously described (Payne et al. 2013b). Oil Red O was eluted with 100% isopropanol and quantified colorimetrically (500nm) on a Bio-Rad plate reader (Bio-Rad Laboratories, Gladesville, NSW, Australia). MSC colony-forming potential was assessed by a colony-forming unit fibroblast (CFU-F) assay employing crystal violet staining methods described previously (Grayson et al. 2006). Briefly, MSCs were seeded (10 cells/cm^2) for 14d and stained with 5% crystal violet (Sigma-Aldrich) for 10min. After washing, colonies >2mm were counted.

2.3.4 Induction of colitis

For induction of colitis, TNBS (Sigma-Aldrich) was dissolved in 30% ethanol to a concentration of 30mg/kg (Nurgali et al. 2011). A total volume of 300μL was instilled by enema into the lumen of the colon through a lubricated silicone catheter approximately 7cm proximal to the anus. For TNBS administration, guinea-pigs were anesthetized with isoflurane (induced at 4%, maintained on 1-4% isoflurane in O_2). Sham-treated guinea-pigs were administered 300 μL sterile PBS only by the same procedure.

2.3.5 Treatment with MSC-based therapies

Guinea-pigs in MSC, CM and UCM-treated groups were anesthetized with isoflurane 3h after TNBS administration (at the peak of acute intestinal inflammation (Pontell et al. 2009)) and administered $1x10^6$ MSCs in 300µL of sterile 0.1M PBS, or 300µL CM, or 300µL UCM by enema into the colon via a silicone catheter. Animals were held at an inverted angle following MSC-based treatments to prevent leakage from the rectum. Guinea-pigs were weighed and monitored daily following treatment. Animals were culled via stunning (a blow to the occipital region) and exsanguination (Nurgali et al. 2009; 2007) at 6h, 24h, 3 days and 7 days after induction of colitis or sham treatment. Segments of the distal colon were collected for histological and immunohistochemical studies. Motility analyses were conducted at 7 days only.

2.3.6 Immunohistochemistry and histology

2.3.6.1 Tissue preparation

Following dissection, tissues were immediately placed in oxygenated 0.1M PBS containing an L-type Ca^{2+} channel blocker, nicardipine (3µm; Sigma-Aldrich), to inhibit smooth muscle contraction. Tissues were cut open along the mesenteric border and then processed for wholemount longitudinal muscle-myenteric plexus (LMMP) preparations and cross sections. For LMMP preparations, colon tissues were pinned flat with the mucosal side up and stretched to maximal capacity without tearing in a Sylgard-lined Petri dish (Dow Corning, Midland, Michigan, USA). Tissues were fixed overnight at 4°C in Zamboni's fixative (2% formaldehyde and 0.2% picric acid) and subsequently washed for 3×10min in dimethyl sulfoxide (DMSO; Sigma-Aldrich) followed by 3×10min in 0.1M PBS to remove fixative. Zamboni's fixative was chosen for tissue fixation to minimize neural tissue autofluorescence. Distal colon samples for LMMP preparations were dissected to expose the myenteric plexus by removing the mucosa, submucosa and circular muscle layers prior to immunohistochemistry. Tissues for cross sections were pinned with the mucosal side up in a Sylgard-lined Petri dish, without stretching. Cross section tissues for immunohistochemistry were

fixed as described above and stored in 50:50 optimum cutting temperature (OCT) compound (Tissue-Tek, Torrance, CA, USA) and 30% sucrose/PBS (Sigma-Aldrich) for 24h at 4°C prior to freezing in liquid nitrogen-cooled isopentane and OCT compound. Subsequently, samples were cryo-sectioned at a 30µm thickness (at least 15 sections from each animal) using a cryostat microtome (Leica CM1850, St. Gallen, Switzerland) and mounted onto glass slides. Cross section tissues for histology were fixed in 10% buffered formalin overnight at 4°C and stored in 70% ethanol until paraffin embedding.

2.3.6.2 Immunohistochemistry

Immunohistochemistry was performed on wholemount LMMP preparations and cross sections of the distal colon as previously described (Nurgali et al. 2011). After a 1h incubation in 10% normal donkey serum (NDS; Merck Millipore, Bayswater, VIC, Australia) diluted in 0.1M PBS-0.1% Triton X-100 at room temperature, the samples were washed with 0.1M PBS-0.1% Triton X-100 (2×5min) and incubated with primary antibodies (Table 2.1) diluted in 2% NDS and 0.1M PBS-0.1% Triton X-100 overnight at room temperature. Tissues were then washed in 0.1M PBS-0.1% Triton X-100 (2×5min) prior to incubation with secondary antibodies (diluted in 2% NDS and 0.1M PBS-0.1% Triton X-100; Table 2.2) for 2h at room temperature. Following 3×10min washes in 0.1M PBS-0.1% Triton X-100, samples were mounted on glass slides with fluorescent mounting medium (DAKO, North Sydney, NSW, Australia).

2.6.3.3 Histology

After fixation, tissues were paraffin embedded, sectioned at 5µm, deparaffinized, cleared, and rehydrated in graded ethanol concentrations for standard hematoxylin and eosin (H&E) and Alcian blue staining. Sections were immersed in xylene (3×4min), 100% ethanol (3min), 90% ethanol (2min), 70% ethanol (2min), rinsed in tap water, hematoxylin (4min) or Alcian blue (30min), rinsed in tap water, Scott's tap water (1min), eosin (3min), rinsed in tap water, 100% ethanol (2×1min), xylene (2×3min) and mounted on glass slides with distrene plasticizer xylene (DPX) mountant.

Table 2.1 Primary antibodies used in this study

Antibody	Host species	Dilution	Supplier	Application in this study
Anti-β-Tubulin class III	Rabbit	1:1000	Abcam, Melbourne, VIC, Australia	Cross sections
Anti-CD45 (clone IH-1)	Mouse	1:200	Abcam	Cross sections and LMMP preparations
Anti-choline acetyltransferase (ChAT)	Goat	1:500	Merck Millipore	LMMP preparations
Anti-Hu (clone 15A7.1)	Mouse	1:500	Merck Millipore	LMMP preparations
Anti-human leukocyte antigen (HLA)-A,B,C (conjugated to fluorescein isothiocyanate (FITC))	Human	1:50	BioLegend	Cross sections
Anti-neuronal nitric oxide synthase (nNOS)	Goat	1:500	Novus Biologicals, Littleton, CO, USA	LMMP preparations
Anti-protein gene product (PGP)-9.5	Chicken	1:500	Abcam	LMMP preparations

Table 2.2 Secondary antibodies used in this study

Antibody	Host species	Dilution	Supplier	Application in this study
Alexa Fluor 594	Donkey anti-chicken	1:200	Jackson Immunoresearch Laboratories, PA, USA	LMMP preparations
Alexa Fluor 594	Donkey anti-mouse	1:200	Jackson Immunoresearch Laboratories	LMMP preparations
Alexa Fluor 594	Donkey anti-rabbit	1:200	Jackson Immunoresearch Laboratories	Cross sections
FITC 488	Donkey anti-goat	1:200	Jackson Immunoresearch Laboratories	LMMP preparations
FITC 488	Donkey anti-mouse	1:200	Jackson Immunoresearch Laboratories	Cross sections and LMMP preparations

2.3.7 Imaging

Confocal microscopy was performed with a Nikon Eclipse Ti confocal laser scanning system (Nikon, Tokyo, Japan). Fluorophores were visualized by a 488nm excitation filter for FITC 488 and a 559nm excitation filter for Alexa 594. Z-series images were acquired at a nominal thickness of 0.5µm (512×512 pixels). Gross morphological damage in H&E-stained colon sections and goblet cell mucin in Alcian blue-stained sections were visualized using an Olympus BX53 microscope (Olympus, Notting Hill, VIC, Australia) and images were captured with CellSense™ software.

2.3.8 Quantitative analyses of immunohistochemical and histological data

In wholemount LMMP preparations, the total number of myenteric neurons immunoreactive (IR) for Hu, nNOS and ChAT, as well as the quantity of CD45-IR cells, were counted within eight randomly captured images per preparation (total area 2mm^2). Infiltration of leukocytes throughout the colon wall was assessed by counting the total number of CD45-IR cells within the mucosa and muscle layers in cross sections (total area 2mm^2). The density of nerve fibers was determined by measuring β-tubulin (III)-IR (average of 8 random areas of 500µm^2). All images were captured under identical acquisition exposure time conditions and calibrated to standardized minimum baseline fluorescence. Images were converted from red, green, and blue (RGB) to grayscale 8 bit then to binary; changes in fluorescence from the baseline were measured using Image J software (National Institutes of Health, Bethesda, MD, USA). The area of immunoreactivity was then expressed as a percentage of the total area examined. Gross morphological damage in H&E-stained colon sections and goblet cell mucin in Alcian blue-stained sections was assessed by histological grading of four parameters: mucosal flattening (0 = normal, 3 = severe flattening), occurrence of hemorrhagic sites (0 = none, 3 = frequent sites), loss of goblet cells (0 = normal, 3 = severe loss of cells) and variation of the circular muscle

(0 = normal, 3 = considerable thickening of muscular layer) (Nurgali et al. 2007). Quantitative analyses were conducted blindly.

2.3.9 Colonic motility

Colonic motility experiments were undertaken by applying methods previously employed (Gwynne et al. 2004b). Immediately following dissection, guinea-pig colon was placed in organ bath chambers superfused with physiological (Krebs) solution (containing (in mM) 118 NaCl, 4.6 KCl, 2.5 $CaCl_2$, 1.2 $MgSO_4$, 1 NaH_2PO_4, 25 $NaHCO_3$, 11 D-glucose, bubbled with 95% O_2 and 5% CO_2) maintained at 37°C and left to naturally expel fecal content. The proximal (oral) and distal (anal) ends of each colon were affixed to cannulae by nylon thread. The oral cannula was connected to a reservoir of Krebs solution (maintained at 15mL), the height of which was adjusted to change the intraluminal pressure (0 to +2cmH_2O), and the anal end was connected to a vertical outflow tube which allowed the back pressure to be maintained at 2cmH_2O (Gwynne et al. 2004b). Organ baths were continuously superfused with oxygenated physiological saline solution, and preparations were left to equilibrate for 30min. A video camera (Logitech Quickcam pro) was positioned ~8 cm above the organ bath to record contractile activity. Videos (2×20min) of each test condition (baseline, +1cmH_2O, and +2cmH_2O intraluminal pressure) were captured and saved directly onto a personal computer in audio video interleaved (AVI) format using VirtualDub software (version 1.9.11). Recordings were later processed and converted to spatiotemporal maps using edge detection software (Scribble v2.0) (Gwynne et al. 2014; 2004b). Spatiotemporal maps plotted the diameter of the colon at any given time point during the recording and enabled contractile motor patterns to be analyzed with MATLAB v2012a software (Gwynne et al. 2004b).

2.3.10 Gene expression analysis

Total RNA was extracted from $1x10^6$ BM-MSCs using a High Pure RNA Isolation Kit (Roche, North Ryde, NSW, Australia) as per the manufacturer's instructions. cDNA was prepared from 0.5µg RNA using an SuperScript III First-Strand

Synthesis System kit for reverse transcriptase-polymerase chain reaction (RT-PCR) and oligo (dT) primers (Invitrogen, Thermo-Fisher Scientific, Scoresby, VIC, Australia; Table 2.3). Polymerase Chain Reaction (PCR) was performed with 1μL cDNA and primer pairs under the following cycling conditions: PCR products were resolved by electrophoresis in 2% agarose gels and the bands visualized under UV light.

Table 2.3 Primers for RT-PCR

Target	Forward	Reverse	Product size
β-actin	CAGAGCCTCGCCTTTGCCG	CTCGCGGTTGGCCTTGGG	405
Brain-derived neurotrophic factor (BDNF)	AGAGGCTTGACATCATTGGC	ACTAATACTGTCACACACGC	276
Nerve growth factor (NGF)	CACACTGAGGTGCATAGCGT	TGATGACCGCTTGCTCCTGT	390
Insulin-like growth factor (IGF)-1	ATGCACACCATGTCCTC	CATCCTGTAGTTCTTGTTTC	390
Neurotrophin (NT)-3	ATCTTACAGGTGAACAAGGT	TCGGTGACTCTTATGCTCCG	459
Hepatocyte growth factor (HGF)	ATGCATCCAAGGTCAAGGAG	TTCCATGTTCTTGTCCCACA	349
Vascular endothelial growth factor (VEGF)	ATGAACTTTCTGCTGTCTTGG	TCACCGCCTCGGCTTGTCACA	516
Tumor necrosis factor-stimulated gene (TSG)-6	AAGCACGGTCTGGCAAATACAAGC	GGGTTGTAGCAATAGGCATCC	268
Transforming growth factor (TGF)-β1	CAGATCCTGTCCAAGCTG	TCGGAGCTCTGATGTGTT	270

2.3.11 Flow cytometric cytokine analysis

MSCs were seeded at a density of 2×10^4 cells/cm^2 in Greiner Bio-One 25cm^2 filter cap flasks (Interpath Services, Heidelberg West, VIC, Australia). After 48h in culture, samples of the media were collected to analyze the secretion of

cytokines. Samples and cytokine standards with known concentrations were prepared according to the manufacturer's instructions using the BD™ Cytometric Bead Array (BD Biosciences, North Ryde, NSW, Australia). Samples were incubated in the dark with cytokine capture beads and phycoerythrin (PE) detection reagent for 2h each before being transferred to fluorescence activated cell sorting (FACS) tubes (BD Biosciences). PE fluorescence was measured via a BDFACS Canto II flow cytometer with FACSDiva v6.1 software.

2.3.12 Antibody array analysis

The RayBio® Label-based (L-Series) Human Antibody Array 1000 kit was used to determine presence of proteins secreted from MSCs and was performed following the manufacturer's instructions (RayBiotech, Norcross, GA, USA). Briefly, samples of equal protein concentrations were incubated with antibody membranes followed by incubation with biotin-conjugated anti-cytokine primary antibodies, as well as Cy3-conjugated streptavidin. Chemiluminescence was used for signal detection on a VersaDoc imaging system (Bio-Rad Laboratories).

2.3.13 Statistical analysis

Statistical differences were determined by one-way or two-way ANOVA with Tukey-Kramer post hoc test for multiple group comparisons using Prism v5.0 (Graphpad Software Inc., La Jolla, CA, USA). Data were considered statistically significant when $P<0.05$. Data were presented as mean±standard error of the mean (SEM), if not specified otherwise.

2.4 Results

2.4.1 Phenotypic and functional validation of MSCs

MSCs were characterized by flow cytometry, differentiation assays, and a CFU-F assay. At passage 4, flow cytometric analysis revealed that MSCs met the ISCT proposed criteria for defining multipotent MSCs. For a population of cells to qualify as MSCs, the minimal requirements of three criteria must be met: 1) ability to adhere to tissue culture plastic; 2) co-expression of certain CD antigens; and 3) capacity to differentiate into osteoblasts, adipocytes, and chondroblasts under standard *in vitro* differentiating conditions (Dominici et al. 2006). Cells expressed MSC markers CD73 and CD90, as well as cell migration molecules CD29 and CD44, and lacked expression of CD34 and CD45 (Fig. 2.1A). MSCs readily differentiated into osteocytes and adipocytes after incubation in osteogenic and adipogenic differentiation media for 14-21d as indicated by positive staining of calcium deposits with Alizarin Red S and lipid vacuoles with Oil Red O, respectively (Fig. 2.1B). Some spontaneous adipogenic differentiation was seen for MSCs cultured in control medium, as described by others (Adamzyk et al. 2013; Zhang and Kilian 2013), but adipogenic differentiation was significantly greater for MSCs cultured in specific medium at 21d ($P<0.05$; Fig. 2.1C). MSCs were subjected to a CFU-F assay with crystal violet labeling. CFU-F assays established a 19% MSC colony-forming efficiency (Fig. 2.1D). A colony-forming efficiency between 15-20% is considered high for BM-MSCs and not indicative of loss of stemness (Ren et al. 2013).

2.4.2 MSCs successively migrate transmurally and engraft at the site of inflammation

To assess the capacity of MSCs to migrate to and engraft at the area of tissue damage and inflammation, segments of the distal colon were collected from guinea-pigs treated with 1) MSCs after TNBS and 2) MSCs only without TNBS (n=3/group/time point). To identify adoptively transferred human MSCs within the guinea-pig colon, cross sections were labeled with anti-HLA-A,B,C antibody to

detect major histocompatibility complex (MHC) class I antigens which are expressed by all human nucleated cells (Fig. 2.2). The successful engraftment of MSCs into the colonic wall was evident by localization of HLA-A,B,C positive cells in the colon sections collected at all time points post induction of colitis (Fig. 2.2A-A^{III}). At 6h after TNBS administration, MSCs were present mostly in the mucosal lamina propria in colon sections from MSC-treated guinea-pigs (Fig. 2.2A). At 24h, 3 days and 7 days after induction of colitis, transmural migration and engraftment of human MSCs into the colon wall to the level of the myenteric ganglia was evident (Fig. 2.2A^{I}-A^{III}). HLA A,B,C-IR cells were absent in colon sections from MSC-only administered animals at all time points demonstrating that MSCs did not home to non-inflamed tissues (Fig. 2.2B-B^{III}).

Figure 2.1. Phenotypic and functional validation of MSCs. Flow cytometric analysis showed MSCs to positively express CD29, CD44, CD73, and CD90, but not CD34 and CD45 (red) compared with isotope controls (blue) **(A)**. After 14d in culture, MSCs were subjected to an osteogenic assay and labeled with Alizarin Red S. Osteogenic differentiation, absent for MSCs cultured in control media **(B^{I})**, was evident when MSCs were cultured in osteogenic differentiation media **(B^{II})**. MSCs were also subjected to adipogenesis assay after 14-21d. Labeling of MSCs with Oil Red O revealed a lack of adipogenesis in control media after 21d **(B^{III})**, but significant adipogenic differentiation of MSCs cultured in adipogenesis media **(B^{IV})**. Quantification of adipogenesis plates for the uptake of Oil Red O at 21d demonstrated a significant increase in MSCs cultured in adipogenesis media compared with control media ($P<0.05$) **(C)**. Crystal violet staining demonstrated MSC colony-forming capacity when subjected to a colony-forming unit fibroblast (CFU-F) assay **(D^{I}).** High-power imaging of CFU-F established formation of separate MSC colonies **(D^{II})**, as well as confirming cells within colonies to display typical MSC phenotype **(D^{III})**. Overall 19% colony-forming efficiency was observed. Scale bars = 500µm (B), 1cm (D^{I}), 1mm (D^{II}), 100µm (D^{III}). Data presented as mean±standard deviation (SD; C).

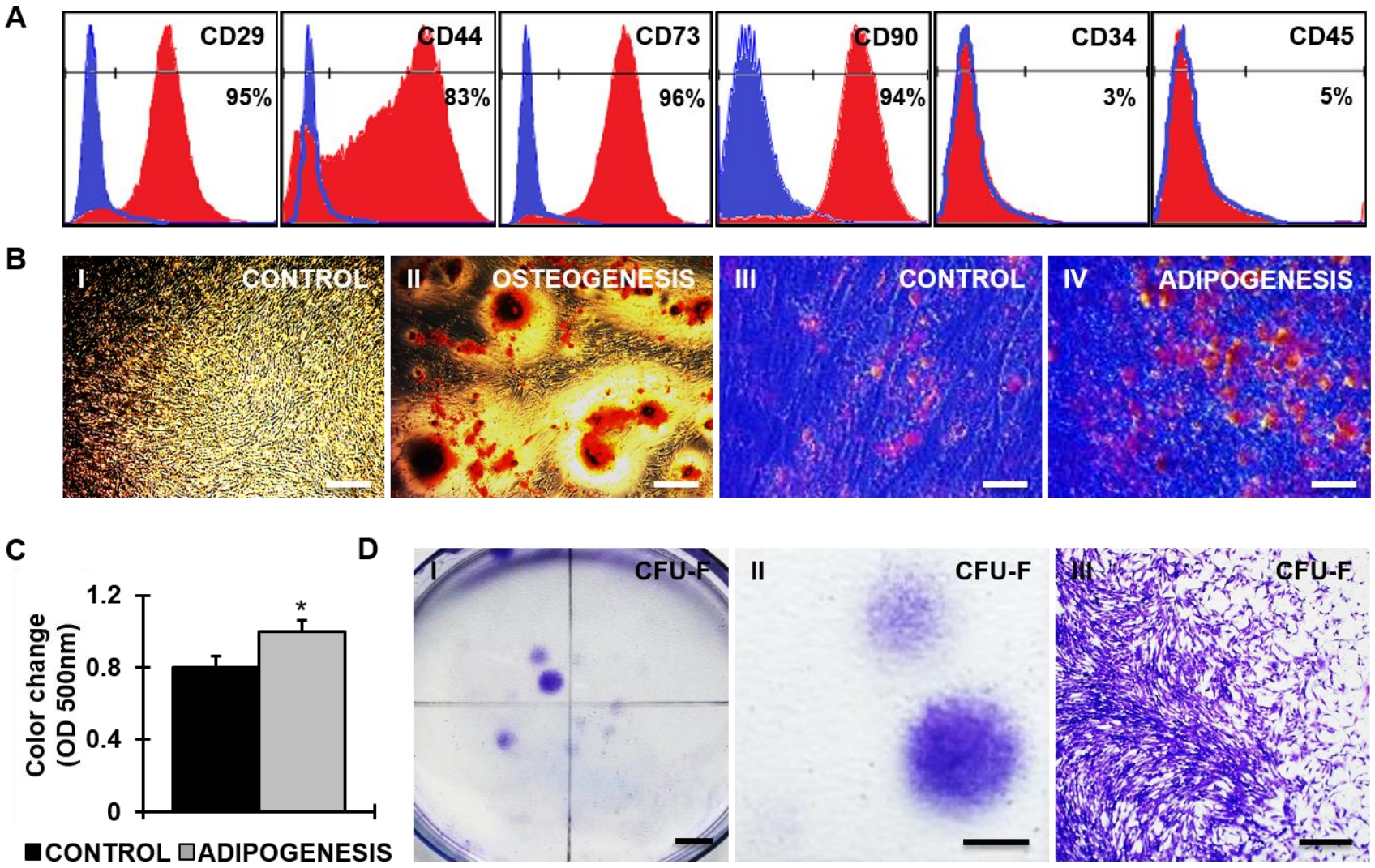
A
CD29
95%
CD44
83%
CD73
96%
CD90
94%
CD34
3%
CD45
5%
B
I
CONTROL
II
OSTEOGENESIS
III
CONTROL
IV
ADIPOGENESIS
C
Color change (OD 500nm)
1.2
0.8
0.4
0
*
CONTROL
ADIPOGENESIS
D
I
CFU-F
II
CFU-F
III
CFU-F

Figure 2.2. MSC migration and engraftment within the colon. Migration and homing of human bone marrow MSCs to the inflamed area of the guinea-pig colon was confirmed using anti-HLA-A,B,C antibody specific to human MHC class I. Fluorescent microscopy confirms MSCs administered 3h after TNBS application were localized mostly in the lamina propria 6h after induction of colitis **(A**; arrows**)**. Transmural engraftment of human MSCs into the colon wall to the level of the myenteric ganglia was evident 24h, 3 days and 7 days post induction of colitis **(A^{I}-A^{III};** arrows**)**. At all time points, HLA-A,B,C-IR cells were not detected in the distal colon from MSC-only treated guinea-pigs, validating absence of MSC homing to non-inflamed tissues **(B-B^{III})**. d = days. Scale bars = 50μm.

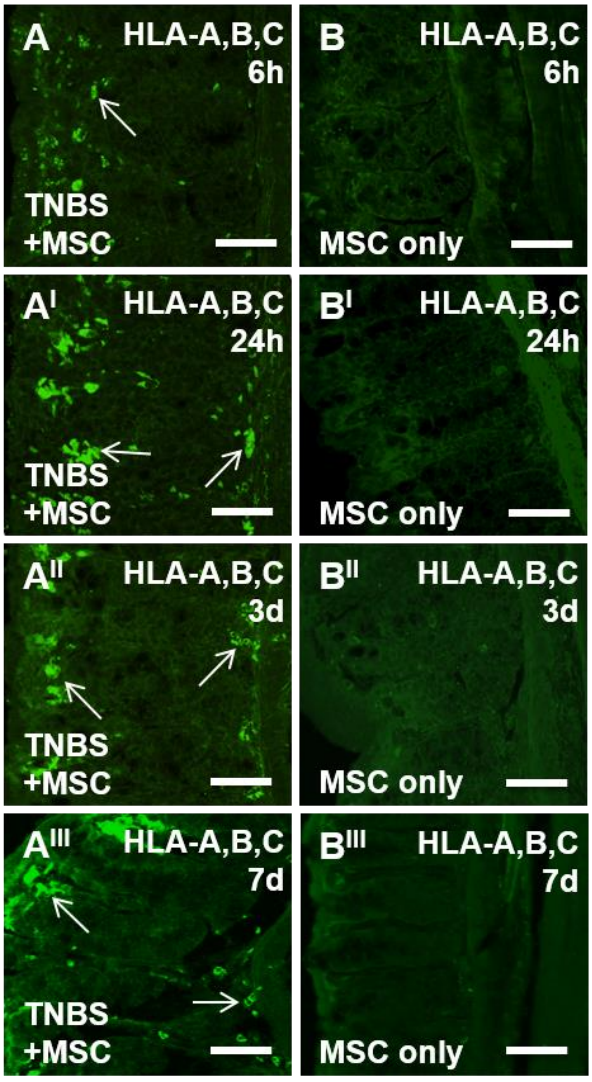
A
HLA-A,B,C
6h
TNBS
+MSC
B
HLA-A,B,C
6h
MSC only
AI
HLA-A,B,C
24h
TNBS
+MSC
BI
HLA-A,B,C
24h
MSC only
AII
HLA-A,B,C
3d
TNBS
+MSC
BII
HLA-A,B,C
3d
MSC only
AIII
HLA-A,B,C
7d
TNBS
+MSC
BIII
HLA-A,B,C
7d
MSC only

2.4.3 MSC and CM treatments prevent TNBS-induced weight loss

Guinea-pig weight was monitored daily prior to and for 7 days following treatment to demonstrate the systemic influence of therapies tested (*n*=5/group/time point; Table 2.4; Fig. 2.3). Control and sham-treated guinea-pigs consistently gained weight over 7 days. At 6h after TNBS administration, there was no change in weight between all groups. TNBS administration caused significant weight loss during the first 3 days compared to control and sham-treated animals. Treatment with MSCs and CM applied by enema 3h after TNBS administration prevented weight loss compared to animals administered with TNBS only. Treatment with UCM did not prevent weight loss compared to control, sham, MSC and CM-treated guinea-pigs. There were no differences in weight between all groups from 4 to 7 days (Table 2.4; Fig. 2.3).

2.4.4 MSC and CM treatments accelerate repair of damaged colonic architecture

Gross morphological assessment of H&E and Alcian blue-stained colon sections enabled definition of changes to colonic architecture and presence of goblet cells 6h, 24h, 3 days and 7 days after induction of TNBS-colitis (*n*=5/group/time point; Figs. 2.4 and 2.5). Normal structural arrangements of goblet cells and crypts, a continuous epithelial cell lining and distinct colonic layers were observed in H&E-stained sections from control and sham-treated animals at 6h, 24h, 3 days and 7 days post treatment (histological score = 0-1 for all; Fig. 2.4A-B^{III}). Alcian blue-stained sections revealed abundant goblet cells within the mucosal glands of control and sham-treated groups (Fig. 2.5A-B^{III}). Conversely, examination of distal colon sections from guinea-pigs in the TNBS-only group showed immune cell infiltration and accumulation in the crypts and submucosal layers, considerable goblet cell loss, glandular disruption and flattening, muscular edema and complete destruction of the epithelial cell lining at 6h (Figs. 2.4C and 2.5C). Immune cell accumulation, flattening of glands, crypt distortion and goblet cell loss persevered 24h post induction of colitis (Figs. 2.4C^{I} and 2.5C^{I}). Some regeneration of the epithelium had occurred by 3 days in TNBS-only administered

animals; crypt morphology remained distorted and goblet cell loss was consistent, but infiltrates of immune cells were less prominent compared to 24h (Figs. 2.4C^{II} and Fig. 2.5C^{II}). By 7 days, immune cell infiltration had diminished and regeneration of the epithelium had advanced further, but epithelial cell loss and glandular disruption persisted (Figs. 2.4C^{III} and 2.5C^{III}). Grading of gross morphological parameters in colon sections from TNBS-administered animals indicated histological score = 3 at 6h, 2-3 at 24h, 2-3 at 3 days, and 2 at 7 days following induction of inflammation. Goblet cell loss, as well as some disruption to glandular structure and epithelial cell lining was observed in colon sections from MSC and CM-treated guinea-pigs at 6h after induction of colitis (histological score = 1-2; Figs. 2.4D-E and 2.5D-E). However, mucosal healing and less flattening of crypts was evidenced when compared to sections from TNBS-only administered guinea-pigs. At 24h post induction of inflammation, sections from MSC and CM-treated animals revealed restoration of goblet cell abundance, as well as accelerated mucosal healing and repair to levels comparable with sham-treated animals (histological score = 0-1; Figs. 2.4D^{I}-E^{I} and 2.5D^{I}-E^{I}). Furthermore, at the 3 day time point, no evidence of goblet cell loss, mucosal damage or disruption to the colonic architecture in MSC-treated and CM-treated colon sections was present (histological score = 0-1; Figs. 2.4D^{II}-E^{II} and 2.5D^{II}-E^{II}). Gross morphology of the colon in MSC-treated and CM-treated animals was comparable to control and sham-treated animals at 7 days post induction of colitis (histological score = 0-1; Figs. 2.4D^{III}, E^{III} and 2.5D^{III}, E^{III}). Sections from UCM-treated animals displayed morphological damage similar to the TNBS-only group at 6h and 24h time points including immune cell infiltration, goblet cell loss, glandular distortion and flattening, muscular edema and destruction of the epithelial cell lining (histological score = 3; Figs. 2.4F-F^{I} and 2.5F-F^{I}). After 3 days, flattening of the glands and muscular edema was still evident similar to TNBS-only administered animals, however some signs of mucosal repair were observed (histological score = 2-3; Figs. 2.4F^{II} and 2.5F^{II}). At 7 days, the colon from UCM-treated animals continued to display evidence of mucosal healing, but morphological changes remained comparable to untreated TNBS-administered animals (histological score = 2; Figs. 2.4F^{III} and 2.5F^{III}). Since no differences were

observed between control and sham-treated animals, only sham-treated animals were used in further experiments.

Table 2.4. Changes in guinea-pig body weight (%) for 7 days following treatment

	0h	6h	24h	2d	3d	4d	5d	6d	7d
Control	100.0	100.6±0.2	102.4±0.5	104.9±0.8	107.4±1.1	109.8±1.3	111.1±1.4	111.9±2.1	113.8±2.0
Sham	100.0	100.6±0.2	102.7±0.6	105.2±0.5	107.4±0.4	110.2±2.1	112.9±1.6	117.8±2.1	119.9±2.4
TNBS	100.0	100.2±0.2	96.1±1.5 ***^^^###†††	97.8±1.7 **^^^###††	98.7±1.1 ***^^^###†††	105.2±2.1	111.2±0.9	114.0±0.8	116.0±0.9
TNBS+MSC	100.0	100.3±0.2	102.1±0.7	104.4±0.8	106.3±0.9	107.5±1.2	111.5±0.5	112.7±0.9	113.9±1.0
TNBS+CM	100.0	100.0±0.1	101.3±0.2	103.5±0.7	107.0±0.7	106.7±1.8	111.2±1.8	113.1±1.7	115.3±1.5
TNBS+UCM	100.0	100.0±0.1	98.8±0.6 **^^^##†††	99.3±0.8 *^^^###†	100.9±1.6 **^^^###†††	106.3±3.5	107.8±3.8	107.7±4.2	109.5±5.0

d = days. *P<0.05, **P<0.01, ***P<0.001 significantly different to control group. ^^^P<0.001 significantly different to sham-treated group. $^{\#\#}P$<0.01, $^{\#\#\#}P$<0.001 significantly different to TNBS+MSC-treated group. $^{\dagger}P$<0.05, $^{\dagger\dagger}P$<0.01, $^{\dagger\dagger\dagger}P$<0.001 significantly different to TNBS+CM-treated group.

Figure 2.3. MSC and CM treatments prevent TNBS-induced weight loss. Total body weight of guinea-pigs was recorded prior to and for 7 days after induction of colitis. No change in guinea-pig weight was observed in all groups at 6h after the induction of colitis. At 24h to 3 days post induction of inflammation, administration of TNBS-only and treatment with UCM induced significant loss of body weight, while treatment with MSCs and CM prevented loss of body weight. d = days. *P<0.05, **P<0.01, ***P<0.001 significantly different to control group. ^^^P<0.001 significantly different to sham-treated group. $^{\#\#}P$<0.01, $^{\#\#\#}P$<0.001 significantly different to TNBS+MSC-treated group. $^{\dagger}P$<0.05, $^{\dagger\dagger}P$<0.01, $^{\dagger\dagger\dagger}P$<0.001 significantly different to TNBS+CM-treated group.

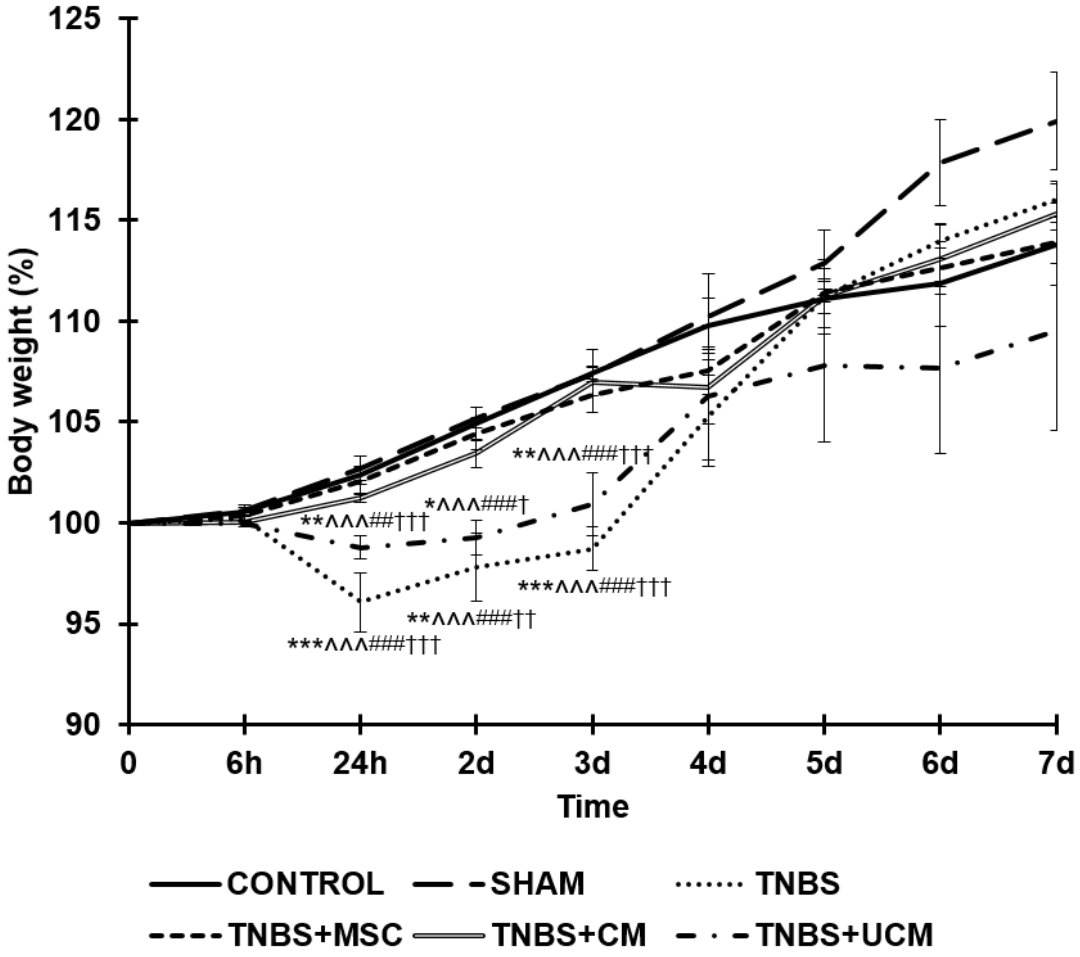
125
120
115
110
105
100
95
90
Body weight (%)
0
6h
24h
2d
3d
4d
5d
6d
7d
Time
**^^^###†††
*^^^###†
**^^^##†††
***^^^###†††
**^^^###††
***^^^###†††
CONTROL
SHAM
TNBS
TNBS+MSC
TNBS+CM
TNBS+UCM

Figure 2.4. MSC and CM treatments prevent TNBS-induced gross morphological damage to the colon. Histological changes to the colonic architecture 6h, 24h, 3 days and 7 days after TNBS application and treatment, as indicated by hematoxylin and eosin (H&E) staining. An intact epithelial lining and systematic arrangement of muscular layers, submucosa, and mucosal glands were observed in colon tissues from control **(A)** and sham-treated **(B-B^{III})** animals at all time points. Immune infiltrate, flattening of the glands, disruption to the epithelial lining and destruction of mucosal epithelium and muscular edema were observed in colon tissues from TNBS-administered **(C-C^{III};** arrows**)** and UCM-treated **(F-F^{III};** arrows**)** guinea-pigs at all time points. Sections from MSC and CM-treated animals revealed initiation of colonic repair at 6h post induction of colitis **(D, E)**. Restoration of colonic architecture was observed at 24h **(C^{I}, D^{I})**, 3 days **(C^{II}, D^{II})** and 7 days **(C^{III}, D^{III})**. d = days. Scale bars = 50µm

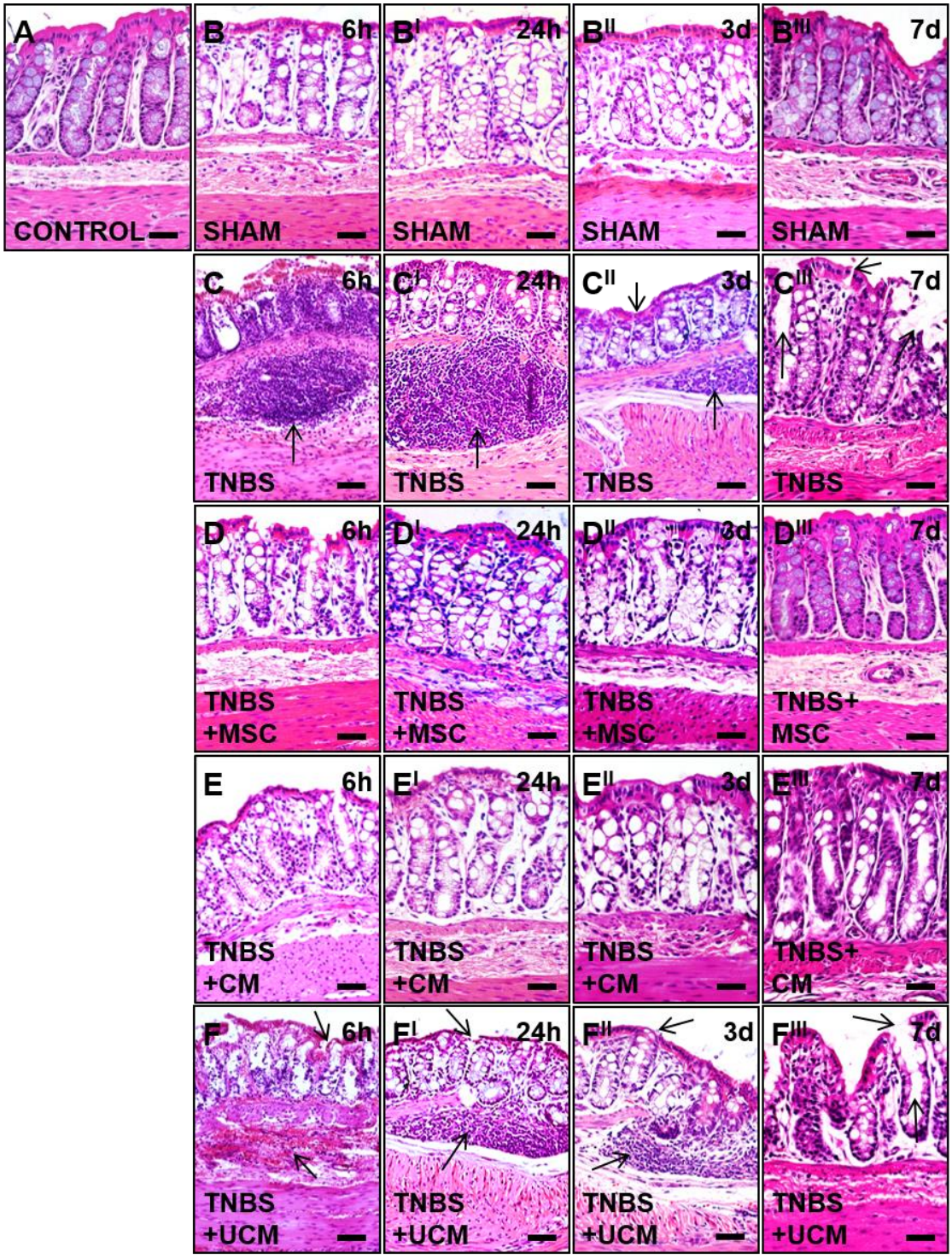
A
CONTROL
B 6h
SHAM
B' 24h
SHAM
B'' 3d
SHAM
B''' 7d
SHAM
C 6h
TNBS
C' 24h
TNBS
C'' 3d
TNBS
C''' 7d
TNBS
D 6h
TNBS
+MSC
D' 24h
TNBS
+MSC
D'' 3d
TNBS
+MSC
D''' 7d
TNBS+
MSC
E 6h
TNBS
+CM
E' 24h
TNBS
+CM
E'' 3d
TNBS
+CM
E''' 7d
TNBS+
CM
F 6h
TNBS
+UCM
F' 24h
TNBS
+UCM
F'' 3d
TNBS
+UCM
F''' 7d
TNBS
+UCM

Figure 2.5. MSC and CM treatments attenuate TNBS-induced goblet cell loss in the colon. Changes to mucin expression 6h, 24h, 3 days and 7 days after TNBS application and treatment, as indicated by Alcian blue staining. Plentiful Alcian blue-positive cells in colon sections from control **(A)** and sham-treated **(B-B^{III})** guinea-pigs at all time points. Less numerous Alcian blue-positive cells were evident in TNBS-administered **(C-C^{III})** and UCM-treated **(F-F^{III})** colon sections at all time points. Conversely, treatment with MSCs **(D-D^{III})** and CM **(E-E^{III})** attenuated TNBS-induced Alcian blue-positive cell loss in the guinea-pig colon after 24h post treatment. d = days. Scale bars = 20µm.

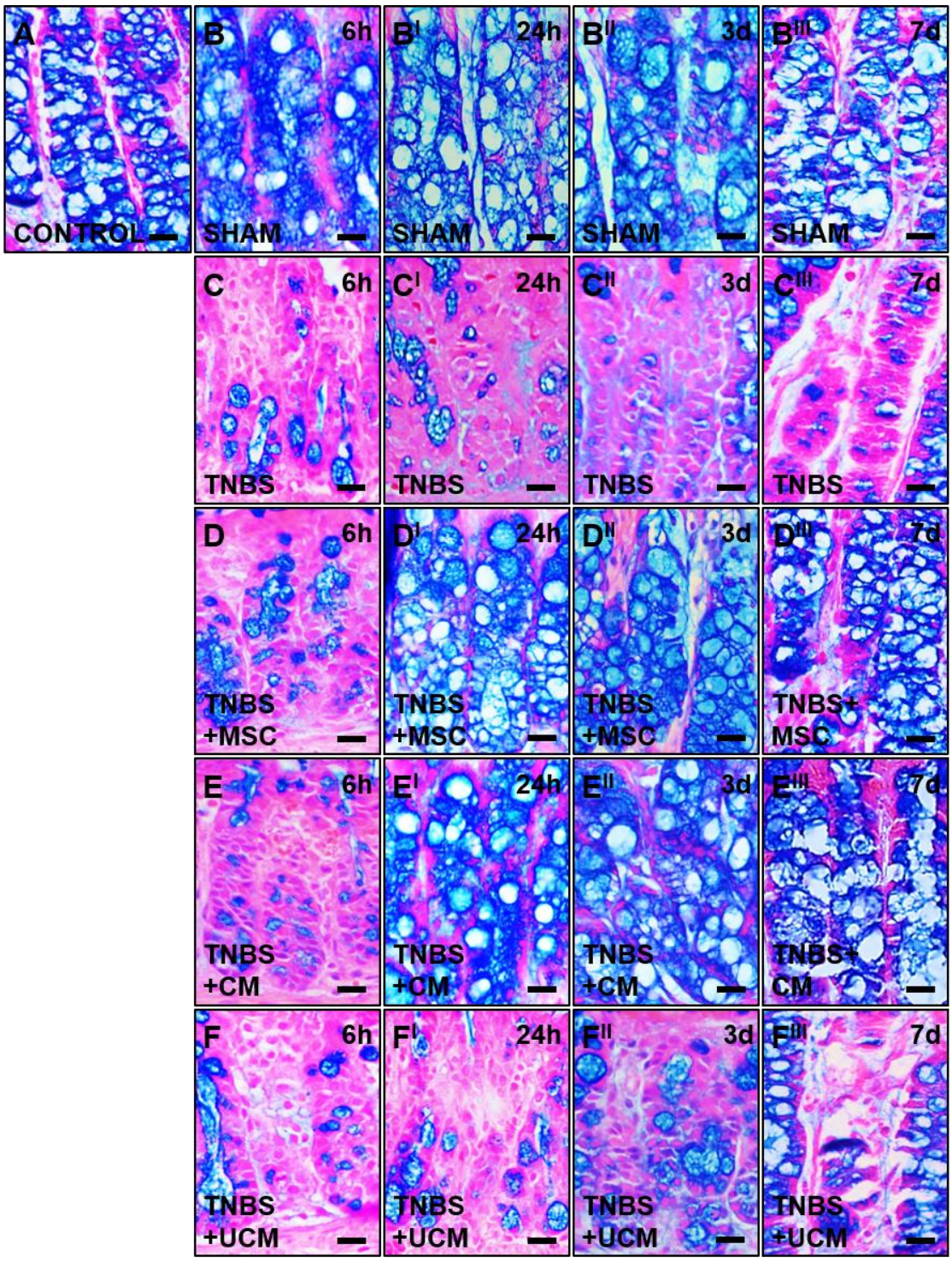
A
CONTROL
B 6h
SHAM
B^I 24h
SHAM
B^II 3d
SHAM
B^III 7d
SHAM
C 6h
TNBS
C^I 24h
TNBS
C^II 3d
TNBS
C^III 7d
TNBS
D 6h
TNBS +MSC
D^I 24h
TNBS +MSC
D^II 3d
TNBS +MSC
D^III 7d
TNBS+ MSC
E 6h
TNBS +CM
E^I 24h
TNBS +CM
E^II 3d
TNBS +CM
E^III 7d
TNBS+ CM
F 6h
TNBS +UCM
F^I 24h
TNBS +UCM
F^II 3d
TNBS +UCM
F^III 7d
TNBS +UCM

2.4.5 MSC and CM treatments attenuated the immune response in the distal colon 24h after induction of inflammation

To measure the severity of colitis and the anti-inflammatory efficacy of the treatments, quantitative analyses of CD45+ leukocytes were performed in colon cross sections and wholemount LMMP preparations (*n*=4/group/time point; Figs. 2.6 and 2.7). In cross sections of the distal colon labeled with anti-CD45 antibody, considerably more leukocytes were present in tissues from TNBS-only (369±10 cells/area) and UCM-treated (379±10 cells/area) animals compared to sham-treated (122±4 cells/area) animals at the 6h time point (*P*<0.001 for both). Sections from MSC (304±14 cells/area) and CM-treated (297±4 cells/area) guinea-pigs revealed a higher number of CD45-IR cells than sham-treated animals (*P*<0.001 for both), but significantly less leukocytes than in sections from TNBS (MSC: *P*<0.01; CM: *P*<0.001) and UCM-treated guinea-pigs (*P*<0.001 for both; Figs. 2.6A-F). At 24h, the numbers of CD45-IR cells were reduced in colon sections from MSC (141±7 cells/area) and CM-treated (142±9 cells/area) guinea-pigs and were similar to the number of CD45-IR cells in sections from sham-treated (120±3 cells/area) animals. CD45-IR cells were identified throughout the thickness of the colon in sections from TNBS-only and UCM-treated animals compared to sections from other groups. The numbers of leukocytes in colon sections from TNBS-only (379±6 cells/area) and UCM-treated (361±10 cells/area) animals remained elevated compared to sham, MSC and CM-treated groups (*P*<0.001 for all; Figs. 2.6A^{I}-E^{I}, F). The numbers of CD45-IR cells in sections from TNBS-only (301±5 cells/area) and UCM-treated (279±7 cells/area) guinea-pigs were slightly reduced by 3 days, but were still higher compared to the number of leukocytes in the sections from sham (121±4 cells/area), MSC (121±2 cells/area) and CM-treated (118±2 cells/area) guinea-pigs (*P*<0.001 for all; Figs. 2.6A^{II}-E^{II}, F). At 7 days post induction of colitis, CD45-IR cells in colon sections from TNBS-administered (258±5 cells/area) and UCM-treated animals (236±13 cells/area) remained elevated when compared to sections from sham (125±7 cells/area), MSC (140±6 cells/area) and CM-treated (137±7 cells/area) animals (*P*<0.001 for all; Figs. 2.6A^{III}-E^{III}, F).

Immune cell infiltration to the level of myenteric ganglia was quantified in wholemount LMMP preparations by double labeling with anti-CD45 antibody and pan-neuronal marker anti-PGP9.5 antibody (Fig. 2.7). At 6h, quantitative analysis of immune cells per $2mm^2$ area showed similar numbers of CD45-IR cells in LMMP preparations of the colon from sham (19±1 cells/area), TNBS-only (26±3 cells/area), MSC (22±2 cells/area), CM (22±1 cells/area), and UCM-treated animals (23±3 cells/area) (Figs. 2.7A-F). After 24h, the number of leukocytes at the level of the myenteric plexus was greater in tissues from TNBS-only (108±7 cells/area) and UCM-treated (100±3 cells/area) animals compared to sections from sham (19±1 cells/area), MSC (39±3 cells/area) and CM-treated (47±3 cells/area) guinea-pigs (P<0.001 for all). However, the numbers of CD45+ cells in colon preparations from MSC and CM-treated animals were higher than in preparations from sham-treated guinea-pigs (MSC: P<0.05; CM: P<0.01; Figs. $2.7A^{I}$-E^{I}, F). By 3 days after induction of inflammation, the numbers of immune cells at the level of the myenteric ganglia in colon preparations from MSC (23±2 cells/area) and CM-treated (27±1 cells/area) animals were comparable to the number of immune cells in preparations from sham-treated (19±1 cells/area) guinea-pigs. The quantity of CD45+ cells in preparations of the distal colon from TNBS-only (77±7 cells/area) and UCM-treated (74±2 cells/area) animals at 3 days was higher when compared to sham, MSC, and CM-treated guinea-pigs (P<0.001 for all; Figs. $2.7A^{II}$-E^{II}, F). At 7 days post induction of colitis, the number of CD45-IR cells remained elevated in TNBS-administered and UCM-treated guinea-pigs when compared to sham, MSC and CM-treated animals (P<0.001 for all; Figs. $2.7A^{III}$-E^{III}, F).

Figure 2.6. MSC and CM treatments reduce leukocyte numbers and infiltration in the distal colon following TNBS-induced colitis. Cross sections of the distal colon were labeled with pan-leukocyte marker anti-CD45 antibody. At 6h, an increase in CD45-IR cells was observed in the mucosa of TNBS-only, MSC, CM and UCM-treated sections compared to sections from sham-treated guinea-pigs **(A-E)**. At 24h, 3 days and 7 days, elevated numbers of CD45-IR cells were prominent transmurally through the layers of the colon wall in sections from TNBS-only **(B^{I}-B^{III})** and UCM-treated **(E^{I}-E^{III})** animals. Treatment with MSCs and CM attenuated the increase of CD45-IR cells at 24h **(C^{I}, D^{I})**, 3 days **(C^{II}, D^{II})** and 7 days **(C^{III}, D^{III})**. d = days. Scale bars = 50μm. Total number of leukocytes counted per 2mm^2 area within the colon wall in cross sections **(F)**. ^^^P<0.001 compared to sham-treated group. $^{\#\#}P$<0.001, $^{\#\#\#}P$<0.001 compared to MSC-treated group. $^{\dagger\dagger\dagger}P$<0.001 compared to CM-treated group.

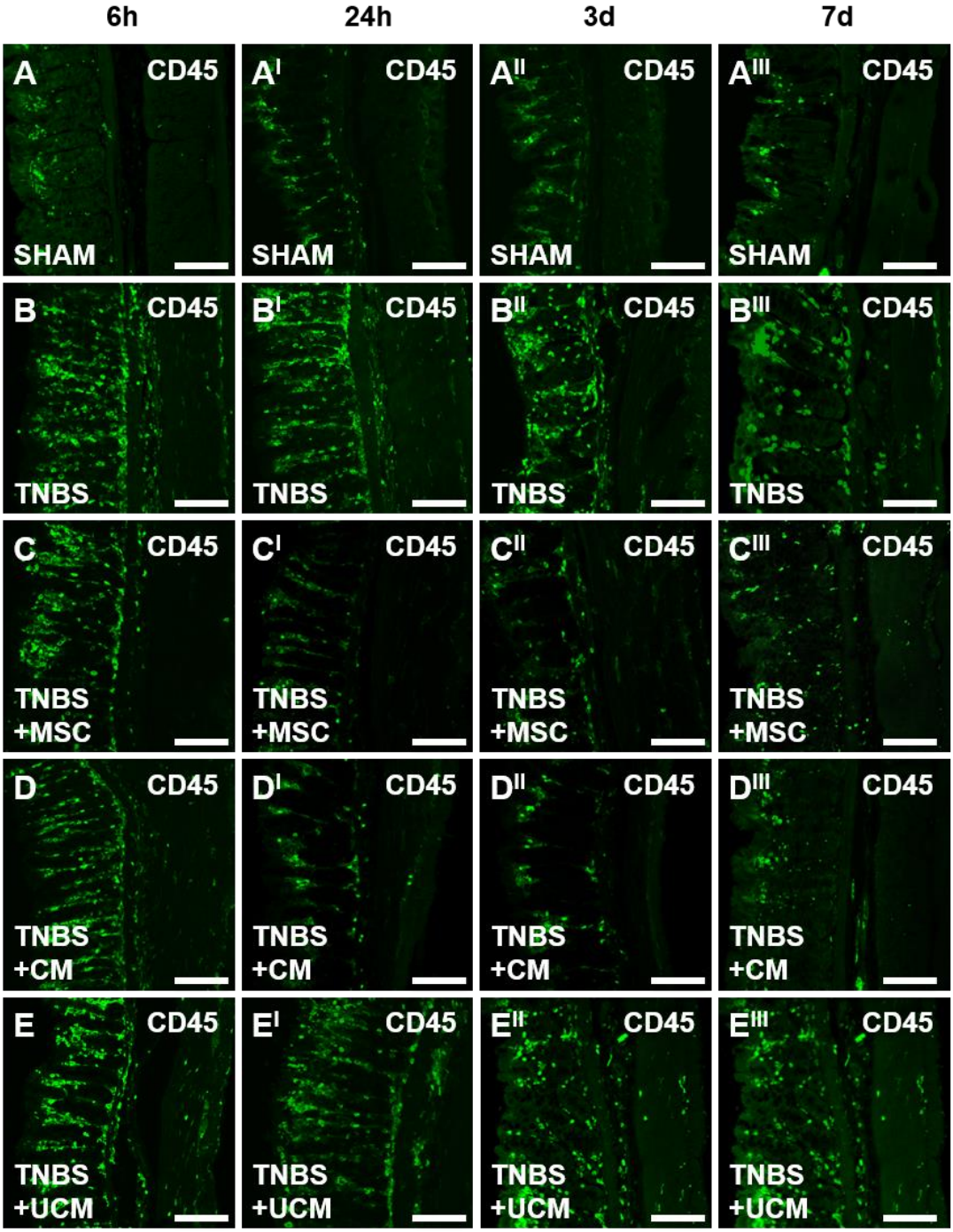
6h
24h
3d
7d
A
CD45
SHAM
AI
CD45
SHAM
AII
CD45
SHAM
AIII
CD45
SHAM
B
CD45
TNBS
BI
CD45
TNBS
BII
CD45
TNBS
BIII
CD45
TNBS
C
CD45
TNBS
+MSC
CI
CD45
TNBS
+MSC
CII
CD45
TNBS
+MSC
CIII
CD45
TNBS
+MSC
D
CD45
TNBS
+CM
DI
CD45
TNBS
+CM
DII
CD45
TNBS
+CM
DIII
CD45
TNBS
+CM
E
CD45
TNBS
+UCM
EI
CD45
TNBS
+UCM
EII
CD45
TNBS
+UCM
EIII
CD45
TNBS
+UCM

F

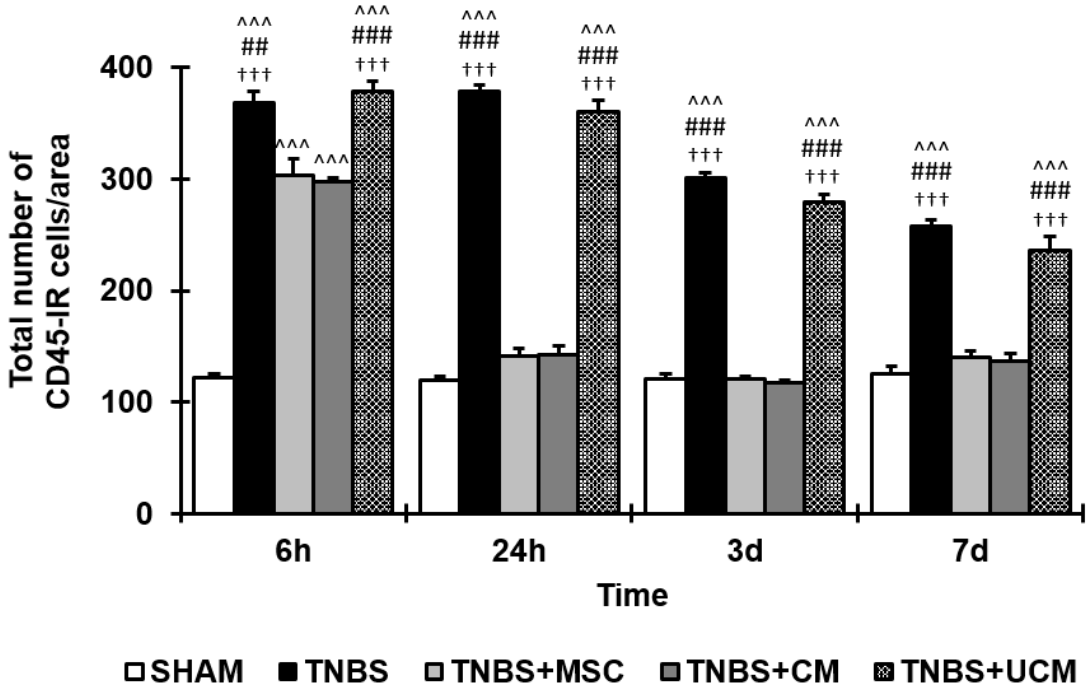
Total number of CD45-IR cells/area
400
300
200
100
0
^^^ ## †††
^^^
^^^
^^^ ### †††
^^^ ### †††
^^^ ### †††
^^^ ### †††
^^^ ### †††
^^^ ### †††
^^^ ### †††
6h
24h
3d
7d
Time
SHAM
TNBS
TNBS+MSC
TNBS+CM
TNBS+UCM

Figure 2.7. MSC and CM treatments reduce leukocyte infiltration at the level of the myenteric ganglia post induction of colitis. LMMP preparations of the distal colon were co-labeled with anti-CD45 and anti-PGP9.5 antibodies. Double-labeling of myenteric neurons with anti-PGP9.5 antibody (red) verified the location of CD45-IR cells (green) surrounding PGP9.5-IR neurons in myenteric ganglia. At 6h, a low level of leukocyte infiltration around the myenteric ganglia was observed in all groups **(A-E)**. At 24h, leukocyte infiltration in LMMP preparations from TNBS-only and UCM-treated animals was elevated in comparison to sham, MSC and CM-treated groups **(A^{I}-E^{I})**. CD45-IR cells were still elevated at 3 and 7 days post induction of colitis in preparations from TNBS-only and UCM-treated animals. Leukocyte numbers in preparations from MSC and CM-treated groups returned to sham-treated levels by 3 continuing to 7 days **(A^{II}-E^{III})**. d = days. Scale bars = 50µm. Total number of leukocytes counted per 2mm^2 area in LMMP preparations of the distal colon **(F)**. ^P<0.05, ^^P<0.01, ^^^P<0.001 compared to sham-treated group. $^{\#\#\#}P$<0.001 significantly different to TNBS+MSC-treated group. $^{\dagger\dagger\dagger}P$<0.001 significantly different to TNBS+CM-treated group.

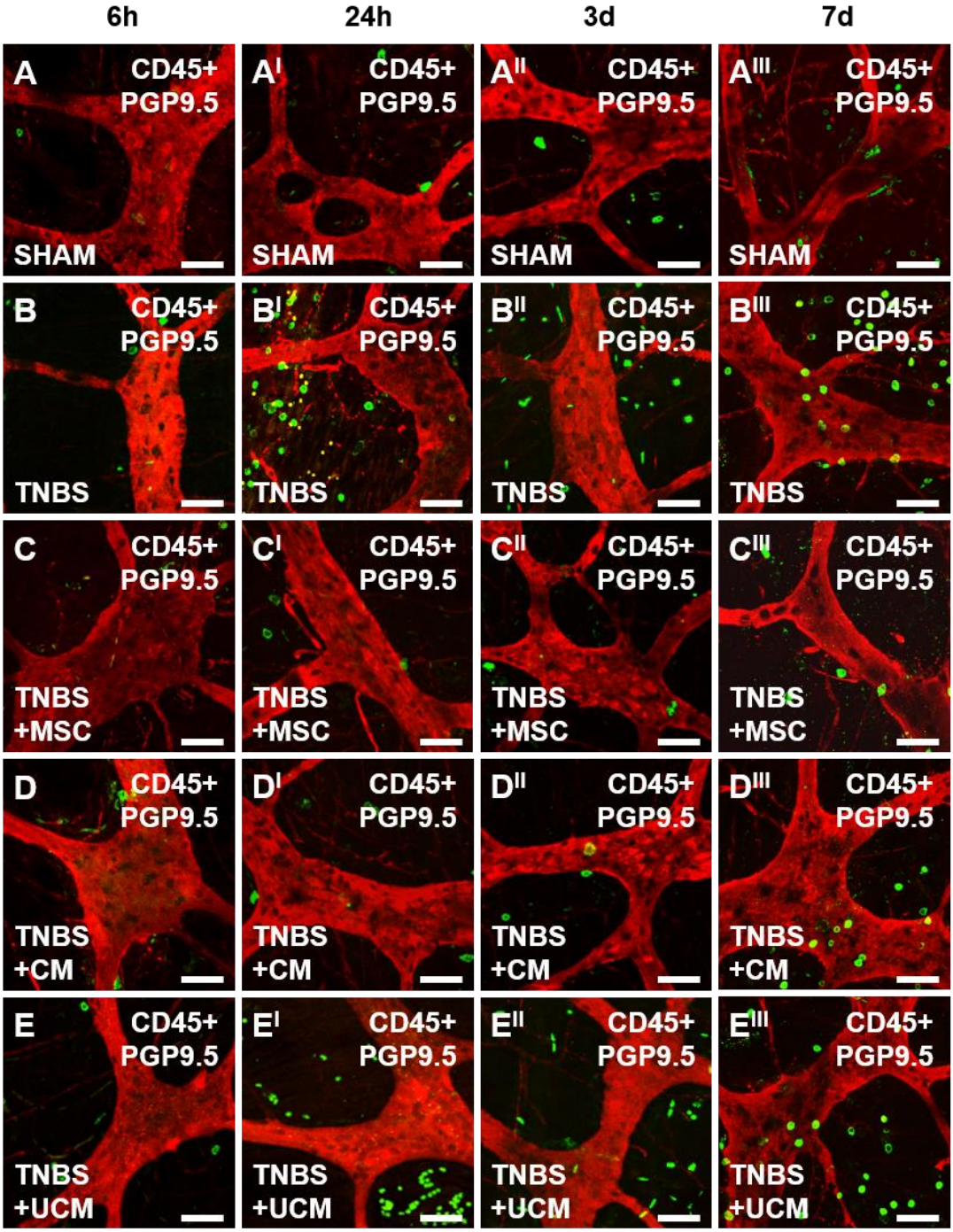
6h
24h
3d
7d
A
CD45+
PGP9.5
SHAM
A^I
CD45+
PGP9.5
SHAM
A^II
CD45+
PGP9.5
SHAM
A^III
CD45+
PGP9.5
SHAM
B
CD45+
PGP9.5
TNBS
B^I
CD45+
PGP9.5
TNBS
B^II
CD45+
PGP9.5
TNBS
B^III
CD45+
PGP9.5
TNBS
C
CD45+
PGP9.5
TNBS
+MSC
C^I
CD45+
PGP9.5
TNBS
+MSC
C^II
CD45+
PGP9.5
TNBS
+MSC
C^III
CD45+
PGP9.5
TNBS
+MSC
D
CD45+
PGP9.5
TNBS
+CM
D^I
CD45+
PGP9.5
TNBS
+CM
D^II
CD45+
PGP9.5
TNBS
+CM
D^III
CD45+
PGP9.5
TNBS
+CM
E
CD45+
PGP9.5
TNBS
+UCM
E^I
CD45+
PGP9.5
TNBS
+UCM
E^II
CD45+
PGP9.5
TNBS
+UCM
E^III
CD45+
PGP9.5
TNBS
+UCM

F

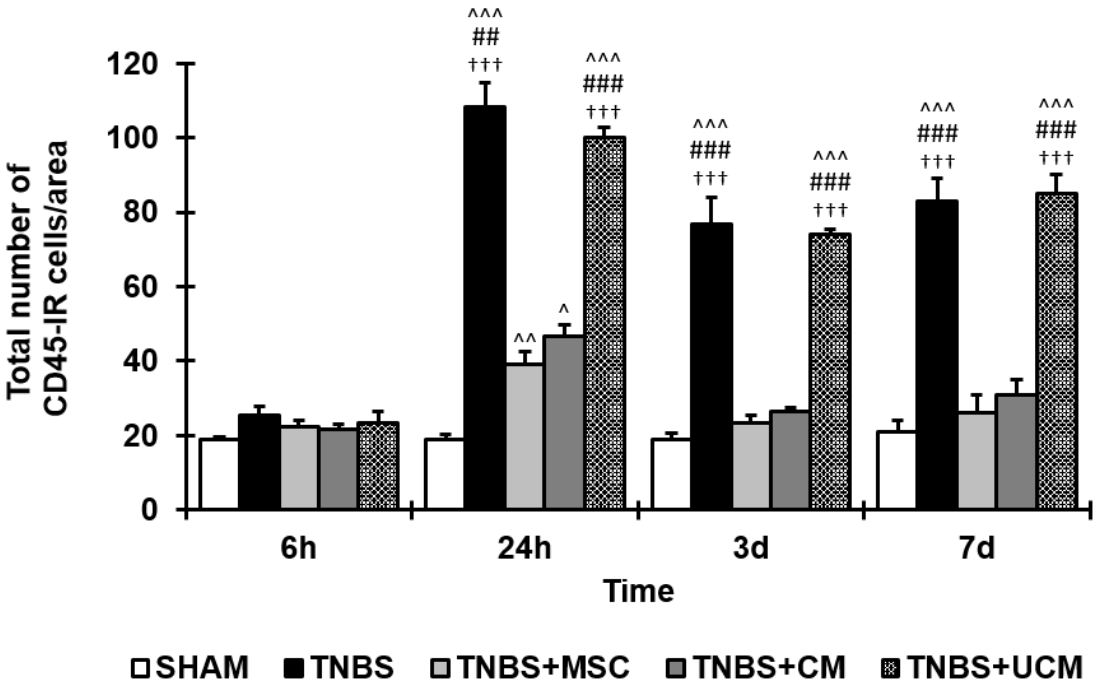
Total number of CD45-IR cells/area
120
100
80
60
40
20
0
^^^ ## †††
^^^ ### †††
^^^ ### †††
^^^ ### †††
^^^ ### †††
^^^ ### †††
^^
^
6h
24h
3d
7d
Time
SHAM
TNBS
TNBS+MSC
TNBS+CM
TNBS+UCM

2.4.6 MSC and CM treatments facilitate regrowth of nerve fibers 24h after induction of colitis

Neuronal cell bodies and processes innervating smooth muscles and mucosa were labeled by an antibody specific to neuronal microtubule protein β-tubulin (III) (*n*=5/group/time point; Fig. 2.8). Orderly distribution of β-tubulin (III)-IR fibers within the mucosal gland cores, submucosal and muscular layers were observed in colon sections from sham-treated guinea-pigs at all time points (Fig. 2.8A-A^{III}). Quantification of fiber density demonstrated the total area of β-tubulin (III)-IR fibers in sections from sham-treated animals was 10.5±0.7%, 10.7±0.7%, 10.4±0.7% and 10.5±0.9% at 6h, 24h, 3 days and 7 days after treatment, respectively (Fig. 2.8F). At all time points following TNBS administration, β-tubulin (III)-IR fibers in colon sections from animals in the TNBS-only and UCM-treated groups were disorganized, fragmented, and dispersed irregularly within the mucosa (Fig. 2.8B-B^{III}, E-E^{III}). Compared to sections from sham-treated animals, quantitative analysis revealed lower β-tubulin (III)-IR fiber density at all time points in colon sections from TNBS-only (6h: 6.5±0.7%, $P<0.001$; 24h: 6.3±0.7%, $P<0.01$; 3 days: 6.8±0.5%, $P<0.01$; 7 days: 6.8±0.3%, $P<0.01$) and UCM-treated (6h: 6.7±0.7%, $P<0.01$; 24h: 6.5±0.7%, $P<0.01$; 3 days: 6.3±0.8%, $P<0.001$; 7 days: 6.7±0.6%, $P<0.01$) guinea-pigs (Fig. 2.8F). Treatment with MSCs and CM did not prevent damage to the nerve fibers 6h after TNBS administration; the distribution and organization of fibers in sections from MSC and CM-treated animals were similar to sections from TNBS-only and UCM-treated guinea-pigs (Fig. 2.8C, D). Subsequently, the density of β-tubulin (III)-IR fibers in sections from MSC (8.0±0.2%) and CM-treated (8.0±0.3%) animals at the 6h time point was less when compared to sham-treated animals ($P<0.05$ for both; Fig. 2.8F). This result suggests that 6h is insufficient time for the regenerative effect of MSC-based treatments to occur. The density of β-tubulin (III)-IR fibers in colon sections from MSC and CM-treated guinea-pigs were comparable to those in sections from sham-treated animals at the 24h (MSC: 9.7±0.7%; CM: 9.6±0.7%), 3 days (MSC: 9.6±0.3%; CM: 9.7±0.4%) and 7 days (MSC: 9.7±0.4%; CM: 9.8±0.7%) time points (Figs. 2.8C^{I}-C^{III}, D^{I}-D^{III}, F). β-Tubulin (III)-IR fiber density in colon sections from MSC and CM-treated guinea-pigs was higher when compared to

sections from TNBS-only and UCM-treated animals at 24h (P<0.05 for all), 3 days (TNBS: P<0.05 for both; UCM: P<0.01 for both) and 7 days (P<0.05 for all), but not after 6h (Fig. 2.8F). Thus, MSC and CM treatments facilitated fiber regeneration and axonal regrowth by 24h after induction of inflammation.

2.4.7 MSC and CM treatments protected against neuronal loss 24h after induction of colitis

To study the effects of MSC and CM treatments on the number of myenteric neurons, neuronal cell bodies were labeled with the pan-neuronal marker anti-Hu antibody in wholemount LMMP preparations of the distal colon (n=5/group/time point; Fig. 2.9). The number of Hu-IR neurons counted within a 2mm^2 area did not differ between all groups at 6h (sham: 264±2 cells/area; TNBS: 260±3 cells/area; MSC: 264±2 cells/area; CM: 264±1 cells/area; UCM: 262±1 cells/area; Figs. 2.9A-F). At 24h after induction of colitis, the number of Hu-IR myenteric neurons decreased in colon preparations from TNBS-only (205±9 cells/area) and UCM-treated (209±7 cells/area) guinea-pigs compared to sham-treated animals (260±2 cells/area; P<0.001 for both). MSC (260±3 cells/area) and CM (255±4 cells/area) treatments attenuated neuronal loss associated with intestinal inflammation at 24h (P<0.001 for all; Figs. 2.9A^{I}-E^{I}, F). At 3 and 7 days, a reduction in the number of Hu-IR neurons was observed in LMMP preparations of the distal colon from TNBS-only (3 days: 202±5 cells/area; 7 days: 192±6 cells/area) and UCM-treated (3 days: 212±4 cells/area; 7 days: 202±6 cells/area) guinea-pigs when compared to preparations from sham (3 days: 261±5 cells/area; 7 days: 263±2 cells/area), MSC (3 days: 260±7 cells/area; 7 days: 261±2 cells/area), and CM-treated (3 days: 254±5 cells/area; 7 days: 258±1 cells/area) animals (P<0.001 for all; Figs. 2.9A^{II}-E^{III}, F).

2.4.8 MSC and CM treatments prevent TNBS-induced changes in the number and proportion of nNOS-IR neurons

Changes in inhibitory and excitatory myenteric neurons underlie inflammation-induced colonic dysmotility (Winston et al. 2013; Neunlist et al. 2003); therefore,

we investigated the effects of MSC-based therapies on these neurons. Inhibitory neurons were identified by using nNOS immunoreactivity in wholemount LMMP preparations of the distal colon (*n*=4/group/time point; Fig. 2.10). The number and proportion of nNOS-IR neurons were comparable between all groups at the 6h time point (sham: 54±2 cells/area, 20.5±0.9%; TNBS: 57±3 cells/area, 21.9±1.1%; MSC: 57±2 cells/area, 21.5±2.1%; CM: 56±2 cells/area, 21.3±1.9%; UCM: 57±3 cells/area, 21.7±2.9%; Figs. 2.10A-G). At 24h, the quantity of nNOS-IR myenteric neurons increased in the colon in TNBS-only (65±1 cells/area) and UCM-treated (66±3 cells/area) guinea-pigs compared to sham (53±1 cells/area; $P<0.01$ for both), MSC (53±2 cells/area; $P<0.01$ for both) and CM-treated (55±2 cells/area; TNBS: $P<0.05$; UCM: $P<0.01$) animals (Figs. 2.10A^{I}-E^{I}, F). The proportion of nNOS-IR neurons to the total number of neurons 24h post induction of colitis was greater in TNBS-only (31.9±1.8%) and UCM-treated (31.7±1.2%) guinea-pigs compared to sham (20.4±0.4%), MSC (20.5±0.7%), and CM-treated (21.4±0.7%) animals ($P<0.001$ for all; Fig. 2.10G). At 3 days, the number of nNOS-IR neurons in preparations of the distal colon from TNBS-only (65±3 cells/area) and UCM-treated (64±2 cells/area) guinea-pigs was higher compared to sham (53±1 cells/area; TNBS: $P<0.01$; UCM: $P<0.05$), MSC (54±2 cells/area; $P<0.05$ for both) and CM-treated (54±2 cells/area; $P<0.05$ for both) animals (Figs. 2.10A^{II}-E^{II}, F). The proportion of nNOS-IR neurons at 3 days was greater in colon preparations from TNBS-only (32.2±2.1%) and UCM-treated (29.9±0.2%) guinea-pigs compared to sham (20.4±0.3%), MSC (20.8±0.9%), and CM-treated (21.1±1.1%) animals ($P<0.001$ for all; Fig. 2.10G). At 7 days post induction of colitis, the number of nNOS-IR neurons in preparations from TNBS-only (65±1 cells/area) and UCM-treated (62±2 cells/area) guinea-pigs continued to be higher than in preparations from sham (53±1 cells/area; TNBS: $P<0.001$; UCM: $P<0.01$), MSC (53±2 cells/area; TNBS: $P<0.001$; UCM: $P<0.01$) and CM-treated (54±1 cells/area; TNBS: $P<0.001$; UCM: $P<0.05$) animals (Figs. 2.10A^{III}-E^{III}, F). Subsequently, the proportion of nNOS-IR neurons was persistently elevated in the colon from TNBS-only (33.7±1.3%) and UCM-treated (30.5±0.9%) guinea-pigs continued to be higher than in preparations from sham (20.1±0.3%), MSC (20.1±0.5%) and CM-treated (21.1±0.5%) animals ($P<0.001$ for all; Figs. 2.10G).

2.4.9 MSC and CM treatments prevent TNBS-induced changes in the number of ChAT-IR neurons

Excitatory neurons were identified using ChAT immunoreactivity in wholemount LMMP preparations of the distal colon (*n*=4/group/time point, Fig. 2.11). The number of ChAT-IR neurons was similar in preparations from all groups at 6h post induction of colitis (sham: 156±2 cells/area; TNBS: 156±3 cells/area; MSC: 152±3 cells/area; CM: 153±2 cells/area; UCM: 146±2 cells/area; Figs. 2.11A-F). The number of ChAT-IR neurons decreased at the 24h time point in TNBS-only (108±2 cells/area) and UCM-treated groups (115±2 cells/area) compared to sham (158±7 cells/area), MSC (155±2 cells/area) and CM (147±3 cells/area) groups (*P*<0.001 for all; Figs 2.11A^{I}-E^{I}, F). At 3 days post induction of colitis, the quantity of ChAT-IR neurons in preparations from sham (155±2 cells/area), MSC (150±4 cells/area) and CM-treated (150±4 cells/area) animals remained higher than in tissues from TNBS-only (111±5 cells/area; *P*<0.01 for all) and UCM-treated (104±4 cells/area; sham: *P*<0.01; MSC: *P*<0.05; CM: *P*<0.05) guinea-pigs (Figs 2.11A^{II}-E^{II}, F). Similar results were found at 7 days where ChAT-IR neurons were significantly reduced in TNBS-only (104±4 cells/area) and UCM-treated (102±5 cells/area) guinea-pigs compared to sham (150±2 cells/area), MSC (146±3 cells/area) and CM-treated (152±1 cells/area) guinea-pigs (*P*<0.001 for all; Figs 2.11A^{III}-E^{III}, F). Changes in the total number of ChAT-IR neurons corresponded with losses in the total number of neurons and there were no significant differences in the proportion of ChAT-IR neurons to the total number of neurons within the distal colon at 6h (sham: 59.2±2.3%; TNBS: 60.2±2.7%; MSC: 57.5±1.3%; CM: 57.9±2.6%; UCM: 55.8±2.7%), 24h (sham: 60.8±3.2%; TNBS: 52.7±5.0%; MSC: 59.8±2.3%; CM: 57.7±2.1%; UCM: 55.0±3.0%), 3 days (sham: 59.3±1.5%; TNBS: 55.2±2.4%; MSC: 57.7±1.3%; CM: 58.9±1.4%; UCM: 53.9±1.2%) or 7 days (sham: 57.0±1.9%; TNBS: 54.3±4.3%; MSC: 55.9±3.2%; CM: 59.0±1.4%; UCM: 50.5±5.1%) post induction of colitis (Fig. 2.11G).

Figure 2.8. MSC and CM treatments facilitate regrowth of nerve fibers in the distal colon following TNBS-induced colitis. Neuronal processes innervating mucosal glands (arrows) in cross sections of the distal colon were identified by neuron specific anti-β-tubulin (III) antibody in cross sections of the distal colon. Orderly distribution of fibers labeled by neuron specific anti-β-tubulin (III) antibody was observed in colon sections from sham-treated guinea-pigs at all time points **(A-A^{III})**. Disorganized, fragmented, and irregularly dispersed fibers were evident within the mucosa of sections from TNBS-only **(B-B^{III})** and UCM-treated **(E-E^{III})** animals at all time points. Damage to nerve fibers was present in sections from MSC and CM-treated animals at 6h **(C, D)**, however regrowth of nerve fibers was observed at 24h **(C^{I}, D^{I})**, 3 days **(C^{II}, D^{II})** and 7 days **(C^{III}, D^{III})** post induction of colitis. d = days. Scale bars = 50μm. Nerve fiber density quantified per 2mm^2 area in cross sections of the distal colon **(F)**. ^P<0.05, ^^P<0.01, ^^^P<0.001 compared to sham-treated group. $^{\#}P$<0.05, $^{\#\#}P$<0.01 significantly different to TNBS+MSC-treated group. $^{\dagger}P$<0.05, $^{\dagger\dagger}P$<0.01 significantly different to TNBS+CM-treated group.

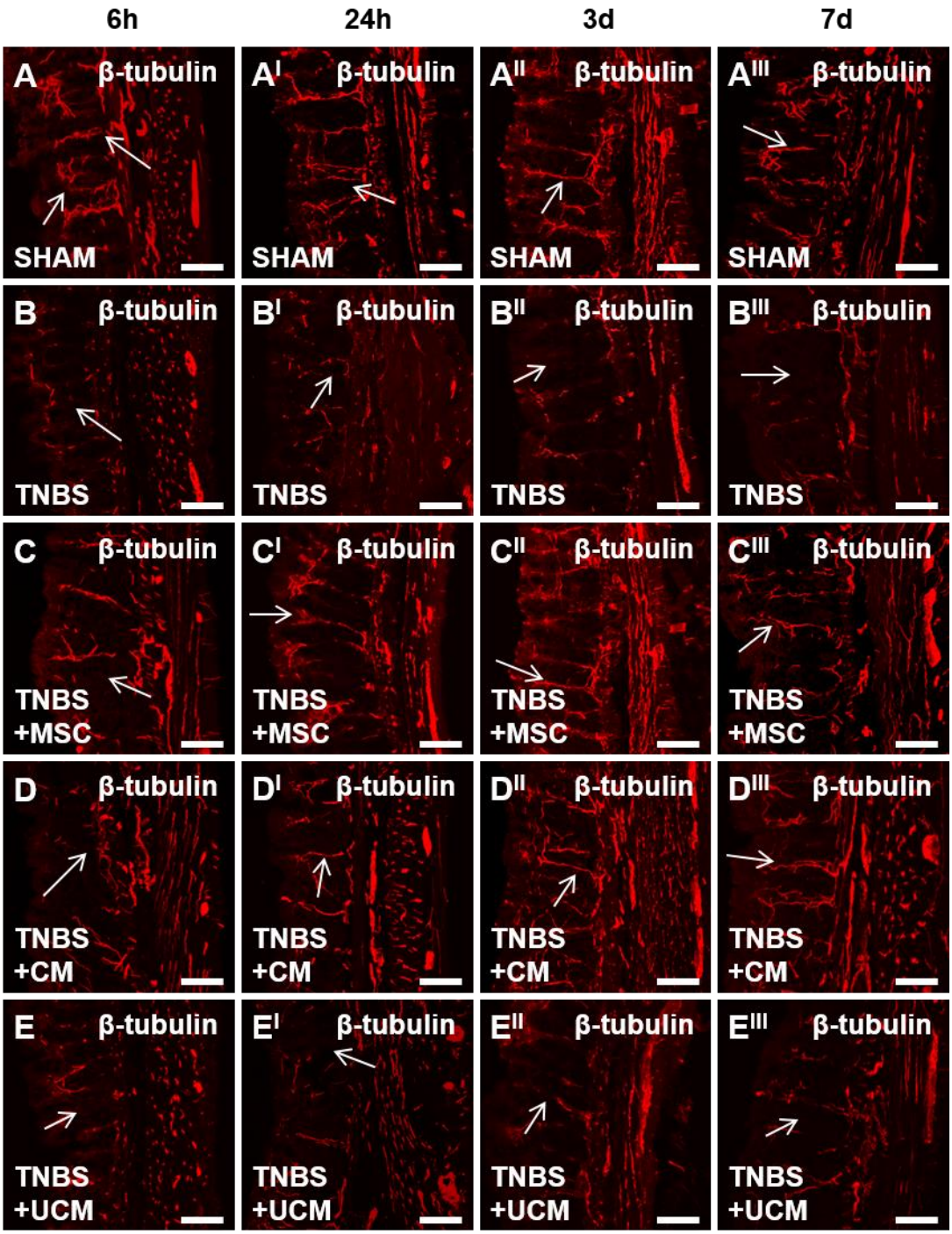
6h
24h
3d
7d
A
β-tubulin
SHAM
AI
AII
AIII
B
TNBS
BI
BII
BIII
C
TNBS
+MSC
CI
CII
CIII
D
TNBS
+CM
DI
DII
DIII
E
TNBS
+UCM
EI
EII
EIII

F

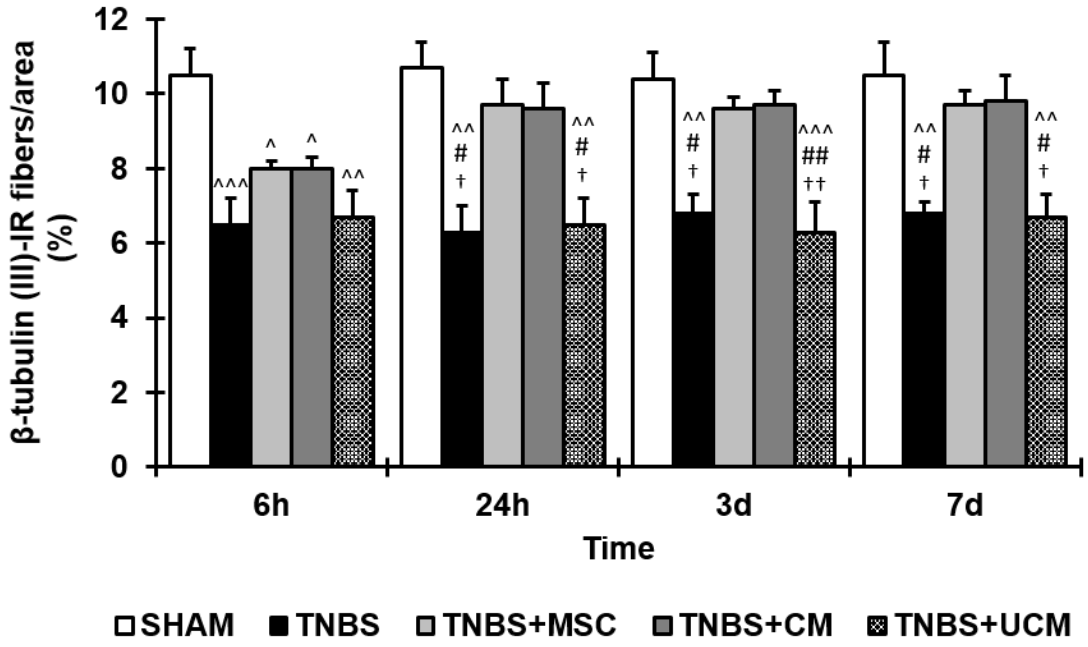
β-tubulin (III)-IR fibers/area (%)
12
10
8
6
4
2
0
^^^
^
^
^^
^^
#
†
^^
#
†
^^
#
†
^^^
##
††
^^
#
†
^^
#
†
6h
24h
3d
7d
Time
SHAM
TNBS
TNBS+MSC
TNBS+CM
TNBS+UCM

Figure 2.9. Effects of MSC and CM treatments on the total number of myenteric neurons. Myenteric neurons were identified by anti-Hu antibody in wholemount LMMP preparations of the distal colon. At 6h post TNBS administration, the number of myenteric neurons was similar across all groups **(A-E)**. Significant loss of neurons was observed in tissues from TNBS-only and UCM-treated when compared to tissues from sham, MSC and CM-treated animals at 24h, 3 days and 7 days post induction of colitis **(A^{I}-E^{III})**. d = days. Scale bars = 50μm. The total number of myenteric neurons per 2mm^2 area in LMMP wholemount preparations **(F)**. ^^^P<0.001 compared to sham-treated group. $^{###}P$<0.001 significantly different to TNBS+MSC-treated group. $^{†††}P$<0.001 significantly different to TNBS+CM-treated group.

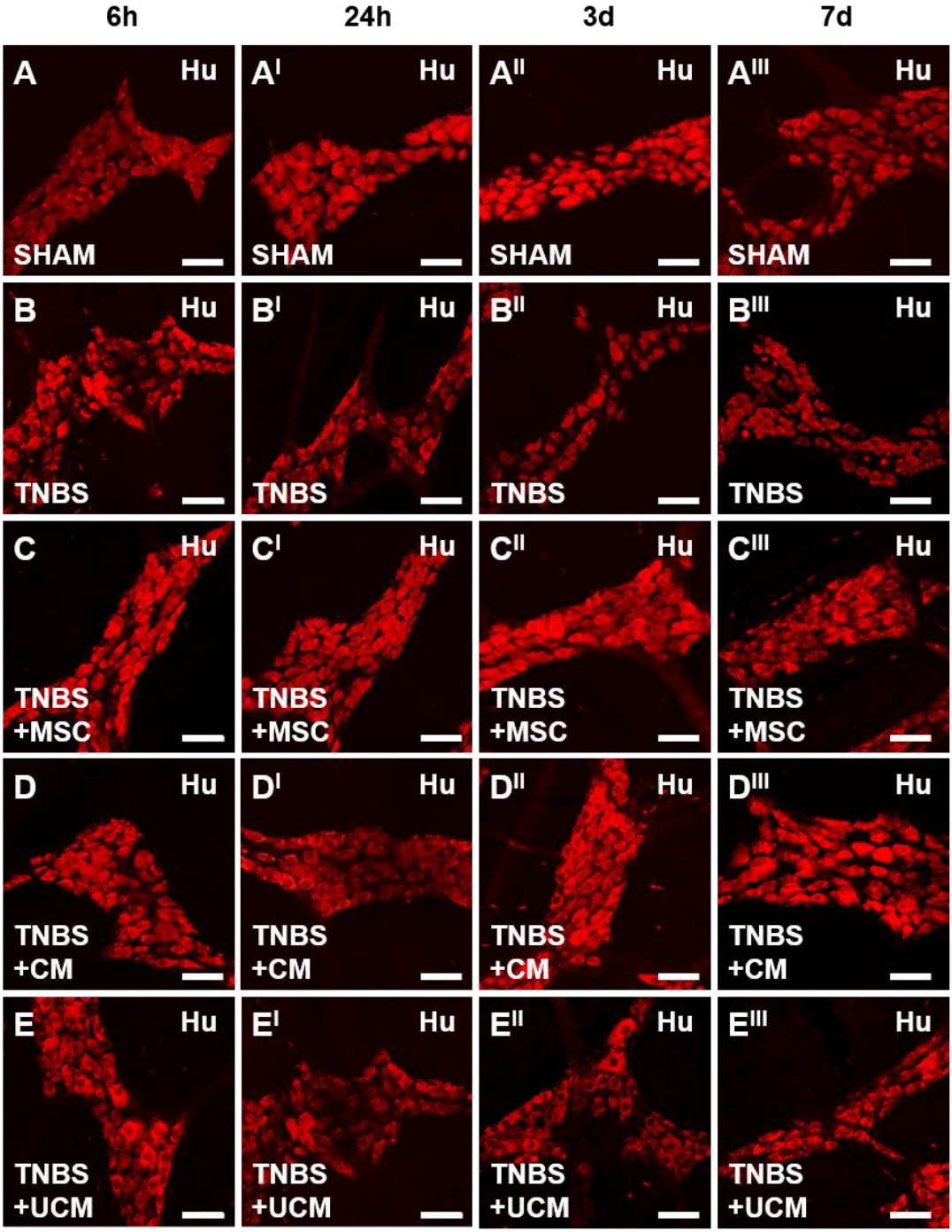
6h
24h
3d
7d
A
Hu
SHAM
A^I
Hu
SHAM
A^II
Hu
SHAM
A^III
Hu
SHAM
B
Hu
TNBS
B^I
Hu
TNBS
B^II
Hu
TNBS
B^III
Hu
TNBS
C
Hu
TNBS
+MSC
C^I
Hu
TNBS
+MSC
C^II
Hu
TNBS
+MSC
C^III
Hu
TNBS
+MSC
D
Hu
TNBS
+CM
D^I
Hu
TNBS
+CM
D^II
Hu
TNBS
+CM
D^III
Hu
TNBS
+CM
E
Hu
TNBS
+UCM
E^I
Hu
TNBS
+UCM
E^II
Hu
TNBS
+UCM
E^III
Hu
TNBS
+UCM

F

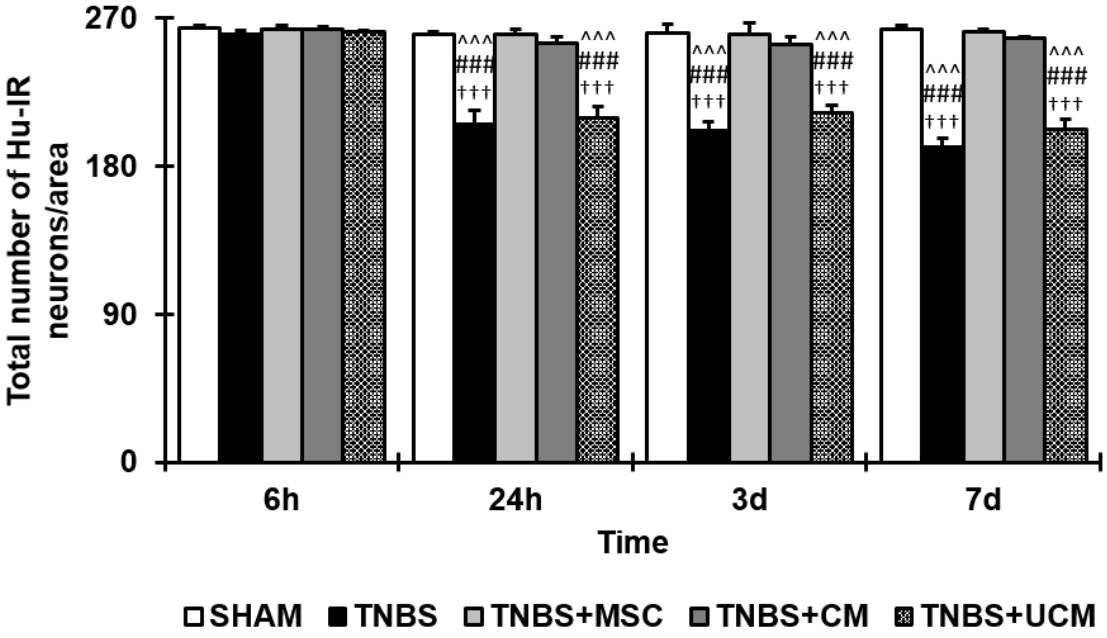
270
180
90
0
Total number of Hu-IR neurons/area
^^^
###
†††
6h
24h
3d
7d
Time
SHAM
TNBS
TNBS+MSC
TNBS+CM
TNBS+UCM

Figure 2.10. Effects of MSC and CM treatments on nNOS-IR myenteric neurons. No changes in nNOS-IR neurons were observed at 6h in any group **(A-E)**. At 24h, 3 days and 7 days, an increase in nNOS-IR neurons was observed in sections from TNBS-only **(B^{I}-B^{III})** and UCM-treated **(E^{I}-E^{III})** animals compared to sham **(A^{I}-A^{III})**, MSC **(C^{I}-C^{II})** and CM-treated groups **(D^{I}-D^{II})**. d = days. Scale bars = 50μm. The total number of nNOS-IR neurons identified by anti-nNOS antibody per $2mm^2$ area **(F)**. The proportion of nNOS-IR neurons to the total number of neurons **(G)**. ^P<0.05, ^^P<0.01, ^^^P<0.001 compared to sham-treated group. $^{\#}P$<0.05, $^{\#\#}P$<0.01, $^{\#\#\#}P$<0.001 significantly different to TNBS+MSC-treated group. $^{\dagger}P$<0.05, $^{\dagger\dagger}P$<0.01, $^{\dagger\dagger\dagger}P$<0.001 significantly different to TNBS+CM-treated group.

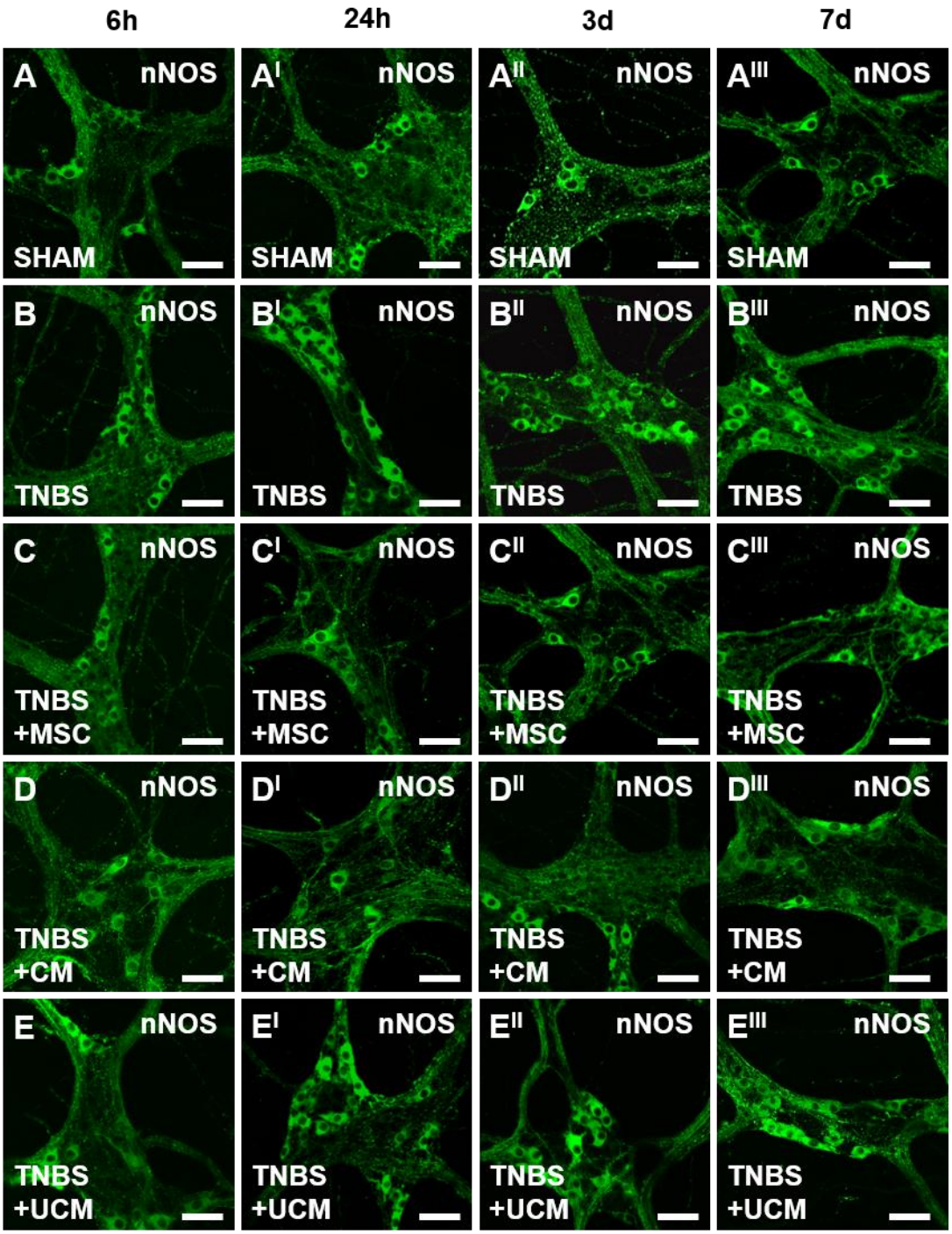
6h
24h
3d
7d
A
nNOS
SHAM
A^I
nNOS
SHAM
A^II
nNOS
SHAM
A^III
nNOS
SHAM
B
nNOS
TNBS
B^I
nNOS
TNBS
B^II
nNOS
TNBS
B^III
nNOS
TNBS
C
nNOS
TNBS
+MSC
C^I
nNOS
TNBS
+MSC
C^II
nNOS
TNBS
+MSC
C^III
nNOS
TNBS
+MSC
D
nNOS
TNBS
+CM
D^I
nNOS
TNBS
+CM
D^II
nNOS
TNBS
+CM
D^III
nNOS
TNBS
+CM
E
nNOS
TNBS
+UCM
E^I
nNOS
TNBS
+UCM
E^II
nNOS
TNBS
+UCM
E^III
nNOS
TNBS
+UCM

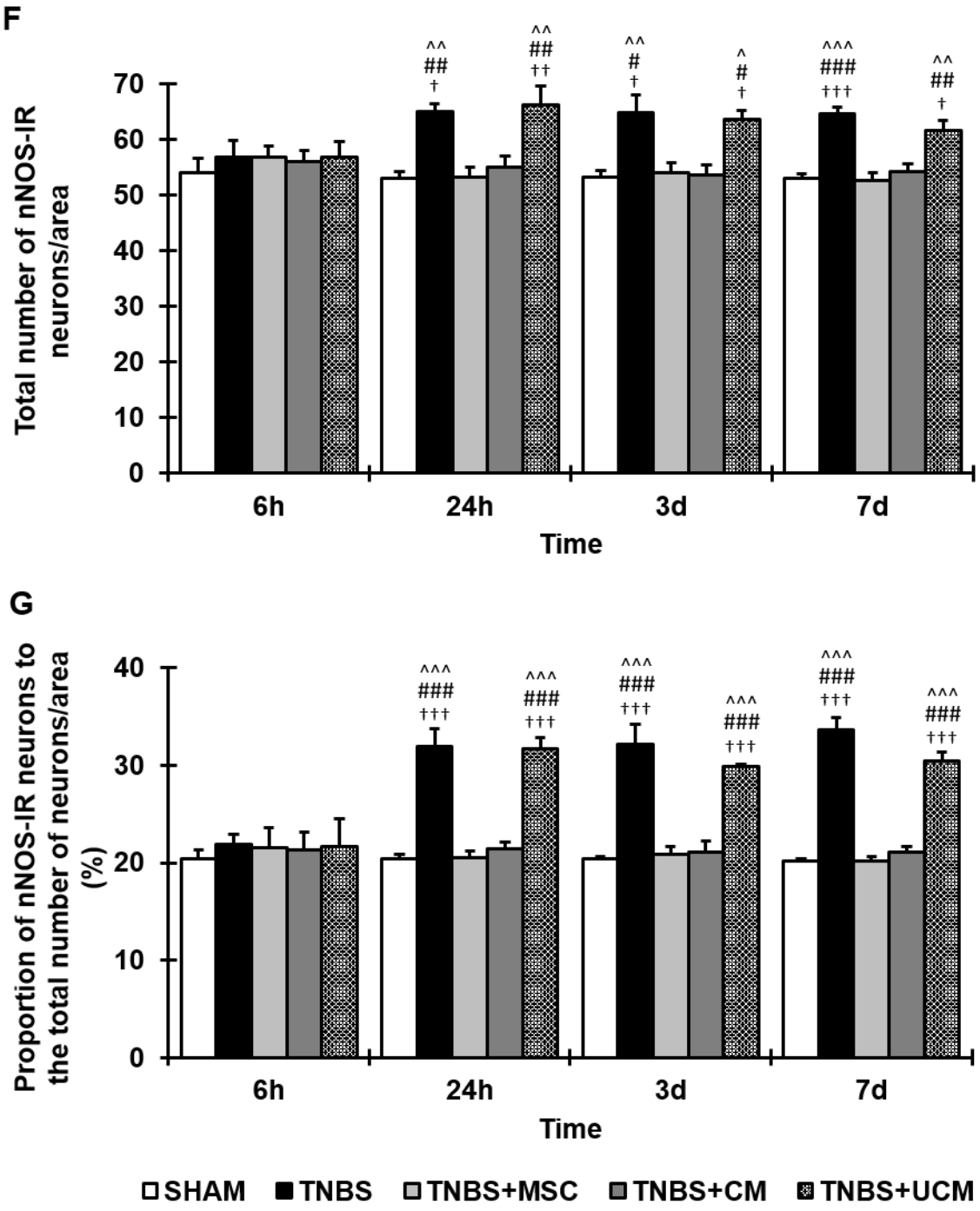
F
Total number of nNOS-IR neurons/area
70
60
50
40
30
20
10
0
^^ ## †
^^ ## ††
^^ # †
^ # †
^^^ ### †††
^^ ## †
6h
24h
3d
7d
Time
G
Proportion of nNOS-IR neurons to the total number of neurons/area (%)
40
30
20
10
0
^^^ ### †††
6h
24h
3d
7d
Time
SHAM
TNBS
TNBS+MSC
TNBS+CM
TNBS+UCM

Figure 2.11. Effects of MSC and CM treatments on ChAT-IR myenteric neurons. No changes in ChAT-IR neurons were observed at 6h post induction of colitis in any group **(A-E)**. At 24h, 3 days and 7 days, a decrease in ChAT-IR neurons was observed in sections from TNBS-only **(B^{I}-B^{III})** and UCM-treated **(E^{I}-E^{III})** animals compared to sham **(A^{I}-A^{III})**, MSC and CM-treated groups **(C^{I}-C^{II}, D^{I}-D^{II})**. d = days. Scale bars = 50μm. The total number of ChAT-IR neurons identified by anti-ChAT antibody per 2mm^2 area **(F)**. The proportion of ChAT-IR neurons to the total number of neurons **(G)**. ^^*P*<0.01, ^^^*P*<0.001 compared to sham-treated group. $^{\#}P$<0.05, $^{\#\#}P$<0.01, $^{\#\#\#}P$<0.001 significantly different to TNBS+MSC-treated group. $^{\dagger}P$<0.05, $^{\dagger\dagger}P$<0.01, $^{\dagger\dagger\dagger}P$<0.001 significantly different to TNBS+CM-treated group.

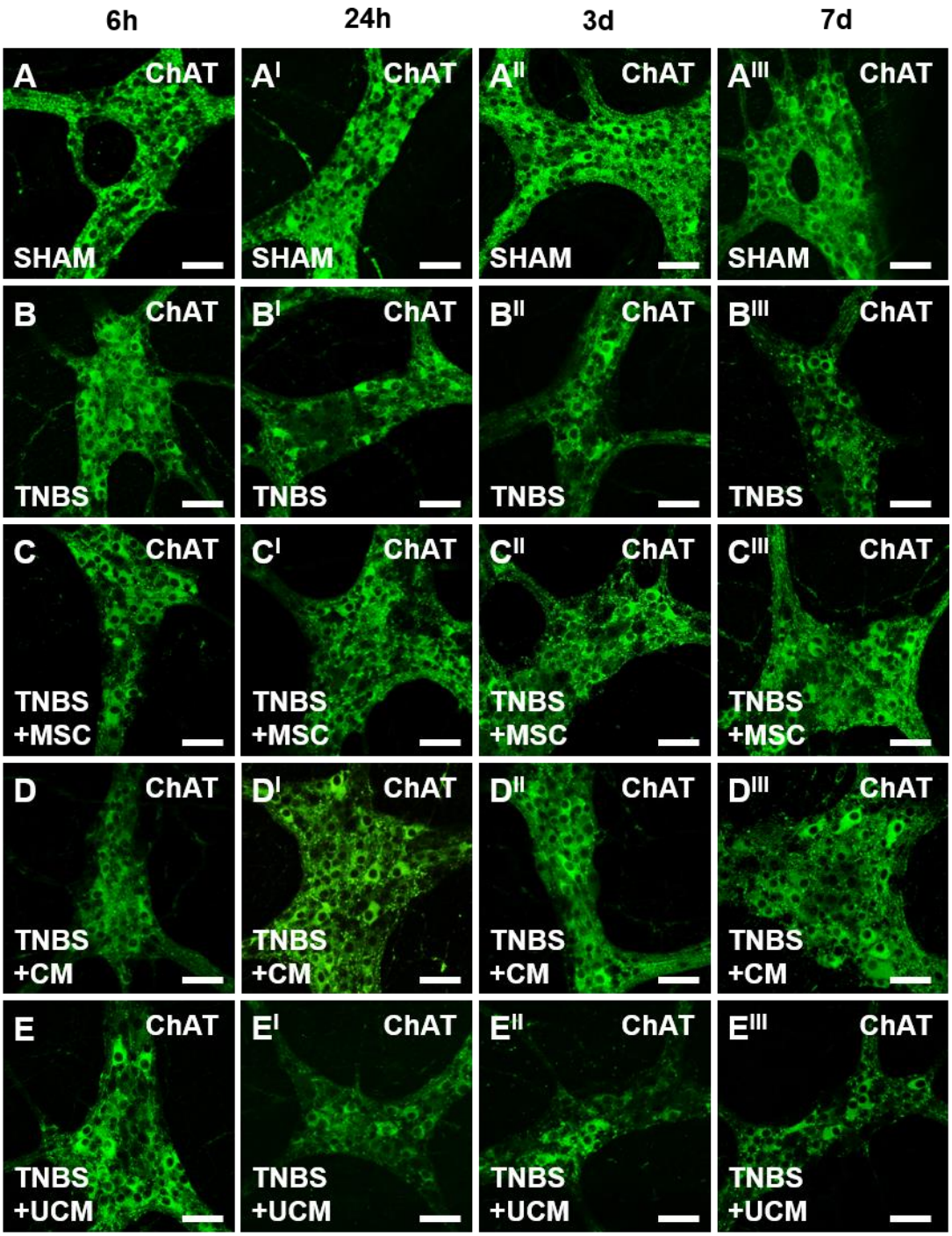
6h
24h
3d
7d
A
ChAT
SHAM
A^I
ChAT
SHAM
A^II
ChAT
SHAM
A^III
ChAT
SHAM
B
ChAT
TNBS
B^I
ChAT
TNBS
B^II
ChAT
TNBS
B^III
ChAT
TNBS
C
ChAT
TNBS
+MSC
C^I
ChAT
TNBS
+MSC
C^II
ChAT
TNBS
+MSC
C^III
ChAT
TNBS
+MSC
D
ChAT
TNBS
+CM
D^I
ChAT
TNBS
+CM
D^II
ChAT
TNBS
+CM
D^III
ChAT
TNBS
+CM
E
ChAT
TNBS
+UCM
E^I
ChAT
TNBS
+UCM
E^II
ChAT
TNBS
+UCM
E^III
ChAT
TNBS
+UCM

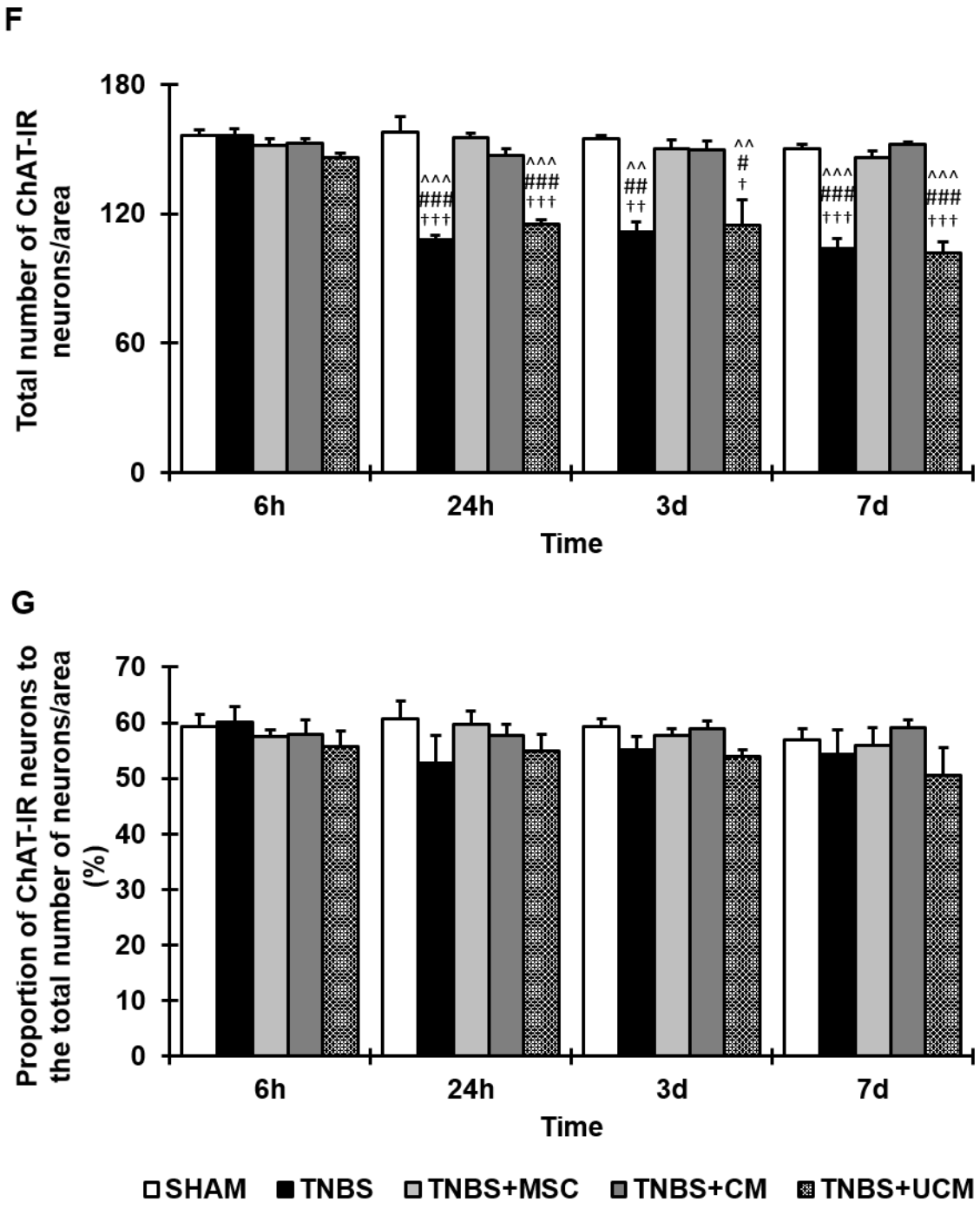
F
Total number of ChAT-IR neurons/area
180
120
60
0
6h
24h
3d
7d
Time
G
Proportion of ChAT-IR neurons to the total number of neurons/area (%)
70
60
50
40
30
20
10
0
6h
24h
3d
7d
Time
SHAM
TNBS
TNBS+MSC
TNBS+CM
TNBS+UCM

2.4.10 MSC and CM treatments prevent TNBS-induced changes in colonic motility

Colonic migrating motor complexes (CMMCs) (constrictions propagating over >50% of the colon segment) were assessed to determine the effectiveness of MSC and CM treatments to prevent TNBS-induced colon dysfunction (Fig. 2.12A). The speed of CMMC propagation, 7 days after TNBS administration (7.5±0.8mm/s; *n*=8) was significantly greater than in sham-treated animals (4.1±0.1mm/s; *n*=5; *P*<0.001; Fig. 2.12B). The frequency of contractions was lower in the colon from TNBS group (1.6±0.1min^{-1}) than from sham-treated guinea-pigs (2.3±0.04min^{-1}; *P*<0.01; Fig. 2.12C). Treatment with MSC and CM (*n*=5 for both) significantly attenuated the speed of CMMC propagation (MSC: 3.8±0.2mm/s; CM: 4.3±0.5mm/s; *P*<0.001 for both) and increased the frequency of contractions (MSC: 2.3±0.1min^{-1}; CM: 2.2±0.2min^{-1}; *P*<0.05 for both; Fig. 2.12B-C). Treatment with UCM (*n*=7) exhibited a decrease in the contraction speed (5.5±0.3mm/s; Fig. 2.12B) and an increase in the CMMC frequency (1.9±0.1min^{-1}; Fig. 2.12C) observed in the colon from TNBS-administered guinea-pigs, however, this effect was not significant when compared to the TNBS group, nor compared with sham, MSC, or CM-treated animals.

2.4.11 Neuroprotective factors released by MSCs

RT-PCR, flow cytometry and antibody array analysis of factors in CM revealed that MSCs used in our study released a substantial number of growth factors, cytokines and proteins exerting neuroprotective effects. Expression of factors with well-known neuroprotective functions have been detected by highly sensitive RT-PCR and flow cytometry techniques. The antibody array method was less sensitive than RT-PCR and flow cytometry, however the capacity to detect great amounts of different target proteins enabled identification of many other neuroprotective factors released by MSCs (Table 2.5).

Figure 2.12. Effects of MSC and CM treatments on propulsive activity of the colon. Spatiotemporal maps of colonic contractile activity define propagating colonic migrating motor complexes (CMMCs; red) 7 days after treatment **(A)**. Quantification of propagation speed (anally propagating whole length contractions (>50% length of the colon)) indicated a significant increase in CMMC velocity in the colon of TNBS-administered guinea-pigs compared to sham, MSC and CM-treated animals **(B)**. Frequency of CMMCs was significantly reduced in the colon of TNBS-administered guinea-pigs compared with sham, MSC and CM-treated animals **(C)**. ^^P<0.01, ^^^P<0.001 compared to sham-treated group. $^{\#}P$<0.05, $^{\#\#\#}P$<0.001 significantly different to TNBS+MSC-treated group. $^{\dagger}P$<0.05, $^{\dagger\dagger\dagger}P$<0.001 significantly different to TNBS+CM-treated group.

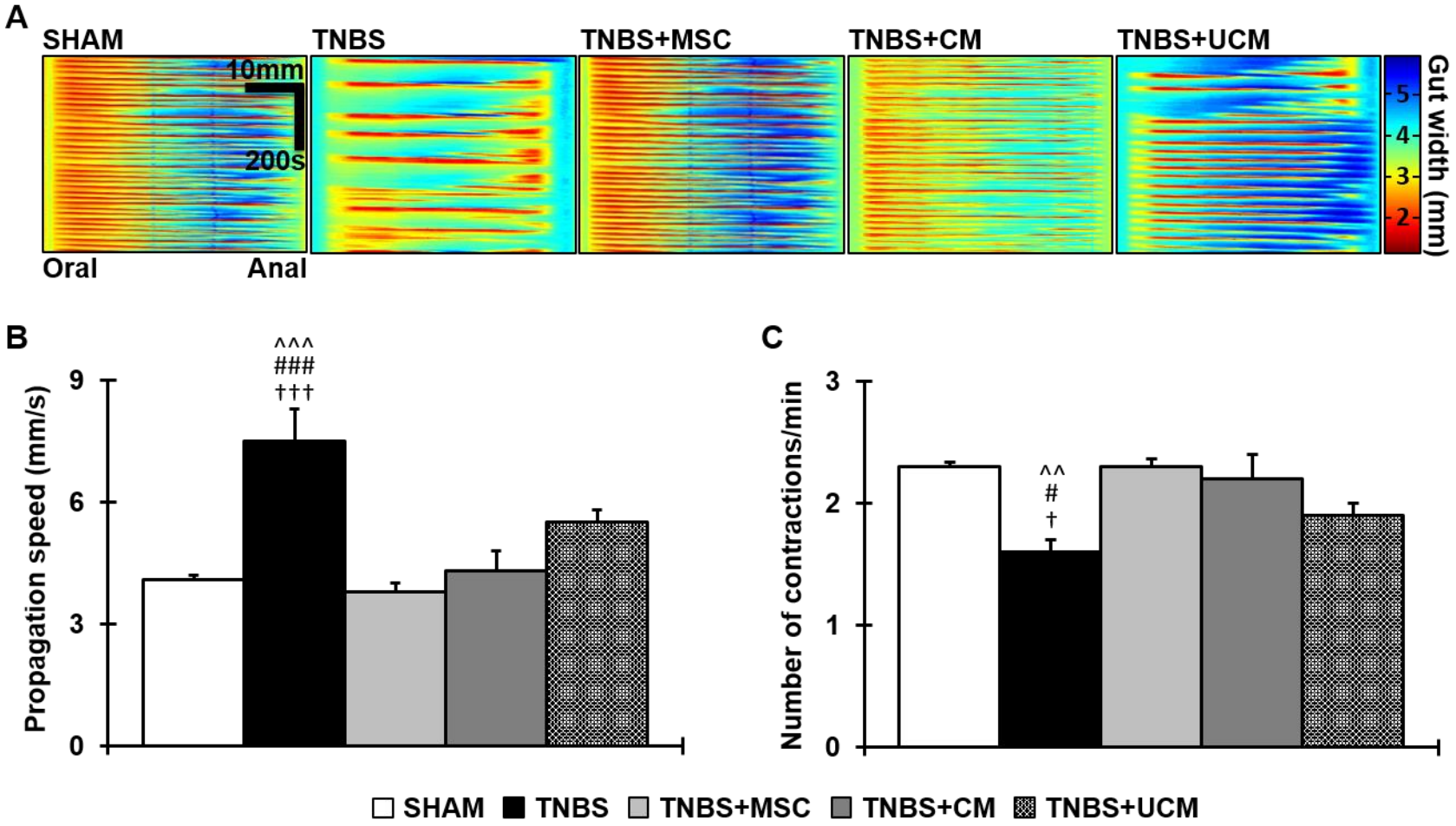
A
SHAM
TNBS
TNBS+MSC
TNBS+CM
TNBS+UCM
10mm
200s
Oral
Anal
Gut width (mm)
5
4
3
2
B
Propagation speed (mm/s)
9
6
3
0
^^^
###
†††
C
Number of contractions/min
3
2
1
0
^^
#
†
SHAM
TNBS
TNBS+MSC
TNBS+CM
TNBS+UCM

Table 2.5 Neuroprotective factors released by MSCs used in this study

Factor	Detection method	Neuroprotective role established in published studies
NGF	RT-PCR	Neuroprotective for hypoxic-ischemic injuries of the brain, optic pathways, and skin, rescues extraocular motoneurons from axotomy-induced cell death (Morcuende et al. 2013; Chiaretti et al. 2011).
NT3	RT-PCR	Neuroprotective against focal cerebral ischemia/reperfusion injury in rats, rescues extraocular motoneurons from axotomy-induced cell death (Zhang et al. 2012; Morcuende et al. 2013).
BDNF	RT-PCR Antibody array	Amplifies neurotransmitter responses and promotes synaptic communication in the ENS, rescues extraocular motoneurons from axotomy-induced cell death (Morcuende et al. 2013; Boesmans et al. 2008).
TSG-6	RT-PCR	Improves neurological function after global cerebral ischemia (Lin et al. 2013).
VEGF	RT-PCR	Protective factor in hypoxia–ischemia, *in vitro* excitotoxicity, motor neuron degeneration and against seizure-induced neuronal loss in hippocampus (Nicoletti et al. 2008).
Glial cell line-derived neurotrophic factor (GDNF)	RT-PCR	Rescues extraocular motoneurons from axotomy-induced cell death, protects enteric glia from apoptosis (Morcuende et al. 2013; Steinkamp et al. 2012).
HGF	RT-PCR	Morphologic and physiological preservation of photoreceptors in rats with photoreceptor degeneration induced by phototoxicity or a gene mutation (Machida et al. 2004).
Interleukin (IL)-6	Flow cytometry	Neuroprotective effect in brain ischemic injury (Jung et al. 2011).

Table 2.5 Neuroprotective factors released by MSCs used in this study (continued)

Factor	Detection method	Neuroprotective role established in published studies
TGF-β1 TGF-β3	RT-PCR Antibody array Flow cytometry	Neuroprotective function following brain ischemia, trauma, sclerosis multiplex, neurodegenerative diseases, infections, and brain tumors (Dobolyi et al. 2012).
IGF-1	RT-PCR	Protects neurons against cell death induced by amyloidogenic derivatives, glucose or serum deprivation relating Alzheimer's disease and other neurodegenerative disorders (Zheng et al. 2000).
Bone morphogenetic protein (BMP)-4	Antibody array	Protects retinal neurons (Fischer et al. 2004).
Cardiotrophin-1	Antibody array	Protects motor, sensory and sympathetic neurons in the peripheral nervous system (Sola et al. 2008).
Frizzled 5	Antibody array	Neuroprotection for nervous system development (Slater et al. 2013).
Glutathione peroxidase (GPX)-3	Antibody array	Neuroprotective in Huntington's disease (Mason et al. 2013).
Activin B	Antibody array	Neuroprotective activity associated with regulation of Bcl-2 family proteins (Kupershmidt et al. 2007).
Axl	Antibody array	Alleviates progression of experimental autoimmune encephalomyelitis, an animal model for multiple sclerosis (Weinger et al. 2011).
Plasminogen activator inhibitor (PAI)-1	Antibody array	Anti-apoptotic role in CNS neurons (Soeda et al. 2008).

Table 2.5 Neuroprotective factors released by MSCs used in this study (continued)

Factor	Detection method	Neuroprotective role established in published studies
Interferon (IFN)-β	Antibody array	Reduces disease burden in relapsing-remitting multiple sclerosis patients (Croze et al. 2013).
Chemokine receptor (CCR)-1	Antibody array	May be associated with specific activities of human MSCs after their migration to the target lesions (Song et al. 2011).
Chordin-Like 1	Antibody array	Promotes neuronal differentiation (Gaughwin et al. 2011).
Fibronectin	Antibody array	Promotes neuron-glial extrasynaptic transmission in Parkinson's disease (Wang et al. 2013b).
Frizzled 1	Antibody array	Neuroprotective for dopaminergic neurons and astrocytes (L'Episcopo et al. 2011).
Glypican 5	Antibody array	Neuroprotective for neuronal development and axon guidance; expression in adult brain tissue suggests a possible role in controlling neurotropic factors and maintaining neural function (Thway et al. 2012).
Gremlin	Antibody array	Protects substantia nigra dopamine neurons and several dopamine cell lines in MPTP mouse model of Parkinson's disease (Phani et al. 2013).
IL-1α	Antibody array	Neuroprotective effect against an excitotoxic challenges with NMDA (Carlson et al. 1999).
Macrophage inflammatory protein (MIP)-1a	Antibody array	Prevents neuronal cell death associated with gp120 (Brenneman et al. 2000).
SPARC/ osteonectin	Antibody array	Retinal ganglion cell neuroprotection (Johnson et al. 2014).
Tissue inhibitor of metalloproteinases (TIMP)-1	Antibody array	Neuroprotective against traumatic and ischemic brain injury in mice (Tejima et al. 2009).

2.5 Discussion

This study is the first to examine the effects of MSC and CM treatments administered by enema on the enteric neurons in the guinea-pig model of TNBS-induced colitis. The objectives of this study were to determine 1) whether MSC-based therapies prevent and/or attenuate enteric neuropathy associated with intestinal inflammation and 2) at which time point these effects are initiated. Key findings revealed that local application of human BM-MSCs and CM 3h after the induction of colitis prevented weight loss, accelerated repair of colonic architecture and regeneration of nerve fibers, reduced immune infiltrate both in the mucosa and at the level of the myenteric ganglia, prevented the loss of myenteric neurons and changes in their subpopulations, and alleviated inflammation-induced changes to GI motility. Substantial number of neuroprotective factors released by MSCs were detected in their secretome. Overall, prominent effects of MSC-based therapies were observed 24h after induction of inflammation in the guinea-pig model of TNBS-induced colitis.

We utilized human BM-MSCs since they are the best characterized and most established as a viable cellular therapy for many pathological conditions in both animal and clinical studies (Li and Ikehara 2013; Hass et al. 2011). Viable human MSCs lack expression of MHC-II, but constitutively express HLA MHC-I molecules on their surface at moderate levels enabling them to escape immune rejection when administered to guinea-pigs, as well as other species (Jacobs et al. 2013; Li et al. 2012; Tse et al. 2003). Both *in vitro* and *in vivo* studies show that MSCs do not elicit a proliferative response from allogeneic lymphocytes, evading normal alloresponses and enabling successful transplantation into diverse allogeneic and xenogeneic locations (Newman et al. 2009; Ren et al. 2008; Ryan et al. 2005).

In vitro culture of MSCs can influence several characteristics important to their *in vivo* efficiency (Sarugaser et al. 2009). We conducted analyses of BM-MSCs to ensure that culture conditions did not affect expression of cell surface markers, cell growth, or their differentiation potential. Subsequently, our results have

shown that MSCs used in this study have all characteristics of MSCs defined by the ISCT (Dominici et al. 2006). The *in vitro* differentiation capacity of MSCs cannot be extrapolated to *in vivo* conditions. This study was performed at 6h, 24h, 3 day and 7 day time points after the induction of colitis; therefore, the capacity to see *in vivo* differentiation into particular cell lineages was restricted. Furthermore, it has also been reported that *in vivo* administered MSCs may not survive long enough for differentiation owing to their limited telomerase activity (Everaert et al. 2012; Burns et al. 2005) and that MSCs frequently exhibit therapeutic benefits without engraftment or differentiation (Prockop 2009). Passage 4 MSCs were employed for *in vivo* experiments in this study because MSC secretion of anti-inflammatory cytokines, neurotrophic factors, and immunomodulating agents is most optimal at early passages, gradually declining with successive passages (Choi et al. 2010).

In hapten-induced colitis, ethanol serves to disrupt the mucosal barrier allowing TNBS to infiltrate the underlying colonic layers and initiate inflammation. The peak of ethanol-induced epithelial damage occurs at 3h (Pontell et al. 2009), therefore this time point was selected for the administration of MSC-based therapies. Timing of administration can impact MSC efficacy (Wei et al. 2013), and previous studies have shown that MSC transplantation at earlier phases of inflammation are optimal for therapeutic effects (Wang et al. 2014c; Bernardo and Fibbe 2013; Karp and Teo 2009).

It is known that chemokine receptors and adhesion molecules expressed by MSCs respond to chemoattractant signals from sites of injury facilitating MSC migratory and homing capacity (Karp and Teo 2009; Liu et al. 2009b). We employed immunolabeling of colon cross sections with anti-HLA-A,B,C antibody to evaluate the successful migration and engraftment of MSCs within the inflamed colon. Results of our study verified the migratory capacity of MSCs throughout the layers of the inflamed colon wall, but not to the uninflamed colon. Progressive MSC homing towards inflamed sites is evidenced by their presence in the colonic mucosa at 6h after induction of colitis and at the level of the myenteric plexus by 24h, 3 days and 7 days post inflammation. The migratory capacity of MSCs is

one of their unique biological attributes. Hence, the significance of these cells migrating throughout the layers of the colon indicates their expression of chemokine receptors and other molecules associated with MSC homing (Karp and Teo 2009). The successful migration and engraftment of MSCs into the inflamed colonic wall observed in our study is consistent with previous reports demonstrating implantation of locally administered MSCs into target tissues, especially in inflammatory conditions (Hayashi et al. 2008; Hu et al. 2007).

This study used the novel approach of MSC application by enema, which has not been previously reported. In contrast to prior studies using systemic IP and IV injections of MSCs, application by enema is less invasive and avoids the initial uptake and accumulation of MSCs within filtering organs, such as the lungs, liver, or spleen associated with IV and IP delivery (Karp and Teo 2009). Direct injection of MSCs into the colonic wall has been investigated (Hayashi et al. 2008), but this is highly invasive and not clinically feasible. Application of MSCs by enema is safe, convenient, and minimally invasive, providing a feasible option for administration in IBD patients without severe complications. Furthermore, enema application is a plausible administration route for CM treatments.

Weight loss associated with TNBS-induced colitis was observed in our study and is consistent with other reports (Lomax et al. 2007a; Linden et al. 2003). Our results indicate that the systemic influences of both MSC and CM treatments applied by enema were actioned rapidly, significantly preventing TNBS-induced weight loss within the first 24h after application and maintaining long-lasting effect, at least for 7 days. TNBS-induced colitis typically involves epithelial cell obliteration and gross morphological damage to the intestinal wall (Dohi and Fujihashi 2006). In our study, administration of MSCs or CM into the distal colon ameliorated epithelial and goblet cell loss, as well as aiding repair of colonic architecture by 24h after induction of colitis and was maintained for at least 7 days. These findings are consistent with previous reports on the therapeutic efficiency of MSCs in other animal models of colitis where MSCs and CM have been shown to protect against ulceration, necrosis of epithelial tissue, and increased permeability of the mucosa (Hayashi et al. 2008; Tanaka et al. 2008).

Administration of TNBS into the distal colon initiates inflammation through a cell-mediated immune response consistent with transmural T1-lymphocyte infiltration (Wirtz et al. 2007; Gotsman et al. 2001). Invasion of immune cells into the level of myenteric ganglia is indicative of an acute inflammatory process, and previous studies have positively correlated the severity of inflammatory infiltrate with the severity of IBD recurrence (Ng et al. 2009; Ferrante et al. 2006). Our results indicate the severity of colitis by infiltration of CD45-IR inflammatory cells through the colonic wall to the level of myenteric ganglia. In this study, we show that MSCs reduce leukocyte infiltrate which is also observed in other disease models (Wei et al. 2013; Galindo et al. 2011; Tanaka et al. 2008). The immunomodulatory mechanisms however, have not been fully elucidated, although it is considered to be through either the production of various soluble factors or by direct interaction with target cells (Burdon et al. 2011; Chen et al. 2008). MSCs exhibit potent modulatory effects on immune cells including T and B lymphocytes, natural killer cells and dendritic cells (Stavely et al. 2014; Duffy et al. 2011). The ability of MSCs to exert their immunosuppressive function requires MSC activation in a pro-inflammatory microenvironment (Crop et al. 2010). Our results indicated that MSC and CM treatments were effective within 24h post inflammation as confirmed by reduced leukocyte numbers throughout the distal colon wall. MSCs were able to continue inhibition of CD45-IR cells for 3 days and can exert long lasting effects up to 7 days. Infiltration of leukocytes to the level of myenteric ganglia was reduced in MSC and CM treated groups at 24h post induction of colitis, but was still higher than in the sham treated group. The level of CD45-IR cells was comparable to the sham group only by 3 days.

Our study demonstrated a loss of myenteric neurons at 24h post induction of colitis. A reduction in the quantity of myenteric neurons following TNBS administration is consistent with previous studies in the guinea-pig intestine (Nurgali et al. 2011; Linden et al. 2005). Neuronal numbers were unaffected at 6h which is consistent with previous findings reporting no change in the total number of myenteric neurons 6h after TNBS administration (Linden et al. 2005). MSC and CM treatments prevented the neuronal loss associated with TNBS-induced inflammation. The number of myenteric neurons in MSC and CM-treated

groups was unchanged at all time points even though the quantity of leukocytes at the level of the myenteric ganglia remained increased at 24h. This indicates that MSC-based therapies are capable of exerting neuroprotective effects independent of anti-inflammatory actions. Some studies have reported the capacity of MSCs to differentiate into cells of neuronal and glial lineage (Bae et al. 2011a; Zeng et al. 2011). Despite evidence that MSCs have the ability to differentiate into neurons and glial cells after appropriate induction *in vitro*, it has been shown that MSCs transplanted into the damaged CNS infrequently differentiate into neural phenotypes (Alexanian et al. 2010; Castro et al. 2002). Limited cellular telomerase activity and a maximum 7 day time point in the current study constrained the likelihood of observing any *in vivo* MSC differentiation into specific cell lineages (Chen et al. 2012a; Everaert et al. 2012; Mirsaidi et al. 2012).

In addition to preventing a reduction in the total number of myenteric neurons, MSCs accelerated regeneration and regrowth of nerve fibers in the colon. Damage to the nerve fibers was observed in all groups at 6h after induction of inflammation. However, regrowth of axons was evident by 24h in MSC and CM treated animals, and nerve fiber density returned to sham levels for at least 7 days. Promotion of axonal regrowth by MSC-based therapies within this study is consistent with previous findings in models of spinal cord injury (Zurita et al. 2008; Deng et al. 2006).

The loss of myenteric neurons in TNBS-administered animals correlated with colonic dysmotility, indicating disruption of the appropriate coordination and activation of motility reflex circuits. TNBS-induced disruption of motility persists at least 7 days after inflammation. Significant differences in velocity and frequency of CMMCs between TNBS-administered and sham-treated animals established in our study validate the functional consequences of inflammation-induced structural alterations to myenteric neurons. Application of MSCs and CM re-established the velocity and frequency of CMMCs. Treatment with UCM had some effect on propagation speed and rate of contraction that was not significant compared with all groups. These changes are probably due to direct effects of

culture medium on intestinal smooth muscles. It has been previously observed that visceral smooth muscles in culture medium display increases in number of contractions, as well as speed of contraction (Chamley-Campbell et al. 1979).

Inhibition of colonic motility observed in TNBS-administered animals correlated with changes in the subpopulations of myenteric neurons immunoreactive to nNOS and ChAT. Our study revealed an increase in the number of nNOS neurons, as well a decrease in the number of ChAT neurons at 24h after induction of colitis. These results are comparable to previous studies in TNBS and dextran sodium sulfate animal models of colitis, as well as in tissues from IBD patients reporting changes in neurochemical coding of enteric neuronal subpopulations (Winston et al. 2013; Boyer et al. 2007; Linden et al. 2005; Neunlist et al. 2003; Belai et al. 1997). It is considered that the increase in the number of nNOS-IR neurons in TNBS-administered guinea-pigs is due to changes in the neurochemical coding of myenteric neurons in response to inflammation rather than neurogenesis, since the maturation of neurons takes 3-6 weeks and the maximum time point of this study is 7 days (Piatti et al. 2011; Boyer et al. 2007). Nitrergic (nNOS) neurons in the myenteric plexus are primarily inhibitory motor neurons responsible for the relaxation of intestinal smooth muscle, while cholinergic (ChAT) neurons are the major excitatory motor neurons of the ENS (Furness 2012). Imbalances in numbers of nNOS and ChAT neurons associate with impaired smooth muscle contractility and intestinal dysmotility (Winston et al. 2013; Chandrasekharan et al. 2011). Furthermore, changes to the distribution of nNOS neurons have been associated with oxidative stress (Bagyanszki and Bodi 2012). We found that MSC-based therapies alleviated the inflammation-induced increase in the number and proportion of nNOS neurons, as well as the loss of ChAT neurons in the myenteric plexus at 24h, 3 days and 7 days.

We found that the efficacy of CM treatment was comparable to MSC therapy. Previous findings in nervous system injury and other pathological conditions highlight the therapeutic potential of soluble factors released by MSCs (Hao et al. 2014; Laroni et al. 2013; Bai et al. 2012; Lee et al. 2012; Voulgari-Kokota et al. 2012; Burdon et al. 2011; Uccelli and Prockop 2010). It is now considered that

the protective mechanisms and endogenous regeneration initiated by MSCs is due to their ability to produce and secrete a wide range of bioactive soluble factors acting as paracrine mediators; directly stimulating target cells and/or instigating nearby cells to release functionally active agents (Caplan and Dennis 2006). The MSC secretome contains anti-apoptotic, neurotrophic and growth factors, as well as neurotransmitters and can promote stimulation of axonal growth, microglial regulation, immunomodulation and re-myelination of host axons (Uccelli et al. 2011; Suzuki and Svendsen 2008; Lepore and Maragakis 2007).

The MSC secretome may be responsible for the therapeutic effect observed in this study via: 1) immunomodulation by reducing *in vivo* levels of pro-inflammatory mediators while simultaneously increasing the production of anti-inflammatory factors in the gut and serum and/or 2) direct neuroprotection of enteric neurons via release of neurotrophic factors. During an inflammatory flare, an array of cytokines and chemokines, reactive oxygen and nitrogen species, prostaglandins and other pro-inflammatory mediators induce profound structural and functional damage to the ENS (Buchholz and Bauer 2010; Mawe et al. 2009; de Winter et al. 2005; Linden et al. 2004). Previous studies in experimental colitis have demonstrated that MSC treatment stimulates upregulation of anti-inflammatory factors including IL-10, indoleamine 2,3-dioxygenase, prostaglandin E2, and TGF-β1, as well as a downregulation of pro-inflammatory mediators such as IL-1β, lL-6, IL-12, IL-17, IFN-γ and TNF-α (Stavely et al. 2014; Chen et al. 2013b; Gonzalez et al. 2009). This immunomodulatory effect of MSC therapy could in turn prevent and/or reduce the damage to enteric neurons and nerve fibers. A direct MSC effect for maintaining enteric neuronal integrity during intestinal inflammation may occur via release of neurotrophic and neuroprotective agents in the MSC secretome. In this study, analysis of CM revealed that MSCs released considerable number of factors under normal culturing conditions including those that have been demonstrated to be neurotrophic and neuroprotective for enteric neurons, as well as factors that have not been studied in the ENS. Previous studies have shown that GDNF protects enteric neurons from apoptosis and promotes the development and survival of many types of

neurons (Sharkey and Savidge 2014; Steinkamp et al. 2012; Bassotti et al. 2006; von Boyen et al. 2006; 2002). Other factors, such as NT, NGF, BDNF, ciliary neurotrophic factor and leukemia inhibitory factor are also involved in modulation of gut inflammation and colonic sensitivity (von Boyen et al. 2006; 2002). In our study, neurotrophic and neuroprotective factors were detected in the secretome of naive MSCs (not exposed to inflammatory conditions). It is plausible that upon placement in an inflammatory milieu, MSCs release a wider array of factors than we have reported in this study. The role of specific MSC-secreted neuroprotective factors in preventing enteric neuronal loss and damage caused by intestinal inflammation needs to be further elucidated.

2.6 Conclusion

In conclusion, this study demonstrated that BM-MSCs have the ability to prevent inflammatory insults to the ENS when administered 3h after induction of colitis. Furthermore, we have shown the equivalent proficiency of CM treatment for exhibiting neuroprotective effects, promoting enteric neuronal repair and functional recovery. Our results clearly support the therapeutic potential of enema-administered MSC and CM treatments for preventing enteric neuropathy associated with TNBS-induced colitis as early as 24h after induction of inflammation even though the inflammatory reaction at the level of the myenteric ganglia has not completely subsided at this time point. This suggests that the neuroprotective efficacy of MSC-based therapies can be exerted independently to their anti-inflammatory effects. Further investigations need to be conducted to define the pathways and specific factors contributing to enteric neuroprotection by MSC-based treatments in acute and chronic inflammatory conditions.

CHAPTER THREE: THE NEUROPROTECTIVE EFFECTS OF HUMAN BONE MARROW MESENCHYMAL STEM CELLS ARE DOSE-DEPENDENT IN TNBS COLITIS

The material presented in this chapter is published and has been reproduced here with the permission of the publisher with minor alterations:

Robinson, A. M., Rahman, A. A., Miller, S., Stavely. R., Sakkal, S., Nurgali, K. 2017. The neuroprotective effects of human bone marrow mesenchymal stem cells are dose-dependent in TNBS colitis. *Stem Cell Res Ther,* 8, 87.

3.1 Summary

Background: The incidence of inflammatory bowel diseases (IBD) is increasing worldwide with patients experiencing severe impacts on their quality of life. It is well accepted that intestinal inflammation associates with extensive damage to the enteric nervous system (ENS), which intrinsically innervates the gastrointestinal tract and regulates all gut functions. Hence, treatments targeting the enteric neurons are plausible for alleviating IBD and associated complications. Mesenchymal stem cells (MSCs) are gaining wide recognition as a potential therapy for many diseases due to their immunomodulatory and neuroprotective qualities. However, there is a large discrepancy regarding appropriate cell doses used in both clinical trials and experimental models of disease. We have previously demonstrated that human bone marrow MSCs exhibit neuroprotective and anti-inflammatory effects in a guinea-pig model of 2,4,6-trinitrobenzene-sulfonate (TNBS)-induced colitis, but an investigation into whether this response is dose-dependent has not been conducted. **Methods:** Hartley guinea-pigs were administered TNBS or sham treatment intra-rectally. Animals in the MSC treatment groups received either 1×10^5, 1×10^6 or 3×10^6 MSCs by enema 3h after induction of colitis. Colon tissues were collected 3 days after TNBS administration to assess the effects of MSC treatments on the level of inflammation and damage to the ENS by immunohistochemical and histological analyses. **Results:** MSCs administered at a low dose, 1×10^5 cells, had little or no effect on the level of immune cell infiltrate and damage to the colonic innervation was similar to the TNBS group. Treatment with 1×10^6 MSCs decreased the quantity of immune infiltrate and damage to nerve processes in the colonic wall, prevented myenteric neuronal loss and changes in neuronal subpopulations. Treatment with 3×10^6 MSCs had similar effects to 1×10^6 MSC treatments. **Conclusions:** The neuroprotective effect of MSCs in TNBS colitis is dose-dependent. Increasing doses higher than 1×10^6 MSCs demonstrates no further therapeutic benefit than 1×10^6 MSCs in preventing enteric neuropathy associated with intestinal inflammation. Furthermore, we have established an

optimal dose of MSCs for future studies investigating intestinal inflammation, the enteric neurons and stem cell therapy in this model.

3.2 Introduction

Many studies report the effectiveness of mesenchymal stem cell (MSC) treatments in attenuating the mechanisms of disease, however some MSC therapies are reported as being ineffective or only demonstrating short-term effectiveness (Nam et al. 2015; Badillo et al. 2008; Meyer et al. 2006; Sudres et al. 2006). Various factors, including cellular dose and timing of administration of MSCs, influence therapeutic efficacy of these cells (Kim and Cho 2015). Hence, it has been suggested that different doses of MSCs might have distinct immune or protective effects (Zhang et al. 2015). There is great variation among clinical trials and experimental models of disease in the injected dosage of MSCs (Sharma et al. 2014; Li et al. 2012), implying that MSCs can effectively treat diseases in a dose-dependent manner (Joo et al. 2010; Kim et al. 2010a; Gonzalez-Rey et al. 2009; Li et al. 2008; Zappia et al. 2005). In addition, defining an optimal MSC dose for both pre-clinical and clinical studies extends to benefits such as reduced production costs, less tissue required for MSC expansion, a lower chance of MSC mutation and a reduced likelihood of MSC accumulation in the filtering organs.

While it has been confirmed that MSCs migrate to sites of intestinal inflammation where they assist in the restoration and repair of the epithelial barrier and damaged tissue via anti-inflammatory actions (He et al. 2012; Gonzalez-Rey et al. 2009; Yabana et al. 2009; Hayashi et al. 2008; Tanaka et al. 2008), there are only a few studies examining the effects of MSC-based therapies in attenuating inflammation-induced enteric neuropathy (Robinson et al. 2015; 2014; Stavely et al. 2015a; 2015b). In these studies, it was concluded that locally applied bone marrow (BM)-MSCs administered at a dose of 1×10^6 are neuroprotective towards enteric neurons compromised by 2,4,6-trinitrobenzene-sulfonate (TNBS)-induced inflammation (Robinson et al. 2015; 2014; Stavely et al. 2015b). These results provide the foundation for examining the neuroprotective potential of MSC therapy in intestinal inflammation. However, no studies have investigated the dose-response relationship of MSCs in protecting enteric neurons from damage and/or death induced by colitis. Therefore, the aim of this study was to investigate

at which dose (1×10^5, 1×10^6 or 3×10^6) human BM-MSCs are most beneficial in protecting and repairing enteric neurons following induction of colitis. This knowledge will define the optimal MSC dosage for treatment of enteric neuropathy associated with TNBS-induced inflammation in a guinea-pig model of colitis, as well as contribute towards future investigations into the mechanisms of MSC-stimulated enteric neuroprotection.

3.3 Materials and methods

3.3.1 Animals

Male and female Hartley guinea-pigs (*n*=20) weighing 140-280g were obtained from South Australian Health and Medical Research Institute (SAHMRI, Adelaide, SA, Australia) and randomly assigned to experimental groups. All animals were housed in a temperature-controlled environment with 12h day/night cycles and had *ad libitum* access to food and water. All animal experiments in this study complied with the guidelines of the National Health and Medical Research Council Australian Code of Practice for the Care and Use of Animals for Scientific Purposes under approval of the Victoria University Animal Experimentation Ethics Committee. All efforts were made to minimize animal suffering.

3.3.2 Cell culture and passaging

Cell culture and passaging was carried out as described in Chapter 2, section 2.3.2. Briefly, MSCs derived from human BM-MSC cell lines BM-7025 and BM-7081 (Tulane University, New Orleans, LA, USA) were plated at an initial density of 60 cells/cm^2 and incubated in complete culture medium (α-minimum essential medium (MEM) supplemented with 16.5% MSC-qualified fetal bovine serum (FBS), 100 U/mL penicillin/streptomycin, and 100X GlutaMAX) (all purchased from Gibco®, Life Technologies, Mulgrave, VIC, Australia) at 37°C. Expansion medium was replenished every 48-72h for 10-14 days until the cells were 70-85% confluent (maximum). MSCs were rinsed in 5mL sterile phosphate buffered solution (PBS) prior to incubation with 3mL TrypLE Select (Gibco®, Life Technologies) for 3min at 37°C to detach cells. Enzymatic activity was neutralized by 8mL of stop solution (α-MEM + 5% FBS) and MSCs were collected and centrifuged at 450*g* for 5min at room temperature. Cells were then resuspended in fresh culture medium and counted using a hemocytometer under a light microscope.

3.3.3 MSC characterization

MSCs were cultured to the fourth passage for all experiments and characterized for their expression of surface antigens, differentiation potential, and colony-forming ability as described in Chapter 2, section 2.3.3. All MSCs utilized in this study met criteria for defining *in vitro* human MSC cultures proposed by the International Society for Cellular Therapy (ISCT) (Dominici et al. 2006).

3.3.4 Induction of colitis

TNBS (Sigma-Aldrich, Castle Hill, NSW, Australia) was dissolved in 30% ethanol to a concentration of 30mg/kg and administered intra-rectally 7 cm proximal to the anus (total volume of 300μL) by a lubricated silicone catheter (Nurgali et al. 2011). For TNBS administration, guinea-pigs were anaesthetized with isoflurane (induced at 4%, maintained on 1-4% isoflurane in O_2) during the procedure. Sham-treated guinea-pigs underwent the same procedure without administration of TNBS.

3.3.5 MSC treatments

Guinea-pigs in the MSC-treated groups were anaesthetized with isoflurane 3h after TNBS administration and administered MSC therapies by enema into the colon via a silicone catheter. MSCs were administered at a dose of 1×10^5, 1×10^6 or 3×10^6 cells in 300μL of sterile 0.1M PBS. The peak of ethanol-induced epithelial damage occurs at 3h in TNBS-induced colitis (Pontell et al. 2009), therefore this time point was selected for the administration of MSCs. Animals were held at an inverted angle following MSC treatments to prevent leakage from the rectum and were weighed and monitored daily following treatment. Guinea-pigs were culled via stunning and exsanguination 3 days after TNBS administration (Nurgali et al. 2009). Sections of the distal colon were collected for histological and immunohistochemical studies.

3.3.6 Immunohistochemistry and histology

3.3.6.1 Tissue preparation

Following dissection, tissues were immediately placed in oxygenated PBS (0.1M, pH7.2) containing an L-type Ca^{2+} channel blocker, nicardipine (3μm; Sigma-Aldrich), to inhibit smooth muscle contraction. Colon tissues were cut open along the mesenteric border, stretched and pinned flat with the mucosal side up for wholemount longitudinal muscle-myenteric plexus (LMMP) preparations; samples for cross sections were not stretched. Tissue samples were fixed overnight at 4°C in Zamboni's fixative (2% formaldehyde and 0.2% picric acid) and subsequently washed for 3×10min in dimethyl sulfoxide (DMSO) (Sigma-Aldrich) and for 3×10min in 0.1M PBS to remove fixative. Zamboni's fixative was chosen for tissue fixation to minimize neural tissue autofluorescence. LMMP distal colon samples were dissected to expose the myenteric plexus by removing the mucosa, submucosa and circular muscle layers prior to immunohistochemistry. Cross section samples for immunohistochemistry were stored in 50:50 optimum cutting temperature (OCT) compound (Tissue-Tek, Torrance, CA, USA) and sucrose solution for 24h at 4°C and subsequently frozen in liquid nitrogen-cooled isopentane and OCT compound. Samples were stored at -80°C until they were cryo-sectioned (30μm) onto glass slides. Samples for histology were fixed in 10% buffered formalin solution overnight at 4°C and stored in 70% ethanol until paraffin embedding.

3.3.6.2 Immunohistochemistry

Immunohistochemistry was performed on distal colon tissues as described in Chapter 2, section 2.3.6.2. Briefly, after a 1h incubation in 10% normal donkey serum (NDS; Merck Millipore, Bayswater, VIC, Australia) diluted in 0.1M PBS-0.1% Triton X-100 at room temperature, samples were washed with 0.1M PBS-0.1% Triton X-100 (2×5min) and incubated with primary antibodies (Table 3.1) diluted in 2% NDS and 0.1M PBS-0.1% Triton X-100 overnight at room temperature. Tissues were then washed in 0.1M PBS-0.1% Triton X-100 (2×5min) prior to incubation with secondary antibodies (diluted in 2% NDS and

Table 3.1 Primary antibodies used in this study

Antibody	Host species	Dilution	Supplier	Application in this study
Anti-β-Tubulin class III	Rabbit	1:1000	Abcam, Melbourne, VIC, Australia	Cross sections
Anti-CD45 (clone IH-1)	Mouse	1:200	Abcam	Cross sections
Anti-choline acetyltransferase (ChAT)	Goat	1:500	Merck Millipore	LMMP preparations
Anti-Hu (clone 15A7.1)	Mouse	1:500	Merck Millipore	LMMP preparations
Anti-neuronal nitric oxide synthase (nNOS)	Goat	1:500	Novus Biologicals, Littleton, CO, USA	LMMP preparations
Anti-human leukocyte antigen (HLA)-A,B,C (conjugated to fluorescein isothiocyanate (FITC))	Human	1:50	BioLegend, San Diego, CA, USA	Cross sections

Table 3.2 Secondary antibodies used in this study

Antibody	Host species	Dilution	Supplier	Application in this study
Alexa Fluor 594	Donkey anti-mouse	1:200	Jackson Immunoresearch Laboratories, PA, USA	LMMP preparations
Alexa Fluor 594	Donkey anti-rabbit	1:200	Jackson Immunoresearch Laboratories	Cross sections
FITC 488	Donkey anti-goat	1:200	Jackson Immunoresearch Laboratories	LMMP preparations
FITC 488	Donkey anti-mouse	1:200	Jackson Immunoresearch Laboratories	Cross sections

0.1M PBS-0.1% Triton X-100; Table 3.2) for 2h at room temperature. Following 3×10min washes in 0.1M PBS-0.1% Triton X-100, samples were mounted on glass slides with fluorescent mounting medium (DAKO, North Sydney, NSW, Australia).

3.3.6.3 Histology

Tissues for histology were paraffin embedded, sectioned at 5µm, deparaffinized, cleared, and rehydrated in graded ethanol concentrations for standard hematoxylin and eosin (H&E) staining as described in Chapter 2, section 2.6.3.3.

3.3.7 Imaging

Confocal microscopy was undertaken on an Eclipse Ti confocal laser scanning system (Nikon, Tokyo, Japan). Fluorophores were visualized by using a 488nm excitation filter for FITC and a 559nm excitation filter for Alexa 594. Z-series images were acquired at a nominal thickness of 0.5µm (512×512 pixels). H&E-stained colon sections were visualized using an Olympus BX53 microscope (Olympus, Notting Hill, VIC, Australia) and images were captured with CellSense™ software.

3.3.8 Quantitative analyses of immunohistochemical and histological data

In wholemount LMMP preparations, the total number of myenteric neurons immunoreactive (IR) for Hu, nNOS and ChAT were counted within eight randomly captured images per preparation (total area 2mm^2), as well as per ganglia (average of ten ganglia per animal). Infiltration of leukocytes throughout the colon wall was assessed by counting the total number of CD45-IR cells within the mucosal (including the mucosa, submucosa and submucosal plexus) and musclar (circular muscle, myenteric plexus, and longitudinal muscle) layers in cross sections (total area 1.5mm^2). The density of nerve fibers was determined by measuring β-tubulin (III)-IR in eight randomly captured images at ×20 magnification. All images were captured under identical acquisition exposure time

conditions and calibrated to standardized minimum baseline fluorescence. Images were converted from red, green, and blue (RGB) to grayscale 8 bit then to binary; changes in fluorescence from the baseline were measured using Image J software (National Institutes of Health, Bethesda, MD, USA). The area of immunoreactivity was then expressed as a percentage of the total area examined. Gross morphological damage in H&E-stained colon sections was assessed by histological grading of four parameters: mucosal flattening (0 = normal, 3 = severe flattening), occurrence of hemorrhagic sites (0 = none, 3 = frequent sites), loss of goblet cells (0 = normal, 3 = severe loss of cells) and variation of the circular muscle (0 = normal, 3 = considerable thickening of muscular layer) (Robinson et al. 2014). Quantitative analyses were conducted blindly.

3.3.9 Statistical analysis

Statistical differences were determined by Student's *t*-test (two-tailed) or one-way ANOVA with Bonferroni post hoc test for multiple group comparisons using Prism v6.0 (Graphpad Software Inc., La Jolla, CA, USA). Data were considered statistically significant when $P<0.05$. Data were presented as mean±standard error of the mean (SEM), if not specified otherwise.

3.4 Results

3.4.1 MSC migration and engraftment at the site of inflammation

The capacity of MSCs to migrate and engraft to the area of tissue damage and inflammation was assessed in sections of the distal colon from guinea-pigs treated with 1×10^5, 1×10^6 or 3×10^6 MSCs administered by enema 3h after the induction of TNBS colitis (*n*=4/group). Transmural migration of MSCs within colon cross sections was identified by labeling with an antibody against HLA-A,B,C, which detects major histocompatibility complex (MHC) class I antigens expressed by all human nucleated cells (Fig. 3.1). MSCs successfully engrafted into the intestinal wall evident by localization of HLA-A,B,C-positive cells in the colon sections collected at 3 days post induction of colitis (Fig. 3.1A-C). HLA-A,B,C-positive cells were present mostly in the mucosal lamina propria in colon sections from guinea-pigs treated with 1×10^5 MSCs (Fig. 3.1A). When administered at higher doses (1×10^6 and 3×10^6), transmural migration and engraftment of human MSCs into the colon wall to the level of the myenteric ganglia was evident (Fig. 3.1B-C).

3.4.2 Effects of MSC treatment on tissue repair

Changes to the colonic architecture 3 days after induction of TNBS-induced colitis were evaluated by gross morphological assessment of H&E-stained colon sections (*n*=4/group; Fig. 3.2). Continuous epithelial cell lining, regular structural arrangements of goblet cells and crypts and defined colonic layers were evident in H&E-stained colon cross sections from sham-treated guinea-pigs (histological score = 0-1; Fig. 3.2A). In contrast, sections from guinea-pigs in the TNBS-only group displayed disruptions to the epithelial lining, goblet cell loss, glandular distortion and flattening of crypts (histological score = 2; Fig. 3.2B). Sections from animals in all MSC-treated groups revealed accelerated healing of the mucosa and repair to levels comparable with sham-treated guinea-pigs (histological score = 0-1 for all; Fig. 3.2C-E).

Figure 3.1. MSC homing within the inflamed colon. The migration and engraftment of MSCs (arrows) to the site of TNBS-induced inflammation in sections of the guinea-pig colon was confirmed using anti-HLA-A,B,C antibody specific to human MHC class I at 3 days post induction of colitis **(A-C)**. Scale bars = 100μm.

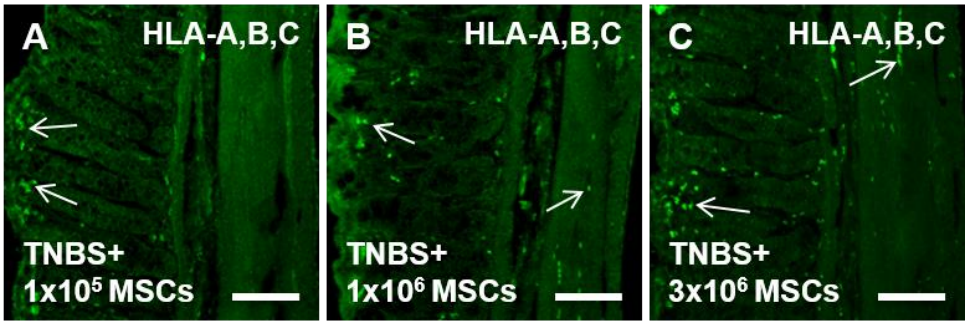
A
HLA-A,B,C
TNBS+
1x10^5 MSCs
B
HLA-A,B,C
TNBS+
1x10^6 MSCs
C
HLA-A,B,C
TNBS+
3x10^6 MSCs

Figure 3.2. Gross morphological changes in the distal colon assessed in H&E-stained cross sections. A complete and continuous epithelial lining and regular arrangement of colonic layers was apparent in sections from sham-treated animals **(A)**. Flattening of the glands, disruption to the epithelial lining and goblet cell loss were evident in sections from TNBS-administered guinea-pigs at 3 days post induction of colitis **(B)**. H&E-stained sections from 1×10^5, 1×10^6 and 3×10^6 MSC-treated animals revealed accelerated repair and restoration of the colonic architecture **(C-E)**. Scale bars = 50 μm.

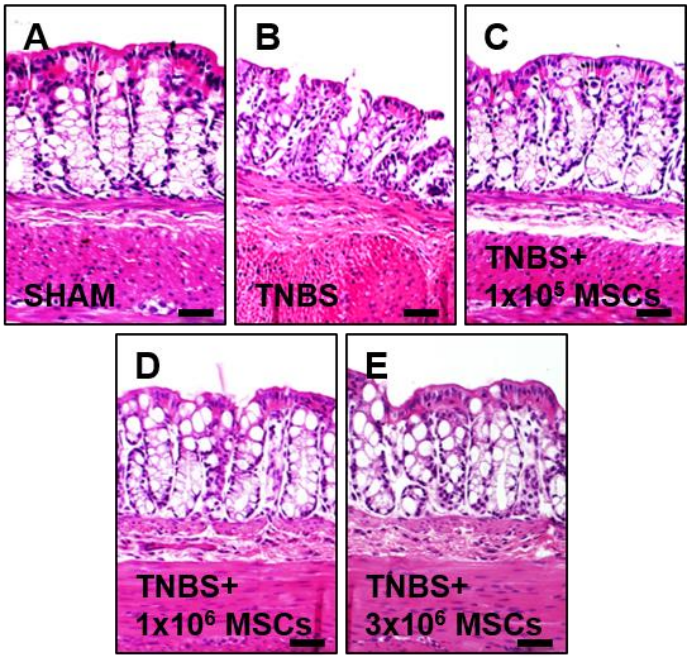
A
SHAM
B
TNBS
C
TNBS+
1x10^5 MSCs
D
TNBS+
1x10^6 MSCs
E
TNBS+
3x10^6 MSCs

3.4.3 Dose-dependent effects of MSC treatments on leukocyte infiltration in the inflamed colon

The severity of colitis and the anti-inflammatory effect of MSC treatments were assessed by quantitative analyses of CD45+ leukocytes in colon cross sections (*n*=4/group; Fig. 3.3). TNBS administration produced an increase in leukocytes within the mucosa and muscular layers at 3 days when compared to sections from sham-treated guinea-pigs (*P*<0.001 for both; Table 3.3; Fig. 3.3A-B, F-G). The TNBS-induced increase in number of leukocytes in the mucosa and muscular layers was reduced by all MSC treatments compared to the TNBS-only group (*P*<0.001 for all). However, leukocyte numbers in both the mucosa and muscular layers of 1×10^5 MSC-treated animals were higher compared to sham, 1×10^6 MSC and 3×10^6 MSC-treated guinea-pigs (*P*<0.001 for all; Table 3.3; Fig. 3.3A-G).

3.4.4 Dose-dependent effects of MSC treatment on nerve fiber regrowth

Nerve fibers innervating smooth muscles and mucosa were identified in cross sections of the guinea-pig distal colon by labeling with an antibody specific to neuronal microtubule protein β-tubulin (III) (*n*=4/group point; Fig. 3.4). Regularly distributed β-tubulin (III)-IR fibers were observed within the mucosal gland cores, submucosal and muscular layers of colon sections from sham-treated guinea-pigs (Fig. 3.4A). Following TNBS administration, β-tubulin (III)-IR fibers within the mucosa were disordered, patchy, and arranged irregularly (Fig. 3.4B). Quantitative analysis confirmed a reduction in β-tubulin (III)-IR fiber density in both mucosa and muscle layers of the colon sections from TNBS-administered guinea-pigs when compared to sections from sham-treated animals (*P*<0.001 for both; Table 3.3; Fig. 3.4F-G). Treatment with 1×10^5 MSCs improved the nerve fiber density in the mucosa compared to the TNBS-only administered group (*P*<0.001). However, the density of fibers in both the mucosa and muscle was still lower compared to the sham-treated group (*P*<0.001 for both; Table 3.3; Fig. 3.4C, F-G). In contrast, the morphology of β-tubulin (III)-IR fibers in mucosal and muscular layers of colon sections from guinea-pigs treated with 1×10^6 and 3×10^6

MSCs were comparable to those in sections from sham-treated animals (Fig. 3.4D-E). When quantified, β-tubulin (III)-IR fiber density in mucosa and muscles in colon sections from 1×10^6 and 3×10^6 MSC-treated guinea-pigs was higher compared to both TNBS-only and 1×10^5 MSC-treated guinea-pigs ($P<0.001$ for all; Table 3.3; Fig. 3.4F-G).

Table 3.3 Dose-dependent effects of MSC treatment on leukocyte infiltration, nerve fiber density and number of myenteric neurons in the inflamed distal colon

	Sham	TNBS	TNBS+ $1x10^5$ MSCs	TNBS+ $1x10^6$ MSCs	TNBS+ $3x10^6$ MSCs
Total no. CD45-IR cells					
Mucosa	341±34	927±31***^^^###†††	686±23***###†††	368±27	425±25
Muscle	33±4	131±1***^^^###†††	83±5***###†††	32±6	29±6
β-tubulin (III)-IR fiber density (%)					
Mucosa	3.3±0.1	1.7±0.1***^^^###†††	2.5±0.1***###†††	3.4±0.1	3.4±0.04
Muscle	5.5±0.2	4.0±0.1***###†††	3.9±0.1***###†††	5.7±0.1	5.5±0.1
Total no. of Hu-IR myenteric neurons					
Ganglia	124±2	108±5*##††	104±2**##††	128±3	127±4
Area	1498±13	1330±41**###†††	1312±20***##†††	1510±19	1513±12
Total no. of nNOS-IR myenteric neurons					
Ganglia	22±1	27±1**###††	27±1***##†††	20±1	22±1
Area	262±12	318±7***##†††	317±5***##†††	277±6	246±3
Proportion of nNOS-IR myenteric neurons (%)					
Ganglia	17±1	26±2***###†††	27±1***###†††	16±1	18±1
Area	17±1	24±1***###†††	24±1***###†††	18±1	16±1

Table 3.3 Dose-dependent effects of MSC treatment on leukocyte infiltration, nerve fiber density and number of myenteric neurons in the inflamed distal colon (continued)

	Sham	TNBS	TNBS+ 1x10^5 MSCs	TNBS+ 1x10^6 MSCs	TNBS+ 3x10^6 MSCs
Total no. of ChAT-IR myenteric neurons					
Ganglia	67±1	52±2$^{**\#\#\dagger\dagger}$	57±2$^{**\#\dagger}$	64±2	65±3
Area	749±29	545±24$^{***\#\#\dagger\dagger\dagger}$	585±23$^{**\#\dagger\dagger}$	708±29	743±14
Proportion of ChAT-IR myenteric neurons (%)					
Ganglia	54±1	49±1	55±1	50±1	52±4
Area	50±2	41±1$^{**\#\dagger}$	45±2	47±2*	49±1*

*P<0.05, **P<0.01, ***P<0.001 when compared to sham-treated guinea-pigs. ^P<0.05, ^^P<0.01, ^^^P<0.001 when compared to 1x10^5 MSC-treated guinea-pigs. $^{\#}P$<0.05, $^{\#\#}P$<0.01, $^{\#\#\#}P$<0.001 when compared to 1x10^6 MSC-treated guinea-pigs. $^{\dagger}P$<0.05, $^{\dagger\dagger}P$<0.01, $^{\dagger\dagger\dagger}P$<0.001 when compared to 3x10^6 MSC-treated guinea-pigs.

Figure 3.3. Effects of MSC treatments on leukocyte infiltration in colon cross sections. Sections of the guinea-pig distal colon were labeled with pan-leukocyte marker anti-CD45 to observe the effects of MSC treatments on leukocyte infiltration. CD45-IR leukocytes were visualized within the mucosa and muscular layers of distal colon sections from guinea-pigs collected at 3 days post induction of colitis **(A-E)**. Scale bars = 100μm. The total number of CD45-IR cells per 1.5mm^2 area quantified in the mucosa **(F)** and muscular **(G)** layers of the colon cross sections. ***P<0.001 when compared to sham-treated guinea-pigs. ^^^P<0.001 when compared to 1x10^5 MSC-treated guinea-pigs. ###P<0.001 when compared to 1x10^6 MSC-treated guinea-pigs. †††P<0.001 when compared to 3x10^6 MSC-treated guinea-pigs.

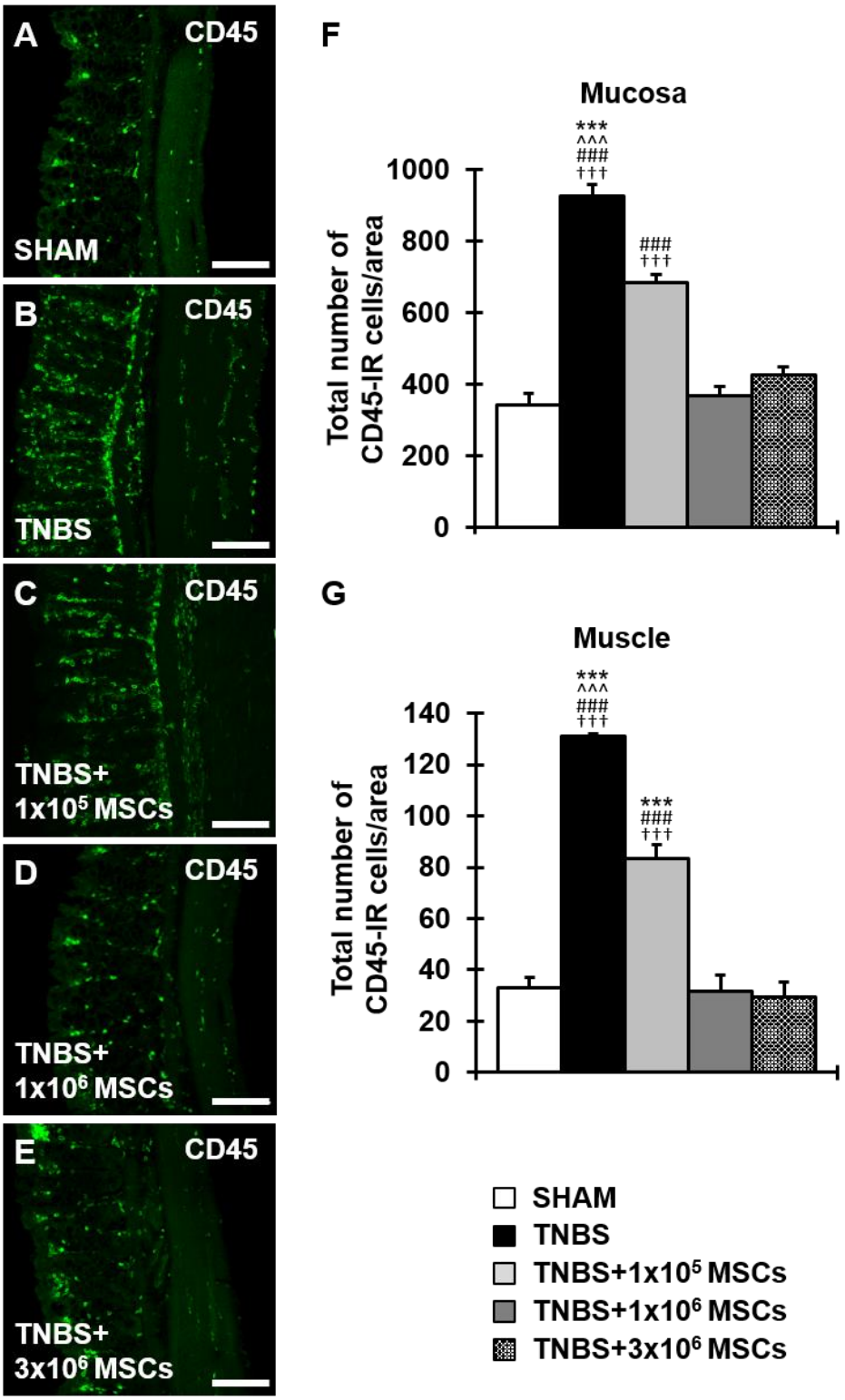
A
CD45
SHAM
B
CD45
TNBS
C
CD45
TNBS+
1x10⁵ MSCs
D
CD45
TNBS+
1x10⁶ MSCs
E
CD45
TNBS+
3x10⁶ MSCs
F
Mucosa
Total number of CD45-IR cells/area
1000
800
600
400
200
0
***
^^^
###
†††
###
†††
G
Muscle
Total number of CD45-IR cells/area
140
120
100
80
60
40
20
0
***
^^^
###
†††
***
###
†††
SHAM
TNBS
TNBS+1x10⁵ MSCs
TNBS+1x10⁶ MSCs
TNBS+3x10⁶ MSCs

Figure 3.4. Effects of MSC treatments on nerve fibers in cross sections of the distal colon. Distribution of fibers labeled by neuron-specific anti-β-tubulin (III) antibody in colon sections from sham-treated, TNBS-only, 1×10^5 MSC-treated, 1×10^6 MSC-treated, and 3×10^6 MSC-treated guinea-pigs at 3 days post induction of colitis **(A-E)**. Scale bars = 100μm. β-tubulin (III)-IR fibers were quantified in the mucosa **(F)** and muscular **(G)** layers of the colon. ***P<0.001 when compared to sham-treated guinea-pigs. ^^^P<0.001 when compared to $1x10^5$ MSC-treated guinea-pigs. ###P<0.001 when compared to $1x10^6$ MSC-treated guinea-pigs. †††P<0.001 when compared to $3x10^6$ MSC-treated guinea-pigs.

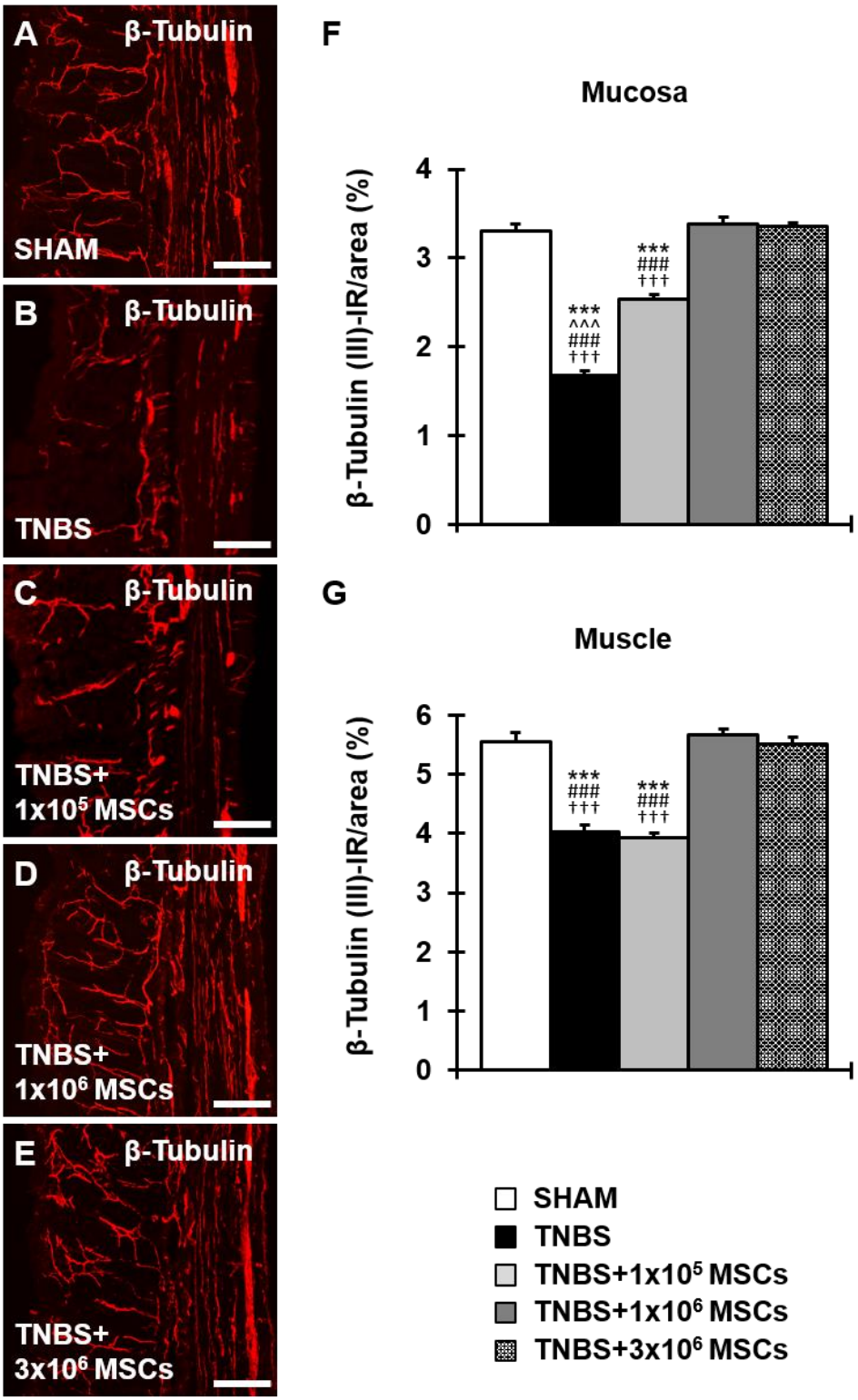
A
β-Tubulin
SHAM
B
β-Tubulin
TNBS
C
β-Tubulin
TNBS+
1x10⁵ MSCs
D
β-Tubulin
TNBS+
1x10⁶ MSCs
E
β-Tubulin
TNBS+
3x10⁶ MSCs
F
Mucosa
β-Tubulin (III)-IR/area (%)
0
1
2
3
4
***
^^^
###
†††
***
###
†††
G
Muscle
β-Tubulin (III)-IR/area (%)
0
1
2
3
4
5
6
***
###
†††
***
###
†††
SHAM
TNBS
TNBS+1x10⁵ MSCs
TNBS+1x10⁶ MSCs
TNBS+3x10⁶ MSCs

3.4.5 Dose-dependent effects of MSC treatment on enteric neuroprotection

To investigate whether 1×10^5, 1×10^6 and 3×10^6 MSC treatments were effective in preventing loss of myenteric neurons, neuronal cell bodies were labeled with the pan-neuronal marker anti-Hu antibody in wholemount LMMP preparations of the distal colon (*n*=4/group; Fig. 3.5). The number of Hu-IR neurons was counted per ganglion and per 2mm^2 area. The number of Hu-IR myenteric neurons was decreased in colon preparations from TNBS-only guinea-pigs compared to sham-treated animals (ganglia: *P*<0.05; area: *P*<0.01; Table 3.3; Fig. 3.5A-B, F-G). Treatments with 1×10^6 and 3×10^6 MSCs attenuated neuronal loss associated with inflammation compared to the TNBS group (ganglia: *P*<0.01 for both; area: *P*<0.001 for both; Table 3.3; Fig. 3.5D-G). However, treatment with 1×10^5 MSCs did not prevent myenteric neuronal loss associated with colitis (ganglia: *P*<0.01 for all; area - sham: *P*<0.001; MSC: *P*<0.01; CM: *P*<0.001; Table 3.3; Fig. 3.5C, F-G).

3.4.6 Dose-dependent effects of MSC treatments on inhibitory myenteric neurons

Changes in inhibitory and excitatory myenteric muscle motor and interneurons underlie inflammation-induced colonic dysmotility, therefore we investigated the effects of MSC-based therapies on these two major subpopulations of neurons. Inhibitory neurons were labeled with anti-nNOS antibody in wholemount LMMP preparations of the distal colon (*n*=4/group; Fig. 3.6). The number of nNOS-IR neurons per ganglion and per area was increased in the myenteric plexus from the TNBS-only group compared with sham-treated animals (ganglia: *P*<0.01; area: *P*<0.001). The proportion of nNOS-IR neurons to the total number of Hu-IR neurons was increased in TNBS-only guinea-pigs compared with sham-treated animals (*P*<0.001 for all; Table 3.3; Fig. 3.6A-B, F-I). The number and proportion of nNOS-IR neurons were comparable between TNBS-only administered guinea-pigs and 1×10^5 MSC-treated animals (Table 3.3; Fig. 3.6C). Thus, nNOS-IR neurons were elevated in preparations from 1×10^5 MSC-treated animals

compared to sham-treated (P<0.001 for both ganglia and area), 1×10^6 MSC-treated (P<0.01 for both ganglia and area) and 3×10^6 MSC-treated (P<0.001 for both ganglia and area) guinea-pigs (Table 3.3; Fig. 3.6F-I). Correspondingly, the proportion of nNOS-IR neurons was also increased (P<0.001 for all). Both 1×10^6 and 3×10^6 MSC treatments prevented the increase in the total number (1×10^6 - ganglia: P<0.001; area: P<0.01; 3×10^6 - ganglia: P<0.01; area: P<0.001) and proportion (P<0.001 for all) of nNOS-IR neurons compared to the TNBS-only group (Table 3.3; Fig. 3.6D-I).

3.4.7 Dose-dependent effects of MSC treatments on excitatory myenteric neurons

Excitatory muscle motor and interneurons were identified using ChAT immunoreactivity in wholemount preparations of the distal colon (n=4/group; Fig. 3.7). Quantification of ChAT-IR neurons revealed a decrease in the TNBS-only group compared to sham-treated guinea-pigs (ganglia: P<0.01; area: P<0.001) (Table 3.3; Fig. 3.7A-B, F, H). The number of ChAT-IR neurons in preparations from 1×10^5 MSC-treated guinea- pigs was comparable to the TNBS-only group, indicating that this dose was not effective in preventing the TNBS-induced decrease in ChAT-IR neurons (Table 3.3; Fig. 3.7C, F, H). ChAT-IR neurons were reduced in 1×10^5 MSC-treated animals compared to sham-treated (P<0.01 for both ganglia and area), 1×10^6 MSC-treated (P<0.05 for both ganglia and area) and 3×10^6 MSC-treated (ganglia: P<0.05; area: P<0.01) guinea-pigs. Treatment with 1×10^6 MSCs (P<0.01 for both ganglia and area) and 3×10^6 MSCs (ganglia: P<0.01; area: P<0.001) prevented the TNBS-induced loss of ChAT-IR neurons, with numbers comparable to the sham-treated group (Table 3.3; Fig. 3.7D-E, F, H). When quantified per ganglia, there were no differences between any groups in the proportion of ChAT-IR neurons to total number of neurons (Fig. 3.7G). However, when quantified per area, the proportion of ChAT-IR neurons to Hu-IR neurons was reduced in TNBS-only administered animals when compared to sham-treated (P<0.01), 1×10^6 MSC-treated (P<0.05) and 3×10^6 MSC-treated (P<0.05) guinea-pigs (Fig. 3.7I).

Figure 3.5. Effects of MSC treatments on the total number of myenteric neurons. Myenteric neurons were identified by anti-Hu antibody in wholemount LMMP preparations of the distal colon from sham-treated, TNBS-only, 1×10^5 MSC-treated, 1×10^6 MSC-treated, and 3×10^6 MSC-treated guinea-pigs 3 days post induction of colitis **(A-E)**. Scale bars = 50μm. The total number of Hu-IR neurons were counted per ganglion (average of ten ganglia) **(F)** and per $2mm^2$ area **(G)** of the colon. **P*<0.05, ***P*<0.01, ****P*<0.001 when compared to sham-treated guinea-pigs. $^{\#\#}P$<0.01, $^{\#\#\#}P$<0.001 when compared to $1x10^6$ MSC-treated guinea-pigs. $^{\dagger\dagger}P$<0.01, $^{\dagger\dagger\dagger}P$<0.001 when compared to $3x10^6$ MSC-treated guinea-pigs.

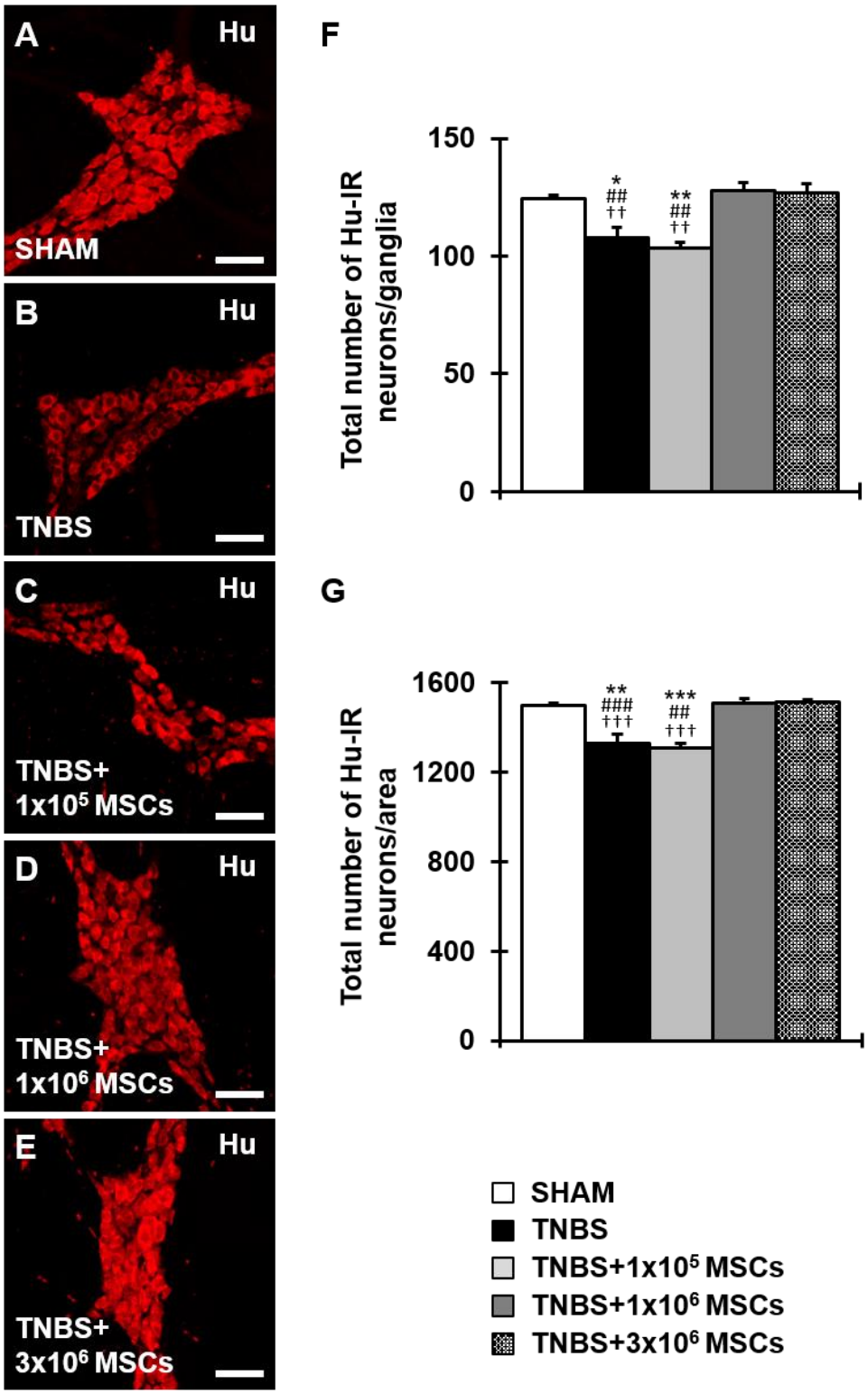
A
Hu
SHAM
B
Hu
TNBS
C
Hu
TNBS+
1x10⁵ MSCs
D
Hu
TNBS+
1x10⁶ MSCs
E
Hu
TNBS+
3x10⁶ MSCs
F
Total number of Hu-IR neurons/ganglia
150
100
50
0
*
##
††
**
##
††
G
Total number of Hu-IR neurons/area
1600
1200
800
400
0
**
###
†††
***
##
†††
SHAM
TNBS
TNBS+1x10⁵ MSCs
TNBS+1x10⁶ MSCs
TNBS+3x10⁶ MSCs

Figure 3.6. Effects of MSC treatments on nNOS-IR myenteric neurons. Inhibitory myenteric neurons were identified by anti-nNOS antibody in wholemount LMMP preparations of the distal colon from sham-treated, TNBS-only, 1×10^5 MSC-treated, 1×10^6 MSC-treated and 3×10^6 MSC-treated guinea-pigs at 3 days post induction of colitis **(A-E)**. Scale bars = 50μm. The total number of nNOS-IR neurons was counted per ganglion (average of ten ganglia) **(F)** and per $2mm^2$ area **(H)** of the colon. The proportion of nNOS-IR neurons to Hu-IR neurons per ganglia **(G)** and per $2mm^2$ area **(I)**. $^{**}P<0.01$, $^{***}P<0.001$ when compared to sham-treated guinea-pigs. $^{\#\#}P<0.01$, $^{\#\#\#}P<0.001$ when compared to $1x10^6$ MSC-treated guinea-pigs. $^{\dagger\dagger}P<0.01$, $^{\dagger\dagger\dagger}P<0.001$ when compared to $3x10^6$ MSC-treated guinea-pigs.

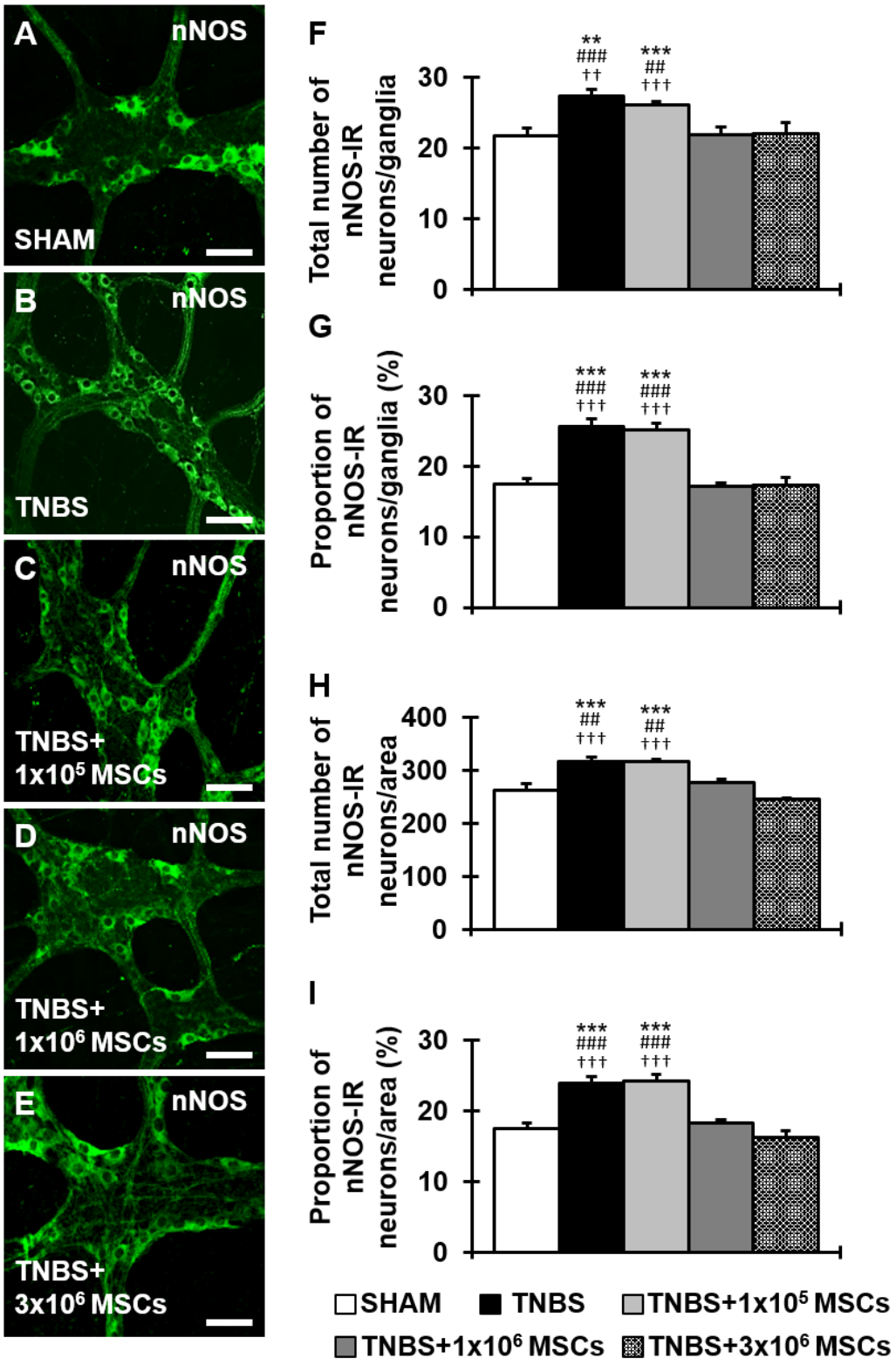
A
nNOS
SHAM
B
nNOS
TNBS
C
nNOS
TNBS+
1x10⁵ MSCs
D
nNOS
TNBS+
1x10⁶ MSCs
E
nNOS
TNBS+
3x10⁶ MSCs
F
Total number of nNOS-IR neurons/ganglia
G
Proportion of nNOS-IR neurons/ganglia (%)
H
Total number of nNOS-IR neurons/area
I
Proportion of nNOS-IR neurons/area (%)
SHAM
TNBS
TNBS+1x10⁵ MSCs
TNBS+1x10⁶ MSCs
TNBS+3x10⁶ MSCs

Figure 3.7. Effects of MSC treatments on ChAT-IR myenteric neurons. Excitatory myenteric neurons were identified by anti-ChAT antibody in wholemount preparations of the distal colon from sham-treated, TNBS-only, 1×10^5 MSC-treated, 1×10^6 MSC-treated and 3×10^6 MSC-treated guinea-pigs **(A-E)**. Scale bars = 50μm. The total number of ChAT-IR neurons were counted per ganglion (average of ten ganglia) **(F)** and per $2mm^2$ area **(H)** of the colon. The proportion of ChAT-IR neurons to Hu-IR neurons per ganglia **(G)** and per area **(I)**. $^{\#\#}P<0.01$, $^{\#\#\#}P<0.001$ when compared to sham-treated guinea-pigs, $^{**}P<0.01$, $^{***}P<0.001$ when compared to TNBS-only administered guinea-pigs, $^{\wedge}P<0.05$, $^{\wedge\wedge}P<0.01$ when compared to 1×10^5 MSC-treated guinea-pigs.

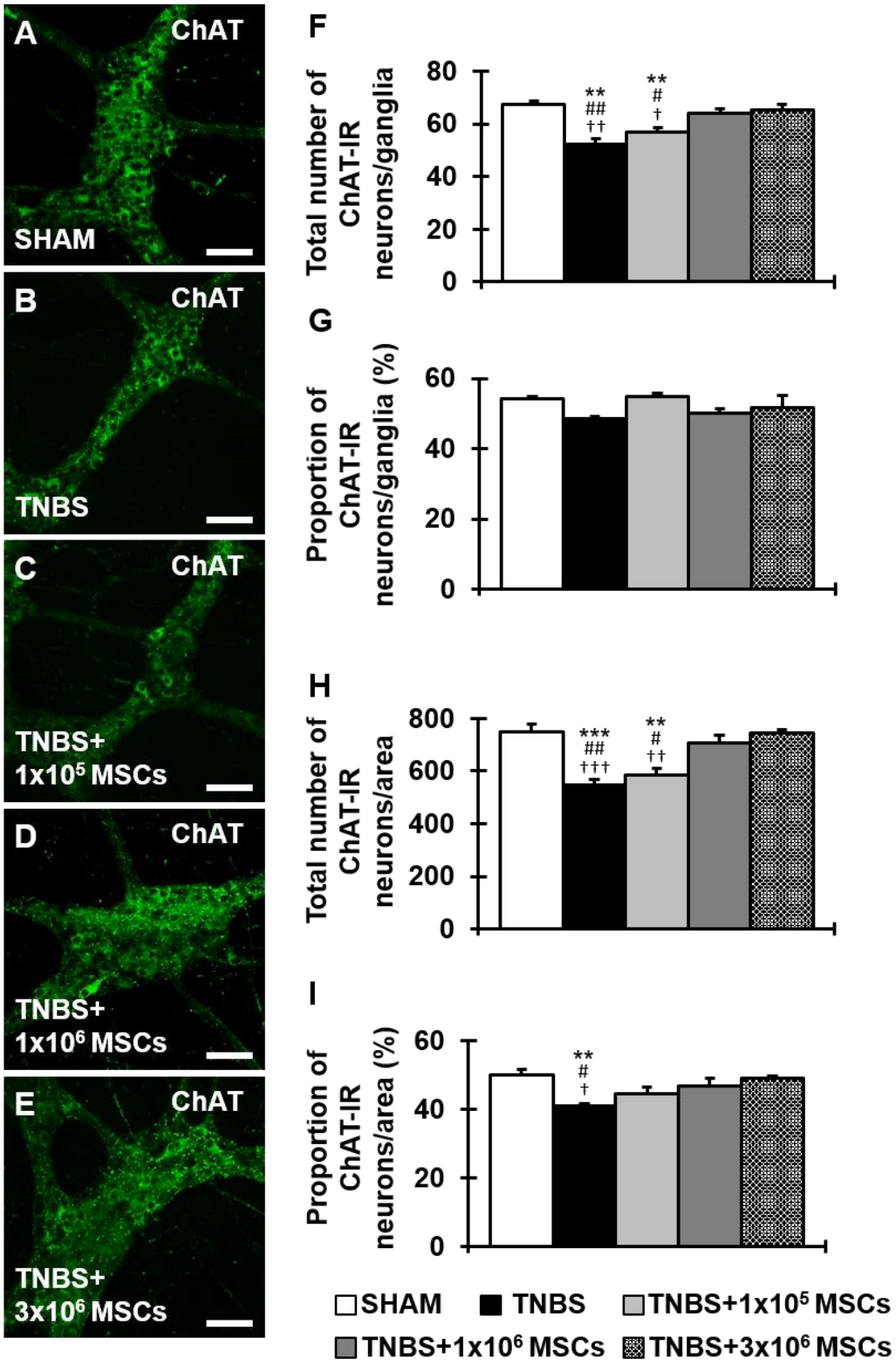
A
ChAT
SHAM
B
ChAT
TNBS
C
ChAT
TNBS+
1x10⁵ MSCs
D
ChAT
TNBS+
1x10⁶ MSCs
E
ChAT
TNBS+
3x10⁶ MSCs
F
Total number of ChAT-IR neurons/ganglia
80
60
40
20
0
** ## ††
** # †
G
Proportion of ChAT-IR neurons/ganglia (%)
60
40
20
0
H
Total number of ChAT-IR neurons/area
800
600
400
200
0
*** ## †††
** # ††
I
Proportion of ChAT-IR neurons/area (%)
60
40
20
0
** # †
SHAM
TNBS
TNBS+1x10⁵ MSCs
TNBS+1x10⁶ MSCs
TNBS+3x10⁶ MSCs

3.5 Discussion

In this study, we compared different doses of human BM-MSCs for their neuroprotective efficacy in a guinea-pig model of TNBS-induced colitis. Both 1×10^6 and 3×10^6 MSC treatments demonstrated therapeutic efficacy in the accelerated repair of colonic architecture, reduced leukocyte infiltration transmurally through the colon wall, regeneration of nerve fibers, and were equally neuroprotective in the amelioration of myenteric neuronal loss and changes to the neurochemical coding of their subpopulations. When administered at a dose of 1×10^5, BM-MSCs offered some therapeutic benefit in healing of the colonic architecture, protection of nerve fibers and the offset of CD45-IR cells in the mucosa, however, were less effective in the attenuation of neuropathy at the level of the myenteric plexus. Thus, a dose of 1×10^6 MSCs is necessary to ameliorate the effects of TNBS-induced inflammation at the level of the myenteric plexus; further increases in dose provide consistent efficacy without promotion of benefit.

In inflammatory bowel disease (IBD) patients with fistulae and luminal inflammation it has been demonstrated that therapy with both BM and adipose MSCs is safe, feasible and efficacious (Forbes et al. 2014; Ciccocioppo et al. 2011; Duijvestein et al. 2010; Garcia-Olmo et al. 2009; 2005). However, there is inconsistency regarding the most effective dose; some studies report reduced disease activity and fistula closure with doses ranging from 3×10^6-60×10^6 MSCs (Molendijk et al. 2015; de la Portilla et al. 2013; Garcia-Olmo et al. 2009; 2005). Additionally, some studies have reported positive outcomes with dose regimes based relative to fistula size (dose range 1×10^6-4×10^7 cells/cm length of fistula (average number of injected cells: 20×10^6-15.8×10^7)) (Cho et al. 2013; Lee et al. 2013b; Ciccocioppo et al. 2011) or patient body weight (1×10^6-2.7×10^6 cells/kg) (Forbes et al. 2014; Duijvestein et al. 2010). In experimental models of colitis, BM-MSCs derived from rats (Fawzy et al. 2013; Castelo-Branco et al. 2012; Tanaka et al. 2011; 2008; Yabana et al. 2009; Hayashi et al. 2008), mice (Liu et al. 2015b; Wang et al. 2014a; Chen et al. 2013b; He et al. 2012), guinea-pigs (Stavely et al. 2015a) and humans (Robinson et al. 2015; 2014; Stavely et al.

2015b; Duijvestein et al. 2011; Zhang et al. 2009b) have been investigated for therapeutic efficacy. In addition, some studies have assessed adipose MSCs derived from these species (Stavely et al. 2015a; 2015b; Liu et al. 2014; Anderson et al. 2013; Castelo-Branco et al. 2012; Gonzalez et al. 2009; Gonzalez-Rey et al. 2009; Ando et al. 2008), as well as human umbilical cord, umbilical cord blood and gingiva (Chao et al. 2016; Kim et al. 2013; Liang et al. 2011; Zhang et al. 2009b). Overall, intravenous, intraperitoneal and local administration of MSCs from various sources and species have been reported to ameliorate experimental colitis however, similarly to clinical trials, there is no consistency regarding the most efficacious dose. Studies report therapeutic efficacy in ameliorating colitis following MSC application with doses of 2×10^3 (Tanaka et al. 2011), 2×10^4 (Yabana et al. 2009), 5×10^5 (Fawzy et al. 2013), 0.5×10^6 (Duijvestein et al. 2011), 1×10^6 (Chao et al. 2016; Liu et al. 2015b; Robinson et al. 2015; 2014; Stavely et al. 2015a; 2015b; Wang et al. 2014a; Anderson et al. 2013; Chen et al. 2013b; He et al. 2012; Duijvestein et al. 2011; Liang et al. 2011; Gonzalez et al. 2009; Gonzalez-Rey et al. 2009), 2×10^6 (Liu et al. 2014; Kim et al. 2013; Castelo-Branco et al. 2012; Zhang et al. 2009b), 5×10^6 (Gonzalez-Rey et al. 2009; Tanaka et al. 2008), 1×10^7 (Ando et al. 2008; Hayashi et al. 2008) MSCs.

In this study, we employed MSCs derived from human BM. Human MSCs are the most characterized, clinically applied as a potential regenerative cell therapy (Mendicino et al. 2014) and defined based upon three minimal criteria (i) plastic adherence, (ii) trilineage differentiation, (iii) surface expression of CD73, CD90, CD105 and absence of expression of CD45, CD34, CD14 or CD11b, CD79α or CD19, and HLA-DR (Dominici et al. 2006). MSCs used in this study were validated according to these guidelines issued by the ISCT. On the other hand, MSCs from animal origin have been defined as cells that fulfil the first two criteria (Li et al. 2012). Comparison of animal and human-derived MSCs has revealed a high degree of concordance (Scuteri et al. 2014; Zavan et al. 2007; Wieczorek et al. 2003). However, differences have been reported in genomic stability (Redaelli et al. 2012; Foudah et al. 2009), differentiation potential (Martinez-Lorenzo et al. 2009), surface antigen expression and immunoregulatory capabilities (Ren et al.

2009) making it difficult to directly extrapolate the results obtained on animal MSCs to human MSCs. MSCs were originally derived from the BM, are the most frequently investigated cell type (Jones and Schafer 2015a) and are often designated as the gold standard in the treatment of various inflammatory conditions (Antunes et al. 2014; Elman et al. 2014; Roemeling-van Rhijn et al. 2013; Hass et al. 2011). Furthermore, human BM-MSCs are the most therapeutic in the treatment of enteric neuropathy and plexitis associated with TNBS-induced colitis (Stavely et al. 2015b).

Of particular relevance to the therapeutic application of MSCs is their fate post-implantation. Ambiguity seen in the efficacy of MSCs, in both animal studies and clinical trials, with therapies being ineffective or only temporarily effective could be due to suboptimal application of MSCs. Previous studies have indicated MSC efficacy may be affected by the timing of delivery (Wei et al. 2013) and administration during the earlier phases of inflammation is favorable for therapeutic results (Wang et al. 2014c; Bernardo and Fibbe 2013; Karp and Teo 2009). Therefore, in consistency with our previous study, BM-MSCs were administered 3h after TNBS; the time point when substantial mucosal damage occurs (Pontell et al. 2009).

The migratory and homing capacity of MSCs is facilitated by their expression of a wide array of chemokine receptors and adhesion molecules that respond to chemoattractant signals released from host cells at the site of injury (Karp and Teo 2009). MHC class I molecules are expressed on the surface of viable human MSCs promoting immune rejection and assisting in engraftment into damaged tissue via the absence of co-stimulatory ligands/receptors and release of immunosuppressive factors (Jacobs et al. 2013; Machado et al. 2013; Li et al. 2012). MSC migration to the area of inflammation and subsequent engraftment into the damaged tissue is an inaugural part of the tissue repair/regeneration process and indispensable for therapeutic efficacy. In this study, we labeled sections of the guinea-pig colon with anti-HLA-A,B,C antibody to evaluate the successful migration and engraftment of MSCs within the inflamed intestinal wall. MSCs engrafted into the mucosa at the initial site of TNBS-induced inflammation

in all MSC-treated groups. However, in sections from guinea-pigs administered 1×10^6 or 3×10^6 MSCs, HLA-A,B,C-positive cells were observed at the level of the myenteric plexus in addition to the mucosal layer. The successful migration and engraftment of enema-applied MSCs into the inflamed colonic wall observed in our study is consistent with previous reports demonstrating implantation of locally administered MSCs into target tissues, especially in inflammatory conditions (Hayashi et al. 2008; Hu et al. 2007). Subsequently, the outcomes of the treatment were more pronounced in animals treated with 1×10^6 and 3×10^6 MSCs compared to those treated with 1×10^5 MSCs. In this study, we did not quantify the proportion of MSCs which migrated to and engrafted in the inflamed colon. Limited studies have quantified the efficiency of MSC transplantation, and those that have quantified MSC engraftment have demonstrated poor engraftment efficiency (approximately 1-20% of transplanted MSCs survive) (Marquardt and Heilshorn 2016; Kean et al. 2013). Most studies investigating the therapeutic effects of MSCs, including our study, administer MSCs in PBS (Hayashi et al. 2008; Hu et al. 2007; Fawzy et al. 2013; He et al. 2012). However, it is plausible to consider that a greater engraftment of MSCs (and thus a reduced number of cells required to attain a therapeutic effect) may be achieved by using viscous, injectable hydrogels or scaffolds as cell carriers since low viscosity saline or PBS seemingly does not hold cells in tissue efficiently (Li et al. 2016a; Li et al. 2016c). This requires further investigation in the guinea-pig model of TNBS-induced colitis.

Reduced disease activity, endoscopic and histopathologic severity of colitis, and infiltration of neutrophils into the colon are commonly evaluated to determine the effectiveness of MSC treatments in both clinical trials and experimental models of IBD. Within these parameters examining the therapeutic efficacy of various MSC doses at the level of the mucosa only, we could conclude that BM-MSCs ameliorate experimental colitis at a dose as low as 1×10^5 MSCs. However, previous studies have reported marked structural and functional changes to the enteric nervous system (ENS) in IBD accompanied by infiltration of inflammatory cells to the submucosa and myenteric plexus (Sokol et al. 2009; Villanacci et al. 2008; Ferrante et al. 2006). Alterations to the ENS persist long after resolution of

acute intestinal inflammation reflected through changes in gut function, colonic dysmotility, hypersensitivity and dysfunction (Mawe 2015; Villanacci et al. 2008), and myenteric plexitis has been shown to be predictive of IBD recurrence (Sokol et al. 2009; Ferrante et al. 2006). Therefore, we further investigated the therapeutic efficacy of varying doses of BM-MSCs at the level of the myenteric plexus.

In this study, MSCs were effective in reducing leukocyte infiltration to the myenteric plexus within the muscular layers of the colon when administered at doses of 1×10^6 and 3×10^6, but not at a dose of 1×10^5. It may be proposed that while some immunomodulatory effect is occurring following application of 1×10^5 MSCs, it is not strong enough to combat all inflammation since leukocyte numbers were reduced at the mucosal level in this group, but not at the myenteric level. While the immunomodulatory mechanisms of MSCs have not been completely elaborated, it is known that in order for MSCs to wield their immunosuppressive capacities, they must be induced by inflammatory cytokines within a pro-inflammatory microenvironment (Crop et al. 2010). The increased numbers of leukocytes in the colonic wall following induction of TNBS colitis provided sufficient pro-inflammatory stimuli for activation of MSCs. Hence, the weaker influence demonstrated by the lower dose of MSCs suggests that the anti-inflammatory effect was hindered by a smaller quantity of MSCs rather than their immunomodulatory capacity. This is reflected by localization of MSCs within the inflamed colon where HLA-A,B,C-positive cells were evident in the mucosa only in sections from 1×10^5 MSC-treated animals.

It is generally considered that the anti-inflammatory properties of MSCs function via direct interaction with target cells and/or production of diverse soluble factors (Burdon et al. 2011; Chen et al. 2008). Many of the MSC-associated biological effects are mediated by paracrine mechanisms engaging the release of cytokines, chemokines and growth factors (Burdon et al. 2011; Ankrum and Karp 2010; Parekkadan and Milwid 2010) and may be exerted by the induction and stimulation of endogenous host progenitor cells to improve the regenerative process (Chen et al. 2013b; Semont et al. 2013). In animal models of colitis, MSC

application efficiently reduces T helper 1 and T helper 17 responses and downregulates pro-inflammatory cytokines (such as tumor necrosis factor-α, interleukin (IL)-1β, IL-6, IL-17, inducible nitric oxide synthase, cyclooxygenase-2 and interferon-γ while enhancing the numbers of regulatory T cells and upregulating anti-inflammatory cytokines (such as IL-10) (Forte et al. 2015; Sala et al. 2015; Yang et al. 2015; Zuo et al. 2015). The proportion of mucosal and peripheral regulatory T cells was also increased after MSC treatment of Crohn's disease fistulae (Ciccocioppo et al. 2011). These findings suggest that the paracrine actions of MSCs have an anti-inflammatory affect in IBD associated with inhibition of nuclear factor kappa B signaling pathways. Furthermore, paracrine actions of MSCs have be shown to diminish free radicals and impede oxidative stress, prevent apoptosis via the extrinsic death receptor signal pathway and the intrinsic mitochondrial signal pathway and stimulate endogenous mechanisms of intestinal epithelial repair (Yang et al. 2015; Semont et al. 2013).

It remains unclear whether changes to the ENS are the cause or the consequence of inflammation; however, in this study TNBS-induced plexitis was associated with damage to nerve fibers and loss of myenteric neurons, as well as changes in their subpopulations. Similar to the limited anti-inflammatory effect discussed above, sections from animals treated with 1×10^5 MSCs revealed some nerve fiber regrowth, but not to the level of sham-treated animals. In contrast, significant regeneration and regrowth of nerve fibers in the colon were associated with 1×10^6 and 3×10^6 MSC treatments in this study. MSCs improve axonal and nerve regeneration through the production of local neurotrophic factors for induction of axonal growth, including brain-derived neurotrophic factor, nerve growth factor and insulin-like growth factor-1 (Petrova 2015; Ladak et al. 2011). Hence, differences in the level and areas of MSC engraftment demonstrated in sections from 1×10^5 MSC-treated animals compared to 1×10^6 and 3×10^6 MSC-treated guinea-pigs maybe associated with a reduction in the expression of neurotrophic factors. However, this needs to be further investigated.

Our study demonstrated a persistent loss of myenteric neurons to be associated with TNBS-induced inflammation in the distal colon of guinea-pigs 3 days after induction of colitis. Consistent with our findings, the quantity of myenteric neurons was found to be reduced in the guinea-pig intestine subsequent to intra-rectal administration of TNBS in previous studies (Robinson et al. 2015; 2014; Stavely et al. 2015a; 2015b; Nurgali et al. 2011; Linden et al. 2005). In this study, neuronal loss was not prevented following treatment with 1×10^5 MSCs and the number of myenteric neurons was comparable to the TNBS-only administered group. On the other hand, doses of 1×10^6 and 3×10^6 MSCs prevented the neuronal loss associated with TNBS-induced inflammation. Similarly, MSCs have been shown to prevent neuronal apoptosis (Wei et al. 2009), increase the survival of motor neurons in amyotrophic lateral sclerosis (ALS) (Marconi et al. 2013; Suzuki et al. 2008) and reduce the loss of dopaminergic neurons in Parkinson's disease (Kim et al. 2009). Furthermore, in a dose-dependent study, 1×10^6 BM-MSCs was optimal to reduce the extent of neural loss in mice with ALS (Kim et al. 2010a).

Enteric neuropathy in intestinal inflammation may be influenced by excessive nitric oxide (Hogaboam et al. 1995), while inflammation-associated loss of ChAT-IR neurons has been associated with decreases in the number of myenteric neurons (Boyer et al. 2005; Linden et al. 2003; Poli et al. 2001; Sanovic et al. 1999). An increase in the total number of nNOS neurons, as well as a decrease in the number of ChAT neurons was revealed 3 days after the induction of colitis. These results are consistent with previous studies using tissues from IBD patients and experimental animals describing alterations in the neurochemical coding of enteric neurons (Winston et al. 2013; Boyer et al. 2007; Linden et al. 2005; Neunlist et al. 2003; Belai et al. 1997). In this study, treatment with 1×10^5 MSCs was not effective in attenuating changes in the neurochemical coding of excitatory and inhibitory myenteric neurons. However, the increase in nNOS-IR neurons, as well as the loss of ChAT-IR neurons was attenuated by 1×10^6 and 3×10^6 MSCs. The neurons of the myenteric plexus are primarily responsible for coordinating muscular contraction (Furness 2012) and prevention of changes to neurochemical coding by MSC treatments has been associated with alleviating TNBS-induced changes to colonic motility (Robinson et al. 2014). Thus,

attenuating changes in the subpopulations of myenteric neurons may alleviate dysmotility associated with intestinal inflammation.

In consistency with our findings, MSCs have been reported to reduce neurological defects and promote functional recovery in experimental models of neurodegenerative diseases (Freedman et al. 2010; Ohtaki et al. 2008; Zhang et al. 2006; Bang et al. 2005; Hofstetter et al. 2002). While the exact mechanisms of MSC neuroprotection remain unknown, MSCs can act via paracrine mechanisms secreting neuro-regulatory molecules, cytokines, growth factors and chemokines, which provide neuroprotective and neurorestorative effects (Uccelli et al. 2008). These effects include enhancing neuronal viability, promoting regeneration of nerve fibers and inducing the proliferation and differentiation of endogenous neural progenitor cells (Singer and Caplan 2011; Skalnikova et al. 2011; Salgado et al. 2010b). Furthermore, studies investigating the MSC secretome suggest that numerous bioactive factors secreted by MSCs mediate neuroprotection via tropic support, immunomodulation and anti-apoptosis (Singer and Caplan 2011; Skalnikova et al. 2011). The exact MSC-mediated signaling network responsible for neuroprotection of enteric neurons requires further investigation.

In this study, we have observed distinct differences between MSC doses in preventing enteric neuropathy associated with intestinal inflammation. From these results, we can determine that a 1×10^5 dose of BM-MSCs is not adequate, whereas doses of 1×10^6 and 3×10^6 demonstrate anti-inflammatory and neuroprotective qualities in TNBS-induced colitis. Although the 3×10^6 dose MSCs contained triple the quantity of cells than the 1×10^6 dose, no differences were evident between the magnitude of cells homing to and engrafting at the site of tissue injury. This suggests a dose saturation indicating that although there is a greater number of cells being transplanted *in vivo*, only the required number migrates and engrafts into the inflamed areas of TNBS-induced colitis. This is consistent with a previous MSC study which revealed the engraftment of osteoprogenitor cells to be saturated and concluded that higher doses of cells would be an ineffective strategy to improve engraftment (Marino et al. 2008).

Furthermore, high dose inhibition of cytokines has also been observed with high concentrations of MSCs (Audet et al. 2002; 2001; Viswanathan et al. 2002).

3.6 Conclusion

In this study we have essentially determined an optimal dose of MSCs for enteric neuroprotection in a guinea-pig model of TNBS-induced colitis. We have demonstrated that the neuroprotective and anti-inflammatory effect of BM-MSCs is dose-dependent in TNBS-induced colitis; BM-MSCs have the ability to prevent inflammatory insults to the ENS when administered at a dose of 1×10^6 cells 3h after induction of colitis, with no further benefit gained from a higher dose. The findings of this study are important for further investigations into the mechanisms of MSC-based enteric neuroprotection, as well as immunomodulation within the inflamed colon, further enabling MSC therapy to continue to advance forward in future studies.

CHAPTER FOUR: ALTERATIONS IN DISTAL COLON INNERVATION AND FUNCTION IN THE *WINNIE* MOUSE MODEL OF SPONTANEOUS CHRONIC COLITIS

The material presented in this chapter is publishers and has been reproduced here with the permission of the publisher with minor alterations:

Rahman, A. A., **Robinson, A. M.**, Jovanovska, V., Eri, E., Nurgali, K. 2015. Alterations in the distal colon innervation in *Winnie* mouse model of spontaneous chronic colitis. *Cell Tissue Res,* 362, 497-512.

Robinson, A. M., Rahman, A. A., Carbone, S. E, Randall-Demllo, S., Filippone, R., Bornstein, J. C., Eri, R., Nurgali, K. 2017. Alterations of colonic function in the *Winnie* mouse model of spontaneous chronic colitis. *Am J Physiol Gastrointest Liver Physiol,* 312, G85-102.

4.1 Summary

Background: The gastrointestinal (GI) tract is innervated by extrinsic sympathetic, parasympathetic and sensory nerve fibers as well as by intrinsic fibers from the neurons in myenteric and submucosal ganglia embedded into the GI wall. Morphological and functional studies of intestinal innervation in animal models are important for understanding the pathophysiology of inflammatory bowel disease (IBD). The *Winnie* mouse, carrying a missense mutation in *Muc2*, is a model for chronic intestinal inflammation demonstrating symptoms closely resembling IBD. Alterations to the immune environment and morphological structure of *Winnie* mouse colon have been identified; however, analyses of distal colon innervation, intestinal transit and colonic functions have not been conducted. **Methods:** In this study, we investigated noradrenergic, cholinergic and sensory nerve fibers and myenteric neurons in the distal colon of *Winnie* compared to C57BL/6 mice using histological and immunohistochemical methods, as well as *in vivo* intestinal transit in radiographic studies and *in vitro* motility of the isolated colon in organ bath experiments. We compared neuromuscular transmission using conventional intracellular recording and smooth muscle contractions using force displacement transducers between the distal colon of *Winnie* and C57BL/6 mice. **Results:** Chronic inflammation in *Winnie* mice was confirmed by detection of lipocalin-2 in fecal samples over 4 weeks, as well as increased leukocyte infiltration and gross morphological damage to the distal colon with thickening of muscle and mucosal layers. The density of sensory, cholinergic and noradrenergic fibers innervating the myenteric plexus, muscle and mucosa significantly decreased in the distal colon of *Winnie* mice compared to C57BL/6 mice, while the total number of myenteric neurons as well as subpopulations of cholinergic and nitrergic neurons remained unchanged. Colonic transit was faster in *Winnie* mice. Motility was altered including decreased frequency and increased speed of colonic migrating motor complexes and increased occurrence of short and fragmented contractions. The mechanisms underlying colon dysfunctions in *Winnie* mice included inhibition of excitatory and fast inhibitory junction potentials, diminished smooth muscle responses to

cholinergic and nitrergic stimulation, and increased number of α-smooth muscle actin-immunoreactive cells. **Conclusions:** Changes in the colon morphology and innervation found in *Winnie* mice have multiple similarities with changes observed in patients with ulcerative colitis. Diminished excitatory responses occur both prejunctionally and postjunctionally and reduced inhibitory purinergic responses are potentially a prejunctional event, while diminished nitrergic inhibitory responses are probably due to a postjunctional mechanism in the *Winnie* mouse colon. Many of these changes are similar to disturbed motor functions in IBD patients indicating that the *Winnie* mouse is a model highly representative of human IBD.

4.2 Introduction

Experimental animal models provide a useful tool for elucidating the etiology and pathophysiological mechanisms of a disease. However, inflammatory bowel disease (IBD) is multifactorial, so it has been difficult to establish a model that closely resembles the pathological symptoms, clinical manifestations, and complexity of the human disease (DeVoss and Diehl 2014). Most experimental models of IBD produce acute colitis via chemicals or nematodes including 2,4,6-trinitrobenzene-sulfonate acid (TNBS), dextran sodium sulfate (DSS), or Trichinella spiralis (*T. spiralis*) (Brierley and Linden 2014). In comparison, there are limited animal models of spontaneous chronic intestinal inflammation, reinforcing the significance of the recently developed *Winnie* mouse model of colitis which is raised from a C57BL/6 background and closely represents the clinical symptoms of IBD.

In *Winnie* mice, chronic intestinal inflammation results from a primary intestinal epithelial defect conferred by a missense mutation, rather than a deletion, in the *Muc2* mucin gene (Eri et al. 2011; Heazlewood et al. 2008). Disruption of *Muc2* biosynthesis initiates alterations to the mucus layers, heightens intestinal permeability, and increases vulnerability to luminal antigens (Heazlewood et al. 2008). Furthermore, the mutation of *Muc2* in *Winnie* mice is comparable to variations in human IBD, where there is a decrease in *Muc2* production and secretion in active ulcerative colitis (UC) (Heazlewood et al. 2008; Van Klinken et al. 1999) and reduced expression of *Muc2* in Crohn's disease (CD) (Buisine et al. 2001). *Winnie* mice develop colitis in the distal region of the colon as indicated by crypt elongation, neutrophilic infiltrates, goblet cell loss, crypt abscesses, limited mucus secretion, and focal epithelial erosions with an UC-like phenotype (Heazlewood et al. 2008). Inflammation is evident by 6 weeks of age and advances over time, resulting in severe colitis by 16 weeks (Eri et al. 2011; McGuckin et al. 2011).

Previous studies consist mainly of histopathological and immunological changes in the gastrointestinal (GI) tract of *Winnie* mice, but a study of the innervation and

functions of the colon, such as transit and motility, in this model has not been performed. Since *Winnie* mice closely mimic human chronic colitis, the aim of the present investigation was to evaluate the intrinsic and extrinsic intestinal innervation, especially in the distal colon. Additionally, we provide the first analysis of intestinal transit and isolated whole colonic motility in the chronically inflamed *Winnie* mouse colon and investigate mechanisms underlying changes in motility, including altered neuromuscular transmission and structural and functional changes in smooth muscles. Our findings crucially translate to human studies where investigation of colonic motility in IBD patients is limited to specific sections of the colon attained from muscle resected during operations (Vrees et al. 2002; Koch et al. 1988).

4.3 Materials and methods

4.3.1 Animals

Male and female *Winnie* mice (12-16 weeks old; 19-29g; *n*=40) were obtained from Monash Animal Services (MAS, Melbourne, Australia). Since the *Winnie* strain was developed from C57BL/6 background, male and female C57BL/6 mice (12wk old; 26-30g; *n*=33), obtained from MAS, were used as controls. All animals were housed in a temperature-controlled environment with 12h day/night cycles and free access to food and water. Mice were humanely euthanized by cervical dislocation and colon tissues were collected for histology, immunohistochemistry, *in vitro* motility, smooth muscle contractile activity, and intracellular electrophysiology experiments. All procedures performed within this study were approved by the Victoria University Animal Experimentation Ethics Committee and were conducted according to the guidelines of the Australian National Health and Medical Research Council.

4.3.2 Analysis of fecal water content and colon length

Fecal water content was calculated following stool collection from *Winnie* and C57BL/6 mice. After collection, stools were immediately weighed (wet weight) and left to air dry. Three days later, stools were re-weighed (dry weight) and the difference between wet and dry weight was calculated. Mouse colon length (from cecum to anus) was measured immediately after dissection from the animal by placing the colon parallel to a ruler and recording its size.

4.3.3 Assessment of fecal lipocalin-2 levels

To assess the level of colonic inflammation in *Winnie* mice, fecal lipocalin (Lcn)-2 was measured. Lcn-2 was quantified by enzyme-linked immunosorbent assay (ELISA), as previously described (Chassaing et al. 2012). Fecal samples were collected from C57BL/6 and *Winnie* mice twice weekly for 4 weeks. Briefly, fecal samples were reconstituted in phosphate buffered saline (PBS)-0.1% Tween 20 (100mg/mL) and vortexed (20min) to form a homogenous fecal suspension.

Samples were then centrifuged for 10min at 12,000rpm and 4°C. Lcn-2 levels were estimated in the supernatants using Duoset murine Lcn-2 ELISA kit (R&D Systems, Minneapolis, MN, USA).

4.3.4 Immunohistochemistry and histology

4.3.4.1 Tissue preparation

Segments of the distal colon were processed in two different ways: (1) wholemount longitudinal muscle-myenteric plexus (LMMP) preparations, and (2) cross sections of the distal colon. The colon was exposed through a midline laparotomy and a 5cm section 2cm from the anus was collected from each animal. Immediately following dissection, colon tissues were placed in oxygenated PBS (pH7.2) containing L-type Ca^{2+} channel blocker, nicardipine (3μM; Sigma-Aldrich, Castle Hill, NSW, Australia). Segments of the distal colon were then cut open along the mesenteric border and pinned flat with the mucosal side up (maximally stretched for LMMP preparations while unstretched for cross sections) in a Sylgard-lined Petri dish (Dow Corning, Midland, Michigan, USA). Tissues for LMMP preparations and cryostat cross sections were fixed with Zamboni's fixative (2% formaldehyde containing 0.2% picric acid) overnight at 4°C and subsequently washed with dimethyl sulfoxide (DMSO; Sigma-Aldrich) for 3×10min followed by 0.1M PBS for 3×10min. Subsequently, LMMP tissues were dissected to expose the myenteric plexus by removing the mucosa, submucosa and circular muscle layers. For cryostat cross section preparations, tissues were cryoprotected (30% sucrose/phosphate buffer; Sigma-Aldrich, Australia) overnight at 4°C then transferred to 50% optimal cutting temperature compound (OCT; Tissue-Tek, Torrance, CA, USA) in 30% sucrose/PBS for 12-24h prior to freezing in 100% OCT. Tissues were sectioned at a 20μm thickness (at least 15 sections from each animal) using a cryostat microtome (Leica CM1850, St. Gallen, Switzerland) and mounted onto glass slides. Tissues for histology were fixed in 10% buffered formalin overnight at 4°C and stored in 70% ethanol until embedding.

4.3.4.2 Immunohistochemistry

Following a 1h incubation in 10% normal donkey serum (NDS; Merck Millipore, Bayswater, VIC, Australia) diluted in 0.1M PBS-0.1% Triton X-100 at room temperature, samples were washed with 0.1M PBS-0.1% Triton X-100 (2×5min) and incubated with primary antibodies (Table 4.1) diluted in 2% NDS and 0.1M PBS-0.1% Triton X-100 overnight at room temperature. The tissues were then washed briefly in 0.1M PBS-0.1% Triton X-100 (2×5min) prior to incubation with secondary antibodies (Table 4.2) diluted in 2% NDS and 0.1M PBS-0.1% Triton X-100 for 2h at room temperature. After 3×10min washes in 0.1M PBS-0.1% Triton X-100, tissues were mounted on glass slides with fluorescent mounting medium (DAKO, North Sydney, NSW, Australia). Cross sections immunolabeled with α-smooth muscle actin (SMA) were incubated for 2min with the fluorescent nucleic acid stain 4′-6-diamidino-2-phenylindole (DAPI; 14nM; Invitrogen, Thermo-Fisher Scientific, Scoresby, VIC, Australia) in between the second and third washes.

4.3.4.3 Histology

For histology, tissues were embedded in paraffin, sectioned at 5μm, deparaffinized, cleared, and rehydrated in graded ethanol concentrations. For hematoxylin and eosin (H&E) staining, sections were immersed in xylene (3×4min), 100% ethanol (3min), 90% ethanol (2min), 70% ethanol (2min), rinsed in tap water, hematoxylin (4min), rinsed in tap water, Scott's tap water (1min), eosin (6min), rinsed in tap water, 100% ethanol (2×1min), xylene (2×3min) and mounted on glass slides with distrene plasticizer xylene (DPX) mountant.

Table 4.1 Primary antibodies used in this study

Antibody	Host species	Dilution	Supplier	Application in this study
Anti-α-smooth muscle actin (α-SMA)	Rabbit	1:1000	Abcam, Melbourne, VIC, Australia	Cross sections
Anti-β-Tubulin class III	Rabbit	1:1000	Abcam	Cross sections
Anti-calcitonin gene-related peptide (CGRP)	Rabbit	1:3000	Sigma-Aldrich	Cross sections and LMMP preparations
Anti-CD45	Rat	1:500	BioLegend, San Diego, CA, USA	Cross sections
Anti-choline acetyltransferase (ChAT)	Goat	1:500	Merck Millipore	LMMP preparations
Anti-neuronal nitric oxide synthase (nNOS)	Goat	1:500	Novus Biologicals, Littleton, CO, USA	LMMP preparations
Anti-protein gene product (PGP)-9.5	Rabbit	1:500	Abcam	LMMP preparations
Anti-tyrosine hydroxylase (TH)	Sheep	1:1000	Merck Millipore	Cross sections and LMMP preparations
Anti-vesicular acetylcholine transporter (VAChT)	Goat	1:500	Merck Millipore	Cross sections and LMMP preparations

Table 4.2 Secondary antibodies used in this study

Antibody	Host species	Dilution	Supplier	Application in this study
Alexa Fluor 488	Donkey anti-rabbit	1:200	Jackson Immunoresearch Laboratories, PA, USA	Cross sections and LMMP preparations
Alexa Fluor 488	Donkey anti-rat	1:200	Jackson Immunoresearch Laboratories	Cross sections
Alexa Fluor 488	Donkey anti-sheep	1:200	Jackson Immunoresearch Laboratories	Cross sections and LMMP preparations
Alexa Fluor 594	Donkey anti-rabbit	1:200	Jackson Immunoresearch Laboratories	Cross sections
Alexa Fluor 647	Donkey anti-goat	1:200	Jackson Immunoresearch Laboratories	Cross sections and LMMP preparations
Alexa Fluor 647	Donkey anti-rabbit	1:200	Jackson Immunoresearch Laboratories	LMMP preparations
Fluorescein isothiocyanate (FITC) 488	Donkey anti-goat	1:200	Jackson Immunoresearch Laboratories	LMMP preparations

4.3.5 Imaging

Immunolabeled distal colon tissues were visualized and imaged by using filter combinations appropriate for the specific fluorophores on a Nikon Eclipse Ti multichannel confocal laser scanning system (Nikon, Tokyo, Japan). such as FITC, Alexa 488 (excitation wavelength 488nm), Alexa 594 (excitation wavelength 559nm), Alexa Fluor 647 (excitation wavelength 640nm) or DAPI (excitation wavelength 405nm). Images (512×512 pixels) were obtained with x20 (dry, 0.75) or x40 (oil immersion, 1.3) lenses. In order to obtain Z-series, neuronal structures were imaged by collecting consecutive optical sections at 0.5-1µm intervals. An Olympus BX53 microscope (Olympus, Notting Hill, VIC, Australia) was used to visualize and image H&E-stained colon sections.

4.3.6 Quantitative analysis of immunohistochemical and histological data

All quantitative analyses were conducted blindly. Images were analyzed using Image J software (National Institute of Health, Bethesda, MD, USA). Muscle and mucosal thicknesses were quantified as described previously (Miampamba and Sharkey 1998). Muscle thickness was measured from the serosa to the submucosa including both longitudinal and circular muscle layers, while mucosal thickness was measured from the submucosa to the luminal surface of mucosa. Infiltration of leukocytes was assessed by measuring the density of CD45-immunoreactive (IR) cells per area (average of eight areas of 500µm^2 per animal at ×20 magnification). Image J software was employed to adjust color images from red, green, and blue (RGB) to 8 bit, after which thresholding to a consistent value was applied to obtain the percentage area of CD45-immunoreactivity. β-Tubulin (III)-IR, CGRP-IR, TH-IR, and VAChT-IR nerve fibers in cross sections of the distal colon were measured from eight images per preparation at ×20 magnification (total area 2mm^2). CGRP-IR, TH-IR and VAChT-IR nerve fibers in LMMP preparations of the distal colon were measured from eight randomly captured images per preparation (total area 2mm^2), as well as per ganglion (all ganglia within meaured area). Images were changed from RGB to 8 bit and made

binary prior to particle analysis with Image J software. The total number of DAPI-IR nuclei of α-SMA-IR cells was counted throughout the muscle thickness including both longitudinal and circular muscle layers (from the serosa to the junction with the submucosa) in eight randomly captured images per preparation at ×40 magnification. Data are expressed as the number of α-SMA-IR cells per 1mm^2 area of distal colon. In LMMP preparations of the distal colon, the average number of PGP9.5-IR, nNOS-IR, and ChAT-IR neurons per ganglion was assessed by measuring ganglionic area and counting the number of myenteric neurons within that area (Gulbransen et al. 2012). Analysis was performed for all ganglia within eight randomly captured images at ×20 magnification (total area 2mm^2) and neuronal counts were normalized to a 0.1mm^2 area of ganglia for direct comparison between groups. Histological scores were developed from the following parameters: aberrant crypt architecture (score range 0-3), increased crypt length (0-3), goblet cell depletion (0-3), crypt abscesses (0-3), leukocyte infiltration (0-3), and epithelial damage and ulceration (0-3) (average of eight areas of 500μm^2 per animal).

4.3.7 Gastrointestinal transit (radiographic study)

GI transit was analyzed using a non-invasive radiological method. Briefly, 0.3mL of suspended barium sulfate (X-OPAQUE-HD; 2.5g/mL; Sigma-Aldrich) was administered to C57BL/6 and *Winnie* mice via oral gavage following 5d acclimatization. Subsequently, serial X-rays were taken using a HiRay Plus Porta610HF X-ray apparatus (50kV, 0.3mA, exposure time 60ms; JOC, Kanagawa, Japan). X-rays were captured using Fujifilm cassettes (24×30cm) immediately after administration of barium sulfate (0min), every 10min for the first 60min, then every 20min through to 250min. Images were developed via a Fujifilm FCR Capsula XLII and analyzed using eFilm 4.0.2 software. Transit speed was calculated as the time (min) taken for the leading edge of the contrast to travel from the stomach to the cecum (orocecal intestine transit time (OCTT)) and from the cecum to the anus (colonic transit time (CTT)).

4.3.8 *In vitro* analysis of isolated whole colon motility

Colonic motility experiments were performed as described in Chapter 2, section 2.3.9. Briefly, colons from C57BL/6 and *Winnie* mice were placed in organ bath chambers superfused with warmed Krebs solution, cannulated at both ends, and positioned horizontally. The oral cannula was attached to a Krebs solution reservoir that was adjusted to maintain intraluminal pressure. A maximum of 2cmH_2O backpressure was provided by an outflow tube coupled to the segment's anal end. A video camera positioned above the organ bath recorded colonic contractile activity (30min equilibration and 2×30min at each test condition (baseline, +1cmH_2O, and +2cmH_2O intraluminal pressure)). Spatiotemporal maps were produced (Scribble v2.0; MATLAB v2012a) and subsequently utilized to analyze colonic contractile activity.

4.3.9 Intracellular electrophysiology

Segments of the distal colon immediately oral to the pelvic brim were dissected in a Sylgard-lined petri dish containing physiological saline. The L-type Ca^{2+} channel blocker nicardipine (2μM) was added to limit the muscle contractions. Tissues were opened along the mesenteric border and pinned down flat, and the mucosa and submucosa were removed by sharp dissection. A full circumference, 1.5cm-long segment of tissue was isolated and re-pinned circular muscle layer uppermost in a Sylgard-lined recording chamber using gold-plated tungsten pins (50μm). The recording chamber was fixed to a stage mounted on a Zeiss Axiovert-200 inverted microscope and superfused with warmed physiological saline (rate 3mL/min) so that the final bath temperature was ~35°C. Preparations were left to equilibrate for 120min before commencing recordings (Carbone et al. 2014; 2012). Circular smooth muscle cells were impaled with borosilicate glass capillary electrodes (1mm outside diameter, 0.58mm inside diameter; Harvard Apparatus, SDR Scientific, Chatswood, NSW, Australia) filled with 5% carboxyfluorescein (Sigma-Aldrich) and 1M KCl in 20mM Tris buffer solution (pH7.0). Electrode resistance ranged from 80-130MΩ. Membrane potential (mV) was recorded with an Axoclamp 2B amplifier (Axon Instruments, Foster City, CA,

USA), digitized at 1-10kHz with a Digidata 1440A interface (Molecular Devices, SDR Scientific), and stored using PClamp 10.0 software (Molecular Devices, SDR Scientific). Focal electrical stimulation was applied 1mm circumferential to the site of impalement using a tungsten electrode (10-50µm tip diameter) connected to an ISO-Flex stimulator controlled by a Master-8 pulse generator (A.M.P. Instruments, Jerusalem, Israel). Unless otherwise specified, a single-pulse, 0.4ms duration electrical stimulus (0-60V) was used to activate nerve fibers, causing motor neurons to release neurotransmitters onto smooth muscle cells. Postjunctional responses were recorded. The resting membrane potential (RMP) of each cell was measured, and its identity was confirmed by viewing carboxyfluorescein labeling *in situ*. For each preparation (*n*), the electrophysiological properties of four to eight cells were averaged for each test condition and then compared with other preparations.

4.3.10 Measurement of contractile force

Experiments were performed using standard organ bath techniques. Freshly excised distal colon was cut into 3mm rings, cleaned of connective tissue and fat, and placed in a custom-built organ bath containing physiological saline (oxygenated with 95% O_2 and 5% CO_2) maintained at 35°C and pH7.4. The colonic rings were then mounted between two small metal hooks attached to force displacement transducers (Zultek Engineering, Hampton, VIC, Australia) and stretched to 0.2g tension. Tissues were allowed to equilibrate for 1h with physiological saline changed every 30min before the start of the experiments (Habiyakare et al. 2014). The colonic rings were examined for their responses to carbachol (a muscarinic receptor agonist), sodium nitroprusside (SNP; nitric oxide (NO) donor), and adenosine 5′-triphosphate (ATP). The dose-response curve for carbachol was evaluated with progressive increases of carbachol dose (1nM-20µM). Increasing concentrations were delivered at 5min (minimum) intervals. Concentration-response curves for SNP (10nM-300µM) and ATP (10µM-3mM) were constructed cumulatively on tissues precontracted with 10µM carbachol (allowed to stabilize for 10min before adding SNP or ATP) with 5min intervals between administrations of increasing concentrations of each drug. The

response to each drug (carbachol, SNP, and ATP) was quantified by comparing the peak response to a baseline control period. The maximum contractile response to carbachol was expressed as a percentage of the contraction induced by 10μM carbachol. The dilating effects of SNP and ATP were expressed as a percentage of the maximum contractile response to carbachol.

4.3.11 Drugs used

ATP (10μM-10mM), atropine (1μM), carbachol (1nM-20μM), Nω-nitro-l-arginine (L-NNA; 1mM), nicardipine (2-3μM), SNP (10nM-1mM) (all from Sigma-Aldrich) and MRS 2500 tetrammonium salt (MRS2500; 1μM; Tocris, In vitro Technologies, Noble Park, VIC, Australia) were prepared as stock solutions and diluted in physiological saline daily before addition to preparations.

4.3.12 Statistical analysis

Statistical analysis was conducted with Prism (v.5.0; GraphPad Software Inc., La Jolla, CA, USA). All values are expressed as mean±SEM. Unpaired *t*-tests were used to compare two sets of data. One-way or two-way ANOVA was used for group comparison of data followed by the Bonferroni's or Tukey-Kramer post hoc tests. For smooth muscle contractility experiments, responses to carbachol, SNP, and ATP were fitted to sigmoid curves. The variable *n* in results refers to the number of animals used for each set of experiments. $P<0.05$ was considered significant.

4.4 Results

4.4.1 Assessment of colonic inflammation

All *Winnie* mice used in this study displayed symptoms of intestinal inflammation: perianal inflammation and bleeding, soiled fur and soft fecal consistency, not forming pellets compared to control mice (Fig. 4.1A-C). There were no gender differences in disease severity in *Winnie* mice. The fecal water content (wet weight minus dry weight) of stools from *Winnie* mice was greater than in stools from C57BL/6 mice (*n*=6/group; *P*<0.001; Table 4.3; Fig. 4.1D). The body weight of all mice was monitored daily for a period of 7 days prior to culling. Average body weight of *Winnie* mice (23.0±1.0g) was less compared to C57BL/6 (27.0±0.2g) mice (*n*=12/group; *P*<0.01; Fig. 4.1E). Immediately following dissection, the length of the colon was measured and recorded showing *Winnie* mice to have longer colons compared to C57BL/6 mice (*n*=6/group; *P*<0.001; Table 4.3; Fig. 4.1F).

Fecal Lcn-2 was quantified by ELISA for *Winnie* (*n*=24) and C57BL/6 (*n*=17) mice. Lcn-2 is a component of granules in neutrophils and is expressed in response to a wide variety of pro-inflammatory stimuli (Kjeldsen et al. 2000). Thus, fecal Lcn-2 is a highly sensitive and broadly dynamic marker of intestinal inflammation (Chassaing et al. 2012). In this study, minimal Lcn-2 was detected in fecal pellets from C57BL/6 mice at any time point (Fig. 4.2A-C), confirming a lack of colonic inflammation. Levels of fecal Lcn-2 in samples from all *Winnie* mice used in this study were consistently higher than C57BL/6 mice at each time point confirming presence of chronic inflammation in the *Winnie* mice (*P*<0.001 for all; Fig. 4.2A-C). Some variation in Lcn-2 levels was observed in individual *Winnie* mice, but not in C57BL/6 mice (examples for *n*=6/group are presented in Fig. 4.2A).

Gross morphological damage was assessed in cross sections to further substantiate the level of inflammation in the distal colon (*n*=6/group; Fig. 4.3A-A^{l}). Consistent with earlier observations (Eri et al. 2011; McGuckin et al. 2011;

Heazlewood et al. 2008), *Winnie* mice exhibited blatant damage to the mucosa and epithelial lining, infiltration of leukocytes, crypt elongation and abscesses, and goblet cell loss (Fig. 4.3A^{I}). No abnormalities were evident in the colon from C57BL/6 mice (Fig. 4.3A). Thickening of the muscle layer is also considered as a histological index of inflammation (Miampamba and Sharkey 1998). The thickness of the colonic muscle layer (total thickness of longitudinal and circular muscles) was significantly higher in *Winnie* mice (101.3±2.8µm) compared to C57BL/6 (88.5±1.2µm) mice (n=4; P<0.05; Fig. 4.3B). *Winnie* mice had a significantly thicker mucosal layer (291.7±10.4µm) compared to C57BL/6 (226.6±8.3µm) mice (n=4; P<0.01; Fig. 4.3C). Histological scoring of H&E-stained sections incorporated the sum of individual scores for various parameters: aberrant crypt architecture, increased crypt length, goblet cell depletion, general leukocyte infiltration, crypt abscesses and epithelial damage and ulceration. Overall histological score was significantly higher in sections from *Winnie* mice compared to sections from C57BL/6 mice (P<0.001; Table 4.3; Fig. 4.3D).

The severity of inflammation was evaluated by immunolabeling with anti-CD45 antibody specific to the leukocyte common antigen in cross sections of the colon (n=6/group; Fig. 4.3E-E^{I}). Quantification of CD45-IR cell density revealed a higher level of leukocyte infiltration throughout the colon wall, as well as in mucosal and muscular layers, in sections from *Winnie* mice compared to C57BL/6 mice (P<0.05 for all; Table 4.3; Fig. 4.3F-H).

Figure 4.1. *Winnie* mouse model of spontaneous chronic colitis. Representative images of C57BL/6 (control) and *Winnie* mice. *Winnie* mice have hunchbacked posture, perianal inflammation, bleeding and soiled fur due to chronic diarrhea **(A-B)**. Soft fecal masses not forming pellets confirm non-watery diarrhea in *Winnie* mice compared to regular pellets in healthy C57BL/6 mice **(C)**. Fecal water content calculated as the difference (Δ) between wet and dry stool weight was higher in *Winnie* mice **(D)**. *Winnie* mice have lower average body weight compared to C57BL/6 mice **(E)**. Variation in colon length between C57BL/6 and *Winnie* mice **(F)**. ***P*<0.01, ****P*<0.001.

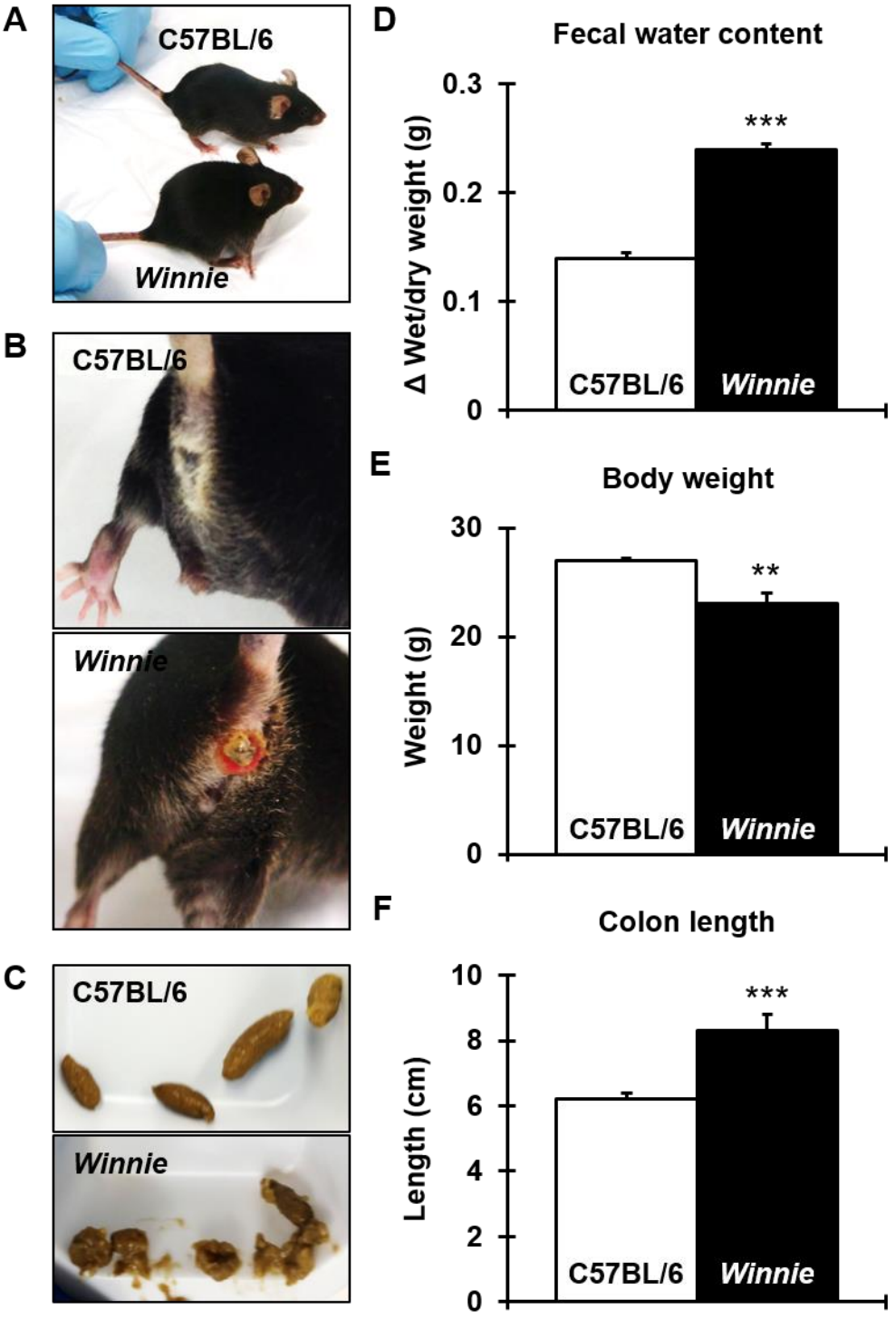
A
C57BL/6
Winnie
B
C57BL/6
Winnie
C
C57BL/6
Winnie
D
Fecal water content
Δ Wet/dry weight (g)
0.3
0.2
0.1
0
***
C57BL/6
Winnie
E
Body weight
Weight (g)
30
20
10
0
**
C57BL/6
Winnie
F
Colon length
Length (cm)
10
8
6
4
2
0
***
C57BL/6
Winnie

Table 4.3 Evaluation of intestinal inflammation

Parameter		**C57BL/6**	***Winnie***
Diarrhea		Absent (hard pellets)	Prominent (loose stools)
Fecal water content (wet weight minus dry weight, g)		0.14±0.005	0.24±0.005***
Colon length (from cecum to anus; cm)		6.2±0.2	8.3±0.5***
Density of CD45+ leukocytes in colon cross sections		5.2±0.6	9.8±1.2*
Density of CD45+ leukocytes in the mucosa of colon cross sections		6.9±0.8	12.2±1.4*
Density of CD45+ leukocytes in the muscle of colon cross sections		2.3±0.3	4.0±0.5*
Parameters for histological scoring	Aberrant crypt architecture (0-3)	0.33±0.05	2.33±0.06***
	Increased crypt length (0-3)	0.25±0.04	2.33±0.05***
	Goblet cell depletion (0-3)	0.25±0.03	2.25±0.03***
	General leukocyte infiltration (0-3)	0.17±0.1	2.25±0.12***
	Crypt abscesses (0-3)	0.25±0.15	2.50±0.15***
	Epithelial damage and ulceration (0-3)	0.33±0.34	2.55±0.35***
Overall histological score (out of 18)		3.1±0.6	14.4±0.6***

*P<0.05, ***P<0.001.

Figure 4.2. Assessment of colonic inflammation with fecal lipocalin (Lcn)-2. Examples of Lcn-2 level quantified in fecal samples from C57BL/6 (C1-C6) and *Winnie* (W1-W6) mice to indicate colonic inflammation. Fecal samples were collected from the same mouse twice weekly for 28d and compared both individually **(A)** and between groups **(B)**. Average fecal Lcn-2 protein levels at the time of tissue collection for *ex vivo* experiments C57BL/6 and *Winnie* mice **(C)**. d = days. ****P*<0.001.

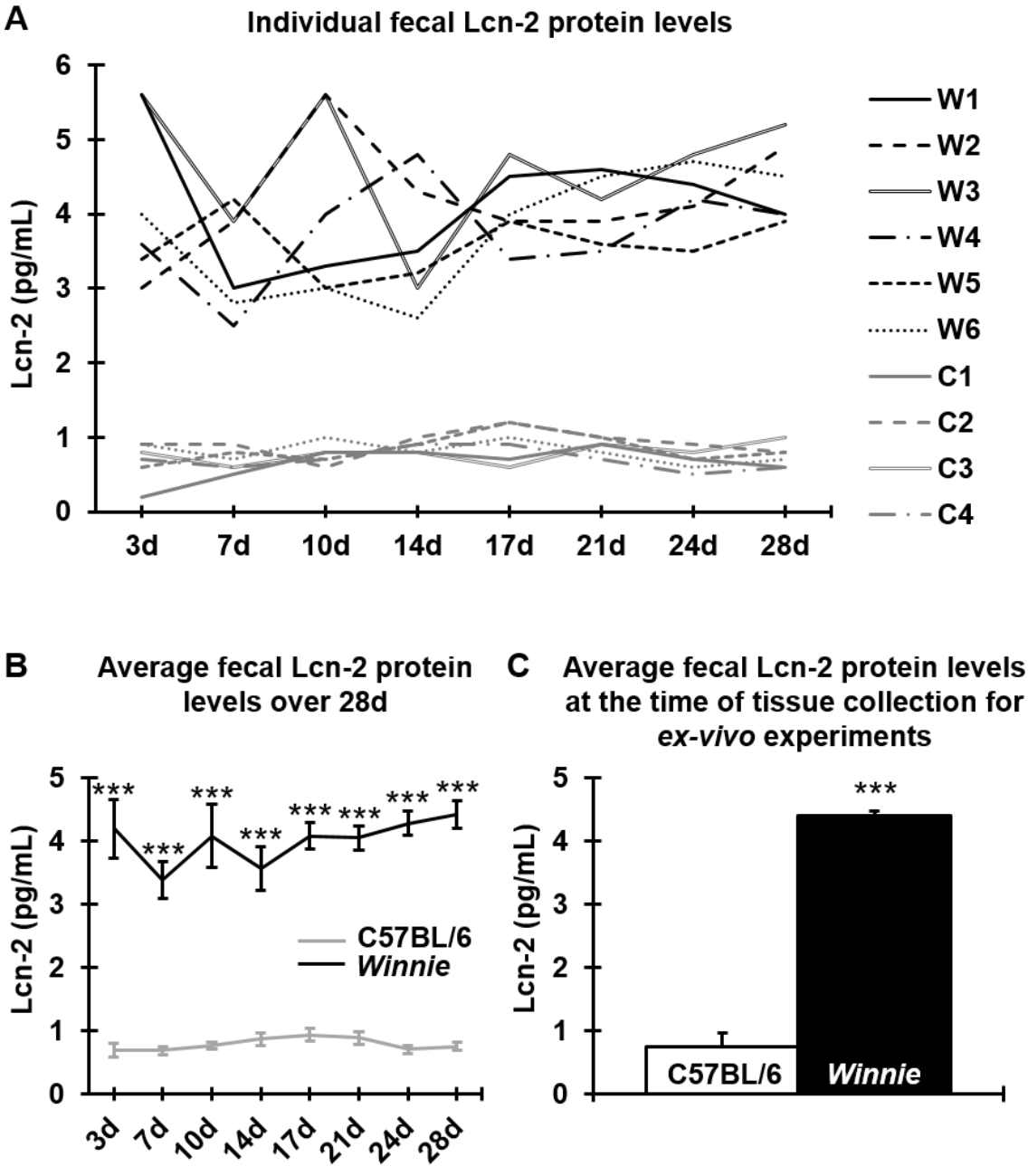
A
Individual fecal Lcn-2 protein levels
Lcn-2 (pg/mL)
0
1
2
3
4
5
6
3d
7d
10d
14d
17d
21d
24d
28d
W1
W2
W3
W4
W5
W6
C1
C2
C3
C4
B
Average fecal Lcn-2 protein levels over 28d
Lcn-2 (pg/mL)
***
C57BL/6
Winnie
C
Average fecal Lcn-2 protein levels at the time of tissue collection for ex-vivo experiments
Lcn-2 (pg/mL)
***
C57BL/6
Winnie

Figure 4.3. Histological and immunohistochemical evidence of colitis in *Winnie* mice. Hematoxylin and eosin (H&E) staining of the distal colon sections from C57BL/6 **(A)** and *Winnie* **(A^I)** mice. Increased thickness of muscle layers and elongation of crypts observed in the distal colon from *Winnie* compared to C57BL/6 mice **(B-C)**. Overall histological score based on the analysis of six individual parameters from H&E-stained sections **(D)**. Anti-CD45 antibody labeling of leukocyte infiltration (arrows) within the colon wall from C57BL/6 **(E)** and *Winnie* **(E^I)** mice. Density of CD45-IR cells in colon cross sections **(F-H)**. Scale bars = 100μm. **P*<0.05, ***P*<0.01, ****P*<0.001.

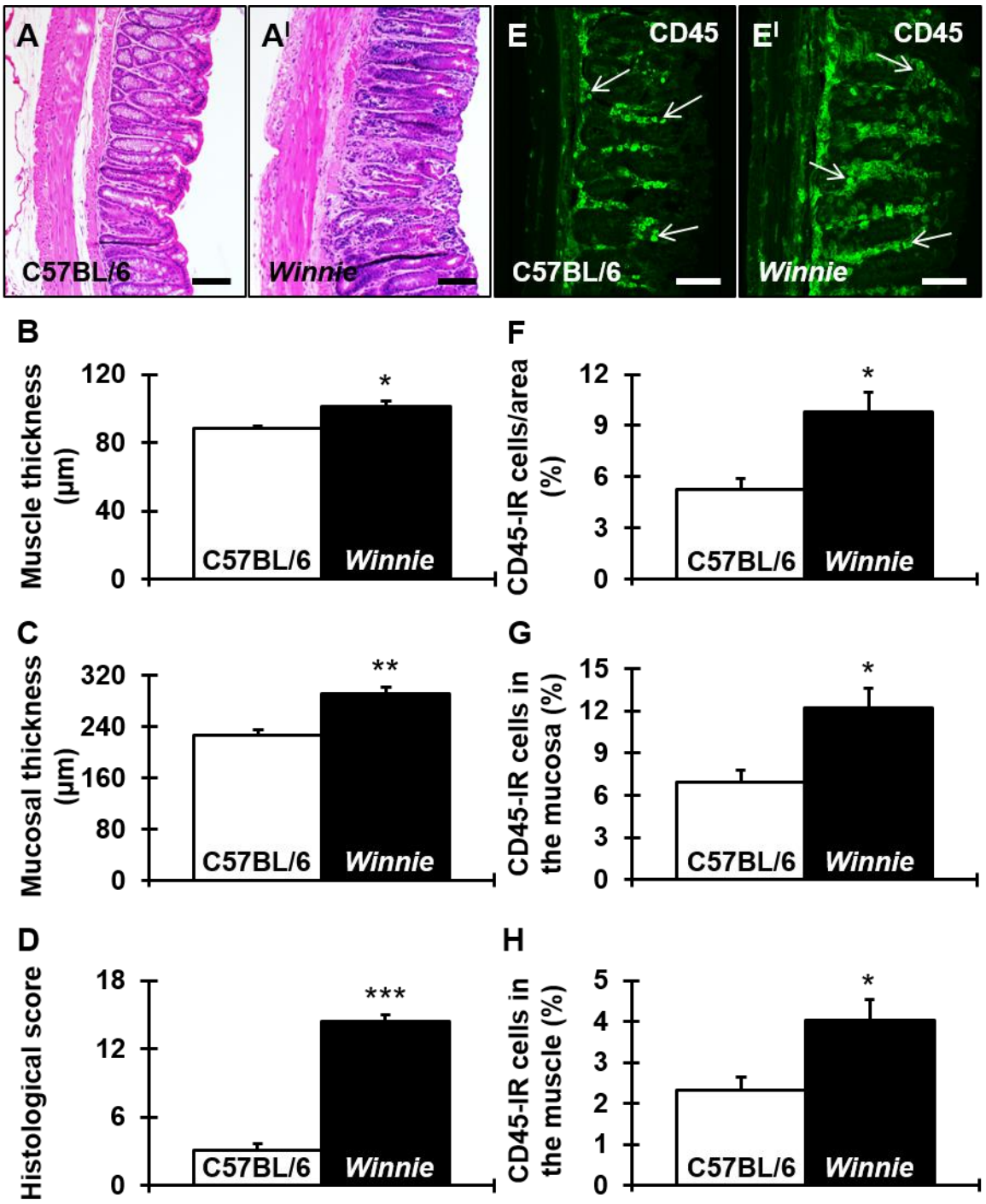
A
C57BL/6
A'
Winnie
E
CD45
C57BL/6
E'
CD45
Winnie
B
Muscle thickness (µm)
120
80
40
0
*
C57BL/6
Winnie
F
CD45-IR cells/area (%)
12
9
6
3
0
*
C57BL/6
Winnie
C
Mucosal thickness (µm)
320
240
160
80
0
**
C57BL/6
Winnie
G
CD45-IR cells in the mucosa (%)
15
12
9
6
3
0
*
C57BL/6
Winnie
D
Histological score
18
12
6
0
***
C57BL/6
Winnie
H
CD45-IR cells in the muscle (%)
5
4
3
2
1
0
*
C57BL/6
Winnie

4.4.2 Changes in the density of nerve fibers in the distal colon of *Winnie* mice

Anti-β-Tubulin (III) antibody was used to identify nerve fibers innervating the mucosa and smooth muscle in cross sections of the distal colon from C57BL/6 and *Winnie* mice (*n*=6/group). Colon sections from C57BL/6 mice showed orderly arrangement of β-Tubulin (III)-IR fibers within the mucosal gland cores, submucosal and muscular layers of the colonic wall (Fig. 4.4A). In contrast, sections from *Winnie* mice showed β-Tubulin (III)-IR fibers to be fragmented, disorderly, and erratically distributed within the mucosa (Fig. 4.4A^{I}). Quantification of fiber density revealed a reduction in β-Tubulin (III)-IR fibers throughout the colon wall in sections from *Winnie* mice (5.7±0.4%) when compared to C57BL/6 mice (9.0±0.5%; *P*<0.01; Fig. 4.4B). In addition, the density of β-Tubulin (III)-IR fibers was less in both the mucosa (C57BL/6: 7.0±0.8%; *Winnie*: 3.4±0.4%; *P*<0.05; Fig. 4.4C) and muscular (C57BL/6: 14.9±0.2%; *Winnie*: 11.8±0.7%; *P*<0.05; Fig. 4.4D) layers in sections from *Winnie* mice.

4.4.3 Changes in the density of cholinergic nerve fibers in the distal colon of *Winnie* mice

Anti-VAChT antibody was used as a marker for cholinergic fibers accumulating acetylcholine (ACh) in synaptic vesicles in both cross sections and wholemount LMMP preparations of the distal colon (*n*=6/group; Figs. 4.5A-A^{I} and 4.6A-A^{I}). The density of cholinergic fibers was decreased throughout the colon wall in the cross section preparations from *Winnie* (2.4±0.3%) compared to C57BL/6 (4.5±0.3%; *P*<0.001) mice (Fig. 4.5B). This result was reflected in reduced VAChT-IR within both mucosal and muscle layers of the colon from *Winnie* (mucosa: 0.7±0.1%; muscle: 7.5±0.9%) compared to C57BL/6 (mucosa: 1.2±0.1%, *P*<0.05; muscle: 14.9±0.7%, *P*<0.001) mice (Fig. 4.5C-D). Similarly, a significant decrease in VAChT-IR fibers within the myenteric ganglia was observed in wholemount LMMP preparations of the distal colon from *Winnie* (ganglia: 24.4±0.7%; area: 5.6±0.3%) compared to C57BL/6 (ganglia: 31.2±1.6%; area: 7.8±0.5%; *P*<0.05 for both) mice (Fig. 4.6B-C).

4.4.4 Changes in the density of noradrenergic nerve fibers in the distal colon of *Winnie* mice

To assess changes in the expression of noradrenergic fibers, we evaluated the density of TH-IR fibers in both cross sections and wholemount LMMP preparations of the distal colon in *Winnie* mice (*n*=6; Figs. 4.7A^{I} and 4.8A^{I}) compared to C57BL/6 mice (*n*=6; Figs. 4.7A and 4.8A). The density of noradrenergic fibers was decreased throughout the colon wall in the cross section preparations from *Winnie* (1.2±0.1%) compared to C57BL/6 (2.6±0.4%; *P*<0.05) mice (Fig. 4.7B). When analysis was isolated to the mucosal (C57BL/6: 1.9±0.2%; *Winnie*: 1.0±0.1%; *P*<0.05; Fig. 4.7C) and muscular (C57BL/6: 4.3±0.7%; *Winnie*: 1.9±0.3%; *P*<0.05; Fig. 4.7D) layers of the colon, the density of TH-IR fibers was consistently less in sections from *Winnie* mice. A significant decrease in the density of TH-IR fibers was observed in LMMP preparations of the distal colon from *Winnie* (ganglia: 14.9±0.5%; area: 3.7±0.1%) compared to C57BL/6 (ganglia: 21.7±0.5%, *P*<0.001; area: 6.0±0.1%, *P*<0.001) mice (Fig. 4.8B-C).

4.4.5 Changes in the density of sensory nerve fibers in the distal colon of *Winnie* mice

Intrinsic primary afferent neurons contain and release CGRP (Grider 2003). Additionally, approximately 85% of spinal afferents and less than 5% of vagal afferents contain CGRP, thus anti-CGRP antibody is recognized as a marker for sensory afferent fibers (Kressel et al. 1994). In this study, immunolabeling using anti-CGRP antibody was carried out to reveal sensory nerve fibers in both cross sections and wholemount LMMP preparations of the distal colon (*n*=6/group; Figs. 4.9 and 4.10). CGRP-IR nerve fibers were widely distributed in the mucosa, myenteric plexus and muscle layers of the colon in C57BL/6, but not *Winnie* mice (Figs. 4.9A-A^{I} and 4.10A-A^{I}). Quantitative analysis revealed a significant decrease in the density of CGRP-IR nerve fibers throughout the colon wall (C57BL/6: 9.4±0.9%; *Winnie*: 3.4±0.2%), as well as in the mucosal (C57BL/6: 8.4±0.5%; *Winnie*: 2.7±0.3%) and muscular layers (C57BL/6: 13.2±1.0%; *Winnie*:

6.7±0.7%), in cross section preparations from *Winnie* compared to C57BL/6 mice (*P*<0.001 for all; Fig. 4.9B-D). Similarly, less CGRP-IR fibers were observed in wholemount LMMP preparations of the distal colon from *Winnie* (ganglia: 20.3±1.4%; area: 4.9±0.6%) when compared to C57BL/6 (ganglia: 27.2±1.4%; area: 6.6±0.3%) mice (ganglia: *P*<0.01; area: *P*<0.05; Fig. 4.10B-C).

Figure 4.4. Nerve fiber density in cross sections of the distal colon from C57BL/6 and *Winnie* mice. Anti-β-Tubulin (III) antibody was used to label nerve fibers in cross sections of the distal colon from C57BL/6 **(A)** and *Winnie* **(A^{l})** mice. Scale bars = 100μm. Quantitative analyses of β-Tubulin (III)-IR throughout the colon wall **(B)**, in the mucosa **(C)** and within the muscular layers **(D)**. **P*<0.05, ***P*<0.01.

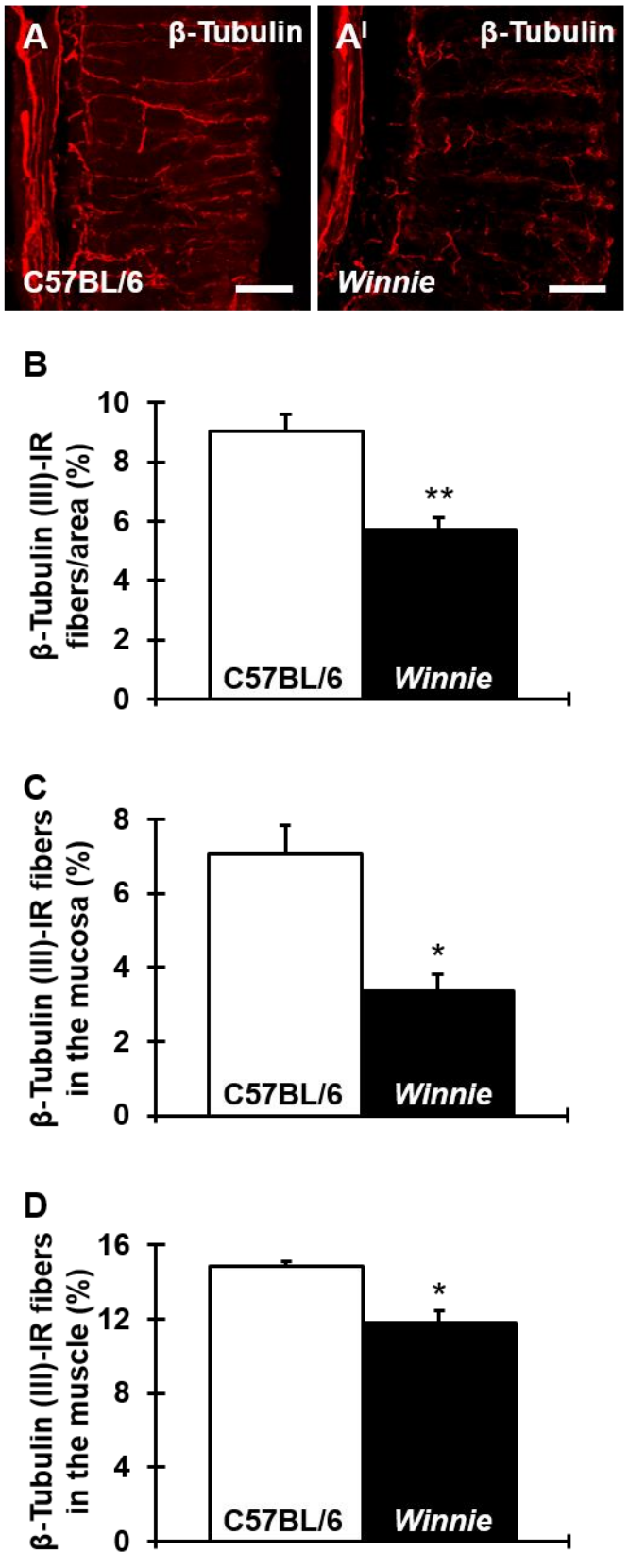
A
β-Tubulin
C57BL/6
A'
β-Tubulin
Winnie
B
β-Tubulin (III)-IR fibers/area (%)
10
8
6
4
2
0
**
C57BL/6
Winnie
C
β-Tubulin (III)-IR fibers in the mucosa (%)
8
6
4
2
0
*
C57BL/6
Winnie
D
β-Tubulin (III)-IR fibers in the muscle (%)
16
12
8
4
0
*
C57BL/6
Winnie

Figure 4.5. Cholinergic nerve fiber density in cross sections of the distal colon from C57BL/6 and *Winnie* mice. Anti-VAChT antibody was used to label cholinergic nerve fibers in cross sections of the distal colon from C57BL/6 **(A)** and *Winnie* **(A^{I})** mice. Scale bars = 100µm. Quantitative analyses of VAChT-IR throughout the colon wall **(B)**, in the mucosa **(C)** and within the muscular layers **(D)**. *P<0.05, ***P<0.001.

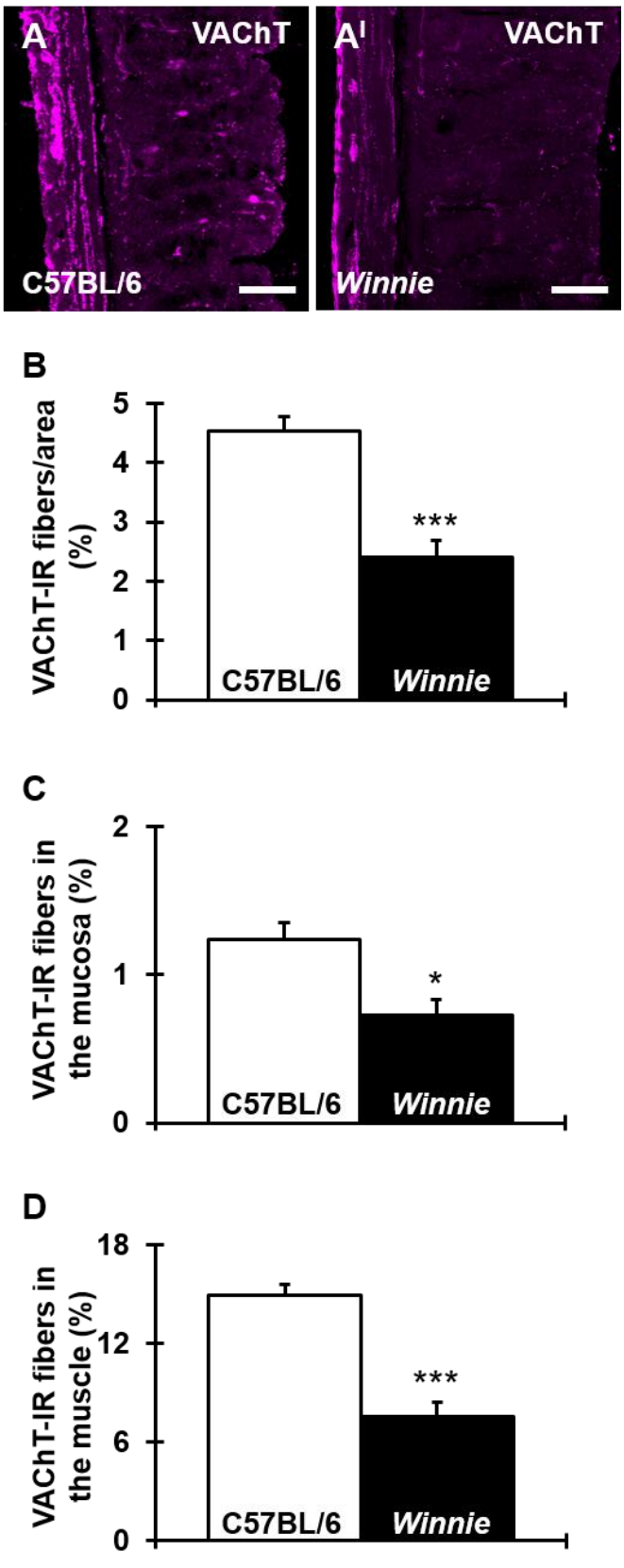
A
VAChT
C57BL/6
A'
VAChT
Winnie
B
VAChT-IR fibers/area (%)
5
4
3
2
1
0
***
C57BL/6
Winnie
C
VAChT-IR fibers in the mucosa (%)
2
1
0
*
C57BL/6
Winnie
D
VAChT-IR fibers in the muscle (%)
18
12
6
0
***
C57BL/6
Winnie

Figure 4.6. Cholinergic nerve fiber density in LMMP preparations of the distal colon from C57BL/6 and *Winnie* mice. Anti-VAChT antibody was used to label cholinergic nerve fibers in LMMP preparations of the distal colon from C57BL/6 **(A)** and *Winnie* **(A^{I})** mice. Scale bars = 100μm. Quantitative analyses of VAChT-IR per ganglion **(B)** and per 2mm^2 area **(C)** of the colon. **P*<0.05.

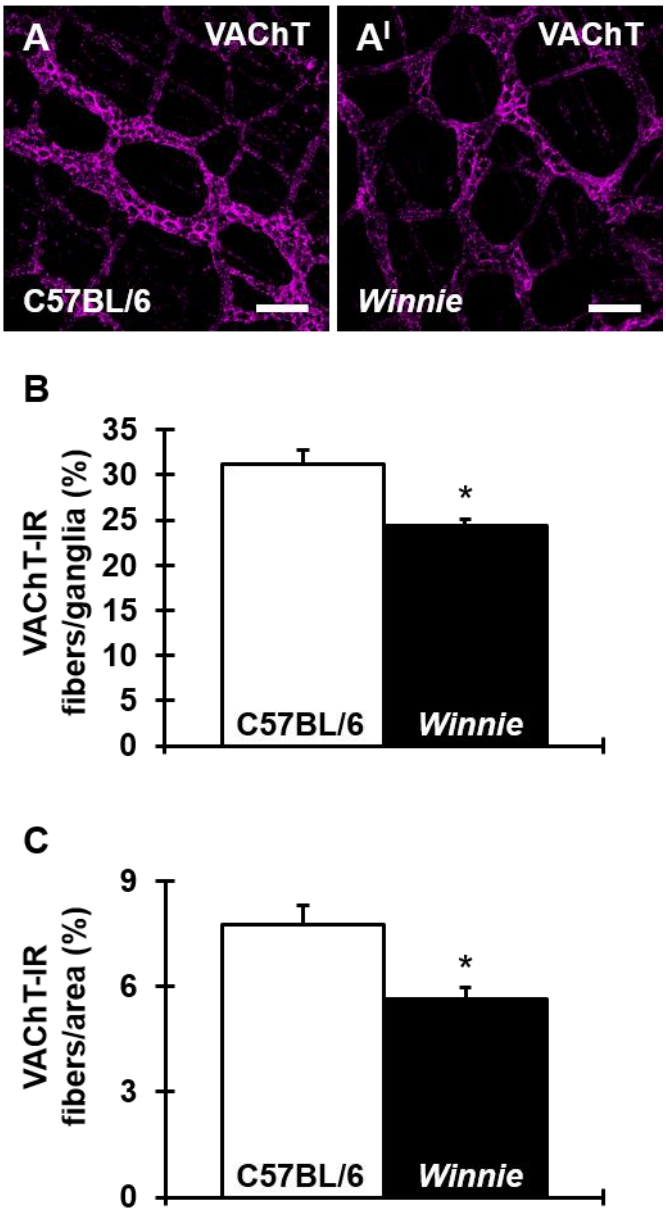
A
VAChT
C57BL/6
A'
VAChT
Winnie
B
VAChT-IR
fibers/ganglia (%)
35
30
25
20
15
10
5
0
*
C57BL/6
Winnie
C
VAChT-IR
fibers/area (%)
9
6
3
0
*
C57BL/6
Winnie

Figure 4.7. Noradrenergic nerve fiber density in cross sections of the distal colon from C57BL/6 and *Winnie* mice. Anti-TH antibody was used to label noradrenergic nerve fibers in cross sections of the distal colon from C57BL/6 **(A)** and *Winnie* **(A^{I})** mice. Scale bars = 100μm. Quantitative analyses of TH-IR throughout the colon wall **(B)**, in the mucosa **(C)** and within the muscular layers **(D)**. **P*<0.05.

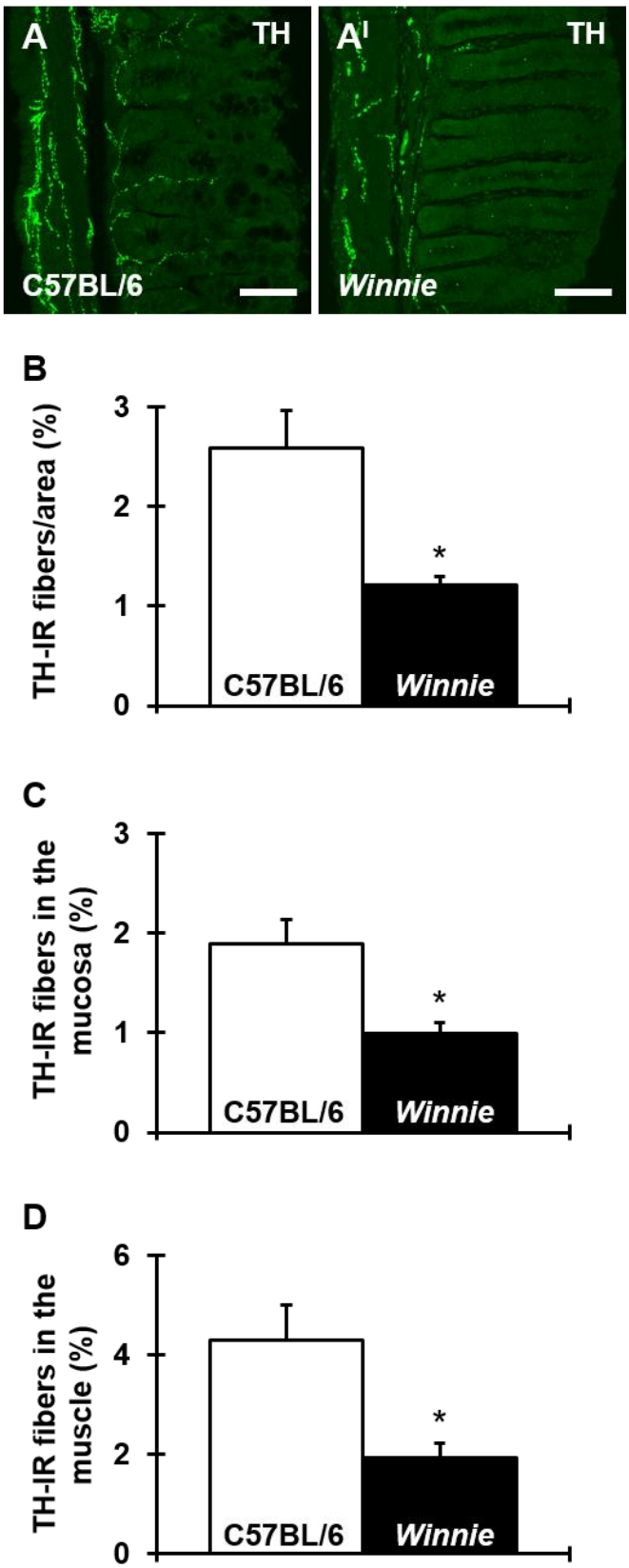
A
TH
C57BL/6
A'
TH
Winnie
B
TH-IR fibers/area (%)
3
2
1
0
*
C57BL/6
Winnie
C
TH-IR fibers in the mucosa (%)
3
2
1
0
*
C57BL/6
Winnie
D
TH-IR fibers in the muscle (%)
6
4
2
0
*
C57BL/6
Winnie

Figure 4.8. Noradrenergic nerve fiber density in LMMP preparations of the distal colon from C57BL/6 and *Winnie* mice. Anti-TH antibody was used to label noradrenergic nerve fibers in LMMP preparations of the distal colon from C57BL/6 **(A)** and *Winnie* **(A^{I})** mice. Scale bars = 100µm. Quantitative analyses of TH-IR per ganglion **(B)** and per 2mm^2 area **(C)** of the colon. ****P*<0.001.

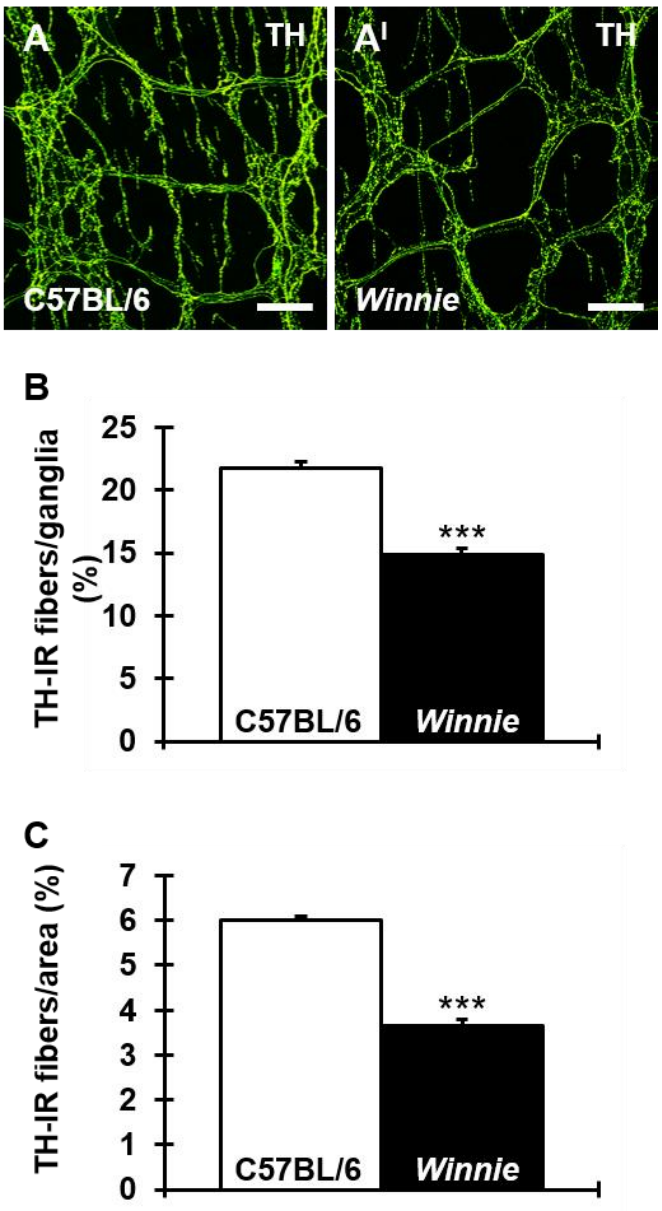
A
TH
C57BL/6
A'
TH
Winnie
B
TH-IR fibers/ganglia (%)
25
20
15
10
5
0
***
C57BL/6
Winnie
C
TH-IR fibers/area (%)
7
6
5
4
3
2
1
0
***
C57BL/6
Winnie

Figure 4.9. Sensory nerve fiber density in cross sections of the distal colon from C57BL/6 and *Winnie* mice. Anti-CGRP antibody was used to label sensory nerve fibers in cross sections of the distal colon from C57BL/6 **(A)** and *Winnie* **(A^{I})** mice. Scale bars = 100μm. Quantitative analyses of CGRP-IR throughout the colon wall **(B)**, in the mucosa **(C)** and within the muscular layers **(D)**. ****P*<0.001.

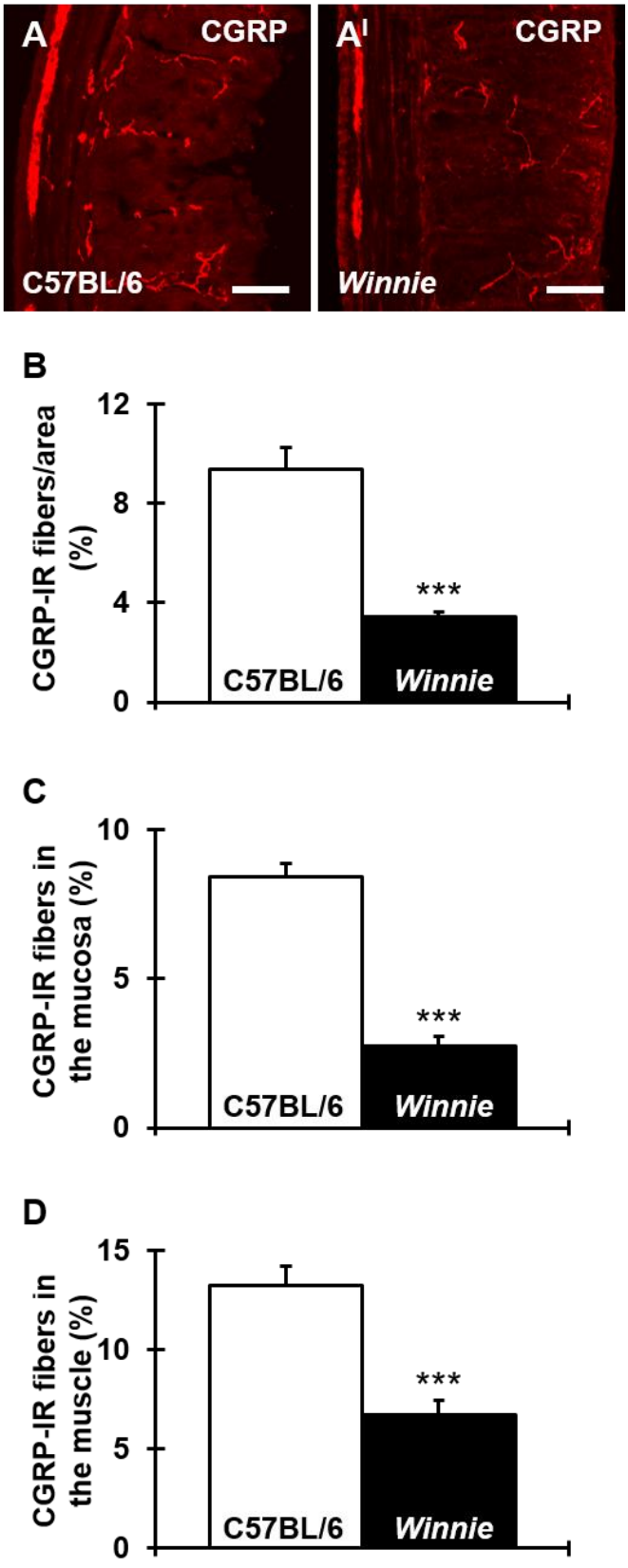
A
CGRP
C57BL/6
A'
CGRP
Winnie
B
CGRP-IR fibers/area (%)
12
8
4
0
***
C57BL/6
Winnie
C
CGRP-IR fibers in the mucosa (%)
10
5
0
***
C57BL/6
Winnie
D
CGRP-IR fibers in the muscle (%)
15
10
5
0
***
C57BL/6
Winnie

Figure 4.10. Sensory nerve fiber density in LMMP preparations of the distal colon from C57BL/6 and *Winnie* mice. Anti-CGRP antibody was used to label sensory nerve fibers in LMMP preparations of the distal colon from C57BL/6 **(A)** and *Winnie* **(A^{I})** mice. Scale bars = 100μm. Quantitative analyses of CGRP-IR per ganglion **(B)** and per 2mm^2 area **(C)** of the colon. *P<0.05, **P<0.01.

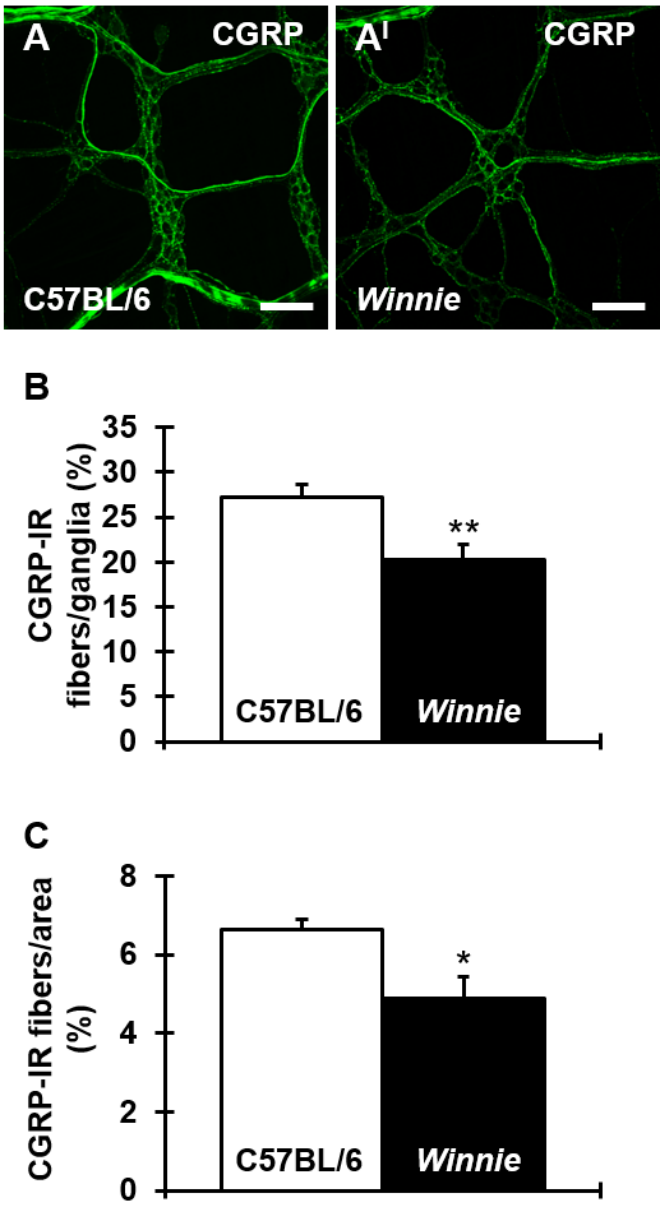
A
CGRP
C57BL/6
A'
CGRP
Winnie
B
CGRP-IR fibers/ganglia (%)
35
30
25
20
15
10
5
0
**
C57BL/6
Winnie
C
CGRP-IR fibers/area (%)
8
6
4
2
0
*
C57BL/6
Winnie

4.4.6 Changes in the average number of PGP9.5-IR and ChAT-IR, but not nNOS-IR myenteric neurons, in the distal colon of *Winnie* mice

The pan-neuronal marker PGP9.5 was used to identify all myenteric neurons in wholemount LMMP preparations of the distal colon from C57BL/6 and *Winnie* mice (*n*=6/group; Fig. 4.11A-A^{I}). The average number of PGP9.5-IR neurons per ganglionic area was 22±0.3 in colons from healthy C57BL/6 mice. A reduced number of PGP9.5-IR neurons were quantified in the inflamed distal colon from *Winnie* mice (19±0.4 cells/ganglionic area; *P*<0.001; Fig. 4.11B). Subsequently, a 14% loss in the ganglionic density of PGP9.5-IR neurons was calculated in tissues from *Winnie* mice (85.8±2.2%) compared to LMMP preparations from C57BL/6 mice (100%; *P*<0.01; Fig. 4.11C).

Anti-nNOS antibody, which identifies predominantly inhibitory muscle motor neurons (Qu et al. 2008), was used to quantify the average number of nNOS-IR neurons in wholemount LMMP preparations of the distal colon (*n*=6/group; Fig. 4.12A-B^{I}). Immunofluorescence staining showed no significant difference in the average number of nNOS-IR neurons counted per ganglionic area (C57BL/6: 7±0.4 cells/ganglionic area; *Winnie*: 7±0.3 cells/ganglionic area; Fig. 4.12C). Hence, ganglionic density of nNOS-IR neurons in tissues from *Winnie* mice (100±6.6%) was similar to tissues from C57BL/6 mice (100%; Fig. 4.12D). The proportion of nNOS-IR neurons to the total number of neurons per ganglionic area was higher in preparations from *Winnie* (37.5±1.2%) when compared to tissues from C57BL/6 (32.1±1.9%) mice (*P*<0.05; Fig. 4.12E). Although there were no changes in the average number of nitrergic neurons between groups, the significant loss of PGP9.5-IR neurons observed in the *Winnie* mouse distal colon ensued the increase in the proportion of nNOS-IR in preparations from *Winnie* mice.

Anti-ChAT antibody labels excitatory muscle motor neurons and was used to identify cholinergic neurons in wholemount LMMP preparations of the distal colon from C57BL/6 and *Winnie* mice (*n*=6/group; Fig. 4.13A-B^{I}). The average number of ChAT-IR neurons per ganglionic area was significantly less in tissues from *Winnie* mice (9±0.3 cells/ganglionic area) when compared to preparations from

C57BL/6 mice (11±0.3 cells/ganglionic area; $P<0.01$; Fig. 4.13C). As a result, the ganglionic density of ChAT-IR neurons was reduced in the *Winnie* mouse distal colon (82.4±4.4%) indicating a 18% loss of cholinergic neurons to be associated with chronic inflammation in this experimental model ($P<0.05$; Fig. 4.13D). The loss of ChAT-IR neurons in tissues from *Winnie* mice corresponded with the loss of PGP9.5-IR neurons. Thus, there were no differences in the proportion of ChAT-IR to PGP-IR neurons between groups (C57BL/6: 51.8±1.3%; *Winnie*: 49.7±2.8%; Fig. 4.13E).

Figure 4.11. The average number of myenteric neurons in the distal colon from C57BL/6 and *Winnie* mice. Anti-PGP9.5 antibody was used to label myenteric neurons in LMMP preparations of the distal colon from C57BL/6 **(A)** and *Winnie* **(A^{I})** mice. Scale bars = 100μm. Quantitative analyses of the average number of PGP9.5-IR neurons normalized to 0.1mm^2 ganglionic area **(B)**. Ganglionic density of PGP9.5-IR neurons in tissues from *Winnie* mice as a percentage of control (100%) **(C)**. ***P*<0.01, ****P*<0.001.

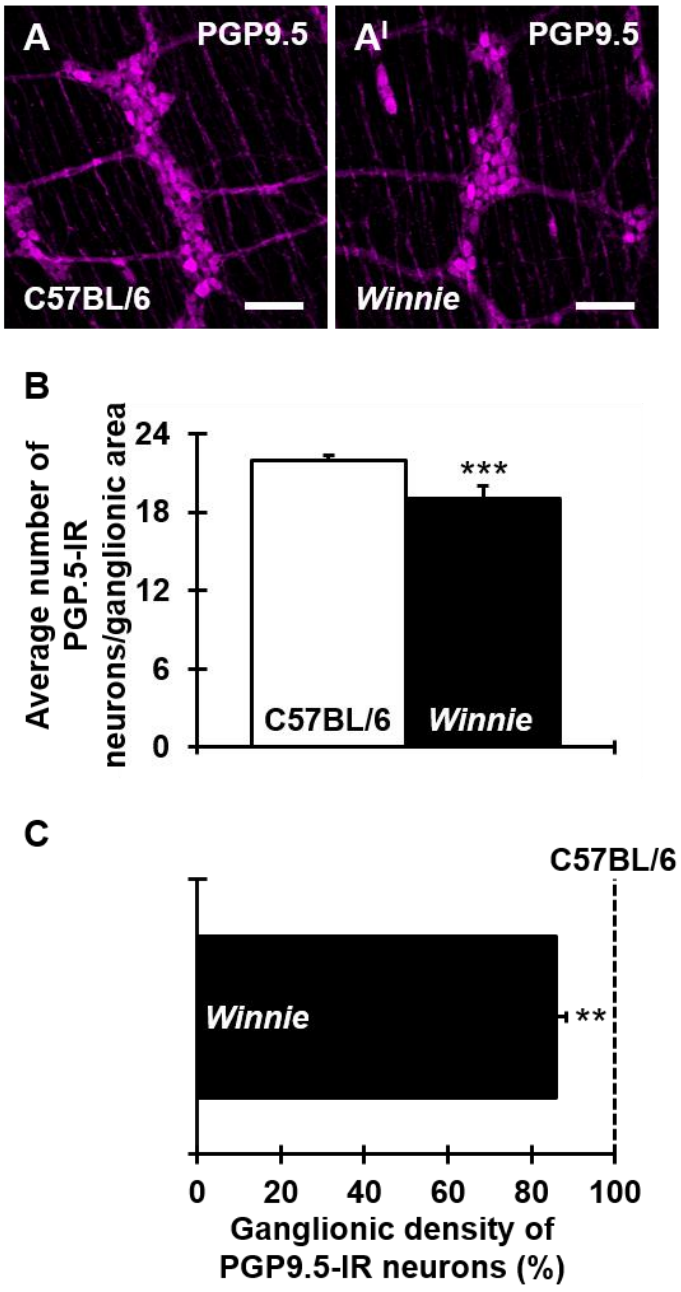
A
PGP9.5
C57BL/6
A'
PGP9.5
Winnie
B
Average number of PGP.5-IR neurons/ganglionic area
24
18
12
6
0
***
C57BL/6
Winnie
C
C57BL/6
Winnie
**
0
20
40
60
80
100
Ganglionic density of PGP9.5-IR neurons (%)

Figure 4.12. The average number of myenteric nitrergic neurons in the distal colon from C57BL/6 and *Winnie* mice. Anti-nNOS antibody was used to label nitrergic neurons in LMMP preparations of the distal colon from C57BL/6 **(A)** and *Winnie* **(B)** mice. The merged images of PGP9.5-IR (red) and nNOS-IR (green) neurons indicate the subpopulation of nNOS-IR neurons within the total population of myenteric neurons **(A^{I}-B^{I})**. Scale bars = 100µm. Quantitative analyses of the average number of nNOS-IR neurons normalized to 0.1mm^2 ganglionic area **(C)**. Ganglionic density of nNOS-IR neurons in tissues from *Winnie* mice as a percentage of control (100%) **(D)**. The proportion of nNOS-IR neurons to PGP9.5-IR neurons per ganglionic area **(E)**. *P<0.05.

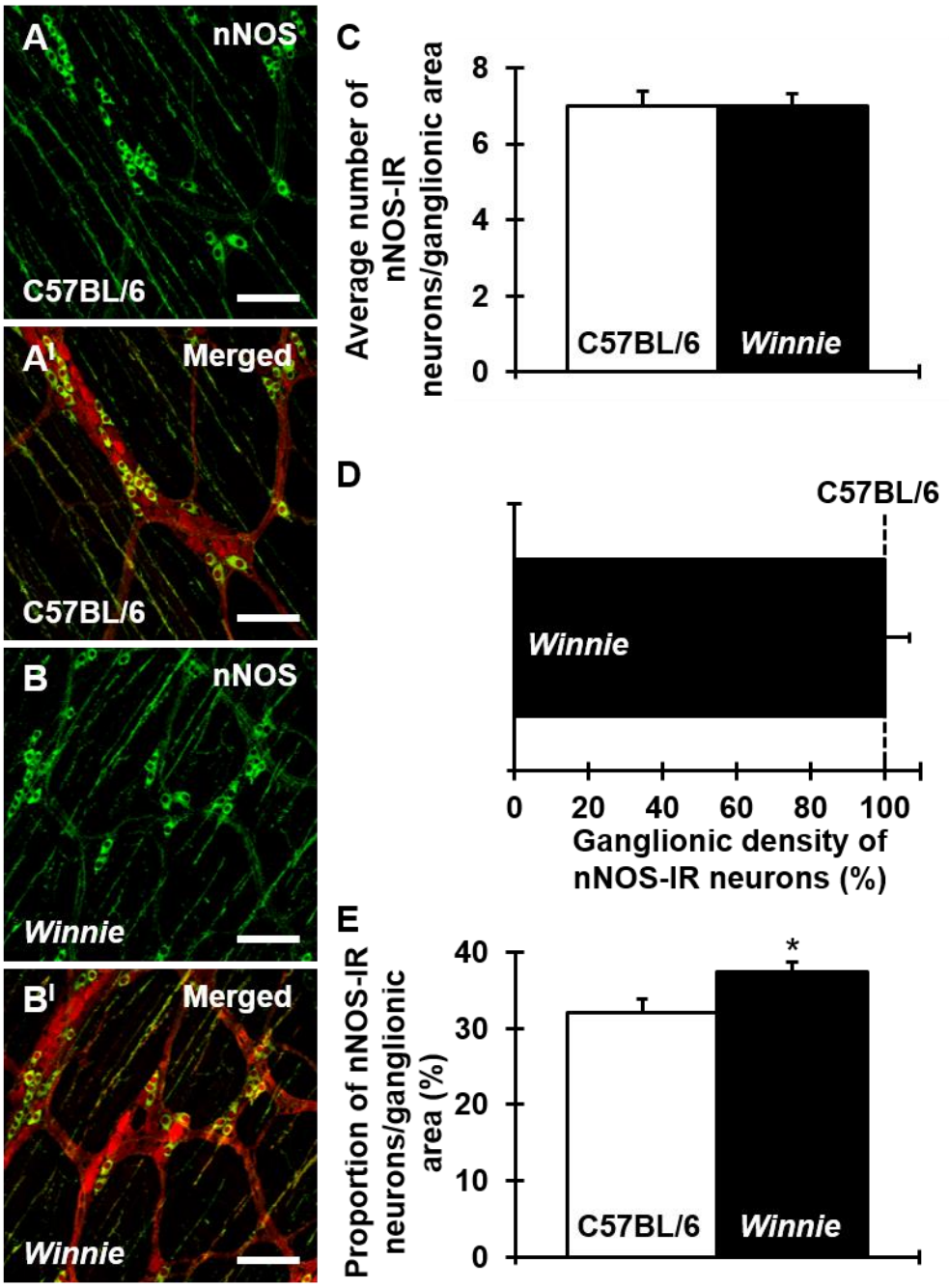
A
nNOS
C57BL/6
A'
Merged
C57BL/6
B
nNOS
Winnie
B'
Merged
Winnie
C
Average number of nNOS-IR neurons/ganglionic area
8
6
4
2
0
C57BL/6
Winnie
D
C57BL/6
Winnie
0
20
40
60
80
100
Ganglionic density of nNOS-IR neurons (%)
E
Proportion of nNOS-IR neurons/ganglionic area (%)
40
30
20
10
0
*
C57BL/6
Winnie

Figure 4.13. The average number of myenteric cholinergic neurons in the distal colon from C57BL/6 and *Winnie* mice. Anti-ChAT antibody was used to label cholinergic neurons in LMMP preparations of the distal colon from C57BL/6 **(A)** and *Winnie* **(B)** mice. The merged images of PGP9.5-IR (red) and ChAT-IR (green) neurons indicate the subpopulation of ChAT-IR neurons within the total population of myenteric neurons **(A^{I}-B^{I})**. Scale bars = 100µm. Quantitative analyses of the average number of ChAT-IR neurons normalized to 0.1mm^2 ganglionic area **(C)**. Ganglionic density of ChAT-IR neurons in tissues from *Winnie* mice as a percentage of control (100%) **(D)**. The proportion of ChAT-IR neurons to PGP9.5-IR neurons per ganglionic area **(E)**. **P*<0.05, ***P*<0.01.

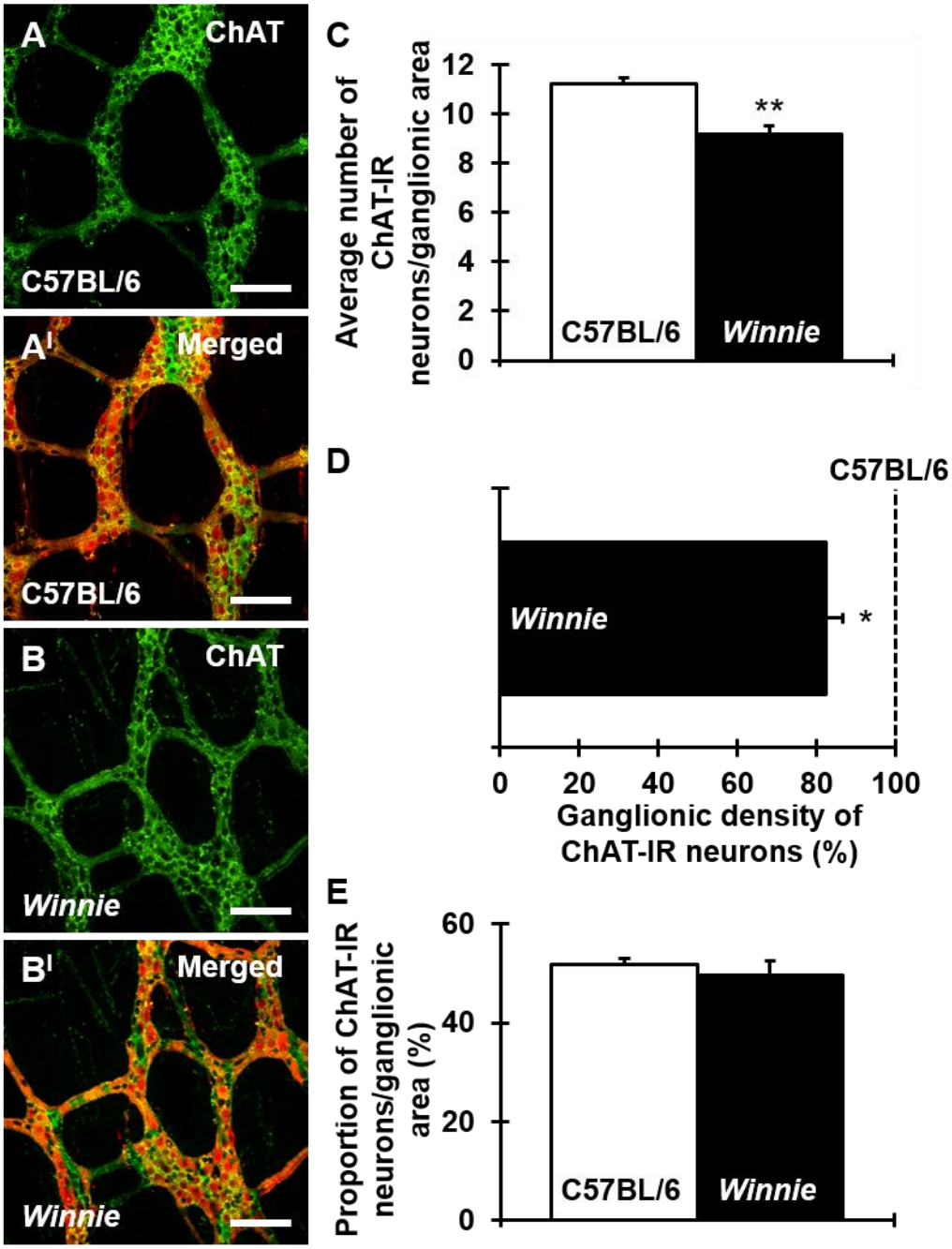
A
ChAT
C57BL/6
A'
Merged
C57BL/6
B
ChAT
Winnie
B'
Merged
Winnie
C
Average number of ChAT-IR neurons/ganglionic area
12
10
8
6
4
2
0
**
C57BL/6
Winnie
D
C57BL/6
Winnie
*
0
20
40
60
80
100
Ganglionic density of ChAT-IR neurons (%)
E
Proportion of ChAT-IR neurons/ganglionic area (%)
60
40
20
0
C57BL/6
Winnie

4.4.7 Altered gastrointestinal transit in *Winnie* mice

To determine differences in GI transit between *Winnie* and C57BL/6 mice (*n*=8/group), radiographic images were used to track barium sulfate from the stomach to the cecum (orocecal intestine transit time (OCTT)), as well as from the cecum to the anus (colonic transit time (CTT); Fig. 4.14A-B). Diarrhea in *Winnie* mice is evident by long size of fecal mass moving from the cecum to the anus compared with the short defined pellets observed in C57BL/6 mice (arrows; Fig. 4.14A-B). Total transit time did not differ between C57BL/6 (221.3±25.7min) and *Winnie* (225.7±19.1min) mice. However, this masked substantial changes in transit within different gut regions. In C57BL/6 mice, OCTT was 164.4±24.5min, and CTT was 56.9±4.5min. In *Winnie* mice, although not statistically significant, OCTT was prolonged (190.0±18.0min) compared with C57BL/6 mice (Fig. 4.14C). On the other hand, CTT was significantly faster in *Winnie* mice (40.0±3.6min; $P<0.05$; Fig. 4.14C).

Figure 4.14. Gastrointestinal transit time in *Winnie* and C57BL/6 mice. Representative X-ray images of C57BL/6 **(A)** and *Winnie* **(B)** mice obtained every 30min from 0-210min after administration of barium sulfate by oral gavage. White arrows indicate long size of fecal mass suggesting diarrhea in *Winnie* mice compared with pellets in the C57BL/6 colon. Transit time (min) for barium sulfate moving from the stomach to the cecum (orocecal intestine transit time (OCTT)) and from the cecum to the anus (colonic transit time (CTT)) in C57BL/6 and *Winnie* mice **(C)**. **P*<0.05.

A C57BL/6

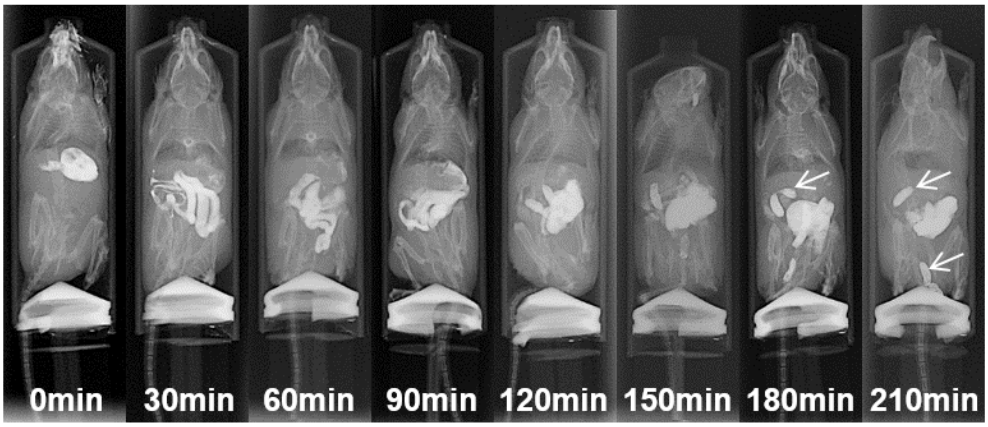

B *Winnie*

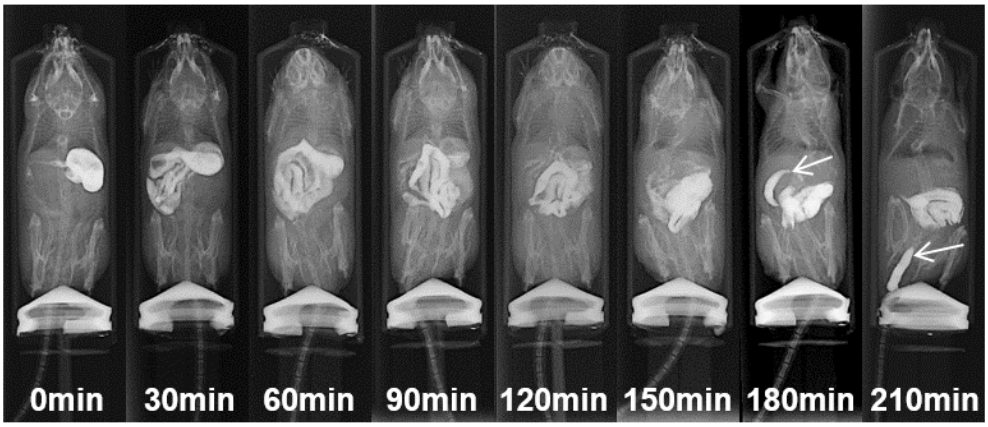

C

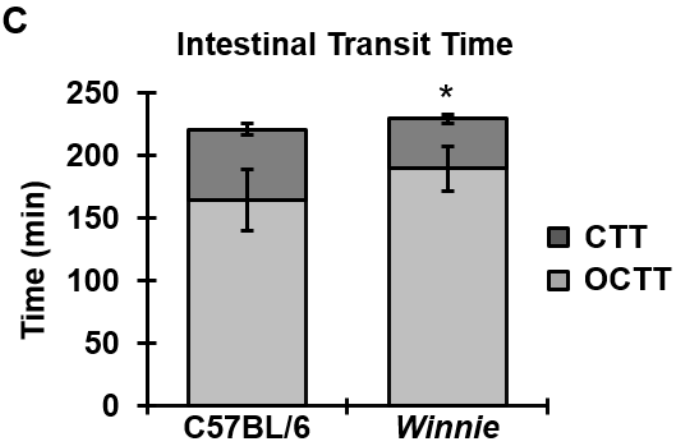

4.4.8 Altered patterns of colon contraction in *Winnie* mice

The total number of contractions was similar in the colons of C57BL/6 (*n*=8; 0cmH_2O: 17.7±1.4min^{-10}; 1cmH_2O: 16.5±1.7min^{-10}; 2cmH_2O: 18.1±1.6min^{-10}) and *Winnie* (*n*=13; 0cmH_2O: 23.0±2.2min^{-10}; 1cmH_2O: 22.3±2.4min^{-10}; 2cmH_2O: 22.1±1.3min^{-10}) mice at all levels of intraluminal pressure. However, further analysis of various types of motor patterns revealed significant differences between *Winnie* and C57BL/6 mice.

Three types of motor patterns (colonic migrating motor complexes (CMMCs), short contractions, and fragmented contractions) were identified and analyzed in the colon of *Winnie* (*n*=13) and C57BL/6 (*n*=8) mice. CMMCs were defined as propagating contractions appearing first at the proximal end and then sequentially over >50% of the distance to the distal end of the colon (Roberts et al. 2008a; 2007). The number of CMMCs was lower in the colon from *Winnie* mice at all levels of intraluminal pressure than in C57BL/6 colon (*P*<0.05 for all; Table 4.4; Fig. 4.15A-B). Similarly, the proportion of contractions identified as CMMCs was less in maps generated from the colons of *Winnie* than C57BL/6 colons (*P*<0.001 for all; Table 4.4; Fig. 4.15C).

Contractions that propagated <50% of the length of the colon were defined as short contractions (Fig. 4.16A). Both the frequency and proportion of short contractions were higher in the colons from *Winnie* mice than those from C57BL/6 mice (*P*<0.05 for all; Table 4.4; Fig. 4.16B-C). With increasing intraluminal pressure, the number and proportion of short contractions did not change significantly in the colons of both groups (Table 4.4; Fig. 4.16B-C). The numbers of short contractions initiated at the proximal, middle, and distal sections of the colon were quantified (Table 4.4; Fig. 4.16D-F). No significant changes in the frequency of short contractions were observed in either proximal or middle sections of the colon from both C57BL/6 and *Winnie* mice (Fig. 4.16D-E). However, increasing intraluminal pressure (>1cmH_2O) reduced the frequency of short contractions in the distal colon from C57BL/6 mice (*P*<0.05; Fig. 4.16F), but not *Winnie* mice, so the frequency of short contractions was significantly higher

in *Winnie* mice at increased levels of intraluminal pressure and was significantly different between the two genotypes (P<0.05; Table 4.4; Fig. 4.16F).

Fragmented contractions were defined as phasic non-propagating contractions occurring concurrently at various locations within the colon. They were easily distinguishable on spatiotemporal maps as distinct segmental contractions (solid arrows) and relaxations (dashed arrows; Fig. 4.17A). The frequency and proportion of fragmented contractions were significantly higher in *Winnie* mice than in C57BL/6 mice, regardless of the intraluminal pressure (Table 4.4; Fig. 4.17B-C). Increased intraluminal pressure initiated heightened numbers and proportion of fragmented contractions in both groups. Because of the low number of fragmented contractions in C57BL/6 colons at 0cmH_2O, we analyzed this in a slightly different way and compared the number of preparations exhibiting at least one fragmented contraction in the recording period between the two genotypes. At a baseline intraluminal pressure, 33±18% of C57BL/6 colons exhibited fragmented contractions, increasing to 44±17% and 56±17% at 1 and 2cmH_2O, respectively. In contrast, more colons from *Winnie* mice exhibited fragmented contractions at baseline and 1cmH_2O intraluminal pressure (77±10% for both; P<0.05 for both); this increased to 85±10% at 2cmH_2O (Fig. 4.17D).

Table 4.4. Parameters of different types of colonic contractions

		Intraluminal pressure		
		0cmH_2O	**1cmH_2O**	**2cmH_2O**
CMMCs				
Frequency (min^{-10})	**C57BL/6**	8.9±1.0	9.5±0.8	10.1±0.9
	Winnie	4.9±1.1*	5.5±1.1*	5.7±1.3*
Proportion (%)	**C57BL/6**	53.0±7.7	59.0±3.4	60.9±3.6
	Winnie	18.7±4.0***	20.9±5.1***	20.7±5.0***
Speed (mm/s)	**C57BL/6**	2.1±0.3	3.0±0.2	3.5±0.5
	Winnie	3.0±0.4^	3.2±0.2^	5.2±0.6*
Length (mm)	**C57BL/6**	35.7±1.7	33.6±1.7	30.8±1.3
	Winnie	34.7±1.8	35.0±1.8	32.4±1.9
Short contractions				
Frequency (min^{-10})	**C57BL/6**	8.5±1.5	6.3±1.3	5.8±1.4
	Winnie	14.2±1.8*	12.8±2.3*	10.4±1.2*
Proportion (%)	**C57BL/6**	45.6±7.3	36.1±3.0	29.9±5.5
	Winnie	60.4±3.7	51.8±6.6*	48.3±5.7*
Proximal colon frequency (min^{-10})	**C57BL/6**	1.1±0.9	0.8±0.4	0.8±0.3
	Winnie	2.9±1.3	1.2±0.7	1.5±0.6
Middle colon frequency (min^{-10})	**C57BL/6**	2.7±1.8	1.1±0.8	2.7±1.4
	Winnie	1.9±1.2	2.0±1.2	1.9±1.2
Distal colon frequency (min^{-10})	**C57BL/6**	25.3±5.0	13.0±2.3$^{\#}$	11.1±1.3$^{\#}$
	Winnie	25.5±4.4	26.2±4.9*	20.3±4.1*
Speed (mm/s)	**C57BL/6**	1.6±0.1†††	1.6±0.1†††	5.1±0.8
	Winnie	1.6±0.1^^	1.8±0.2^	2.7±0.3**
Length (mm)	**C57BL/6**	5.5±0.6	5.4±0.6	10.6±1.2
	Winnie	5.5±0.5	4.1±0.6	12.0±0.9
Fragmented contractions				
Frequency (min^{-10})	**C57BL/6**	0.3±0.2	0.7±0.4	2.3±0.7$^{\#}$
	Winnie	3.9±1.0**	4.0±0.6***	6.9±1.7*

Table 4.4 Parameters of different types of colonic contractions (continued)

		Intraluminal pressure		
		1cmH_2O	**1cmH_2O**	**1cmH_2O**
Fragmented contractions				
Proportion (%)	**C57BL/6**	1.5±0.7	5.0±3.0	13.8±4.2$^{\#}$
	Winnie	21.0±5.8*	21.9±4.2**	31.4±7.2*
Speed (mm/s)	**C57BL/6**	1.6±0.2††	2.3±0.7†	4.3±0.8
	Winnie	2.6±0.4	2.4±0.4^	3.8±0.5
Length (mm)	**C57BL/6**	23.9±2.1	25.8±3.9	26.5±3.9
	Winnie	25.6±1.3	26.5±1.0	31.2±1.5

*P<0.05, **P<0.01, ***P<0.001 significantly different to C57BL/6 at the same level of intraluminal pressure. ^P<0.05, ^^P<0.01 significantly different to *Winnie* at 2cmH_2O. $^{\dagger}P$<0.05, $^{\dagger\dagger}P$<0.01, $^{\dagger\dagger\dagger}P$<0.001 significantly different to C57BL/6 at 2cmH_2O. $^{\#}P$<0.05 significantly different to C57BL/6 at 0cmH_2O.

Figure 4.15. Frequency and proportion of colonic migrating motor complexes in *Winnie* and C57BL/6 mice. Examples of spatiotemporal maps depicting colonic contractions (red) and relaxations (blue) of whole length colons from C57BL/6 and *Winnie* mice. Black arrows indicate colonic migrating motor complexes (CMMCs) that propagate >50% of colon length **(A)**. Frequency of CMMCs per 10min counted at baseline (0cmH_2O), 1cmH_2O, and 2cmH_2O intraluminal pressure **(B**). The proportion of CMMCs to the total number of contractions was calculated at each level of intraluminal pressure **(C)**. *P<0.05, ***P<0.001 significantly different to C57BL/6 at the same level of intraluminal pressure.

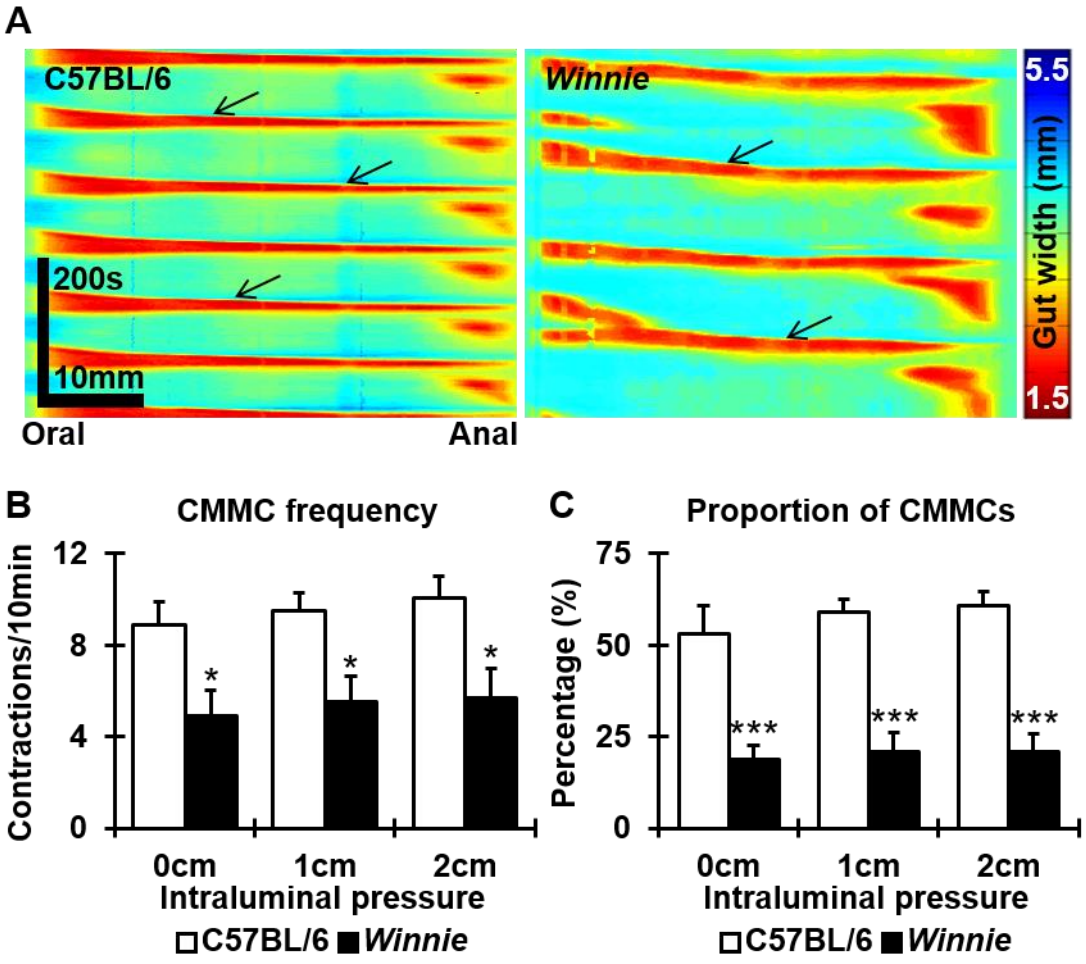
A
C57BL/6
Winnie
200s
10mm
Oral
Anal
5.5
Gut width (mm)
1.5
B
CMMC frequency
Contractions/10min
12
8
4
0
*
*
*
0cm
1cm
2cm
Intraluminal pressure
C57BL/6
Winnie
C
Proportion of CMMCs
Percentage (%)
75
50
25
0
***
***
***
0cm
1cm
2cm
Intraluminal pressure
C57BL/6
Winnie

Figure 4.16. Frequency and proportion of short contractions in *Winnie* and C57BL/6 mice. Examples of spatiotemporal map depicting short contractions that propagate <50% colon length in the proximal (P), middle (M), and distal (D) sections of the *Winnie* mouse colon **(A)**. Total number of short contractions counted in the colons from C57BL/6 and *Winnie* mice at baseline (0cmH_2O), 1cmH_2O, and 2cmH_2O intraluminal pressure **(B)**. The proportion of short contractions to the total number of contractions was calculated at each level of intraluminal pressure **(C)**. Frequency of short contractions occurring in the proximal **(D)**, middle **(E)**, and distal **(F)** sections of the C57BL/6 and *Winnie* mouse colon. **P*<0.05 compared to C57BL/6 at the same level of intraluminal pressure. $^{\#}P$<0.05 compared to C57BL/6 at 0cmH_2O.

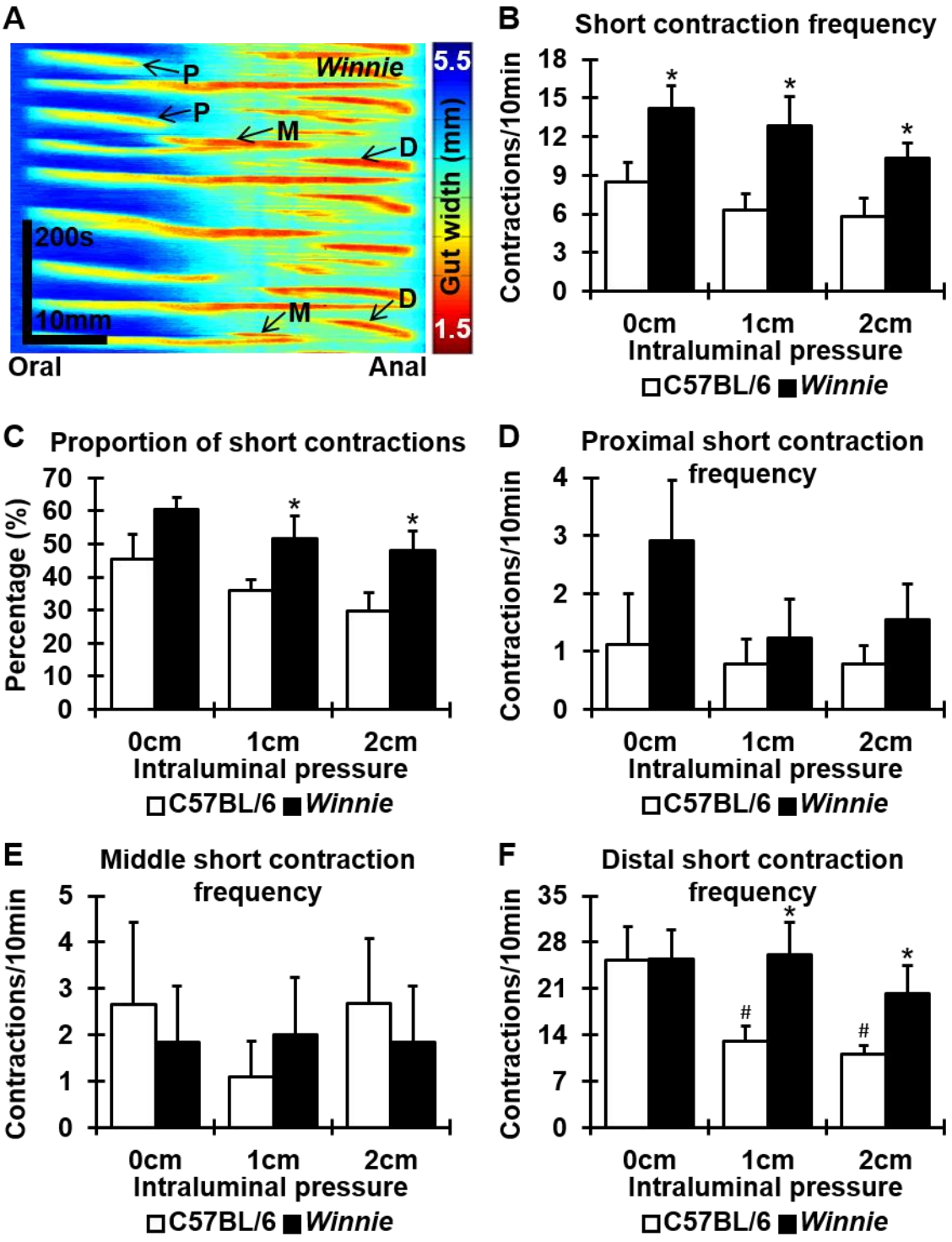
A
P
P
M
D
M
D
Winnie
200s
10mm
Oral
Anal
5.5
Gut width (mm)
1.5
B
Short contraction frequency
Contractions/10min
0cm
1cm
2cm
Intraluminal pressure
C57BL/6
Winnie
C
Proportion of short contractions
Percentage (%)
D
Proximal short contraction frequency
E
Middle short contraction frequency
F
Distal short contraction frequency

Figure 4.17. Frequency and proportion of fragmented contractions in *Winnie* and C57BL/6 mice. Images captured from a video recording of an *in vitro* colonic motility organ bath experiment and corresponding spatiotemporal map demonstrating fragmented contractions in the *Winnie* mouse colon. Solid arrows indicate contraction, and dashed arrows represent relaxation **(A)**. Frequency of fragmented contractions in the colons from C57BL/6 and *Winnie* mice at baseline (0cmH_2O), 1cmH_2O, and 2cmH_2O intraluminal pressure **(B)**. The proportion of fragmented contractions to the total number of contractions was calculated at each level of intraluminal pressure **(C)**. Line graph demonstrating the proportion of C57BL/6 and *Winnie* mice which generated fragmented contractions at each level of intraluminal pressure **(D)**. Scale bars = 10mm. **P*<0.05, ***P*<0.01, ****P*<0.001 compared to C57BL/6 at the same level of intraluminal pressure. $^{\#}P$<0.05 compared to C57BL/6 at 0cmH_2O.

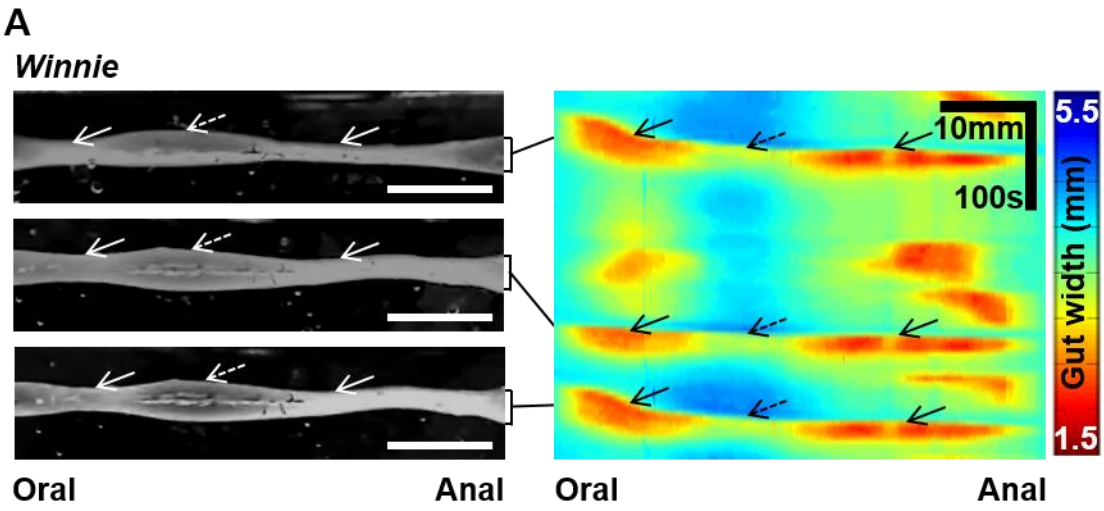
A
Winnie
10mm
100s
5.5
Gut width (mm)
1.5
Oral
Anal
Oral
Anal

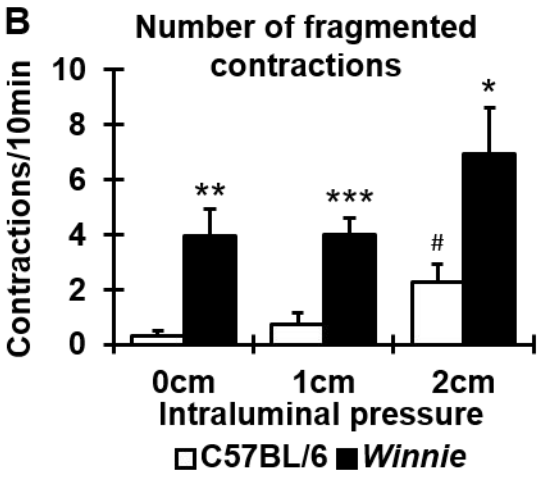
B
Number of fragmented contractions
Contractions/10min
10
8
6
4
2
0
**
***
#
*
0cm
1cm
2cm
Intraluminal pressure
C57BL/6
Winnie

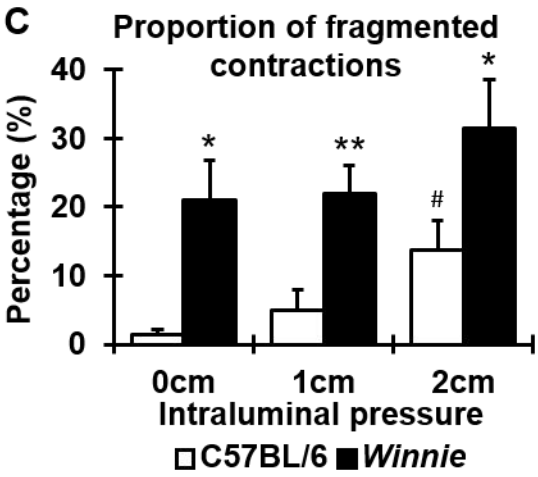
C
Proportion of fragmented contractions
Percentage (%)
40
30
20
10
0
*
**
#
*
0cm
1cm
2cm
Intraluminal pressure
C57BL/6
Winnie

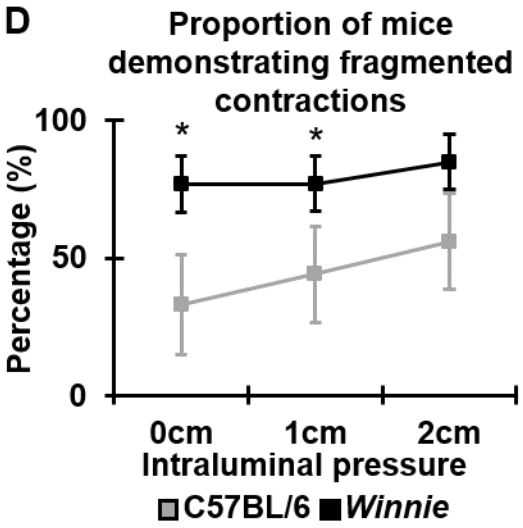
D
Proportion of mice demonstrating fragmented contractions
Percentage (%)
100
50
0
*
*
0cm
1cm
2cm
Intraluminal pressure
C57BL/6
Winnie

4.4.9 Speed and length of colonic contractions in *Winnie* and C57BL/6 mice

CMMCs propagated more rapidly in the colons from *Winnie* mice when intraluminal pressure was increased from 0 to 2cmH_2O (*n*=13; *P*<0.05; Table 4.4; Fig. 4.18A), but there were no changes in CMMC speed in colons from C57BL/6 mice (*n*=8). When intraluminal pressure was increased from baseline to 1cmH_2O, the propagation speed of short contractions remained constant in both *Winnie* and C57BL/6 colons (Table 4.4; Fig. 4.18B). At 2cmH_2O, short contractions propagated more rapidly in C57BL/6 than in *Winnie* colons (*P*<0.01), but the propagation speed increased significantly in each genotype (Table 4.4; Fig. 4.18B). The speed of propagation of fragmented contractions did not differ between C57BL/6 and *Winnie* mice; faster contraction speeds were recorded as intraluminal pressure was increased to 2cmH_2O in both groups (Table 4.4; Fig. 4.18C).

CMMCs propagated over similar distances in the colon in both C57BL/6 (*n*=8) and *Winnie* (*n*=13) mice regardless of intraluminal pressure. Similarly, short and fragmented contraction lengths did not differ between *Winnie* and C57BL/6 mice (Table 4.4).

4.4.10 Phases of contraction in the colons from *Winnie* and C57BL/6 mice

The individual properties of contractions were compared between C57BL/6 (*n*=8) and *Winnie* (*n*=13) mice at the proximal, middle, and distal regions of the colon by tracking the diameter independent of the type of contraction (Gwynne et al. 2004b). Several parameters were analyzed from these traces including duration of contraction, quiescence (time at the baseline resting diameter between contractions), and contraction interval (time from the beginning to the end of the contraction-relaxation cycle; Fig. 4.19A-B^{I}).

In the proximal colon, the duration of contraction was similar in *Winnie* and C57BL/6 mice, reducing in both groups as intraluminal pressure increased

(1cmH_2O: *P*<0.01; 2cmH_2O: *P*<0.05; Table 4.5), whereas the time of quiescence decreased in *Winnie* mice only (*P*<0.05; Table 4.5). Subsequently, at 2cmH_2O, quiescence was shorter in the colons from *Winnie* mice compared with the colons from C57BL/6 mice (*P*<0.05; Table 4.5). The contraction interval in the proximal colon decreased as intraluminal pressure increased in both *Winnie* and C57BL/6 mice (Table 4.5). In the middle colon, there were no changes in the duration of contraction or quiescence in both C57BL/6 and *Winnie* mice. As a result, there were no differences measured in the contraction intervals of the middle colon in either group (Table 4.5).

The total constriction and relaxation activity (duration of contraction) was greater in the distal colons from *Winnie* mice than from C57BL/6 mice across all levels of pressure (*P*<0.05 for all; Table 4.5; Fig. 4.19C). Quiescence of the distal colon was decreased in *Winnie* mice at 2cmH_2O of intraluminal pressure compared with C57BL/6 mice (*P*<0.05; Table 4.5; Fig. 4.19D). Similarly, contraction intervals were shorter in *Winnie* mice than in C57BL/6 mice at 2cmH_2O (*P*<0.05; Table 4.5).

To investigate possible mechanisms underlying these changes in the patterns and properties of colonic motility induced by intestinal inflammation, we examined three possible causes: changes in neuromuscular transmission, changes in intestinal smooth muscle function, and changes in intestinal smooth muscle structure. These were examined in segments of the distal colon only, since most changes in the phases of contraction were evident in this section of the colon.

Figure 4.18. Colonic migrating motor complex, short contraction, and fragmented contraction speed in *Winnie* and C57BL/6 mice. The speed of colonic migrating motor complexes (CMMCs) **(A)**, short contractions **(B)**, and fragmented contractions **(C)** was measured from spatiotemporal maps generated from the colons of C57BL/6 and *Winnie* mice at baseline, 1cmH_2O, and 2cmH_2O intraluminal pressure. *P<0.05, **P<0.01 significantly different to C57BL/6 at the same level of intraluminal pressure. ^P<0.05, ^^P<0.01 significantly different to *Winnie* at 2cmH_2O. $^{\dagger}P$<0.05, $^{\dagger\dagger}P$<0.01, $^{\dagger\dagger\dagger}P$<0.001 significantly different to C57BL/6 at 2cmH_2O.

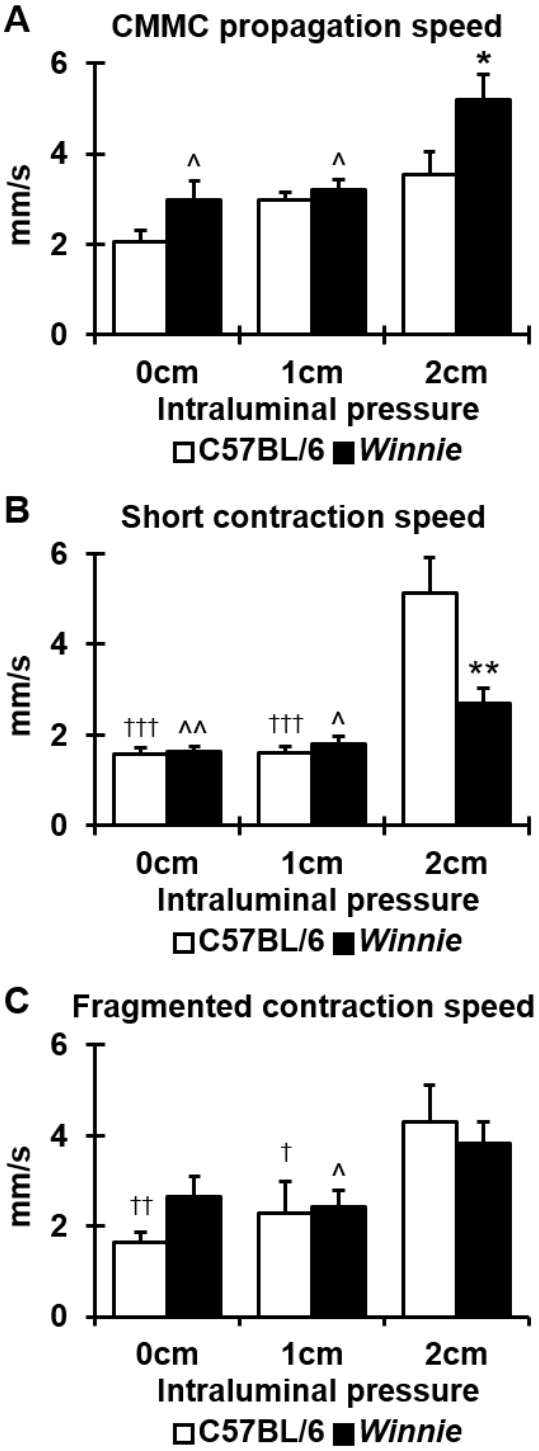
A
CMMC propagation speed
mm/s
6
4
2
0
*
^
^
0cm
1cm
2cm
Intraluminal pressure
C57BL/6
Winnie
B
Short contraction speed
mm/s
6
4
2
0
†††
^^
†††
^
**
0cm
1cm
2cm
Intraluminal pressure
C57BL/6
Winnie
C
Fragmented contraction speed
mm/s
6
4
2
0
††
†
^
0cm
1cm
2cm
Intraluminal pressure
C57BL/6
Winnie

Figure 4.19. Variations in duration of contraction and quiescence in the distal colon. Parameters of contractions were evaluated at the distal section of the colon independent of the type of contraction in spatiotemporal maps from C57BL/6 **(A)** and *Winnie* mice **(B)**. Traces of contractility at a specific location along the colon plotted changes in the gut width against time **(A^I, B^I)**. The duration of contractile activity **(C)** and quiescence **(D)** was measured from traces of colonic motor patterns at distal section of the C57BL/6 and *Winnie* mouse colon. **P*<0.05 compared to C57BL/6 at the same level of intraluminal pressure.

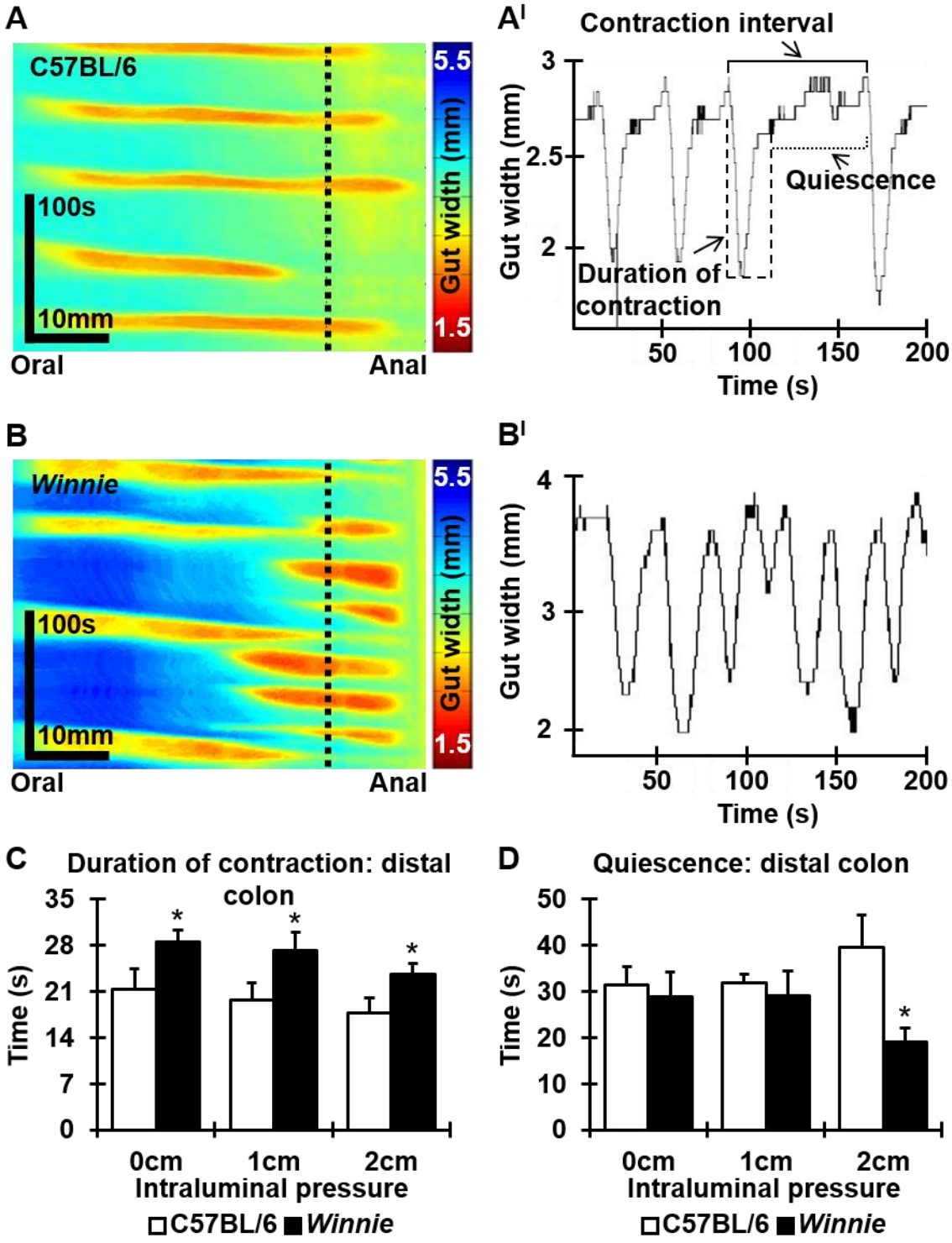
A
C57BL/6
100s
10mm
Oral
Anal
5.5
Gut width (mm)
1.5
A'
Contraction interval
Quiescence
Duration of contraction
Gut width (mm)
Time (s)
B
Winnie
B'
C
Duration of contraction: distal colon
Time (s)
0cm
1cm
2cm
Intraluminal pressure
C57BL/6
Winnie
D
Quiescence: distal colon

Table 4.5. Phases of colonic contraction

		Intraluminal pressure		
		0cmH_2O	**1cmH_2O**	**2cmH_2O**
Proximal colon				
Duration of contraction (s)	**C57BL/6**	39.4±3.9†	33.9±3.5	26.1±1.7
	Winnie	44.1±3.4^^	37.7±2.4	30.5±2.7
Quiescence (s)	**C57BL/6**	36.1±5.9	35.3±2.3	26.9±3.2
	Winnie	36.8±6.8^	26.4±4.7	15.4±3.6*
Contraction interval (s)	**C57BL/6**	82.4±10.0†	57.9±5.8	52.9±4.6
	Winnie	80.9±8.8^^	64.1±6.3^	45.8±5.5
Middle colon				
Duration of contraction (s)	**C57BL/6**	34.1±5.7	31.8±6.4	25.1±2.5
	Winnie	37.1±6.4	35.1±3.5	30.6±2.1
Quiescence (s)	**C57BL/6**	44.7±9.8	35.3±6.8	34.2±7.0
	Winnie	35.1±2.7	35.5±6.6	25.3±4.1
Contraction interval (s)	**C57BL/6**	78.8±15.1	60.2±12.3	59.3±8.6
	Winnie	72.2±6.7	70.3±6.4	52.5±5.2
Distal colon				
Duration of contraction (s)	**C57BL/6**	21.3±3.1	19.7±2.6	17.7±2.4
	Winnie	28.5±1.7*	27.1±2.8*	23.5±1.7*
Quiescence (s)	**C57BL/6**	31.4±3.9	31.8±2.0	39.7±7.0
	Winnie	28.9±5.4	29.1±5.4	19.1±2.9*
Contraction interval (s)	**C57BL/6**	53.4±6.4	51.2±3.9	60.6±7.3
	Winnie	61.2±6.1^^	51.5±6.4	40.8±3.7*

*P<0.05 compared to C57BL/6 at the same level of intraluminal pressure. ^P<0.01, ^^P<0.01 compared to *Winnie* at 2cmH_2O. †P<0.05 compared to C57B/L6 at 2cmH_2O.

4.4.11 Altered neuromuscular transmission in the distal colon of *Winnie* mice

To evaluate the role of neuromuscular transmission in colonic dysmotility observed in *Winnie* mice, intracellular recordings from circular smooth muscle cells in the C57BL/6 and *Winnie* mouse colon were compared. Focal electrical stimulation of nerve fibers innervating the circular muscle layer evoked junction potentials in muscle cells. Inhibitory and excitatory neuromuscular junction potentials were identified as purinergic fast inhibitory junction potentials (fIJPs), nitrergic slow inhibitory junction potentials (sIJPs), and cholinergic excitatory junction potentials (EJPs) using various antagonists.

Single-pulse electrical stimuli evoked fIJPs in control physiological solution (Fig. 4.20A). In both the C57BL/6 (n=12) and *Winnie* (n=14) mouse colon, the amplitudes of these fIJPs increased with larger electrical stimuli (single-pulse, 0.4ms duration, 0-60V; data not shown). The amplitudes of fIJPs evoked by a 30V electrical stimulus differed significantly between the two genotypes (C57BL/6: -24.4±1.2mV; *Winnie*: -17.9±2.8mV; P<0.05; Fig. 4.20B). Addition of the purinergic P2Y1 receptor antagonist, MRS2500 (1µM), inhibited the fIJPs.

A short, high-frequency train of electrical stimuli (3 pulses at 20Hz, 20V, 0.5ms duration) was used to generate sIJPs (Fig. 4.20C). The amplitudes of sIJPs did not differ between the C57BL/6 (-6.8±0.8mV) and *Winnie* (-6.6±0.8mV) colon (Fig. 4.20D). Addition of a NO synthase inhibitor L-NNA (1mM) in the presence of MRS2500 (1µM) blocked the sIJPs.

High-frequency stimulus trains (3 pulses, 20Hz, 20V, 0.5ms pulse duration) in the presence of MRS2500 and L-NNA, blocking the fIJPs and sIJPs, evoked EJPs (Fig. 4.20E). The amplitudes of EJPs in colonic smooth muscle cells of C57BL/6 mice (7.7±0.7mV) were greater than those from the *Winnie* mice (5.9±0.9mV; P<0.05; Fig. 4.20F). In both genotypes, EJPs were inhibited by the muscarinic antagonist atropine (1µM; C57BL/6 from 7.4±0.7 to 1.4±0.2mV; *Winnie* from 6.8±0.8 to 1.3±0.1mV; P<0.001 for both).

In control Krebs solution, the RMPs of colonic smooth muscle cells from C57BL/6 (-41.9±0.7mV) and *Winnie* (-40.7±1.5mV) mice were not significantly different. Addition of MRS2500, L-NNA, and atropine did not affect RMP.

Figure 4.20. Intracellular electrophysiological recordings of excitatory and inhibitory junction potentials from colonic smooth muscle cells. Representative traces of purinergic fast inhibitory junction potentials (fIJPs; *stimulus artifact) **(A)**. Quantitative analysis of fIJP amplitudes in the colonic smooth muscle cells from C57BL/6 and *Winnie* mice **(B)**. Representative traces of nitrergic slow inhibitory junction potentials (sIJPs) **(C)**. Amplitudes of sIJP in the colonic smooth muscle cells from C57BL/6 and *Winnie* mice **(D)**. Representative traces of excitatory junction potentials (EJPs) **(E)**. Amplitudes of EJPs in the colonic smooth muscle cells from C57BL/6 and *Winnie* mice **(F)**. *$P<0.05$.

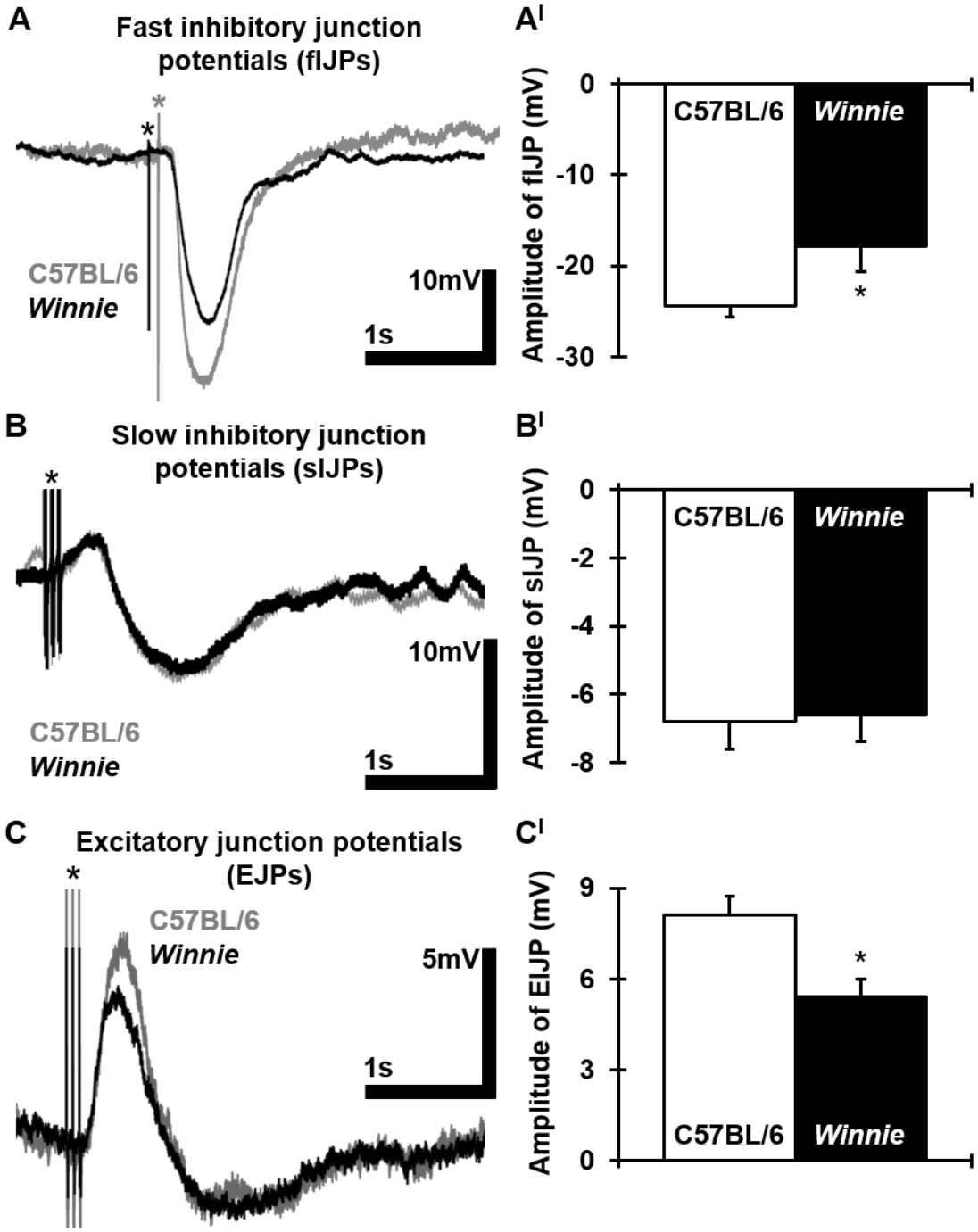
A
Fast inhibitory junction potentials (fIJPs)
C57BL/6
Winnie
10mV
1s
A'
Amplitude of fIJP (mV)
0
-10
-20
-30
C57BL/6
Winnie
B
Slow inhibitory junction potentials (sIJPs)
C57BL/6
Winnie
10mV
1s
B'
Amplitude of sIJP (mV)
0
-2
-4
-6
-8
C57BL/6
Winnie
C
Excitatory junction potentials (EJPs)
C57BL/6
Winnie
5mV
1s
C'
Amplitude of EIJP (mV)
9
6
3
0
C57BL/6
Winnie

4.4.12 Smooth muscle responses to carbachol and sodium nitroprusside (SNP) are altered in the distal colon of *Winnie* mice

To investigate the role of smooth muscle function in colonic dysmotility observed in *Winnie* mice, we examined circular smooth muscle contractile responses to common excitatory and inhibitory agents. Addition of carbachol (1nM-20μM) to the organ bath containing excised colonic rings evoked a dose-dependent and significant increase in contractile force in both C57BL/6 (*n*=6) and *Winnie* (*n*=6) mice. However, the magnitude of contractions evoked by carbachol was significantly lower in preparations from *Winnie* mice compared with those from C57BL/6 mice at 5μM ($P<0.001$), 10μM ($P<0.001$), and 20μM ($P<0.001$) doses (Fig. 4.21A-A^{I}). SNP (10nM-300μM) relaxed carbachol-preconstricted colonic rings from both C57BL/6 (*n*=6) and *Winnie* (*n*=6) mice (Fig. 4.21B). The magnitude of this relaxation was significantly reduced in *Winnie* mice compared with C57BL/6 mice at 10μM ($P<0.01$), 100μM ($P<0.01$), and 300μM ($P<0.001$; Fig. 4.21B^{I}). ATP (10μM-3mM) induced relaxation of carbachol-preconstricted colonic rings from both C57BL/6 (*n*=6) and *Winnie* (*n*=6) mice with no difference between the groups (Fig. 4.21C-C^{I}).

4.4.13 Hyperplasia of smooth muscle cells in the distal colon of *Winnie* mice

The changes in muscle function described above may be due to morphological changes in muscle structure. To determine whether chronic inflammation causes hyperplasia of smooth muscle cells in *Winnie* mice, cross sections of the distal colon were labeled with α-SMA antibody to label smooth muscle cells and DAPI to label nuclei (*n*=5/group; Fig. 4.22A-B^{II}). The numbers of α-SMA-IR circular and longitudinal muscle cells counterstained with DAPI were significantly increased in the muscle layers of the colon in the cross section preparations from *Winnie* (618±16 cells/mm^2) compared with C57BL/6 (329±9 cells/mm^2; $P<0.001$) mice (Fig. 4.22C).

Figure 4.21. Smooth muscle cell response to carbachol, SNP, and ATP. Representative traces recorded from smooth muscle contraction (g) of the colonic rings from C57BL/6 and *Winnie* mice at baseline and following application of 10µM carbachol **(A)**, 100µM SNP **(B)**, and 300µM ATP **(C)**. Cumulative log dose-response curves to carbachol (1nM-20µM) in colonic preparations from C57BL/6 and *Winnie* mice **(A^I)**. Cumulative log dose-response curves to SNP (10nM-300µM) **(B^I)** and ATP (10µM-3mM) **(C^I)** in colonic smooth muscle preparations precontracted with 10µM carbachol (100%) in C57BL/6 and *Winnie* mice. Peak effects are shown as percentage change from respective basal values. $^{**}P<0.01$, $^{***}P<0.001$.

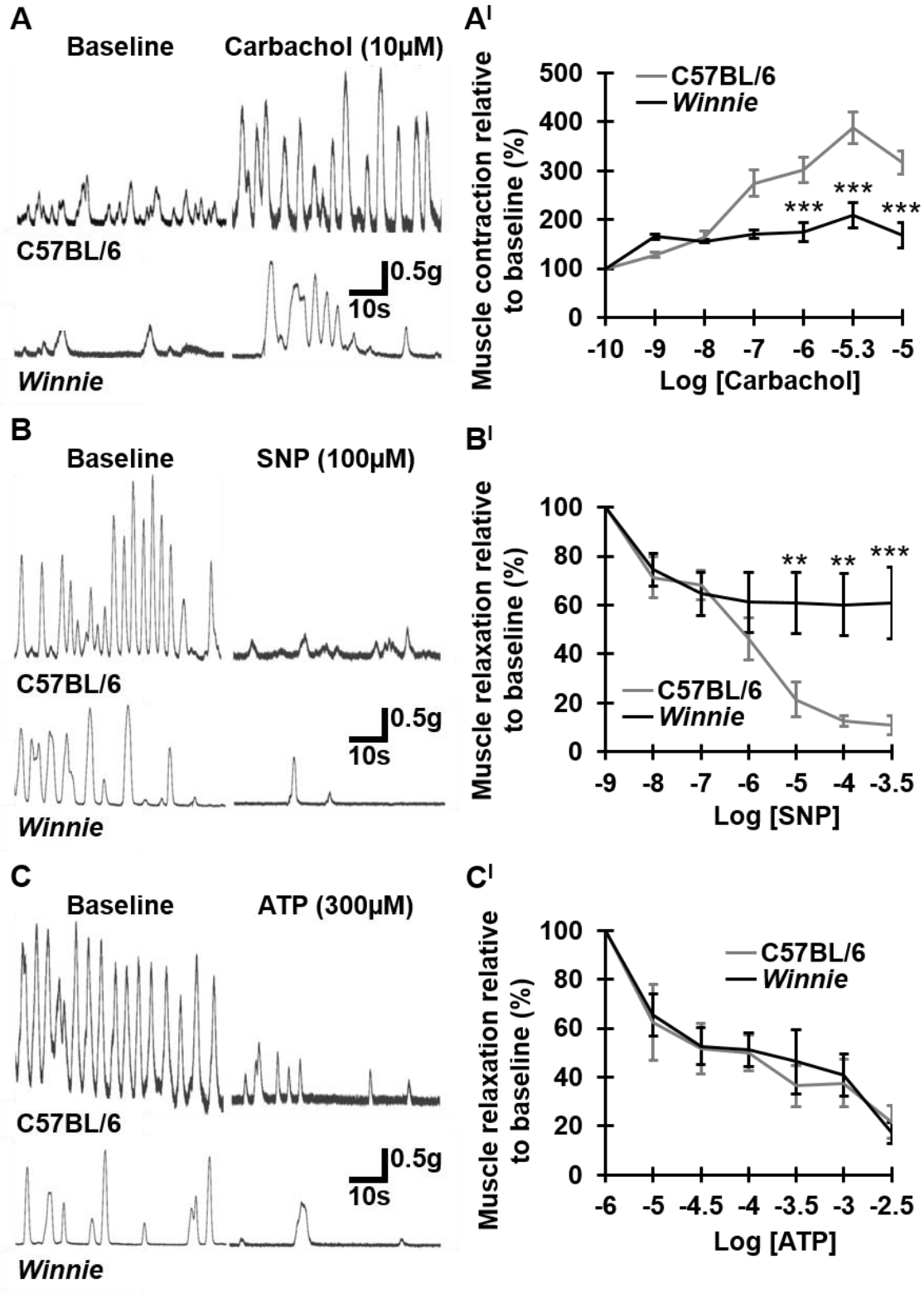
A
Baseline
Carbachol (10μM)
C57BL/6
0.5g
10s
Winnie
A'
Muscle contraction relative to baseline (%)
500
400
300
200
100
0
C57BL/6
Winnie
***
***
***
-10
-9
-8
-7
-6
-5.3
-5
Log [Carbachol]
B
Baseline
SNP (100μM)
C57BL/6
0.5g
10s
Winnie
B'
Muscle relaxation relative to baseline (%)
100
80
60
40
20
0
**
**
***
C57BL/6
Winnie
-9
-8
-7
-6
-5
-4
-3.5
Log [SNP]
C
Baseline
ATP (300μM)
C57BL/6
0.5g
10s
Winnie
C'
Muscle relaxation relative to baseline (%)
100
80
60
40
20
0
C57BL/6
Winnie
-6
-5
-4.5
-4
-3.5
-3
-2.5
Log [ATP]

Figure 4.22. Hyperplasia of smooth muscle cells in the distal colon of *Winnie* mice. Colon cross sections from C57BL/6 and *Winnie* mice were labeled with α-SMA antibody to identify smooth muscle cells **(A, B)** and counterstained with DAPI **(A^{I}, B^{I})**. Merged images depicting DAPI stained nuclei in α-SMA-IR cells within colon cross sections **(A^{II}, B^{II})**. Quantitative analysis of α-SMA-IR cells in the circular and longitudinal muscle layers of the colon ($1mm^2$) **(C)**. Scale bars = 50µm. ****P*<0.001.

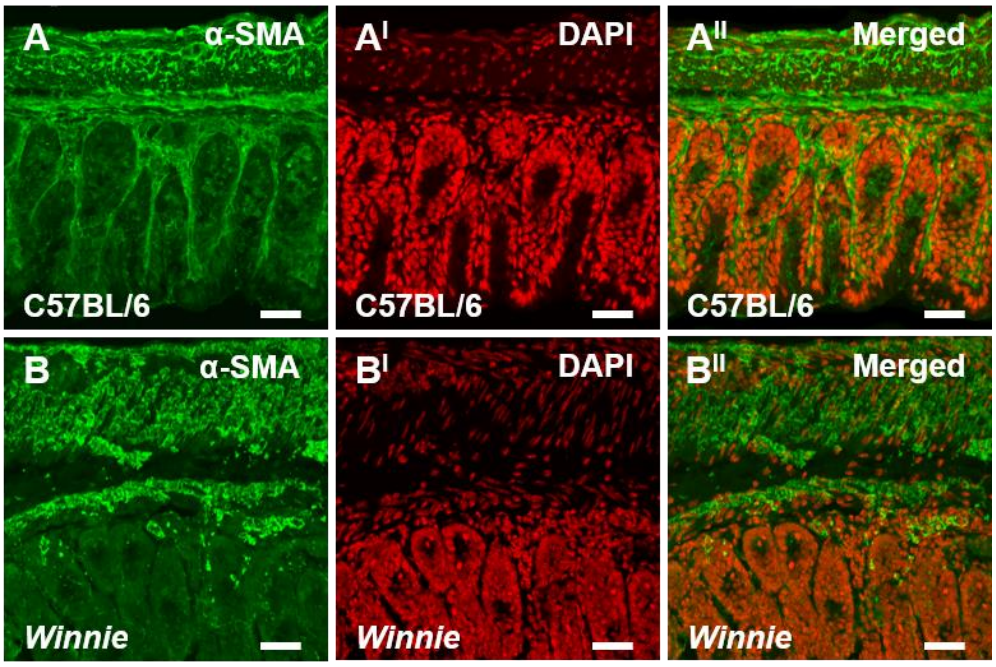
A
α-SMA
C57BL/6
A^I
DAPI
C57BL/6
A^II
Merged
C57BL/6
B
α-SMA
Winnie
B^I
DAPI
Winnie
B^II
Merged
Winnie

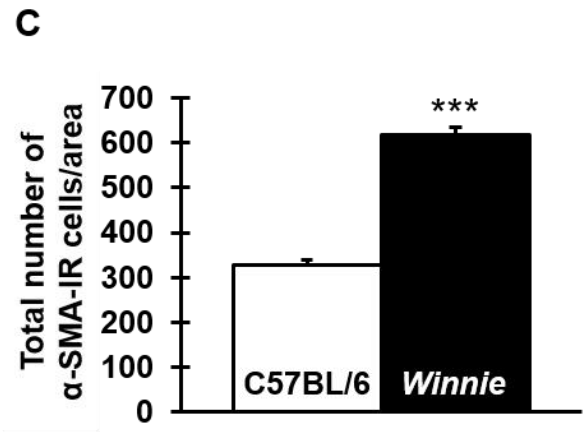
C
Total number of α-SMA-IR cells/area
700
600
500
400
300
200
100
0
***
C57BL/6
Winnie

4.5 Discussion

This study provides the first investigation of intestinal innervation, as well as *in vivo* GI transit and in-depth analysis of colonic function in an animal model of spontaneously occurring chronic intestinal inflammation. Chronic inflammation in the distal colon of *Winnie* mice was confirmed by thickening of muscle and mucosal layers, increased CD45-immunoreactivity, high fecal Lcn-2 protein levels measured over a 4wk period and distinct gross morphological damage to the colon. The ganglionic density of myenteric neurons, as well as the density of sensory, cholinergic and noradrenergic fibers innervating the myenteric plexus, muscle and mucosa significantly decreased in the distal colon of *Winnie* mice compared to C57BL/6 mice. Here, we report that *Winnie* mice exhibit alterations in small intestinal and colonic transit, in patterns of colonic motility, and in parameters of contractions. Furthermore, we provide novel data about the mechanisms underlying changes in *Winnie* colonic motility implicating impaired neuromuscular transmission, as well as altered contractile activity and morphology of colonic smooth muscle cells.

Animal models of IBD have provided significant contributions to understanding pathophysiological mechanisms as well as development of novel therapeutic strategies for IBD (Mizoguchi and Mizoguchi 2010; Xavier and Podolsky 2007). Although animal models have their limitations and do not reproduce all the pathogenic and clinical features of human IBD, each animal model provides an invaluable tool to study complex physiological and biochemical disease aspects that are difficult to address in humans (Dothel et al. 2013; Elson et al. 1995). The *Winnie* mice used in our study develop inflammation in the colon with multiple similarities to human UC, including goblet cell pathology, depleted mucus layer, and distal gradient of colitis, as well as a characteristic immune profile (Eri et al. 2011; McGuckin et al. 2011; Heazlewood et al. 2008; Lourenssen et al. 2005). The manifestation of clinical symptoms in *Winnie* mice starts at the age of 6 weeks when animals become young adults. Colitis in *Winnie* mice has a chronic and relapsing nature, a major feature of human IBD. *Winnie* mice carry only a point mutation in the *Muc2* gene leading to spontaneous colitis unlike chemically-

induced models and some other chronic models which require pathogens to develop colitis (e.g., IL-10$^{-/-}$ mice) (Uhlig and Powrie 2009; Wirtz and Neurath 2007).

In this study, we used 12-16wk-old *Winnie* mice, all of which had active colitis with symptoms of perianal bleeding and diarrhea confirmed by increased fecal water content and Lcn-2 over 4 consecutive weeks, and lack of weight gain. Acute diarrhea lasting for <14d is generally associated with bacterial, viral, or parasitic infection. On the other hand, diarrhea that persists for at least 4 weeks is most likely caused by alterations in GI transit and motility (Collins 2007). Chronic inflammation induced morphological changes in the *Winnie* mouse colon including increase in its length and marked thickening of the intestinal wall which may contribute to colonic dysmotility present in these mice. Together with the mucosal damage and leukocyte infiltration observed in all *Winnie* mice in this study, these are the hallmark features of chronic intestinal inflammation. Muscular hypertrophy, changes in colon length and similar gross morphological changes have been described previously in other models of chronic intestinal inflammation (Rivera-Nieves et al. 2003; Elson et al. 1995).

Inflammation in *Winnie* mice was associated with significant structural damage to the colonic innervation which was investigated for the first time in this study. The results of this study have demonstrated decrease in the density of nerve fibers, including cholinergic, noradrenergic and sensory fibers, projecting to the myenteric plexus, as well as reductions in the average number of myenteric neurons in the distal colon from *Winnie* mice.

Significant reduction in the density of VAChT-IR cholinergic nerve fibers observed in the colon tissues from *Winnie* mice in our study is consistent with previous work conducted in colon tissues from UC patients (Jonsson et al. 2007). It has been established that ACh attenuates the release of pro-inflammatory cytokines (Ulloa 2005; Borovikova et al. 2000) and thereby could control systemic inflammation and modulate immune response. Other studies further demonstrated that cholinergic pathways also modulated experimental colitis in rats by using acetylcholinesterase inhibitors (Miceli and Jacobson 2003) or vagotomy (Ghia et

al. 2006). Previous studies showed impaired release of ACh from the inflamed rat intestine (Collins et al. 1989). Alterations in functions of cholinergic fibers in *Winnie* mice should be further investigated.

Noradrenergic neurons of the sympathetic celiac and the superior mesenteric ganglia innervate the smooth muscles and enteric ganglia in the colon and modulate motility, secretion, blood flow, and immune system activation (Cervi et al. 2014; Lomax et al. 2010; Straub et al. 2008; Vasina et al. 2008). The results of our study demonstrated that the density of noradrenergic nerve fibers identified by TH immunoreactivity was significantly reduced in the colon tissues from *Winnie* mice. This is consistent with the results of previous studies in patients with CD (Straub et al. 2008; Belai et al. 1997), and in mouse models of DSS and TNBS-induced colitis (Lomax et al. 2007b; Straub et al. 2005). A large body of evidence obtained from animal models of GI inflammation indicated marked changes in sympathetic neuronal excitability (Dong et al. 2008), neurotransmitter release (Blandizzi et al. 2003; Swain et al. 1991) and structure of noradrenergic nerve fibers (Straub et al. 2008; Magro et al. 2002; Dvorak and Silen 1985; Dvorak et al. 1980). Decreased colonic mucosal norepinephrine concentration was observed in CD patients (Magro et al. 2002). In addition, colitis impairs noradrenergic regulation of submucosal arterioles and mesenteric arteries (Birch et al. 2008; Lomax et al. 2007b).

Anti-CGRP antibody was used to label sensory fibers including extrinsic spinal and vagal primary sensory afferent as well as intrinsic sensory fibers containing and releasing CGRP (Qu et al. 2008; Grider 2003; Kressel et al. 1994). In this study, we observed reductions in the density of CGRP-IR fibers in the distal colon of *Winnie* mice. Similarly, CGRP was found to be reduced in the inflamed bowel in animal models of chemically-induced colitis (Miampamba and Sharkey 1998; Miampamba et al. 1992; Eysselein et al. 1991). Moreover, tissues from patients with CD and UC also showed a decrease in the number and density of CGRP-positive nerve fibers in the colonic mucosa (Eysselein et al. 1992; Koch et al. 1987).

Our data demonstrated that, although significant reduction in all types of fibers analyzed in this study was observed, CGRP-IR fibers were the most affected compared to other types of fibers in *Winnie* mice with the loss of about 65% of CGRP-IR fibers in cross sections. CGRP-IR sensory fibers extensively supply the mucosa and submucosa where chronic inflammation is the most prominent in *Winnie* mice. CGRP released from sensory nerve fibers plays important anti-inflammatory and protective roles: it facilitates mucus production and controls blood flow in the GI mucosa (Holzer 2007). It has been suggested that during inflammation there is a sustained increased release of CGRP, leading to depletion of CGRP fibers (Eysselein et al. 1992). Loss of CGRP-IR sensory fibers and sensory neuron dysfunction impair mucosal protection (Holzer 2007). The loss of about 52% of TH-IR noradrenergic fibers within myenteric ganglia observed in our study might contribute to impairment of motility, secretion, blood flow and GI immunity in *Winnie* mice which needs to be further investigated. It was suggested that the loss of noradrenergic fibers is a pro-inflammatory signal in the chronic phase of the intestinal inflammation (Straub et al. 2008). On the other hand, the density of VAChT-IR cholinergic fibers was less reduced in cross sections of the colon from *Winnie* mice. This might be due to the extensive projection of cholinergic fibers to the muscle layer where immune infiltration is less prominent. Nevertheless, concurrent significant reduction of VAChT-IR fibers within the myenteric ganglia suggests that excitatory cholinergic neurotransmission is reduced, leading to impaired motility and symptoms of diarrhea observed in *Winnie* mice. Whether the loss of nerve fibers in *Winnie* mice is a result of chronic inflammation or whether *Winnie* mice are born with altered intestinal innervation which contributes to initial pathological changes in the mucosa leading to inflammation needs to be further elucidated.

In this study, we have demonstrated a substantial loss of myenteric neurons in the *Winnie* mouse distal colon. These results are consistent with previous reports in both experimental models of colitis and tissues from IBD patients (Brown et al. 2016; Bernardini et al. 2012; Sarnelli et al. 2009; Linden et al. 2005). However, while enteric neuronal loss associated with intestinal inflammation has been repeatedly reported, some studies have demonstrated increases or no change in

the number of myenteric neurons (Table 4.6). Variability within the literature may be attributable to the method of analyzing the number of myenteric neurons within the inflamed gut. In this study, we normalized the number of neurons to the ganglionic area and observed decreases in neuronal density consistent with other studies using this method of analysis (Brown et al. 2016; Bernardini et al. 2012; Gulbransen et al. 2012). The mean ganglionic area, relative to the microscopic field area, is increased in UC patients (Bernardini et al. 2012). Thus, reports of increases or no changes to neuronal numbers associated with intestinal inflammation may be due to absence of normalization to account for size differences between the ganglion. It has been suggested that the loss of enteric neurons in the inflamed bowel may be due to the infiltration of neutrophils into the myenteric ganglia (Boyer et al. 2005) and/or activation of the P2X7 receptor, pannexin-1-signaling complex (Gulbransen et al. 2012).

Our results demonstrated that the number of cholinergic (ChAT-IR excitatory muscle motor and interneurons) neurons decreased in the distal colon of *Winnie* mice, but the density of nitrergic (nNOS-IR inhibitory muscle motor and interneurons) neurons were unaltered. These results are consistent with findings in animal models of colitis (da Silva et al. 2015; Winston et al. 2013) and in patients with UC (Neunlist et al. 2003). While there were no changes in the density of nNOS-IR neurons in *Winnie* mice, simultaneous decrease in the number of PGP9.5-IR neurons caused an increase in the proportion of nNOS-IR neurons. Imbalances in the number and/or proportion of inhibitory and excitatory myenteric neurons underlie impaired smooth muscle contractility and colonic dysmotility induced by inflammation (Robinson et al. 2014; Winston et al. 2013; Neunlist et al. 2003). Furthermore, reductions in the density of nerve fibers observed in *Winnie* mice might lead to decreased neuropeptide release and changes in the neurotransmission affecting alterations to GI functions.

Table 4.6 Effect of intestinal inflammation on the number of neurons in the myenteric plexus

Species	Pathology/model	Tissue studied	Preparations	Number of neurons	Reference
Human	UC	Colon	Transverse sections	Threefold increase	(Storsteen et al. 1953)
Human	UC	Colon	Cross sections	61% decrease	(Bernardini et al. 2012)
Human	UC	Colon	LMMP preparations	No change	(Neunlist et al. 2003)
Human	UC	Colon	Transverse sections	No change	(Villanacci et al. 2008)
Guinea-pig	TNBS	Colon	LMMP preparations	15% decrease	(Linden et al. 2005)
Mouse	DNBS	Colon	LMMP preparations	50% decrease	(Boyer et al. 2005)
Mouse	DNBS	Colon	LMMP preparations	24% decrease	(Brown et al. 2016)
Mouse	DNBS, DSS, Oxazolone, $IL10^{-/-}$	Colon	LMMP preparations	20-30% decrease	(Gulbransen et al. 2012)
Mouse	*Muc2* mutation	Colon	LMMP preparations	20% decrease	(Rahman et al. 2016)
Rat	DNBS	Colon	Cross sections	50% decrease	(Sanovic et al. 1999)
Rat	TNBS	Colon	LMMP preparations	33% decrease	(Lin et al. 2005)
Rat	TNBS	Colon	LMMP preparations	20% decrease	(Sarnelli et al. 2009)
Rat	DSS	Colon	LMMP preparations	No change	(Winston et al. 2013)

UC = ulcerative colitis, TNBS = 2,4,6-trinitrobenzene sulfonic acid, DNBS = 2,4-dinitrobenzene sulfonic acid, DSS = dextran sodium sulfate.

Similar to IBD and irritable bowel syndrome-diarrhea predominant patients, chronic diarrhea in *Winnie* mice was associated with a faster colonic transit time (Deiteren et al. 2010; Manabe et al. 2010; Camilleri et al. 2008; Sadik et al. 2008; Hebden et al. 2000). Compared with healthy control mice, OCTT was also altered in *Winnie* mice in this study. Previous studies examining murine GI transit times via the movements of radiopaque markers, as well as other methods (i.e., phenol red meal test), have reported that the orocecal or small intestinal transit time is greater than colonic transit time in wild-type or control mice (Myagmarjalbuu et al. 2013; Qiu et al. 2008). Furthermore, in experimental models of intestinal inflammation such as TNBS-induced colitis (Storr et al. 2008), croton oil-induced diarrhea (Izzo and Sharkey 2010), and intraperitoneal lipopolysaccharide injection (Duncan et al. 2008; Mathison et al. 2004), small intestinal transit is reported to be inhibited. It is considered that increased OCTTs may be due to electrical uncoupling and focal increase in slow-wave frequency, which lead to orally propagating contractions slowing the transit in the proximal small intestine (Der et al. 2000). Consistent with our results, many clinical studies report delays in small intestine transit to be correlated with IBD (Fischer et al. 2017; Niv et al. 2014; Sadik et al. 2008). Moreover, it has been suggested that changes in intestinal transit resulting from inflammation, particularly faster CTT, correlate with changes in colonic motility (Capasso et al. 2014; Reddy et al. 1991).

Colonic dysmotility, hypersensitivity, and dysfunction result from intestinal inflammation and reflect changes in smooth muscle function and/or the enteric nervous system (ENS) (Aldini et al. 2012; Wadie et al. 2012; Hoffman et al. 2011; Smith and Smid 2005; Vrees et al. 2002; O'Brien and Phillips 1996). In human studies, the majority of data were obtained from muscle resected at the time of operation. Therefore, investigation of colonic motility in IBD patients is usually limited to analyzing colonic segments rather than the whole colon (Vrees et al. 2002; Koch et al. 1988). Hence, it is unsurprising that most of our knowledge regarding motility dysfunction in colonic inflammation has come from animal models. Changes in motor function have been described in animals with acute colitis induced by a variety of inflammatory stimuli, including infection, chemical irritation, and immune activation. These studies have mostly investigated smooth

muscle contractility in sections of the colon rather than analysis of whole colon motility (Aldini et al. 2012; Wadie et al. 2012; Kinoshita et al. 2006; Kiyosue et al. 2006). Smooth muscle contractility has been examined in colon sections from animal models of chronic colitis, such as IL-10$^{-/-}$ mice, as well as from mice with chronic DSS-induced colitis (Park et al. 2015; Aldini et al. 2012; Ohama et al. 2007). Although these experiments provide valuable information about the functional properties of isolated colonic smooth muscles, evaluation of the role of the ENS in inflammation-induced colonic dysmotility can only be achieved via studies of the whole organ. There are currently no in-depth analyses of isolated whole colon motility in a murine model of chronic colitis.

Our spatiotemporal maps of isolated colonic motility revealed distinct rhythmic recurring patterns of motor activity in control C57BL/6 mice, consistent with previous studies (Spencer et al. 2013; Roberts et al. 2008a; Bush et al. 2001; 2000). Alterations in both spatial and temporal characteristics of colonic motility were evident in *Winnie* mice. Notably, colonic motility in the C57BL/6 and *Winnie* mouse differed in the absence of external stimuli, as well as in response to rising intraluminal pressure. *Winnie* mice showed a high number of fragmented contractions in the colon. Fragmented contractions in the colon of C57BL/6 mice have previously been associated with variations in nitrergic innervation in different colonic regions (Chen et al. 2013a; Wang et al. 2009a). Importantly, our study is the first to report fragmented contractions in an experimental model of colitis. Previous studies have shown that the membrane potential of the circular layer is maintained under tonic neurogenic inhibition in the interval between CMMCs (Spencer et al. 1998; Fida et al. 1997). Periodic withdrawal of tonic inhibition, or disinhibition, can lead to generation of contractions (Spencer et al. 1998). Therefore, coinciding with a decrease in CMMCs, the amplified occurrence of fragmented contractions may indicate disruption to neural inhibition and circuitry regulating CMMC generation.

We observed an increased frequency of short or segmenting contractions between CMMCs in the *Winnie* mice colon. Spatially disorganized short contractions were also observed in C57BL/6 mice. This is consistent with

previous studies describing this type of motor pattern in normal intestinal motility (Roberts et al. 2007). The segmenting motor pattern varies from peristalsis in that it comprises only stationary or very short distance contractions. Hence, it is considered to be a specialized motor pattern for mixing and absorption (Fung et al. 2010; Huizinga and Chen 2014). Although short contractions were evident in all regions of the *Winnie* and C57BL/6 mouse colon, they were most frequent at the distal end with no constant or predictable pattern of occurrence. Under normal conditions, short contractions have been reported to make up a high proportion of activity in the distal colon (Bampton et al. 2002); however, we observed an exaggerated increase in spontaneous activity in the *Winnie* distal colon.

The chronic intestinal inflammation in the *Winnie* mouse colon is associated with fewer propulsive propagating contractions and promotion of short contractions. In *Winnie* mice, loss of *Muc2* leads to a thinner mucus layer allowing increased intestinal permeability and thus enhanced susceptibility to luminal toxins normally within the gut. The extended mixing period observed in the colons from *Winnie* mice might suggest slower colonic transit, contrary to what was seen *in vivo*. However, the faster CMMC propagation seen in this study suggests a mechanism for the faster colonic transit *in vivo* and the non-secretory diarrhea and changes to absorption described in UC (Van Klinken et al. 1999). This would also contribute to soft stools and increased fecal water content observed in *Winnie* mice. An increased propagation of contraction would reduce the contact time of fecal material with the inflamed mucosa and diminish absorption of water and electrolytes (Sarna 2010). Thus, clinical symptoms such as diarrhea may be associated with inhibited absorption in the colon of *Winnie* mice. This requires further investigation.

Altered colonic motility in *Winnie* mice may result from challenges to ENS output and/or the regulatory mechanisms of smooth muscle cells. Chronic inflammation-induced changes to motility in *Winnie* mice are associated with changes to neuromuscular transmission, including decreased purinergic fIJPs and cholinergic EJPs. The amplitude of fIJPs in the *Winnie* colon was significantly different from those in C57BL/6 mice. The fIJPs are mediated by ATP acting at

P2Y1 receptors and represent the rapid purinergic component of the IJP (Mutafova-Yambolieva et al. 2007). A reduction in purinergic inhibitory transmission in the inflamed colon is consistent with previous reports in guinea-pig TNBS-colitis and mouse DSS-colitis (Roberts et al. 2013; Strong et al. 2010), where it has been concluded that an inflammation-induced decrease in the synthesis and release of purines contributes to a reduced purinergic neuromuscular transmission (Roberts et al. 2013). Inhibition of P2Y1 receptors slows propulsive motility in TNBS-inflamed guinea-pigs (Strong et al. 2010). Exogenously applied ATP to precontracted distal colon rings produced comparable responses in *Winnie* and C57BL/6 tissue. Similar findings were reported in TNBS-colitis (Strong et al. 2010). Thus, we conclude that interruptions to purinergic neurotransmission, but not alterations in the smooth muscle response to ATP, contribute to inflammation-induced changes in colonic motility in *Winnie* mice.

EJPs are predominantly mediated by ACh released from cholinergic neurons acting at smooth muscle receptors to cause contraction (Spencer and Smith 2001). The amplitudes of EJPs were reduced in the *Winnie* mouse colon, in contrast to previous studies of the effects of acute TNBS- and DSS-induced colitis on neuromuscular transmission which reported no change in EJP amplitudes (Roberts et al. 2013; Strong et al. 2010). Our data are consistent with our finding of reductions in density of cholinergic nerve fibers innervating the distal colon of *Winnie* mice, something that has also been described in UC patients (Jonsson et al. 2007).

Smooth muscle contractility in response to cholinergic stimulation is also impaired in the *Winnie* distal colon. In contrast, no change in ACh-mediated contractile force was reported in the colon of IL-10$^{-/-}$ mice with chronic inflammation (Park et al. 2015). IL-10$^{-/-}$ mice provide an IBD model that closely resembles human CD (Hale and Greer 2012), whereas *Winnie* mice appear to model UC (Eri et al. 2011). In addition, these authors used colonic sections, rather than colonic rings as employed in our study. Intestinal muscle hypocontractility is seen in isolated colonic muscle strips from both patients with UC and animal models of acute

colonic inflammation (Qureshi et al. 2010; Sato et al. 2007; Shi and Sarna 1999; Annese et al. 1997; Martinolle et al. 1997; Grossi et al. 1993; Reddy et al. 1991; Koch et al. 1988).

Our study identified changes in both excitatory neuromuscular transmission and the smooth muscle response to carbachol suggesting that colonic dysmotility in *Winnie* mouse may result from both alterations to ENS output and smooth muscle cell function. Cholinergic innervation mediates the rapid component of the CMMC (Bywater et al. 1989). Thus, reduced CMMC frequency in the *Winnie* mouse colon may be due to impaired cholinergic output from the ENS.

The slow nitrergic component of the IJP (sIJP) involves activation of NO and cyclic guanosine monophosphate (GMP) (Strong et al. 2010). *Winnie* and C57BL/6 mice had similar sIJPs in the distal colon, consistent with our findings of no changes to the number of nNOS neurons in the distal colon of *Winnie* mice when compared with C57BL/6 mice. Normal nitrergic sIJPs have been reported in acute TNBS-colitis (Strong et al. 2010). The reasons for this apparent protection of nitrergic neuromuscular transmission are uncertain.

Exogenously applied NO donor SNP evoked a reduced level of smooth muscle relaxation in the distal colon from *Winnie* mice. NO-mediated relaxation of distal colon smooth muscle is also impaired in chronically inflamed IL-$10^{-/-}$ mice (Park et al. 2015). Similar findings have been observed in acute intestinal inflammation where smooth muscle relaxation in response to NO donor was decreased (Rajagopal et al. 2015; van Bergeijk et al. 1998). Release of inhibitory neurotransmitters suppresses contractile activity of the circular muscle (Farrell and Savage 2012; Roberts et al. 2007; Spencer et al. 1998). Subsequent to downregulatory mechanisms, smooth muscle response to NO is inhibited by high endogenous NO production as demonstrated by increased concentrations of NO in intestinal mucosa of IBD patients (Rachmilewitz et al. 1995; Middleton et al. 1993; Tepperman et al. 1993).

An impaired smooth muscle cell response may be associated with changes to muscle structure (Nair et al. 2014; Blennerhassett et al. 1999). We found that the

number of smooth muscle cells in the *Winnie* distal colon was significantly greater than in the C57BL/6 colon which is consistent with the increased muscle thickness of the distal colon in *Winnie* mice. A thickened intestinal wall occurs because of both hypertrophy and hyperplasia of the smooth muscle cells and is characteristic of inflammation in human disease and in animal models of intestinal inflammation (Finkelstone et al. 2012; Blennerhassett et al. 1999; 1992). It has been suggested that an increased number of cells with an altered contractile nature may challenge normal intestinal motility and is a cumulative risk for future obstruction, stricture formation, and fibrosis (Nair et al. 2014). Chronic inflammation in the *Winnie* distal colon would accentuate hyperplasia of smooth muscle cells in the colon wall, which may be associated with changes in smooth muscle function. Cooperation between neurally induced pacemaker activity by interstitial cells of Cajal and enteric neural programs in the *Winnie* mouse colon needs to be further investigated.

4.6 Conclusion

In conclusion, the present study demonstrates that chronic colitis in *Winnie* mice is associated with dysmotility and significant impairment of distal colon innervation. Furthermore, we found that cholinergic and purinergic neuromuscular transmission, as well as the smooth muscle cell responses to cholinergic and nitrergic stimulation, is altered in the chronically inflamed *Winnie* mouse colon. The reduced inhibitory purinergic responses are probably a prejunctional event, whereas diminished inhibitory nitrergic responses in the *Winnie* mouse colon may be due to a postjunctional mechanism. Diminished excitatory responses occurred both prejunctionally and postjunctionally. Myenteric neuronal loss and changes in cholinergic, noradrenergic and sensory innervation, as well as intestinal transit and colonic function observed in *Winnie* mice are similar to those seen in IBD patients; thus, this model is highly representative of human IBD and should be useful for studying chronic intestinal inflammation.

CHAPTER FIVE: FECAL MICROBIOTA AND METABOLOME IN A MOUSE MODEL OF SPONTANEOUS CHRONIC COLITIS: RELEVANCE TO HUMAN INFLAMMATORY BOWEL DISEASE

The material presented in this chapter is published and has been reproduced here with the permission of the publisher with minor alterations:

Robinson, A. M., Gondalia, S. V., Karpe, A. V., Eri, R., Beale, D. J., Morrison, P. D., Palombo, E. A., Nurgali, K. 2016. Fecal microbiota and metabolome in a mouse model of spontaneous chronic colitis: Relevance to human inflammatory bowel disease. *Inflamm Bowel Dis,* 22, 2627-87.

5.1 Summary

Background: Dysbiosis of the gut microbiota may be involved in the pathogenesis of inflammatory bowel disease (IBD). However, the mechanisms underlying the role of the intestinal microbiome and metabolome in IBD onset and its alteration during active treatment and recovery remain unknown. Animal models of chronic intestinal inflammation with similar microbial and metabolomic profiles would enable investigation of these mechanisms and development of more effective treatments. Recently, the *Winnie* mouse model of colitis closely representing the clinical symptoms and characteristics of human IBD has been developed. In this study, we have analyzed fecal microbial and metabolomic profiles in *Winnie* mice and discussed their relevance to human IBD. **Methods:** The 16S rRNA gene was sequenced from fecal DNA of *Winnie* and C57BL/6 mice to define operational taxonomic units at ≥97% similarity threshold. Metabolomic profiling of the same fecal samples was performed by gas chromatography-mass spectrometry. **Results:** Microbial richness, diversity, and evenness were not altered by chronic intestinal inflammation in *Winnie* mice. However, composition of the dominant microbiota was disturbed, and prominent differences were evident at the phylum, class, order, family, genus and, species levels of the intestinal microbiome in fecal samples from *Winnie* mice, similar to observations in patients with IBD. Metabolomic profiling revealed that chronic colitis in *Winnie* mice upregulated production of metabolites and altered several metabolic pathways, mostly affecting amino acid synthesis and breakdown of monosaccharides to short chain fatty acids. **Conclusions:** Significant dysbiosis in the *Winnie* mouse gut replicates many changes observed in patients with IBD. These results provide justification for the suitability of this model to investigate mechanisms underlying the role of intestinal microbiota and metabolome in the pathophysiology of IBD.

5.2 Introduction

The gastrointestinal (GI) tract harbors a highly diverse collection of microorganisms. The intestinal microbiota are involved in complex interactions between host mucosal epithelial and immune cells to shape fundamental physiological, metabolic, and immunological processes (Bakhtiar et al. 2013; Ley et al. 2008; Gill et al. 2006). Disruption to this symbiotic homeostasis and abnormal interactions between a host's immune system and gut microbiota have been implicated in the pathogenesis of several GI disorders, including inflammatory bowel disease (IBD), functional dyspepsia, irritable bowel syndrome, diabetes and obesity (Sartor and Mazmanian 2012; Sartor 2008; Ley et al. 2006). However, it remains unclear whether this dysbiosis is a cause or consequence of these disorders.

It is generally considered that IBD occurs due to inappropriate activation of intestinal mucosal immunity and an imbalanced mucosal immune response to commensal bacteria in genetically susceptible hosts (Chassaing and Darfeuille-Michaud 2011). Persuasive evidence supporting an integral role for intestinal microbiota in IBD is provided by experimental models, where animals develop colitis in conventional environments, but not in the absence of commensal microbiota in germ-free conditions (Liu et al. 2013; Sartor 2008; Elson et al. 2005). Furthermore, fecal and intestinal microbiota of IBD patients are characterized by decreased biodiversity and abnormal compositions (Manichanh et al. 2012; Qin et al. 2010), as well as disturbed metabolites (Thibault et al. 2010; Sartor 2008). Loss of beneficial microbes can provide opportunity for the emergence of disease-promoting microbes producing metabolites with negative effects on the intestine under inflammatory conditions (Dalal and Chang 2014). Collectively, these findings suggest the intestinal microbiota might play a role in initiating, maintaining, and determining the phenotype of intestinal inflammatory disease. However, the mechanisms underlying the role of the GI microbiome and metabolome in IBD onset and its alteration in the course of active treatment and recovery are still unknown.

Most intestinal microbiotas are anaerobic and difficult to identify using culture-dependent methods (Suau et al. 1999). However, advances in DNA sequencing methods and development of culture-independent techniques have enabled the high-throughput phylogenetic study of microbial ecology and composition during IBD, in addition to examining the underlying molecular and metabolic mechanisms (Goodman et al. 2011; Schloss and Handelsman 2005). Currently, most detailed knowledge is available with respect to the microbial composition of feces because fecal material can be collected non-invasively and contains a large biomass of microbial cells. The large intestine has a rather uniform composition of luminal intestinal microorganisms, and fecal material seems to represent the colonic microbiota composition best (Eckburg et al. 2005).

Experimental animal models provide an opportunity to identify gut microbial community members and functions in IBD, and host-microbiota responses to therapies. This can be difficult to discern in humans given their genetic diversity and variability in environmental and treatment exposures (Huttenhower et al. 2014; Kostic et al. 2013). Many experimental models of IBD evoke acute colitis via chemicals or nematodes (Brierley and Linden 2014). In contrast, limited models of chronic intestinal inflammation exist. Recently, the *Winnie* mouse model of colitis has been developed which closely represents the clinical symptoms of IBD, including bloody stools, diarrhea, and weight loss (Eri et al. 2011; Heazlewood et al. 2008). A primary intestinal epithelial defect in the mucin *Muc2* gene alters intestinal barrier permeability and activates the interleukin (IL)-23/Th17 pathway in *Winnie* mice causing the development of spontaneous chronic intestinal inflammation (Eri et al. 2011; Heazlewood et al. 2008). Additionally, defects in Paneth and goblet cells of the *Winnie* mouse intestine heighten their vulnerability to luminal antigens (McGuckin et al. 2011).

Previous studies have described changes to histopathology, immunology, and intestinal innervation in the *Winnie* GI tract (Rahman et al. 2016; 2015; Shabala et al. 2013; Eri et al. 2011; Heazlewood et al. 2008). However, studies reporting the microbiome and metabolome signatures of *Winnie* mice with spontaneous chronic colitis are lacking. We chose to profile fecal samples from *Winnie* mice

rather than mucosal samples, since fecal material is highly representative of the colonic microbiome and metabolome, non-invasive to attain, and able to be compared to the majority of other studies investigating gut microbiota and metabolites in IBD patients. In this study, we investigated variations in microbial phyla, class and order, as well as more intricate differences at the family, genus and species levels between *Winnie* and C57BL/6 mice. In addition, we assessed the metabolic profiles of fecal samples from both phenotypes to determine changes in metabolites produced by the intestinal bacteria during colonic inflammation. The findings of this study will substantiate the *Winnie* mouse model of colitis to be appropriate in studying IBD-related microbiota, as well as provide assistance in targeting changes in microbiota as a therapy for intestinal inflammation.

5.3 Materials and methods

5.3.1 Sample collection and DNA extraction

Fecal samples were collected from *Winnie* (12wk old; *n*=10) and C57BL/6 (12wk old; *n*=10) mice and stored at -80°C until microbial DNA was extracted. DNA was extracted from 0.25g of each fecal sample using MoBio PowerFecal® DNA Isolation Kit (Geneworks, Thebarton, South Australia) according to the manufacturer's instructions. Briefly, homogenization and lysis of cells was performed with a FastPrep-24® instrument (MP Biomedical, Seven Hills, NSW Australia) at 6.5m/s for 45s. Contaminating non-DNA organic and inorganic matter were then removed using patented Inhibitor Removal Technology®. A high concentration salt solution was added to assist the DNA bind to the silica spin filters before the DNA was cleaned with an ethanol-based wash solution to remove residual salt and other contaminants. Finally, a sterile elution buffer (10mM Tris) released the DNA from the spin column filter, yielding DNA that was ready for downstream applications. All centrifugation steps were carried out in a Heraeus Fresco-17™ centrifuge (Thermo Scientific, Scoresby, VIC, Australia) for 1min at 13,000*g*.

5.3.2 High-throughput sequence analysis

The samples underwent high-throughput sequencing on the Illumina MiSeq platform at the Australian Genome Research facility (University of Queensland, Brisbane, Australia). Paired-end reads were assembled by aligning the forward and reverse reads using join_paired_ends.py. Primers were trimmed using Seqtk (version 1.0). Trimmed sequences were processed using Quantitative Insights into Microbial Ecology (QIIME 1.9) 4 USEARCH2,3 (version 8.0.1623) software (Caporaso et al. 2010). Briefly, de-multiplexing and quality filtering were performed using the split_libraries_fastq.py script for each data set. Operational Taxonomic Units (OTUs) were *de novo* picked at 97% sequence similarity following the USEARCH pipeline and representative sequences of each cluster were used to assign taxonomy through matching against the Blast 2.2.22

database. Evaluations present at each taxonomic level, including percentage compilations, represent all sequences resolved to their primary identification or their closest relative. Alpha diversity using alpha_diversity.py script was performed for species richness, Good's coverage, Chao1, Shannon-Wiener's diversity index and Simpson's index. Weighted and unweighted UniFrac distance matrices were obtained through Jack-knifed beta diversities in QIIME and Principal Coordinate Analysis (PCoA) plots were obtained. Sample clustering and statistical analysis were carried out in R environment and SPSS (version 23).

5.3.3 Metabolomic analysis

Fecal samples from the same *Winnie* (*n*=6) and C57BL/6 (*n*=4) mice were collected for metabolic profiling. Freeze dried fecal samples (40±2mg) were derivatized prior to analyses by gas chromatography-mass spectrometry (GC-MS) as described previously (Ng et al. 2012). Briefly, 1mL of methanol was added to the samples, immediately ^{13}C-stearic acid (10µg/mL; HPLC grade; Sigma-Aldrich, Castle Hill, NSW, Australia) was added as an internal standard. The sample was than vortexed for 2min and centrifuged at 572.5*g* and 4°C for 15min. 50µL of supernatant was transferred to a clean tube and dried in an RVC 2-18 centrifugal evaporator at 210*g* and 37°C (Vacubrand GMBH, Wertheim, Germany). All samples were stored at -80°C until further use.

5.3.3.1 Sample silyl derivatization

In order to derivatize the samples for GC-MS analysis, 40µL methoxamine HCl (2% in pyridine) was added to each sample and incubated for 45min at 37°C. To complete the derivatization, silylation was performed by adding 70µL BSTFA in 1% TMCS. Samples were then incubated for an additional 1h at 70°C. Pre-derivatized ^{13}C-Sorbitol (Kovats Retention Index=1918.76; m/z=620.00; 10µg/mL; HPLC grade; Sigma-Aldrich) was added as the second internal standard in order to verify instrument stability over the run time. Samples were then vortexed and centrifuged at 15682*g* for 5min before transferring to GC-MS vials.

5.3.3.2 Single quadrupole GC-MS

The derivatized samples were analyzed using an Agilent 6890B Gas Chromatograph (GC) oven coupled with a 5973A Mass spectrometer (MS) detector (Agilent Technologies, Mulgrave, VIC, Australia) as described previously (Beale et al. 2014; 2013). Five replicates per sample were used for GC-MS analyses. Data acquisition and processing were performed using MassHunter. Qualitative identification of the compounds was performed according to the Metabolomics Standard Initiative (MSI) Chemical Analysis Workgroup (Sumner et al. 2007) using standard GC-MS reference metabolite libraries of Wiley, NIST 11 and NIST EPA/NIH.

5.3.4 Statistical analysis

Two-tailed *t*-tests were used to compare two sets of data, assuming unequal variance. $P<0.05$ was considered significant. The data generated by mass spectral analyses were normalized with respect to internal standards (RSD=19.28%), where a magnitude of 1-fold change (FC) referred to the concentration of 10mg/L. Statistical analysis was performed using SIMCA 14 (Umetrics AG, Umea, Sweden) and MetaboAnalyst 3.0 (TMIC, Edmonton, Canada). For metabolome: an unsupervised statistical approach using Principal Component Analysis (PCA) was undertaken on the data, with no clear separation being observed. To accommodate the outliers and enable differentiation between the groups based on metabolic pattern, a Partial Least Square-Discriminant Analysis (PLS-DA) was employed (Wold et al. 2001). The normalized observational distance between X modal plane (DModX) was used to find the residual standard of variables in PLS-DA model.

5.4 Results

5.4.1 16S rRNA sequencing and bioinformatics analysis of fecal samples from C57BL/6 and *Winnie* mice

A large quantity of gut bacteria and their metabolic products are present in feces creating an ideal biological sample to assess functional changes of the gut microbiome. To compare compositional differences in gut microbiota between healthy C57BL/6 control mice and *Winnie* mice with chronic colonic inflammation, we used 16S rRNA sequencing with fecal samples collected from 20 animals (C57BL/6: *n*=10, *Winnie*: *n*=10). Total DNA was extracted from the fecal samples and polymerase chain reaction (PCR) amplicons spanning the 16S rRNA V3-V4 hypervariable region were sequenced. High-quality pyrosequencing yielded a total of 919,819 sequences from 20 fecal samples with an average of 45,990 reads per sample (range: 22,580-68,027) (C57BL/6: 24,242±3,808 reads per sample, range: 11,551-48,907; *Winnie*: 35,072±4,072 reads per sample, range: 21,330-53,756 [see Appendix A, Table S1]; Fig. 5.1A). To characterize the microbial communities, sequences were clustered into OTUs at a ≥97% similarity threshold. Following removal of low-quality or chimeric sequences, 11,551 high-quality sequences per sample were available for analysis. The rarefaction curve of most samples approached saturation indicating sufficient reads for comparisons (data not shown).

5.4.2 Microbial richness, diversity and evenness of fecal samples

Library coverage was calculated by Good's formula (C57BL/6: 88-94%; *Winnie*: 90-97%) indicating that the 16S rRNA gene sequences from each sample encompassed the majority of the microbiota in each mouse ([see Appendix A, Table S1]; Fig. 5.1B). The effect of chronic colonic inflammation on fecal microbiota α-diversity was assessed based on OTU richness (Chao1), diversity (Shannon-Wiener diversity index) and evenness (Simpson index). Community richness did not differ significantly between C57BL/6 and *Winnie* mice (*P*=0.18; [see Appendix A, Table S1]; Fig. 5.1C). Similarly, there were no statistically

significant differences in the diversity (*P*=0.72) or evenness (*P*=0.42) of the groups ([see Appendix A, Table S1]; Fig. 5.1D-E).

Trends in community-level diversity differences were further probed by exploring the amount of diversity shared between samples (β-diversity) using an unsupervised multivariate statistical technique, PCoA. Applying unweighted UniFrac, the first three axes of the PCoA, plotted in Fig. 5.1F, were sufficient to account for 55% of the total variability. The relative contribution to variability for each successive axis decreased. The first principal coordinate (PC1) captured 28% of intersample variance revealing a sharp distinction between the gut microbiota of C57BL/6 and *Winnie* mice. PC2 captured 18% and PC3 9% of variance further separating samples based on individual subject (Fig. 5.1F). Taken together, these results suggest that the gut microbiota of C57BL/6 and *Winnie* mice show both compositional individuality and temporal stability in their distal gut microbiota.

Figure 5.1. Species richness estimates and diversity indices between fecal samples from C57BL/6 and *Winnie* mice. Microbiota communities were profiled from healthy C57BL/6 mice and *Winnie* mice with chronic colonic inflammation. Number of reads per sample in each phenotype **(A)**. Library coverage calculated by Good's formula **(B)**. Chao's richness estimate detected in each group **(C)**. Community diversity and evenness assessed by calculating the Shannon H' (diversity) **(D)** and Simpson E (evenness) **(E)** indices based on microarray phylotype abundance data. Principle coordinate analysis (PCoA) of communities in C57BL/6 versus *Winnie* mice based on unweighted UniFrac distance **(F)**.

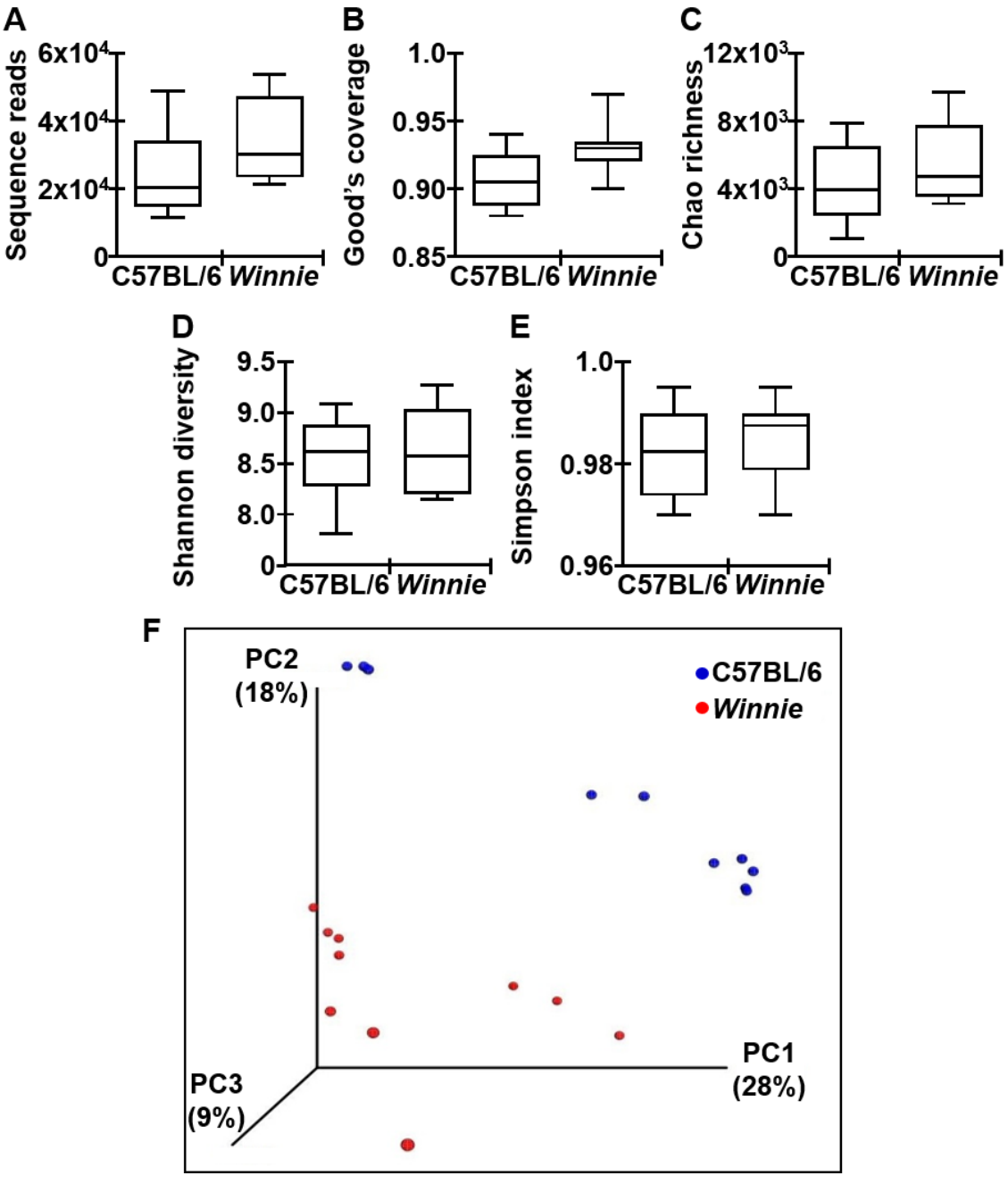
A
Sequence reads
6x10^4
4x10^4
2x10^4
0
C57BL/6
Winnie
B
Good's coverage
1.0
0.95
0.90
0.85
C57BL/6
Winnie
C
Chao richness
12x10^3
8x10^3
4x10^3
0
C57BL/6
Winnie
D
Shannon diversity
9.5
9.0
8.5
8.0
0
C57BL/6
Winnie
E
Simpson index
1.0
0.98
0.96
C57BL/6
Winnie
F
PC2
(18%)
C57BL/6
Winnie
PC1
(28%)
PC3
(9%)

5.4.3 Differences in the gut microbiome at the phylum level in fecal samples from C57BL/6 and *Winnie* mice

In this study, 12 bacterial phyla were identified in all fecal samples (Fig. 5.2). A majority of the core OTUs were represented by two phyla: *Bacteroidetes and Firmicutes,* which have repeatedly been described as major and functionally significant components of the human intestinal microbiota (Jandhyala et al. 2015). Although *Winnie* mice shared the majority of the same OTUs as healthy controls, quantities of core OTUs varied. *In both phenotypes, Bacteriodetes* was the most profuse phylum. Although the abundance of the *Bacteriodetes* phylum was less in fecal samples from *Winnie* mice (62.0±4.0%) compared to samples from C57BL/6 mice (66.4±6.2%), the result was not statistically significant (Fig. 5.2). Similarly, while the *Firmicutes* phylum was increased in samples from *Winnie* mice (26.6±3.5% vs 22.0±6.4%), statistical significance was lacking (Fig. 5.2). The *Bacteriodetes* to *Firmicutes* ratio was higher in samples from C57BL/6 mice (3:1) compared to *Winnie* mice (2:1). *Actinobacteria*, *Chloroflexi*, *Cyanobacteria*, *Deferribacteres*, *Nitrospirae*, *Proteobacteria*, *TM7*, *Tenericutes*, *Verrucomicrobia* and an *Unknown* phylum were also identified in fecal samples from both phenotypes (Fig. 5.2A). A greater abundance of *Actinobacteria* (1.0±0.3% (113.6±35.8 OTUs) vs 0.1±0.0% (8.6±3.0 OTUs); $P<0.01$), *Cyanobacteria* (0.1±0.0% (9.8±3.4 OTUs) vs 0.0±0.0% (2.1±1.0 OTUs); $P<0.05$) and *Proteobacteria* (4.1±0.8% (471.9±91.9 OTUs) vs 2.3±0.3% (262.3±38.5 OTUs); $P<0.05$) were represented in samples from *Winnie* mice, while *Tenericutes* (0.0±0.1% (2.3±2.1 OTUs) vs 0.3±0.3% (32.7±8.4 OTUs); $P<0.05$) and an *Unknown* phylum (4.3±0.3% (492.0±30.9 OTUs) vs 5.7±0.3% (659.5±29.5 OTUs); $P<0.01$) were reduced (Fig. 5.2B). No changes were evident in *Verrucomicrobia* (1.7±0.6% vs 2.1±1.5%), *Deferribacteres* (0.2±0.1% vs 0.8±0.4%), *TM7* (0.1±0.1% vs 0.3±0.1%), *Nitrospirae* (0.0±0.0% vs 0.0±0.0%) and *Chloroflexi* phylum (0.0±0.0% vs 0.0±0.0%; Fig. 5.2B).

Figure 5.2. Phylum level changes in fecal gut communities. The composition and relative abundance estimates of bacterial phylum (%) measured in fecal samples from *Winnie* and C57BL/6 mice **(A)**. Quantitative analysis depicting significant changes in phyla distribution between phenotypes **(B)**. **P*<0.05, ***P*<0.01.

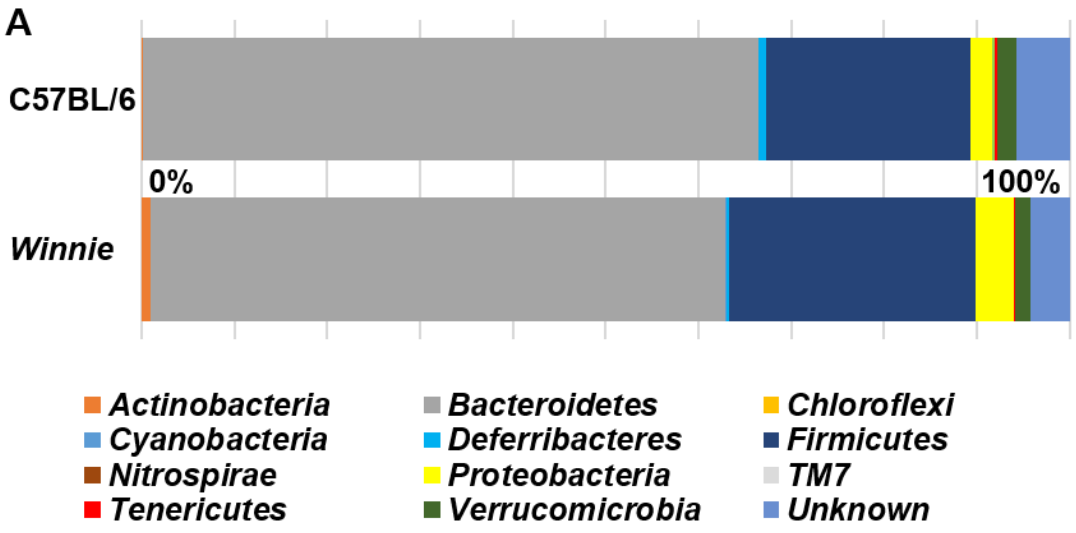
A
C57BL/6
0%
100%
Winnie
Actinobacteria
Bacteroidetes
Chloroflexi
Cyanobacteria
Deferribacteres
Firmicutes
Nitrospirae
Proteobacteria
TM7
Tenericutes
Verrucomicrobia
Unknown

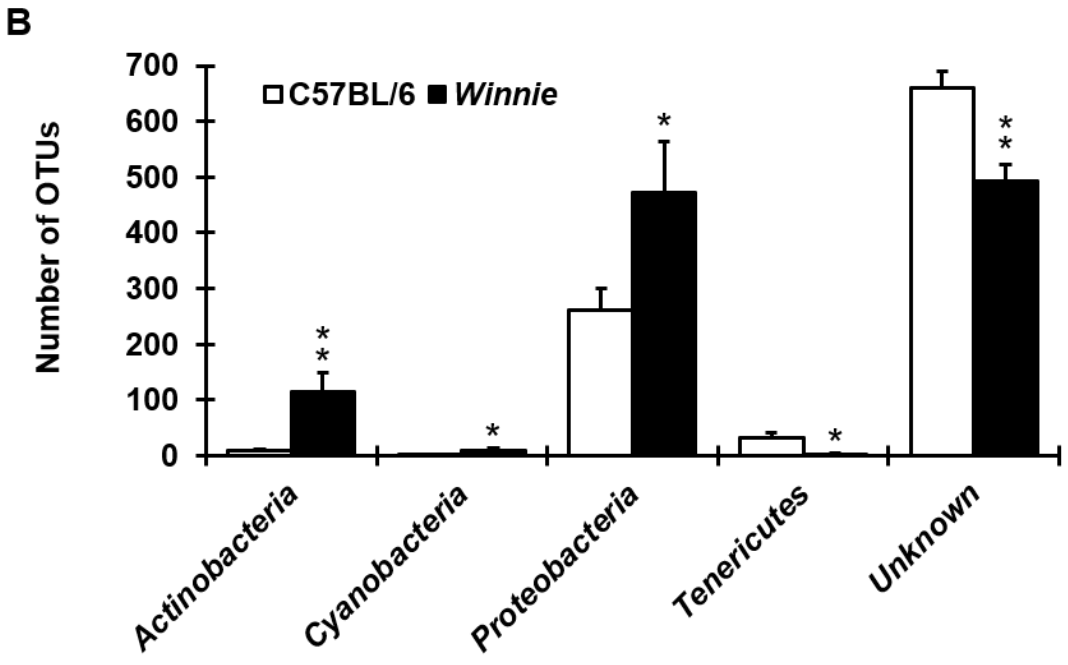
B
Number of OTUs
700
600
500
400
300
200
100
0
C57BL/6
Winnie
Actinobacteria
Cyanobacteria
Proteobacteria
Tenericutes
Unknown

5.4.4 Class differences in the gut microbiome in fecal samples from C57BL/6 and *Winnie* mice

From the 12 identified phyla in samples from both phenotypes, 22 microbial classes were recognized (Fig. 5.3A). *Clostridia* (*Winnie*: 20.5±3.2%, 2366.2±371.4 OTUs; C57BL/6: 21.0±6.5%, 2424.9±746.0 OTUs) and *Erysipelotrichi* (*Winnie*: 4.5±1.2%, 514.8±143.1 OTUs; C57BL/6: 0.5±0.4%, 61.0±47.1 OTUs; $P<0.01$; Fig. 5.3B) from *Firmicutes* phylum, as well as *Bacteroidia* (*Winnie*: 62.0±4.0%, 7158.4±466.6 OTUs; C57BL/6: 66.4±6.2%, 7666.6±715.0 OTUs) from *Bacteroidetes* phylum were the most prevalent in *Winnie* mice. Within the *Actinobacteria* phylum, 2 classes of bacteria were increased in samples from *Winnie* mice when compared to healthy controls: *Actinobacteria* (*Winnie*: 76.8±32.5 OTUs; C57BL/6: 5.7±3.1 OTUs; $P<0.05$) and *Coriobacteria* (*Winnie*: 36.7±12.4 OTUs; C57BL/6: 2.9±1.2 OTUs; $P<0.05$). Similarly, *4C0d-2* (*Winnie*: 9.5±3.3 OTUs; C57BL/6: 2.1±1.0 OTUs; $P<0.05$) from *Cyanobacteria* and *Bacilli* (*Winnie*: 191.3±58.9 OTUs; C57BL/6: 58.5±19.7 OTUs; $P<0.05$) from *Firmicutes* phylum were also increased in the fecal samples from *Winnie* mice with chronic colonic inflammation (Fig. 5.3B). On the other hand, *Mollicutes* (*Winnie*: 2.3±2.1 OTUs; C57BL/6: 32.7±8.4 OTUs; $P<0.05$) from *Tenericutes* were reduced (Fig. 5.3B).

5.4.5 Changes to microbial order in fecal samples from C57BL/6 and *Winnie* mice

From the fecal samples of both phenotypes, 28 orders of bacteria were identified (Fig. 5.4A). The most dominant orders were *Clostridiales* (*Winnie*: 20.5±3.2%, 2366.2±371.4 OTUs; C57BL/6: 21.0±6.5%, 2424.9±746.0 OTUs) from *Firmicutes* phylum and *Bacteroidales* (*Winnie*: 62.0±4.0%, 7158.4±466.6 OTUs; C57BL/6: 66.4±6.2%, 7666.6±715.0 OTUs) from *Bacteroidetes* phylum. Within the *Actinobacteria* phylum, 2 orders of bacteria were increased in samples from *Winnie* mice when compared to healthy controls: *Bifidobacteriales* (class *Actinobacteria*) (*Winnie*: 76.8±32.5 OTUs; C57BL/6: 5.7±3.1 OTUs; $P<0.05$) and *Coriobacteriales* (class *Coriobacteria*) (*Winnie*: 36.7±12.4 OTUs; C57BL/6:

2.9±1.2 OTUs; *P*<0.05). Equally, *Erysipelotrichales* (class *Erysipelotrichi*) (*Winnie*: 514.8±143.1 OTUs; C57BL/6: 61.0±47.1 OTUs; *P*<0.01) and *Lactobacillales* (class *Bacilli*) (*Winnie*: 191.3±58.9 OTUs; C57BL/6: 55.8±18.9 OTUs; *P*<0.05) from *Firmicutes* phylum, as well as *YS2* (class *4C0d-2*) (*Winnie*: 9.5±3.3 OTUs; C57BL/6: 2.1±1.0 OTUs; *P*<0.05) from *Cyanobacteria* were also increased in the fecal samples from *Winnie* mice (Fig. 5.4B). Alternatively, *Anaeroplasmatales* (*Winnie*: 0.1±0.1 OTUs; C57BL/6: 11.2±3.5 OTUs; *P*<0.01) and *RF39* (both from class *Mollicutes*) (*Winnie*: 2.1±2.1 OTUs; C57BL/6: 21.5±7.9 OTUs; *P*<0.05) from *Tenericutes* were reduced (Fig. 5.4B).

Figure 5.3. Class level changes in fecal gut communities. The composition and relative abundance estimates of bacterial classes (%) measured in fecal samples from *Winnie* and C57BL/6 mice **(A)**. Quantitative analysis depicting significant changes in class distribution between phenotypes **(B)**. *P<0.05, **P<0.01.

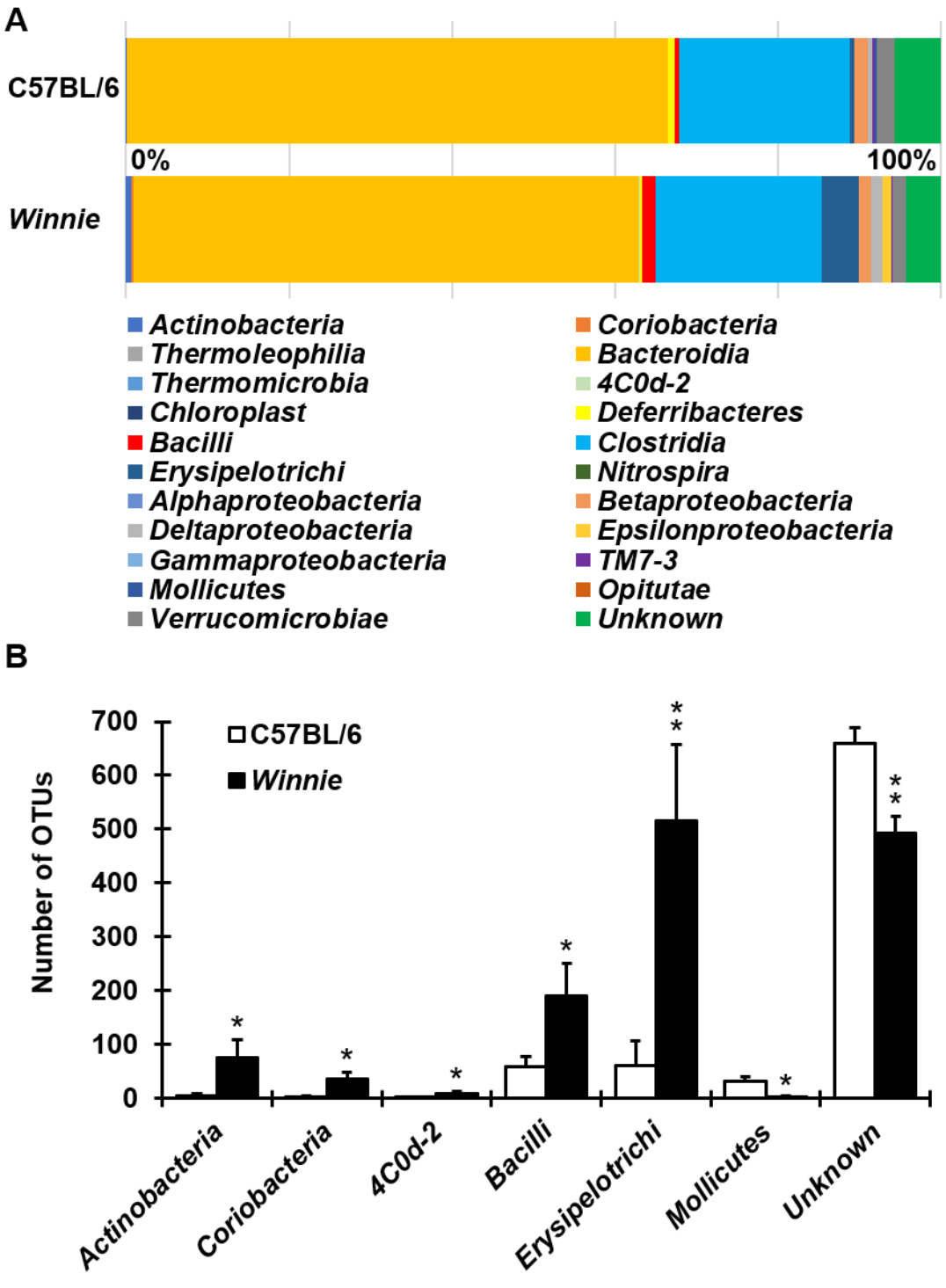
A
C57BL/6
0%
100%
Winnie
Actinobacteria
Coriobacteria
Thermoleophilia
Bacteroidia
Thermomicrobia
4C0d-2
Chloroplast
Deferribacteres
Bacilli
Clostridia
Erysipelotrichi
Nitrospira
Alphaproteobacteria
Betaproteobacteria
Deltaproteobacteria
Epsilonproteobacteria
Gammaproteobacteria
TM7-3
Mollicutes
Opitutae
Verrucomicrobiae
Unknown
B
Number of OTUs
700
600
500
400
300
200
100
0
C57BL/6
Winnie
Actinobacteria
Coriobacteria
4C0d-2
Bacilli
Erysipelotrichi
Mollicutes
Unknown

Figure 5.4. Order level changes in fecal gut communities. The composition and relative abundance estimates of bacterial orders (%) measured in fecal samples from *Winnie* and C57BL/6 mice **(A)**. Quantitative analysis depicting significant changes in order distribution between phenotypes **(B)**. **P*<0.05, ***P*<0.01.

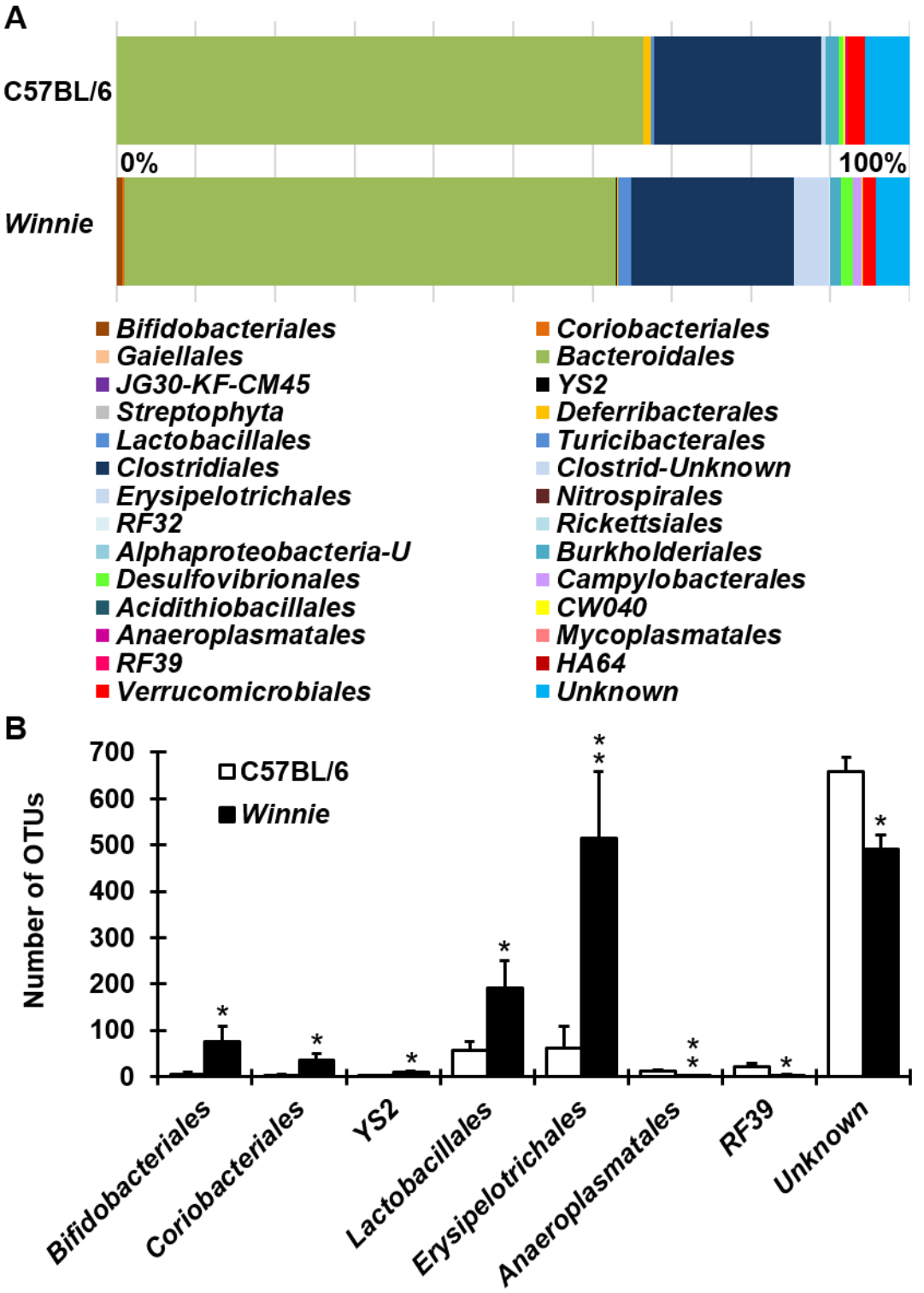
A
C57BL/6
Winnie
0%
100%
Bifidobacteriales
Coriobacteriales
Gaiellales
Bacteroidales
JG30-KF-CM45
YS2
Streptophyta
Deferribacterales
Lactobacillales
Turicibacterales
Clostridiales
Clostrid-Unknown
Erysipelotrichales
Nitrospirales
RF32
Rickettsiales
Alphaproteobacteria-U
Burkholderiales
Desulfovibrionales
Campylobacterales
Acidithiobacillales
CW040
Anaeroplasmatales
Mycoplasmatales
RF39
HA64
Verrucomicrobiales
Unknown
B
Number of OTUs
700
600
500
400
300
200
100
0
C57BL/6
Winnie
Bifidobacteriales
Coriobacteriales
YS2
Lactobacillales
Erysipelotrichales
Anaeroplasmatales
RF39
Unknown

5.4.6 Changes in fecal microbiota at the family level in *Winnie* mice

Analysis of fecal samples from *Winnie* and C57BL/6 mice showed variances in the bacterial families present contributing to the differences in β-diversity and grouping (Fig. 5.5A). The most abundant distribution of microbial family was *S24-7* (phylum *Bacteroidetes*, class *Bacteroidia*, order *Bacteroidales*) followed by an *unknown Clostridiales* (phylum *Firmicutes*, class *Clostridia*, order *Clostridiales*). Amongst identified bacterial families, six were more abundant in samples from *Winnie* mice compared to samples from C57BL/6 mice: *Bifidobacteriaceae (Winnie*: 76.8±32.5 OTUs; C57BL/6: 5.7±3.1 OTUs; $P<0.05$) and *Coriobacteriaceae (Winnie*: 36.7±12.4 OTUs; C57BL/6: 2.9±1.2 OTUs; $P<0.05$) from *Actinobacteria* phylum, *unknown YS2 (Winnie*: 9.5±3.3 OTUs; C57BL/6: 2.1±1.0 OTUs; $P<0.05$) from *Cyanobacteria* phylum, *Lactobacilliaceae (Winnie*: 191.2±59.0 OTUs; C57BL/6: 55.8±18.9 OTUs; $P<0.05$) and *Erysipelotrichaceae (Winnie*: 514.8±143.1 OTUs; C57BL/6: 61.0±47.1 OTUs; $P<0.01$) from *Firmicutes* phylum and *Oxalobacteraceae (Winnie*: 1.3±0.5 OTUs; C57BL/6: 0.1±0.1 OTUs; $P<0.05$) from *Proteobacteria* phylum (Fig. 5.5B). The increases in *Bifidobacteriaceae* and *Coriobacteriaceae* in samples from *Winnie* mice correlate with the greater abundance of the *Actinobacteria* phylum in this group. Additionally, increases in the *Lactobacilliaceae and Erysipelotrichaceae* families, as well as in the *Oxalobacteraceae* family and in the *unknown YS2* family associate with increases in the *Firmicutes*, *Proteobacteria* and *Cyanobacteria* phyla in samples from *Winnie* mice. Certain bacterial families were reduced in samples from *Winnie* mice including *Prevotellaceae (Winnie*: 287.6±78.9 OTUs; C57BL/6: 739.3±128.6 OTUs*;* $P<0.01$), *[Barnesiellaceae] (Winnie*: 0.1±0.1 OTUs; C57BL/6: 4.2±1.8 OTUs; $P<0.05$) and *[Paraprevotellaceae] (Winnie*: 167.9±68.7 OTUs; C57BL/6: 839.2±175.2 OTUs; $P<0.01$) from *Bacteroidetes* phylum; *Dehalobacteriaceae (Winnie*: 9.9±5.7 OTUs; C57BL/6: 69.5±24.9 OTUs*,* $P<0.05$) and *Peptococcaceae (Winnie*: 0.0±0.0 OTUs; C57BL/6: 1.7±0.8 OTUs*,* $P<0.05$) from *Firmicutes* phylum; *Anaeroplasmataceae (Winnie*: 0.1±0.1 OTUs; C57BL/6: 11.2±3.5 OTUs; $P<0.01$) and *unknown RF39 (Winnie*: 2.1±2.1 OTUs; C57BL/6: 21.5±7.9 OTUs; $P<0.05$) from *Tenericutes* phylum (Fig. 5.5B).

Figure 5.5. Changes in bacterial families present in fecal samples from *Winnie* mice. The composition and relative abundance estimates of bacterial families (%) measured in fecal samples from *Winnie* and C57BL/6 mice **(A)**. Quantitative analysis depicting significant changes in order distribution between phenotypes **(B)**. *P<0.05, **P<0.01.

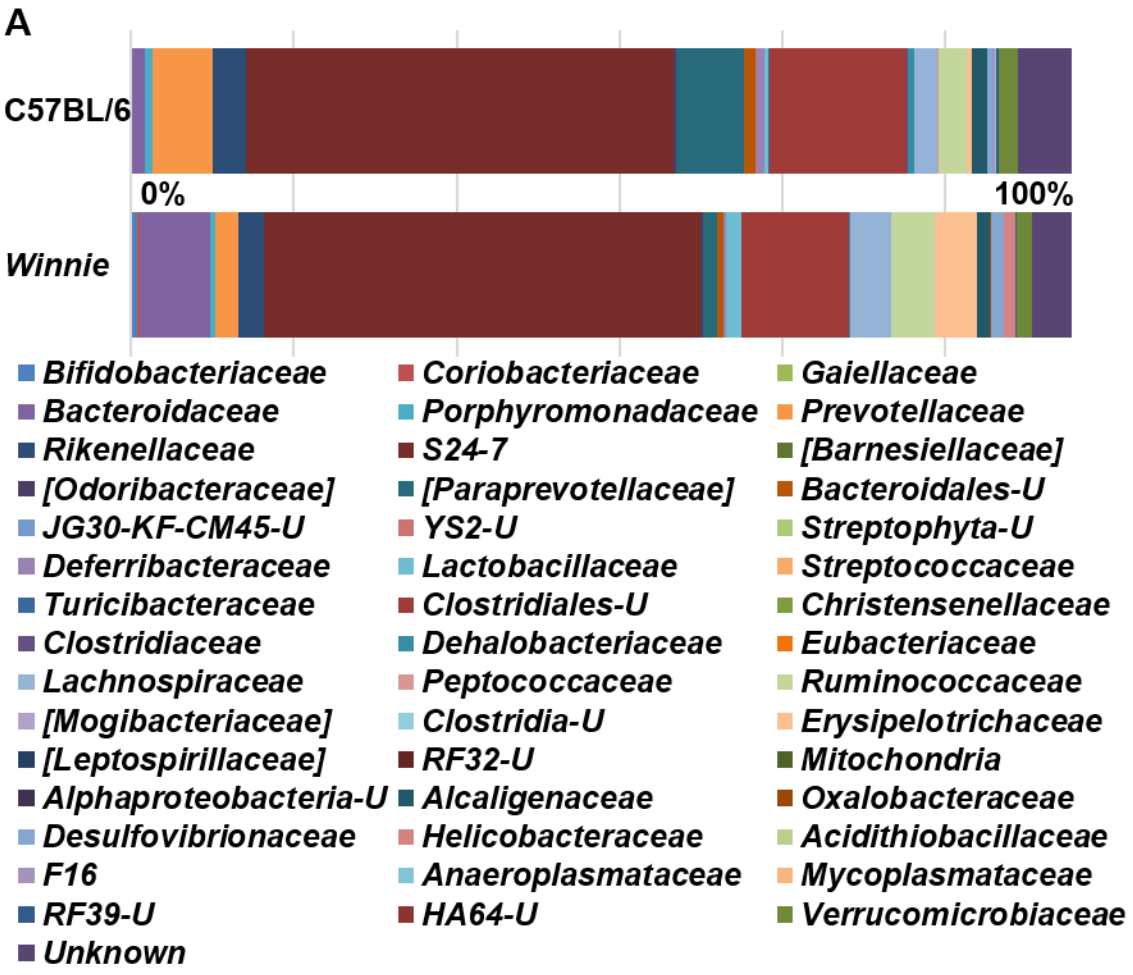
A
C57BL/6
0%
100%
Winnie
Bifidobacteriaceae
Coriobacteriaceae
Gaiellaceae
Bacteroidaceae
Porphyromonadaceae
Prevotellaceae
Rikenellaceae
S24-7
[Barnesiellaceae]
[Odoribacteraceae]
[Paraprevotellaceae]
Bacteroidales-U
JG30-KF-CM45-U
YS2-U
Streptophyta-U
Deferribacteraceae
Lactobacillaceae
Streptococcaceae
Turicibacteraceae
Clostridiales-U
Christensenellaceae
Clostridiaceae
Dehalobacteriaceae
Eubacteriaceae
Lachnospiraceae
Peptococcaceae
Ruminococcaceae
[Mogibacteriaceae]
Clostridia-U
Erysipelotrichaceae
[Leptospirillaceae]
RF32-U
Mitochondria
Alphaproteobacteria-U
Alcaligenaceae
Oxalobacteraceae
Desulfovibrionaceae
Helicobacteraceae
Acidithiobacillaceae
F16
Anaeroplasmataceae
Mycoplasmataceae
RF39-U
HA64-U
Verrucomicrobiaceae
Unknown

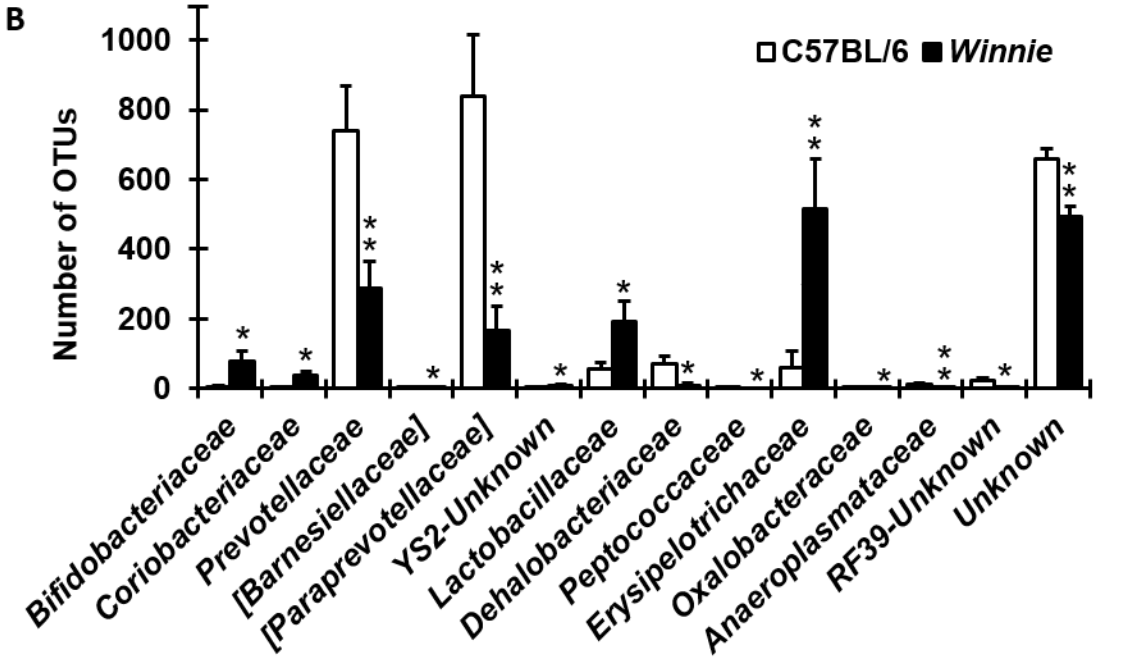
B
C57BL/6
Winnie
Number of OTUs
1000
800
600
400
200
0
Bifidobacteriaceae
Coriobacteriaceae
Prevotellaceae
[Barnesiellaceae]
[Paraprevotellaceae]
YS2-Unknown
Lactobacillaceae
Dehalobacteriaceae
Peptococcaceae
Erysipelotrichaceae
Oxalobacteraceae
Anaeroplasmataceae
RF39-Unknown
Unknown

5.4.7 Genus level differences of microbiota in fecal samples from *Winnie* and healthy C57BL/6 mice

At the genus level, distribution of microbiota in samples from *Winnie* mice was markedly different to samples from C57BL/6 mice (Fig. 5.6A). Specifically, the abundance of *Bifidobacterium (Winnie*: 76.8±32.5 OTUs; C57BL/6: 5.7±3.1 OTUs*; P*<0.05) and *unknown Coriobacteriaceae (Winnie*: 22.2±6.0 OTUs; C57BL/6: 1.6±0.7 OTUs*; P*<0.01) from *Actinobacteria* phylum, *AF12 (Winnie*: 27.2±12.1 OTUs; C57BL/6: 0.0±0.0 OTUs*, P*<0.05) from *Bacteroidetes* phylum, *unknown YS2 (Winnie*: 9.5±3.3 OTUs; C57BL/6: 2.1±1.0 OTUs*; P*<0.05) from *Cyanobacteria* phylum, *Lactobacillus (Winnie*: 191.2±59.0 OTUs; C57BL/6: 55.8±18.9 OTUs*, P*<0.05) and *Allobaculum (Winnie*: 506.7±145.5 OTUs; C57BL/6: 58.9±47.0 OTUs*; P*<0.01) from *Firmicutes* phylum, *Oxalobacter (Winnie*: 1.3±0.5 OTUs; C57BL/6: 0.0±0.0 OTUs*; P*<0.05), *unknown Desulfovibrionaceae (Winnie*: 54.7±13.6 OTUs; C57BL/6: 1.1±0.5 OTUs*; P*<0.001) and *unknown Helicobacteraceae (Winnie*: 27.7±12.3 OTUs; C57BL/6: 0.0±0.0 OTUs*; P*<0.05) from *Proteobacteria* phylum were all increased in fecal samples from *Winnie* mice (Fig. 5.6B). On the other hand, certain microbial families were reduced in the samples from *Winnie* mice: *unknown Prevotellaceae (Winnie*: 8.9±3.3 OTUs; C57BL/6: 533.8±101.4 OTUs*; P*<0.001), *unknown [Barnesiellaceae] (Winnie*: 0.1±0.1 OTUs; C57BL/6: 4.2±1.8 OTUs*; P*<0.05) and *[Prevotella] (Winnie*: 167.9±68.7 OTUs; C57BL/6: 839.2±175.2 OTUs*; P*<0.01) from *Bacteroidetes* phylum, *Dehalobacterium (Winnie*: 9.9±5.7 OTUs; C57BL/6: 69.0±25.0 OTUs*; P*<0.05) and *unknown Peptococcaceae (Winnie*: 0.0±0.0 OTUs; C57BL/6: 1.7±0.8 OTUs*; P*<0.05) from *Proteobacteria* phylum, as well as *Anaeroplasma (Winnie*: 0.1±0.1 OTUs; C57BL/6: 11.2±3.1 OTUs*; P*<0.01) and *unknown RF39 (Winnie*: 2.1±2.1 OTUs; C57BL/6: 21.5±7.9 OTUs*; P*<0.05) from *Tenericutes* phylum (Fig. 5.6B).

Figure 5.6. Genus level changes in fecal samples from *Winnie* mice. The genus level composition and relative abundance estimates (%) measured in fecal samples from *Winnie* and C57BL/6 mice **(A)**. Quantitative analysis depicting significant changes in order distribution between phenotypes **(B)**. *P<0.05, **P<0.01, ***P<0.001.

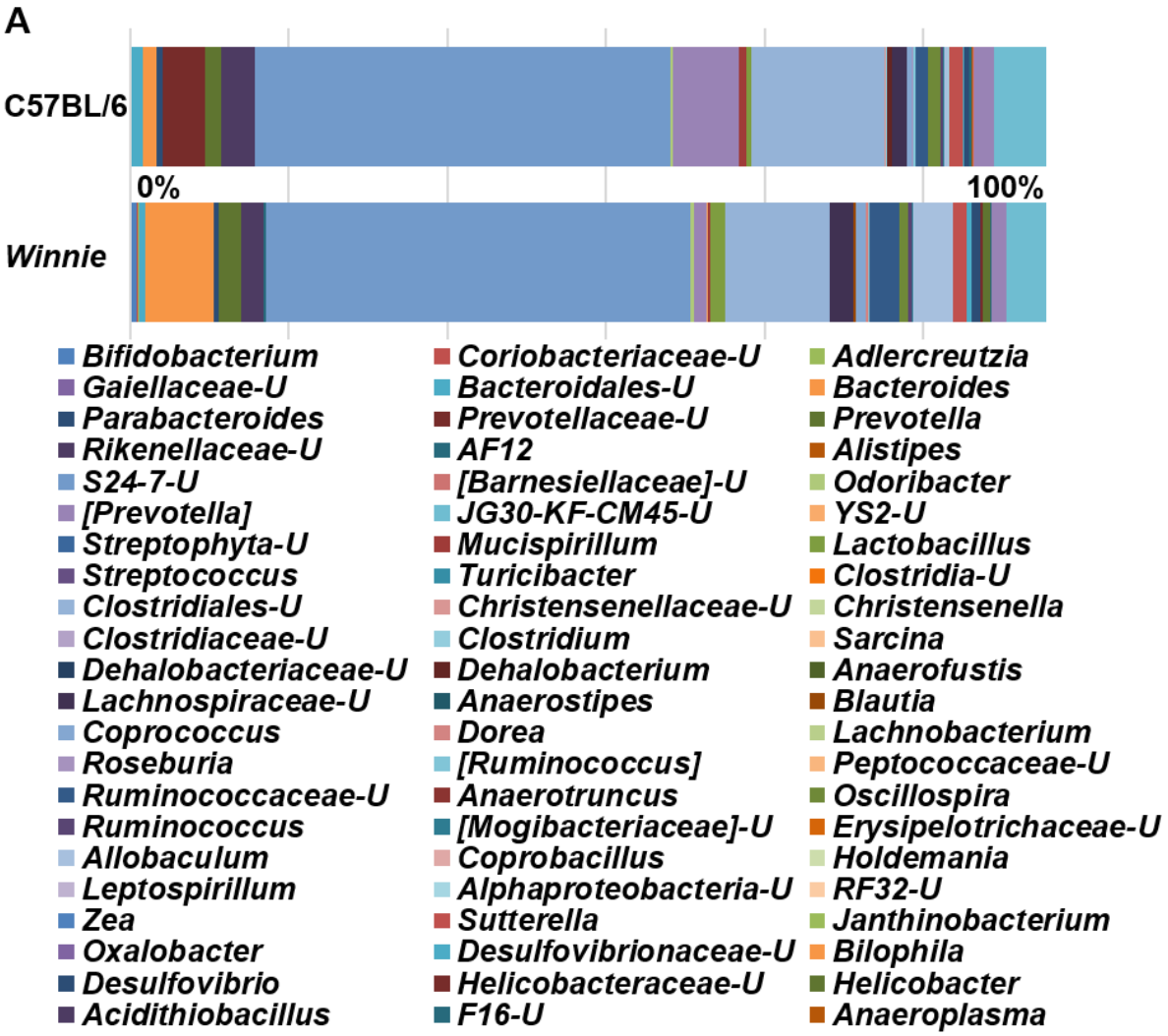
A
C57BL/6
0%
100%
Winnie
Bifidobacterium
Coriobacteriaceae-U
Adlercreutzia
Gaiellaceae-U
Bacteroidales-U
Bacteroides
Parabacteroides
Prevotellaceae-U
Prevotella
Rikenellaceae-U
AF12
Alistipes
S24-7-U
[Barnesiellaceae]-U
Odoribacter
[Prevotella]
JG30-KF-CM45-U
YS2-U
Streptophyta-U
Mucispirillum
Lactobacillus
Streptococcus
Turicibacter
Clostridia-U
Clostridiales-U
Christensenellaceae-U
Christensenella
Clostridiaceae-U
Clostridium
Sarcina
Dehalobacteriaceae-U
Dehalobacterium
Anaerofustis
Lachnospiraceae-U
Anaerostipes
Blautia
Coprococcus
Dorea
Lachnobacterium
Roseburia
[Ruminococcus]
Peptococcaceae-U
Ruminococcaceae-U
Anaerotruncus
Oscillospira
Ruminococcus
[Mogibacteriaceae]-U
Erysipelotrichaceae-U
Allobaculum
Coprobacillus
Holdemania
Leptospirillum
Alphaproteobacteria-U
RF32-U
Zea
Sutterella
Janthinobacterium
Oxalobacter
Desulfovibrionaceae-U
Bilophila
Desulfovibrio
Helicobacteraceae-U
Helicobacter
Acidithiobacillus
F16-U
Anaeroplasma
B
Number of OTUs
1000
800
600
400
200
0
C57BL/6
Winnie
Bifidobacterium
Coriobacteriaceae-U
Prevotellaceae-U
AF12
[Barnesiellaceae]-U
[Prevotella]
YS2-U
Lactobacillus
Dehalobacterium
Peptococcaceae-U
Allobaculum
Oxalobacter
Desulfovibrionaceae-U
Helicobacteraceae-U
Anaeroplasma
RF39-U
Unknown

5.4.8 Species level differences of microbiota in fecal samples from *Winnie* and healthy C57BL/6 mice

In this study, 88 species were identified in the fecal samples analyzed and 19 of these species differed between phenotypes (Fig. 5.7A). In samples from *Winnie* mice, there was an increased abundance of species from *Actinobacteria* phylum, including *unknown Bifidobacterium (Winnie*: 13.7±5.8 OTUs; C57BL/6: 0.7±0.4 OTUs*; P*<0.05), *Bifidobacterium longum (Winnie*: 0.5±0.2 OTUs; C57BL/6: 0.0±0.0 OTUs*; P*<0.05), *Bifidobacterium pseudolongum (Winnie*: 61.4±26.6 OTUs; C57BL/6: 4.9±2.6 OTUs*, P*<0.05) and *unknown Coriobacteriaceae (Winnie*: 22.2±6.0 OTUs; C57BL/6: 1.6±0.7 OTUs*; P*<0.01). In addition, *unknown AF12 (Winnie*: 27.2±12.0 OTUs; C57BL/6: 0.0±0.0 OTUs*; P*<0.05) from *Bacteroidetes* phylum, *unknown YS2 (Winnie*: 9.5±3.3 OTUs; C57BL/6: 2.1±1.0 OTUs*; P*<0.05) from *Cyanobacteria* phylum, *unknown Lactobacillus (Winnie*: 191.2±59.0 OTUs; C57BL/6: 55.8±18.9 OTUs*; P*<0.05) and *unknown Allobaculum (Winnie*: 506.7±145.5 OTUs; C57BL/6: 58.9±47.0 OTUs*; P*<0.01) from *Firmicutes* phylum, *Oxalobacter formigenes (Winnie*: 1.3±0.5 OTUs; C57BL/6: 0.0±0.0 OTUs*; P*<0.01), *unknown Desulfovibrionaceae (Winnie*: 54.7±13.6 OTUs; C57BL/6: 1.1±0.5 OTUs*; P*<0.001), and *unknown Helicobacteraceae (Winnie*: 27.7±12.3 OTUs; C57BL/6: 0.0±0.0 OTUs*, P*<0.05) from *Proteobacteria* phylum were increased in samples from *Winnie* mice (Fig. 5.7B). Certain bacterial species were found to be decreased in samples from *Winnie* mice, including: *unknown Prevotellaceae (Winnie*: 8.9±3.3 OTUs; C57BL/6: 533.8±101.4 OTUs*; P*<0.001), *unknown [Barnesiellaceae] (Winnie*: 0.1±0.1 OTUs; C57BL/6: 4.2±1.8 OTUs*; P*<0.05) and *[Prevotella] (Winnie*: 167.9±68.7 OTUs; C57BL/6: 839.2±175.2 OTUs*; P*<0.01) from *Bacteroidetes* phylum, *unknown Dehalobacterium (Winnie*: 9.9±5.7 OTUs; C57BL/6: 69.0±25.0 OTUs*; P*<0.05) and *unknown Peptococcaceae (Winnie*: 0.0±0.0 OTUs; C57BL/6: 1.7±0.8 OTUs*; P*<0.05) from *Proteobacteria* phylum, as well as *unknown Anaeroplasma (Winnie*: 0.1±0.1 OTUs; C57BL/6: 11.2±3.1 OTUs*; P*<0.01) and *unknown RF39 (Winnie*: 2.1±2.1 OTUs; C57BL/6: 21.5±7.9 OTUs*; P*<0.05) from *Tenericutes* phylum (Fig. 5.7B).

Figure 5.7. Species level changes in fecal samples from *Winnie* mice. The species level composition and relative abundance estimates (%) measured in fecal samples from *Winnie* and C57BL/6 mice **(A)**. Quantitative analysis depicting significant changes in order distribution between phenotypes **(B)**. **P*<0.05, ***P*<0.01, ****P*<0.001.


A
C57BL/6
0%
100%
Winnie
Bifidobacterium-U
Adolescentis
Animalis
Bifidobacterium-Longum
Bifidobacterium-Pseudolongum
Coriobacteriaceae-U
Adlercreutzia-U
Gaiellaceae-U
Bacteroidales-U
Bacteroides-U
Bacteroides-Acidifaciens
Bacteroides-Ovatus
Bacteroides-Uniformis
Parabacteroides-U
Parabacteroides-Distasonis
Parabacteroides-Gordonii
Prevotellaceae-U
Prevotella-U
Prevotella-Copri
Prevotella-Stercorea
Rikenellaceae-U
AF12-U
Alistipes-Massiliensis
S24-7-U
[Barnesiellaceae]-U
Odoribacter-U
[Prevotella]-U
JG30-KF-CM45-U
YS2-U
Streptophyta-U
Mucispirillum-Schaedleri
Lactobacillus-U
Lactobacillus-Reuteri
Streptococcus-U
Turicibacter-U
Clostridia-U
Clostridiales-U
Christensenellaceae-U
Christensenella-U
Clostridiaceae-U
Clostridium-U
Clostridium-Perfringens
Sarcina-U
Dehalobacteriaceae-U
Dehalobacterium-U
Anaerofustis-U
Lachnospiraceae-U
Anaerostipes-U
Blautia-U
Blautia-Producta
Coprococcus-U
Dorea-U
Lachnobacterium-U
Roseburia-U
[Ruminococcus]-Gnavus
Peptococcaceae-U
Ruminococcaceae-U
Anaerotruncus-U
Oscillospira-U
Ruminococcus-U
[Mogibacteriaceae]-U
Erysipelotrichaceae-U
Allobaculum-U
Coprobacillus-U
Coprobacillus-Cateniformis
Holdemania-U
Leptospirillum-U
Alphaproteobacteria-U
RF32-U
Zea-Luxurians
Sutterella-U
Janthinobacterium-U
Oxalobacter-Formigenes
Desulfovibrionaceae-U
Bilophila-U
Desulfovibrio-U
Desulfovibrio-C21_C20
Helicobacteraceae-U
Helicobacter-U
Helicobacter-Apodemus
Acidithiobacillus-Caldus
F16-U
Anaeroplasma-U
Mycoplasmataceae-U
RF39-U
HA64-U
Akkermansia-Muciniphila
Unknown

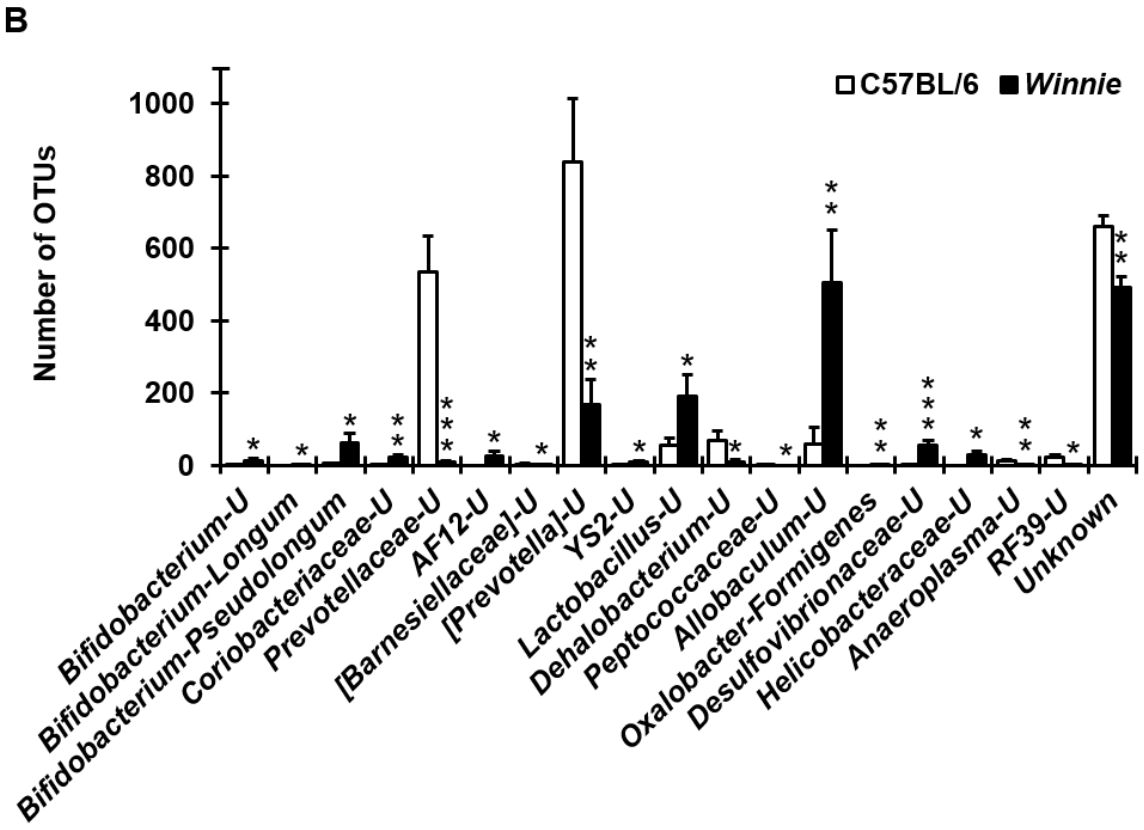
B
C57BL/6
Winnie
Number of OTUs
1000
800
600
400
200
0
Bifidobacterium-U
Bifidobacterium-Longum
Bifidobacterium-Pseudolongum
Coriobacteriaceae-U
Prevotellaceae-U
AF12-U
[Barnesiellaceae]-U
[Prevotella]-U
YS2-U
Lactobacillus-U
Dehalobacterium-U
Peptococcaceae-U
Allobaculum-U
Oxalobacter-Formigenes
Desulfovibrionaceae-U
Helicobacteraceae-U
Anaeroplasma-U
RF39-U
Unknown

5.4.9 Metabolome profiling of fecal samples from *Winnie* and healthy C56BL/6 mice

GC-MS metabolic profiling of fecal samples from *Winnie* (*n*=6) and C57BL/6 (*n*=4) mice yielded a total of 154 metabolites. An unsupervised statistical approach using PCA was undertaken. The model showed three PCs accounting for 31.4% (component 1) and 17.2% (component 2) variance in the data with good predictabilities (R^2X(cum)=88% and Q^2(cum)=63.9%) [see Appendix A, Fig. S1]. Although metabolic profiles were differentiated, no clear separation was observed and consequently the predictability of the model remained unsatisfactory (albeit good). Therefore, a supervised form of discriminant analysis, PLS-DA, that relies on the class membership of each observation was applied. The PLS-DA model, based on significant components, accounted for 30.5% (component 1) and 6.26% (component 2) of the data variance, with higher predictabilities of R^2X(cum)=93.4%, R^2Y(cum)=97.3% and Q^2(cum)=86.2% [see Appendix A, Fig. S2A-B]. Hence, PLS-DA better yielded metabolite discrimination compared to PCA analysis indicating a distinct separation between sample groups. In a DModX model using critical value (Dcrit), the F-distribution based size of the observational model area of the PCA was calculated to be 1.23. Any values greater than this number were considered as the moderate outliers [see Appendix A, Fig. S2C].

Of the 154 metabolites analyzed by PLS-DA, 74 were significantly different in samples from *Winnie* compared to C57BL/6 mice based on their FC and statistical significance, as based on FC value ≥2.0 and *P* value ≤ 0.05 (Table 5.1; Fig. 5.8). The structures of these metabolites were diverse, including carbohydrates (CHOs), amino acids, derivatives of CHO and amino acid metabolism, carboxylic acids, fatty acids, alcohols, aldehydes, alkanes and phenolic compounds. In particular, samples from *Winnie* mice showed an increased presence of CHOs and CHO conjugates, alcohols, carboxylic acids and derivatives. Certain amino acid derivatives and lipid metabolites were also several fold higher in *Winnie* mice feces compared to C57BL/6 samples (Table 5.1; Fig. 5.8). On the other hand, samples from *Winnie* mice revealed significantly

fewer amino acid, peptides and amines, as well as lipid metabolites than in samples from C57BL/6 mice (Table 5.1). Overall, fecal metabolomic profiling demonstrated inflammation-associated alterations in metabolites produced by the gut microbiome and, in particular, inhibition of monosaccharide breakdown to short chain fatty acids (SCFAs), as well as hindrance of amino acid metabolism.

Table 5.1. Metabolites identified in fecal samples from *Winnie* (FC>2.0) and C57BL/6 (FC<2.0) mice analyzed by PLS-DA and *t*-test of GC-MS data

Metabolites	Kovats RI	FC	*P* Value	m/z	InChI key	KEGG ID
1-O-Methyl-alpha-D-Galactoside	2394.8	10.0	0.000	194.2	HOVAGTYPODGVJG-PZRMXXKTSA-N	C03619
Tyramine (3TMS)	1907.1	7.5	0.000	353.7	WDQQWJKBIMOZAK-UHFFFAOYSA-N	C00483
N,O-Bis(trimethylsilyl)-L-phenylalanine/Phenylalanine (2TMS)	1646.7	5.7	0.000	309.6	DWNFNBPPSFIIBG-UHFFFAOYSA-N	C00079
Butanal, 2,3,4-tris[(trimethylsilyl)oxy]-3-[[(trimethylsilyl)oxy]methyl]-, O-methyloxime, (S)-	1658.5	5.3	0.000	467.9	OKWPSPPSKQXZNS-WFVLPUPGSA-N	C01412
(+/-)-2,3-Butanediol diTMS	1048.9	5.3	0.000	234.5	ZAPDHFWCOMITJN-UHFFFAOYSA-N	C03044
Xylose, D- (1MEOX) (4TMS)	1660.4	5.2	0.000	467.9	ZBEJHGUYYNELJI-RQSRTLBHSA-N	C00181
Ferulic acid, cis- (2TMS)	2085.2	5.1	0.001	338.5	UQBSUVIBJIXFQT-LUAWRHEFSA-N	C01494
Butane, 2,3-bis(trimethylsiloxy)-	1062.0	4.8	0.000	234.5	ZAPDHFWCOMITJN-UHFFFAOYSA-N	C03044

Table 5.1. Metabolites identified in fecal samples from *Winnie* (FC>2.0) and C57BL/6 (FC<2.0) mice analyzed by PLS-DA and *t*-test of GC-MS data (continued)

Metabolites	Kovats RI	FC	*P* Value	m/z	InChI key	KEGG ID
Ribose, D- (1MEOX) (4TMS)	1664.3	4.7	0.000	467.9	ZBEJHGUYYNELJI-KSZLIROESA-N	C00121
Uridine TMS	3038.8	4.4	0.000	532.9	GQVVRBIFPVSHCQ-XFQGIKGNSA-N	C00299
Inositol, 1,2,3,4,5,6-hexakis-O-(trimethylsilyl)-, D-chiro-	2080.5	4.3	0.001	613.2	FRTKXRNTVMCAKI-UHFFFAOYSA-N	C00137
Neo-Inositol, 1,2,3,4,5,6-hexakis-O-(trimethylsilyl)-	2080.8	4.3	0.001	613.2	FRTKXRNTVMCAKI-HPEVMFQJSA-N	
Fructose, D- (1MEOX) (5TMS)	1667.6	4.1	0.000	570.1	ACDMQGXCXUQPRR-QQLONMSUSA-N	C00095
Pyruvic acid (1MEOX) (1TMS)	1059.6	4.0	0.000	189.3	RDATZQIINHXKAG-SOFGYWHQSA-N	C00022
1-phenyl-1-(2-trimethylsilylcyclopentyl)ethanol	1063.7	4.0	0.000	122.2	WRMNZCZEMHIOCP-UHFFFAOYSA-N	C05853
Trimethylsiloxy-trimethylsilylmethyl-phenylsulphide	1063.2	3.8	0.000	73.0		C00850

Table 5.1. Metabolites identified in fecal samples from *Winnie* (FC>2.0) and C57BL/6 (FC<2.0) mice analyzed by PLS-DA and *t*-test of GC-MS data (continued)

Metabolites	Kovats RI	FC	*P* Value	m/z	InChI key	KEGG ID
Phosphoric acid (3TMS)	1311.6	3.8	0.000	314.5	QJMMCGKXBZVAEI-UHFFFAOYSA-N	C00009
Xylose, D- (1MEOX) (4TMS)	1699.3	3.7	0.000	467.9	ZBEJHGUYYNELJI-RQSRTLBHSA-N	C00181
(-)-Perillyl alcohol	1699.3	3.7	0.000	152.2	NDTYTMIUWGWIMO-UHFFFAOYSA-N	C02452
D-(+)-Glucose	1698.8	3.7	0.000	180.2	GZCGUPFRVQAUEE-SLPGGIOYSA-N	C00031
Compound_105	2112.1	3.7	0.013			
Oxalic acid dihydrate	1050.4	3.6	0.000	126.1	GEVPUGOOGXGPIO-UHFFFAOYSA-N	C00209
Compound_106	2224.0	3.4	0.000			
3-(trimethylsilyl)-1,1-diethoxypropane	1687.2	3.3	0.002			
Glycine, N-(2-methyl-1-oxobutyl)-, trimethylsilyl ester	1682.1	3.3	0.001	231.4	SZZJQCDMJUGIOJ-UHFFFAOYSA-N	C00037
Mucic acid	1681.8	3.3	0.001	210.1	DSLZVSRJTYRBFB-DUHBMQHGSA-N	C00879

Table 5.1. Metabolites identified in fecal samples from *Winnie* (FC>2.0) and C57BL/6 (FC<2.0) mice analyzed by PLS-DA and *t*-test of GC-MS data (continued)

Metabolites	Kovats RI	FC	*P* Value	m/z	InChI key	KEGG ID
3-Oxalomalate	1565.5	3.3	0.001	229.1	RTAVNKBUIDTTIZ-UHFFFAOYSA-N	C01990
Sinapyl alcohol	2102.0	3.2	0.020	210.2	LZFOPEXOUVTGJS-ONEGZZNKSA-N	C02325
Benzenepropanoic acid, 3-[(trimethylsilyl)oxy]-, trimethylsilyl ester	1723.0	3.2	0.013	310.5	BDAIEAHTVSLQPN-UHFFFAOYSA-N	C05629
S-t-Butyl ester of (3-Trimethylsilyloxy-2-cyclopentenyl)-thioacetic acid	1501.8	3.0	0.000	86.5	SGLOKVXGLTZLJN-UHFFFAOYSA-N	
1H-Indole-1-acetic acid	2219.1	2.9	0.000	247.4	QSNYXYIMLGVIJP-UHFFFAOYSA-N	
2-Methyl-4-phenyl-4-trimethylsilylbutan-2-ol	1226.6	2.7	0.000	164.2	YXVSKJDFNJFXAJ-UHFFFAOYSA-N	
D-Ribulose	1677.8	2.7	0.004	230.1	FNZLKVNUWIIPSJ-UHNVWZDZSA-N	C00309
Fucose, DL- (1MEOX) (4TMS)	1715.0	2.7	0.000	481.9	SXUVIFIZLGMRBJ-PYXDERCCSA-N	C01019

Table 5.1. Metabolites identified in fecal samples from *Winnie* (FC>2.0) and C57BL/6 (FC<2.0) mice analyzed by PLS-DA and *t*-test of GC-MS data (continued)

Metabolites	Kovats RI	FC	*P* Value	m/z	InChI key	KEGG ID
Lithocholic acid	1226.1	2.7	0.000	376.6	SMEROWZSTRWXGI-VKPXTEDRSA-N	C03990
Oleic acid, trimethylsilyl ester	2220.0	2.7	0.001	354.6	GAODWSYPSJBKGB-SEYXRHQNSA-N	C00712
Shikimic acid-3-phosphate	1368.1	2.6	0.000	254.1	QYOJSKGCWNAKGW-PBXRRBTRSA-N	
Octadecanoic acid, n- (1TMS)	2244.1	2.6	0.000	356.7	DDLPZVTUKLKVQB-UHFFFAOYSA-N	C01530
Ethanimidic acid, N-(trimethylsilyl)-, trimethylsilyl ester	1157.3	2.6	0.000	203.4	SIOVKLKJSOKLIF-UHFFFAOYSA-N	C06244
Glycerol (3TMS)	1314.8	2.6	0.000	308.6	JQUGYGVCECHKBA-UHFFFAOYSA-N	C00116
Phytol mixture of isomers	1727.7	2.4	0.023	296.5	BOTWFXYSPFMFNR-PYDDKJGSSA-N	C01389
3-Methyl-2-phenyl-4-trimethylsilylbutan-2-ol	2610.2	2.3	0.001	164.2	KZVSJCRPDWUPEP-UHFFFAOYSA-N	

Table 5.1. Metabolites identified in fecal samples from *Winnie* (FC>2.0) and C57BL/6 (FC<2.0) mice analyzed by PLS-DA and *t*-test of GC-MS data (continued)

Metabolites	Kovats RI	FC	*P* Value	m/z	InChI key	KEGG ID
2-Hydroxypyridine	1047.4	2.3	0.000	95.1	UBQKCCHYAOITMY-UHFFFAOYSA-N	C02502
Benzenepropanoic acid, .alpha.-[(trimethylsilyl)oxy]-, trimethylsilyl ester	1616.7	2.3	0.000	398.7	ZSYIYFFJWIPCPN-UHFFFAOYSA-N	
L-(-)-3-Phenyllactic acid	1616.7	2.3	0.000	166.2	VOXXWSYKYCBWHO-UHFFFAOYSA-N	C05607
Compound_1	1048.9	2.2	0.000			
9,12-Octadecadienoic acid (Z,Z)-, trimethylsilyl ester	2256.3	2.2	0.000	352.6	MXGBYOVWUYSJSN-UTJQPWESSA-N	C01595
Trimethylsilyl 3-(3,4-bis[(trimethylsilyl)oxy]phenyl)-2-[(trimethylsilyl)oxy]propanoate	2052.6	2.2	0.000	486.9	YUBNYNACEYYZIC-UHFFFAOYSA-N	
Inulobiose (impurity: Sucrose)	2491.6	2.2	0.005	342.3		C01711
alpha-D-Glucose-1-phosphate, dipotassium salt dihydrate	2491.5	2.2	0.005	260.1	HXXFSFRBOHSIMQ-VFUOTHLCSA-N	
(3-Carboxypropyl) Trimethylammonium chloride	1252.1	2.2	0.000	181.7	GNRKTORAJTTYIW-UHFFFAOYSA-N	C01996

Table 5.1. Metabolites identified in fecal samples from *Winnie* (FC>2.0) and C57BL/6 (FC<2.0) mice analyzed by PLS-DA and *t*-test of GC-MS data (continued)

Metabolites	Kovats RI	FC	*P* Value	m/z	InChI key	KEGG ID
Methionine, DL- (2TMS)	1560.2	2.2	0.003	293.6	JATQZWJTOMUJCG-JTQLQIEISA-N	C00073
Heptadecanoic acid, trimethylsilyl ester	2137.9	2.1	0.000	342.6	KCEZRIREPDDPDI-UHFFFAOYSA-N	C16536
Glycerol (3TMS)	1314.8	2.1	0.000	308.6	JQUGYGVCECHKBA-UHFFFAOYSA-N	C00116
heptadecanoic acid tert-butyl-dimethylsilyl ester	2110.9	2.1	0.000	384.7	PADPNPKFJSPJIC-UHFFFAOYSA-N	
Hexadecanoic acid, n- (1TMS)	2042.1	2.0	0.000	328.6	HKNNSWCACQFVIK-UHFFFAOYSA-N	C00249
Sebacic acid, bis(trimethylsilyl) ester	2416.3	0.4	0.000	346.6	BDACUOPQFMCPLO-UHFFFAOYSA-N	C08277
Putrescine 4TMS	1730.9	0.3	0.005	376.9	HALMUIBMTWWREW-UHFFFAOYSA-N	C00134
Tyrosine, DL- (3TMS)	1931.9	0.3	0.002	397.7	WMWBCQXPKSQMOK-UHFFFAOYSA-N	C00082
L-Isoleucine, N-(trimethylsilyl)-, trimethylsilyl ester	1335.4	0.3	0.046	275.5	JQJPJSDLFYVVEY-GHMZBOCLSA-N	C00407

Table 5.1. Metabolites identified in fecal samples from *Winnie* (FC>2.0) and C57BL/6 (FC<2.0) mice analyzed by PLS-DA and *t*-test of GC-MS data (continued)

Metabolites	Kovats RI	FC	*P* Value	m/z	InChI key	KEGG ID
L-Norleucine, N-(trimethylsilyl)-, trimethylsilyl ester	1335.0	0.3	0.046	275.5	PYFDJFOVTXNRGI-UHFFFAOYSA-N	C01933
Glycine (2TMS)	1161.9	0.3	0.002	219.4	SPAJELCPLFYXLX-UHFFFAOYSA-N	C00037
Cadaverine 4TMS	1830.7	0.2	0.034	390.9	VLLJOGZFMDUFGI-UHFFFAOYSA-N	C01672
2-Piperidinecarboxylic acid, 1-(trimethylsilyl)-, trimethylsilyl ester	1406.3	0.2	0.016	273.5	CPDPZJUOATWIOD-UHFFFAOYSA-N	C00408
Butyric acid, 4-amino- (2TMS)	1570.9	0.2	0.020	247.5	ZRQMOACDJFMJPD-UHFFFAOYSA-N	C00246
Phenylalanine 1TM, 3-phenyl-, trimethylsilyl ester, DL-	1592.9	0.1	0.000	237.4	NBXFAHHUVWSAFQ-NSHDSACASA-N	C00079

Figure 5.8. Differences in the metabolic profiles of fecal microbiota in *Winnie* mice compared to control. Volcano plot demonstrating discrimination between the metabolic profiles of fecal samples from *Winnie* and C57BL/6 mice. Metabolites marked with triangles (▲) represent statistically significant metabolites from *Winnie*, while circles (●) represent metabolites from C57BL/6 mice. Remaining metabolites, marked as diamonds (◆), represent metabolites that were not statistically significant. Lines represent FC value threshold levels of 2.0 (X-axis) and *P* value threshold level of 0.05 (Y-axis).

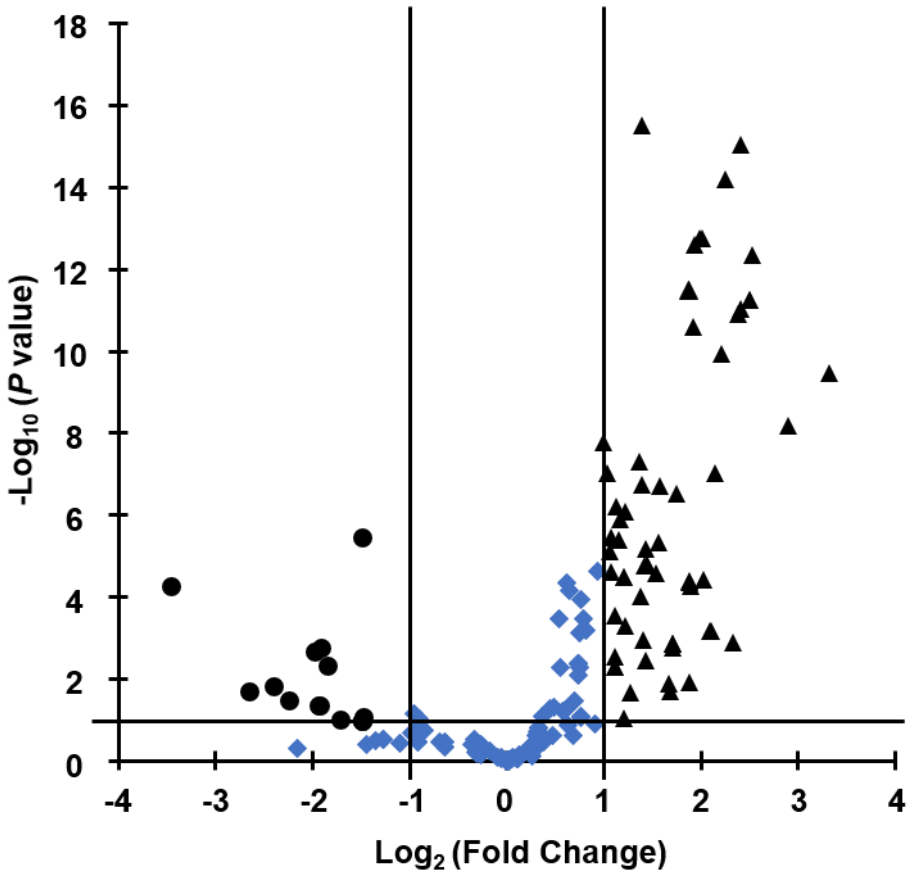
18
16
14
12
10
8
6
4
2
0
-Log10 (P value)
-4
-3
-2
-1
0
1
2
3
4
Log2 (Fold Change)

5.5 Discussion

In this study, we identified the microbial composition and metabolomic profile of fecal samples from *Winnie* mice with spontaneous chronic colitis. Notable differences in the fecal microbiome were evident at all formal levels of bacterial taxonomy, the rank-based classification, including the phylum, class, order, family, genus and species divisions. In general, the abundance of members from the *Actinobacteria* and *Proteobacteria* was greater, while less *Bacteroidetes* and *Tenericutes* present in samples from *Winnie* mice. Metabolomic profiling of fecal samples indicated substantial changes to metabolites generated by the gut bacteria in *Winnie* mice compared to healthy C57BL/6 mice. Specifically, defects in SCFA production and monosaccharide breakdown, as well as hindrance to amino acid metabolism, were observed in the inflamed *Winnie* mouse colon.

The equilibrium of the dominant microbiota was disturbed in the fecal samples from *Winnie* mice, despite species diversity remaining high. Abnormal composition of the intestinal microbiome, such as imbalance between beneficial and harmful microbes, has consistently been reported in IBD patients and animal models of colitis (He et al. 2016; Rooks et al. 2014; Manichanh et al. 2012; Ott et al. 2004; Seksik et al. 2003). In this study, 12 bacterial phyla were identified, with *Bacteroidetes* and *Firmicutes* dominating in both groups. Consistent with our results, multiple studies have demonstrated *Bacteroidetes* and *Firmicutes* to be the two most numerically prevalent bacteria in the human gut (Khor et al. 2011; Waterman et al. 2011; Frank et al. 2007; Eckburg et al. 2005). *Bacteroidetes* inhabit the mucosal surface of the intestinal tract where they modulate immune and intestinal functions (Lathrop et al. 2011; Comelli et al. 2008; Mazmanian et al. 2005; Hooper et al. 2001) while maintaining a mostly beneficial relationship with the host (Hooper et al. 2012; Hooper and Macpherson 2010). Although not statistically significant, a 4% decrease in *Bacteroidetes* was observed in samples from *Winnie* mice when compared to C57BL/6 mice. Several studies have reported reductions in *Bacteroidetes* to associate with IBD (Krogius-Kurikka et al. 2009; Frank et al. 2007; Scanlan et al. 2006). However, other studies have not found any significant alterations (Zitomersky et al. 2013; Andoh et al. 2011;

Bibiloni et al. 2006; Manichanh et al. 2006) or even reported an increased abundance of *Bacteroidetes* (Lucke et al. 2006; Kleessen et al. 2002; Neut et al. 2002). Thus, no clear consensus has been reached about total gut *Bacteroidetes* levels in patients with IBD (Walker et al. 2011; Gophna et al. 2006).

The abundance of the *Prevotellaceae* family from the *Bacteroidetes* phyla was significantly reduced in samples from *Winnie* mice, further evident at the genus and species levels. This is consistent with depleted species from the *Prevotellaceae* family and members of the lineage *Prevotellaceae-Prevotella* found in IBD patients (Juste et al. 2014; Lepage et al. 2011; Willing et al. 2010). On the other hand, increasing trends were demonstrated in *Bacteroides* species and the *AF12* genus from the *Rikenellaceae* family, which has been linked with inflammation in dextran sodium sulfate (DSS)-induced colitis (Schwab et al. 2014), was increased in fecal samples from *Winnie* mice.

Preceding proteomic data in IBD patients implies that specific opportunistic *Bacteroides* pathogens are intensified at the expense of *Prevotella* species (Juste et al. 2014), which could rationalize the shifts within *Bacteroidetes* in this study. Other studies have established decreased mucus secretion, reduced production of glycosylated *Muc2* and increased intestinal permeability in both *Winnie* mice and ulcerative colitis (UC) patients (Heazlewood et al. 2008; Van Klinken et al. 1999; Tytgat et al. 1996). Additionally, elevated levels of bacterial mucin desulfating sulfatases have been associated with active UC (Tsai et al. 1995). This suggests that changes in the *Bacteroidetes* phyla may contribute to and promote chronic inflammation by impairing the function of the epithelial cell barrier via production of mucin desulfating sulfatases (Lucke et al. 2006; Tsai et al. 1995).

There was a 4% increase in the quantity of *Firmicutes* in samples from *Winnie* mice. In contrast, a reduced abundance of the *Firmicutes* phylum has been consistently noted in patients with IBD (Peterson et al. 2008; Frank et al. 2007; Gophna et al. 2006; Manichanh et al. 2006; Scanlan et al. 2006; Sokol et al. 2006). However, the only other study investigating the microbiome in mice with spontaneous chronic colitis also observed increases in *Firmicutes* (Alkadhi et al.

2014). Similar to *Bacteroidetes*, there were shifts in the diversity of *Firmicutes* in samples from *Winnie* mice, which has also been described in patients with IBD (Frank et al. 2007; Manichanh et al. 2006; Ott et al. 2004). Within the *Firmicutes*, order *Clostridiales* and families *Dehalobacterium*, *Peptococcaceae*, and *Clostridiaceae* decreased. A decrease in the *Clostridium* groups has been reported in human studies (Willing et al. 2010; Manichanh et al. 2006). However, *Lactobacilli* were increased in samples from *Winnie* mice, consistent with findings in patients with Crohn's disease (CD) (Wang et al. 2014b). The importance of *Erysipelotrichaceae*, which increased in samples from *Winnie* mice, in inflammation-related disorders of the GI tract is highlighted by the fact that they have been found to be enriched in colorectal cancer (Chen et al. 2012b). Changes in the levels of *Erysipelotrichaceae* in patients with IBD or animal models of IBD have also been observed; however, the evidence does not seem to be consistent (Schaubeck et al. 2016; Labbe et al. 2014; Dey et al. 2013; Craven et al. 2012).

In this study, *Actinobacteria* was increased in samples from *Winnie* mice. Correspondingly, enrichment in *Actinobacteria* is associated with IBD (Wang et al. 2014b) and in mice with spontaneous colitis (Alkadhi et al. 2014). Furthermore, fecal samples from *Winnie* mice comprised increased *Bifidobacterium*, similar to findings in studies investigating the IBD microbiome (Wang et al. 2014b; Willing et al. 2010). Previous reports have indicated that *Bifidobacterium animalis* induced mild colonic inflammation and immune responses in germ-free IL-10-deficient mice (Moran et al. 2009), whereas *B. longum* diverted immune responses toward a pro-inflammatory profile (Medina et al. 2007). However, *Bifidobacterium* are generally considered to exert protective activities against pathogens, and *Bifidobacteria*-containing probiotics have been shown to be effective in reducing the severity of gut inflammation (Preising et al. 2010; Rastall et al. 2005).

The *Tenericutes* phylum, *Anaeroplasmataceae* family, and genus *Anaeroplasma* were reduced in samples from *Winnie* mice. It has been suggested that *Tenericutes* is involved in IBD because of their ability to adhere to and fuse with

epithelial and immune cells (Roediger and Macfarlane 2002). Furthermore, increased GI transit rates are associated with decreased levels of *Anaeroplasmataceae* (Kashyap et al. 2013) and therefore, diarrhea observed in all *Winnie* mice (Heazlewood et al. 2008) may play a role in the reduced distribution of *Tenericutes* in this study. In humans, reductions in *Anaeroplasmataceae* is evident in UC (Willing et al. 2010), but there are contradictory reports regarding the distribution of *Tenericutes* in murine models of IBD (Nagalingam et al. 2011; Hoffmann et al. 2009).

Significantly, more *Proteobacteria* were present in fecal samples from *Winnie* mice when compared with samples from C57BL/6 mice. The most often reported incidence of microbial expansion in IBD is that of *Proteobacteria* (Lupp et al. 2007). Hence, multiple classes of *Proteobacteria* are associated with IBD, including *Alphaproteobacteria*, *Betaproteobacteria*, *Gammaproteobacteria, Deltaproteobacteria*, and *Epsilonproteobacteria* (Mukhopadhya et al. 2012; Lepage et al. 2011). Consistent with our findings, increased *Proteobacteria* were reported in both the feces and appendix of *Winnie* mice (Alkadhi et al. 2014). The increase in *Proteobacteria* observed in samples from *Winnie* mice in this study was mostly due to a class of *Betaproteobacteria*, order *Burkholderiales,* family *Oxalobacteraceae*, and species *Oxalobacter formigenes*. Increased *Oxalobacteraceae* has also been reported in CD (Chiodini et al. 2015). Of the *Epsilonproteobacteria*, it is noteworthy that the *Helicobacter* species of the *Helicobacteraceae* family were present in samples from *Winnie* mice, but not in samples from C57BL/6 mice. This is consistent with a previous study which reported *Helicobacter* in all mice with spontaneous chronic colitis (Alkadhi et al. 2014). *Helicobacteraceae* are strongly associated with clinical IBD, although it is not clear whether its presence is a risk or causative factor in the etiology of the disease (Yu et al. 2015; Thomson et al. 2011). Additionally, enterohepatic *Helicobacter* species can trigger persistent intestinal inflammation and elicit diarrhea in susceptible laboratory animals (Yu et al. 2015; Shomer et al. 1998).

Expansion of the members of *Enterobacteriaceae* family is described in patients with IBD (Frank et al. 2007), consistent with what is reported in murine models of

IBD (Petersen and Round 2014). However, in this study, no *Enterobacteriaceae*, such as *Escherichia coli*, were identified in samples from *Winnie* mice. This may be correlated with the genetic mutation of the *Muc2* mucin in this phenotype. Generally, because of high mucin expression in IBD, *E. coli* are able to thrive because they can use mucin as their primary energy source. However, there is a decrease/depletion in bacteria related to *E. coli* when the *Muc* gene is knocked out or its expression is blocked (Ren et al. 2012b; Stringer et al. 2009).

In this study, metabolomic analysis of fecal samples was performed to assess metabolite profiles pertaining to chronic intestinal inflammation in *Winnie* mice. The intestinal microbiota is directly involved in the metabolism of proteins, free amino acids, and CHOs, producing metabolites that influence signaling pathways in epithelial cells, modulate the mucosal immune system of the host, and play a direct role in health and disease (Nicholson et al. 2012; Blachier et al. 2007; Schaible and Kaufmann 2005). Our results revealed significant variation in CHO and amino acid metabolism in *Winnie* mice when compared with healthy C57BL/6 mice.

Branched-chain amino acids (BCAAs) isoleucine and leucine, as well as other amino acids phenylalanine, glycine, and tyrosine were significantly reduced in samples from *Winnie* mice suggesting increased gut protein putrefaction. In support of our findings, decreased levels of these amino acids are reported in the colonic mucosa of patients with IBD (Vigsnaes et al. 2013; Ooi et al. 2011; Balasubramanian et al. 2009). In contrast, one study reported increased fecal BCAA metabolites to be associated with CD (Marchesi et al. 2007). Overall, metabolomic analysis of fecal samples from patients with IBD demonstrates major perturbation of amino acid metabolism (Bjerrum et al. 2015) resulting in reduced amino acid biosynthesis and CHO metabolism in favor of nutrient uptake (Morgan et al. 2012). A decrease in amino acids can instigate a stress response in the host subsequently inducing intestinal epithelial cell autophagy. This may be involved in the pathogenesis and/or increase the risk of IBD (Tattoli et al. 2012; Shiomi et al. 2011). It has been demonstrated that several amino acids, including glycine, are radical scavengers in epithelial injury, exhibiting anti-inflammatory

activity and efficacy in attenuating intestinal inflammation in animal models of colitis (Andou et al. 2009; Tsune et al. 2003).

Fecal levels of leucine and isoleucine are positively correlated with *Prevotella*, *Alistipes* and *Barnesiella*, but negatively associated with *Bacteroides* (Neis et al. 2015). This correlates with our findings where a reduction in *Prevotellaceae* and (*Prevotella*), as well as increasing levels of *Bacteroides* accompanied reductions in BCAAs. In addition, *Alistipes* were present in samples from healthy C57BL/6 mice, but absent in samples from *Winnie* mice. Therefore, the reduction in BCAA metabolites in *Winnie* mice may be due to the reduction in BCAA metabolizing bacteria. Reduction in these amino acids may also be attributed to chronic inflammation and decreased muscle protein metabolism that may lead to deterioration of the mucosal lining (Mercier et al. 2002). Previous studies have shown that species belonging to the genera *Clostridium* and *Bacteroides* have a high capacity to ferment phenylalanine to phenolic compounds such as phenylpropionate, phenyl acetate, and/or phenyllactate (Smith and Macfarlane 1996; Elsden et al. 1976). Furthermore, UC has been associated with the production of phenolic compounds through proteolytic and peptidolytic activities of the gut microbiota (Smith and Macfarlane 1997). *Clostridium* are key participants in tyrosine metabolism, which correlates to the decreases in *Dehalobacterium* and *Peptococcaceae* species observed in the samples from *Winnie* mice in this study.

Similar to our findings, the sulfur-containing amino acid methionine was increased in fecal samples from patients with CD (Morgan et al. 2012). As homocysteine is easily convertible to methionine, this may indicate a mechanism of maintaining redox homeostasis. Alternatively, this may be connected to the increase in CHO metabolism observed in samples from *Winnie* mice, as cysteine can be metabolized to pyruvate (Morgan et al. 2012). Sulfate-reducing activity in the human colon is predominantly performed by members of the *Desulfovibrio* genus in the *Deltaproteobacteria* class (Scanlan et al. 2009). These sulfate-reducing bacteria are positively associated with inflammation (Devkota et al.

2012). Importantly, in this study, the increase in methionine corresponded with an increase in *Desulfovibrio* in samples from *Winnie* mice.

The levels of amino acid derivatives tyramine, putrescine, and cadaverine were altered in the *Winnie* mouse metabolome. Dysregulation of amines is associated with inflammation, as well as various other pathological conditions (Pegg 2009). Tyramine, which was increased in samples from *Winnie* mice, has a strong cytotoxic effect and elevated levels have been correlated with GI symptoms including nausea, abdominal cramping, and diarrhea (Linares et al. 2016). Studies assessing fecal levels of tyramine and IBD are lacking. However, the increased tyramine level observed in *Winnie* mice in this study correlates with the decreased levels of tyrosine in this phenotype. Conversely, putrescine and cadaverine were reduced in the fecal samples from *Winnie* mice. These primary amines are indispensable for intestinal mucosal barrier function and gut tissue maturation (Matsumoto et al. 2012; Matsumoto and Benno 2007). Depletion of putrescine levels causes G_1 phase growth arrest in intestinal epithelial (IEC)-6 cells (Li et al. 1999), alters the sensitivity of IEC-6 cells to apoptotic stimulus (Li et al. 2001), and is accompanied by rapid induction of nuclear factor kappa B (NF-κB) activation (Pfeffer et al. 2001). In patients with IBD, NF-κB activation is markedly increased, strongly influencing the course of mucosal inflammation through its capacity to promote the expression of various pro-inflammatory genes (Atreya et al. 2008). *Clostridium*, *Bacteroides*, and *Lactobacillus* are involved in putrescine and cadaverine metabolism (Matsumoto and Benno 2007; Noack et al. 2000). In this study, reduced putrescine and cadaverine levels in fecal samples from *Winnie* mice correlate with decreases in the *Clostridum* group. Furthermore, in addition to the *Muc2* mutation, it is possible that mucosal inflammation in the *Winnie* mouse colon may be stimulated by NF-κB activation as a result of decreased putrescine.

CHO malabsorption may occur in IBD because of the adverse inflammatory effects on digestive enzymes (Ziambaras et al. 1996) or inflammatory infiltrates acting as a nutrient diffusion barrier (Lee et al. 1988). In this study, several monosaccharides including glucose, fructose, xylose, ribose, ribulose, and

fucose were increased in samples from *Winnie* mice. In support of our findings, excessive amounts of these monosaccharides have been reported in the fecal samples of various animal models of colitis (Minamoto et al. 2015; Jump et al. 2014; Hong et al. 2010). Alterations of glucose metabolism are related with markers of systemic and intestinal inflammation (Pradhan et al. 2003). The malabsorption of fructose is frequent in both CD and UC (Barrett et al. 2009) and associated with fostering growth of detrimental commensal enteric bacteria (Whitehead et al. 2011). Accelerated whole gut motility is associated with high ribose resulting in malabsorption, diarrhea, and disturbed energy homeostasis (Liu et al. 2016b; van der Burg et al. 2011; Gross and Zollner 1991). Although fucose, a common component of many glycans and glycolipids, is protective in several disease models, fucosylated glycans can also provide adhesion sites or receptors for pathogens (Stahl et al. 2011; Coddens et al. 2009). As such, colonic fucosylation was shown to increase during local inflammation in humans (Miyoshi et al. 2011). Furthermore, genetic markers identified as IBD susceptibility genes are involved in glycosylation pathways, including hepatocyte nuclear factor 4 alpha which regulates fucose metabolism and fucosyltransferase-2 which adds fucose to glycoproteins (Huttenhower et al. 2014; Theodoratou et al. 2014; McGovern et al. 2010). An increased abundance of many genes related to CHO transport is associated with CD (Morgan et al. 2012). Hence, rapid delivery of these monosaccharides to the colonic microbiota may play a role in the pathophysiology of IBD (Gibson and Shepherd 2005). Additionally, the increased ribose in samples from *Winnie* mice correlates with diarrhea and disrupted colonic motility previously described in this phenotype (Robinson et al. 2017a; Rahman et al. 2015).

The fermentation of sugar alcohols by gut bacteria and the gases produced, such as hydrogen and methane, can produce flatulence, abdominal cramping, abdominal bloating, and diarrhea (Hayes et al. 2014). Furthermore, sugar alcohols have been shown to result in malabsorption of other energy nutrients, in addition to the sugar alcohol itself (Wolever et al. 2002). Particular sugar alcohols including glycerol, inositol, and neo-inositol were increased in samples from *Winnie* mice. Similar to our findings, an elevated level of glycerol has been

reported in the feces of patients with CD (Marchesi et al. 2007), as well as in the colonic mucosa of rats with IBD (Varma et al. 2007). Increases in glycerol in samples from *Winnie* mice may be reflective of increases in total colonic lipid concentration during inflammation. Alterations in colonic mucosal lipid profiles are demonstrated in UC and animal models of colitis (Nieto et al. 1998; Nishida et al. 1987). Increased colonic glycerol levels can also occur through microbial synthesis, release from desquamated epithelial cells, intestinal clearing of endogenous plasma glycerol, disrupted fat absorption in the small intestine, and inhibition of its absorption by certain products of fermentation (Casas and Dobrogosz 2011; Fujimoto et al. 2007; Kato et al. 2005).

Glycosyl compound galactoside and mucic acid, a sugar acid, were increased in samples from *Winnie* mice. There are no reports investigating either of these metabolites and their effect *Faecalibacterium* on IBD pathogenesis. However, bacterial enzyme activities, especially β-D-galactosidase, a glycoside hydrolase enzyme that catalyzes the hydrolysis of galactosides into monosaccharides, are decreased in fecal extracts from patients with CD (Favier et al. 1997). Therefore, a reduction in this enzyme may result in accumulation of galactosides as observed in the fecal samples from *Winnie* mice. Elevated sugar acids encourage the growth of pathogenic bacteria in the intestinal mucosa (Horne et al. 2009). High levels of mucic acid have also been linked to a high fat diet and positively correlated with albuminuria in patients with type 2 diabetes (Hwang et al. 2015; Hirayama et al. 2012). Thus, the increased concentration of mucic acid in fecal samples from *Winnie* mice may be associated with an overall heightening of the disease state.

The composition of the gut microbiota shifts with increased presence of complex glycans. As such, microorganisms that prefer these glycans, such as *Bacteroidetes, Lactobacillus*, and *Bifidobacterium* species, become more prevalent (Koropatkin et al. 2012). Other gut microbes involved in fermentation of undigested CHOs are *Ruminococcus* and *Roseburia* species, as well as some members from the *Clostridium, Eubacterium*, and *Enterococcus* groups (Bernalier-Donadille 2010). Lactic acid bacteria, particularly the *Lactobacilli*,

represent the best characterized group of fructophilic and glycerol microbes, but *Bifidobacterium* and are also involved in metabolism of this monosaccharide (Payne et al. 2012a; Endo et al. 2009). Overall, the increase in CHO metabolites in samples from *Winnie* mice correlates with increases in *Lactobacillus* and *Bifidobacterium*.

A principal energy source for colonic epithelial cells, SCFAs are known to enhance the integrity of the intestinal epithelial barrier and modulate the GI immune response (Lara-Villoslada et al. 2006; Wong et al. 2006). Fecal SCFA content is correlated with various diseases, including IBD, thereby reinforcing the essential role of SCFAs in maintaining the health of colonic mucosa (Floch and Hong-Curtiss 2001). In this study, it was found that SCFA butyric acid was decreased significantly in samples from *Winnie* mice. Similar to our findings, patients with IBD have defective butyrate metabolism and diminished concentrations of butyric acid metabolites (Takaishi et al. 2008; Hallert et al. 2003; Vernia et al. 1988). Reduced butyric acid in *Winnie* mice feces is relevant to their augmented level of colonic inflammation; butyric acid has widely acknowledged anti-inflammatory effects, inhibiting NF-κB activation and reducing the formation of pro-inflammatory cytokines (Inan et al. 2000; Segain et al. 2000). Furthermore, butyric acid fortifies the colonic defense barrier, reducing its permeability and increasing production of mucins and antimicrobial peptides (Hamer et al. 2008). As such, enemas of butyric acid have been suggested to play an important role in the prevention and treatment of distal UC (Breuer et al. 1997) and CD disease (Di Sabatino et al. 2005).

Most butyrate-producing bacteria found in human feces belong to the *Clostridia* (Louis and Flint 2009), corresponding to the decreases in certain species within this class in samples from *Winnie* mice. The *Ruminococcaceae* and *Lachnospiraceae* families from *Clostridium* clusters IV and XIVa are also adept at fermenting various substrates to butyrate (Onrust et al. 2015). Interestingly, these families were found to increase in samples from *Winnie* mice. One reason for this may be that both clusters include additional non-butyrate-producing species. Furthermore, epithelial butyrate metabolism may be inhibited by hydrogen sulfide

released by excess numbers of sulfate-reducing bacteria (Pitcher and Cummings 1996). As mentioned above, most sulfate-reducing bacteria belong to the genus *Desulfovibrio* (Scanlan et al. 2009). Therefore, in this study, the increase of *Desulfovibrio* in samples from *Winnie* mice suggests a possible explanation for the imbalance of butyric acid metabolites and butyric acid-producing bacteria.

Long chain fatty acids hexadecanoic acid, heptadecanoic acid, and octadecanoic acid were heightened 2- to 3-fold in samples from *Winnie* mice when compared with samples from healthy C57BL/6 mice. In correlation with our findings, levels of long chain fatty acids are increased in IBD (Antharam et al. 2016; Jansson et al. 2009; Romanato et al. 2009). Hexadecanoic acid is an indicator of adipocyte lipolysis (Sarosiek et al. 2016) and has been shown to promote inflammation (Kim et al. 2010b). Furthermore, hexadecenoic acid has been characterized as a toll-like receptor-2 and toll-like receptor-4 ligand to induce inflammatory cytokines (Nguyen et al. 2007; Senn 2006; Shi et al. 2006). The high concentrations of hexadecanoic acid observed in our study and in investigations associated with IBD suggest enhanced lipolysis within the colon. Mostly, *Lactobacillus* species metabolize hexadecanoic acid, whereas other intestinal bacteria such as *Akkermansia*, *Enterococcus*, *Prevotella*, and *Clostridium* cluster XI also possess the ability to metabolize this fatty acid, but at a much lower level (Chen et al. 2015). Thus, the increased numbers of *Lactobacillus* observed in fecal samples from *Winnie* mice in this study correlate with the increase in hexadanoic acid.

In addition to SCFAs, polyunsaturated fatty acids contribute significantly to enterocyte function and pathology. In this study, we observed increased quantities of oleic and 9,12-octadecadienoic acids in samples from *Winnie* mice. In support of these findings, increased concentrations of these polyunsaturated fatty acids were observed in fecal samples from patients with CD (Jansson et al. 2009), whereas certain lipids implicating the role of oleic acid biogenesis in the mechanism of colitis were found in the serum of mice with DSS-induced colitis (Chen et al. 2012b). The *Lactobacillales*, specifically *Bacilli*, have been reported to be responsible for hydrogenation of oleic acid (Kishino et al. 2013), which corresponds to the increase in these microbiota in samples from *Winnie* mice.

Several carboxylic acid metabolites including thiocarboxylic acid (thioacetic acid), keto acid (pyruvic acid), and dicarboxylic acid (oxalate), as well as tricarboxylic acid and phenylcarboxylic acids were increased in samples from *Winnie* mice when compared with healthy controls in this study. In UC, irritation to the colonic mucosa is affected by the production of thioacetic acid in addition to hydrogen sulfide and sulfide (Parcell 2002). Increased intestinal thioacetic acid produced by sulfur-producing bacteria, *Desulfovibrio*, may result in impairment of colonic epithelial cells and subsequent inflammation (Jansson et al. 2009; Roediger 1998; Roediger et al. 1997). Hence, increases in thioacetic acid and *Desulfovibrio* species in samples from *Winnie* mice correlate to disruptions in thiocarboxylic acid metabolism and microbial shifting observed in human UC. Higher concentrations of pyruvic acid are also reported in fecal samples of patients with IBD (Huda-Faujan et al. 2010; Takaishi et al. 2008; Vernia et al. 1988). Shifts in levels of pyruvic acid may be caused by a number of nonspecific factors, but suggest changes in mitochondrial function, as well as glucose oxidative and nonoxidative metabolisms (Campbell et al. 2014). Furthermore, in association with the excessive glucose evident in samples from *Winnie* mice, the increased pyruvate concentration may reflect reduced efficiency of glucose oxidative metabolism. Importantly, proficient glucose/pyruvate oxidation accompanies improved metabolic health. The lactic acid bacteria are responsible for converting pyruvic acid into lactic acid. No differences in the lactic acid bacteria were observed between samples from *Winnie* and C57BL/6 mice in this study, indicating that elevated pyruvic acid levels in *Winnie* mice are most likely due to mitochondrial dysfunction or disrupted glucose metabolism.

The toxin oxalate, which was increased 3-fold in samples from *Winnie* mice, is formed endogenously as a waste product of metabolism. The bacterium primarily responsible is the strict anaerobe *Oxalobacter formigenes*, which was correspondingly increased in *Winnie* mice. Oxalate that is not degraded by the colonic microbiota can be excreted in the feces or urine or can accumulate in the kidneys as calcium oxalate stones (Miller and Dearing 2013). High level of urinary oxalate has been reported in patients with IBD (Kumar et al. 2004; Bohles et al. 1988). In contrast to our findings, increased urinary oxalate excretion was

associated with the absence of colonization with *Oxalobacter formigenes* (Kumar et al. 2004). Fatty acids and bile acids increase the permeability of colonic oxalate affecting the absorption and secretion of oxalate to the colon (Viana et al. 2007). Therefore, the levels of oxalate in *Winnie* mice may exceed the capacity of *Oxalobacter formigenes,* despite the increased members found in this study.

Volatile compounds, such as alcohols, aldehydes, alkanes, ketones, and esters, are products of diverse metabolic pathways and the result of complex interactions between the colonic intestinal cells, fecal microbes, mucosal integrity, and invading pathogens (Arasaradnam et al. 2009; Korpi et al. 2009). In this study, the alcohol 2,3-butanediol was observed in samples from *Winnie* mice, but not in samples from C57BL/6 mice. There are no studies focusing on 2,3-butanediol and IBD. However, 2,3-butanediol is present in <5% of healthy adults (Hsieh et al. 2007). It has been suggested that 2,3-butanediol production is upregulated in a glucose-rich environment to prevent hyperacidification (Yoon and Mekalanos 2006). Therefore, 2,3-butanediol synthesis may be upregulated in *Winnie* mice subsequent to excess glucose manifestation. Additionally, 2,3-butanediol can be produced by some *Bacillus*, of which some members were increased in samples from *Winnie* mice.

The aldehydes, butanal and propanal and the alkane, butane were predominantly observed in samples from *Winnie* mice. Similar to our results, aldehydes and alkanes are significantly elevated in patients with IBD (Ahmed et al. 2016; Hicks et al. 2015; Pelli et al. 1999). Increased aldehyde levels prospectively represent oxidative stress and correspondingly, there is considerable evidence linking markers of oxidative stress to IBD (Rezaie et al. 2007). Disruptions to the intestinal barrier function associated with intestinal inflammation can instigate oxidative stress and produce reactive oxygen species. In turn, reactive oxygen species seem to have a predominant role in instigating the production of alkanes in inflamed tissues, manufacturing propane, butane, and ethane from BCAAs (Kurada et al. 2015). Hence, elevated aldehydes and alkane production in the *Winnie* mouse intestine suggest increases in lipid peroxidation and oxidative stress.

High levels of salicylic alcohol and shikimate-3-phosphate were observed in fecal samples from *Winnie* mice. Salicylic alcohol metabolism and the shikimate pathway are necessary for the synthesis of important metabolites, such as aromatic amino acids, folic acid, and ubiquinone (Bochkov et al. 2012). Salican hydrolyzes in the GI tract to yield salicylic alcohol and glucose, thus increased levels of glucose in samples from *Winnie* mice correlate with the increases in salicylic alcohol. Furthermore, salicyl alcohol is oxidized into salicylic acid on absorption in the colon which suggests malabsorption of this metabolite in chronic inflammation. Bacteria involved in metabolism of shikimate include *Firmicutes* and *Bifidobacteria* which is consistent with shifts in these bacteria observed in this study. *Proteobacteria* has been associated with endogenous alcohol production (Ren et al. 2007). Hence, amplified members of this phylum could account for the high levels of alcohols in fecal samples from *Winnie* mice. Importantly, excess endogenous alcohol production may contribute to a constant source of oxidative stress (Michail et al. 2015).

5.6 Conclusion

In this study, we have provided evidence of microbial shifts and subsequent alteration to the metabolic profiles of fecal samples from *Winnie* mice with chronic inflammation of the colon. In particular, we have observed significant dysbiosis in the *Winnie* mouse gut reflected by changes similar to those noted in patients with IBD. These changes correlated with increases in CHO metabolites and decreases in amino acid metabolites, thereby generating disrupted CHO, fat, and amino acid profiles in fecal samples from *Winnie* mice. Collectively, these results point to mechanisms of oxidative stress and malabsorption of nutrients in the colon, both of which are reported in IBD. Furthermore, alterations in the microbiota and metabolome associate with variations in the enteric nervous system previously reported in the distal colon of this phenotype. It can therefore be concluded that the *Winnie* mouse model of spontaneous chronic colitis is an appropriate animal model for studying mechanisms underlying the role of intestinal microbiota and metabolome in the pathophysiology of IBD.

CHAPTER SIX: A SINGLE DOSE OF MESENCHYMAL STEM CELL TREATMENT DOES NOT EXERT BENEFICIAL EFFECTS ON ENTERIC NEUROPATHY IN THE *WINNIE* MOUSE MODEL OF SPONTANEOUSLY OCCURRING CHRONIC COLITIS

6.1 Summary

Background: Our previous studies have demonstrated the beneficial effects of mesenchymal stem cell (MSC)-based treatments in attenuating disease symptoms, immune response and enteric neuropathy in acute models of colitis. Although inflammatory bowel disease (IBD) incorporates acute flares of gut inflammation, it is well established as a chronic and progressive disease. There has been some investigation into cellular therapy for the treatment of symptoms and immunological changes associated with chronic gut inflammation, however no studies have investigated the therapeutic effect of MSCs for the attenuation of enteric neuropathy in a chronic model of colitis. The *Winnie* mouse model of spontaneously occurring chronic colitis has been demonstrated to be highly representative of human IBD. Therefore, we have chosen this animal model to investigate the short-term and long-term effects of MSC treatment in moderating inflammation and damage to the enteric nervous system (ENS) associated with chronic colitis. **Methods:** *Winnie* mice with chronic colonic inflammation received a single dose of 1×10^6 human bone marrow-derived MSCs or 100µL phosphate buffered saline (PBS) by enema. C57BL/6 mice received 100µL PBS. Colon tissues were collected at 3 and 60 days post MSC administration to evaluate the short-term and long-term effects of MSC treatment on the extent of inflammation and enteric neuropathy by histological and immunohistochemical analyses. **Results:** Treatment with MSCs had no effect on the level of inflammation or damage to the ENS associated with chronic colitis at either 3 or 60 days post treatment. **Conclusions:** A single dose of human bone marrow-derived MSCs is ineffective in attenuating chronic colonic inflammation and associated enteric neuropathy in the *Winnie* mouse model of colitis. Studies investigating the therapeutic effects of higher and/or multiple doses of MSCs in moderating ENS damage in the chronically inflamed *Winnie* mouse colon are warranted.

6.2 Introduction

In cases of acute inflammation, mesenchymal stem cells (MSCs) have been shown to respond quickly and vigorously to the injury (Joyce et al. 2010). Hence, various studies have established the benefits of MSC-based treatments in an array of diseases (Robinson et al. 2017b; 2015; 2014; Gao et al. 2016; Zhao et al. 2016; Stavely et al. 2015a; 2015b; Farini et al. 2014; Tanna and Sachan 2014; Galindo et al. 2011; Kassis et al. 2008; Zheng et al. 2008). In particular, *in vivo* application of MSCs has been successful for acute inflammatory events including sepsis (Nemeth et al. 2009), acute renal failure (Bruno et al. 2009), myocardial infarction (Nagaya et al. 2004) and acute lung injury (Matthay et al. 2010). In acute neurodegenerative diseases such as ischemic stroke or spinal cord injury (SCI), MSCs have been demonstrated to ameliorate post-stroke/SCI functional impairments (Melo et al. 2017; Yousefifard et al. 2016; Onda et al. 2008; Li et al. 2002).

Many inflammatory bowel disease (IBD) patients suffer from acute flares of gut inflammation interspersed with remissions due to the relapsing nature of the disease (Bielefeldt et al. 2009; Carter et al. 2004). In animal models of acute colitis, MSCs have been demonstrated to suppress disease activity (Chen et al. 2013b; He et al. 2012; Liang et al. 2011; Gonzalez et al. 2009), systemically reduce pro-inflammatory cytokines interferon-γ, interleukin (IL)-17, IL-6, and tumor necrosis factor-α and elevate anti-inflammatory cytokine IL-10 (Akiyama et al. 2012; He et al. 2012; Liang et al. 2011; Gonzalez et al. 2009; Gonzalez-Rey et al. 2009), as well as impede inflammation-induced enteric neuropathy in the colon (Chapter 2 and Chapter 3). Nonetheless, IBD is well established as a chronic and progressive disease (Neurath 2017; de Souza and Fiocchi 2016; Kaser et al. 2010); therefore, animal models of acute colitis do not completely reproduce the complexity of human IBD (DeVoss and Diehl 2014; Wirtz and Neurath 2007).

Given the extensive therapeutic potential of MSCs, it is feasible that they will be appropriate for treatment of numerous chronic diseases. MSCs have been

successfully applied in experimental models of chronic kidney disease (Ebrahimi et al. 2013; Zhu et al. 2013; Eirin et al. 2012; Franquesa et al. 2012; Choi et al. 2009; Ezquer et al. 2008; Lee et al. 2006), chronic pancreatitis (Zhou et al. 2013) and chronic obstructive pulmonary disease (Stessuk et al. 2013; Ribeiro-Paes et al. 2011). Furthermore, MSCs have provided therapeutic effect in chronic untreatable neurodegenerative diseases, delaying loss of motor neurons and prolonging motor performance in models of amyotrophic lateral sclerosis (Vercelli et al. 2008), as well as functional improvement and decreased demyelination in experimental multiple sclerosis (Karussis and Kassis 2008; Zhang et al. 2005). The beneficial outcomes of MSC treatment in these chronic diseases is thought to be due to paracrine effects, promotion of repair, suppression of inflammatory cytokines and overall anti-inflammatory activity of MSCs (Cheng et al. 2017; Eirin and Lerman 2014; Zhou et al. 2013; Joyce et al. 2010).

MSCs have been demonstrated to protect against inflammation and lessen disease progression in the IL-10$^{-/-}$ mouse model of chronic colitis (Jung et al. 2015). However, no studies have investigated the therapeutic effect of MSCs for the attenuation of enteric neuropathy in a chronic model of IBD. Previously, we have shown changes in gastrointestinal (GI) histopathology, immunology, microbiota and intestinal innervation in the *Winnie* mouse model of spontaneous chronic colitis (Robinson et al. 2017a; 2016; Rahman et al. 2016; 2015). Thus, we have chosen this experimental model to investigate the potential of MSC treatment in attenuating enteric neuropathy associated with chronic colitis. Furthermore, most studies have focused on the prevention and attenuation of inflammation in a relatively short period after administration of MSCs, therefore in this study we will investigate the long-term, as well as the short-term, effects of a single dose of bone marrow (BM)-MSCs in *Winnie* mice with chronic colitis.

6.3 Materials and methods

6.3.1 Animals

Winnie (12wk old; 19-29g; *n*=16) and C57BL/6 (12wk old; 25-30g; *n*=8) were obtained from Monash Animal Services (MAS, Melbourne, Australia). All animals were housed in a temperature-controlled environment with 12h day/night cycles and free access to food and water. All procedures performed within this study were approved by the Victoria University Animal Experimentation Ethics Committee and were conducted according to the guidelines of the Australian National Health and Medical Research Council.

6.3.2 MSC culture, passaging and characterization

Cell culture and passaging were carried out as described in Chapter 2, section 2.3.2. Briefly, pre-established cell lines of human BM-MSCs (Tulane University, New Orleans, LA, USA) were cultured until the fourth passage. Cells were plated at an initial density of 60 cells/cm^2 and incubated in expansion medium (α-minimum essential medium (MEM) supplemented with 16.5% MSC-qualified fetal bovine serum (FBS), 100 U/mL penicillin/streptomycin, and 100X GlutaMAX) (Gibco®, Life Technologies, Mulgrave, VIC, Australia) at 37°C. Expansion medium was replenished every 48-72h for 10-14 days until the cells were 70-85% confluent (maximum). MSCs were trypsinized and collected for *in vivo* treatment of *Winnie* mice. As described in Chapter 2, section 2.3.3, MSCs were characterized for their expression of surface antigens, differentiation potential, and colony-forming ability. All MSCs utilized in this study met criteria for defining *in vitro* human MSC cultures proposed by the International Society for Cellular Therapy (ISCT) (Dominici et al. 2006).

6.3.3 MSC treatments

Winnie mice in the short-term and long-term MSC treatment groups were anaesthetized with isoflurane (induced at 3%, maintained on 1-3% isoflurane in O_2) and administered 1×10^6 MSCs in 100µL of sterile phosphate buffered solution

(PBS) by enema into the colon via a silicone catheter. Sham-treated *Winnie* and C57BL/6 mice underwent the same procedure but were administered 100µL of sterile PBS only. Animals were held at an inverted angle following MSC treatments to prevent leakage from the rectum and were monitored daily following treatment. Mice were culled via cervical dislocation at 3 (short-term) or 60 days (long-term) after MSC or sham treatments. Colon tissues were used for histology and immunohistochemistry experiments.

6.3.4 Analysis of fecal water content and colon length

Fecal water content was calculated as described in Chapter 4, section 4.3.2. Briefly, following collection, stools from C57BL/6+sham, *Winnie*+sham, and *Winnie*+MSC-treated mice were immediately weighed to ascertain the wet weight. After 3 days, stools were re-weighed to establish the dry weight. The difference between wet and dry weight was then calculated. Immediately after dissection, the length of the colon from cecum to anus was measured by placing the colon parallel to a ruler.

6.3.5 Assessment of fecal lipocalin-2 levels

To assess the level of colonic inflammation in *Winnie* mice prior to and after treatment, levels of fecal lipocalin (Lcn)-2 were measured as described in Chapter 4, section 4.3.3 (Chassaing et al. 2012). For the short-term time point study, fecal samples were collected from mice prior to treatment and then at 3 days after treatment (immediately before culling). For the long-term time point study, fecal samples were collected prior to treatment and then twice weekly over 60 days following treatment. Briefly, fecal samples were reconstituted and vortexed to form a homogenous fecal suspension. Levels of fecal Lcn-2 were estimated in the supernatants using Duoset murine Lcn-2 ELISA kit (R&D Systems, Minneapolis, MN, USA).

6.3.6 Immunohistochemistry and histology

Immunohistochemistry and histology were performed as described in Chapter 4, section 4.3.4.

6.3.6.1 Tissue preparation

Distal colon tissues were processed for wholemount longitudinal muscle-myenteric plexus (LMMP) preparations and cross sections. Tissues for LMMP and cryostat cross sections were cut open along the mesenteric border, pinned flat with the mucosal side up and fixed overnight with Zamboni's fixative (2% formaldehyde containing 0.2% picric acid) at 4°C. After fixative removal, the mucosa, submucosa and circular muscle layers were removed from LMMP colon preparations via fine dissection to expose the myenteric plexus. Cross section preparations were cryoprotected and subsequently frozen in liquid nitrogen-cooled isopentane and optimal cutting temperature (OCT; Tissue-Tek, Torrance, CA, USA) compound. Samples were stored at -80°C until they were cryo-sectioned (20µm) onto glass slides for immunohistochemistry. Tissues for histology were fixed in 10% buffered formalin overnight at 4°C and stored in 70% ethanol until embedding.

6.3.6.2 Immunohistochemistry

Following a 1h incubation in 10% normal donkey serum (NDS; Merck Millipore, Bayswater, VIC, Australia), samples were incubated with primary antibodies (Table 6.1) overnight at room temperature. Tissues were then washed and incubated with secondary antibodies (Table 6.2) for 2h at room temperature prior to mounting with fluorescent mounting medium (DAKO, North Sydney, NSW, Australia).

6.3.6.3 Histology

For histology, tissues were embedded in paraffin, sectioned at 5µm, deparaffinized, cleared, and rehydrated in graded ethanol concentrations for hematoxylin and eosin (H&E) and Alcian blue staining.

Table 6.1 Primary antibodies used in this study

Antibody	Host species	Dilution	Supplier	Application in this study
Anti-β-Tubulin class III	Rabbit	1:1000	Abcam, Melbourne, VIC, Australia	Cross sections
Anti-calcitonin gene-related peptide (CGRP)	Rabbit	1:3000	Sigma-Aldrich, Castle Hill, NSW, Australia	LMMP preparations
Anti-CD45	Rat	1:500	BioLegend, San Diego, CA, USA	Cross sections
Anti-choline acetyltransferase (ChAT)	Goat	1:500	Merck Millipore	LMMP preparations
Anti-human leukocyte antigen (HLA)-A,B,C (conjugated to fluorescein isothiocyanate (FITC))	Human	1:50	BioLegend	Cross sections
Anti-neuronal nitric oxide synthase (nNOS)	Goat	1:500	Novus Biologicals, Littleton, CO, USA	LMMP preparations
Anti-protein gene product (PGP)-9.5	Rabbit	1:500	Abcam	LMMP preparations
Anti-tyrosine hydroxylase (TH)	Sheep	1:1000	Merck Millipore	LMMP preparations
Anti-vesicular acetylcholine transporter (VAChT)	Goat	1:500	Merck Millipore	LMMP preparations

Table 6.2 Secondary antibodies used in this study

Antibody	Host species	Dilution	Supplier	Application in this study
Alexa Fluor 488	Donkey anti-rat	1:200	Jackson Immunoresearch Laboratories, PA, USA	Cross sections
Alexa Fluor 488	Donkey anti-sheep	1:200	Jackson Immunoresearch Laboratories	LMMP preparations
Alexa Fluor 488	Donkey anti-rabbit	1:200	Jackson Immunoresearch Laboratories	LMMP preparations
Alexa Fluor 594	Donkey anti-rabbit	1:200	Jackson Immunoresearch Laboratories	Cross sections
Alexa Fluor 647	Donkey anti-goat	1:200	Jackson Immunoresearch Laboratories	LMMP preparations
Alexa Fluor 647	Donkey anti-rabbit	1:200	Jackson Immunoresearch Laboratories	LMMP preparations
FITC 488	Donkey anti-goat	1:200	Jackson Immunoresearch Laboratories	LMMP preparations

6.3.7 Imaging

Images were captured using a Nikon Eclipse Ti multichannel confocal laser scanning system (Nikon, Tokyo, Japan). Immunolabeled sections were visualized and imaged by using filter combinations appropriate for the specific fluorophores such as FITC, Alexa 488 (excitation wavelength 488nm), Alexa 594 (excitation wavelength 559nm) or Alexa Fluor 647 (excitation wavelength 640nm). Z-series images were acquired at a nominal thickness of 0.5µm (512×512 pixels). H&E-stained colon sections were visualized and imaged with CellSense™ software using an Olympus BX53 microscope (Olympus, Notting Hill, VIC, Australia).

6.3.8 Quantitative analysis of immunohistochemical and histological data

Images were analyzed using Image J software (National Institute of Health, Bethesda, MD, USA) as described in Chapter 4, section 4.3.6. The density of β-Tubulin (III)-immunoreactive (IR) fibers and CD45-IR cells was measured per area (average of eight areas of 500µm^2 per animal at ×20 magnification) in colon cross sections. CGRP-IR, TH-IR and VAChT-IR nerve fibers in LMMP preparations of the distal colon were measured from eight randomly captured images per preparation (total area 2mm^2), as well as per ganglion (all ganglia within measured area). All images were captured under identical acquisition exposure time conditions and calibrated to standardized minimum baseline fluorescence. Changes in fluorescence from the baseline were calculated and the area of immunoreactivity was then expressed as a percentage. Myenteric neuronal density was assessed in wholemount LMMP preparations immunolabeled with anti-PGP9.5, anti-nNOS, and anti-ChAT antibodies. The area of all ganglia randomly captured in eight images at ×20 magnification (total area 2mm^2) was measured and the number of neurons within each ganglionic area recorded. The number of neurons was normalized to a 0.1mm^2 area of ganglia for direct comparison between groups. Histological scores were developed from the following parameters: aberrant crypt architecture (score range 0-3), increased crypt length (0-3), goblet cell depletion (0-3), crypt

abscesses (0-3), leukocyte infiltration (0-3), and epithelial damage and ulceration (0-3) (average of eight areas of 500µm^2 per animal). All quantitative analyses were conducted blindly.

6.3.9 Statistical analysis

Statistical differences were determined using Prism v7.0 (Graphpad Software Inc., La Jolla, CA, USA). Data were considered statistically significant when $P<0.05$. Data were presented as mean±standard error of the mean (SEM), if not specified otherwise.

6.4 Results

6.4.1 MSCs are evident at the site of inflammation 3 days after administration

To determine whether locally administered human MSCs migrated to and engrafted within the area of tissue damage and inflammation, sections of the distal colon were collected from *Winnie*+MSC-treated mice at 3 and 60 days post treatment and labeled with anti-human HLA-A,B,C antibody (*n*=4/group; Fig. 6.1). Anti-HLA-A,B,C antibody distinguishes major histocompatibility complex (MHC) class I antigens which are found on the surface of all human nucleated cells. MSC migration and engraftment into the colon wall was evident by the presence of HLA-A,B,C-IR cells in sections from MSC-treated *Winnie* mice at 3 days post treatment (Fig. 6.1A). However, no HLA-A,B,C-IR cells were identified in sections from MSC-treated *Winnie* mice at 60 days after treatment (Fig. 6.1B).

6.4.2 Assessment of the short-term and long-term effects of MSC treatment on colonic inflammation in *Winnie* mice

C57BL/6+sham-treated mice did not display any symptoms of inflammation prior to or following sham treatment (*n*=4/group). Furthermore, the fecal matter of control mice was consistently firm with distinct pellet formation and absence of diarrhea (Table 6.3; Fig. 6.2A-A^{I}, D-D^{I}). In this investigation, all *Winnie* mice exhibited signs of intestinal inflammation, including perianal bleeding, soiled fur, diarrhea, soft fecal consistency and inability to form pellets, before treatment (Fig. 6.2B-C, E-F). Furthermore, a higher fecal water content (P<0.001) and lower body weight (P<0.01) was calculated in *Winnie* mice before treatment when compared to C57BL/6 mice (Table 6.3; Fig. 6.3A-B). *Winnie*+sham-treated mice continued to display signs of intestinal inflammation 3 and 60 days post treatment (*n*=4/group; Table 6.3; Fig. 6.2B^{I}, E^{I}). Treatment with MSCs did not provide any effect in alleviating symptoms; perianal bleeding and inflammation with soft fecal consistency, not forming pellets and diarrhea, was observed in *Winnie*+MSC-treated mice at both 3 and 60 days post treatment (*n*=4/group; Table 6.3; Fig.

6.2C^{I}, F^{I}). The fecal water content of stools from *Winnie*+sham and *Winnie*+MSC-treated was higher than in samples from C57BL/6+sham-treated mice following treatment (*n*=4/group; *P*<0.001 for all; Table 6.3; Fig. 6.3A). At 3 and 60 days post treatment, the average body weight of *Winnie*+sham-treated mice was less than C57BL/6+sham-treated mice (*n*=4/group; 3 days: *P*<0.001; 60 days: *P*<0.01; Table 6.3; Fig. 6.3B). Additionally, the colon length of *Winnie*+sham-treated mice was significantly longer than C57BL/6+sham-treated mice (*n*=4/group; 3 days: *P*<0.001; 60 days: *P*<0.01; Table 6.3; Fig. 6.3C). The body weight and colon length of MSC-treated *Winnie* mice was similar to sham-treated *Winnie* mice and significantly different to C57BL/6+sham-treated mice at 3 and 60 days post treatment (*n*=4/group; *P*<0.01 for all; Table 6.3; Fig. 6.3B-C).

Fecal Lcn-2 was quantified by ELISA in samples from C57BL/6+sham, *Winnie*+sham and *Winnie*+MSC-treated mice prior to and post treatment (*n*=4/group). Before treatment, the level of fecal Lcn-2 was higher in sham (4.5±0.7pg/mL) and MSC-treated (4.4±0.4pg/mL) *Winnie* mice groups when compared to C57BL/6 mice (0.7±0.2pg/mL), indicating colonic inflammation in *Winnie*, but not C57BL/6 mice (*P*<0.001 for both; Fig. 6.4A). At 3 days, levels of fecal Lcn-2 in samples from sham-treated *Winnie* mice (4.2±0.2pg/mL) remained higher than in samples from C57BL/6+sham-treated mice (0.7±0.1pg/mL; *P*<0.001; Fig. 6.4A). Similarly, at 60 days post treatment, Lcn-2 was significantly greater in fecal samples from *Winnie*+sham-treated (4.2±0.4pg/mL) when compared to samples from C57BL/6+sham-treated (0.8±0.1pg/mL) mice (*P*<0.001; Fig. 6.4A). The levels of fecal Lcn-2 in samples from MSC-treated *Winnie* mice remained similar to pre-treatment values and comparable to samples from sham-treated *Winnie* mice at both 3 (4.1±0.1pg/mL) and 60 days (4.4±0.5pg/mL) post treatment. Consequently, Lcn-2 was significantly higher in fecal samples from *Winnie*+MSC-treated mice when compared to C57BL/6+sham-treated mice at both time points (*P*<0.001 for both; Fig. 6.4A). When measured twice weekly during the 60 day experimental period, fecal Lcn-2 levels in samples from C57BL/6+sham-treated mice were consistently lower than in samples from *Winnie*+sham and *Winnie*+MSC-treated mice (*P*<0.001 for all; [see Appendix B, Table S2]; Fig. 6.4B).

Gross morphological damage was assessed in H&E and Alcian blue-stained colon sections to substantiate the short-term and long-term effects of MSC treatment on changes to the colonic architecture associated with intestinal inflammation (*n*=4/group; Fig. 6.5). Sections from C57BL/6+sham-treated mice at both time points showed continuous epithelial cell lining, distinct colonic layers and regular arrangements of goblet cell and crypt structures (Fig. 6.5). Conversely, at 3 and 60 days post treatment, damage to the epithelial cell lining and mucosa, crypt elongation, loss of goblet cells and leukocyte infiltration was evident in sections from *Winnie*+sham-treated mice (Fig. 6.5). Sections from MSC-treated *Winnie* mice were comparable to sham-treated *Winnie* mice at both time points (Fig. 6.5). These observations were confirmed with histological scoring of sections which combined individual scores of the following parameters: aberrant crypt architecture, increased crypt length, goblet cell depletion, general leukocyte infiltration, crypt abscesses and epithelial damage and ulceration (Table 6.3). Histological scores were significantly higher in sections from *Winnie*+sham-treated mice when compared to C57BL/6+sham-treated mice at both 3 and 60 days post treatment. The overall histological scores for MSC-treated *Winnie* mice at these time points were comparable to sham-treated *Winnie* mice and significantly greater than C57BL/6+sham-treated mice (Table 6.3).

The thickness of the mucosal (3 days: 199.8±4.3μm; 60 days: 203.5±5.9μm) and muscular (3 days: 85.5±4.0μm; 60 days: 88.8±2.1μm) layers of colon cross sections from C57BL/6+sham-treated mice was consistent from 3 to 60 days post treatment (*n*=4/group). Both the mucosal and smooth muscle layer of distal colon sections from *Winnie*+sham-treated mice was thicker than in sections from C57BL/6+sham-treated mice at 3 (mucosa: 281.3±11.0μm; muscle: 100.8±4.5μm) and 60 days (mucosa: 283.0±9.8μm; muscle: 105.3±4.6μm) following treatment (*n*=4/group; mucosa: $P<0.001$ for both; muscle: $P<0.05$ for both). The thickness of layers in colon sections from MSC-treated *Winnie* mice at 3 (mucosa: 278.5±14.0μm; muscle: 103.8±4.3μm) and 60 days (mucosa: 279.8±10.5μm; muscle: 103.0±3.6μm) post treatment was comparable to sections from *Winnie*+sham-treated mice and greater than in sections from

C57BL/6+sham-treated mice (*n*=4/group; mucosa: *P*<0.001 for both; muscle: *P*<0.05 for both).

Cross sections of the distal colon were immunolabeled with anti-CD45 antibody, specific to the leukocyte common antigen, to evaluate the short-term and long-term effects of MSC treatment on the severity of inflammation throughout the colon wall (*n*=4/group; Fig. 6.6). Overall, sections from *Winnie*+sham and *Winnie*+MSC-treated mice exhibited more CD45-IR cells than in sections from C57BL/6+sham-treated mice at 3 and 60 days post treatment (Fig. 6.6A-C^{I}). These observations were supported by quantification of CD45-IR cell density. Distal colon sections from C57BL/6+sham-treated mice revealed low numbers of leukocytes when measured throughout the whole section, as well as when isolated to the mucosa and muscle layers at both time points (Table 6.3; Fig. 6.6D-F). The level of leukocyte infiltration in sections from sham-treated *Winnie* mice was higher when compared to sections from C57BL/6+sham-treated mice at 3 and 60 days post treatment (*P*<0.001 for both; Table 6.3; Fig. 6.6D). CD45-IR in sections from *Winnie*+MSC-treated mice at 3 and 60 days was comparable to sham-treated *Winnie* mice, and significantly higher than tissues from C57BL/6+sham-treated mice (*P*<0.001 for both; Table 6.3; Fig. 6.6D). Similarly, the density of CD45-IR cells was higher in the mucosal and muscle layers of colon sections from *Winnie*+sham (mucosa - 3 days: *P*<0.05; 60 days: *P*<0.001; muscle - 3 days: *P*<0.05; 60 days: *P*<0.01) and *Winnie*+MSC-treated (mucosa - 3 days: *P*<0.05; 60 days: *P*<0.01; muscle - 3 days: *P*<0.05; 60 days: *P*<0.05) when compared to C57BL/6+sham-treated mice following treatment (Table 6.3; Fig. 6.6E-F).

Hence, a single dose of MSCs did not have any short-term or long-term effect on symptoms, fecal Lcn-2 levels, gross morphological damage to the colonic architecture, or immune cell infiltration associated with chronic colonic inflammation in *Winnie* mice.

Figure 6.1. MSC migration and engraftment within the inflamed colon. Migration and engraftment of human BM-MSCs to the inflamed area of the *Winnie* mouse colon was investigated using anti-HLA-A,B,C antibody, specific to human MHC class I. Enema applied MSCs were localized in the mucosal layer of the colon wall at 3 days post treatment **(A;** arrows**)**. At 60 days post treatment, HLA-A,B,C-IR cells were not detected in the distal colon from MSC-treated *Winnie* mice **(B)**. d = days. Scale bars = 50μm.

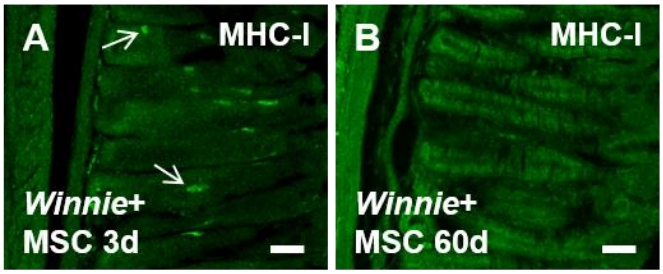
A
MHC-I
Winnie+
MSC 3d
B
MHC-I
Winnie+
MSC 60d

Table 6.3 Evaluation of intestinal inflammation

	C57BL/6+sham			*Winnie*+sham			*Winnie*+MSC		
Parameter	**BT**	**3d**	**60d**	**BT**	**3d**	**60d**	**BT**	**3d**	**60d**
Symptoms									
Diarrhea	A	A	A	P	P	P	P	P	P
Body weight (g)	26.7± 0.6	27.6± 0.4	30.0± 1.0	22.5± 0.9**	23.2± 0.7***	26.0± 0.4**	22.8± 0.9**	23.5± 0.9**	26.3± 0.5**
Fecal water content (g)	0.15± 0.01	0.14± 0.01	0.15± 0.02	0.25± 0.02***	0.24± 0.01***	0.23± 0.003***	0.26± 0.01***	0.23± 0.01***	0.25± 0.01***
Colon length (cm)	-	6.3± 0.2	6.4± 0.2	-	8.2± 0.2***	7.9± 0.2**	-	8.0± 0.4**	7.8± 0.4**
Leukocyte infiltration									
Density of CD45-IR cells in colon cross sections (%)	-	5.4± 0.3	5.3± 0.3	-	9.2± 0.6***	9.3± 0.3***	-	8.9± 0.2***	9.3± 0.3***
Density of CD45-IR cells in the mucosa (%)	-	6.9± 0.3	6.8± 1.0	-	10.1± 1.0*	11.1± 0.4***	-	10.0± 0.6*	10.6±0.5 **
Density of CD45-IR cells in the muscle (%)	-	2.3± 0.2	2.5± 0.3	-	4.3± 0.6*	4.9± 0.5**	-	4.1± 0.7*	4.4± 0.5*

Table 6.3 Evaluation of intestinal inflammation (continued)

	C57BL/6+sham			*Winnie*+sham			*Winnie*+MSC		
Parameter	**BT**	**3d**	**60d**	**BT**	**3d**	**60d**	**BT**	**3d**	**60d**
Histological scoring									
Aberrant crypt architecture (0-3)	-	0.5± 0.3	0.3± 0.3	-	2.3± 0.3*	2.3± 0.5**	-	2.3± 0.3*	2.0± 0.6*
Increased crypt length (0-3)	-	0.3± 0.3	0.3± 0.3	-	2.5± 0.3***	2.8± 0.5***	-	2.8± 0.3***	2.5± 0.5***
Goblet cell depletion (0-3)	-	0.5± 0.3	0.5± 0.3	-	2.0± 0.0*	2.3± 0.5**	-	2.0± 0.4*	2.0± 0.4*
General leukocyte infiltration (0-3)	-	0.8± 0.3	0.8± 0.3	-	2.3± 0.3*	2.3± 0.5*	-	2.3± 0.5*	2.5± 0.3*
Crypt abscesses (0-3)	-	0.5± 0.3	0.5± 0.3	-	2.5± 0.3***	2.8± 0.3***	-	2.5± 0.3***	2.5± 0.3***
Epithelial damage and ulceration (0-3)	-	0.8±0.3	0.8± 0.3	-	2.5± 0.3*	2.5± 0.5*	-	2.5± 0.5*	2.3± 0.5*
Overall histological score (out of 18)	-	3.5±0.9	3.0± 0.7	-	14.0± 0.9***	14.8± 1.3***	-	14.3± 1.5***	13.8± 1.7***

BT = before treatment, d = days, A = absent, P = prominent. *P<0.05, **P<0.01, ***P<0.001 when compared to C57BL/6+sham-treated mice.

Figure 6.2. The short-term and long-term effects of MSC treatment on pellet formation. Fecal samples collected from C57BL/6+sham, *Winnie*+sham, and *Winnie*+MSC-treated mice pre treatment **(A-F)**, as well as 3 **(A^{I}-C^{I})** and 60 days **(D^{I}-F^{I})** post treatment. d = days.

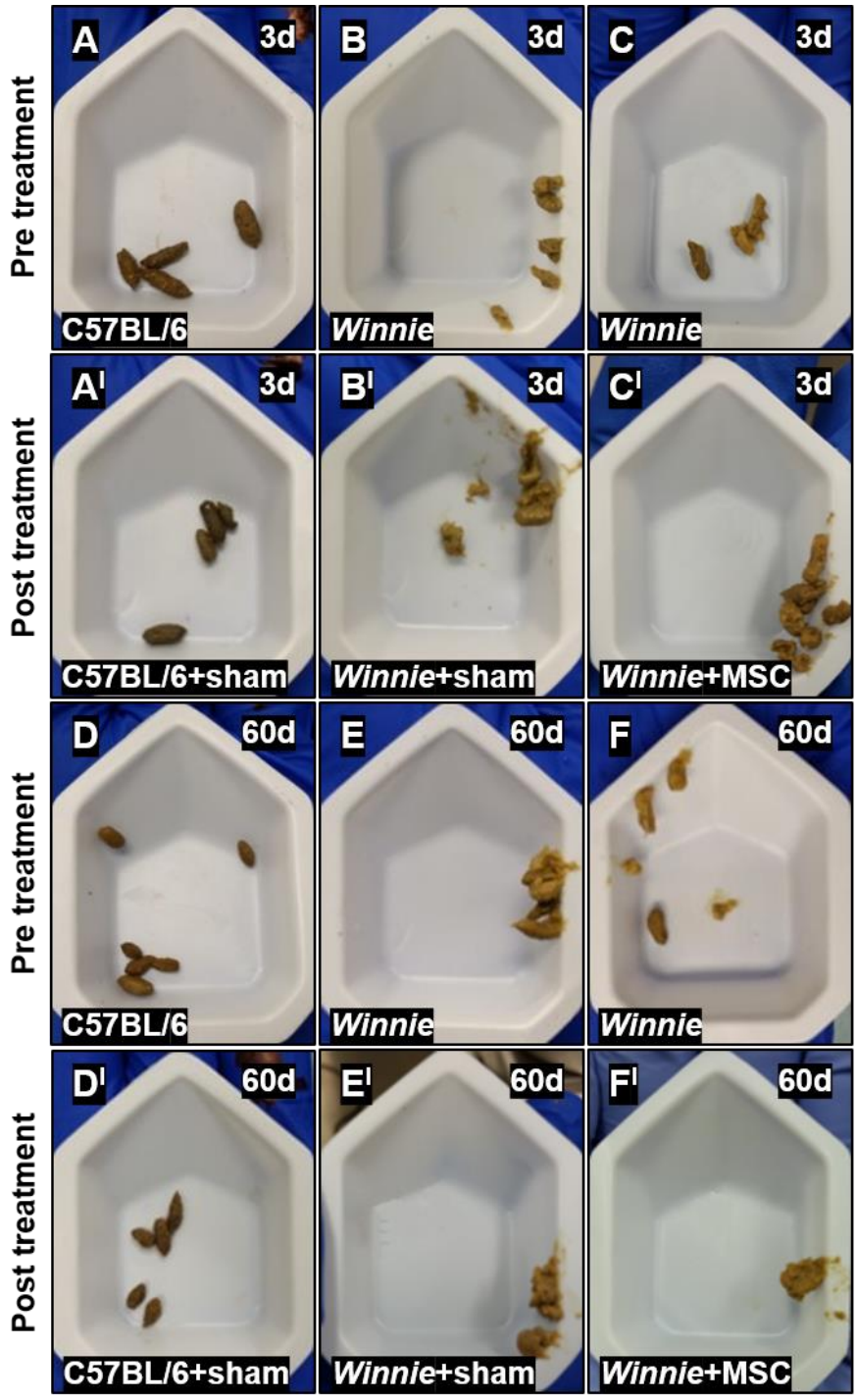
Pre treatment
Post treatment
Pre treatment
Post treatment
A
3d
C57BL/6
B
3d
Winnie
C
3d
Winnie
A'
3d
C57BL/6+sham
B'
3d
Winnie+sham
C'
3d
Winnie+MSC
D
60d
C57BL/6
E
60d
Winnie
F
60d
Winnie
D'
60d
C57BL/6+sham
E'
60d
Winnie+sham
F'
60d
Winnie+MSC

Figure 6.3. The short-term and long-term effects of MSC treatment on fecal water content, body weight and colon length. Fecal water content (wet weight minus dry weight) of stools **(A)**, body weight **(B)**, and colon length **(C)** of C57BL/6+sham, *Winnie*+sham, and *Winnie*+MSC-treated mice before treatment, as well as 3 and 60 days post treatment. d = days. ***P*<0.01, ****P*<0.001 when compared to C57BL/6+sham-treated mice.

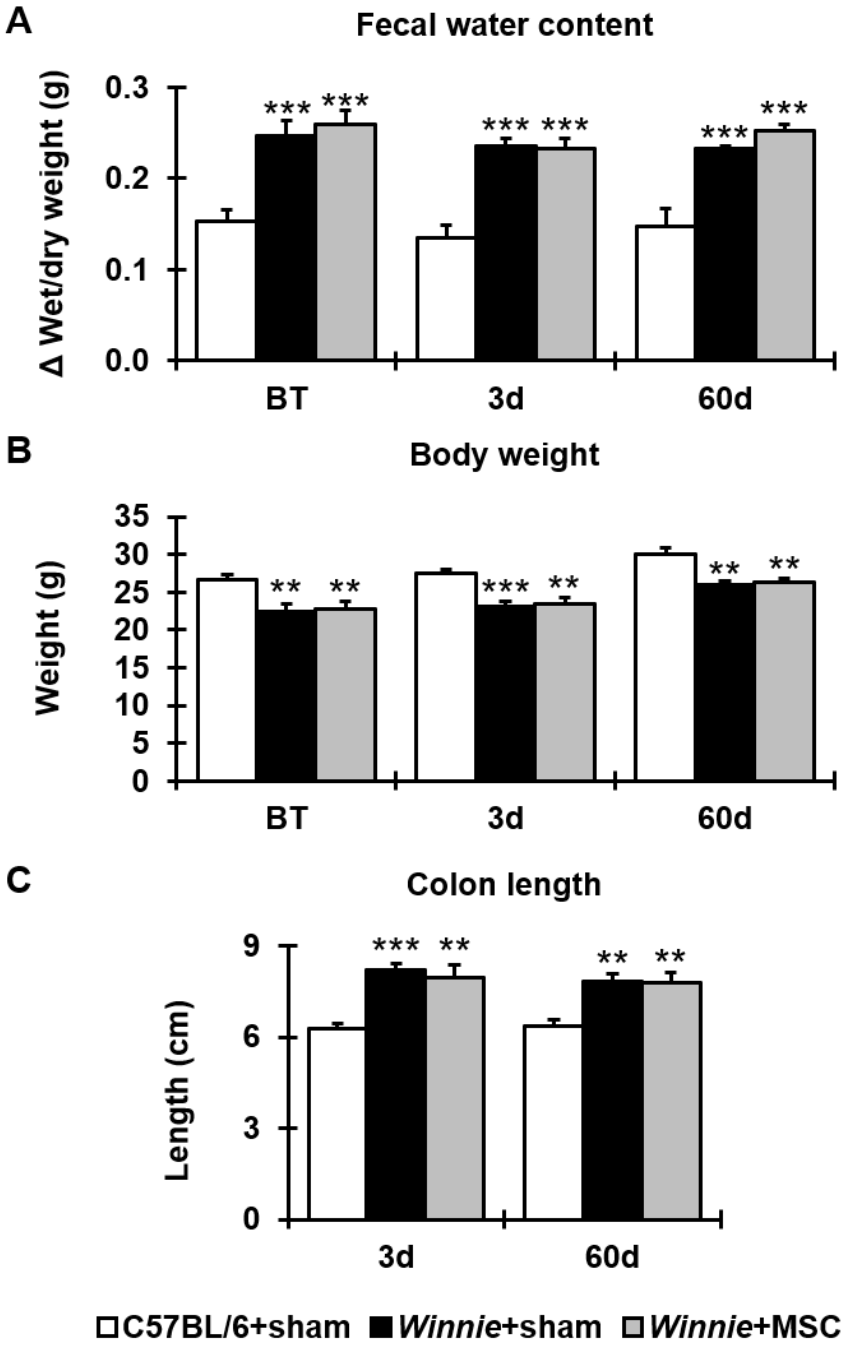
A
Fecal water content
Δ Wet/dry weight (g)
0.3
0.2
0.1
0.0
***
***
***
***
***
***
BT
3d
60d
B
Body weight
Weight (g)
35
30
25
20
15
10
5
0
**
**
***
**
**
**
BT
3d
60d
C
Colon length
Length (cm)
9
6
3
0
***
**
**
**
3d
60d
C57BL/6+sham
Winnie+sham
Winnie+MSC

Figure 6.4. Assessment of the short-term and long-term effects of MSC treatment on colonic inflammation with fecal lipocalin (Lcn)-2. Average Lcn-2 levels quantified in fecal samples from C57BL/6+sham, *Winnie*+sham, and *Winnie*+MSC-treated mice before treatment (BT), as well as 3 and 60 days post treatment **(A)**. Fecal samples were collected twice weekly for 60 days to assess any changes in the level of intestinal inflammation during the experimental period **(B)**. d = days. ****P*<0.001 when compared to C57BL/6+sham-treated mice.

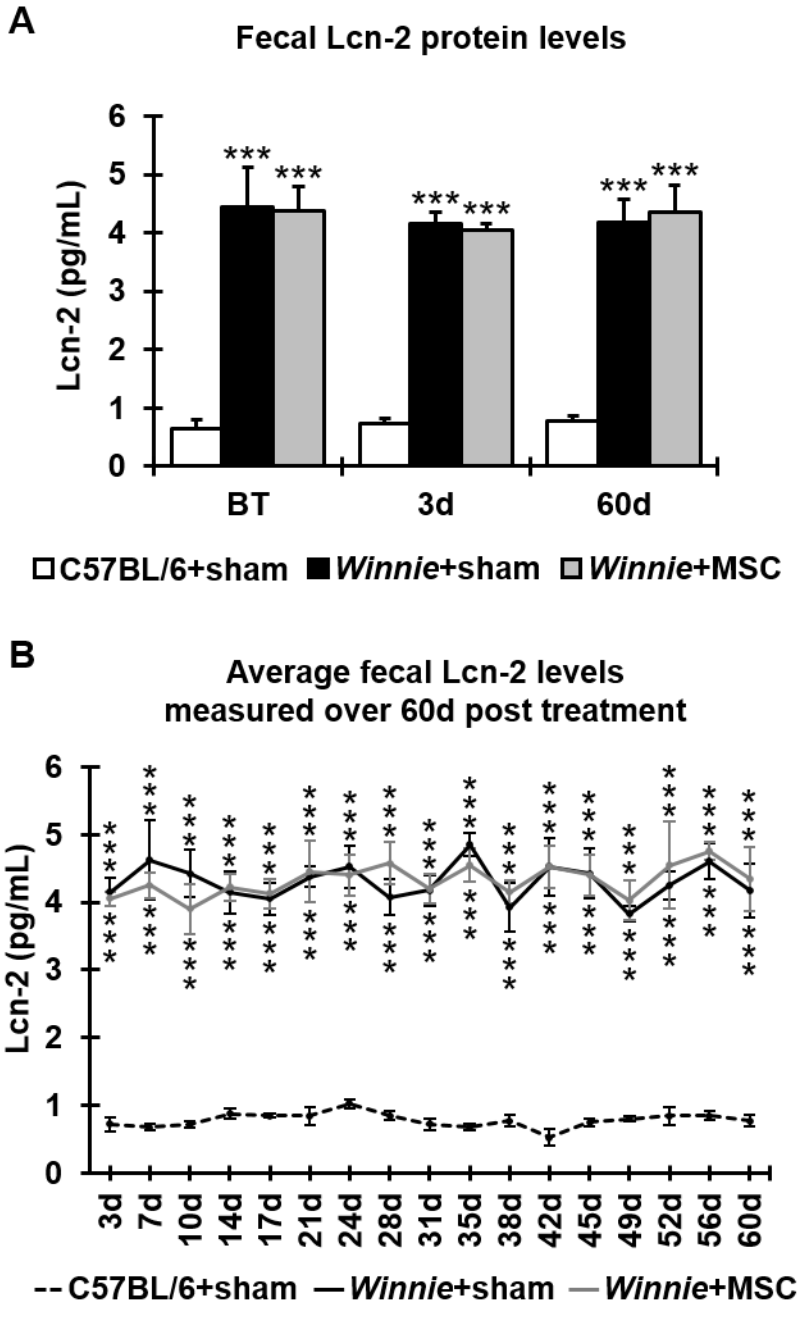
A
Fecal Lcn-2 protein levels
Lcn-2 (pg/mL)
0
1
2
3
4
5
6
***
BT
3d
60d
C57BL/6+sham
Winnie+sham
Winnie+MSC
B
Average fecal Lcn-2 levels
measured over 60d post treatment
Lcn-2 (pg/mL)
3d
7d
10d
14d
17d
21d
24d
28d
31d
35d
38d
42d
45d
49d
52d
56d
60d
C57BL/6+sham
Winnie+sham
Winnie+MSC

Figure 6.5. Histological assessment of the short-term and long-term effects of MSC treatment on colonic inflammation in *Winnie* mice. Gross morphological changes to the colonic architecture and mucin expression was assessed by hematoxylin and eosin (H&E) **(A)** and Alcian blue **(B)** staining of cross sections of the distal colon from C57BL/6+sham, *Winnie*+sham, and *Winnie*+MSC-treated mice 3 and 60 days post treatment. d = days. Scale bars = 50μm (A), 20μm (B).

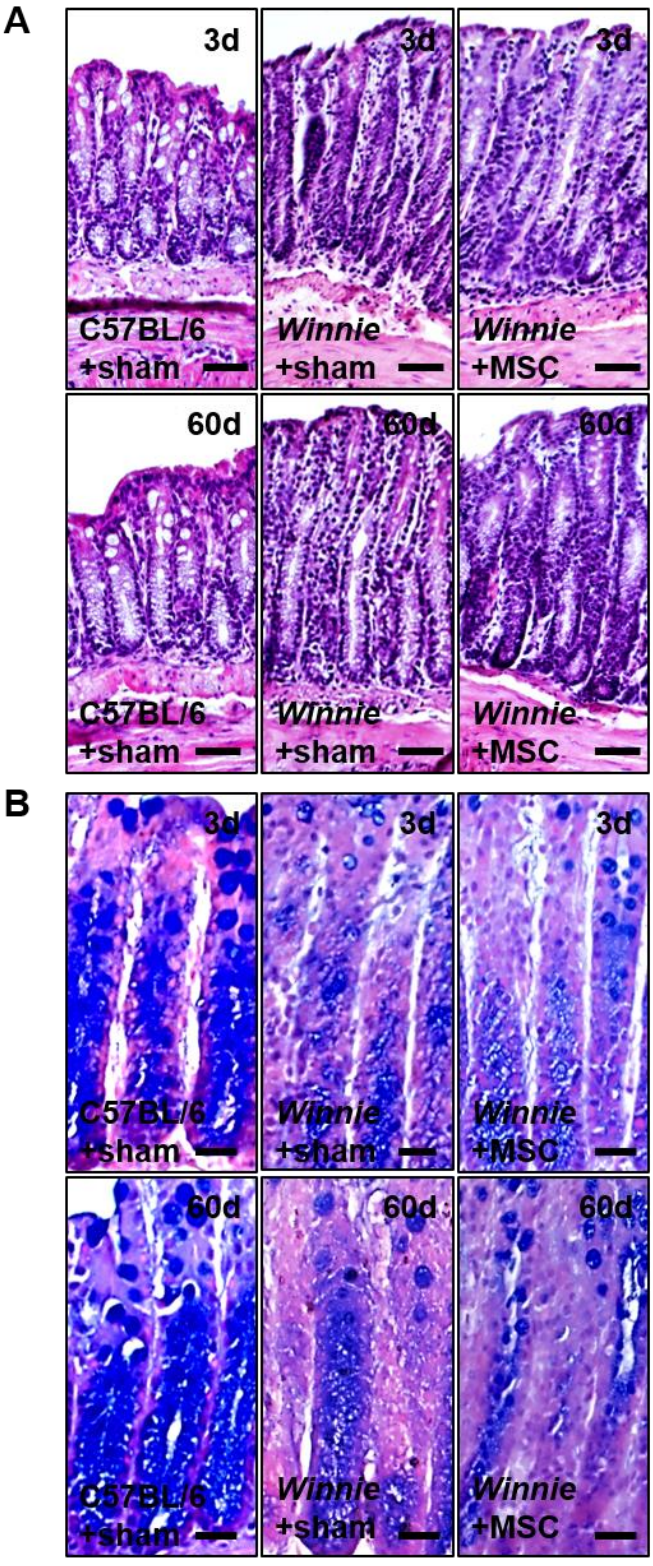
A
3d
3d
3d
C57BL/6
+sham
Winnie
+sham
Winnie
+MSC
60d
60d
60d
C57BL/6
+sham
Winnie
+sham
Winnie
+MSC
B
3d
3d
3d
C57BL/6
+sham
Winnie
+sham
Winnie
+MSC
60d
60d
60d
C57BL/6
+sham
Winnie
+sham
Winnie
+MSC

Figure 6.6. Short-term and long-term effects of MSC treatment on leukocyte infiltration in *Winnie* mice. Anti-CD45 antibody was used to label infiltrating leukocytes within the colon wall from C57BL/6+sham, *Winnie*+sham, and *Winnie*+MSC-treated mice 3 and 60 days post treatment **(A-C^{I})**. d = days. Scale bars = 100µm. Quantitative analyses of CD45-IR cells throughout the colon wall **(D)**, in the mucosa **(E)** and within the muscular layers **(F)**. **P*<0.05, ***P*<0.01, ****P*<0.001 when compared to C57BL/6+sham-treated mice.

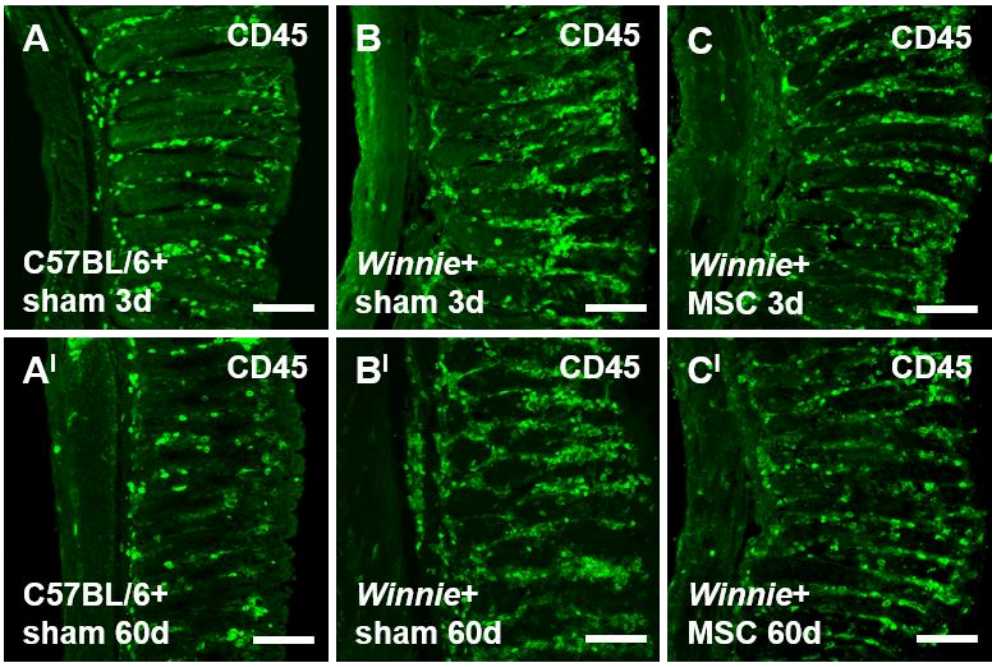
A
CD45
C57BL/6+
sham 3d
B
CD45
Winnie+
sham 3d
C
CD45
Winnie+
MSC 3d
AI
CD45
C57BL/6+
sham 60d
BI
CD45
Winnie+
sham 60d
CI
CD45
Winnie+
MSC 60d

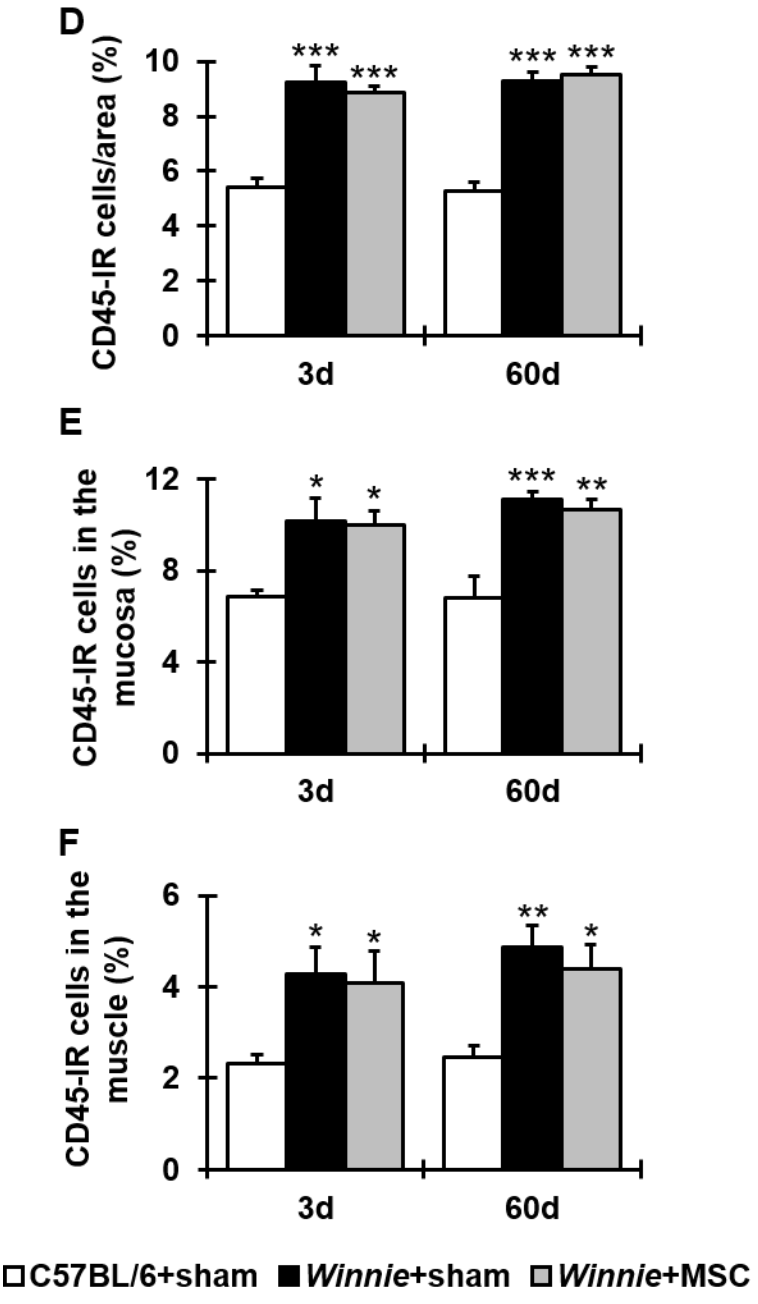
D
CD45-IR cells/area (%)
10
8
6
4
2
0
***
***
***
***
3d
60d
E
CD45-IR cells in the mucosa (%)
12
8
4
0
*
*
***
**
3d
60d
F
CD45-IR cells in the muscle (%)
6
4
2
0
*
*
**
*
3d
60d
C57BL/6+sham
Winnie+sham
Winnie+MSC

6.4.3 No changes in the density of nerve fibers in the distal colon of *Winnie* mice at 3 and 60 days post MSC treatment

Nerve fibers in the mucosa and smooth muscle of the distal colon were identified with anti-β-Tubulin (III) antibody in cross sections from C57BL/6+sham, *Winnie*+sham and *Winnie*+MSC-treated mice (n=4/group; Fig. 6.7A-C^{I}). Sections from all C57BL/6+sham-treated mice revealed systematic arrangement of β-Tubulin (III)-IR fibers within the mucosal and muscular layers of the colonic wall (Fig. 6.7A-A^{I}). β-Tubulin (III)-IR fibers were broken and irregularly dispersed in colon sections from sham-treated *Winnie* mice at 3 and 60 days post treatment (Fig. 6.7B-B^{I}). Similar arrangements of β-Tubulin (III)-IR fibers were observed in sections from MSC-treated *Winnie* mice at both time points (Fig. 6.7C-C^{I}). Quantification of β-Tubulin (III)-IR fibers supported these observations revealing a reduced nerve fiber density throughout the colon wall in sections from *Winnie*+sham (3 days: 4.8±0.6%; 60 days: 5.2±0.2%) and *Winnie*+MSC-treated (3 days: 5.6±0.5%; 60 days: 5.2±0.5%) mice when compared to C57BL/6+sham-treated mice (3 days: 8.9±0.7%; 60 days: 9.0±0.3%) at both 3 and 60 days post treatment (P<0.001 for all; Fig. 6.7D). When analysis was isolated to the mucosal and muscular layers of the colon, sections from *Winnie*+sham (mucosa: 2.8±0.4%; muscle: 10.3±1.3%) and *Winnie*+MSC-treated (mucosa: 3.5±0.5%; muscle: 11.1±1.0%) mice showed consistently diminished nerve fiber densities at 3 days post treatment when compared to C57BL/6+sham-treated mice (mucosa: 7.2±0.9%, P<0.001 for both; muscle: 14.7±0.2%, P<0.05 for both; Fig. 6.7E-F). Similar results were evident at 60 days following treatment when β-Tubulin (III)-IR fiber density was greater in the mucosa and smooth muscle of distal colon sections from C57BL/6+sham-treated (mucosa: 6.7±0.5%; muscle: 14.7±0.3%) compared to *Winnie*+sham (mucosa: 3.2±0.2%; muscle: 11.2±0.9%) and *Winnie*+MSC-treated (mucosa: 2.9±0.1%; muscle: 11.2±0.2%) mice (mucosa: P<0.001 for both; muscle: P<0.05 for both; Fig. 6.7E-F). No changes in nerve fiber density were evident in colon sections from *Winnie*+sham when compared to *Winnie*+MSC-treated mice at either time point.

6.4.4 No changes in the density of cholinergic nerve fibers in the distal colon of *Winnie* mice at 3 and 60 days post MSC treatment

Cholinergic fibers were identified by anti-VAChT antibody in wholemount LMMP preparations of the distal colon from C57BL/6+sham, *Winnie*+sham, and *Winnie*+MSC-treated mice at 3 and 60 days post treatment (*n*=4/group; Fig. 6.8A-C^{I}). VAChT-IR fibers were plentiful within the myenteric plexus of tissues from C57BL/6+sham-treated mice at both 3 (ganglia: 31.2±1.7%; area: 8.3±0.4%) and 60 days (ganglia: 29.7±0.8%; area: 7.8±0.4%) following treatment (Fig. 6.8A-A^{I}, D-E). There was a significant reduction in the density of VAChT-IR fibers in tissues from *Winnie*+sham (ganglia: 24.0±0.8%; area: 5.7±0.3%) and *Winnie*+MSC-treated (ganglia: 24.5±0.9%; area: 6.2±0.1%) mice when compared to C57BL/6+sham-treated mice at 3 days post treatment (*P*<0.001 for all; (Fig. 6.8B, C, D-E). Similarly, diminished cholinergic fibers were quantified in LMMP preparations from *Winnie*+sham (ganglia: 24.7±0.4%; area: 5.5±0.2%) and *Winnie*+MSC-treated (ganglia: 24.2±0.8%; area: 5.3±0.2%) mice when compared to C57BL/6+sham-treated mice at 60 days post treatment (ganglia: *P*<0.01 for both; area: *P*<0.001 for both; Fig. 6.8B^{I}, C^{I}, D-E). There were no differences in cholinergic fiber density in LMMP preparations of the distal colon from *Winnie*+sham and *Winnie*+MSC-treated mice when measured per ganglion or per area at either time point (Fig. 6.8D-E).

6.4.5 No changes in the density of noradrenergic nerve fibers in the distal colon of *Winnie* mice at 3 and 60 days post MSC treatment

To assess the short-term and long-term effects of MSC treatment on noradrenergic nerve fibers, we evaluated changes in their expression by quantifying the density of TH-IR fibers in LMMP preparations of the colon from C57BL/6+sham, *Winnie*+sham and *Winnie*+MSC-treated mice 3 and 60 days post treatment (*n*=4/group; Fig. 6.9A-C^{I}). TH-IR fibers were abundantly distributed throughout the myenteric plexus of C57BL/6+sham-treated mice at 3 (ganglia: 22.9±0.9%; area: 6.1±0.1%) and 60 days (ganglia: 23.1±0.6%; area: 6.3±0.1%) post treatment (Fig. 6.9A-A^{I}, D-E). The density of TH-IR fibers was

significantly less in LMMP preparations of the distal colon from *Winnie*+sham-treated (ganglia: 15.1±0.5%; area: 3.6±0.1%) and *Winnie*+MSC-treated (ganglia: 14.9±0.7%; area: 3.7±0.2%) mice at 3 days when compared to tissues from C57BL/6+sham-treated mice (P<0.001 for all; Fig. 6.9B, C, D-E). Similarly, when compared to colons from C57BL/6+sham-treated mice at 60 days post treatment, TH-IR fibers were reduced in LMMP preparations from *Winnie*+sham-treated (ganglia: 15.3±0.4%; area: 3.7±0.1%) and *Winnie*+MSC-treated (ganglia: 15.4±1.0%; area: 3.5±0.1%) mice (P<0.001 for all; Fig. 6.9B^{I}, C^{I}, D-E). There was no difference in TH-IR fiber density in colon tissues from *Winnie*+sham-treated and *Winnie*+MSC-treated mice at either time point.

6.4.6 No changes in the density of sensory nerve fibers in the distal colon of *Winnie* mice at 3 and 60 days post MSC treatment

Sensory nerve fibers were labeled with anti-CGRP antibody in wholemount LMMP preparations of the distal colon from C57BL/6+sham, *Winnie*+sham and *Winnie*+MSC-treated mice 3 and 60 days post treatment (n=4/group; Fig. 6.10A-C^{I}). CGRP-IR fibers were liberally dispersed throughout the myenteric plexus in LMMP preparations from C57BL/6+sham-treated mice (Fig. 6.10A-A^{I}). Less extensive sensory fiber IR was observed in tissues from *Winnie*+sham and *Winnie*+MSC-treated mice at 3 and 60 days post treatment (Fig. 6.10B-C^{I}). Quantitative analyses revealed significantly less CGRP-IR fibers in preparations from *Winnie*+sham (ganglia: 18.9±0.6%; area: 4.9±0.2%) and *Winnie*+MSC-treated mice (ganglia: 20.5±0.9%; area: 5.0±0.4%) when compared to C57BL/6+sham-treated mice (ganglia: 28.9±0.9%; area: 6.7±0.3%) at 3 days after treatment (P<0.001 for all; Fig. 6.10D-E). Similarly, at 60 days post treatment, there was a higher density of sensory fibers in LMMP preparations in C57BL/6+sham-treated mice (ganglia: 28.7±1.0%; area: 6.7±0.2%) than sham-treated (ganglia: 19.6±1.7%; area: 4.8±0.4%) and MSC-treated (ganglia: 20.9±1.4%; area: 4.8±0.3%) *Winnie* mice (P<0.01 for all; Fig. 6.10D-E). There were no differences in the density of sensory fibers in samples from *Winnie*+sham-treated and *Winnie*+MSC-treated at both time points.

Figure 6.7. Short-term and long-term effects of MSC treatment on nerve fiber density in *Winnie* mice. Nerve fibers were labeled with anti-β-Tubulin (III) antibody in cross sections of the distal colon from C57BL/6+sham, *Winnie*+sham and *Winnie*+MSC-treated mice 3 and 60 days post treatment **(A-C^{I})**. d = days. Scale bars = 100μm. Quantitative analyses of β-Tubulin (III)-IR fibers throughout the colon wall **(D)**, in the mucosa **(E)** and within the muscular layers **(F)**. **P*<0.05, ****P*<0.001 when compared to C57BL/6+sham-treated mice.

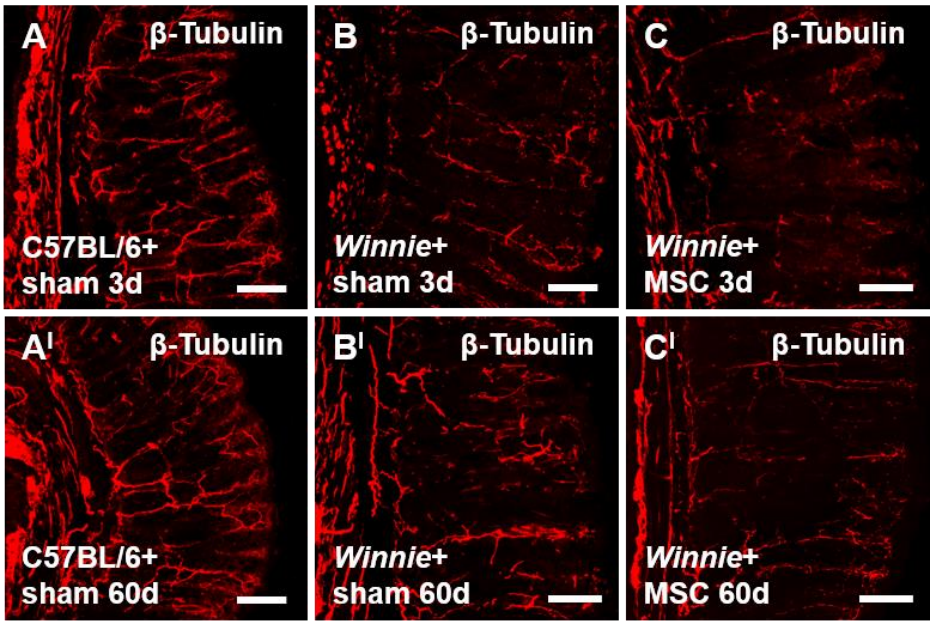
A
β-Tubulin
C57BL/6+
sham 3d
B
β-Tubulin
Winnie+
sham 3d
C
β-Tubulin
Winnie+
MSC 3d
A'
β-Tubulin
C57BL/6+
sham 60d
B'
β-Tubulin
Winnie+
sham 60d
C'
β-Tubulin
Winnie+
MSC 60d

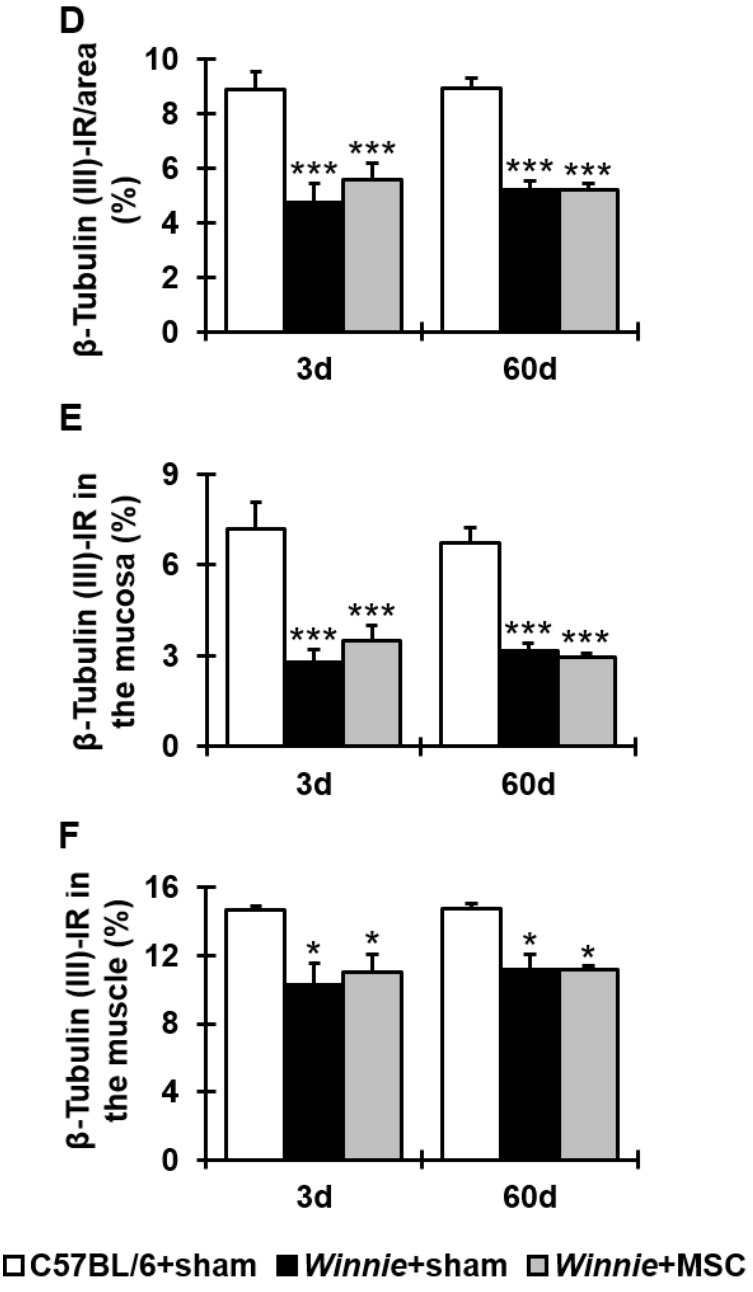
D
β-Tubulin (III)-IR/area (%)
10
8
6
4
2
0
***
***
***
***
3d
60d
E
β-Tubulin (III)-IR in the mucosa (%)
9
6
3
0
***
***
***
***
3d
60d
F
β-Tubulin (III)-IR in the muscle (%)
16
12
8
4
0
*
*
*
*
3d
60d
C57BL/6+sham
Winnie+sham
Winnie+MSC

Figure 6.8. Short-term and long-term effects of MSC treatment on cholinergic nerve fiber density in *Winnie* mice. Anti-VAChT antibody was used to label cholinergic nerve fibers in LMMP preparations of the distal colon from C57BL/6+sham, *Winnie*+sham and *Winnie*+MSC-treated mice 3 and 60 days post treatment **(A-C^{I})**. d = days. Scale bars = 100µm. Quantitative analyses of VAChT-IR fibers per ganglion **(D)** and per 2mm^2 area **(E)** of the colon. ***P*<0.01, ****P*<0.001 when compared to C57BL/6+sham-treated mice.

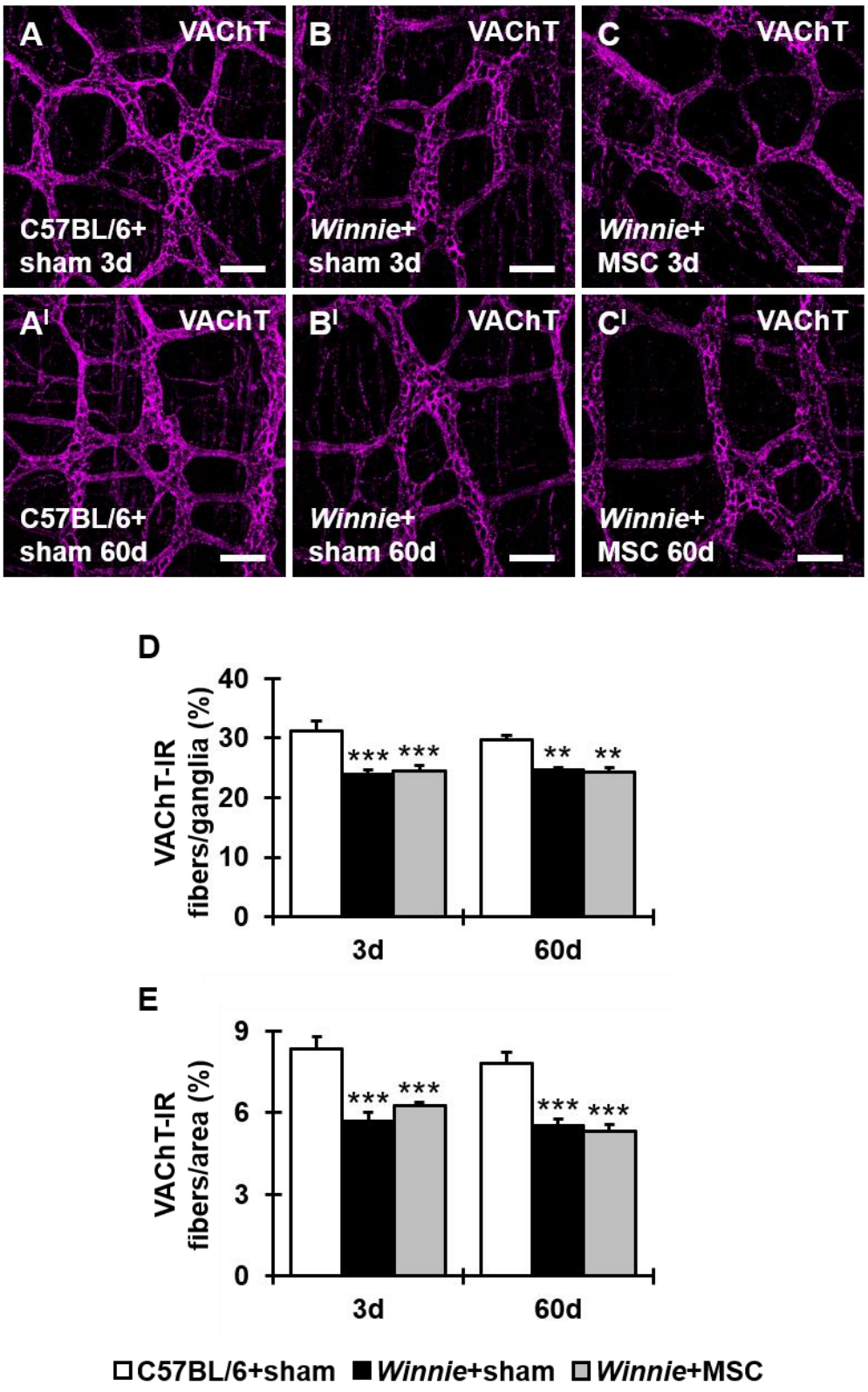
A
VAChT
C57BL/6+
sham 3d
B
VAChT
Winnie+
sham 3d
C
VAChT
Winnie+
MSC 3d
A'
VAChT
C57BL/6+
sham 60d
B'
VAChT
Winnie+
sham 60d
C'
VAChT
Winnie+
MSC 60d
D
VAChT-IR
fibers/ganglia (%)
40
30
20
10
0
***
***
**
**
3d
60d
E
VAChT-IR
fibers/area (%)
9
6
3
0
***
***
***
***
3d
60d
C57BL/6+sham
Winnie+sham
Winnie+MSC

Figure 6.9. Short-term and long-term effects of MSC treatment on noradrenergic nerve fiber density in *Winnie* mice. Noradrenergic nerve fibers in LMMP preparations of the distal colon from C57BL/6+sham, *Winnie*+sham and *Winnie*+MSC-treated mice 3 and 60 days post treatment were identified by anti-TH antibody **(A-C^{I})**. d = days. Scale bars = 100µm. Quantitative analyses of TH-IR fibers per ganglion **(D)** and per 2mm^2 area **(E)** of the colon. ****P*<0.001 when compared to C57BL/6+sham-treated mice.

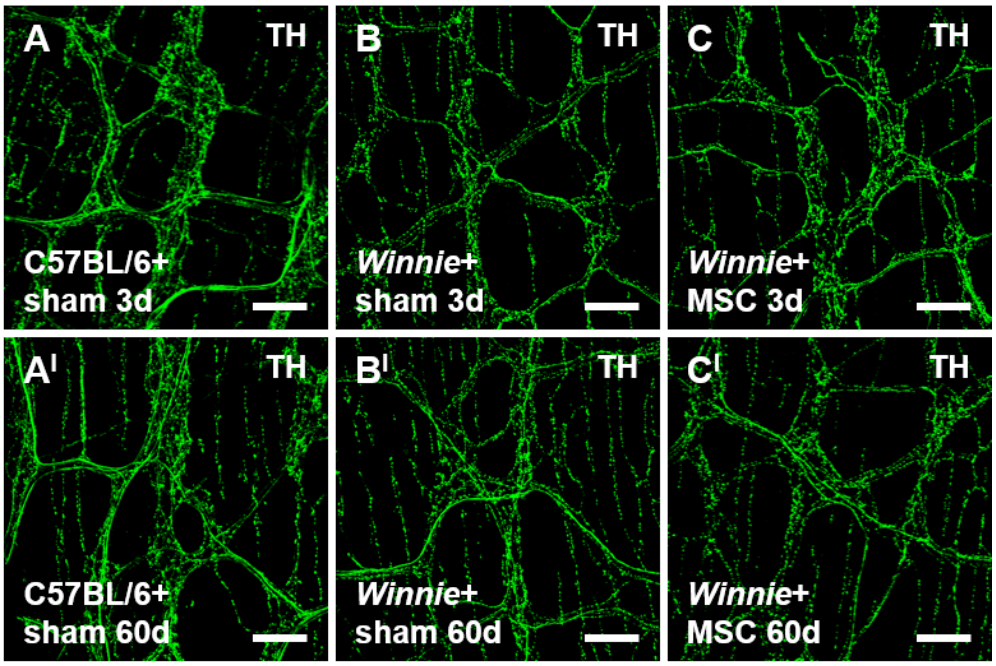
A
TH
C57BL/6+
sham 3d
B
TH
Winnie+
sham 3d
C
TH
Winnie+
MSC 3d
AI
TH
C57BL/6+
sham 60d
BI
TH
Winnie+
sham 60d
CI
TH
Winnie+
MSC 60d

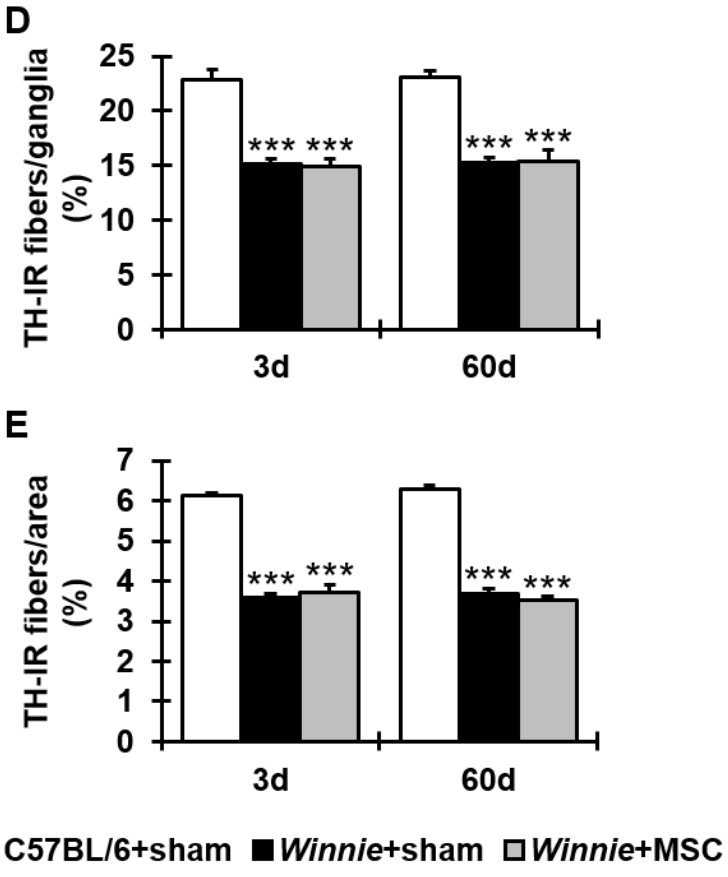
D
TH-IR fibers/ganglia (%)
25
20
15
10
5
0
***
***
***
***
3d
60d
E
TH-IR fibers/area (%)
7
6
5
4
3
2
1
0
***
***
***
***
3d
60d
C57BL/6+sham
Winnie+sham
Winnie+MSC

Figure 6.10. Short-term and long-term effects of MSC treatment on sensory nerve fiber density in *Winnie* mice. Anti-CGRP antibody was used to identify sensory nerve fibers in LMMP preparations of the distal colon from C57BL/6+sham, *Winnie*+sham and *Winnie*+MSC-treated mice 3 and 60 days post treatment **(A-C^{I})**. d = days. Scale bars = 100μm. Quantitative analyses of CGRP-IR fibers per ganglion **(D)** and per 2mm^2 area **(E)** of the colon. ***P*<0.01, ****P*<0.001 when compared to C57BL/6+sham-treated mice.

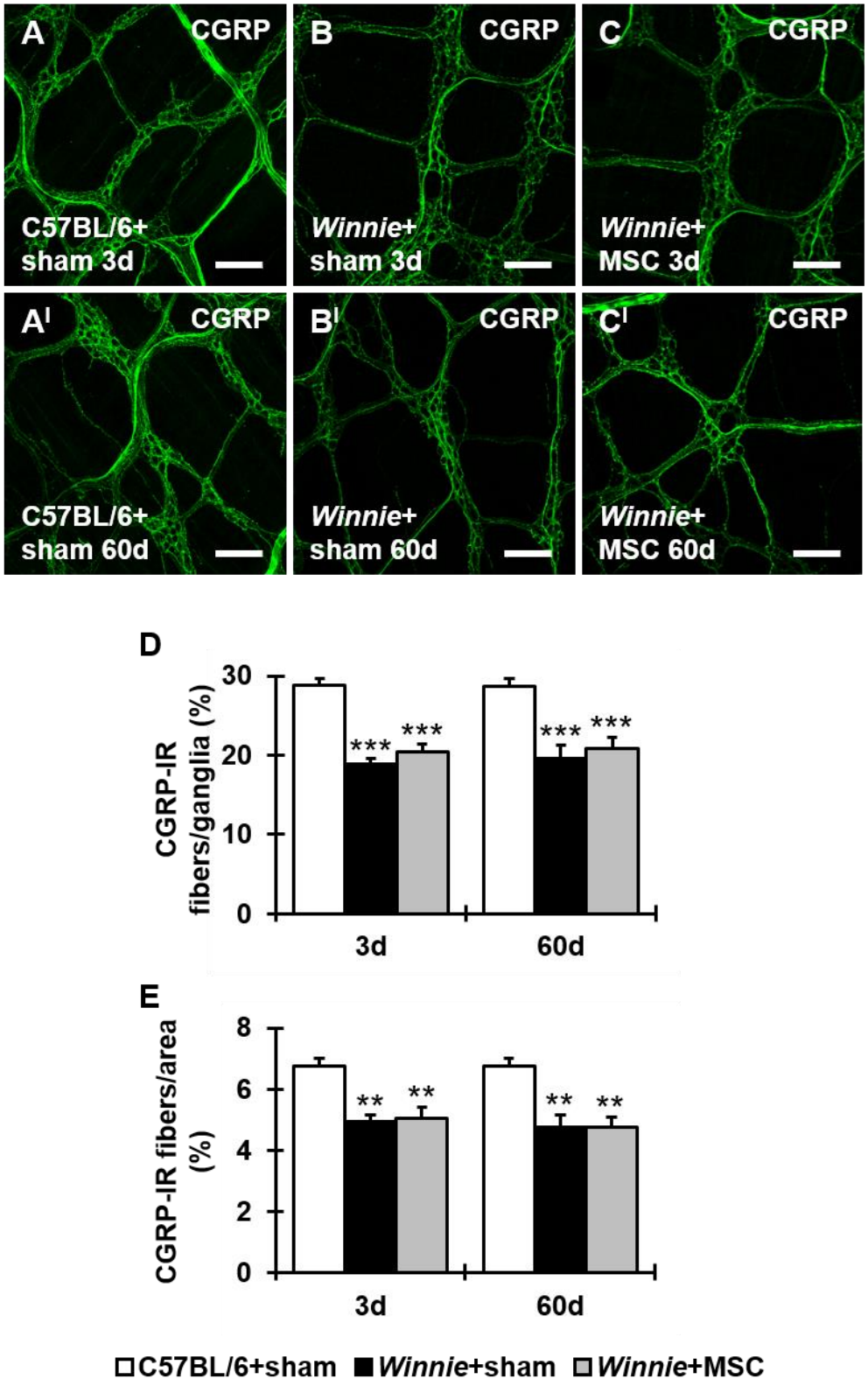
A
CGRP
C57BL/6+
sham 3d
B
CGRP
Winnie+
sham 3d
C
CGRP
Winnie+
MSC 3d
AI
CGRP
C57BL/6+
sham 60d
BI
CGRP
Winnie+
sham 60d
CI
CGRP
Winnie+
MSC 60d
D
CGRP-IR
fibers/ganglia (%)
30
20
10
0
***
***
***
***
3d
60d
E
CGRP-IR fibers/area
(%)
8
6
4
2
0
**
**
**
**
3d
60d
C57BL/6+sham
Winnie+sham
Winnie+MSC

6.4.7 No changes in the average number of myenteric neurons in the distal colon of *Winnie* mice at 3 and 60 days post MSC treatment

The average number and percentage of myenteric neurons per ganglionic area was calculated in wholemount LMMP preparations of the distal colon from C57BL/6+sham, *Winnie*+sham, and *Winnie*+MSC-treated mice 3 and 60 days post treatment using the pan-neuronal marker PGP9.5 (n=4/group; Fig. 6.11A-C^{I}). In tissues from C57BL/6+sham-treated mice, the average number of PGP9.5-IR neurons per ganglionic area was 22±0.7 and 22±0.3 at 3 and 60 days post treatment, respectively (Fig. 6.11D). Prominent neuronal loss was evident in tissues from *Winnie* mice in the sham treatment groups when compared to LMMP preparations from C57BL/6+sham-treated mice at both time points (3 days: 18±0.2 cells/ganglionic area; 60 days: 18±0.4 cells/ganglionic area; P<0.001 for both; Fig. 6.11D). Subsequently, the percent ganglionic density of PGP9.5-IR neurons in tissues from *Winnie*+sham-treated mice (3 days: 83.9±1.9%; 60 days: 82.2±3.0%; P<0.001 for both) was reduced relative to control (100%; Fig. 6.11E). In samples from MSC treated *Winnie* mice, the number of neurons per ganglionic area, as well as the percent neuronal density, was similar at 3 (18±0.2 cells/ganglionic area; 82.4±3.3%) and 60 days (18±0.4 cells/ganglionic area; 83.6±2.5%) post treatment, comparable to tissues from *Winnie*+sham-treated mice. At both time points, LMMP preparations from *Winnie*+MSC-treated mice exhibited a lower average number and percentage of PGP9.5-IR neurons per ganglionic area than tissues from C57BL/6+sham-treated mice (P<0.001 for all; Fig. 6.11D-E).

6.4.8 No changes in the average number of nNOS-IR myenteric neurons in the distal colon of *Winnie* mice at 3 and 60 days post MSC treatment

Nitrergic myenteric neurons were identified in wholemount LMMP preparations of the distal colon using anti-nNOS antibody (n=4/group; Fig. 6.12A-F). In addition, LMMP preparations were co-labeled with anti-PGP9.5 antibody to demonstrate the subpopulation of nNOS-IR neurons within the total population of myenteric

neurons (Fig. 6.12A^{I}-F^{I}). In tissues from C57BL/6+sham-treated mice, the average number of nNOS-IR neurons per ganglionic area was consistent from 3 (7±0.2 cells/ganglionic area) to 60 days (7±0.3 cells/ganglionic area) post treatment (Fig. 6.12G). The average number of nNOS-IR neurons per ganglionic area in tissues from *Winnie*+sham (3 days: 7±0.2 cells/ganglionic area; 60 days: 7±0.3 cells/ganglionic area) and *Winnie*+MSC-treated (3 days: 7±0.4 cells/ganglionic area; 60 days: 7±0.4 cells/ganglionic area) mice were comparable to tissues from C57BL/6+sham-treated mice at both time points (Fig. 4.12G). Consequently, there was no difference in the ganglionic density of nNOS-IR neurons in distal colon samples from any group (*Winnie*+sham - 3 days: 96.3±5.1%; 60 days: 93.6±4.0%; *Winnie*+MSC - 3 days: 92.5±3.3%; 60 days: 95.0±2.6%) relative to control (100%; Fig. 4.12H). Although there were no changes in the average number of nNOS-IR neurons in tissues from *Winnie*+sham or *Winnie*+MSC-treated mice, loss of myenteric neurons established an increased proportion of nNOS-IR neurons to PGP9.5-IR neurons (*Winnie*+sham - 3 days: 38.1±1.4%; 60 days: 37.4±0.8%; *Winnie*+MSC - 3 days: 37.5±1.4%; 60 days: 36.9±0.9%) when compared to C57BL/6+sham-treated mice (3 days: 33.5±0.6%; 60 days: 32.9±1.2%) at both time points (P<0.05 for all; Fig. 4.12I).

6.4.9 No changes in the average number of ChAT-IR myenteric neurons in the distal colon of *Winnie* mice at 3 and 60 days post MSC treatment

Anti-ChAT antibody was used to quantify the average number of cholinergic neurons in wholemount LMMP preparations of the distal colon from C57BL/6+sham, *Winnie*+sham, and *Winnie*+MSC mice at 3 and 60 days post treatment (n=4/group; Fig. 6.13A-F). Tissues were also labeled with anti-PGP9.5 antibody to verify the subpopulation of ChAT-IR neurons within the total population of myenteric neurons (Fig. 6.13A^{I}-F^{I}). The average number of ChAT-IR neurons per ganglionic area and the proportion of ChAT-IR to PGP9.5-IR neurons in tissues from C57BL/6+sham-treated mice was similar at 3 (12±0.7 cells per ganglionic area; 51.5±2.5%) and 60 days (11±0.6 cells per ganglionic

area; 51.9±3.0%) post treatment (Fig. 6.13G, I). Less ChAT-IR neurons were counted in tissues from *Winnie*+sham-treated when compared to C57BL/6+sham-treated at both time points (3 days: 9±0.2 cells per ganglionic area; 60 days: 9±0.4 cells per ganglionic area; $P<0.05$ for both; Fig. 6.13G). Thus, the ganglionic density of ChAT-IR neurons was reduced in samples from sham treated *Winnie* mice relative to control tissues (3 days: 79.5±3.3%, $P<0.01$; 60 days: 81.9±6.3%, $P<0.05$; Fig. 6.13H). In tissues from *Winnie*+MSC-treated mice, the average number and density of ChAT-IR neurons per ganglionic area at 3 (9±0.7 cells per ganglionic area, $P<0.05$; 80.7±2.7%, $P<0.01$) and 60 days (9±0.4 cells per ganglionic area, $P<0.05$; 79.3±6.3%, $P<0.01$) post treatment was comparable to samples from *Winnie*+sham-treated mice and significantly less than in preparations from C57BL/6+sham-treated mice (Fig. 6.13G-H). No differences in the proportion of ChAT-IR neurons to the total number of neurons was found between groups due to the concurrent loss of PGP9.5-IR and ChAT-IR neurons in samples from *Winnie*+sham (3 days: 49.2±1.3; 60 days: 51.3±2.3) and *Winnie*+MSC-treated (3 days: 51.7±4.0; 60 days: 49.0±1.8) mice (Fig. 6.13I).

Figure 6.11. Short-term and long-term effects of MSC treatment on the average number of myenteric neurons in *Winnie* mice. Anti-PGP9.5 antibody was used to label myenteric neurons in LMMP preparations of the distal colon from C57BL/6+sham, *Winnie*+sham, and *Winnie*+MSC-treated mice 3 and 60 days post treatment **(A-C^{I})**. d = days. Scale bars = 100µm. Quantitative analyses of the average number of PGP9.5-IR neurons normalized to 0.1mm^2 ganglionic area **(D)**. Ganglionic density of PGP9.5-IR neurons in tissues from *Winnie* mice as a percentage of control (100%) **(E)**. ***P<0.001 when compared to C57BL/6+sham-treated mice.

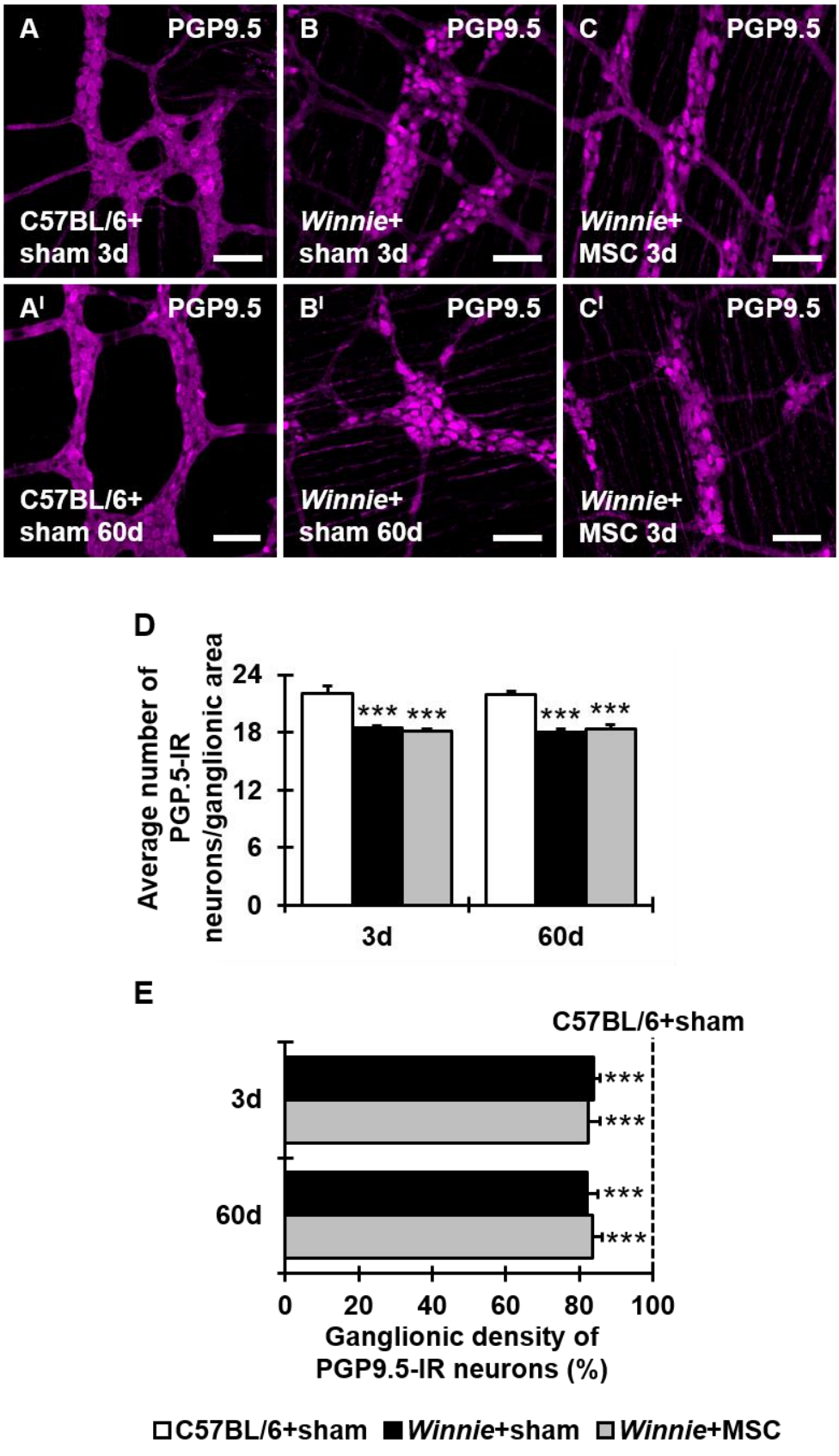
A
PGP9.5
C57BL/6+
sham 3d
B
PGP9.5
Winnie+
sham 3d
C
PGP9.5
Winnie+
MSC 3d
A'
PGP9.5
C57BL/6+
sham 60d
B'
PGP9.5
Winnie+
sham 60d
C'
PGP9.5
Winnie+
MSC 3d
D
Average number of PGP.5-IR neurons/ganglionic area
24
18
12
6
0
***
***
***
***
3d
60d
E
C57BL/6+sham
3d
60d
***
***
***
***
0
20
40
60
80
100
Ganglionic density of PGP9.5-IR neurons (%)
C57BL/6+sham
Winnie+sham
Winnie+MSC

Figure 6.12. Short-term and long-term effects of MSC treatment on the average number of nNOS-IR myenteric neurons in *Winnie* mice. Anti-nNOS antibody was used to label myenteric nitrergic neurons in LMMP preparations of the distal colon from C57BL/6+sham, *Winnie*+sham, and *Winnie*+MSC-treated mice 3 and 60 days post treatment **(A-F)**. Merged images of nNOS-IR (green) and PGP9.5-IR (red) neurons indicate the subpopulation of nNOS-IR neurons within the total population of myenteric neurons **(A^{I}-F^{I})**. d = days. Scale bars = 100µm. Quantitative analyses of the average number of nNOS-IR neurons normalized to 0.1mm^2 ganglionic area **(G)**. Ganglionic density of nNOS-IR neurons in tissues from *Winnie* mice as a percentage of control (100%) **(H)**. The proportion of nNOS-IR neurons to PGP9.5-IR neurons **(I)**. **P*<0.05 when compared to C57BL/6+sham-treated mice.

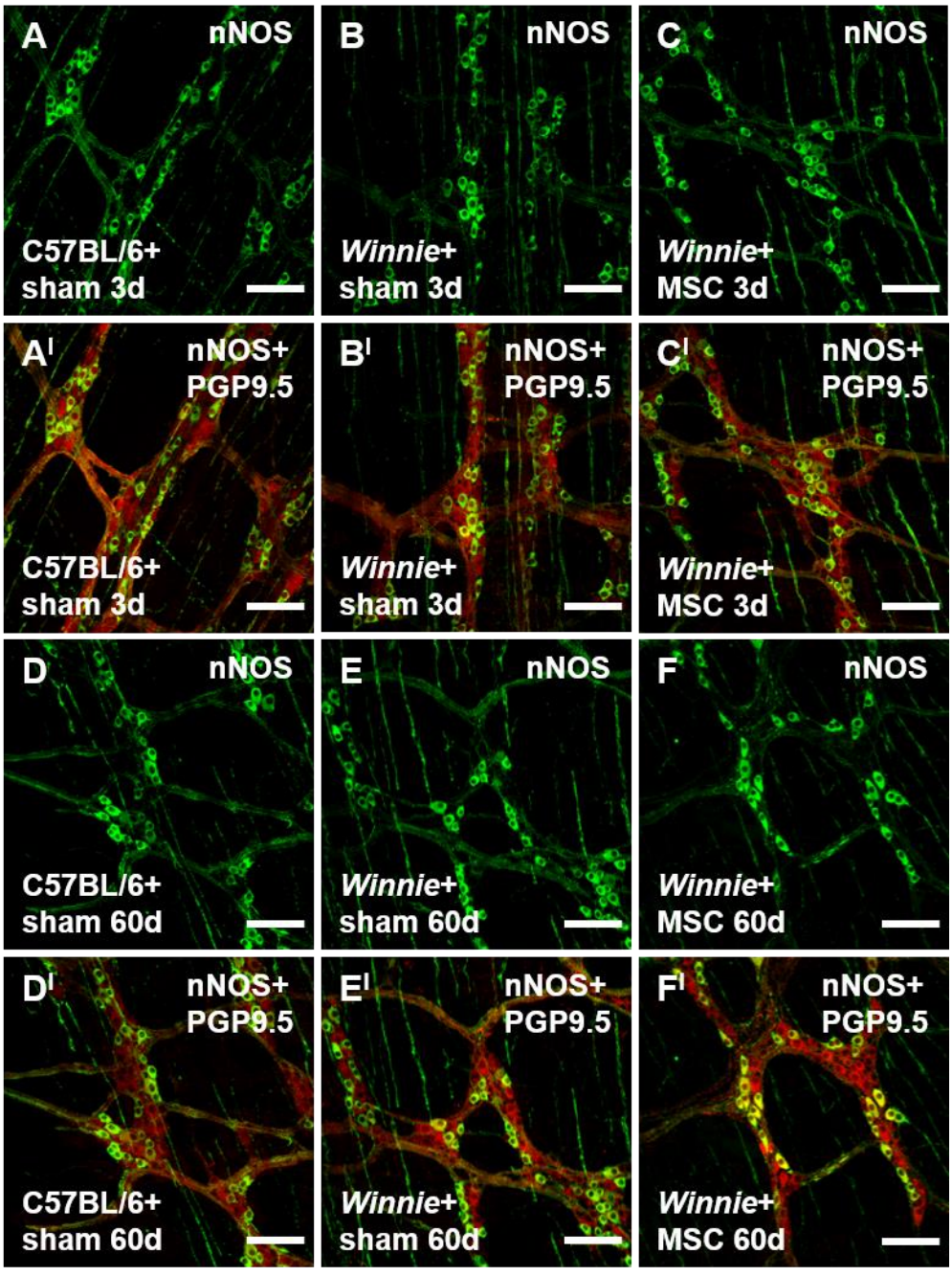
A
nNOS
C57BL/6+
sham 3d
B
nNOS
Winnie+
sham 3d
C
nNOS
Winnie+
MSC 3d
A'
nNOS+
PGP9.5
C57BL/6+
sham 3d
B'
nNOS+
PGP9.5
Winnie+
sham 3d
C'
nNOS+
PGP9.5
Winnie+
MSC 3d
D
nNOS
C57BL/6+
sham 60d
E
nNOS
Winnie+
sham 60d
F
nNOS
Winnie+
MSC 60d
D'
nNOS+
PGP9.5
C57BL/6+
sham 60d
E'
nNOS+
PGP9.5
Winnie+
sham 60d
F'
nNOS+
PGP9.5
Winnie+
MSC 60d

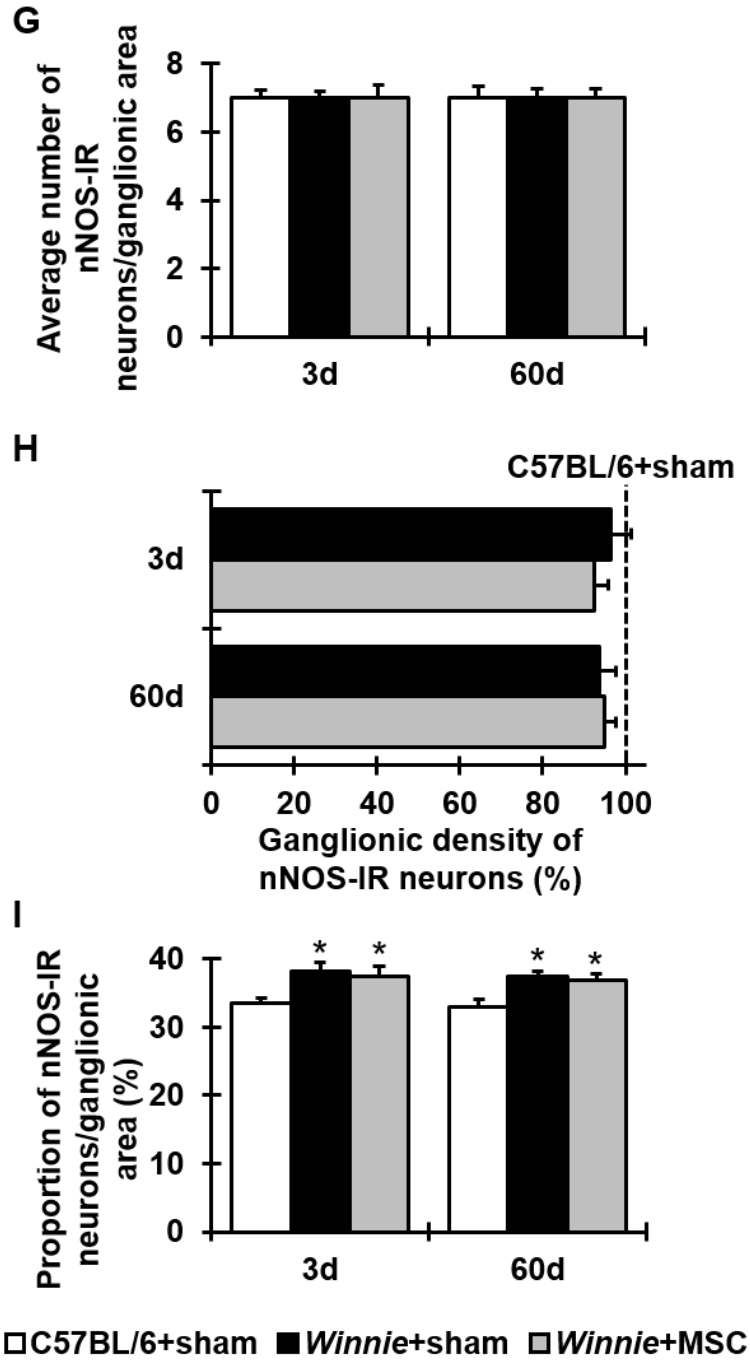
G
Average number of nNOS-IR neurons/ganglionic area
8
6
4
2
0
3d
60d
H
C57BL/6+sham
3d
60d
0
20
40
60
80
100
Ganglionic density of nNOS-IR neurons (%)
I
Proportion of nNOS-IR neurons/ganglionic area (%)
40
30
20
10
0
*
*
*
*
3d
60d
C57BL/6+sham
Winnie+sham
Winnie+MSC

Figure 6.13. Short-term and long-term effects of MSC treatment on the average number of ChAT-IR myenteric neurons in *Winnie* mice. Anti-ChAT antibody was used to label myenteric cholinergic neurons in LMMP preparations of the distal colon from C57BL/6+sham, *Winnie*+sham, and *Winnie*+MSC-treated mice 3 and 60 days post treatment **(A-F)**. Merged images of ChAT-IR (green) and neurons PGP9.5-IR (red) indicate the subpopulation of ChAT-IR neurons within the total population of myenteric neurons **(A^{I}-F^{I})**. d = days. Scale bars = 100µm. Quantitative analyses of the average number of ChAT-IR neurons normalized to 0.1mm^2 ganglionic area **(G)**. Ganglionic density of ChAT-IR neurons in tissues from *Winnie* mice as a percentage of control (100%) **(H)**. The proportion of ChAT-IR neurons to PGP9.5-IR neurons **(I)**. **P*<0.05, ***P*<0.01 when compared to C57BL/6+sham-treated mice.

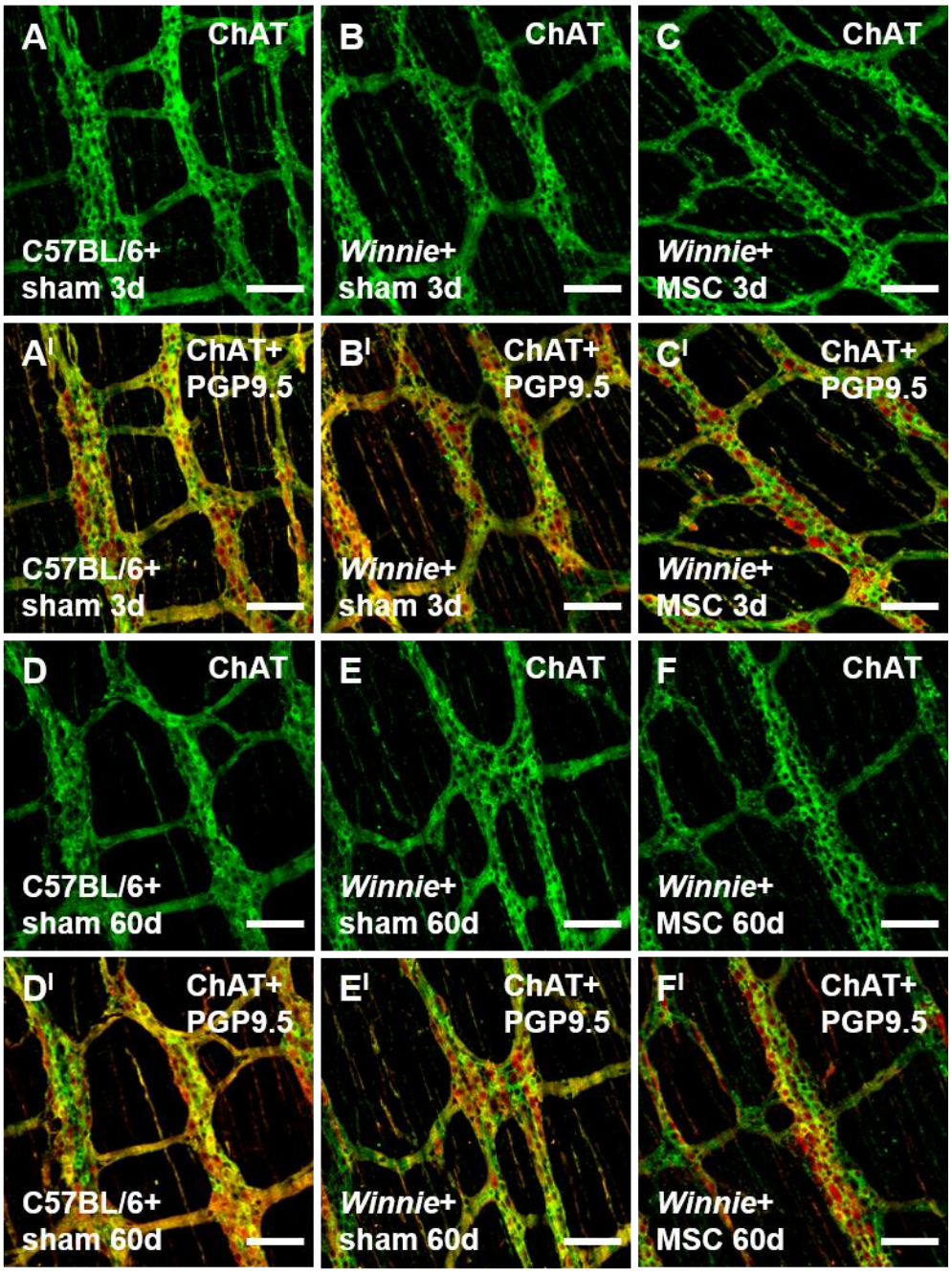
A
ChAT
C57BL/6+
sham 3d
B
ChAT
Winnie+
sham 3d
C
ChAT
Winnie+
MSC 3d
AI
ChAT+
PGP9.5
C57BL/6+
sham 3d
BI
ChAT+
PGP9.5
Winnie+
sham 3d
CI
ChAT+
PGP9.5
Winnie+
MSC 3d
D
ChAT
C57BL/6+
sham 60d
E
ChAT
Winnie+
sham 60d
F
ChAT
Winnie+
MSC 60d
DI
ChAT+
PGP9.5
C57BL/6+
sham 60d
EI
ChAT+
PGP9.5
Winnie+
sham 60d
FI
ChAT+
PGP9.5
Winnie+
MSC 60d

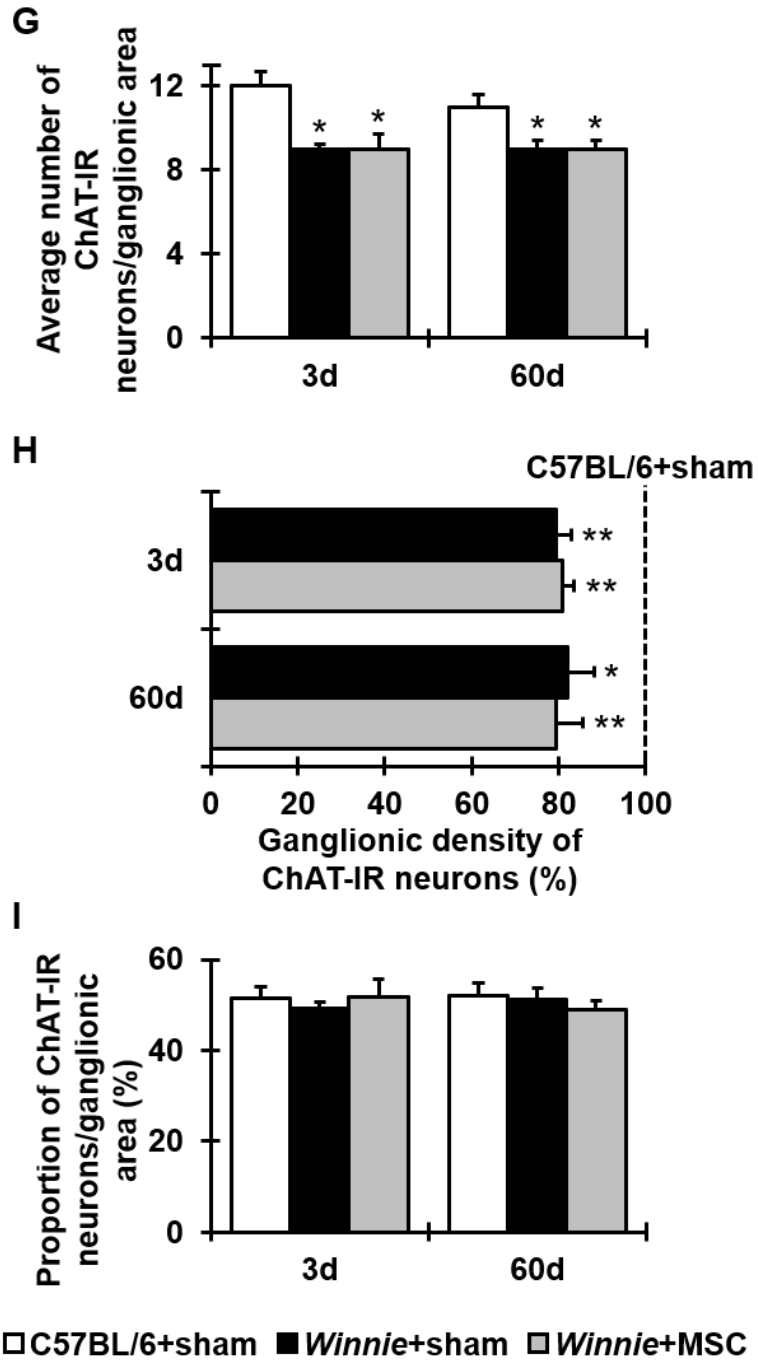
G
Average number of ChAT-IR neurons/ganglionic area
12
8
4
0
*
*
*
*
3d
60d
H
C57BL/6+sham
3d
60d
**
**
*
**
0
20
40
60
80
100
Ganglionic density of ChAT-IR neurons (%)
I
Proportion of ChAT-IR neurons/ganglionic area (%)
60
40
20
0
3d
60d
C57BL/6+sham
Winnie+sham
Winnie+MSC

6.5 Discussion

This is the first investigation of the short-term and long-term effects of MSC treatment on chronic intestinal inflammation in the *Winnie* mouse model of spontaneously occurring colitis. In this study, we found that a single dose of 1×10^6 human BM-MSCs administered by enema had no effects on symptoms of gut inflammation, levels of fecal Lcn-2, leukocyte infiltration throughout the colon wall or enteric neuropathy associated with chronic intestinal inflammation in the distal colon of *Winnie* mice at either 3 or 60 days post treatment.

Chronic intestinal inflammation in *Winnie* mice is associated with significant changes to the ENS, including impairment of cholinergic, noradrenergic and sensory innervation, myenteric neuronal loss, intestinal transit, colonic motility, smooth muscle cell responses and neuromuscular transmission (Robinson et al. 2017a; Rahman et al. 2016; 2015). Changes in histopathology, immunology and intestinal permeability, as well as alterations of the microbiota and metabolome in the *Winnie* mouse colon have also been reported (Robinson et al. 2016; Eri et al. 2011; Heazlewood et al. 2008). Collectively, these findings provide evidence that changes to the structure and function of the GI tract in *Winnie* mice are consistent with those seen in IBD patients, and that this experimental model is highly representative of the human disease. Therefore, the use of the *Winnie* mouse model within this study was highly appropriate to test the effects of MSC treatment on enteric neuropathy associated with chronic inflammation.

In preceding studies, we have shown that BM-MSCs attenuated gross morphological damage, nerve fiber injury and immune cell infiltration, as well as prevented enteric neuropathy associated with TNBS-colitis, an animal model of acute intestinal inflammation (Chapter 2 and Chapter 3). However, in this study, MSC administration had no effect on chronic intestinal inflammation and associated enteric neuropathy in the *Winnie* mouse model of spontaneously occurring colitis. Advantageous effects of MSC-based therapies have been reported in chronic disease. Nonetheless, consistent with our findings, many studies have demonstrated beneficial effects of MSC therapy in acute disease

without such positive effects in the chronic stage of the same disorder. MSCs successfully ameliorated the severity of experimental autoimmune encephalomyelitis (EAE) if administered early, but had no effect after disease reached a chronic phase (Zappia et al. 2005). In experimental models of acute kidney injury and acute liver failure, MSCs have been shown to promote functional improvements, but their effect in chronic fibrotic kidney disease and chronic liver injury models has been less effective (O'Connor et al. 2016; Kim and Cho 2013; Banas et al. 2008; Carvalho et al. 2008; Kuo et al. 2008). Other studies suggest that MSCs are less effective in chronic graft-versus-host disease (GvHD) than acute GvHD (Kuzmina et al. 2012; Lucchini et al. 2010; Weng et al. 2010; Muller et al. 2008). In addition, BM-MSC transplantation does not have any significant effect on hyperalgesia unless it is given during the first 4d after injury (Hosseini et al. 2015). Together, these results are consistent with an MSC-induced therapeutic effect occurring only during the early inflammatory phase of disease (Bernardo and Fibbe 2013; Zappia et al. 2005). Several reasons may account for inefficacy of MSC treatment in chronic diseases, including the source of cells, conditions of expansion, route of delivery, dosage and characteristics of the host (Sargent and Miller 2016).

It is unlikely that the ineffectiveness of MSC treatment in this study was due to the cell source. Human MSCs are the most utilized stem cell type in clinical trials due to their safety, regenerative capacity, and ease of isolation (Trounson and McDonald 2015). In 2006, the ISCT defined the minimal criteria to define human MSCs (Dominici et al. 2006). In this study, human MSCs were validated according to these guidelines. MSCs were originally discovered in the BM and despite only representing a minute fraction (0.001-0.01%) of the total population of BM nucleated cells (Jones and Schafer 2015b; Pittenger et al. 1999), their adherent nature enables them to be isolated and rapidly expanded *in vitro* (Choi et al. 2010; Garcia-Bosch et al. 2010; Barry and Murphy 2004). Human BM-MSCs have been investigated for therapeutic use more extensively than any other MSC subtype and are taken as a standard for the comparison of MSCs from other sources (Jones and Schafer 2015b; Ullah et al. 2015; Hass et al. 2011; Jones and McGonagle 2008; Muguruma et al. 2006). Furthermore, we have previously

demonstrated beneficial effects of human BM-MSCs from the same donors in the prevention and attenuation of acute TNBS-induced colitis (Chapter 2 and Chapter 3).

Seeding density, number of passages, basal medium, and growth supplements are all cell culture variables which may have an important impact on MSC function (De Becker and Riet 2016; Jung et al. 2012). In this study, MSCs were seeded at a low density of 60 cells/cm^2. There is mounting evidence in the literature stating that seeding MSCs at low densities (0.5-1000 cells/cm^2) results in the most rapid proliferation and the highest percentage of multipotent cells (Sotiropoulou et al. 2006; Sekiya et al. 2002; Colter et al. 2001; 2000). BM-MSCs were cultured to the fourth passage in α-MEM supplemented with FBS in this study. In early passages (<5), optimal amounts of anti-inflammatory cytokines, immunomodulators, neurotrophic factors and growth factors are released by MSCs, progressively decreasing with additional passaging (Choi et al. 2010). Previous studies have shown that α-MEM is the premium culture medium for isolation, proliferation and expansion of MSCs (Chen et al. 2009; Barlow et al. 2008; Sotiropoulou et al. 2006). Growth factors, adhesion factors, and vital nutrients essential for MSC culture are provided by media supplements, such as FBS and platelet lysate (Diez et al. 2015). Human MSCs are frequently cultured in media supplemented with FBS and subsequently, FBS-based media remains the gold standard for MSC isolation and expansion (Sotiropoulou et al. 2006; Caterson et al. 2002). In this study, we used MSC qualified FBS which is validated to successfully support the differentiation and culture of human MSCs according to ISCT guidelines. Overall, the conditions of MSC expansion employed within this study are equivalent to the culture conditions we have previously described (Robinson et al. 2017b; 2015; 2014; Stavely et al. 2015b). Hence, it is not plausible that the conditions of MSC expansion explain the inefficacy of MSC treatments within this study.

We chose to administer MSCs by enema in this study, since we have previously demonstrated beneficial effects of MSCs delivered by this route (Robinson et al. 2017b; 2015; 2014; Stavely et al. 2015a; 2015b). The most common route of

MSC administration in animal models and clinical studies is systemic intravenous (IV) injection (Nacif et al. 2015; Manieri and Stappenbeck 2011; Kurtz 2008), however MSCs administered via this route can become trapped in the lung due to their large cell size (Assis et al. 2010; Crop et al. 2010; Fischer et al. 2009; Schrepfer et al. 2007). Hence, although IV administered MSCs can home to the inflamed intestine, only a minute quantity of the transplanted MSCs are detected despite large numbers of cells injected (Moussa et al. 2017; Semont et al. 2010). Previous studies have reported a transient engraftment of IV administered MSCs into the colon peaking at 24h to 2 days post injection and undetectable after 7 days (Parekkadan et al. 2011; Gonzalez-Rey et al. 2009). Long-term engraftment of IV infused MSCs may be low due to an inability of MSCs to survive and engraft (von Bahr et al. 2012). It is considered that local injection may be more beneficial; the necessity for cell homing to the injured site is eliminated and more MSCs are available to participate in healing and repair (Manieri and Stappenbeck 2011).

In this study, MSCs engrafted into the colon wall, as identified by anti-HLA,A,B,C antibody, at 3 days post administration. However, MSCs were undetectable in the colon sections from MSC-treated *Winnie* mice at 60 days after treatment. In consistency with our results, locally administered MSCs were engrafted in the lamina propria of rats with colorectal tumors 3 days after administration and lasted at least 35 days (Katsuno et al. 2013). Other studies have reported MSCs administered locally in tissues remain present up to several weeks (Abouelkheir et al. 2016; Boulland et al. 2012; Hu et al. 2012; Nam et al. 2012), but are undetected after several months (Abouelkheir et al. 2016). These findings suggest that it is improbable that the route of delivery is the reason MSCs had no effect in this study.

A single dose of $1x10^6$ MSCs was ineffective in attenuating chronic intestinal inflammation in *Winnie* mice in this study. Consistent with our results, a single dose of MSCs did not improve functional recovery after moderate traumatic brain injury (Harting et al. 2009), impact on chronic progressive EAE (Payne et al. 2013a; Harris et al. 2012), attenuate diabetic cardiomyopathy (Calligaris and Conget 2013), restore glucose homeostasis in type 2 diabetes (Hao et al. 2013),

affect the incidence and severity of GvHD (Sudres et al. 2006), or improve the condition of osteoarthritis (Ozeki et al. 2016). On the other hand, some other studies report therapeutic effects of MSC treatment with a single dose of MSCs (Ebrahimi et al. 2013; Zhu et al. 2013; Eirin et al. 2012; Ezquer et al. 2008). Differences observed between these studies may relate to the number of MSCs administered in a single dose, given that varying doses of MSCs can exert diverse effects on healing or cytokine expression (Saether et al. 2014). In clinical trials and experimental models of disease, there are substantial disparities in the dosage of applied MSCs (Sharma et al. 2014; Li et al. 2012) indicating that the therapeutic effects of MSCs are dose-dependent (Joo et al. 2010; Kim et al. 2010a; Gonzalez-Rey et al. 2009; Li et al. 2008; Zappia et al. 2005). The microenvironment significantly influences the fate of grafted MSCs and subsequently, the outcome of cellular therapies (Liu et al. 2016a; Parekkadan and Milwid 2010). Within a few days post administration, transplanted MSCs face cell death due to anoikis and harsh environmental conditions (Robey et al. 2008). Chronic inflammation and associated oxidative stress have been shown to increase anoikis, as well as hinder the recruitment and survival of transplanted MSCs (Chang et al. 2013; Song et al. 2010; Khansari et al. 2009). Therefore, in an established chronic inflammatory environment, it may be challenging for MSCs to exert immunomodulatory functions (Nam et al. 2015; Kim and Cho 2013). The inefficacy of a single dose of $1x10^6$ MSCs in the current study may be due to an insufficient quantity of transplanted MSCs to overcome the perils of the microenvironment and attenuate the disease state.

While a single dose of MSCs has proven to be ineffective in this study, a multiple dose regimen may be efficacious against chronic inflammation in the *Winnie* mouse model of colitis. Previous studies have reported that multiple injections of MSCs improved neurological function in chronic EAE (Harris et al. 2012), effectively restored glucose homeostasis in diabetic mice (Bhansali et al. 2015; El-Tantawy and Haleem 2014; Hao et al. 2013; Ezquer et al. 2011), controlled lethal GvHD (Sudres et al. 2006), inhibited progression and attenuated synovitis in osteoarthritis (Ozeki et al. 2016), and effectively relieved liver cirrhosis (Hong et al. 2014). The possible underlying mechanism is that multiple infusions of

MSCs are necessary to maintain both the number and the efficacy of MSCs to sustain a long-term biological response and improve pathological conditions (Hong et al. 2014; Parekkadan and Milwid 2010).

6.6 Conclusion

In conclusion, we have demonstrated that a single dose of $1x10^6$ MSCs administered by enema has no effect on chronic intestinal inflammation or associated enteric neuropathy in the *Winnie* mouse model of spontaneously occurring colitis. The inefficiency of administered MSCs in this study may be due to an insufficient number of transplanted cells able to combat the microenvironment of the chronically inflamed *Winnie* mouse colon. Therefore, further studies investigating the effects of varying doses and/or multiple applications of MSCs on enteric neuropathy associated with chronic inflammation in *Winnie* mice are warranted.

CHAPTER SEVEN: MULTIPLE HIGH DOSE MESENCHYMAL STEM CELL TREATMENTS AVERT INFLAMMATION AND ENTERIC NERVE FIBER DAMAGE IN THE *WINNIE* MOUSE MODEL OF SPONTANEOUSLY OCCURRING CHRONIC COLITIS

7.1 Summary

Background: We have demonstrated the neuroprotective and anti-inflammatory effects of mesenchymal stem cell (MSC)-based therapy in acute models of colitis. Conversely, limited studies have investigated the efficacy of MSC treatment in experimental models of chronic colitis. Our studies have shown that a single dose of MSCs was ineffective in attenuating inflammation and enteric neuropathy in the *Winnie* mouse model of spontaneously occurring colitis. Multiple administrations of MSCs have been demonstrated to be more efficacious than single dose administration in various experimental models of disease. Furthermore, many studies, including our study in an acute model of colitis, have shown MSC-induced therapeutic effects to be dose-dependent. Therefore, in this study we investigated whether multiple administrations of high and low dose MSCs can attenuate inflammation and enteric neuropathy in *Winnie* mice. **Methods:** *Winnie* mice with chronic colonic inflammation received multiple administrations of high dose (HD) MSC (4×10^6 cells ×2, 2×10^6 cells ×2), low dose (LD) MSC (1×10^6 cells ×4) or sham (100µL phosphate buffered saline ×4) treatments by enema. C57BL/6 mice received multiple (×4) sham treatments. Colon tissues were collected at 3 and 60 days post treatment for histological and immunohistochemical analyses. **Results:** Multiple HD MSC treatments attenuated clinical signs of colitis, reduced fecal lipocalin-2 levels, promoted healing of the colonic architecture, decreased leukocyte infiltration throughout the colon wall, and facilitated nerve fiber regeneration in the *Winnie* mouse colon. Multiple LD MSC treatments had no effect. **Conclusion:** Multiple HD MSC treatments administered by enema ameliorated inflammation and associated enteric nerve fiber damage in *Winnie* mice. Since multiple LD MSC treatments had no effect, it can be concluded that efficacy of MSCs in *Winnie* mice is dose-dependent. Studies investigating whether multiple HD MSC treatments are effective in restoring motility, smooth muscle cell response and neurotransmission functions in the *Winnie* mouse colon are warranted.

7.2 Introduction

Most studies demonstrating therapeutic effects of MSC treatments in experimental colitis incorporate acute models of intestinal inflammation (Nikolic et al. 2018; Robinson et al. 2017b; 2015; 2014; Chao et al. 2016; Stavely et al. 2015a; 2015b; Onishi et al. 2015; Chen et al. 2013b; Liang et al. 2011; Hayashi et al. 2008; Tanaka et al. 2008). Conversely, studies investigating MSCs in chronic colitis are limited and report variable results. A single dose of MSCs suppressed inflammation and disease progression in the IL-$10^{-/-}$ mouse model of chronic colitis (Jung et al. 2015), but had no effect in attenuating colonic inflammation and associated enteric neuropathy in the *Winnie* mouse colon (Chapter 6). Another study reported that although a single dose of MSCs was ineffective, dose-dependent therapeutic effects of MSCs were evident after multiple applications in DSS-induced chronic colitis (Yu et al. 2017). Therefore, whether MSCs induce therapeutic effects in chronic models of colitis may depend on the concentration and number of MSC doses, as well as type of experimental model investigated.

There is great controversy in the literature regarding optimal dosing in MSC cell-based therapies (Florea et al. 2017; Golpanian et al. 2016; Nitkin and Bonfield 2016). Some studies, including our study in an acute model of colitis (Chapter 3), report the therapeutic efficacy of MSCs to be dose-dependent (Kim et al. 2015; Richardson et al. 2013; Joo et al. 2010; Schuleri et al. 2009), whereas other investigations describe MSCs to exert effects in a non-dose-dependent manner (Lee et al. 2017; Saether et al. 2014; Hashemi et al. 2008). Furthermore, there are inconsistencies in the definitions of “low” versus “high dose” between studies. Defining an optimal MSC dose has numerous advantages for both pre-clinical and clinical studies including a lower economic burden, smaller quantities of MSCs required for expansion, and a reduced likelihood of MSC mutation (Lee et al. 2017; Robinson et al. 2017b).

The rationale for using multiple MSC doses for greater therapeutic effect has been supported in the literature (Ayache and Chalah 2016). Multiple

administrations of MSCs have been demonstrated to be more effective than a single administration of MSCs in improving left ventricular cardiac function in experimental models of myocardial infarction (Guo et al. 2017; Reich et al. 2016; Tokita et al. 2016), recovering neurological function in experimental autoimmune encephalomyelitis (Harris et al. 2012), enhancing motor performance and preventing motor neuron loss in experimental amyotrophic lateral sclerosis (Zhang et al. 2009a), restoring glucose homeostasis in diabetic mice (Li et al. 2016b; Aali et al. 2014; Hao et al. 2013), and improving fertility after endometrial injury (Zhang et al. 2018). Why multiple MSC dosing, but not a single dose, produces therapeutic effects in certain disease models is unclear. However, it is hypothesized that multiple doses of MSCs may yield cumulative beneficial effects and be crucial for the sustained production of immunomodulatory and trophic factors necessary to exceed a therapeutic threshold (Tokita et al. 2016; Harris et al. 2012; Zhang et al. 2009a). It has also been suggested that the initial MSC application prepares an appropriate environment in which survival, docking and homing of incoming MSCs is facilitated (Aali et al. 2014). Thus, repeated doses of MSCs may provide therapeutic superiority in amelioration of disease.

Since *Winnie* mice have been demonstrated to be highly representative of human inflammatory bowel disease (IBD) (Robinson et al. 2017a; 2016; Rahman et al. 2016; Eri et al. 2011; Heazlewood et al. 2008), they are appropriate to test the therapeutic efficacy of cellular therapies. It has been concluded previously that a single dose of $1x10^6$ MSCs is ineffective in attenuating colitis in *Winnie* mice. No studies have examined the effect of multiple MSC applications in *Winnie* mice or whether the efficacy of MSCs in this experimental model are dose-dependent. Therefore, the aim of this study was to investigate whether multiple LD and HD MSC treatments administered by enema are effective in attenuating inflammation and enteric neuropathy in the *Winnie* mouse colon.

7.3 Materials and methods

7.3.1 Animals

Winnie (12wk old; 19-29g; *n*=30) and C57BL/6 (12wk old; 25-30g; *n*=10) were obtained from Monash Animal Services (MAS, Melbourne, Australia). All animals were housed in a temperature-controlled environment with 12h day/night cycles and had *ad libitum* access to food and water. All procedures performed within this study were approved by the Victoria University Animal Experimentation Ethics Committee and were conducted according to the guidelines of the Australian National Health and Medical Research Council.

7.3.2 MSC culture, passaging and characterization

Cell culture and passaging were carried out as described in Chapter 2, section 2.3.2. Briefly, pre-established cell lines of human BM-MSCs (Tulane University, New Orleans, LA, USA) were plated at an initial density of 60 cells/cm^2 and incubated in expansion medium (α-minimum essential medium (MEM) supplemented with 16.5% MSC-qualified fetal bovine serum (FBS), 100 U/mL penicillin/streptomycin, and 100X GlutaMAX) (Gibco®, Life Technologies, Mulgrave, VIC, Australia) at 37°C. Expansion medium was replaced every 48-72h for 10-14 days until the cells were 70-85% confluent (maximum). MSCs were cultured to the fourth passage for all experiments, after which they were trypsinized and collected for *in vivo* treatment of *Winnie* mice. MSCs were characterized for their expression of surface antigens, differentiation potential, and colony-forming ability as described in Chapter 2, section 2.3.3. All MSCs utilized in this study met the International Society for Cellular Therapy's (ISCT) criteria for defining *in vitro* human MSC cultures (Dominici et al. 2006).

7.3.3 MSC treatments

MSC or sham treatments were administered by enema into the colon via a lubricated silicone catheter twice weekly for two consecutive weeks (Table 7.1). MSCs were suspended in 100μL of sterile phosphate buffered solution (PBS) for

application. All mice were anaesthetized with isoflurane (induced at 3%, maintained on 1-3% isoflurane in O_2) during the treatment procedures. At 3 or 60 days after the conclusion of the treatment regime, mice were culled via cervical dislocation and colon tissues were collected for histology and immunohistochemistry experiments.

Table 7.1 Treatment schedule for *Winnie* and C57BL/6 mice

Group	Week 1		Week 2	
	Treatment #1	***Treatment #2***	***Treatment #3***	***Treatment #4***
C57BL/6+sham	100µL PBS	100µL PBS	100µL PBS	100µL PBS
Winnie+sham	100µL PBS	100µL PBS	100µL PBS	100µL PBS
Winnie+LD MSC	1×10^6 MSCs	1×10^6 MSCs	1×10^6 MSCs	1×10^6 MSCs
Winnie+HD MSC	4×10^6 MSCs	4×10^6 MSCs	2×10^6 MSCs	2×10^6 MSCs

7.3.4 Analysis of fecal water content and colon length

Fecal water content and colon length was calculated as described in Chapter 4, section 4.3.2. Briefly, stools from all C57BL/6+sham, *Winnie*+sham, and *Winnie*+MSC-treated mice were immediately weighed after collection to ascertain the wet weight. Stools were re-weighed 3 days later to establish the dry weight and the difference between wet and dry weight was calculated. Colon length was determined by measuring the colon from cecum to anus immediately after dissection.

7.3.5 Assessment of fecal lipocalin-2 levels

Fecal lipocalin (Lcn)-2 levels were determined as described in Chapter 4, section 4.3.3 (Chassaing et al. 2012). Briefly, fecal samples were collected from *Winnie* and C57BL/6 mice immediately prior to treatment and twice weekly over 60 days following treatment. Samples were then reconstituted and vortexed to form a homogenous fecal suspension. Lcn-2 levels were measured using Duoset murine

Lcn-2 ELISA kit (R&D Systems, Minneapolis, MN, USA) as per manufacturer's instructions.

7.3.6 Immunohistochemistry and histology

Immunohistochemistry and histology were performed as described in Chapter 4, section 4.3.4.

7.3.6.1 Tissue preparation

Segments of the distal colon were processed for wholemount longitudinal muscle-myenteric plexus (LMMP) preparations and cross sections. After dissection from the animal, colon tissues were cut open along the mesenteric border, pinned flat with the mucosal side up and fixed overnight with Zamboni's fixative (2% formaldehyde containing 0.2% picric acid; LMMP and cryostat cross sections) or 10% buffered formalin (histology cross sections) at 4°C. For LMMP preparations, the myenteric plexus was exposed by removing the mucosa, submucosa and circular muscle layers via fine dissection. For cryostat cross sections, tissues were frozen in liquid nitrogen-cooled isopentane and optimal cutting temperature (OCT; Tissue-Tek, Torrance, CA, USA) compound, then stored at -80°C until they were cryo-sectioned (20µm) onto glass slides for immunohistochemistry. Tissues for histology cross sections were stored in 70% ethanol until embedding.

7.3.6.2 Immunohistochemistry

Immunohistochemistry was performed on LMMP and cross sections of the distal colon. Briefly, colon tissues were incubated with 10% normal donkey serum (NDS; Merck Millipore, Bayswater, VIC, Australia) for 1h, primary antibodies (Table 7.2) for 24h, and secondary antibodies (Table 7.3) for 2h, all at room temperature prior to mounting with fluorescent mounting medium (DAKO, North Sydney, NSW, Australia).

Table 7.2 Primary antibodies used in this study

Antibody	Host species	Dilution	Supplier	Application in this study
Anti-β-Tubulin class III	Rabbit	1:1000	Abcam, Melbourne, VIC, Australia	Cross sections
Anti-calcitonin gene-related peptide (CGRP)	Rabbit	1:3000	Sigma-Aldrich, Castle Hill, NSW, Australia	LMMP preparations
Anti-CD45	Rat	1:500	BioLegend, San Diego, CA, USA	Cross sections
Anti-choline acetyltransferase (ChAT)	Goat	1:500	Merck Millipore	LMMP preparations
Anti-human leukocyte antigen (HLA)-A,B,C (conjugated to fluorescein isothiocyanate (FITC))	Human	1:50	BioLegend	Cross sections
Anti-neuronal nitric oxide synthase (nNOS)	Goat	1:500	Novus Biologicals, Littleton, CO, USA	LMMP preparations
Anti-protein gene product (PGP)-9.5	Rabbit	1:500	Abcam	LMMP preparations
Anti-tyrosine hydroxylase (TH)	Sheep	1:1000	Merck Millipore	LMMP preparations
Anti-vesicular acetylcholine transporter (VAChT)	Goat	1:500	Merck Millipore	LMMP preparations

Table 7.3 Secondary antibodies used in this study

Antibody	Host species	Dilution	Supplier	Application in this study
Alexa Fluor 488	Donkey anti-rabbit	1:200	Jackson Immunoresearch Laboratories, PA, USA	LMMP preparations
Alexa Fluor 488	Donkey anti-rat	1:200	Jackson Immunoresearch Laboratories	Cross sections
Alexa Fluor 488	Donkey anti-sheep	1:200	Jackson Immunoresearch Laboratories	LMMP preparations
Alexa Fluor 594	Donkey anti-rabbit	1:200	Jackson Immunoresearch Laboratories	Cross sections and LMMP preparations
Alexa Fluor 647	Donkey anti-goat	1:200	Jackson Immunoresearch Laboratories	LMMP preparations
Alexa Fluor 647	Donkey anti-rabbit	1:200	Jackson Immunoresearch Laboratories	LMMP preparations
FITC 488	Donkey anti-goat	1:200	Jackson Immunoresearch Laboratories	LMMP preparations

7.3.6.3 Histology

For histology cross sections, tissues were paraffin embedded, sectioned by microtome (5µm), deparaffinized, cleared, and rehydrated in graded ethanol concentrations for hematoxylin and eosin (H&E) and Alcian blue staining.

7.3.7 Imaging

Immunolabeled LMMP preparations and cross sections of the distal colon were visualized and imaged with a Nikon Eclipse Ti multichannel confocal laser scanning system (Nikon, Tokyo, Japan) as described in Chapter 6, section 6.3.7. An Olympus BX53 microscope (Olympus, Notting Hill, VIC, Australia) was used to visualize H&E-stained colon sections. Images were captured with CellSense™ software.

7.3.8 Quantitative analysis of immunohistochemical and histological data

Image analysis was conducted as described in Chapter 4, section 4.3.6. Briefly, all images were analyzed blindly using Image J software (National Institute of Health, Bethesda, MD, USA). In cross sections of the distal colon, β-Tubulin (III)-immunoreactive (IR) fiber and CD45-IR cell density was measured per area (average of eight areas of 500µm^2 per animal). Sensory (CGRP-IR), noradrenergic (TH-IR), and cholinergic (VAChT-IR) nerve fibers in the myenteric plexus were measured from eight randomly captured images per LMMP preparation (total area 2mm^2), as well as per ganglion (all ganglia within measured area). The area of immunoreactivity was expressed as a percentage of the total area examined. The number and density of PGP9.5-IR, nNOS-IR, and ChAT-IR myenteric neurons per ganglionic area was measured in wholemount LMMP preparations (all ganglia within a 2mm^2 total area). Neuronal numbers were normalized to a 0.1mm^2 area of ganglia for direct comparison between groups. Histological scores encompassed aberrant crypt architecture (score range 0-3), increased crypt length (0-3), goblet cell depletion (0-3), crypt

abscesses (0-3), leukocyte infiltration (0-3), and epithelial damage and ulceration (0-3) (average of eight areas of 500μm^2 per animal).

7.3.9 Statistical analysis

Prism v7.0 (Graphpad Software Inc., La Jolla, CA, USA) was used to conduct statistical analyses. Data were considered statistically significant when $P<0.05$. Data were presented as mean±standard error of the mean (SEM), if not specified otherwise.

7.4 Results

7.4.1 MSCs engraft at the site of colonic inflammation at 3 days post treatment

MSCs were identified in sections of the distal colon from *Winnie*+MSC-treated mice with anti-HLA-A,B,C antibody which detects MHC-I antigens present on all human nucleated cells (*n*=5/group; Fig. 7.1). At 3 days post treatment, engraftment of MSCs at the site of colonic tissue damage and inflammation was evident by the presence of HLA-A,B,C-IR cells in sections from all MSC-treated *Winnie* mice (Fig. 7.1A-B). MSC engraftment within the colon wall was observed to be more extensive in sections from HD MSC-treated *Winnie* mice than in sections from LD MSC-treated *Winnie* mice at this time point. HLA-A,B,C-IR cells were absent in sections from both LD and HD MSC-treated *Winnie* mice at 60 days post treatment, indicating that no MSCs engrafted within the colonic layers of *Winnie* mice at this time point (Fig. 7.1A^{I}-B^{I}).

Figure 7.1. Engraftment of MSCs within the colon. Engraftment of human MSCs at the site of colonic inflammation in *Winnie* mice was ascertained using anti-HLA-A,B,C antibody specific to human MHC class I. HLA-A,B,C-IR cells were localized in colon sections from LD and HD MSC-treated *Winnie* mice at 3 days **(A-B;** arrows**)**, but not 60 days **(A^{I}-B^{I})** post treatment. d = days. Scale bars = 50μm.

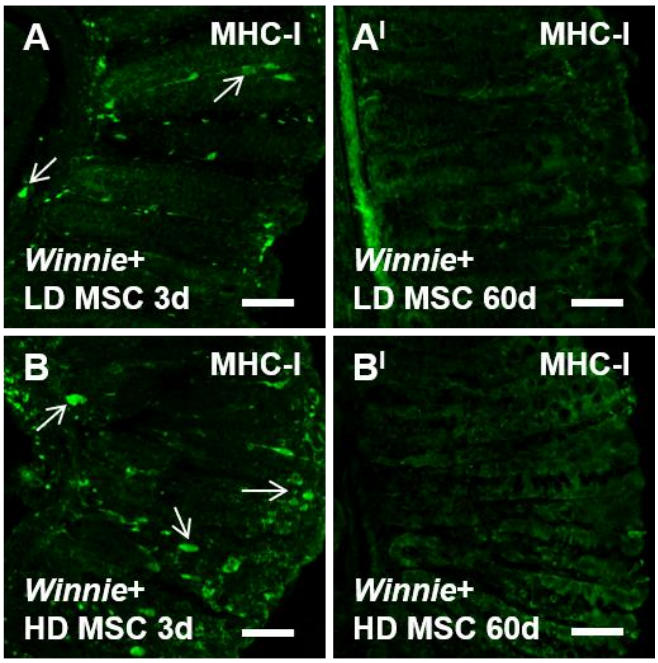
A
MHC-I
Winnie+
LD MSC 3d
A'
MHC-I
Winnie+
LD MSC 60d
B
MHC-I
Winnie+
HD MSC 3d
B'
MHC-I
Winnie+
HD MSC 60d

7.4.2 Multiple HD MSC treatments alleviate colonic inflammation in *Winnie* mice

C57BL/6 mice did not show any signs of intestinal inflammation or any other symptoms before or at 3 and 60 days post sham treatment (*n*=5/group; Table 7.4). Accordingly, the formation of pellets with firm consistency was repeatedly observed in fecal samples collected from control mice during this study (Fig. 7.2A-A^{I}, E-E^{I}). Before treatment, all *Winnie* mice used in this study presented with symptoms of intestinal inflammation, including perianal bleeding, soiled fur, diarrhea and soft fecal consistency, not forming pellets, (*n*=5/group; Table 7.4; Fig. 7.2B-D, F-H). When compared to C57BL/6 mice, *Winnie* mice had a higher fecal water content and lower body weight prior to treatment (*P*<0.001 for all; Table 7.4; Fig. 7.3A-B). *Winnie* mice in the sham treatment groups continued to display signs of intestinal inflammation at both 3 and 60 days post treatment with higher fecal water content, reduced body weight, and lack of pellet formation when compared to C57BL/6+sham-treated mice (*P*<0.001 for all; Table 7.4; 7.2B^{I}, F^{I}; Fig. 7.3A-B). Repeated application of LD MSCs did not affect stool consistency or alleviate signs of intestinal inflammation in *Winnie* mice at either time point (Fig. 7.2C^{I}, G^{I}). Subsequently, fecal water content was higher and body weight was lower in LD MSC-treated *Winnie* mice when compared to C57BL/6+sham-treated mice post treatment (*P*<0.001 for all; Table 7.4; Fig. 7.3A-B). MSCs administered at a HD alleviated diarrhea, perianal bleeding and soiled fur in *Winnie* mice at 3 days post treatment. Furthermore, fecal samples collected from HD MSC-treated mice demonstrated pellet formation with firm consistency (Fig. 7.2D^{I}). At 3 days post treatment, the body weight and fecal water content of HD MSC-treated *Winnie* mice was comparable to C57BL/6+sham-treated mice and significantly different to sham-treated (fecal water content: *P*<0.001; body weight: *P*<0.01) and LD MSC-treated (fecal water content: *P*<0.001; body weight: *P*<0.05) *Winnie* mice (Table 7.4; Fig. 7.3A-B). The effects of HD MSC treatment were maintained for 60 days (fecal water content - *Winnie*+sham: *P*<0.001; *Winnie*+LD MSC: *P*<0.01; body weight - *Winnie*+sham: *P*<0.05; *Winnie*+LD MSC: *P*<0.05; Table 7.4; Fig. 7.2H^{I}; Fig. 7.3 A-B). Colons from sham-treated and LD MSC-treated *Winnie* mice were longer

than the colons from C57BL/6+sham-treated mice at 3 and 60 days post treatment (*n*=5/group; *P*<0.001 for all; Fig. 7.3C). However, at both time points, colon length of HD MSC-treated *Winnie* mice was comparable to C57BL/6+sham-treated mice and less than sham-treated (3 days: *P*<0.05; 60 days: *P*<0.001) and LD MSC-treated (3 days: *P*<0.05; 60 days: *P*<0.001) *Winnie* mice (*n*=5/group; Fig. 7.3C).

Fecal Lcn-2 was quantified by ELISA to verify intestinal inflammation in *Winnie* mice pre-treatment, as well as to assess the effects of MSC treatment in attenuating colonic inflammation 3 and 60 days post treatment (Fig. 7.4). Fecal samples from C57BL/6+sham-treated mice revealed minimal levels of Lcn-2 before treatment (0.8±0.1pg/mL) continuing at 3 (0.8±0.1pg/mL) and 60 days (0.8±0.02pg/mL) post treatment, confirming a lack of colonic inflammation. (*n*=5; Fig. 7.4A). Before treatment, levels of Lcn-2 were higher in samples from *Winnie* mice in all groups (*Winnie*+sham: 4.1±0.4pg/mL; *Winnie*+LD MSC: 4.3±0.3pg/mL; *Winnie*+HD MSC: 4.7±0.1pg/mL) when compared to C57BL/6 mice, indicating the presence of colonic inflammation (*n*=5/group; *P*<0.001 for all; Fig. 7.4A). In fecal samples from *Winnie*+sham-treated (3 days: 4.3±0.3pg/mL; 60 days: 4.2±0.2pg/mL) and *Winnie*+LD MSC-treated (3 days: 4.1±0.1pg/mL; 60 days: 4.4±0.1pg/mL) mice, levels of Lcn-2 were significantly higher than in samples from C57BL/6+sham-treated mice at 3 and 60 days post treatment (*P*<0.001 for all; Fig. 7.4A). At 3 days post treatment, Lcn-2 levels were reduced in samples from *Winnie*+HD MSC-treated mice, comparable to C57BL/6+sham-treated mice and significantly less than in samples from *Winnie*+sham and *Winnie*+LD MSC-treated mice at this time point (1.2±0.1pg/mL; *P*<0.001 for both; Fig. 7.4A). At 60 days post treatment, the quantity of fecal Lcn-2 in samples from HD MSC-treated *Winnie* mice was consistently lower than in samples *Winnie*+sham and *Winnie*+LD MSC-treated mice (1.6±0.1pg/mL; *P*<0.001 for both; Fig. 7.4A). Although administration of HD MSCs had long lasting effects in attenuating colonic inflammation, Lcn-2 levels in fecal samples from HD MSC-treated *Winnie* mice were higher than in samples from C57BL/6+sham-treated mice at 60 days post treatment (*P*<0.05). In addition, fecal Lcn-2 values were measured twice weekly over the 60 day experimental period to assess any

variation in levels of colonic inflammation ([see Appendix C, Table S3]; Fig. 7.4B). At all time points measured, Lcn-2 values in samples from *Winnie*+sham and *Winnie*+LD MSC-treated mice were consistently higher than in samples from C57BL/6+sham-treated and *Winnie*+HD MSC-treated mice (P<0.001 for all; Fig. 7.4B). A gradual increase in fecal Lcn-2 levels is depicted in HD MSC-treated *Winnie* mice from 21d post treatment, however for the majority of the experimental period, Lcn-2 values were comparable to control mice (Fig. 7.4B).

The effects of multiple LD and HD MSC treatments on inflammation-induced damage to the colonic architecture was assessed in H&E and Alcian blue-stained sections of the distal colon at 3 and 60 days post treatment (Fig. 7.5). At both time points, sections from C57BL/6+sham-treated mice revealed orderly arrangement of the colonic layers, crypts and glands, plentiful mucin secreting cells, and continuous epithelial lining (n=5/group; Fig. 7.5A-A^{I}, E-E^{I}). Subsequently, histological scores for colon sections from control mice were minimal (Table 7.4). On the other hand, sections from *Winnie*+sham-treated mice showed elongation of crypts with increased immune cell infiltrate, damage to the mucosa and epithelial lining, and goblet cell loss at 3 and 60 days post treatment (n=5/group; Fig. 7.5B-B^{I}, F-F^{I}). Histological scores for colon sections from sham-treated *Winnie* mice were significantly higher than C57BL/6+sham-treated mice at both time points (P<0.001 for all; Table 7.4). Inflammation induced damage to the gross morphology of the colon was not alleviated by multiple LD MSC treatments reflected by histological scores comparable to sections from *Winnie*+sham-treated mice and significantly higher than sections from control mice (P<0.001 for all; Table 7.4; Fig. 7.5C-C^{I}, G-G^{I}). At 3 days post treatment, sections from HD MSC-treated mice revealed healing of the mucosa, epithelial lining and overall colonic architecture, as well as reduced immune infiltrate and restoration of mucin secreting goblet cells (Fig. 7.5D-D^{I}). Furthermore, the attenuation of gross morphological damage to the colon was maintained for 60 days in sections from HD MSC-treated *Winnie* mice (Fig. 7.5H-H^{I}). The histological scores of colon sections from *Winnie*+HD MSC-treated mice were comparable to sections from C57BL/6+sham-treated mice and less than sections

from *Winnie*+sham-treated and *Winnie*+LD MSC-treated mice at both 3 and 60 days post treatment (P<0.001 for all; Table 7.4).

Anti-CD45 antibody, a pan leukocyte marker, was used to measure the degree of inflammation throughout the colon wall in cross sections from C57BL/6 and *Winnie* mice at 3 and 60 days post treatment (n=5/group; Fig. 7.6A-D^{I}). Few leukocytes were observed in sections from C57BL/6+sham-treated mice at both time points (Fig. 7.6A-A^{I}). These observations were verified by analysis of CD45-IR cell density, confirming a lack of inflammation in the colons from C57BL/6+sham-treated mice (Table 7.4; Fig. 7.6E-G). Conversely, copious amounts of leukocytes were evident in sections from *Winnie*+sham-treated mice at 3 and 60 days post treatment, indicating active inflammation within the colon (Fig. 7.6B-B^{I}). Quantification confirmed significantly higher densities of CD45-IR cells throughout the colon wall, as well as when isolated to the mucosal and muscle layers, in tissues from sham-treated *Winnie* mice when compared to sections from C57BL/6+sham-treated mice (P<0.001 for all; Table 7.4; Fig. 7.6E-G). Multiple LD MSC treatments did not affect the number of leukocytes within the colonic layers at either 3 or 60 days post treatment (Fig. 7.6C-C^{I}). Quantification revealed the density of CD45-IR cells in sections from *Winnie*+LD MSC-treated mice to be comparable to sections from *Winnie*+sham-treated mice and higher than in sections from C57BL/6+sham-treated mice (P<0.001 for all; Table 7.4; Fig. 7.6E-G). Diminished levels of leukocytes were observed in sections from HD MSC-treated *Winnie* mice (Fig. 7.6D-D^{I}). Analysis of CD45-IR cell density in colon sections from *Winnie*+HD MSC-treated mice revealed comparable results to sections from C57BL/6+sham-treated mice post treatment. Although the density of CD45-IR cells had risen slightly in sections from *Winnie*+HD MSC-treated mice at 60 days when compared to values calculated at 3 days, there was no statistical difference between time points. Furthermore, quantification confirmed less leukocyte infiltration in the colon sections from *Winnie*+HD MSC-treated mice when compared to *Winnie*+sham-treated (3 days - P<0.001 for all; 60 days - area: P<0.001; mucosa: P<0.001; muscle: P<0.05) and *Winnie*+LD MSC-treated mice (3 days - area: P<0.001; mucosa: P<0.001;

muscle: $P<0.05$; 60 days - area: $P<0.01$; mucosa: $P<0.001$; muscle: $P<0.05$; Table 7.4; Fig. 7.6E-G).

Table 7.4 Evaluation of intestinal inflammation

	C57BL/6+sham			*Winnie*+sham			*Winnie*+LD MSC			*Winnie*+HD MSC		
Parameter	**BT**	**3d**	**60d**	**BT**	**3d**	**60d**	**BT**	**3d**	**60d**	**BT**	**3d**	**60d**
Symptoms												
Diarrhea	A	A	A	P	P	P	P	P	P	P	A	A
Body weight (g)	27.6± 0.3	28.2± 1.1	28.9± 0.6	22.8± 0.6 ***	23.3± 0.6 ***^^	24.2± 0.4 ***^	23.7± 0.7 ***	23.9± 0.6 ***^	24.5± 0.4 ***^	23.9± 0.4 ***	26.5± 0.8 #	26.9± 0.3 ##
Fecal water content (g)	0.15± 0.01	0.15± 0.01	0.14± 0.01	0.24± 0.01 ***	0.25± 0.01 ***^^^	0.25± 0.01 ***^^^	0.23± 0.01 ***	0.24± 0.01 ***^^^	0.24± 0.02 ***^^	0.24± 0.01 ***	0.16± 0.01 ###	0.18± 0.01 ##
Colon length (cm)	-	6.4± 0.2	6.4± 0.1	-	7.9± 0.1 ***^	8.1± 0.2 ***^	-	7.9± 0.2 ***^^^	8.0± 0.3 ***^^^	-	7.0± 0.2	6.8± 0.2
Leukocyte infiltration												
Density of CD45-IR cells in colon cross sections (%)	-	5.3± 0.2	5.6± 0.4	-	9.4± 0.4 ***^^^	9.5± 0.5 ***^^^	-	8.8± 0.5 ***^^^	9.0± 0.4 ***^^^	-	5.9± 0.1	7.0± 0.2
Density of CD45-IR cells in the mucosa (%)	-	7.1± 0.3	6.7± 0.4	-	10.7± 0.5 ***^^^	10.9± 0.4 ***^^^	-	10.6± 0.3 ***^^^	11.1± 0.5 ***^^^	-	7.0± 0.3	8.1± 0.3

Table 7.4 Evaluation of intestinal inflammation (continued)

	C57BL/6+sham			*Winnie*+sham			*Winnie*+LD MSC			*Winnie*+HD MSC		
Parameter	**BT**	**3d**	**60d**	**BT**	**3d**	**60d**	**BT**	**3d**	**60d**	**BT**	**3d**	**60d**
Density of CD45-IR cells in the muscle (%)	-	2.3± 0.1	2.6± 0.1	-	4.9± 0.4 ***^^^	4.8± 0.1 ***^	-	4.0± 0.3 ***^	4.8± 0.5 ***^	-	2.9± 0.1	3.5± 0.3
Histological scoring												
Aberrant crypt architecture (0-3)	-	0.6± 0.2	0.2± 0.2	-	2.4± 0.2 ***^^^	2.4± 0.4 ***^^^	-	2.4± 0.2 ***^^^	2.2± 0.5 ***^^^	-	0.6± 0.2	0.4± 0.2
Increased crypt length (0-3)	-	0.4± 0.2	0.2± 0.2	-	2.6± 0.2 ***^^^	2.8± 0.2 ***^^^	-	2.8± 0.2 ***^^^	2.6± 0.4 ***^^^	-	0.6± 0.2	1.0± 0.3
Goblet cell depletion (0-3)	-	0.6± 0.2	0.6± 0.2	-	2.2± 0.2 **^^	2.2± 0.4 **^^	-	2.2± 0.4 **^^	2.0± 0.3 **^	-	0.6± 0.2	0.8± 0.2
General leukocyte infiltration (0-3)	-	0.6± 0.2	0.8± 0.2	-	2.4± 0.2 ***^^	2.4± 0.4 ***^^^	-	2.6± 0.2 ***^^^	2.6± 0.2 ***^^^	-	1.2± 0.2	1.0± 0.0
Crypt abscesses (0-3)	-	0.6± 0.2	0.6± 0.2	-	2.4± 0.2 ***^^	2.8± 0.2 ***^^^	-	2.4± 0.2 ***^^^	2.4± 0.2 ***^^^	-	0.4± 0.2	0.4± 0.2

Table 7.4 Evaluation of intestinal inflammation (continued)

	C57BL/6+sham			*Winnie*+sham			*Winnie*+LD MSC			*Winnie*+HD MSC		
Parameter	**BT**	**3d**	**60d**	**BT**	**3d**	**60d**	**BT**	**3d**	**60d**	**BT**	**3d**	**60d**
Epithelial damage and ulceration (0-3)	-	0.8± 0.2	0.8± 0.2	-	2.4± 0.2 **^^	2.6± 0.4 ***^^^	-	2.4± 0.4 **^^	2.4± 0.4 **^^^	-	0.8± 0.2	0.6± 0.2
Overall histological score (out of 18)	-	3.6± 0.7	3.2± 0.6	-	14.4± 0.8 ***^^^	15.2± 1.1 ***^^^	-	14.8± 1.2 ***^^^	14.2± 1.4 ^^^***	-	4.2± 0.7	4.2± 0.4

BT = before treatment, d = days, A = absent, P = prominent. **P*<0.05, ***P*<0.01, ****P*<0.001 when compared to C57BL/6+sham-treated mice. ^*P*<0.05, ^^*P*<0.01, ^^^*P*<0.001 when compared to *Winnie*+HD MSC-treated mice. $^{\#}P$<0.05, $^{\#\#}P$<0.01, $^{\#\#\#}P$<0.001 when compared to *Winnie*+HD MSC-treated mice BT.

Figure 7.2. Effects of multiple LD and HD MSC treatments on pellet formation. Fecal samples were collected from C57BL/6+sham, *Winnie*+sham, *Winnie*+LD MSC, and *Winnie*+HD MSC-treated mice before treatment **(A-H)**, as well as 3 **(A^{I}-D^{I})** and 60 days **(E^{I}-H^{I})** post treatment. d = days.


Pre treatment
Post treatment
Pre treatment
Post treatment
A
3d
C57BL/6
B
3d
Winnie
C
3d
Winnie
D
3d
Winnie
A'
3d
C57BL/6+sham
B'
3d
Winnie+sham
C'
3d
Winnie+LD MSC
D'
3d
Winnie+HD MSC
E
60d
C57BL/6
F
60d
Winnie
G
60d
Winnie
H
60d
Winnie
E'
60d
C57BL/6+sham
F'
60d
Winnie+sham
G'
60d
Winnie+LD MSC
H'
60d
Winnie+HD MSC

Figure 7.3. Effects of multiple LD and HD MSC treatments on fecal water content, body weight and colon length. Water content (wet weight minus dry weight) of stools **(A)**, body weight **(B)**, and colon length **(C)** of C57BL/6+sham, *Winnie*+sham, *Winnie*+LD MSC, and *Winnie*+HD MSC-treated mice before treatment, as well as 3 and 60 days post treatment. d = days. ***P<0.001 when compared to C57BL/6+sham-treated mice. ^P<0.05, ^^P<0.01, ^^^P<0.001 when compared to *Winnie*+HD MSC-treated mice. $^{\#}P$<0.05, $^{\#\#}P$<0.01, $^{\#\#\#}P$<0.001 when compared to *Winnie*+HD MSC-treated mice BT.

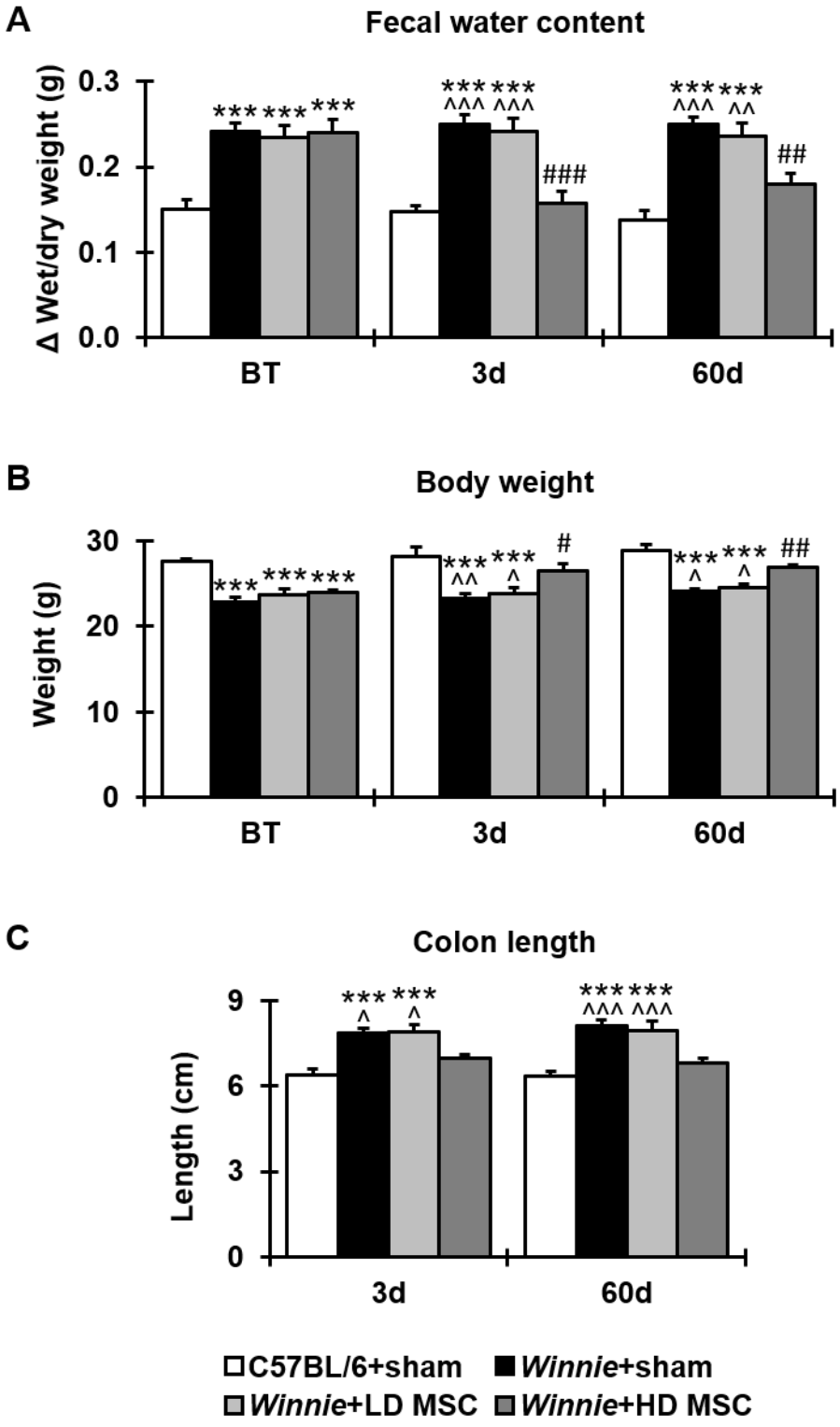
A
Fecal water content
Δ Wet/dry weight (g)
0.3
0.2
0.1
0.0
BT
3d
60d
B
Body weight
Weight (g)
30
20
10
0
C
Colon length
Length (cm)
9
6
3
0
C57BL/6+sham
Winnie+sham
Winnie+LD MSC
Winnie+HD MSC

Figure 7.4. Effects of multiple LD and HD MSC treatments on fecal lipocalin (Lcn)-2. Average Lcn-2 levels quantified in fecal samples from C57BL/6+sham, *Winnie*+sham, *Winnie*+LD MSC and *Winnie*+HD MSC-treated mice before treatment (BT), as well as 3 and 60 days post treatment **(A)**. Fecal samples were collected twice weekly for 60 days to assess any changes in the level of intestinal inflammation during the experimental period **(B)**. d = days. **P*<0.05, ***P*<0.01, ****P*<0.001 when compared to C57BL/6+sham-treated mice. ^^^*P*<0.001 when compared to *Winnie*+HD MSC-treated mice.

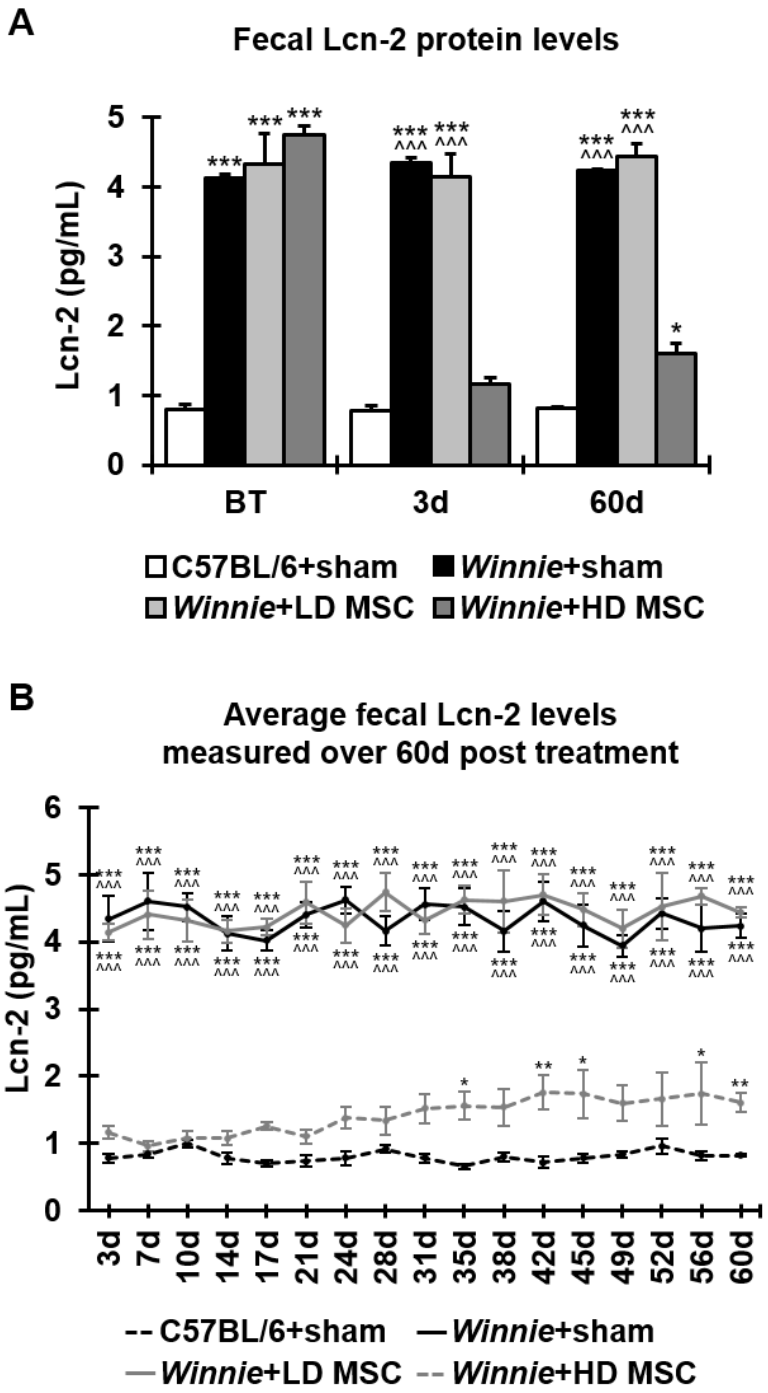
A
Fecal Lcn-2 protein levels
Lcn-2 (pg/mL)
0
1
2
3
4
5
BT
3d
60d
C57BL/6+sham
Winnie+sham
Winnie+LD MSC
Winnie+HD MSC
B
Average fecal Lcn-2 levels
measured over 60d post treatment
Lcn-2 (pg/mL)
0
1
2
3
4
5
6
3d
7d
10d
14d
17d
21d
24d
28d
31d
35d
38d
42d
45d
49d
52d
56d
60d
C57BL/6+sham
Winnie+sham
Winnie+LD MSC
Winnie+HD MSC

Figure 7.5. Effects of multiple LD and HD MSC treatments on inflammation-induced changes to the colonic architecture. Cross sections of the distal colon from C57BL/6+sham, *Winnie*+sham, *Winnie*+LD MSC and *Winnie*+HD MSC-treated mice were stained with hematoxylin and eosin (H&E) **(A-D^{I})** and Alcian blue **(E-H^{I})** to assess the effects of MSC treatments on changes to the colonic architecture and mucin expressing cells induced by chronic inflammation. d = days. Scale bars = 50μm (A-D^{I}), 20μm (E-H^{I}).

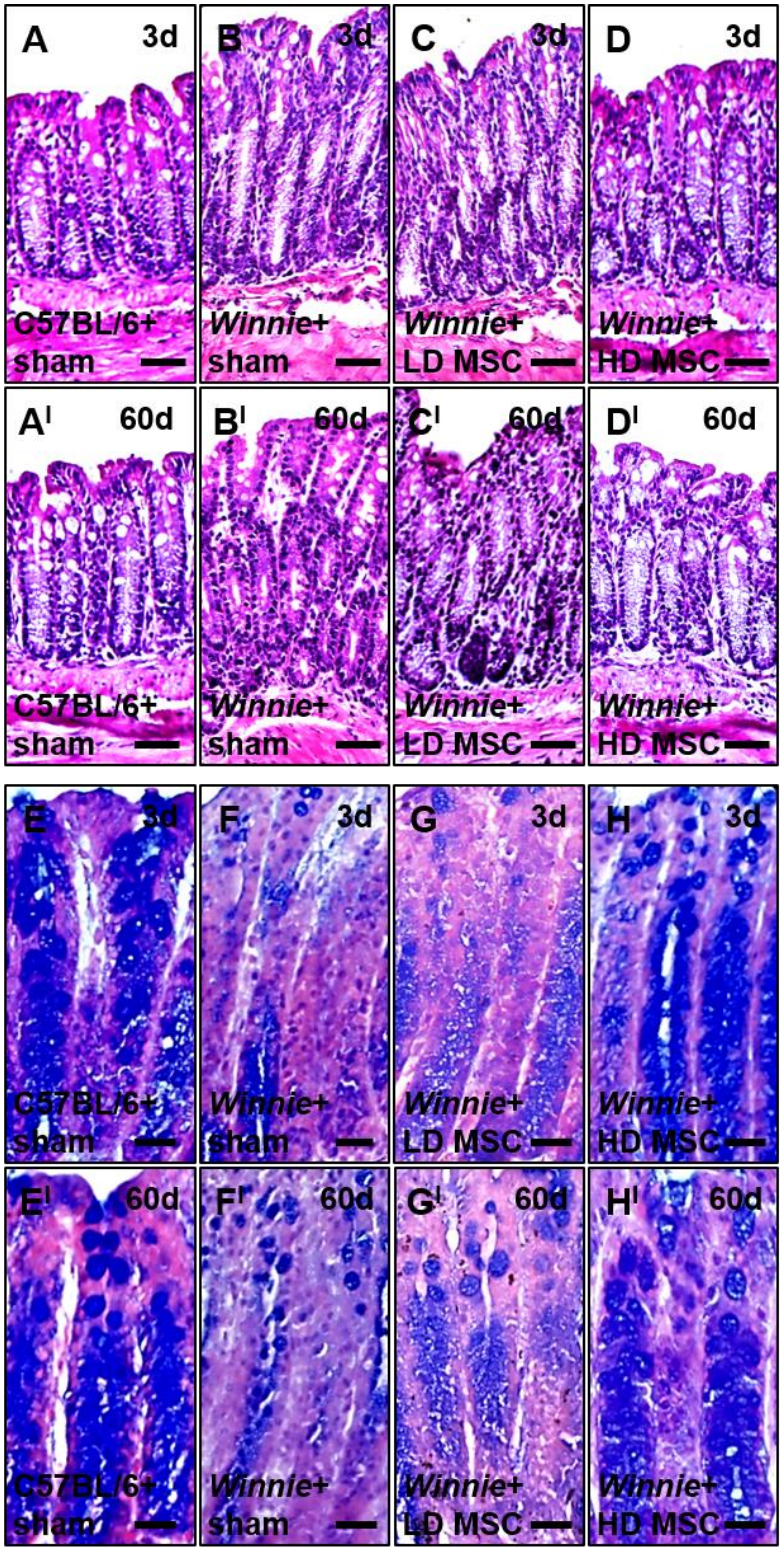
A 3d
B 3d
C 3d
D 3d
C57BL/6+ sham
Winnie+ sham
Winnie+ LD MSC
Winnie+ HD MSC
A' 60d
B' 60d
C' 60d
D' 60d
C57BL/6+ sham
Winnie+ sham
Winnie+ LD MSC
Winnie+ HD MSC
E 3d
F 3d
G 3d
H 3d
C57BL/6+ sham
Winnie+ sham
Winnie+ LD MSC
Winnie+ HD MSC
E' 60d
F' 60d
G' 60d
H' 60d
C57BL/6+ sham
Winnie+ sham
Winnie+ LD MSC
Winnie+ HD MSC

Figure 7.6. Effects of multiple LD and HD MSC treatments on leukocyte infiltration in the chronically inflamed distal colon. Leukocyte infiltration in distal colon sections from C57BL/6+sham, *Winnie*+sham, *Winnie*+LD MSC, and *Winnie*+HD MSC-treated mice was assessed with anti-CD45 antibody, a pan leukocyte marker, at 3 **(A-D)** and 60 days **(A^I-D^I)** post treatment. d = days. Scale bars = 100µm. Quantitative analyses of CD45-IR cells throughout the colon wall **(E)**, in the mucosa **(F)** and within the muscular layers **(G)**. ***P<0.001 when compared to C57BL/6+sham-treated mice. ^P<0.05, ^^P<0.01, ^^^P<0.001 when compared to *Winnie*+HD MSC-treated mice.

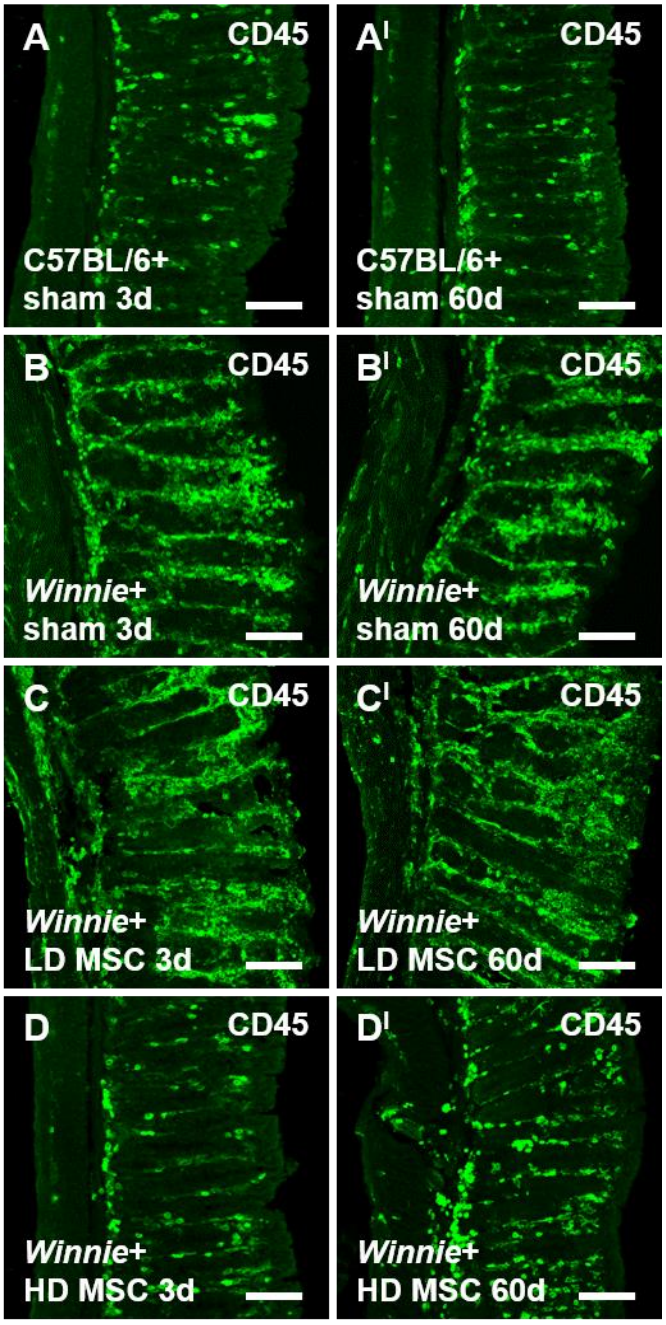
A
CD45
C57BL/6+
sham 3d
A'
CD45
C57BL/6+
sham 60d
B
CD45
Winnie+
sham 3d
B'
CD45
Winnie+
sham 60d
C
CD45
Winnie+
LD MSC 3d
C'
CD45
Winnie+
LD MSC 60d
D
CD45
Winnie+
HD MSC 3d
D'
CD45
Winnie+
HD MSC 60d

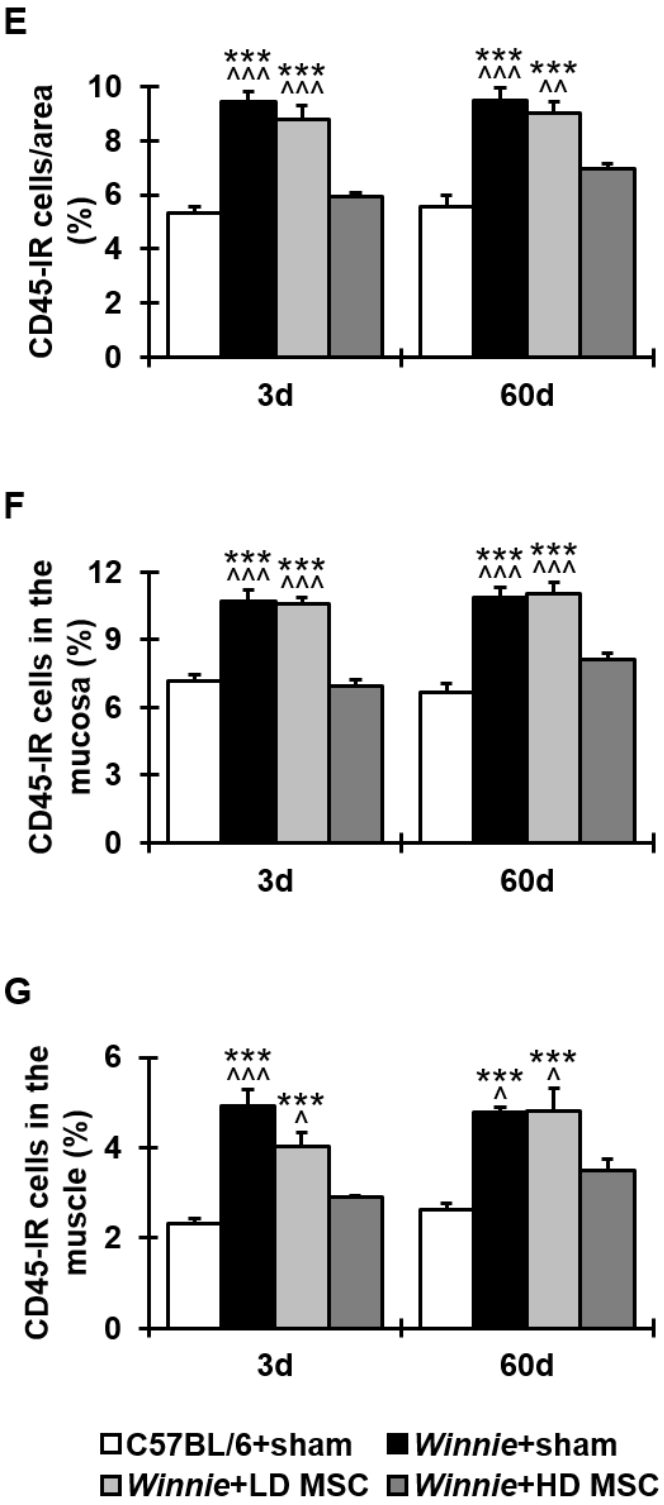
E
CD45-IR cells/area (%)
10
8
6
4
2
0
***
^^^
***
^^^
***
^^^
***
^^
3d
60d
F
CD45-IR cells in the mucosa (%)
12
9
6
3
0
***
^^^
***
^^^
***
^^^
***
^^^
3d
60d
G
CD45-IR cells in the muscle (%)
6
4
2
0
***
^^^
***
^
***
^
***
^
3d
60d
C57BL/6+sham
Winnie+sham
Winnie+LD MSC
Winnie+HD MSC

7.4.3 Multiple HD MSC treatments facilitate nerve regeneration in the chronically inflamed colon

Anti-β-Tubulin (III) antibody was used to label nerve fibers within the mucosal and muscular layers in the distal colon from C57BL/6 and *Winnie* mice at 3 and 60 days post treatment (*n*=5/group; Fig. 7.7A-D^{I}). In colon sections from C57BL/6+sham-treated mice, β-Tubulin (III)-IR fibers were arranged in an orderly manner, prominent in the smooth muscle and projecting from the submucosal layers through the mucosal glands (3 days - area: 9.0±0.2%; mucosa: 6.3±0.6%; muscle: 15.3±0.2%; 60 days - area: 8.9±0.4%; mucosa: 6.4±0.4%; muscle: 15.0±0.6%; Fig. 7.7A-A^{I}, E-G). In contrast, sections from *Winnie*+sham-treated mice showed disorganization and fragmentation of β-Tubulin (III)-IR fibers at both 3 and 60 days post treatment (Fig. 7.7B-B^{I}). Quantification confirmed these observations revealing less abundant β-Tubulin (III)-IR fiber density in sections from *Winnie*+sham-treated (3 days - area: 6.0±0.4%, *P*<0.001; mucosa: 3.8±0.5%, *P*<0.001; muscle: 12.4±0.7%, *P*<0.01; 60 days - area: 5.8±0.1%, *P*<0.001; mucosa: 3.6±0.1%, *P*<0.001; muscle: 11.7±0.5%, *P*<0.01) when compared to C57BL/6+sham-treated mice (Fig. 7.7E-G). Similarly, in sections from LD MSC-treated *Winnie* mice, β-Tubulin (III)-IR nerve fibers were broken and irregularly dispersed (Fig. 7.7C-C^{I}). The density of nerve fibers in sections from *Winnie*+LD MSC-treated mice was comparable to sections from *Winnie*+sham-treated mice and significantly less than in sections from C57BL/6+sham-treated mice at both 3 (area: 5.8±0.4%, *P*<0.001; mucosa: 3.1±0.4%, *P*<0.001; muscle: 12.5±0.9%, *P*<0.05) and 60 days (area: 5.8±0.2%, *P*<0.001; mucosa: 3.2±0.3%, *P*<0.001; muscle: 12.0±0.4%, *P*<0.01) post treatment (Fig. 7.7E-G). Hence, LD MSC treatments did affect any nerve fiber regeneration in the *Winnie* mouse colon. At both 3 and 60 days post treatment, β-tubulin (III)-IR nerve fibers were systematically and prominently distributed throughout the mucosal and muscular layers in sections from *Winnie*+HD MSC-treated mice (Fig. 7.7D-D^{I}). Analysis revealed multiple HD MSC treatments facilitated nerve fiber regeneration by 3 (area: 9.4±0.4%; mucosa: 6.5±0.2%; muscle: 15.3±0.7%) continuing to 60 days (area: 8.9±0.2%; mucosa: 5.8±0.2%; muscle: 14.3±0.5%) post treatment; the density of β-Tubulin (III)-IR nerve fibers

in sections from *Winnie*+HD MSC-treated mice was comparable to sections from C57BL/6+sham-treated mice and higher than in sections from *Winnie*+sham-treated (3 days - area: $P<0.001$; mucosa: $P<0.001$; muscle: $P<0.01$; 60 days - area: $P<0.001$; mucosa: $P<0.01$; muscle: $P<0.05$) and *Winnie*+LD MSC-treated (3 days - area: $P<0.001$; mucosa: $P<0.001$; muscle: $P<0.05$; 60 days - area: $P<0.001$; mucosa: $P<0.001$; muscle: $P<0.05$) mice (Fig. 7.7E-G).

7.4.4 Multiple HD MSC treatments promote cholinergic fiber regeneration in the *Winnie* mouse distal colon

Cholinergic nerve fibers were identified with anti-VAChT antibody in LMMP preparations of the distal colon from C57BL/6+sham, *Winnie*+sham, *Winnie*+LD MSC, and *Winnie*+HD MSC-treated mice at 3 and 60 days post treatment (Fig. 7.8A-D^{I}). VAChT-IR fibers were extensively distributed within the myenteric plexus of tissues from C57BL/6+sham-treated mice at 3 (ganglia: 30.9±1.7%; area: 8.0±0.6%) and 60 days (ganglia: 30.7±1.5%; area: 8.1±0.5%) post treatment. In tissues from *Winnie*+sham-treated mice, there was a substantial decrease in the density of cholinergic fibers when compared to C57BL/6+sham-treated mice at both time points (3 days - ganglia: 23.5±0.7%; area: 5.7±0.1%; 60 days - ganglia: 23.9±1.1%; area: 5.4±0.2%; $P<0.001$ for all; Fig. 7.8E-F). At 3 and 60 days after multiple LD MSC treatments, the density of VAChT-IR fibers in tissues from *Winnie*+MSC-treated mice were comparable to tissues from *Winnie*+sham-treated mice and less than in LMMP preparations from C57BL/6+sham-treated mice (3 days - ganglia: 23.9±0.9%, $P<0.001$; area: 6.1±0.1%, $P<0.01$; 60 days - ganglia: 23.7±0.5%; area: 5.8±0.3%, $P<0.001$ for both; Fig. 7.8E-F). In tissues from *Winnie*+HD MSC-treated mice, VAChT-IR fibers abundantly encompassed neurons and processes of ganglia in LMMP preparations at 3 days post treatment. Quantification of cholinergic fibers showed VAChT-IR fiber density in tissues from *Winnie*+HD MSC-treated mice (ganglia: 28.0±0.7%; area: 7.8±0.4%) was comparable to samples from C57BL/6+sham-treated mice at 3 days and higher than in samples from *Winnie*+sham (ganglia: $P<0.05$; area: $P<0.01$) and *Winnie*+LD MSC-treated ($P<0.05$ for both) mice (Fig. 7.8E-F). The effect of multiple HD MSC treatments on cholinergic fiber

regeneration did not last long term. By 60 days post treatment, VAChT-IR fiber density in tissues from *Winnie*+HD MSC-treated mice (ganglia: 24.6±0.8%; area: 6.4±0.5%) was reduced to levels comparable with tissues from *Winnie*+sham and *Winnie*+LD MSC-treated mice, considerably less than in samples from C57BL/6+sham-treated mice (ganglia: $P<0.01$; area: $P<0.05$).

7.4.5 Multiple HD MSC treatments support noradrenergic fiber regeneration in the *Winnie* mouse distal colon

LMMP preparations of the distal colon from C57BL/6+sham, *Winnie*+sham, *Winnie*+LD MSC, and *Winnie*+HD MSC-treated mice were labeled with anti-TH antibody to identify noradrenergic fibers at 3 and 60 days post treatment (Fig. 7.9A-D^{I}). In tissues from C57BL/6+sham-treated mice, profuse noradrenergic fibers were evident within and around the myenteric ganglia at the 3 (ganglia: 22.4±0.8%; area: 6.1±0.1%) and 60 days (ganglia: 22.6±0.7%; area: 6.0±0.2%) time points (Fig. 7.9A-A^{I}, E-F). TH-IR nerve fiber density was reduced at 3 (ganglia: 15.2±0.3%; area: 3.6±0.2%) continuing to 60 days (ganglia: 15.1±0.7%; area: 3.4±0.4%) post treatment in LMMP preparations from *Winnie*+sham-treated mice when compared to tissues from C57BL/6+sham-treated mice ($P<0.001$ for all; Fig. 7.9B-B^{I}, E-F). Multiple LD MSC treatments had no effect on noradrenergic fibers in the *Winnie* mouse distal colon. Subsequently, TH-IR fiber density in tissues from *Winnie*+LD MSC-treated mice at 3 (ganglia: 14.6±0.4%; area: 3.6±0.1%) and 60 days (ganglia: 14.7±0.3%; area: 3.7±0.2%) was comparable to LMMP preparations from *Winnie*+sham-treated mice and less than in samples from C57BL/6+sham-treated mice ($P<0.001$ for all; Fig. 7.9C-C^{I}, E-F). At 3 days post treatment, TH-IR fiber density in tissues from *Winnie*+HD MSC-treated mice (ganglia: 20.4±0.4%; area: 5.5±0.2%) was increased when compared to *Winnie*+sham ($P<0.001$ for both) and *Winnie*+LD MSC-treated ($P<0.001$ for both) mice, comparable to samples from C57BL/6+sham-treated mice (Fig. 7.9D-D^{I}, E-F). By 60 days post treatment, the density of noradrenergic fibers in tissues from *Winnie*+HD MSC-treated mice (ganglia: 17.9±0.7%; area: 5.1±0.2%) remained higher than in LMMP preparations from *Winnie*+sham and *Winnie*+LD MSC-treated mice (ganglia: $P<0.01$ for both; area: $P<0.001$ for both), however were

significantly less than in tissues from C57BL/6+sham-treated mice (ganglia: $P<0.001$; area: $P<0.01$).

7.4.6 Multiple HD MSC treatments facilitate sensory nerve fiber regeneration in the *Winnie* mouse distal colon

Sensory nerve fibers were labeled with anti-CGRP antibody in LMMP preparations of the distal colon from C57BL/6+sham, *Winnie*+sham, *Winnie*+LD MSC, and *Winnie*+HD MSC-treated mice at 3 and 60 days post treatment (Fig. 7.10A-D^{I}). In tissues from C57BL/6+sham-treated mice, sensory fibers were abundant throughout the myenteric plexus and CGRP-IR fiber density was consistent from 3 (ganglia: 28.5±1.2%; area: 6.6±0.2%) to 60 days (ganglia: 28.6±0.9%; area: 6.8±0.5%) post treatment (Fig. 7.10E-F). When compared to samples from control mice, the density of CGRP-IR fibers was reduced in distal colon preparations from *Winnie*+sham-treated mice at both 3 (ganglia: 20.5±0.4%; area: 4.6±0.2%) and 60 days (ganglia: 20.6±0.8%; area: 4.7±0.1%) after treatment ($P<0.001$ for all; Fig. 7.10E-F). Tissues from *Winnie*+LD MSC-treated mice revealed comparable CGRP-IR fiber densities to LMMP preparations from *Winnie*+sham-treated mice; a reduction in sensory fiber density when compared to tissues from C57BL/6+sham-treated mice (3 days - ganglia: 19.6±1.0%; area: 4.7±0.2%; 60 days - ganglia: 21.1±0.7%; area: 4.6±0.2%; $P<0.001$ for all; Fig. 7.10E-F). Multiple treatments of HD MSCs facilitated sensory nerve fiber regeneration by 3 (ganglia: 29.3±1.3%; area: 6.1±0.5%) maintaining to 60 days (ganglia: 25.0±1.0%; area: 5.7±0.3%) post treatment in preparations from *Winnie*+HD MSC-treated mice to levels comparable with C57BL/6+sham tissues. Thus, CGRP-IR fiber density was higher in tissues from *Winnie*+HD MSC-treated mice when compared to samples from *Winnie*+sham (3 days - ganglia: $P<0.001$; area: $P<0.01$; 60 days: $P<0.05$ for both) and *Winnie*+LD MSC-treated (3 days - ganglia: $P<0.001$; area: $P<0.05$; 60 days: $P<0.05$ for both) mice at both time points (Fig. 7.10E-F).

Figure 7.7. Effects of multiple LD and HD MSC treatments on nerve fiber density in the chronically inflamed distal colon. Nerve fibers in distal colon sections from C57BL/6+sham, *Winnie*+sham, *Winnie*+LD MSC, and *Winnie*+HD MSC-treated mice were identified with anti-β-Tubulin (III) antibody at 3 **(A-D)** and 60 days **(A^I-D^I)** post treatment. d = days. Scale bars = 100μm. Quantitative analyses of β-Tubulin (III)-IR fibers within the wall of the colon **(E)**, in the mucosa only **(F)** and within the muscular layers only **(G)**. **P*<0.05, ***P*<0.01, ****P*<0.001 when compared to C57BL/6+sham-treated mice. ^*P*<0.05, ^^*P*<0.01, ^^^*P*<0.001 when compared to *Winnie*+HD MSC-treated mice.

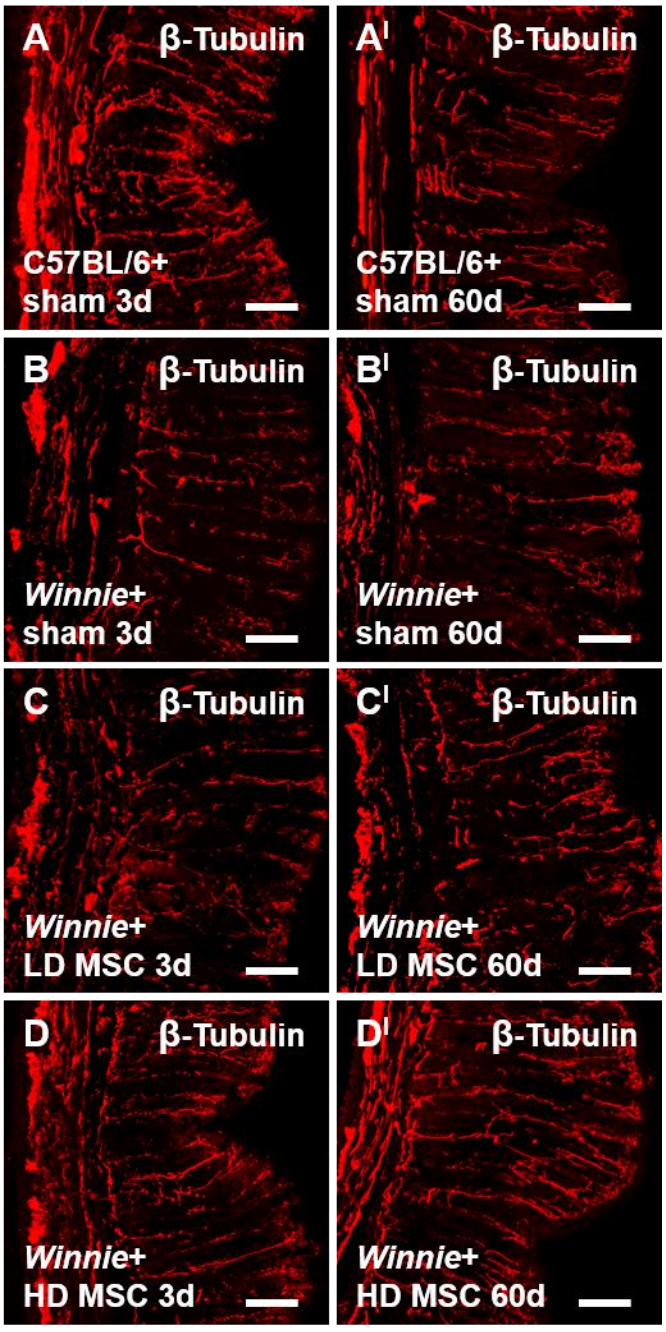
A
β-Tubulin
C57BL/6+
sham 3d
A'
β-Tubulin
C57BL/6+
sham 60d
B
β-Tubulin
Winnie+
sham 3d
B'
β-Tubulin
Winnie+
sham 60d
C
β-Tubulin
Winnie+
LD MSC 3d
C'
β-Tubulin
Winnie+
LD MSC 60d
D
β-Tubulin
Winnie+
HD MSC 3d
D'
β-Tubulin
Winnie+
HD MSC 60d

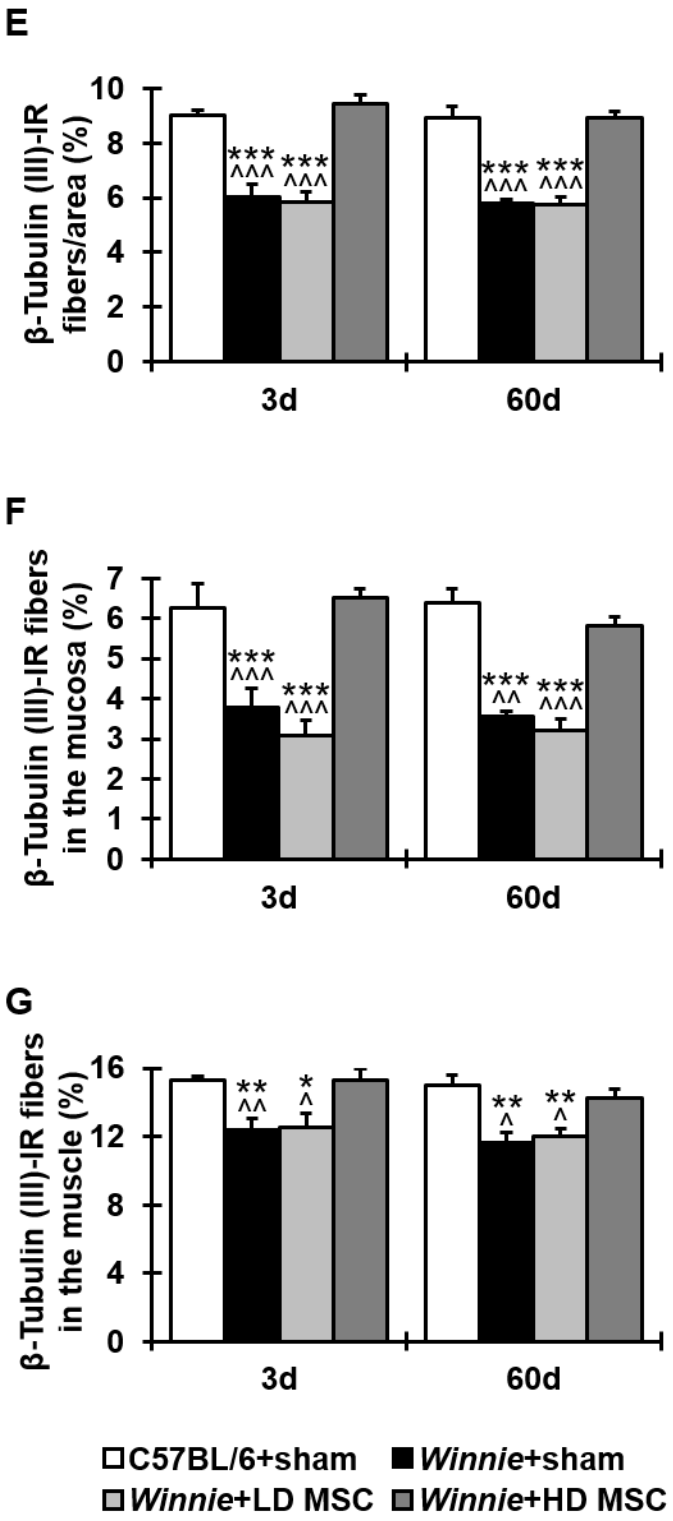
E
β-Tubulin (III)-IR fibers/area (%)
10
8
6
4
2
0
***
^^^
***
^^^
***
^^^
***
^^^
3d
60d
F
β-Tubulin (III)-IR fibers in the mucosa (%)
7
6
5
4
3
2
1
0
***
^^^
***
^^^
***
^^
***
^^^
3d
60d
G
β-Tubulin (III)-IR fibers in the muscle (%)
16
12
8
4
0
**
^^
*
^
**
^
**
^
3d
60d
C57BL/6+sham
Winnie+sham
Winnie+LD MSC
Winnie+HD MSC

Figure 7.8. Effects of multiple LD and HD MSC treatments on cholinergic nerve fibers within the myenteric plexus of the *Winnie* mouse colon. Cholinergic nerve fibers in LMMP preparations of the distal colon from C57BL/6+sham, *Winnie*+sham, *Winnie*+LD MSC, and *Winnie*+HD MSC-treated mice were distinguished with anti-VAChT antibody at 3 **(A-D)** and 60 days **(A^I-D^I)** post treatment. d = days. Scale bars = 100μm. Quantitative analyses of VAChT-IR fibers per ganglion **(E)** and per 2mm^2 area **(F)**. *P<0.05, **P<0.01, ***P<0.001 when compared to C57BL/6+sham-treated mice. ^P<0.05, ^^P<0.01 when compared to *Winnie*+HD MSC-treated mice.

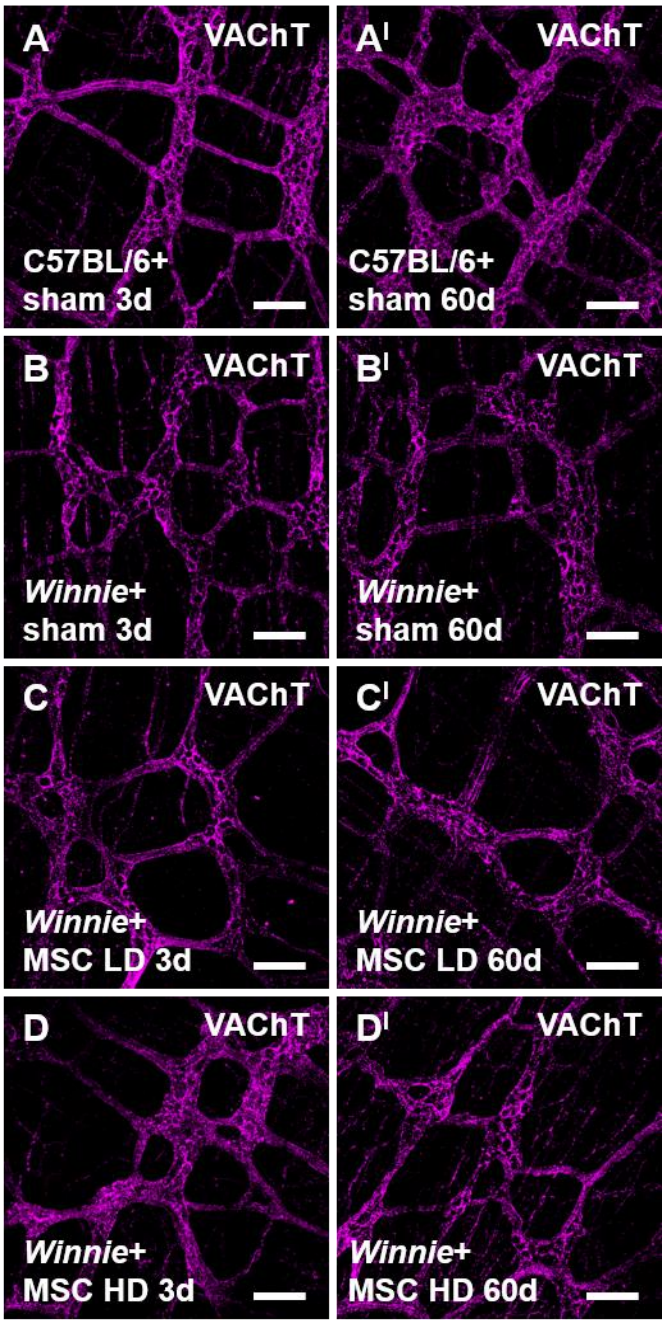
A
VAChT
C57BL/6+
sham 3d
A'
VAChT
C57BL/6+
sham 60d
B
VAChT
Winnie+
sham 3d
B'
VAChT
Winnie+
sham 60d
C
VAChT
Winnie+
MSC LD 3d
C'
VAChT
Winnie+
MSC LD 60d
D
VAChT
Winnie+
MSC HD 3d
D'
VAChT
Winnie+
MSC HD 60d

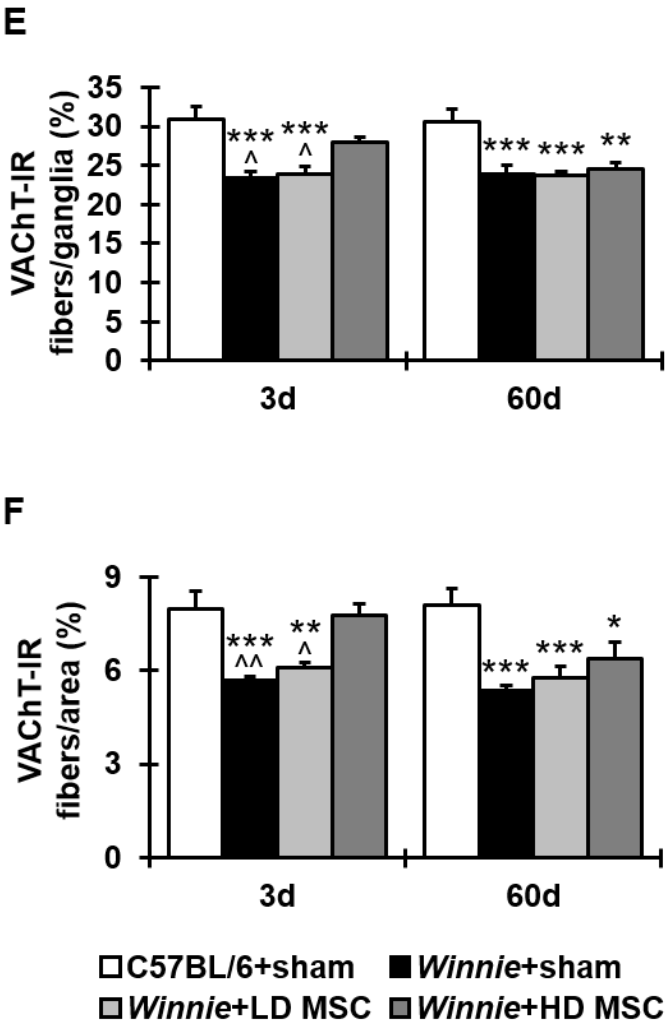
E
VAChT-IR fibers/ganglia (%)
35
30
25
20
15
10
5
0
***
^
***
^
***
***
**
3d
60d
F
VAChT-IR fibers/area (%)
9
6
3
0
***
^^
**
^
***
***
*
3d
60d
C57BL/6+sham
Winnie+sham
Winnie+LD MSC
Winnie+HD MSC

Figure 7.9. Effects of multiple LD and HD MSC treatments on noradrenergic nerve fibers within the myenteric plexus of the *Winnie* mouse colon. Noradrenergic nerve fibers in LMMP preparations of the distal colon from C57BL/6+sham, *Winnie*+sham, *Winnie*+LD MSC, and *Winnie*+HD MSC-treated mice were distinguished with anti-TH antibody at 3 **(A-D)** and 60 days **(A^I-D^I)** post treatment. d = days. Scale bars = 100µm. Quantitative analyses of TH-IR fibers per ganglion **(E)** and per 2mm^2 area **(F)**. ***P*<0.01, ****P*<0.001 when compared to C57BL/6+sham-treated mice. ^^*P*<0.01, ^^^*P*<0.001 when compared to *Winnie*+HD MSC-treated mice.

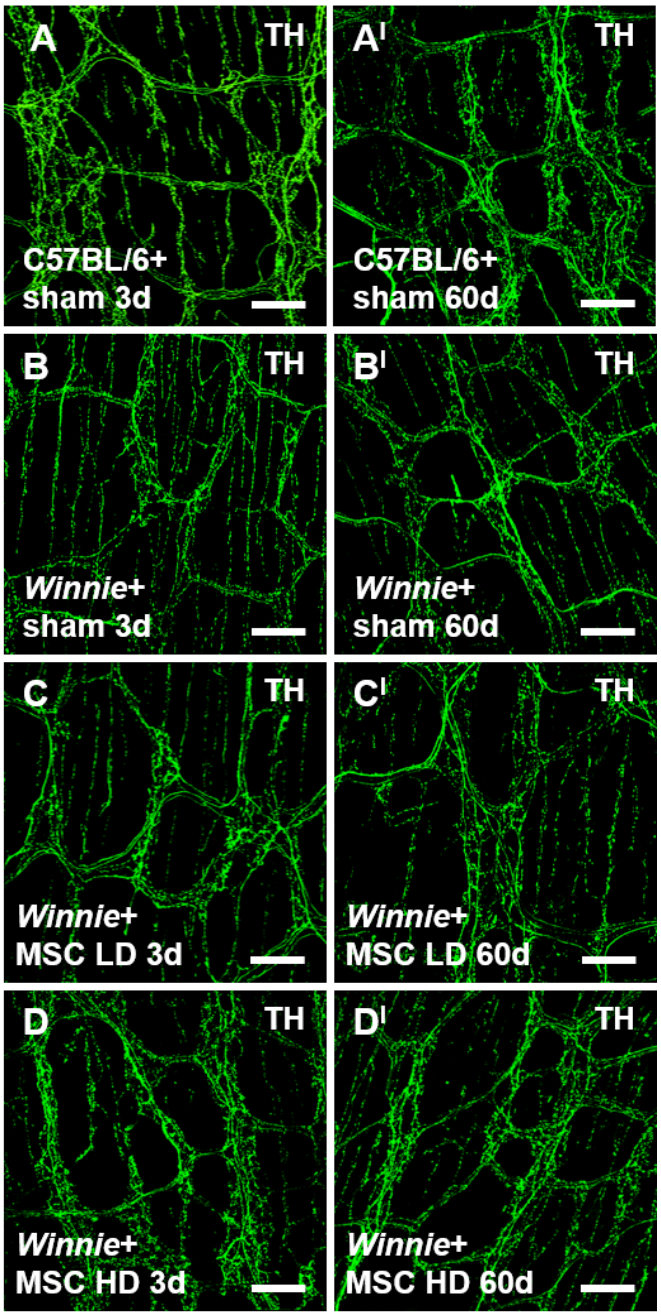
A
TH
C57BL/6+
sham 3d
A'
TH
C57BL/6+
sham 60d
B
TH
Winnie+
sham 3d
B'
TH
Winnie+
sham 60d
C
TH
Winnie+
MSC LD 3d
C'
TH
Winnie+
MSC LD 60d
D
TH
Winnie+
MSC HD 3d
D'
TH
Winnie+
MSC HD 60d

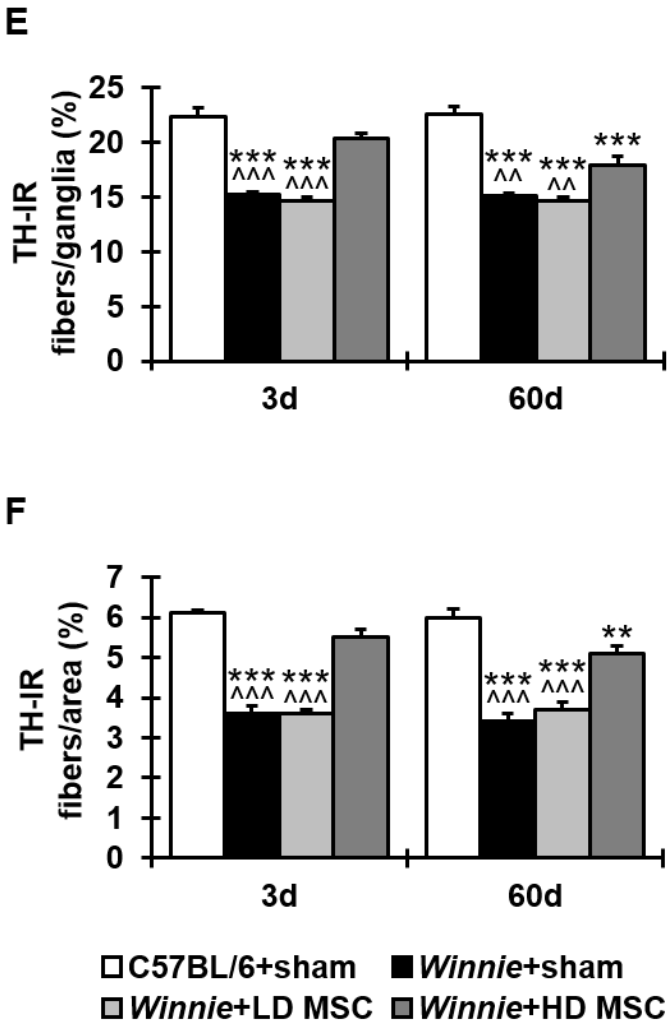
E
TH-IR fibers/ganglia (%)
25
20
15
10
5
0
***
^^^
***
^^^
***
^^
***
^^
***
3d
60d
F
TH-IR fibers/area (%)
7
6
5
4
3
2
1
0
***
^^^
***
^^^
***
^^^
***
^^^
**
3d
60d
C57BL/6+sham
Winnie+sham
Winnie+LD MSC
Winnie+HD MSC

Figure 7.10. Effects of multiple LD and HD MSC treatments on sensory nerve fibers within the myenteric plexus of the *Winnie* mouse colon. Sensory nerve fibers were identified with anti-CGRP antibody in LMMP preparations of the distal colon from C57BL/6+sham, *Winnie*+sham, *Winnie*+LD MSC, and *Winnie*+HD MSC-treated mice at 3 **(A-D)** and 60 days **(A^I-D^I)** post treatment. d = days. Scale bars = 100µm. Quantitative analyses of CGRP-IR fibers per ganglion **(E)** and per 2mm^2 area **(F)**. ****P*<0.001 when compared to C57BL/6+sham-treated mice. ^*P*<0.05, ^^*P*<0.01, ^^^*P*<0.001 when compared to *Winnie*+HD MSC-treated mice.

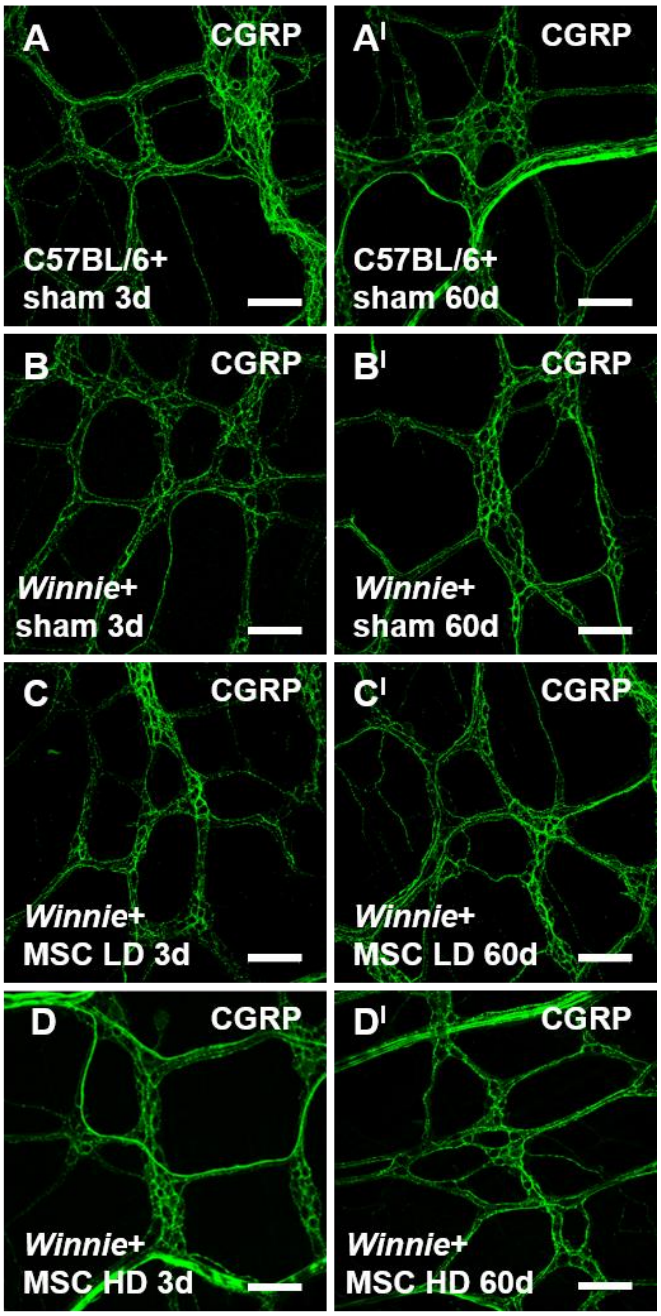
A
CGRP
C57BL/6+
sham 3d
A'
CGRP
C57BL/6+
sham 60d
B
CGRP
Winnie+
sham 3d
B'
CGRP
Winnie+
sham 60d
C
CGRP
Winnie+
MSC LD 3d
C'
CGRP
Winnie+
MSC LD 60d
D
CGRP
Winnie+
MSC HD 3d
D'
CGRP
Winnie+
MSC HD 60d

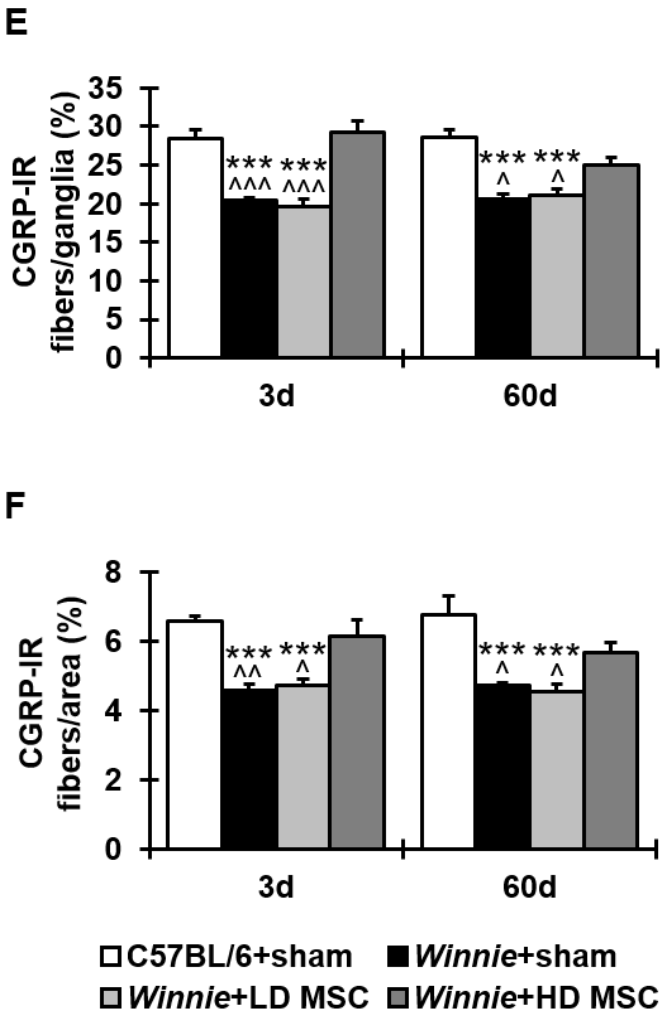
E
CGRP-IR fibers/ganglia (%)
35
30
25
20
15
10
5
0
*** ^^^
*** ^^^
*** ^
*** ^
3d
60d
F
CGRP-IR fibers/area (%)
8
6
4
2
0
*** ^^
*** ^
*** ^
*** ^
3d
60d
C57BL/6+sham
Winnie+sham
Winnie+LD MSC
Winnie+HD MSC

7.4.7 Multiple MSC treatments have no effect on the average number of myenteric neurons in the chronically inflamed distal colon

Myenteric neurons in LMMP preparations from C57BL/6+sham, *Winnie*+sham, *Winnie*+LD MSC, and *Winnie*+HD MSC-treated mice were identified with anti-PGP9.5 antibody, a pan neuronal marker, at 3 and 60 days post treatment (Fig. 7.11A-D^{I}). In tissues from C57BL/6+sham-treated mice, the average number of PGP9.5-IR neurons per ganglionic area was 22±0.5 and 22±0.4 at 3 and 60 days post treatment, respectively (Fig. 7.11E). A reduction in the average number and density of neurons per ganglionic area was consistently recorded in LMMP preparations from *Winnie*+sham-treated mice at 3 (18±0.6 cells/ganglionic area; 82.7±3.4%) and 60 days (18±0.5 cells/ganglionic area; 82.8±3.4%) when compared to tissues from C57BL/6+sham-treated mice (P<0.001 for all; Fig. 7.11E-F). Tissues from *Winnie*+LD MSC (3 days: 18±0.5 cells/ganglionic area; 60 days: 18±0.6 cells/ganglionic area; P<0.001 for both) and *Winnie*+HD MSC-treated (3 days: 20±0.5 cells/ganglionic area, P<0.05; 60 days: 19±0.4 cells/ganglionic area, P<0.01) mice showed comparable average numbers of neurons per ganglionic area as samples from *Winnie*+sham-treated mice, significantly less than in tissues from C57BL/6+sham-treated mice (Fig. 7.11E). The ganglionic density of PGP9.5-IR neurons reflected these numbers, confirming that neither LD or HD MSC treatments had effect on the number of myenteric neurons in the *Winnie* mouse distal colon at 3 (LD MSC: 81.7±3.1%, P<0.001; HD MSC: 89.4±3.5%, P<0.05) or 60 days (LD MSC: 83.0±3.3%, P<0.001; HD MSC: 87.8±1.0%, P<0.05) post treatment.

7.4.8 Multiple MSC treatments have no effect on the average number of nitrergic myenteric neurons in the *Winnie* mouse distal colon

Anti-nNOS antibody was used to label nitrergic neurons in wholemount LMMP preparations of the distal colon from C57BL/6+sham, *Winnie*+sham, *Winnie*+LD MSC, and *Winnie*+HD MSC-treated mice 3 and 60 days following treatment (Fig. 7.12A-D^{I}). Consistent mean numbers of nNOS-IR neurons per ganglionic area were analyzed in tissues from C57BL/6+sham-treated mice at 3 (7±0.3

cells/ganglionic area) and 60 days (7±0.2 cells/ganglionic area) post treatment (Fig. 7.12E). No differences in average nitrergic neuron numbers were observed between tissues from *Winnie*+sham (3 days: 7±0.3 cells/ganglionic area; 60 days: 7±0.3 cells/ganglionic area), *Winnie*+LD MSC (3 days: 7±0.3 cells/ganglionic area; 60 days: 7±0.1 cells/ganglionic area), and *Winnie*+HD MSC-treated (3 days: 7±0.2 cells/ganglionic area; 60 days: 7±0.2 cells/ganglionic area) mice at either time point, comparable to samples from C57BL/6+sham-treated mice (Fig. 7.12E). Subsequently, there was no differences in the nNOS-IR neuronal density in tissues from any *Winnie* group relative to control tissues (*Winnie*+sham - 3 days: 95.9±6.3%; 60 days: 91.9±1.8%; *Winnie*+LD MSC - 3 days: 94.64.53%; 60 days: 90.8±3.0%; *Winnie*+HD MSC - 3 days: 100.8±5.7%; 60 days: 97.3±4.4%; Fig. 7.12F). While there were no changes in the average number of nNOS-IR neurons in tissues from treated *Winnie* mice, loss of PGP9.5-IR neurons founded an increased proportion of nNOS-IR neurons to PGP9.5-IR neurons (*Winnie*+sham - 3 days: 38.5±2.0%, $P<0.001$; 60 days: 37.3±0.7%, $P<0.05$; *Winnie*+LD MSC - 3 days: 38.4±1.0%, $P<0.001$; 60 days: 36.8±1.2%, $P<0.05$; *Winnie*+HD MSC - 3 days: 37.4±0.9%, $P<0.01$; 60 days: 37.0±0.7%, $P<0.05$) when compared to C57BL/6+sham-treated mice (3 days: 33.3±1.2%; 60 days: 33.6±1.3%) at both time points post treatment (Fig. 7.12G).

7.4.9 Multiple MSC treatments have no effect on the average number of cholinergic myenteric neurons in the *Winnie* mouse distal colon

Cholinergic neurons were identified with anti-ChAT antibody in LMMP preparations of the distal colon from C57BL/6+sham, *Winnie*+sham, *Winnie*+LD MSC, and *Winnie*+HD MSC-treated mice 3 and 60 days post treatment (Fig. 7.13A-D^{I}). At both time points, the average number of ChAT-IR neurons per ganglionic area was lower in tissues from *Winnie*+sham-treated mice (3 days: 9±0.3 cells/ganglionic area; 60 days: 9±0.3 cells/ganglionic area) when compared to samples from C57BL/6+sham-treated mice (3 days: 12±0.5 cells/ganglionic area; 60 days: 12±0.4 cells/ganglionic area; $P<0.01$ for both; Fig. 7.13E). Correspondingly, the ganglionic density of ChAT-IR neurons in preparations from *Winnie*+sham-treated mice was decreased relative to control tissues (3 days:

82.2±5.6%; 60 days: 80.3±4.6%; *P*<0.01 for both; Fig. 7.13F). In tissues from *Winnie*+LD MSC (3 days: 10±0.3 cells/ganglionic area; 82.7±3.7%; 60 days: 9±0.4 cells/ganglionic area; 80.7±2.8%) and *Winnie*+HD MSC-treated mice (3 days: 10±0.4 cells/ganglionic area; 86.3±3.5%; 60 days: 10±0.5 cells/ganglionic area; 87.0±2.2%), the average number and density of ChAT-IR neurons per ganglionic area at 3 and 60 days post treatment were comparable to LMMP preparations from *Winnie*+sham-treated mice, significantly less than in tissues from C57BL/6+sham-treated mice (*Winnie*+LD MSC: *P*<0.01 for all; *Winnie*+HD MSC: *P*<0.05 for all; Fig. 7.13E-F). No differences in the proportion of excitatory neurons per ganglionic area were calculated between groups due to the simultaneous decrease in ChAT-IR and PGP9.5 neurons in tissues from *Winnie* mice (C57BL/6+sham - 3 days: 52.6±3.4%; 60 days: 52.1±2.8%; *Winnie*+sham - 3 days: 51.6±1.6%; 60 days: 50.3±1.8%; *Winnie*+LD MSC - 3 days: 53.0±2.4%; 60 days: 50.8±3.1%; *Winnie*+HD MSC - 3 days: 50.4±1.2%; 60 days: 50.3±1.7%; Fig. 7.13G).

Figure 7.11. The effects of multiple LD and HD MSC treatments on the average number of myenteric neurons in the chronically inflamed colon. Anti-PGP9.5 antibody was used to label myenteric neurons in LMMP preparations of the distal colon from C57BL/6+sham, *Winnie*+sham, *Winnie*+LD MSC, and *Winnie*+HD MSC-treated mice at 3 and 60 days post treatment **(A-D^{I})**. d = days. Scale bars = 100µm. Quantitative analyses of the average number of PGP9.5-IR neurons normalized to 0.1mm^2 ganglionic area **(E)**. Ganglionic density of PGP9.5-IR neurons in tissues from *Winnie* mice as a percentage of control (100%) **(F)**. **P*<0.05, ***P*<0.01, ****P*<0.001 when compared to C57BL/6+sham-treated mice.

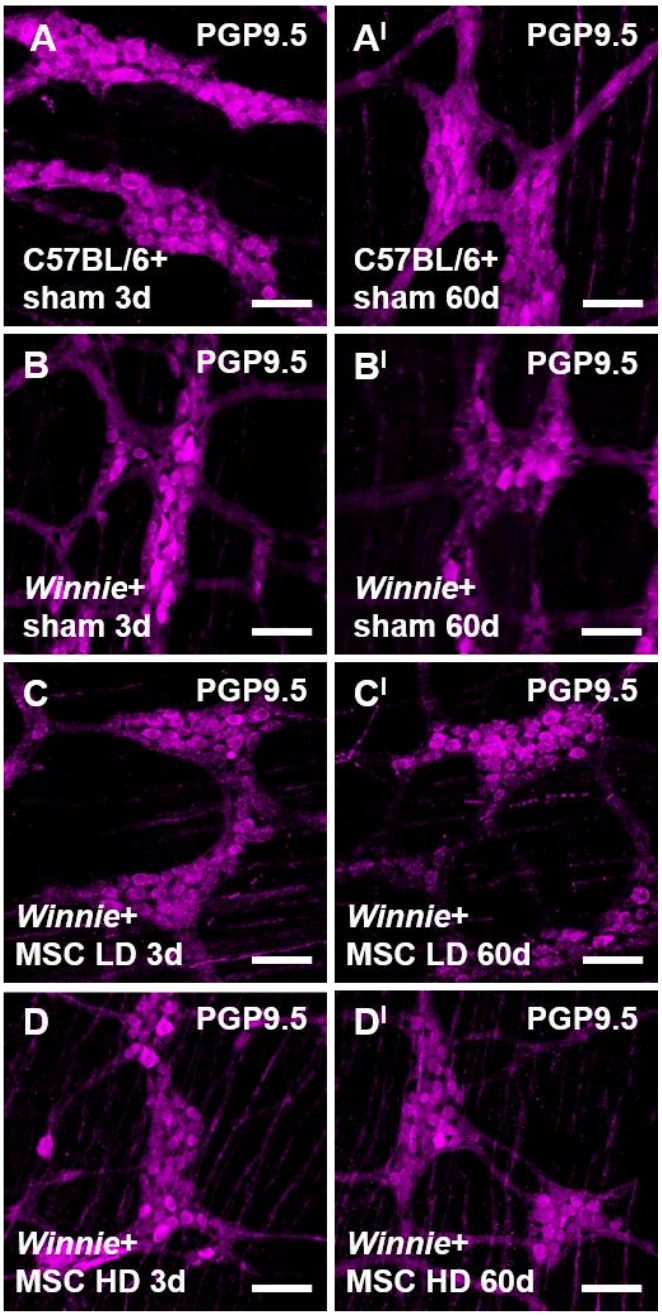
A
PGP9.5
C57BL/6+
sham 3d
A'
PGP9.5
C57BL/6+
sham 60d
B
PGP9.5
Winnie+
sham 3d
B'
PGP9.5
Winnie+
sham 60d
C
PGP9.5
Winnie+
MSC LD 3d
C'
PGP9.5
Winnie+
MSC LD 60d
D
PGP9.5
Winnie+
MSC HD 3d
D'
PGP9.5
Winnie+
MSC HD 60d

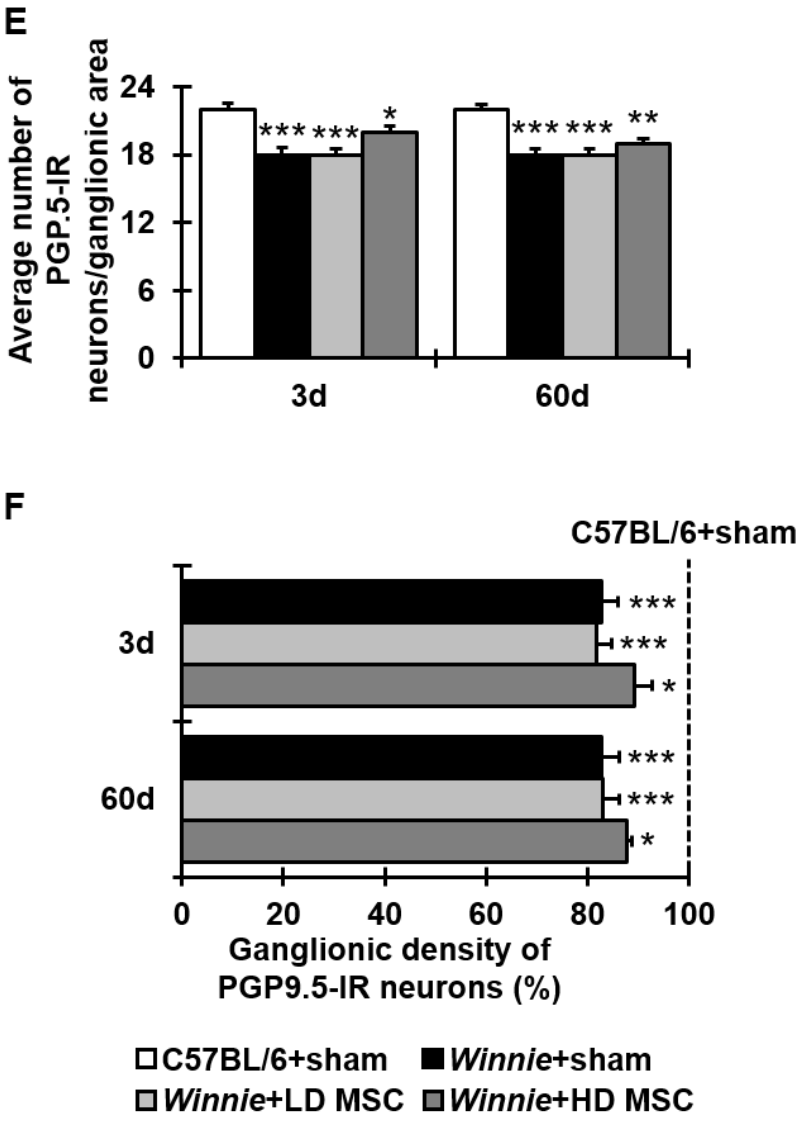
E
Average number of PGP.5-IR neurons/ganglionic area
24
18
12
6
0
***
***
*
***
***
**
3d
60d
F
C57BL/6+sham
3d
60d
***
***
*
***
***
*
0
20
40
60
80
100
Ganglionic density of PGP9.5-IR neurons (%)
C57BL/6+sham
Winnie+sham
Winnie+LD MSC
Winnie+HD MSC

Figure 7.12. The effects of multiple LD and HD MSC treatments on the average number of nNOS-IR myenteric neurons in the *Winnie* mouse colon. Anti-nNOS antibody was used to label nitrergic myenteric neurons in LMMP preparations of the distal colon from C57BL/6+sham, *Winnie*+sham, *Winnie*+LD MSC, and *Winnie*+HD MSC-treated mice at 3 and 60 days post treatment **(A-D^{I})**. d = days. Scale bars = 100µm. Quantitative analyses of the average number of nNOS-IR neurons normalized to 0.1mm^2 ganglionic area **(E)**. Ganglionic density of nNOS-IR neurons in tissues from *Winnie* mice as a percentage of control (100%) **(F)**. The proportion of nNOS-IR neurons to PGP9.5-IR neurons **(H)**. **P*<0.05, ***P*<0.01, ****P*<0.001 when compared to C57BL/6+sham-treated mice.

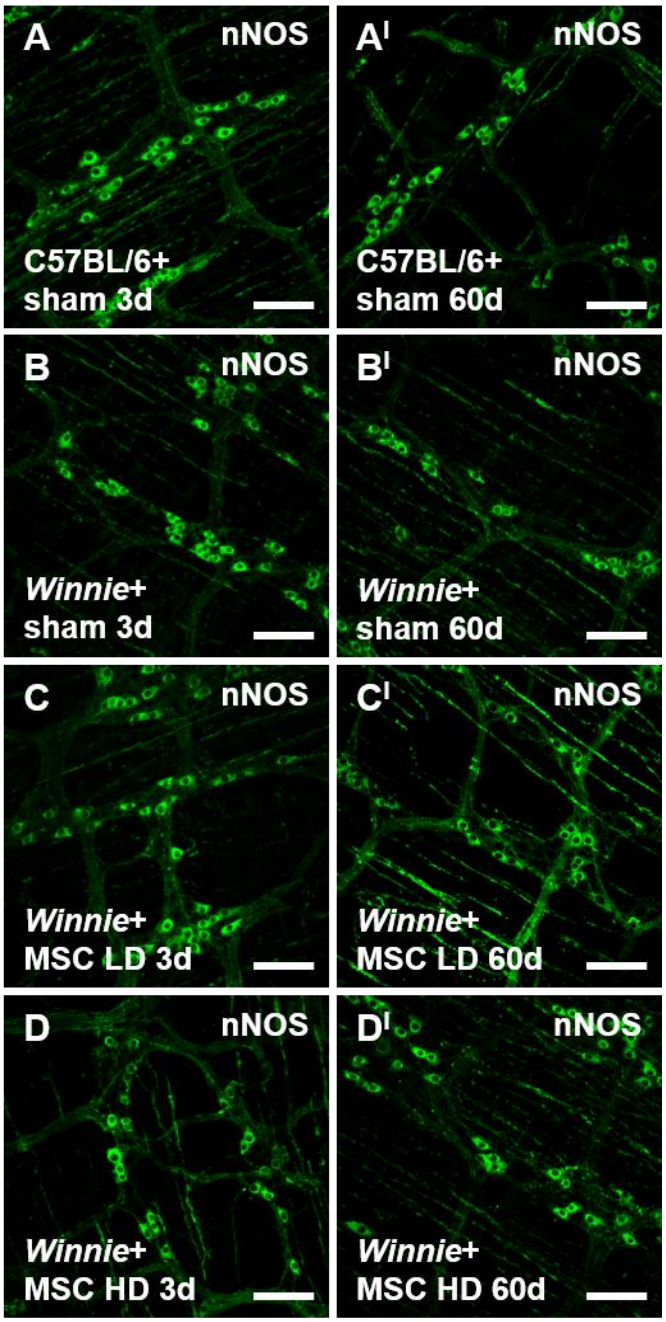
A
nNOS
C57BL/6+
sham 3d
A'
nNOS
C57BL/6+
sham 60d
B
nNOS
Winnie+
sham 3d
B'
nNOS
Winnie+
sham 60d
C
nNOS
Winnie+
MSC LD 3d
C'
nNOS
Winnie+
MSC LD 60d
D
nNOS
Winnie+
MSC HD 3d
D'
nNOS
Winnie+
MSC HD 60d

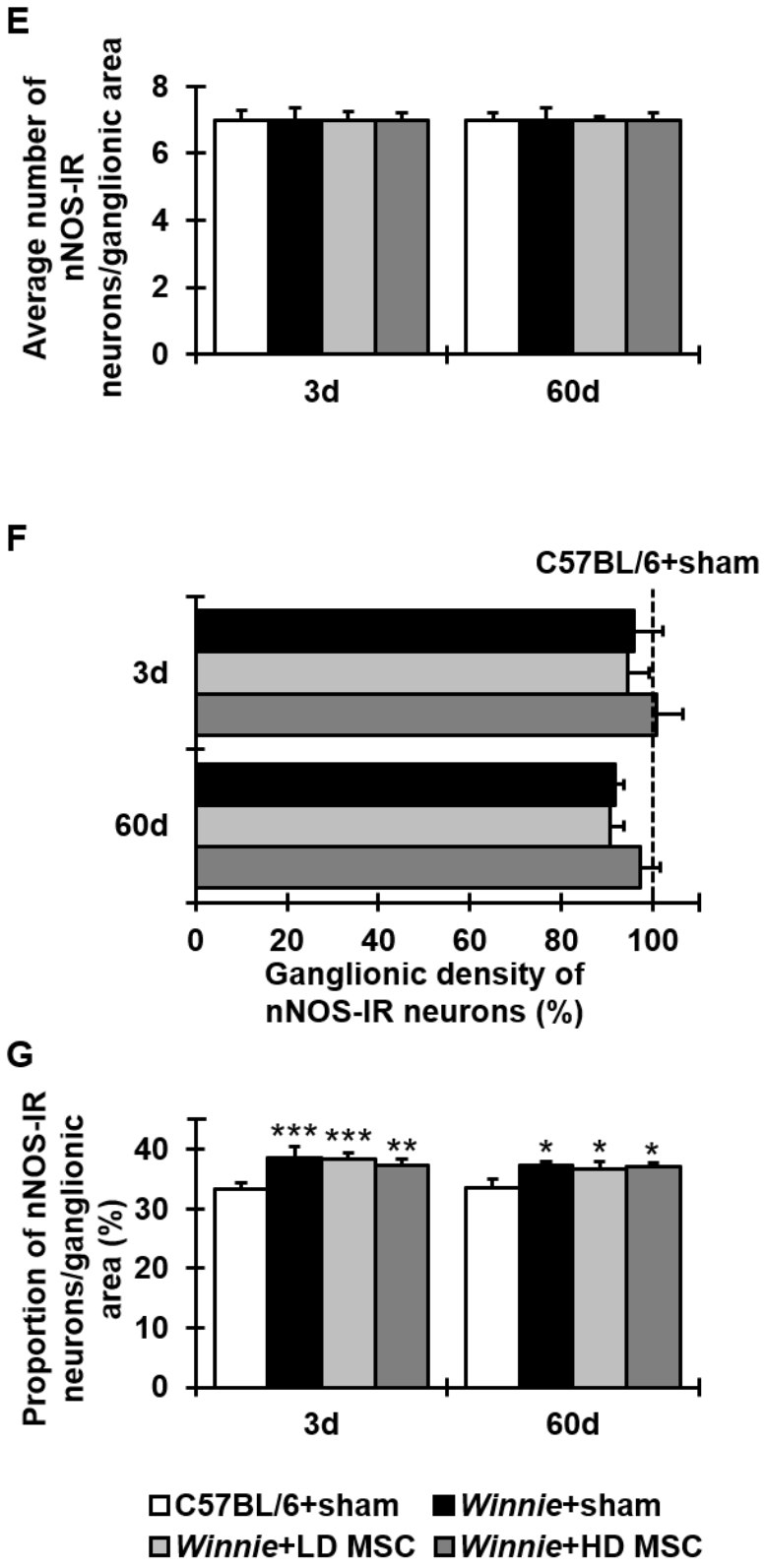
E
Average number of nNOS-IR neurons/ganglionic area
8
6
4
2
0
3d
60d
F
C57BL/6+sham
3d
60d
0
20
40
60
80
100
Ganglionic density of nNOS-IR neurons (%)
G
Proportion of nNOS-IR neurons/ganglionic area (%)
40
30
20
10
0
***
***
**
*
*
*
3d
60d
C57BL/6+sham
Winnie+sham
Winnie+LD MSC
Winnie+HD MSC

Figure 7.13. The effects of multiple LD and HD MSC treatments on the average number of ChAT-IR myenteric neurons in the *Winnie* mouse colon. Anti-ChAT antibody was used to label cholinergic myenteric neurons in LMMP preparations of the distal colon from C57BL/6+sham, *Winnie*+sham, *Winnie*+LD MSC, and *Winnie*+HD MSC-treated mice at 3 and 60 days post treatment **(A-D^{I})**. d = days. Scale bars = 100µm. Quantitative analyses of the average number of ChAT-IR neurons normalized to 0.1mm^2 ganglionic area **(E)**. Ganglionic density of ChAT-IR neurons in tissues from *Winnie* mice as a percentage of control (100%) **(F)**. The proportion of ChAT-IR neurons to PGP9.5-IR neurons **(H)**. **P*<0.05, ***P*<0.01 when compared to C57BL/6+sham-treated mice.

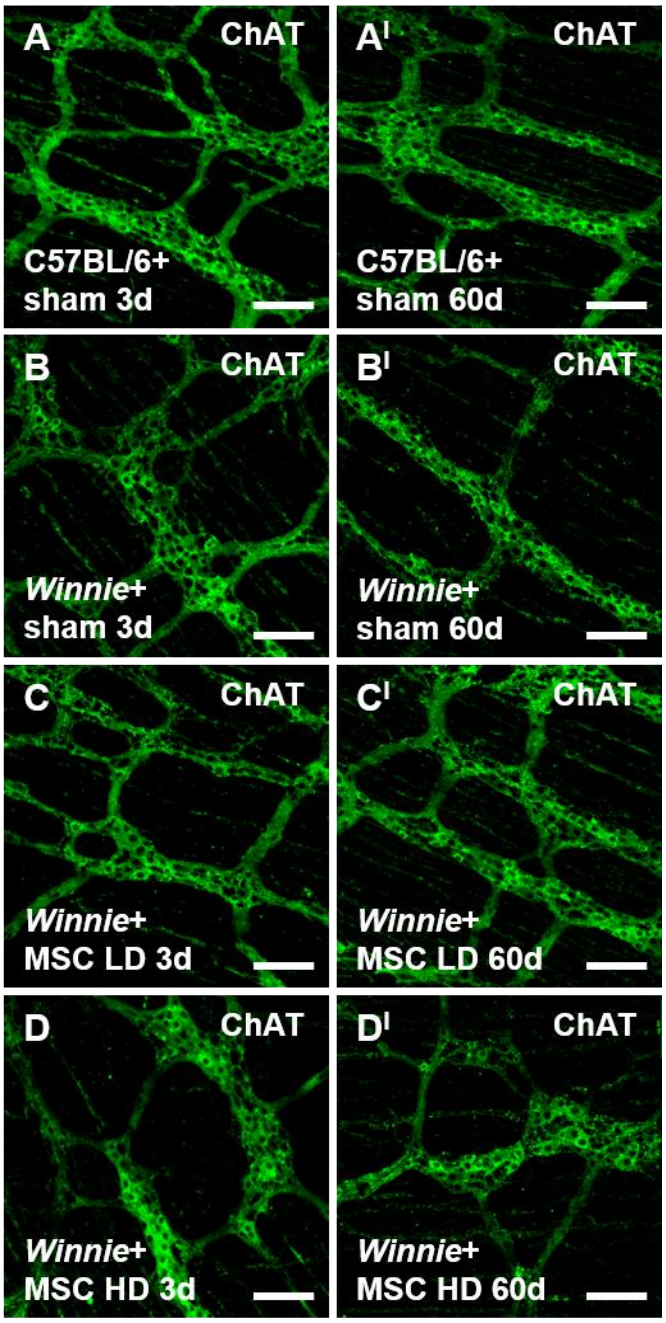
A
ChAT
C57BL/6+
sham 3d
A'
ChAT
C57BL/6+
sham 60d
B
ChAT
Winnie+
sham 3d
B'
ChAT
Winnie+
sham 60d
C
ChAT
Winnie+
MSC LD 3d
C'
ChAT
Winnie+
MSC LD 60d
D
ChAT
Winnie+
MSC HD 3d
D'
ChAT
Winnie+
MSC HD 60d

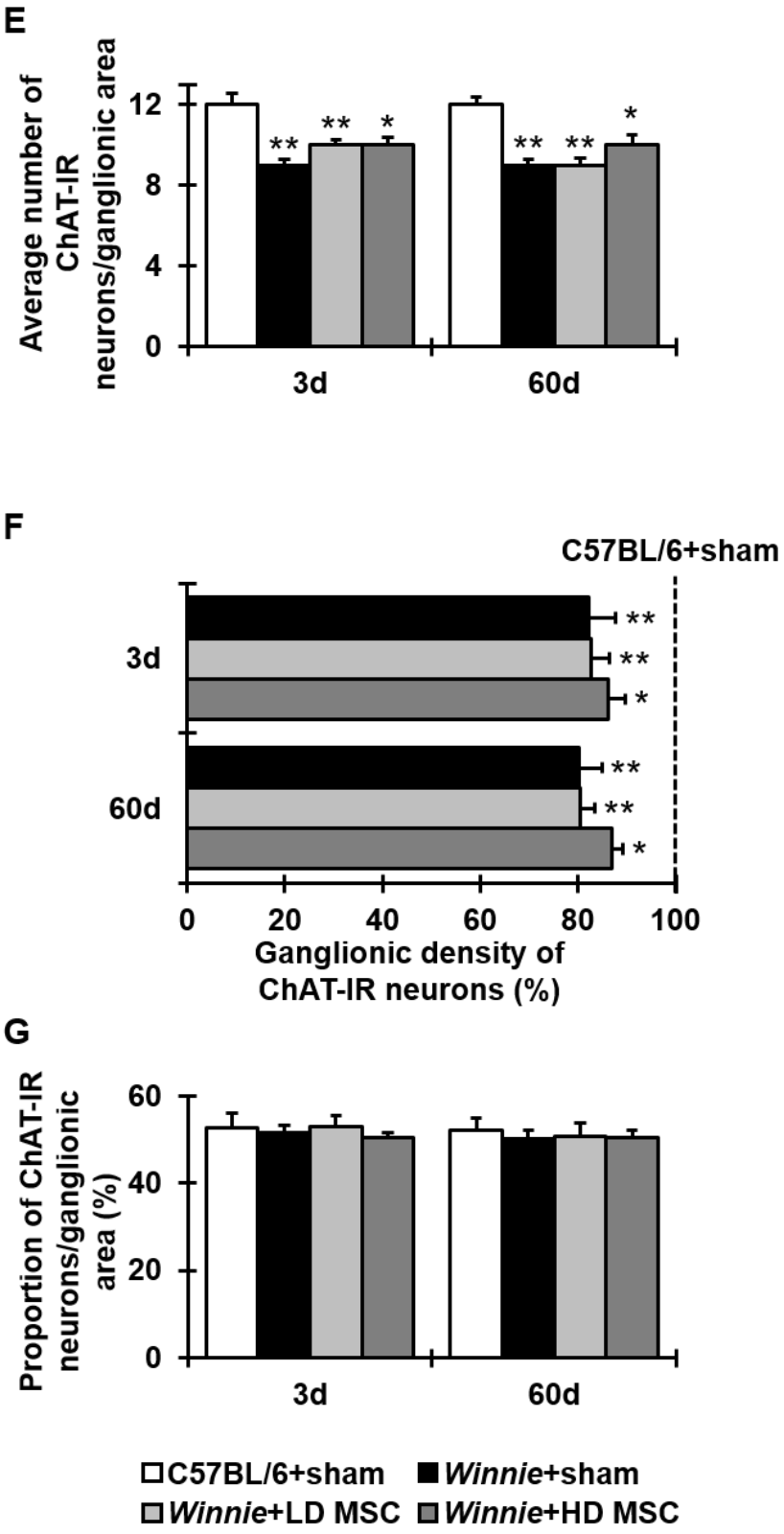
E
Average number of ChAT-IR neurons/ganglionic area
12
8
4
0
**
**
*
**
**
*
3d
60d
F
C57BL/6+sham
3d
60d
**
**
*
**
**
*
0
20
40
60
80
100
Ganglionic density of ChAT-IR neurons (%)
G
Proportion of ChAT-IR neurons/ganglionic area (%)
60
40
20
0
3d
60d
C57BL/6+sham
Winnie+sham
Winnie+LD MSC
Winnie+HD MSC

7.5 Discussion

This is the first study to examine the effects of multiple MSC treatments in the *Winnie* mouse model of spontaneously occurring chronic colitis. The efficacy of LD and HD MSC treatments were investigated at both a short-term (3 day) and long-term (60 day) time point. In this study, we found that multiple HD MSC treatments administered by enema attenuated inflammation and facilitated nerve fiber regeneration in the distal colon of *Winnie* mice at 3 days post treatment. The beneficial effects of HD MSC treatments in the inflamed colon were mostly sustained long-term for up to 60 days. Conversely, we established that multiple LD MSC treatments have no effect in alleviating colonic inflammation or associated enteric neuropathy in *Winnie* mice. Hence, the therapeutic effects of multiple BM-MSC treatments administered by enema into the *Winnie* mouse colon are dose-dependent.

In colon sections from both LD and HD MSC-treated *Winnie* mice, localization of enema administered MSCs were evident at 3 days post treatment. A greater quantity of engrafted MSCs were observed in the colon sections from HD MSC-treated than LD MSC-treated mice. In consistency with our findings, localization and engraftment of MSCs in injured tissues is reported to be significantly greater when administered at higher doses (Li et al. 2016b; Fernandez-Garcia et al. 2015; Saether et al. 2014; Muller-Ehmsen et al. 2006). At 60 days post treatment, there was no MSC engraftment in the colons from *Winnie* mice in any group. Similarly, transient engraftment of MSCs in the intestine was observed within a few days of transplantation (Han et al. 2017; Sala et al. 2015; Semont et al. 2013; Castelo-Branco et al. 2012; Gonzalez-Rey et al. 2009; Hayashi et al. 2008; Tanaka et al. 2008). The length of time that administered MSCs engraft in the colon varies between studies, however, there is general consensus that cell numbers dramatically decline after a few days and are undetectable within a few weeks (Moussa et al. 2017; Sala et al. 2015; Semont et al. 2013; Gonzalez-Rey et al. 2009).

Symptoms of perianal bleeding, diarrhea and lack of weight gain confirmed active colitis in all *Winnie* mice before treatment. Alterations to the consistency, frequency and water content of stools is associated with active colitis in IBD patients and experimental models of colitis, including *Winnie* mice (Chen et al. 2017; Rahman et al. 2015; Fierer et al. 2012; Waljee et al. 2009). These changes are consistent with weakening of normal colonic sodium and/or chloride uptake mechanisms, thereby eliminating the driving force for luminal passive water absorption and promoting diarrhea (Spehlmann et al. 2009). Furthermore, dysmotility and increased transit times in the *Winnie* mouse colon deprives fecal material of adequate exposure to the mucosa for absorption of water and electrolytes, resulting in loose stools (Robinson et al. 2017a). A distinct formation of pellets, absence of diarrhea and a reduced fecal water content was consistently observed in samples from control mice, indicating that the epithelium was not compromised by inflammation. Following treatment, we did not observe any changes to average body weight, stool consistency or fecal water content in sham-treated and LD MSC-treated *Winnie* mice. However, pellet formation, absence of diarrhea and a reduced fecal water content was observed in samples from HD MSC-treated mice long-term. These results suggest that a multiple HD MSC treatment regime was efficacious in restoring the integrity of the epithelial barrier to enhance water absorption from the lumen.

In *Winnie* mice, chronic inflammation induces morphological changes including increased colon length and marked thickening of the intestinal wall, as well as mucosal damage and heightened leukocyte infiltration in the distal colon (Rahman et al. 2015). Sham-treated *Winnie* mice exhibited all afore mentioned changes confirming the severity of inflammation at 3 and 60 days post treatment. Colon length and thickness, damage to the architecture of the colon and density of leukocytes remained comparable to sham-treated *Winnie* mice after LD MSC treatment. Conversely, multiple HD MSC treatments attenuated the severity of inflammation in *Winnie* mice evidenced by a decrease in colon length and thickness, healing of the colonic architecture and reduced leukocyte infiltration throughout the colon wall for up to 60 days. In consistency with our results, many studies have demonstrated the capacity for BM-MSCs, as well as MSCs derived

from adipose, umbilical cord, amnion and gingiva tissue, to reduce the overall disease activity of acute experimental colitis: attenuating reduction in body weight and diarrhea, ameliorating colonic transmural inflammation, improving histological scores and suppressing infiltration of inflammatory cells (Robinson et al. 2017b; 2015; 2014; Song et al. 2017; Chao et al. 2016; Lee et al. 2016; Jung et al. 2015; Onishi et al. 2015; Perez-Merino et al. 2015; Sala et al. 2015; Stavely et al. 2015a; 2015b; Chen et al. 2013b; Fawzy et al. 2013; Liang et al. 2011; Gonzalez et al. 2009; Zhang et al. 2009b; Hayashi et al. 2008; Yu et al. 2017; Goncalves et al. 2014; Nikolic et al. 2018; Tanaka et al. 2008). In contrast to our study, most studies reporting attenuation of colitis implement only a single administration of MSCs (Robinson et al. 2017b; 2015; 2014; Song et al. 2017; Chao et al. 2016; Jung et al. 2015; Onishi et al. 2015; Perez-Merino et al. 2015; Sala et al. 2015; Stavely et al. 2015a; 2015b; Chen et al. 2013b; Fawzy et al. 2013; He et al. 2012; Gonzalez et al. 2009; Zhang et al. 2009b; Hayashi et al. 2008). Few studies have investigated a multiple MSC treatment regime in experimental colitis and generally describe reductions in disease activity and histological scores (Nikolic et al. 2018; Lee et al. 2016; Tang et al. 2015; Liang et al. 2011; Tanaka et al. 2008). Of these studies, there is great variation in the number of MSC treatments administered (2 (Yu et al. 2017; Tang et al. 2015; Goncalves et al. 2014; Liang et al. 2011), 3 (Lee et al. 2016; Tanaka et al. 2008), 4 (Yu et al. 2017), 7 (Nikolic et al. 2018)). The frequency of MSC treatments also fluctuates between studies (daily for 2d (Liang et al. 2011), daily for 7 days (Nikolic et al. 2018), 1×wk (Yu et al. 2017), 2×wk (Yu et al. 2017; Goncalves et al. 2014), 3×wk (Lee et al. 2016; Tanaka et al. 2008), 1×2wk (Tang et al. 2015)). Furthermore, there is much diversity regarding the dose of MSCs reported to exhibit therapeutic effect (2×10^5 MSCs (Tang et al. 2015), 1×10^6 MSCs (Yu et al. 2017; Goncalves et al. 2014; Liang et al. 2011), 2×10^6 MSCs (Nikolic et al. 2018), 5×10^6 MSCs (Tanaka et al. 2008), 1×10^7 MSCs (Lee et al. 2016)).

While multiple administrations of LD MSCs were ineffective in alleviating inflammation in *Winnie* mice in this study, single or repeated MSC applications using comparable doses have been shown to be efficacious in other studies. This may be attributable to variations in the inflammatory milieu *in vivo*; MSCs are

extremely contingent on environmental inflammatory conditions (Kim and Cho 2013). Studies examining the effects of MSC treatment on experimental colitis most commonly employ acute models of intestinal inflammation, such as TNBS and DSS-induced colitis (Nikolic et al. 2018; Robinson et al. 2017b; 2015; 2014; Song et al. 2017; Chao et al. 2016; Liu et al. 2015b; Onishi et al. 2015; Sala et al. 2015; Stavely et al. 2015a; 2015b; Goncalves et al. 2014; Chen et al. 2013b; He et al. 2012; Liang et al. 2011; Gonzalez et al. 2009; Zhang et al. 2009b; Hayashi et al. 2008; Tanaka et al. 2008). Limited studies have investigated MSCs in chronic colitis. Only one study investigating the effect of tonsil derived MSCs on chronic DSS colitis followed a similar number, frequency and dose regime as the LD part of our investigation (Yu et al. 2017). In consistency with our results, these authors found that multiple administrations of $1x10^6$ MSCs did not have effect on disease activity (Yu et al. 2017). It may be postulated that the increased MSC numbers present in the colons from mice with repeated HD MSC treatments heighten the expression of anti-inflammatory and immunosuppressive factors secreted by MSCs to a level sufficient to overcome the impediments of the chronic inflammatory environment.

Intestinal innervation is impaired in the distal colon of *Winnie* mice (Rahman et al. 2015). In consistency with these results, reductions in the density of sensory, noradrenergic, and cholinergic fibers were observed in LMMP preparations of the distal colon from *Winnie*+sham-treated mice when compared to tissues from C57BL/6+sham-treated mice in this study. While LD MSC treatments had no effect, multiple administrations of HD MSCs facilitated regeneration of β-Tubulin (III)-IR, CGRP-IR, TH-IR, and VAChT-IR nerve fibers in the myenteric plexus of the *Winnie* mouse colon at 3 days post treatment. The increase in β-Tubulin (III)-IR and CGRP-IR fiber density was maintained for 60 days. In consistency with our findings, regeneration of β-tubulin (III)-IR fibers has been reported at 3 days after MSC administration in rat spinal transection (Qiu et al. 2015) and infusion of MSC conditioned medium in an animal model of cerebral ischemia (Tsai et al. 2014), and maintained up to 36 weeks in canine spinal cord transection (Han et al. 2018). In addition, CGRP-IR nerve fibers were increased in the injured spinal cord at 4, 8 and 36 weeks post MSC transplantation (Han et al. 2018; Novikova

et al. 2018; Onuma-Ukegawa et al. 2015; Ding et al. 2009). In this study, we found that although HD MSCs facilitated regeneration of VAChT-IR and TH-IR fibers at 3 days, the increase in cholinergic and noradrenergic fiber density was not maintained at the 60 day time point when compared to control tissues. Similar to our results, regeneration of cholinergic fibers was observed 7 days after MSC transplantation, but not at 60 days in a rat model of lumbar ventral root avulsion (Torres-Espin et al. 2013a). Other studies have demonstrated MSC-induced regeneration of TH-IR nerve fibers to be maintained for 11 days and 42 days in experimental models of peripheral nerve injury (Lopatina et al. 2011; Kamada et al. 2005), as well as up to 50 days in experimental Parkinson's disease (Sadan et al. 2009). These studies suggest that multiple treatments of HD MSCs are capable of supporting VAChT-IR and TH-IR fiber regeneration for longer than 3 days in *Winnie* mice, however further investigation is necessitated to reveal the exact time point for which cholinergic and noradrenergic fiber regrowth is sustained.

In response to local cues such as hypoxia, apoptosis, or inflammation, transplanted MSCs exert tropic support by secreting a variety of factors, such as growth factors, trophic factors, cytokines and chemokines, that directly or indirectly stimulate tissue repair and regeneration (Fu et al. 2017; Hofer and Tuan 2016). The aptitude of MSCs to augment nerve fiber regeneration is attributable to their capacity to increase the expression of growth factors and neurotrophic factors, such as vascular endothelial growth factor, basic fibroblast growth factor, hepatocyte growth factor, brain-derived neurotrophic factor (BDNF), nerve growth factor (NGF), glial cell-derived neurotrophic factor (GDNF), ciliary-derived neurotrophic factor, and neurotrophin (NT) (Mohammadi et al. 2013; Marconi et al. 2012; Lopatina et al. 2011; Sebben et al. 2011; Ribeiro-Resende et al. 2009; Rodrigues Hell et al. 2009; Wei et al. 2009; Rehman et al. 2004). These factors have been shown to promote cholinergic, sympathetic, and sensory nerve fibers in experimental regeneration models (Yu et al. 2014; Kuihua et al. 2014; Tang et al. 2013; de Boer et al. 2012; Scholz et al. 2010; Glueckert et al. 2008; Katsui et al. 2008; Kemp et al. 2008; Dezawa et al. 2004; Boyd and Gordon 2003; 2002; Jakeman et al. 1998). Previously, we have shown that BM-MSCs from the same

cell line utilized in this study secrete BDNF, NT, NGF, and GDNF (Chapter 2). These findings suggest that the short-term regenerative effects demonstrated by repeated administrations of HD MSCs in this study were enhanced by neurotrophic factors secreted by MSCs *in vivo*. However, few MSCs survive for more than one week after transplantation (Parekkadan and Milwid 2010) suggesting that the long-term effects of MSCs on β-Tubulin (III)-IR and CGRP-IR are most likely mediated by paracrine mechanisms (Maguire 2013). However, these paracrine mechanisms did not sustain TH-IR and VAChT-IR fiber density long-term which requires further investigation. Conceivably, nerve fiber regeneration was not evident in the *Winnie* mouse colon following repeated LD MSC treatments due to an inadequate number of cells to express sufficient amounts of neurotrophic factors.

The loss of myenteric neurons observed in colons from sham-treated *Winnie* mice in this study was not attenuated by multiple administrations of LD or HD MSCs. It has been demonstrated that MSCs provide a neuroprotective effect against inflammation-induced neuronal loss in acute TNBS colitis (Robinson et al. 2017b; 2015; 2014; Stavely et al. 2015a; 2015b). However, in these studies MSCs are administered close to the onset of colonic inflammation, therefore neuronal loss is prevented rather than restored through the formation of new neurons. Conversely, in the *Winnie* mouse colon, neuronal loss is established prior to MSC administration. While MSCs have the potential for neuronal differentiation *in vitro* (Bae et al. 2011a; Jang et al. 2010), it remains controversial whether MSCs can differentiate to neurons with functional characteristics *in vivo*. Furthermore, in consistency with our results, the majority of homing and engraftment studies have demonstrated minimal or absent long-term engraftment of MSCs, thereby eliminating the prospect of neuronal differentiation (Parekkadan and Milwid 2010). Our results show that slightly more PGP9.5-IR neurons per ganglionic area were counted in colons from HD MSC-treated *Winnie* mice than in tissues from sham-treated *Winnie* mice. This observation may be due to direct or indirect secretion of neurotrophic factors by MSCs protecting the remaining neurons, enabling them to survive and regenerate fibers (Mesentier-Louro et al. 2014).

7.6 Conclusion

Here we have demonstrated for the first time that multiple administrations of HD MSCs attenuated inflammation and facilitated regeneration of nerve fibers in the *Winnie* mouse model of chronic colitis. Most of the beneficial effects were maintained long-term for up to 60 days post treatment. Based on the therapeutic effects observed with repeated administration of HD, but not LD, MSCs in this study, it can be concluded that the efficacy of MSC treatment on colonic inflammation is dose-dependent in *Winnie* mice. Further investigations are warranted to examine whether HD MSC treatments are effective in restoring dysmotility and impaired smooth muscle cell responses previously demonstrated in the *Winnie* mouse colon.

CHAPTER EIGHT: GENERAL DISCUSSION, FUTURE DIRECTIONS AND CONCLUSIONS

8.1 General discussion

Although not associated with mortality, severe symptoms and complications, along with the relapsing nature of inflammatory bowel disease (IBD), cause significant impairment to patient's quality of life (Fakhoury et al. 2014; Kalafateli et al. 2013; Umanskiy and Fichera 2010). Many studies involving experimental models of colitis and tissues from IBD patients demonstrate the detrimental effects of intestinal inflammation on the enteric nervous system (ENS) (Nurgali et al. 2011; 2009; 2007; Villanacci et al. 2008; De Giorgio et al. 2002; Sanovic et al. 1999). Damage to the structure and function of the ENS is considered to play a major role in the generation of symptoms associated with IBD.

The mechanisms underlying the pathogenesis of IBD are unknown, thus current treatments are focused only on the prevention of symptoms once they arise (Sandborn et al. 2014). Existing therapies can provide short-term symptom relief in some patients however they can be associated with adverse effects, loss of patient response, or no response at all (Nitzan et al. 2016; Williams et al. 2011; D'Haens 2007; Irving et al. 2007; Van Dieren et al. 2007). Furthermore, no current IBD treatments focus on the attenuation of enteric neuropathy that is clearly associated with intestinal inflammation. The basis of this thesis was to examine a novel treatment for IBD which targets enteric neurons.

Mesenchymal stem cells (MSCs) have been shown to participate in tissue repair and regeneration in various inflammatory, autoimmune, and neurodegenerative disorders (Galindo et al. 2011; da Silva Meirelles et al. 2009; Kassis et al. 2008; Zheng et al. 2008). The capacity of MSCs to migrate to the site of tissue damage and exert anti-inflammatory, immunomodulating and neuroprotective effects via paracrine actions makes them an ideal candidate for the treatment of IBD (Wang et al. 2012a; Spaeth et al. 2008; Liu et al. 2007; Ortiz et al. 2003). Previous studies have demonstrated that systemic and locally administered MSCs derived from various sources ameliorate colitis, promoting intestinal repair, decreasing inflammation and modulating the immune response (Liu et al. 2014; Castelo-Branco et al. 2012; Liang et al. 2011; Gonzalez-Rey et al. 2009; Ando et al. 2008;

Hayashi et al. 2008; Tanaka et al. 2008). However, no studies investigated the effects of MSC therapy on damage to the ENS associated with intestinal inflammation. Hence, the studies within this thesis are the first to investigate the therapeutic effects of MSC treatment on enteric neuropathy associated with IBD.

This thesis can be divided into three main sections: 1) an investigation into whether MSC and CM treatments can avert enteric neuropathy in an acute model of colitis, 2) establishment of a chronic model of colitis that is highly representative of human IBD, and 3) an examination of MSC treatment in this chronic model of colitis.

8.1.1 MSC therapy for the treatment of enteric neuropathy associated with acute TNBS-induced colitis in guinea-pigs

In Chapter 2, we investigated whether enema applied human bone marrow (BM)-MSCs and conditioned medium (CM) are efficacious in averting enteric neuropathy in the guinea-pig model of 2,4,6-trinitrobenzene sulfonic acid (TNBS)-induced colitis. Colon tissues were collected at 6h, 24h, 3 days, and 7 days post induction of colitis for histology, immunohistochemistry and motility experiments. The results of this chapter demonstrated that both MSCs and CM attenuate inflammation and prevent enteric neuropathy and colonic dysmotility associated with intestinal inflammation. Furthermore, we established that MSC-based therapies start exerting their neuroprotective effects by 24h post treatment and maintain these effects for at least 7 days. The neuroprotective effects of MSCs and CM were independent of the anti-inflammatory effects since the inflammatory reaction in the myenteric plexus did not subside until 3 days.

The application of MSCs by enema is reported for the first time in Chapter 2. Systemic administration of MSCs can be associated with large numbers of cells becoming trapped in the lungs and other filtering organs, however local application positions the MSCs at, or near, the injury site to ensure the maximum number of cells are available to participate in the repair of damaged tissues (Manieri and Stappenbeck 2011). Additionally, application by enema offers a

feasible option for MSC administration in IBD patients because it is safe, convenient and minimally invasive.

The myenteric neuronal loss and nerve fiber damage in the TNBS-inflamed colon described in Chapter 2 was consistent with previous studies in the guinea-pig intestine (Nurgali et al. 2011; 2007; Linden et al. 2005; 2003). We also observed changes to the neurochemical coding of myenteric neurons to be associated with TNBS colitis, comparable to other studies (Winston et al. 2013; Boyer et al. 2007; Linden et al. 2005; Neunlist et al. 2003; Belai et al. 1997). Alterations to the neurochemical coding and loss of myenteric neurons induced by TNBS correlated with colonic dysmotility, indicating disruptions in the intrinsic motor circuits. In colons from MSC and CM-treated guinea-pigs, neuronal loss was prevented, and regeneration of nerve fibers was evident by 24h maintained for 7 days post treatment. Correspondingly, colonic motor patterns were comparable to sham-treated animals at 7 days. It was considered that the neuroprotective effects of MSC-based therapy on enteric neurons observed in Chapter 2 were due to soluble factors released by MSCs *in vivo*, rather than the differentiation of MSCs into neural phenotypes. There are two reasons for these conclusions: 1) neuroprotective effects were also observed with CM treatment, and 2) limited cellular telomerase activity and a maximum 7 day time point hindered the prospect of any *in vivo* MSC differentiation specific cell lineages (Chen et al. 2012a; Everaert et al. 2012; Mirsaidi et al. 2012). Examination of the CM revealed that MSCs secrete numerous neuroprotective factors under normal culturing conditions, some of which have been demonstrated as neurotrophic and neuroprotective for enteric neurons including nerve growth factor (NGF), neurotrophin (NT)-3, brain-derived neurotrophic factor (BDNF), and glial cell line-derived neurotrophic factor (GDNF) (Sharkey and Savidge 2014; Steinkamp et al. 2012; Bassotti et al. 2006; von Boyen et al. 2006; 2002).

Extensive leukocyte infiltration through the colonic wall to the level of myenteric ganglia indicated the acute inflammatory process in TNBS-administered guinea-pigs; the severity of inflammatory infiltrate is positively correlated with the severity of IBD (Ng et al. 2009; Ferrante et al. 2006). MSC-based treatments reduced

leukocyte infiltrate consistent with observations in other disease models (Wei et al. 2013; Galindo et al. 2011; Tanaka et al. 2008). The anti-inflammatory effects were maintained for up to 7 days. Although the exact mechanisms underlying immunomodulation by MSCs have not been fully elucidated, it is generally considered that their anti-inflammatory effects occur indirectly through the production of soluble factors or via direct interaction with target cells (Burdon et al. 2011; Chen et al. 2008). In unpublished data from our group, evaluation of the CM reveled many factors with anti-inflammatory properties, however the role that these factors play in the TNBS-inflamed colon requires further investigation.

In Chapter 3, we investigated whether the efficacy of MSCs in acute colitis, as described in Chapter 2, were dose-dependent. We investigated the effects of three differing doses of MSCs: 1×10^5, 1×10^6, and 3×10^6 MSCs, at 3 days post induction of colitis. This study established that the neuroprotective and anti-inflammatory effects of BM-MSCs in TNBS inflammation are dose-dependent; 1×10^5 MSCs accelerated healing of the colonic architecture but had no effect on enteric neuronal loss and nerve fiber degeneration, 1×10^6 MSCs exhibited comparable effects to those reported in Chapter 2, 3×10^6 MSCs provided effects consistent with 1×10^6 MSCs without further benefit. Hence, it was concluded that the optimal dose of MSCs for the treatment of enteric neuropathy associated with TNBS is 1×10^6 MSCs. There is inconsistency regarding the most effective dose of MSCs in both clinical studies and experimental models of IBD (Molendijk et al. 2015; de la Portilla et al. 2013; Fawzy et al. 2013; Garcia-Olmo et al. 2009; 2005; Gonzalez et al. 2009; Ando et al. 2008; Tanaka et al. 2008). However, there is general agreement that an optimal dose of MSCs is required to observe the greatest therapeutic effect. Given that this thesis provides novel evidence for the neuroprotective effects of MSCs in acute TNBS-induced colitis, the establishment of an optimal MSC dose is significant for future investigations into the mechanisms of MSC-based enteric neuroprotection.

Overall, the findings of Chapter 2 and Chapter 3 determine that MSC-based therapies are highly efficacious for the treatment of acute colitis, providing rapid

and long lasting anti-inflammatory and neuroprotective effects in a dose-dependent manner.

8.1.2 Characterization of the *Winnie* mouse model of spontaneously occurring chronic colitis

Since we established that treatment with MSCs averts enteric neuropathy associated with acute colitis, the next step was to investigate the efficacy of MSC therapy in a suitable chronic model of colitis Currently, there are more than 60 established experimental models of colitis. However, most of these models represent the acute inflammatory flares associated with IBD (Mizoguchi 2012). Chronic models of colitis representative of IBD are limited, which is somewhat surprising since IBD is defined as a chronic inflammatory disease. Dextran sulfate sodium (DSS)-induced colitis is the most commonly used model of chronic colitis, however this model is not an accurate mimic of human IBD and symptoms reverse as soon as DSS is removed (Kiesler et al. 2015; De Fazio et al. 2014). Chronic models that truly exhibit the spontaneous relapsing inflammation that is characteristic of IBD are even scarcer. Spontaneous colitis develops in interleukin (IL)-$10^{-/-}$ mice, however their pathogenic relevance is questionable as the deletion of IL-10 gene products, as well as the presence of pathogenic bacteria essential to induce symptoms, suggests they do not fully represent the underlying mechanisms of the disease (Cominelli et al. 2017). Another model of spontaneously occurring colitis is the *Winnie* mouse in which chronic intestinal inflammation results from a primary intestinal epithelial defect conferred by a missense mutation, rather than a deletion, in the *Muc2* mucin gene (Eri et al. 2011; Heazlewood et al. 2008). In *Winnie* mice, the mutation of *Muc2* is comparable to human IBD, where the production and secretion *Muc2* is reduced in active ulcerative colitis (UC) (Heazlewood et al. 2008; Van Klinken et al. 1999) and the expression of *Muc2* is decreased in Crohn's disease (CD) (Buisine et al. 2001). Previous studies have characterized the histopathological and immunological changes in the *Winnie* mouse colon (Eri et al. 2011; McGuckin et al. 2011; Heazlewood et al. 2008; Lourenssen et al. 2005), however analyses of

distal colon innervation, intestinal transit, colonic function, and microbiota have not been conducted.

In Chapter 4, we reported for the first time that innervation of the *Winnie* mouse colon is significantly impaired by chronic inflammation. The density of the all nerve fibers innervating the *Winnie* mouse colon were reduced independent of fiber function. Reductions in the density of sensory, noradrenergic, and cholinergic nerve fibers are observed in IBD patients (Straub et al. 2008; Jonsson et al. 2007; Belai et al. 1997; Eysselein et al. 1992; Koch et al. 1987). Loss of these fiber types in the *Winnie* mouse colon may exacerbate inflammation since they are known to exert anti-inflammatory actions; sensory nerve fibers stimulate the production of mucus for protection of the mucosa and sympathetic and cholinergic neurotransmitters inhibit secretion of pro-inflammatory cytokines (Straub et al. 2008; Holzer 2007; Ulloa 2005; Borovikova et al. 2000). Loss of enteric neurons, with corresponding decreases in number of choline acetyltransferase-IR subpopulations, were evident in the *Winnie* mouse colon which is consistent with previous findings in UC patients (Bernardini et al. 2012). There were no changes in the number of neuronal nitric oxide synthase (nNOS)-IR neurons, however an increase in the proportion of nNOS-IR neurons in the distal colon of *Winnie* mice was observed due to the decrease in the total number of neurons.

Similar to the findings in Chapter 2, loss of myenteric neurons and imbalances in the number and/or proportion of inhibitory and excitatory myenteric neurons affected disruptions in colonic motility in *Winnie* mice. Decreases in the number of colonic migrating motor complexes (CMMCs) corresponded to an increase in fragmented contractions indicating disruption to neural inhibition and circuitry regulating CMMC generation. Increases in the velocity of contractions paralleled a faster colonic transit which may explain chronic diarrhea observed in *Winnie* mice. Chronic diarrhea is a predominant symptom of IBD and its association with active inflammation in these patients is well established (Deiteren et al. 2010; Manabe et al. 2010; Camilleri et al. 2008; Sadik et al. 2008; Hebden et al. 2000).

In Chapter 4, we also addressed the mechanisms that could potentially underlie the observed changes in colonic motility and transit associated with chronic intestinal inflammation. We established that inhibited neuromuscular transmission, including decreases in purinergic fast inhibitory junction potentials and cholinergic excitatory junction potentials, as well as diminished smooth muscle cell responses are responsible for altered motor patterns in the *Winnie* mouse colon. These findings are highly significant since they determine that colonic dysmotility in *Winnie* mouse results from both alterations to ENS output and smooth muscle cell function, comparable to findings in IBD patients and animal models of colitis (Roberts et al. 2013; Strong et al. 2010; Qureshi et al. 2010; Annese et al. 1997; Reddy et al. 1991; Koch et al. 1988).

In Chapter 5, we provided further evidence signifying the relevance of *Winnie* mice as a model to study human IBD. This chapter examined the microbiota and metabolome of fecal samples from *Winnie* mice compared to healthy C57BL/6 mice, finding differences in the fecal microbiome at all formal levels of bacterial taxonomy, including the phylum, class, order, family, genus and species divisions, as well as diminished capacity for amino acid metabolism, production of short chain fatty acids, and breakdown of monosaccharides. While the exact mechanisms of IBD pathogenesis remain unknown, there is substantial evidence to support an integral role for intestinal microbiota in the disease process (Liu et al. 2013; Sartor 2008; Elson et al. 2005). Similar to the findings in Chapter 5, the microbiota of IBD patients are characterized by abnormal compositions (Manichanh et al. 2012; Qin et al. 2010), as well as disturbed metabolites (Manichanh et al. 2012; Thibault et al. 2010; Sartor 2008; Ott et al. 2004). In *Winnie* mice, a thinner mucus layer, due to loss of *Muc2*, increases intestinal permeability, which has also been described in IBD patients (Michielan and D'Inca 2015). A heightened intestinal permeability enhances susceptibility to microbes and toxins normally contained within the lumen leading to imbalances in the gut microbiome and aberrant immune activation, a hallmark feature of IBD (Chichlowski and Hale 2008). Intestinal microbial shifts and subsequent alteration to the metabolic profiles described in *Winnie* mice have been associated with ENS anomalies, colonic dysmotility, and GI symptoms of IBD, such as nausea,

abdominal bloating and cramping, and diarrhea (Linares et al. 2016; Hayes et al. 2014; Brun et al. 2013). Given the findings presented in Chapters 4 and 5, it is clear that the *Winnie* mouse model of spontaneously occurring colitis demonstrates many characteristics observed in IBD patients. Therefore, the main conclusion of these chapters, is that the *Winnie* mouse is highly relevant to human IBD and is extremely significant for future studies investigating the underlying mechanisms of IBD pathogenesis.

8.1.3 MSC therapy for the treatment of enteric neuropathy in the *Winnie* mouse model of spontaneously occurring chronic colitis

Chapters 6 and 7 investigate the effects of MSC treatment on the enteric neuropathy associated with chronic inflammation in the *Winnie* mouse colon described in Chapter 4. In Chapter 2, we reported the beneficial effects of a single 1×10^6 MSC dose in acute TNBS colitis, therefore we hypothesized that this dosage would demonstrate therapeutic effects in the chronically inflamed *Winnie* mouse colon. In Chapter 6, we showed that a single dose of 1×10^6 MSCs did not provide any anti-inflammatory or neurotrophic effects in *Winnie* mice at 3 or 60 days post treatment. In consistency with our findings, a single dose of MSCs did not provide therapeutic effect in other chronic disease models, including multiple sclerosis and osteoarthritis (Ozeki et al. 2016; Payne et al. 2013a; Harris et al. 2012). Conversely, some studies report that a single dose of MSCs is beneficial for chronic diseases, such as kidney disease and type 1 diabetes (Ebrahimi et al. 2013; Zhu et al. 2013; Eirin et al. 2012; Ezquer et al. 2008). Limited studies have investigated the effects of a single administration of MSCs in chronic colitis with conflicting results. Similar to our findings, a single dose of 1×10^6 was was ineffective in attenuating chronic DSS-induced colitis (Yu et al. 2017), however another study report that MSCs reduced disease activity in IL-$10^{-/-}$ mice (Jung et al. 2015). This study administered MSCs at a higher dose than we administered into *Winnie* mice. Variabilities in the number of MSCs administered in a single application may explain why a single dose of MSCs is effective in some studies but not in others; differences in the number of cells available to participate in tissue repair has diverse effects on healing capacity and expression of soluble

factors (Nam et al. 2015; Saether et al. 2014; Kim and Cho 2013). It is therefore possible that the effectiveness of a single MSC dose in *Winnie* mice may be dose-dependent. However, since there is growing support for the application of multiple MSC doses to achieve therapeutic effect, we elected to explore the effects of differing doses of MSCs administered multiple times in Chapter 7.

In Chapter 7, we investigated the anti-inflammatory and neurotrophic effects of multiple administrations of MSCs at a low dose (LD) and a high dose (HD) in the *Winnie* mouse model of chronic colitis at 3 and 60 days post treatment. When administered at a HD, multiple MSC treatments are effective in attenuating inflammation and nerve fiber damage in the *Winnie* mouse colon at 3 days post treatment. Most of the therapeutic effects induced by HD MSC administration were maintained until 60 days post treatment. Conversely multiple administrations of LD MSCs did not have effect, demonstrating similar results to those obtained with a single dose of MSCs in Chapter 6.

In HD MSC-treated *Winnie* mice, pellet formation, absence of diarrhea, and reduced fecal water content correlated with healing of the colonic architecture. MSCs have been demonstrated to release factors known to participate in healing of the intestinal epithelium *in vitro* (Watanabe et al. 2014; Ando et al. 2008; Zvonic et al. 2007; Rehman et al. 2004). Hence, it is plausible to consider that the release of such factors contributes to the restoration of the epithelial barrier in the *Winnie* mouse colon, enhancing water absorption from the lumen and leading to formation of pellets rather than persistent diarrhea. Reductions in fecal lipocalin (Lcn)-2 and leukocyte infiltration throughout the colon wall indicated the anti-inflammatory effect of HD MSCs. As discussed earlier, the anti-inflammatory and immunomodulating actions of MSCs are considered to involve direct cell-cell interactions, as well as indirect interactions via the release of soluble factors (Burdon et al. 2011; Chen et al. 2008). It is well known that the immunomodulation capacity of MSCs requires activation by a pro-inflammatory environment (Ren et al. 2008; Krampera et al. 2006). This suggests that administration of LD MSCs into the chronically inflamed *Winnie* mouse colon would activate these cells to exert anti-inflammatory effects. However, chronic inflammation has been shown

to increase anoikis and hinder the survival of transplanted MSCs, therefore the inflammatory milieu of the *Winnie* mouse colon may be too challenging for LD MSCs to demonstrate immunomodulating and anti-inflammatory effects (Chang et al. 2013; Song et al. 2010; Khansari et al. 2009). Conversely, the increased number of MSCs in HD treatments may be sufficient to overcome these barriers.

HD MSC treatments promoted the regeneration of nerve fibers in the *Winnie* mouse colon, which is consistent with other neural disease models (Onuma-Ukegawa et al. 2015; Qiu et al. 2015; Torres-Espin et al. 2013a; Lopatina et al. 2011). As mentioned above, the capacity of MSCs to enhance nerve fiber regeneration is attributable to their release of growth factors and neurotrophic factors. Evaluation of CM from the MSCs used in this thesis demonstrated that our MSCs release factors that have been shown to promote cholinergic, sympathetic, and sensory nerve fibers in experimental regeneration models, such as BDNF, GDNF, NGF and NT (Yu et al. 2014; Kuihua et al. 2014; Tang et al. 2013; de Boer et al. 2012; Scholz et al. 2010; Glueckert et al. 2008; Katsui et al. 2008; Kemp et al. 2008; Dezawa et al. 2004; Boyd and Gordon 2003; 2002; Jakeman et al. 1998). HD MSC treatments were not efficacious for restoring neuronal loss in the colon of *Winnie* mice. While some studies have demonstrated the potential for MSCs differentiate into neural cells *in vitro* (Bae et al. 2011a; Jang et al. 2010), it is controversial as to whether these cells demonstrate functional characteristics *in vivo*. Additionally, it is consistently shown that engrafted MSCs survive short-term *in vivo*, thus there is minimal or absent long-term engraftment of MSCs nulling the prospect of neuronal differentiation (Parekkadan and Milwid 2010). Overall, the findings in Chapters 6 and 7 indicate that the anti-inflammatory and neurotrophic effects of MSCs in the *Winnie* mouse model of spontaneously occurring chronic colitis are dose-dependent with the dose range higher than for acute colitis.

8.2 Future directions

Several of the factors detected in the CM described in Chapter 2 have been demonstrated as neuroprotective and neurotrophic for enteric neurons, however whether the remaining factors provide neuroprotection for the ENS is currently unknown. Further studies are required to assess the role of these factors in the ENS. Furthermore, we analyzed the secretome of naive MSCs. MSCs are activated by the local microenvironment and respond to these cues by secreting a site-specific array of bioactive molecules (Kean et al. 2013). Hence, it is plausible to consider that under the inflammatory conditions in TNBS-induced colitis, the CM may secrete a wider range of neuroprotective factors than described in Chapter 2. Evaluation of the MSC secretome in a simulated inflammatory milieu and investigations into whether these factors are neurotrophic or neuroprotective for enteric neurons will provide further insight into the mechanisms of MSC-induced neuroprotection in the ENS.

In Chapter 2, we observed substantial myenteric neuronal loss at 24h, but not at 6h post induction of colitis which was consistent with previous findings (Linden et al. 2005). Administration of MSCs and CM prevented the reduction in the total number of enteric neurons at 24h. Hence, it was concluded that MSCs start to exert their neuroprotective effects by 24h after TNBS administration. It has been reported that loss of neurons in the guinea-pig colon occurs by 12h after administration of TNBS (Linden et al. 2005), therefore it is possible that MSCs may start to exert neuroprotective effects prior to the 24h time point. The unpredictable and relapsing nature of IBD means that the exact timing of acute inflammation initiation is unknown. Therefore, whether this warrants further investigation is questionable.

In Chapters 4 and 5, we provided a detailed characterization of the *Winnie* mouse model of spontaneously occurring chronic colitis, including changes to innervation, intestinal transit, colonic motility, neuromuscular transmission and smooth muscle cell responses. Loss of nerve fibers and enteric neurons in the *Winnie* mouse colon produces disruptions in colonic motility and faster colonic

transit which can be correlated to chronic diarrhea observed in this model. An increase in the propulsion of contents along the colon would reduce the contact time of fecal material with the mucosa and diminish absorption of water and electrolytes (Sarna 2010). Furthermore, increased fecal water content observed in *Winnie* mice may be associated with impaired absorption. Alterations to absorptive and secretory functions are described in colons from UC patients and suggested to play a role in the persistent diarrhea reported by these patients (Gustafsson et al. 2012; Van Klinken et al. 1999). Whether there is impairment of these functions in the inflamed *Winnie* mouse colon is unknown. Therefore, an investigation of absorption and secretion capacities in the *Winnie* mouse colon would be useful for future studies incorporating this model to aid understanding of the mechanisms underlying IBD.

In Chapter 6, we demonstrated that a single dose of MSCs is ineffective in attenuating inflammation and enteric neuropathy in the *Winnie* mouse colon. While some studies investigating the effects of single dose MSC administration support our findings, others do not. This may be due to varying numbers of MSCs per dose and suggests that the effectiveness of a single MSC dose in *Winnie* mice may be dose-dependent. Although we demonstrate the therapeutic effects of multiple administrations of HD MSCs in Chapter 7, a study investigating whether a single dose is effective at higher doses may be valuable. The prospect of a single dose versus a multiple dose regime would be more beneficial to a clinical setting, saving time, costs, and patient stress.

The anti-inflammatory and neuroprotective effects of multiple administrations of HD MSCs in the *Winnie* mouse colon were demonstrated in Chapter 7. The establishment of an optimal MSC dosing regimen for the attenuation of inflammation and regeneration of nerve fibers in chronic colitis is a leading step for many future studies. In Chapters 4 and 5, we validated the relevance of the *Winnie* mouse model of chronic colitis to human IBD. Further studies should investigate the efficacy of multiple HD MSC treatments in attenuating colonic dysmotility and transit, as well as changes in neuromuscular transmission and smooth muscle cell responses. Analysis of the microbiota and metabolome in

fecal samples from *Winnie* mice treated with HD MSCs should be conducted. Additionally, systemic routes of administration should be tested since they are currently in use for IBD patients in clinical studies. The findings of such investigations would be highly significant and beneficial to future clinical investigations.

8.3 General conclusions

The studies within this thesis have provided many novel findings which have contributed to the existing literature and will assist future investigations. In Chapters 2 and 3, we showed that MSC-based therapies administered by enema attenuate inflammation and avert enteric neuropathy and colonic dysmotility associated with acute TNBS-induced colitis in guinea-pigs in a dose-dependent manner. Acute inflammatory flares that are a hallmark feature of IBD, therefore the anti-inflammary, immunomodulatory and neuroprotecive effects of MSCs and CM demonstrated in this model are highly translational to clinical investigations. Chapters 4 and 5 provide novel investigations and characterization of a chronic model of IBD. These studies provided substantial evidence that the *Winnie* mouse model of spontaneously occurring chronic colitis is highly representative of human IBD and extremely relevant for use in investigations into IBD pathogenesis. Chapters 6 and 7 established that the anti-inflammatory and neurotrophic effects of MSCs are dose-dependent in the chronically inflamed *Winnie* mouse colon. These chapters establish the optimal dose of MSCs for the attenuation of colonic inflammation and regeneration of nerve fibers in *Winnie* mice. Overall, the results of these studies show that a higher dose of MSCs administered multiple times is required in chronic colitis as compared to acute colitis. Collectively, the results of these chapters are significant for clinical application and for future investigations into the mechanisms of MSC therapy in acute and chronic colitis. Future studies into the effects of HD MSC treatments on changes to colonic motility and transit, neuromuscular transmission and smooth muscle responses are necessitated for continuation of the studies presented in this thesis.

CHAPTER NINE: REFERENCES

Aali, E., Mirzamohammadi, S., Ghaznavi, H., Madjd, Z., Larijani, B., Rayegan, S., Sharifi, A. M. 2014. A comparative study of mesenchymal stem cell transplantation with its paracrine effect on control of hyperglycemia in type 1 diabetic rats. *J Diabetes Metab Disord,* 13, 76.

Aberra, F. N., Lichtenstein, G. R. 2005. Monitoring of immunomodulators in inflammatory bowel disease. *Aliment Pharmacol Ther,* 21, 307-19.

Abouelkheir, M., El Tantawy, D. A., Saad, M. A., Abdelrahman, K. M., Sobh, M. A., Lotfy, A., Sobh, M. A. 2016. Mesenchymal stem cells versus their conditioned medium in the treatment of cisplatin-induced acute kidney injury: Evaluation of efficacy and cellular side effects. *Int J Clin Exp Med,* 9, 23222-34.

Abraham, C., Cho, J. H. 2009. Inflammatory bowel disease. *N Engl J Med,* 361, 2066-78.

Adamzyk, C., Emonds, T., Falkenstein, J., Tolba, R., Jahnen-Dechent, W., Lethaus, B., Neuss, S. 2013. Different culture media affect proliferation, surface epitope expression, and differentiation of ovine MSC. *Stem Cells Int,* 2013, 387324.

Aggarwal, S., Pittenger, M. F. 2005. Human mesenchymal stem cells modulate allogeneic immune cell responses. *Blood,* 105, 1815-22.

Ahmed, I., Greenwood, R., Costello, B., Ratcliffe, N., Probert, C. S. 2016. Investigation of faecal volatile organic metabolites as novel diagnostic biomarkers in inflammatory bowel disease. *Aliment Pharmacol Ther,* 43, 596-611.

Akiyama, K., Chen, C., Wang, D., Xu, X., Qu, C., Yamaza, T., Cai, T., Chen, W., Sun, L., Shi, S. 2012. Mesenchymal stem cell-induced immunoregulation involves FAS ligand/FAS-mediated T cell apoptosis. *Cell Stem Cell,* 10, 544-55.

Al Jumah, M. A., Abumaree, M. H. 2012. The immunomodulatory and neuroprotective effects of mesenchymal stem cells (MSCs) in experimental autoimmune encephalomyelitis (EAE): A model of multiple sclerosis (MS). *Int J Mol Sci,* 13, 9298-331.

Aldini, R., Budriesi, R., Roda, G., Micucci, M., Ioan, P., D'Errico-Grigioni, A., Sartini, A., Guidetti, E., Marocchi, M., Cevenini, M., Rosini, F., Montagnani, M., Chiarini, A., Mazzella, G. 2012. Curcuma longa extract exerts a myorelaxant effect on the ileum and colon in a mouse experimental colitis model, independent of the anti-inflammatory effect. *PLoS One,* 7, e44650.

Alex, G., Clerc, N., Kunze, W. A., Furness, J. B. 2002. Responses of myenteric S neurones to low frequency stimulation of their synaptic inputs. *Neuroscience,* 110, 361-73.

Alex, G., Kunze, W. A., Furness, J. B., Clerc, N. 2001. Comparison of the effects of neurokinin-3 receptor blockade on two forms of slow synaptic transmission in myenteric AH neurons. *Neuroscience,* 104, 263-9.

Alexanian, A. R., Kwok, W. M., Pravdic, D., Maiman, D. J., Fehlings, M. G. 2010. Survival of neurally induced mesenchymal cells may determine degree of motor recovery in injured spinal cord rats. *Restor Neurol Neurosci,* 28, 761-7.

Alkadhi, S., Kunde, D., Cheluvappa, R., Randall-Demllo, S., Eri, R. 2014. The murine appendiceal microbiome is altered in spontaneous colitis and its pathological progression. *Gut Pathog,* 6, 25.

An, S. Y., Han, J., Lim, H. J., Park, S. Y., Kim, J. H., Do, B. R., Kim, J. H. 2014. Valproic acid promotes differentiation of hepatocyte-like cells from whole human umbilical cord-derived mesenchymal stem cells. *Tissue Cell,* 46, 127-35.

Ananthakrishnan, A. N. 2015. Epidemiology and risk factors for IBD. *Nat Rev Gastroenterol Hepatol,* 12, 205-17.

Anderson, P., Souza-Moreira, L., Morell, M., Caro, M., O'Valle, F., Gonzalez-Rey, E., Delgado, M. 2013. Adipose-derived mesenchymal stromal cells induce immunomodulatory macrophages which protect from experimental colitis and sepsis. *Gut,* 62, 1131-41.

Ando, Y., Inaba, M., Sakaguchi, Y., Tsuda, M., Quan, G. K., Omae, M., Okazaki, K., Ikehara, S. 2008. Subcutaneous adipose tissue-derived stem cells facilitate colonic mucosal recovery from 2,4,6-trinitrobenzene sulfonic acid (TNBS)-induced colitis in rats. *Inflamm Bowel Dis,* 14, 826-38.

Andoh, A., Imaeda, H., Aomatsu, T., Inatomi, O., Bamba, S., Sasaki, M., Saito, Y., Tsujikawa, T., Fujiyama, Y. 2011. Comparison of the fecal microbiota profiles between ulcerative colitis and Crohn's disease using terminal restriction fragment length polymorphism analysis. *J Gastroenterol,* 46, 479-86.

Andou, A., Hisamatsu, T., Okamoto, S., Chinen, H., Kamada, N., Kobayashi, T., Hashimoto, M., Okutsu, T., Shimbo, K., Takeda, T., Matsumoto, H., Sato, A., Ohtsu, H., Suzuki, M., Hibi, T. 2009. Dietary histidine ameliorates murine colitis by inhibition of proinflammatory cytokine production from macrophages. *Gastroenterology,* 136, 564-74.e2.

Ankrum, J., Karp, J. M. 2010. Mesenchymal stem cell therapy: Two steps forward, one step back. *Trends Mol Med,* 16, 203-9.

Anlauf, M., Schäfer, M. K. H., Eiden, L., Weihe, E. 2003. Chemical coding of the human gastrointestinal nervous system: Cholinergic, VIPergic, and catecholaminergic phenotypes. *J Comp Neurol,* 459, 90-111.

Annese, V., Bassotti, G., Napolitano, G., Usai, P., Andriulli, A., Vantrappen, G. 1997. Gastrointestinal motility disorders in patients with inactive Crohn's disease. *Scand J Gastroenterol,* 32, 1107-17.

Antharam, V. C., McEwen, D. C., Garrett, T. J., Dossey, A. T., Li, E. C., Kozlov, A. N., Mesbah, Z., Wang, G. P. 2016. An integrated metabolomic and microbiome analysis identified specific gut microbiota associated with fecal cholesterol and coprostanol in *Clostridium difficile* infection. *PLoS One,* 11, e0148824.

Antunes, M. A., Laffey, J. G., Pelosi, P., Rocco, P. R. 2014. Mesenchymal stem cell trials for pulmonary diseases. *J Cell Biochem,* 115, 1023-32.

Arasaradnam, R. P., Pharaoh, M. W., Williams, G. J., Nwokolo, C. U., Bardhan, K. D., Kumar, S. 2009. Colonic fermentation--more than meets the nose. *Med Hypotheses,* 73, 753-6.

Ardizzone, S., Porro, G. B. 2002. Inflammatory bowel disease: New insights into pathogenesis and treatment. *J Intern Med,* 252, 475-96.

Assis, A. C., Carvalho, J. L., Jacoby, B. A., Ferreira, R. L., Castanheira, P., Diniz, S. O., Cardoso, V. N., Goes, A. M., Ferreira, A. J. 2010. Time-dependent migration of systemically delivered bone marrow mesenchymal stem cells to the infarcted heart. *Cell Transplant,* 19, 219-30.

Atreya, I., Atreya, R., Neurath, M. F. 2008. NF-kappaB in inflammatory bowel disease. *J Intern Med,* 263, 591-6.

Audet, J., Miller, C. L., Eaves, C. J., Piret, J. M. 2002. Common and distinct features of cytokine effects on hematopoietic stem and progenitor cells revealed by dose-response surface analysis. *Biotechnol Bioeng,* 80, 393-404.

Audet, J., Miller, C. L., Rose-John, S., Piret, J. M., Eaves, C. J. 2001. Distinct role of gp130 activation in promoting self-renewal divisions by mitogenically stimulated murine hematopoietic stem cells. *Proc Natl Acad Sci U S A,* 98, 1757-62.

Ayache, S. S., Chalah, M. A. 2016. Stem cells therapy in multiple sclerosis - a new hope for progressive forms. *J Stem Cells Regen Med,* 12, 49-51.

Badillo, A. T., Peranteau, W. H., Heaton, T. E., Quinn, C., Flake, A. W. 2008. Murine bone marrow derived stromal progenitor cells fail to prevent or treat acute graft-versus-host disease. *Br J Haematol,* 141, 224-34.

Bae, K. S., Park, J. B., Kim, H. S., Kim, D. S., Park, D. J., Kang, S. J. 2011a. Neuron-like differentiation of bone marrow-derived mesenchymal stem cells. *Yonsei Med J,* 52, 401-12.

Bae, K. S., Park, J. B., Kim, H. S., Kim, D. S., Park, D. J., Kang, S. J. 2011b. Neuron-like differentiation of bone marrow-derived mesenchymal stem cells. *Yonsei Med J,* 52, 401-12.

Bagyanszki, M., Bodi, N. 2012. Diabetes-related alterations in the enteric nervous system and its microenvironment. *World J Diabetes,* 3, 80-93.

Bai, L., Lennon, D. P., Caplan, A. I., DeChant, A., Hecker, J., Kranso, J., Zaremba, A., Miller, R. H. 2012. Hepatocyte growth factor mediates mesenchymal stem cell-induced recovery in multiple sclerosis models. *Nat Neurosci,* 15, 862-70.

Bai, L., Lennon, D. P., Eaton, V., Maier, K., Caplan, A. I., Miller, S. D., Miller, R. H. 2009. Human bone marrow-derived mesenchymal stem cells induce Th2-polarized immune response and promote endogenous repair in animal models of multiple sclerosis. *Glia,* 57, 1192-203.

Bakhtiar, S. M., LeBlanc, J. G., Salvucci, E., Ali, A., Martin, R., Langella, P., Chatel, J. M., Miyoshi, A., Bermudez-Humaran, L. G., Azevedo, V. 2013. Implications of the human microbiome in inflammatory bowel diseases. *FEMS Microbiol Lett,* 342, 10-7.

Balasubramanian, K., Kumar, S., Singh, R. R., Sharma, U., Ahuja, V., Makharia, G. K., Jagannathan, N. R. 2009. Metabolism of the colonic mucosa in patients with inflammatory bowel diseases: An *in vitro* proton magnetic resonance spectroscopy study. *Magn Reson Imaging,* 27, 79-86.

Ball, S. G., Shuttleworth, C. A., Kielty, C. M. 2007. Vascular endothelial growth factor can signal through platelet-derived growth factor receptors. *J Cell Biol,* 177, 489-500.

Bampton, P. A., Dinning, P. G., Kennedy, M. L., Lubowski, D. Z., Cook, I. J. 2002. The proximal colonic motor response to rectal mechanical and chemical stimulation. *Am J Physiol Gastrointest Liver Physiol,* 282, G443-9.

Banas, A., Teratani, T., Yamamoto, Y., Tokuhara, M., Takeshita, F., Osaki, M., Kawamata, M., Kato, T., Okochi, H., Ochiya, T. 2008. IFATS collection: *In vivo* therapeutic potential of human adipose tissue mesenchymal stem cells after transplantation into mice with liver injury. *Stem Cells,* 26, 2705-12.

Bang, O. Y., Lee, J. S., Lee, P. H., Lee, G. 2005. Autologous mesenchymal stem cell transplantation in stroke patients. *Ann Neurol,* 57, 874-82.

Bannaga, A. S., Selinger, C. P. 2015. Inflammatory bowel disease and anxiety: Links, risks, and challenges faced. *Clin Exp Gastroenterol,* 8, 111-7.

Bao, X., Wei, J., Feng, M., Lu, S., Li, G., Dou, W., Ma, W., Ma, S., An, Y., Qin, C., Zhao, R. C., Wang, R. 2011. Transplantation of human bone marrow-derived mesenchymal stem cells promotes behavioral recovery and endogenous neurogenesis after cerebral ischemia in rats. *Brain Res,* 1367, 103-13.

Barlow, S., Brooke, G., Chatterjee, K., Price, G., Pelekanos, R., Rossetti, T., Doody, M., Venter, D., Pain, S., Gilshenan, K., Atkinson, K. 2008. Comparison of human placenta- and bone marrow-derived multipotent mesenchymal stem cells. *Stem Cells Dev,* 17, 1095-107.

Barrett, J. S., Irving, P. M., Shepherd, S. J., Muir, J. G., Gibson, P. R. 2009. Comparison of the prevalence of fructose and lactose malabsorption across chronic intestinal disorders. *Aliment Pharmacol Ther,* 30, 165-74.

Barry, F. P., Murphy, J. M. 2004. Mesenchymal stem cells: Clinical applications and biological characterization. *Int J Biochem Cell Biol,* 36, 568-84.

Bassotti, G., Villanacci, V., Antonelli, E., Morelli, A., Salerni, B. 2007. Enteric glial cells: New players in gastrointestinal motility? *Lab Invest,* 87, 628-32.

Bassotti, G., Villanacci, V., Maurer, C. A., Fisogni, S., Di Fabio, F., Cadei, M., Morelli, A., Panagiotis, T., Cathomas, G., Salerni, B. 2006. The role of glial cells and apoptosis of enteric neurones in the neuropathology of intractable slow transit constipation. *Gut,* 55, 41-6.

Baumgart, D. C., Carding, S. R. 2007. Inflammatory bowel disease: Cause and immunobiology. *The Lancet,* 369, 1627-40.

Baumgart, D. C., Sandborn, W. J. 2007. Inflammatory bowel disease: Clinical aspects and established and evolving therapies. *Lancet,* 369, 1641-57.

Beale, D. J., Marney, D., Marlow, D. R., Morrison, P. D., Dunn, M. S., Key, C., Palombo, E. A. 2013. Metabolomic analysis of *Cryptosporidium parvum* oocysts in water: A proof of concept demonstration. *Environ Pollut,* 174, 201-3.

Beale, D. J., Morrison, P. D., Palombo, E. A. 2014. Detection of Listeria in milk using non-targeted metabolic profiling of *Listeria monocytogenes*: A proof-of-concept application. *Food Control,* 42, 343-6.

Becker, C., Neurath, M. F., Wirtz, S. 2015a. The intestinal microbiota in inflammatory bowel disease. *ILAR J,* 56, 192-204.

Becker, H. M., Grigat, D., Ghosh, S., Kaplan, G. G., Dieleman, L., Wine, E., Fedorak, R. N., Fernandes, A., Panaccione, R., Barkema, H. W. 2015b. Living with inflammatory bowel disease: A Crohn's and Colitis Canada survey. *Can J Gastroenterol Hepatol,* 29, 77-84.

Belai, A., Boulos, P. B., Robson, T., Burnstock, G. 1997. Neurochemical coding in the small intestine of patients with Crohn's disease. *Gut,* 40, 767-74.

Bernalier-Donadille, A. 2010. [Fermentative metabolism by the human gut microbiota]. *Gastroenterol Clin Biol,* 34, S16-22.

Bernardini, N., Segnani, C., Ippolito, C., De Giorgio, R., Colucci, R., Faussone-Pellegrini, M. S., Chiarugi, M., Campani, D., Castagna, M., Mattii, L., Blandizzi, C., Dolfi, A. 2012. Immunohistochemical analysis of myenteric ganglia and interstitial cells of Cajal in ulcerative colitis. *J Cell Mol Med,* 16, 318-27.

Bernardo, M. E., Fibbe, W. E. 2013. Mesenchymal stromal cells: Sensors and switchers of inflammation. *Cell Stem Cell,* 13, 392-402.

Bernstein, C. N., Fried, M., Krabshuis, J. H., Cohen, H., Eliakim, R., Fedail, S., Gearry, R., Goh, K. L., Hamid, S., Khan, A. G., LeMair, A. W., Malfertheiner, Ouyang, Q., Rey, J. F., Sood, A., Steinwurz, F., Thomsen, O. O., Thomson, A., Watermeyer, G. 2010. World Gastroenterology Organization Practice Guidelines for the diagnosis and management of IBD in 2010. *Inflamm Bowel Dis,* 16, 112-24.

Bhansali, S., Kumar, V., Saikia, U. N., Medhi, B., Jha, V., Bhansali, A., Dutta, P. 2015. Effect of mesenchymal stem cells transplantation on glycaemic profile & their localization in streptozotocin induced diabetic Wistar rats. *Indian J Med Res,* 142, 63-71.

Bibiloni, R., Mangold, M., Madsen, K. L., Fedorak, R. N., Tannock, G. W. 2006. The bacteriology of biopsies differs between newly diagnosed, untreated, Crohn's disease and ulcerative colitis patients. *J Med Microbiol,* 55, 1141-9.

Bielefeldt, K., Davis, B., Binion, D. G. 2009. Pain and inflammatory bowel disease. *Inflamm Bowel Dis,* 15, 778-88.

Birch, D., Knight, G. E., Boulos, P. B., Burnstock, G. 2008. Analysis of innervation of human mesenteric vessels in non-inflamed and inflamed bowel - a confocal and functional study. *Neurogastroenterol Motil,* 20, 660-70.

Bjerrum, J. T., Wang, Y., Hao, F., Coskun, M., Ludwig, C., Gunther, U., Nielsen, O. H. 2015. Metabonomics of human fecal extracts characterize ulcerative colitis, Crohn's disease and healthy individuals. *Metabolomics,* 11, 122-33.

Blachier, F., Mariotti, F., Huneau, J. F., Tome, D. 2007. Effects of amino acid-derived luminal metabolites on the colonic epithelium and physiopathological consequences. *Amino Acids,* 33, 547-62.

Blandizzi, C., Fornai, M., Colucci, R., Baschiera, F., Barbara, G., De Giorgio, R., De Ponti, F., Breschi, M. C., Del Tacca, M. 2003. Altered prejunctional modulation of intestinal cholinergic and noradrenergic pathways by α2-adrenoceptors in the presence of experimental colitis. *Br J Pharmacol,* 139, 309-20.

Blennerhassett, M. G., Bovell, F. M., Lourenssen, S., McHugh, K. M. 1999. Characteristics of inflammation-induced hypertrophy of rat intestinal smooth muscle cell. *Dig Dis Sci,* 44, 1265-72.

Blennerhassett, M. G., Vignjevic, P., Vermillion, D. L., Collins, S. M. 1992. Inflammation causes hyperplasia and hypertrophy in smooth muscle of rat small intestine. *Am J Physiol,* 262, G1041-6.

Bochkov, D. V., Sysolyatin, S. V., Kalashnikov, A. I., Surmacheva, I. A. 2012. Shikimic acid: Review of its analytical, isolation, and purification techniques from plant and microbial sources. *J Chem Biol,* 5, 5-17.

Bodger, K. 2011. Cost effectiveness of treatments for inflammatory bowel disease. *Pharmacoeconomics,* 29, 387-401.

Boesmans, W., Gomes, P., Janssens, J., Tack, J., Vanden Berghe, P. 2008. Brain-derived neurotrophic factor amplifies neurotransmitter responses and promotes synaptic communication in the enteric nervous system. *Gut,* 57, 314-22.

Bohles, H., Beifuss, O. J., Brandl, U., Pichl, J., Akcetin, Z., Demling, L. 1988. Urinary factors of kidney stone formation in patients with Crohn's disease. *Klin Wochenschr,* 66, 87-91.

Boirivant, M., Cossu, A. 2012. Inflammatory bowel disease. *Oral Dis,* 18, 1-15.

Borm, M. E. A., Bouma, G. 2004. Animal models of inflammatory bowel disease. *Drug Discov Today Dis Models* 1, 437-43.

Bornstein, J. C. 2006. Intrinsic sensory neurons of mouse gut--toward a detailed knowledge of enteric neural circuitry across species. Focus on "characterization of myenteric sensory neurons in the mouse small intestine". *J Neurophysiol,* 96, 973-4.

Bornstein, J. C. 2008. Purinergic mechanisms in the control of gastrointestinal motility. *Purinergic Signal,* 4, 197-212.

Bornstein, J. C., Costa, M., Grider, J. R. 2004. Enteric motor and interneuronal circuits controlling motility. *Neurogastroenterol Motil,* 16 Suppl 1, 34-8.

Bornstein, J. C., Furness, J. B., Kunze, W. A. A., Bertrand, P. P. 2002. Enteric reflexes that influence motility. *In:* BROOKES, S. J. H. & COSTA, M. (eds.) *Innervation of the gastrointestinal tract.* London: Taylor Francis.

Bornstein, J. C., Hendriks, R., Furness, J. B., Trussell, D. C. 1991. Ramifications of the axons of AH-neurons injected with the intracellular marker biocytin in the myenteric plexus of the guinea pig small intestine. *J Comp Neurol,* 314, 437-51.

Borovikova, L. V., Ivanova, S., Zhang, M., Yang, H., Botchkina, G. I., Watkins, L. R., Wang, H., Abumrad, N., Eaton, J. W., Tracey, K. J. 2000. Vagus nerve stimulation attenuates the systemic inflammatory response to endotoxin. *Nature,* 405, 458-62.

Boulland, J. L., Leung, D. S., Thuen, M., Vik-Mo, E., Joel, M., Perreault, M. C., Langmoen, I. A., Haraldseth, O., Glover, J. C. 2012. Evaluation of intracellular labeling with micron-sized particles of iron oxide (MPIOs) as a general tool for *in vitro* and *in vivo* tracking of human stem and progenitor cells. *Cell Transplant,* 21, 1743-59.

Boyd, J. G., Gordon, T. 2002. A dose-dependent facilitation and inhibition of peripheral nerve regeneration by brain-derived neurotrophic factor. *Eur J Neurosci,* 15, 613-26.

Boyd, J. G., Gordon, T. 2003. Glial cell line-derived neurotrophic factor and brain-derived neurotrophic factor sustain the axonal regeneration of chronically axotomized motoneurons in vivo. *Exp Neurol,* 183, 610-9.

Boyer, L., Ghoreishi, M., Templeman, V., Vallance, B. A., Buchan, A. M., Jevon, G., Jacobson, K. 2005. Myenteric plexus injury and apoptosis in experimental colitis. *Auton Neurosci,* 117, 41-53.

Boyer, L., Sidpra, D., Jevon, G., Buchan, A. M., Jacobson, K. 2007. Differential responses of VIPergic and nitrergic neurons in paediatric patients with Crohn's disease. *Auton Neurosci,* 134, 106-14.

Bravo, B., Gallego, M. I., Flores, A. I., Bornstein, R., Puente-Bedia, A., Hernandez, J., de la Torre, P., Garcia-Zaragoza, E., Perez-Tavarez, R., Grande, J., Ballester, A., Ballester, S. 2016. Restrained Th17 response and myeloid cell infiltration into the central nervous system by human decidua-derived mesenchymal stem cells during experimental autoimmune encephalomyelitis. *Stem Cell Res Ther,* 7, 43.

Brehmer, A., Schrodl, F., Neuhuber, W. 1999. Morphological classifications of enteric neurons--100 years after Dogiel. *Anat Embryol (Berl),* 200, 125-35.

Brenneman, D. E., Hauser, J., Spong, C. Y., Phillips, T. M. 2000. Chemokines released from astroglia by vasoactive intestinal peptide. Mechanism of neuroprotection from HIV envelope protein toxicity. *Ann N Y Acad Sci,* 921, 109-14.

Breuer, R. I., Soergel, K. H., Lashner, B. A., Christ, M. L., Hanauer, S. B., Vanagunas, A., Harig, J. M., Keshavarzian, A., Robinson, M., Sellin, J. H., Weinberg, D., Vidican, D. E., Flemal, K. L., Rademaker, A. W. 1997. Short chain fatty acid rectal irrigation for left-sided ulcerative colitis: A randomised, placebo controlled trial. *Gut,* 40, 485-91.

Brierley, S. M., Linden, D. R. 2014. Neuroplasticity and dysfunction after gastrointestinal inflammation. *Nat Rev Gastroenterol Hepatol,* 11, 611-27.

Brierley, S. M., Nichols, K., Grasby, D. J., Waterman, S. A. 2001. Neural mechanisms underlying migrating motor complex formation in mouse isolated colon. *Br J Pharmacol,* 132, 507-17.

Brookes, S. J., Song, Z. M., Ramsay, G. A., Costa, M. 1995. Long aboral projections of Dogiel type II, AH neurons within the myenteric plexus of the guinea pig small intestine. *J Neurosci,* 15, 4013-22.

Brown, I. A. M., McClain, J. L., Watson, R. E., Patel, B. A., Gulbransen, B. D. 2016. Enteric glia mediate neuron death in colitis through purinergic pathways that require connexin-43 and nitric oxide. *Cell Mol Gastroenterol Hepatol,* 2, 77-91.

Browning, K. N., Travagli, R. A. 2014. Central nervous system control of gastrointestinal motility and secretion and modulation of gastrointestinal functions. *Compr Physiol,* 4, 1339-68.

Brun, P., Giron, M. C., Qesari, M., Porzionato, A., Caputi, V., Zoppellaro, C., Banzato, S., Grillo, A. R., Spagnol, L., De Caro, R., Pizzuti, D., Barbieri, V., Rosato, A., Sturniolo, G. C., Martines, D., Zaninotto, G., Palu, G., Castagliuolo, I. 2013. Toll-like receptor 2 regulates intestinal inflammation by controlling integrity of the enteric nervous system. *Gastroenterology,* 145, 1323-33.

Bruno, S., Grange, C., Deregibus, M. C., Calogero, R. A., Saviozzi, S., Collino, F., Morando, L., Busca, A., Falda, M., Bussolati, B., Tetta, C., Camussi, G. 2009. Mesenchymal stem cell-derived microvesicles protect against acute tubular injury. *J Am Soc Nephrol,* 20, 1053-67.

Buchholz, B. M., Bauer, A. J. 2010. Membrane TLR signaling mechanisms in the gastrointestinal tract during sepsis. *Neurogastroenterol Motil,* 22, 232-45.

Buisine, M. P., Desreumaux, P., Leteurtre, E., Copin, M. C., Colombel, J. F., Porchet, N., Aubert, J. P. 2001. Mucin gene expression in intestinal epithelial cells in Crohn's disease. *Gut,* 49, 544-51.

Buisson, A., Chevaux, J. B., Allen, P. B., Bommelaer, G., Peyrin-Biroulet, L. 2012. The natural history of postoperative Crohn's disease recurrence. *Aliment Pharmacol Ther,* 35, 625-33.

Burdon, T. J., Paul, A., Noiseux, N., Prakash, S., Shum-Tim, D. 2011. Bone marrow stem cell derived paracrine factors for regenerative medicine: Current perspectives and therapeutic potential. *Bone Marrow Res,* 2011, 207326.

Burisch, J., Jess, T., Martinato, M., Lakatos, P. L. 2013. The burden of inflammatory bowel disease in Europe. *J Crohns Colitis,* 7, 322-37.

Burns, J. S., Abdallah, B. M., Guldberg, P., Rygaard, J., Schroder, H. D., Kassem, M. 2005. Tumorigenic heterogeneity in cancer stem cells evolved from long-term cultures of telomerase-immortalized human mesenchymal stem cells. *Cancer Res,* 65, 3126-35.

Bush, T. G., Spencer, N. J., Watters, N., Sanders, K. M., Smith, T. K. 2000. Spontaneous migrating motor complexes occur in both the terminal ileum and colon of the C57BL/6 mouse *in vitro*. *Autonom Neurosci,* 84, 162-8.

Bush, T. G., Spencer, N. J., Watters, N., Sanders, K. M., Smith, T. K. 2001. Effects of alosetron on spontaneous migrating motor complexes in murine small and large bowel *in vitro*. *Am J Physiol Gastrointest Liver Physiol,* 281, G974-83.

Bussolati, B. 2011. Stem cells for organ repair: Support or replace? *Organogenesis,* 7, 95.

Bywater, R. A., Small, R. C., Taylor, G. S. 1989. Neurogenic slow depolarizations and rapid oscillations in the membrane potential of circular muscle of mouse colon. *J Physiol,* 413, 505-19.

Calligaris, S. D., Conget, P. 2013. Intravenous administration of bone marrow-derived multipotent mesenchymal stromal cells has a neutral effect on obesity-induced diabetic cardiomyopathy. *Biol Res,* 46, 251-5.

Camilleri, M., McKinzie, S., Busciglio, I., Low, P. A., Sweetser, S., Burton, D., Baxter, K., Ryks, M., Zinsmeister, A. R. 2008. Prospective study of motor, sensory, psychological and autonomic functions in patients with irritable bowel syndrome. *Clin Gastroenterol Hepatol,* 6, 772-81.

Campbell, C., Grapov, D., Fiehn, O., Chandler, C. J., Burnett, D. J., Souza, E. C., Casazza, G. A., Gustafson, M. B., Keim, N. L., Newman, J. W., Hunter, G. R., Fernandez, J. R., Garvey, W. T., Harper, M. E., Hoppel, C. L., Meissen, J. K., Take, K., Adams, S. H. 2014. Improved metabolic health alters host metabolism in parallel with changes in systemic xeno-metabolites of gut origin. *PLoS One,* 9, e84260.

Capasso, R., Orlando, P., Pagano, E., Aveta, T., Buono, L., Borrelli, F., Di Marzo, V., Izzo, A. A. 2014. Palmitoylethanolamide normalizes intestinal motility in a model of post-inflammatory accelerated transit: involvement of CB(1) receptors and TRPV1 channels. *Br J Pharmacol,* 171, 4026-37.

Caplan, A. I., Dennis, J. E. 2006. Mesenchymal stem cells as trophic mediators. *J Cell Biochem,* 98, 1076-84.

Caporaso, J. G., Kuczynski, J., Stombaugh, J., Bittinger, K., Bushman, F. D., Costello, E. K., Fierer, N., Pena, A. G., Goodrich, J. K., Gordon, J. I., Huttley, G. A., Kelley, S. T., Knights, D., Koenig, J. E., Ley, R. E., Lozupone, C. A., McDonald, D., Muegge, B. D., Pirrung, M., Reeder, J., Sevinsky, J. R., Turnbaugh, P. J., Walters, W. A., Widmann, J., Yatsunenko, T., Zaneveld, J., Knight, R. 2010. QIIME allows analysis of high-throughput community sequencing data. *Nat Methods,* 7, 335-6.

Carbone, S. E., Wattchow, D. A., Spencer, N. J., Brookes, S. J. 2012. Loss of responsiveness of circular smooth muscle cells from the guinea pig ileum is associated with changes in gap junction coupling. *Am J Physiol Gastrointest Liver Physiol,* 302, G1434-44.

Carbone, S. E., Wattchow, D. A., Spencer, N. J., Hibberd, T. J., Brookes, S. J. H. 2014. Damage from dissection is associated with reduced neuro-musclar transmission and gap junction coupling between circular muscle cells of guinea pig ileum, *in vitro*. *Front Physiol,* 5, 319.

Carlson, N. G., Wieggel, W. A., Chen, J., Bacchi, A., Rogers, S. W., Gahring, L. C. 1999. Inflammatory cytokines IL-1 alpha, IL-1 beta, IL-6, and TNF-alpha impart neuroprotection to an excitotoxin through distinct pathways. *J Immunol,* 163, 3963-8.

Carter, M., Lobo, A., Travis, S. 2004. Guidelines for the management of inflammatory bowel disease in adults. *Gut,* 53, v1-16.

Carvalho, A. B., Quintanilha, L. F., Dias, J. V., Paredes, B. D., Mannheimer, E. G., Carvalho, F. G., Asensi, K. D., Gutfilen, B., Fonseca, L. M. B., Resende, C. M. C., Rezende, G. F. M., Takiya, C. M., de Carvalho, A. C. C., Goldenberg, R. C. S. 2008. Bone marrow multipotent mesenchymal stromal cells do not reduce fibrosis or improve function in a rat model of severe chronic liver injury. *Stem Cells,* 26, 1307-14.

Casas, I. A., Dobrogosz, W. J. 2011. Validation of the probiotic concept: *Lactobacillus reuteri* confers broad-spectrum protection against disease in humans and animals. *Microb Ecol Health Dis,* 12, 247-85

Castelo-Branco, M. T. L., Soares, I. D. P., Lopes, D. V., Buongusto, F., Martinusso, C. A., do Rosario, A., Souza, S. A. L., Gutfilen, B., Fonseca, L. M. B., Elia, C., Madi, K., Schanaider, A., Rossi, M. I. D., Souza, H. S. P. 2012. Intraperitoneal but not intravenous cryopreserved mesenchymal stromal cells home to the inflamed colon and ameliorate experimental colitis. *PLoS One,* 7, e33360.

Castro, R. F., Jackson, K. A., Goodell, M. A., Robertson, C. S., Liu, H., Shine, H. D. 2002. Failure of bone marrow cells to transdifferentiate into neural cells *in vivo*. *Science,* 297, 1299.

Caterson, E. J., Nesti, L. J., Danielson, K. G., Tuan, R. S. 2002. Human marrow-derived mesenchymal progenitor cells: Isolation, culture expansion, and analysis of differentiation. *Mol Biotechnol,* 20, 245-56.

Cerquetella, M., Spaterna, A., Laus, F., Tesei, B., Rossi, G., Antonelli, E., Villanacci, V., Bassotti, G. 2010. Inflammatory bowel disease in the dog: differences and similarities with humans. *World J Gastroenterol,* 16, 1050-6.

Cervi, A. L., Lukewich, M. K., Lomax, A. E. 2014. Neural regulation of gastrointestinal inflammation: Role of the sympathetic nervous system. *Auton Neurosci,* 182, 83-8.

Chamley-Campbell, J., Campbell, G. R., Ross, R. 1979. The smooth muscle cell in culture. *Physiol Rev,* 59, 1-61.

Chan, H. C., Ng, S. C. 2017. Emerging biologics in inflammatory bowel disease. *J Gastroenterol,* 52, 141-50.

Chande, N., Tsoulis, D. J., MacDonald, J. K. 2013. Azathioprine or 6-mercaptopurine for induction of remission in Crohn's disease. *Cochrane Database Syst Rev*, CD000545.

Chandrasekharan, B., Anitha, M., Blatt, R., Shahnavaz, N., Kooby, D., Staley, C., Mwangi, S., Jones, D. P., Sitaraman, S. V., Srinivasan, S. 2011. Colonic motor dysfunction in human diabetes is associated with enteric neuronal loss and increased oxidative stress. *Neurogastroenterol Motil,* 23, 131-8, e26.

Chang, W., Song, B. W., Moon, J. Y., Cha, M. J., Ham, O., Lee, S. Y., Choi, E., Choi, E., Hwang, K. C. 2013. Anti-death strategies against oxidative stress in grafted mesenchymal stem cells. *Histol Histopathol,* 28, 1529-36.

Chao, K., Zhang, S., Qiu, Y., Chen, X., Zhang, X., Cai, C., Peng, Y., Mao, R., Pevsner-Fischer, M., Ben-Horin, S., Elinav, E., Zeng, Z., Chen, B., He, Y., Xiang, A. P., Chen, M. 2016. Human umbilical cord-derived mesenchymal stem cells protect against experimental colitis via CD5+ B regulatory cells. *Stem Cell Res Ther,* 7, 109.

Charpentier, C., Salleron, J., Savoye, G., Fumery, M., Merle, V., Laberenne, J.-E., Vasseur, F., Dupas, J.-L., Cortot, A., Dauchet, L., Peyrin-Biroulet, L., Lerebours, E., Colombel, J.-F., Gower-Rousseau, C. 2014. Natural history of elderly-onset inflammatory bowel disease: a population-based cohort study. *Gut,* 63, 423-32.

Chassaing, B., Darfeuille-Michaud, A. 2011. The commensal microbiota and enteropathogens in the pathogenesis of inflammatory bowel diseases. *Gastroenterology,* 140, 1720-28.

Chassaing, B., Srinivasan, G., Delgado, M. A., Young, A. N., Gewirtz, A. T., Vijay-Kumar, M. 2012. Fecal lipocalin 2, a sensitive and broadly dynamic non-invasive biomarker for intestinal inflammation. *PLoS One,* 7, e44328.

Chaudhari, S., Desai, J. S., Adam, A., Mishra, P. 2014. Inflammatory bowel disease: An idiopathic disease and its treatment. *Int J Pharm Res Rev,* 3, 106-14.

Chen, H. H., Decot, V., Ouyang, J. P., Stoltz, J. F., Bensoussan, D., de Isla, N. G. 2009. *In vitro* initial expansion of mesenchymal stem cells is influenced by the culture parameters used in the isolation process. *Biomed Mater Eng,* 19, 301-9.

Chen, H. T., Lee, M. J., Chen, C. H., Chuang, S. C., Chang, L. F., Ho, M. L., Hung, S. H., Fu, Y. C., Wang, Y. H., Wang, H. I., Wang, G. J., Kang, L., Chang, J. K. 2012a. Proliferation and differentiation potential of human

adipose-derived mesenchymal stem cells isolated from elderly patients with osteoporotic fractures. *J Cell Mol Med,* 16, 582-92.
Chen, J. H., Zhang, Q., Yu, Y., Li, K., Liao, H., Jiang, L., Hong, L., Du, X., Hu, X., Chen, S., Yin, S., Gao, Q., Yin, X., Luo, H., Huizinga, J. D. 2013a. Neurogenic and myogenic properties of pan-colonic motor patterns and their spatiotemporal organization in rats. *PLoS One,* 8, e60474.
Chen, L., Tredget, E. E., Wu, P. Y. G., Wu, Y. 2008. Paracrine factors of mesenchymal stem cells recruit macrophages and endothelial lineage cells and enhance wound healing. *PLoS One,* 3, e1886.
Chen, L., Zhou, Z., Yang, Y., Chen, N., Xiang, H. 2017. Therapeutic effect of imiquimod on dextran sulfate sodium-induced ulcerative colitis in mice. *PLoS One,* 12, e0186138.
Chen, P., Torralba, M., Tan, J., Embree, M., Zengler, K., Starkel, P., van Pijkeren, J. P., DePew, J., Loomba, R., Ho, S. B., Bajaj, J. S., Mutlu, E. A., Keshavarzian, A., Tsukamoto, H., Nelson, K. E., Fouts, D. E., Schnabl, B. 2015. Supplementation of saturated long-chain fatty acids maintains intestinal eubiosis and reduces ethanol-induced liver injury in mice. *Gastroenterology,* 148, 203-14.e16.
Chen, Q. Q., Yan, L., Wang, C. Z., Wang, W. H., Shi, H., Su, B. B., Zeng, Q. H., Du, H. T., Wan, J. 2013b. Mesenchymal stem cells alleviate TNBS-induced colitis by modulating inflammatory and autoimmune responses. *World J Gastroenterol,* 19, 4702-17.
Chen, W., Liu, F., Ling, Z., Tong, X., Xiang, C. 2012b. Human intestinal lumen and mucosa-associated microbiota in patients with colorectal cancer. *PLoS One,* 7, e39743.
Cheng, S. L., Lin, C. H., Yao, C. L. 2017. Mesenchymal stem cell administration in patients with chronic obstructive pulmonary disease: State of the science. *Stem Cells Int,* 2017, 8916570.
Chiaretti, A., Falsini, B., Aloe, L., Pierri, F., Fantacci, C., Riccardi, R. 2011. Neuroprotective role of nerve growth factor in hypoxicischemic injury. From brain to skin. *Arch Ital Biol,* 149, 275-82.
Chichlowski, M., Hale, L. P. 2008. Bacterial-mucosal interactions in inflammatory bowel disease: An alliance gone bad. *Am J Physiol Gastrointest Liver Physiol,* 295, G1139-49.
Chiodini, R. J., Dowd, S. E., Chamberlin, W. M., Galandiuk, S., Davis, B., Glassing, A. 2015. Microbial population differentials between mucosal and submucosal intestinal tissues in advanced Crohn's disease of the ileum. *PLoS One,* 10, e0134382.
Cho, Y. B., Lee, W. Y., Park, K. J., Kim, M., Yoo, H. W., Yu, C. S. 2013. Autologous adipose tissue-derived stem cells for the treatment of Crohn's fistula: A phase I clinical study. *Cell Transplant,* 22, 279-85.
Cho, Y. B., Park, K. J., Yoon, S. N., Song, K. H., Kim, D. S., Jung, S. H., Kim, M., Jeong, H. Y., Yu, C. S. 2015. Long-term results of adipose-derived stem cell therapy for the treatment of Crohn’s fistula. *Stem Cells Transl Med,* 4, 532-7.
Choi, M. R., Kim, H. Y., Park, J. Y., Lee, T. Y., Baik, C. S., Chai, Y. G., Jung, K. H., Park, K. S., Roh, W., Kim, K. S., Kim, S. H. 2010. Selection of optimal passage of bone marrow-derived mesenchymal stem cells for stem cell

therapy in patients with amyotrophic lateral sclerosis. *Neurosci Lett,* 472, 94-8.

Choi, S., Park, M., Kim, J., Hwang, S., Park, S., Lee, Y. 2009. The role of mesenchymal stem cells in the functional improvement of chronic renal failure. *Stem Cells Dev,* 18, 521-9.

Christofi, F. L. 2008. Purinergic receptors and gastrointestinal secretomotor function. *Purinergic Signal,* 4, 213-36.

Chung, H. J., Chung, W. H., Lee, J. H., Chung, D. J., Yang, W. J., Lee, A. J., Choi, C. B., Chang, H. S., Kim, D. H., Suh, H. J., Lee, D. H., Hwang, S. H., Do, S. H., Kim, H. Y. 2016. Expression of neurotrophic factors in injured spinal cord after transplantation of human-umbilical cord blood stem cells in rats. *J Vet Sci,* 17, 97-102.

Chung, T. N., Kim, J. H., Choi, B. Y., Chung, S. P., Kwon, S. W., Suh, S. W. 2015. Adipose-derived mesenchymal stem cells reduce neuronal death after transient global cerebral ischemia through prevention of blood-brain barrier disruption and endothelial damage. *Stem Cells Transl Med,* 4, 178-85.

Ciccocioppo, R., Bernardo, M. E., Sgarella, A., Maccario, R., Avanzini, M. A., Ubezio, C., Minelli, A., Alvisi, C., Vanoli, A., Calliada, F., Dionigi, P., Perotti, C., Locatelli, F., Corazza, G. R. 2011. Autologous bone marrow-derived mesenchymal stromal cells in the treatment of fistulising Crohn's disease. *Gut,* 60, 788-98.

Coddens, A., Diswall, M., Angstrom, J., Breimer, M. E., Goddeeris, B., Cox, E., Teneberg, S. 2009. Recognition of blood group ABH type 1 determinants by the FedF adhesin of F18-fimbriated *Escherichia coli*. *J Biol Chem,* 284, 9713-26.

Cohen, J. A. 2013. Mesenchymal stem cell transplantation in multiple sclerosis. *J Neurol Sci,* 333, 43-9.

Cohen, J. L., Strong, S. A., Hyman, N. H., Buie, W. D., Dunn, G. D., Ko, C. Y., Fleshner, P. R., Stahl, T. J., Kim, D. G., Bastawrous, A. L., Perry, W. B., Cataldo, P. A., Rafferty, J. F., Ellis, C. N., Rakinic, J., Gregorcyk, S., Shellito, P. C., Kilkenny, J. W., 3rd, Ternent, C. A., Koltun, W., Tjandra, J. J., Orsay, C. P., Whiteford, M. H., Penzer, J. R. 2005. Practice parameters for the surgical treatment of ulcerative colitis. *Dis Colon Rectum,* 48, 1997-2009.

Collins, S. M. 2007. Translating symptoms into mechanisms: Functional GI disorders. *Adv Physiol Educ,* 31, 329-31.

Collins, S. M., Blennerhassett, P. A., Blennerhassett, M. G., Vermillion, D. L. 1989. Impaired acetylcholine release from the myenteric plexus of Trichinella-infected rats. *Am J Physiol,* 257, G898-903.

Colombel, J. F., Sandborn, W. J., Rutgeerts, P., Enns, R., Hanauer, S. B., Panaccione, R., Schreiber, S., Byczkowski, D., Li, J., Kent, J. D., Pollack, P. F. 2007. Adalimumab for maintenance of clinical response and remission in patients with Crohn's disease: the CHARM trial. *Gastroenterology,* 132, 52-65.

Colter, D. C., Class, R., DiGirolamo, C. M., Prockop, D. J. 2000. Rapid expansion of recycling stem cells in cultures of plastic-adherent cells from human bone marrow. *Proc Natl Acad Sci U S A,* 97, 3213-8.

Colter, D. C., Sekiya, I., Prockop, D. J. 2001. Identification of a subpopulation of rapidly self-renewing and multipotential adult stem cells in colonies of human marrow stromal cells. *Proc Natl Acad Sci U S A,* 98, 7841-5.

Comelli, E. M., Simmering, R., Faure, M., Donnicola, D., Mansourian, R., Rochat, F., Corthesy-Theulaz, I., Cherbut, C. 2008. Multifaceted transcriptional regulation of the murine intestinal mucus layer by endogenous microbiota. *Genomics,* 91, 70-7.

Cominelli, F., Arseneau, K. O., Rodriguez-Palacios, A., Pizarro, T. T. 2017. Uncovering pathogenic mechanisms of inflammatory bowel disease using mouse models of Crohn's disease-like ileitis: What is the right model? *Cell Mol Gastroenterol Hepatol,* 4, 19-32.

Conrad, K., Roggenbuck, D., Laass, M. W. 2014. Diagnosis and classification of ulcerative colitis. *Autoimmun Rev,* 13, 463-6.

Constantin, G., Marconi, S., Rossi, B., Angiari, S., Calderan, L., Anghileri, E., Gini, B., Bach, S. D., Martinello, M., Bifari, F., Galie, M., Turano, E., Budui, S., Sbarbati, A., Krampera, M., Bonetti, B. 2009. Adipose-derived mesenchymal stem cells ameliorate chronic experimental autoimmune encephalomyelitis. *Stem Cells* 27, 2624-35.

Coors, M. E., Glover, J. J., Juengst, E. T., Sikela, J. M. 2010. The ethics of using transgenic non-human primates to study what makes us human. *Nat Rev Genet,* 11, 658-62.

Corcione, A., Benvenuto, F., Ferretti, E., Giunti, D., Cappiello, V., Cazzanti, F., Risso, M., Gualandi, F., Mancardi, G. L., Pistoia, V., Uccelli, A. 2006. Human mesenchymal stem cells modulate B-cell functions. *Blood,* 107, 367-72.

Cosnes, J., Gower–Rousseau, C., Seksik, P., Cortot, A. 2011. Epidemiology and natural history of inflammatory bowel diseases. *Gastroenterology,* 140, 1785-94.e4.

Costa, M., Brookes, S., Hennig, G. 2000. Anatomy and physiology of the enteric nervous system. *Gut,* 47, iv15-9.

Costa, M., Brookes, S. H. 2008. Architecture of enteric neural circuits involved in intestinal motility. *Eur Rev Med Pharmacol Sci,* 12 Suppl 1, 3-19.

Cova, L., Armentero, M.-T., Zennaro, E., Calzarossa, C., Bossolasco, P., Busca, G., Lambertenghi Deliliers, G., Polli, E., Nappi, G., Silani, V., Blandini, F. 2010. Multiple neurogenic and neurorescue effects of human mesenchymal stem cell after transplantation in an experimental model of Parkinson's disease. *Brain Res,* 1311, 12-27.

Craven, M., Egan, C. E., Dowd, S. E., McDonough, S. P., Dogan, B., Denkers, E. Y., Bowman, D., Scherl, E. J., Simpson, K. W. 2012. Inflammation drives dysbiosis and bacterial invasion in murine models of ileal Crohn's disease. *PLoS One,* 7, e41594.

Croft, A. P., Przyborski, S. A. 2009. Mesenchymal stem cells expressing neural antigens instruct a neurogenic cell fate on neural stem cells. *Exp Neurol,* 216, 329-41.

Crohn's & Colitis Australia. 2017. *Annual review* [Online]. Camberwell, VIC, Australia. Available: https://www.crohnsandcolitis.com.au/site/wp-content/uploads/CCA_AnnualReport2017_WEB_FINAL.pdf [Accessed 10 August 2018].

Crop, M. J., Baan, C. C., Korevaar, S. S., Ijzermans, J. N. M., Pescatori, M., Stubbs, A. P., van Ijcken, W. F. J., Dahlke, M. H., Eggenhofer, E., Weimar, W., Hoogduijn, M. J. 2010. Inflammatory conditions affect gene expression and function of human adipose tissue-derived mesenchymal stem cells. *Clin Exp Immunol,* 162, 474-86.

Croze, E., Yamaguchi, K. D., Knappertz, V., Reder, A. T., Salamon, H. 2013. Interferon-beta-1b-induced short- and long-term signatures of treatment activity in multiple sclerosis. *Pharmacogenomics J,* 13, 443-51.

D'Haens, G. 2007. Risks and benefits of biologic therapy for inflammatory bowel diseases. *Gut,* 56, 725-32.

da Silva Meirelles, L., Chagastelles, P. C., Nardi, N. B. 2006. Mesenchymal stem cells reside in virtually all post-natal organs and tissues. *J Cell Sci,* 119, 2204-13.

da Silva Meirelles, L., Sand, T. T., Harman, R. J., Lennon, D. P., Caplan, A. I. 2009. MSC frequency correlates with blood vessel density in equine adipose tissue. *Tissue Eng Part A,* 15, 221-9.

da Silva, M. V., Marosti, A. R., Mendes, C. E., Palombit, K., Castelucci, P. 2015. Differential effects of experimental ulcerative colitis on P2X7 receptor expression in enteric neurons. *Histochem Cell Biol,* 143, 171-84.

Dadon-Nachum, M., Sadan, O., Srugo, I., Melamed, E., Offen, D. 2011. Differentiated mesenchymal stem cells for sciatic nerve injury. *Stem Cell Rev,* 7, 664-71.

Dalal, S. R., Chang, E. B. 2014. The microbial basis of inflammatory bowel diseases. *J Clin Invest,* 124, 4190-6.

Datta, I., Mishra, S., Mohanty, L., Pulikkot, S., Joshi, P. G. 2011. Neuronal plasticity of human Wharton's jelly mesenchymal stromal cells to the dopaminergic cell type compared with human bone marrow mesenchymal stromal cells. *Cytotherapy,* 13, 918-32.

Davis, D. R., Dockerty, M. B., Mayo, C. W. 1955. The myenteric plexus in regional enteritis: A study of the number of ganglion cells in the ileum in 24 cases. *Surg Gynecol Obstet,* 101, 208-16.

De Becker, A., Riet, I. V. 2016. Homing and migration of mesenchymal stromal cells: How to improve the efficacy of cell therapy? *World J Stem Cells,* 8, 73-87.

De Boer, A. G., Bennebroek Evertsz, F., Stokkers, P. C., Bockting, C. L., Sanderman, R., Hommes, D. W., Sprangers, M. A., Frings-Dresen, M. H. 2016. Employment status, difficulties at work and quality of life in inflammatory bowel disease patients. *Eur J Gastroenterol Hepatol,* 28, 1130-6.

de Boer, R., Borntraeger, A., Knight Andrew, M., Hébert-Blouin, M. N., Spinner Robert, J., Malessy Martijn, J. A., Yaszemski Michael, J., Windebank Anthony, J. 2012. Short- and long-term peripheral nerve regeneration using a poly-lactic-co-glycolic-acid scaffold containing nerve growth factor and glial cell line-derived neurotrophic factor releasing microspheres. *J Biomed Mater Res A,* 100, 2139-46.

De Fazio, L., Cavazza, E., Spisni, E., Strillacci, A., Centanni, M., Candela, M., Pratico, C., Campieri, M., Ricci, C., Valerii, M. C. 2014. Longitudinal analysis of inflammation and microbiota dynamics in a model of mild

chronic dextran sulfate sodium-induced colitis in mice. *World J Gastroenterol,* 20, 2051-61.
De Giorgio, R., Barbara, G., Stanghellini, V., De Ponti, F., Salvioli, B., Tonini, M., Velio, P., Bassotti, G., Corinaldesi, R. 2002. Clinical and morphofunctional features of idiopathic myenteric ganglionitis underlying severe intestinal motor dysfunction: A study of three cases. *Am J Gastroenterol,* 97, 2454-9.
De Giorgio, R., Giancola, F., Boschetti, E., Abdo, H., Lardeux, B., Neunlist, M. 2012. Enteric glia and neuroprotection: Basic and clinical aspects. *Am J Physiol Gastrointest Liver Physiol,* 303, G887-93.
de Jonge, W. J. 2013. The gut's little brain in control of intestinal immunity. *ISRN Gastroenterol,* 2013, 630159.
de la Portilla, F., Alba, F., Garcia-Olmo, D., Herrerias, J. M., Gonzalez, F. X., Galindo, A. 2013. Expanded allogeneic adipose-derived stem cells (eASCs) for the treatment of complex perianal fistula in Crohn's disease: results from a multicenter phase I/IIa clinical trial. *Int J Colorectal Dis,* 28, 313-23.
De Luca, A., Verardi, R., Neva, A., Benzoni, P., Crescini, E., Xia, E., Almici, C., Calza, S., Dell'Era, P. 2013. Comparative analysis of mesenchymal stromal cells biological properties. *ISRN Stem Cells,* 2013, 674671.
de Silva, S., Devlin, S., Panaccione, R. 2010. Optimizing the safety of biologic therapy for IBD. *Nat Rev Gastroenterol Hepatol,* 7, 93-101.
de Souza, H. S., Fiocchi, C. 2016. Immunopathogenesis of IBD: Current state of the art. *Nat Rev Gastroenterol Hepatol,* 13, 13-27.
de Winter, B. Y., van Nassauw, L., de Man, J. G., de Jonge, F., Bredenoord, A. J., Seerden, T. C., Herman, A. G., Timmermans, J. P., Pelckmans, P. A. 2005. Role of oxidative stress in the pathogenesis of septic ileus in mice. *Neurogastroenterol Motil,* 17, 251-61.
de Witte, S. F., Franquesa, M., Baan, C. C., Hoogduijn, M. J. 2015. Toward development of imesenchymal stem cells for immunomodulatory therapy. *Front Immunol,* 6, 648.
Deiteren, A., Camilleri, M., Bharucha, A. E., Burton, D., McKinzie, S., Rao, A. S., Zinsmeister, A. R. 2010. Performance characteristics of scintigraphic colon transit measurement in health and irritable bowel syndrome and relationship to bowel functions. *Neurogastroenterol Motil,* 22, 415-23, e95.
Deloose, E., Janssen, P., Depoortere, I., Tack, J. 2012. The migrating motor complex: Control mechanisms and its role in health and disease. *Nat Rev Gastroenterol Hepatol,* 9, 271-85.
Demir, I. E., Schafer, K. H., Tieftrunk, E., Friess, H., Ceyhan, G. O. 2013. Neural plasticity in the gastrointestinal tract: Chronic inflammation, neurotrophic signals, and hypersensitivity. *Acta Neuropathol,* 125, 491-509.
Deng, Y. B., Liu, X. G., Liu, Z. G., Liu, X. L., Liu, Y., Zhou, G. Q. 2006. Implantation of BM mesenchymal stem cells into injured spinal cord elicits *de novo* neurogenesis and functional recovery: Evidence from a study in rhesus monkeys. *Cytotherapy,* 8, 210-14.
Der, T., Bercik, P., Donnelly, G., Jackson, T., Berezin, I., Collins, S. M., Huizinga, J. D. 2000. Interstitial cells of cajal and inflammation-induced motor dysfunction in the mouse small intestine. *Gastroenterology,* 119, 1590-9.

Devkota, S., Wang, Y., Musch, M. W., Leone, V., Fehlner-Peach, H., Nadimpalli, A., Antonopoulos, D. A., Jabri, B., Chang, E. B. 2012. Dietary-fat-induced taurocholic acid promotes pathobiont expansion and colitis in IL10-/- mice. *Nature,* 487, 104-8.

DeVoss, J., Diehl, L. 2014. Murine models of inflammatory bowel disease (IBD): Challenges of modeling human disease. *Toxicol Pathol,* 42, 99-110.

Dey, N., Soergel, D. A., Repo, S., Brenner, S. E. 2013. Association of gut microbiota with post-operative clinical course in Crohn's disease. *BMC Gastroenterol,* 13, 131.

Dezawa, M., Kanno, H., Hoshino, M., Cho, H., Matsumoto, N., Itokazu, Y., Tajima, N., Yamada, H., Sawada, H., Ishikawa, H., Mimura, T., Kitada, M., Suzuki, Y., Ide, C. 2004. Specific induction of neuronal cells from bone marrow stromal cells and application for autologous transplantation. *J Clin Invest,* 113, 1701-10.

Di Sabatino, A., Morera, R., Ciccocioppo, R., Cazzola, P., Gotti, S., Tinozzi, F. P., Tinozzi, S., Corazza, G. R. 2005. Oral butyrate for mildly to moderately active Crohn's disease. *Aliment Pharmacol Ther,* 22, 789-94.

Diez, J. M., Bauman, E., Gajardo, R., Jorquera, J. I. 2015. Culture of human mesenchymal stem cells using a candidate pharmaceutical grade xeno-free cell culture supplement derived from industrial human plasma pools. *Stem Cell Res Ther,* 6, 28.

Dignass, A., Eliakim, R., Magro, F., Maaser, C., Chowers, Y., Geboes, K., Mantzaris, G., Reinisch, W., Colombel, J.-F., Vermeire, S., Travis, S., Lindsay, J. O., Van Assche, G. 2012. Second European evidence-based consensus on the diagnosis and management of ulcerative colitis Part 1: Definitions and diagnosis. *J Crohns Colitis,* 6, 965-90.

Dignass, A., Van Assche, G., Lindsay, J. O., Lemann, M., Soderholm, J., Colombel, J. F., Danese, S., D'Hoore, A., Gassull, M., Gomollon, F., Hommes, D. W., Michetti, P., O'Morain, C., Oresland, T., Windsor, A., Stange, E. F., Travis, S. P. 2010. The second European evidence-based Consensus on the diagnosis and management of Crohn's disease: Current management. *J Crohns Colitis,* 4, 28-62.

Dignass, A. U. 2001. Mechanisms and modulation of intestinal epithelial repair. *Inflamm Bowel Dis,* 7, 68-77.

Ding, Y., Yan, Q., Ruan, J.-W., Zhang, Y.-Q., Li, W.-J., Zhang, Y.-J., Li, Y., Dong, H., Zeng, Y.-S. 2009. Electro-acupuncture promotes survival, differentiation of the bone marrow mesenchymal stem cells as well as functional recovery in the spinal cord-transected rats. *BMC Neurosci,* 10, 35.

Djouad, F., Charbonnier, L. M., Bouffi, C., Louis-Plence, P., Bony, C., Apparailly, F., Cantos, C., Jorgensen, C., Noel, D. 2007. Mesenchymal stem cells inhibit the differentiation of dendritic cells through an interleukin-6-dependent mechanism. *Stem Cells,* 25, 2025-32.

Dobolyi, A., Vincze, C., Pal, G., Lovas, G. 2012. The neuroprotective functions of transforming growth factor beta proteins. *Int J Mol Sci,* 13, 8219-58.

Dohi, T., Fujihashi, K. 2006. Type 1 and 2 T helper cell-mediated colitis. *Curr Opin Gastroenterol,* 22, 651-7.

Dominici, M., Le Blanc, K., Mueller, I., Slaper-Cortenbach, I., Marini, F., Krause, D., Deans, R., Keating, A., Prockop, D., Horwitz, E. 2006. Minimal criteria for defining multipotent mesenchymal stromal cells. The International Society for Cellular Therapy position statement. *Cytotherapy,* 8, 315-7.

Dong, X. X., Thacker, M., Pontell, L., Furness, J. B., Nurgali, K. 2008. Effects of intestinal inflammation on specific subgroups of guinea-pig celiac ganglion neurons. *Neurosci Lett,* 444, 231-5.

Dothel, G., Vasina, V., Barbara, G., De Ponti, F. 2013. Animal models of chemically induced intestinal inflammation: Predictivity and ethical issues. *Pharmacol Ther,* 139, 71-86.

Duffy, M. M., Ritter, T., Ceredig, R., Griffin, M. D. 2011. Mesenchymal stem cell effects on T-cell effector pathways. *Stem Cell Res Ther,* 2, 34.

Duijvestein, M., Vos, A. C. W., Roelofs, H., Wildenberg, M. E., Wendrich, B. B., Verspaget, H. W., Kooy-Winkelaar, E. M. C., Koning, F., Zwaginga, J. J., Fidder, H. H., Verhaar, A. P., Fibbe, W. E., van den Brink, G. R., Hommes, D. W. 2010. Autologous bone marrow-derived mesenchymal stromal cell treatment for refractory luminal Crohn's disease: Results of a phase I study. *Gut,* 59, 1662-9.

Duijvestein, M., Wildenberg, M. E., Welling, M. M., Hennink, S., Molendijk, I., van Zuylen, V. L., Bosse, T., Vos, A. C. W., de Jonge-Muller, E. S. M., Roelofs, H., van der Weerd, L., Verspaget, H. W., Fibbe, W. E., te Velde, A. A., van den Brink, G. R., Hommes, D. W. 2011. Pretreatment with interferon-γ enhances the therapeutic activity of mesenchymal stromal cells in animal models of colitis. *Stem Cells,* 29, 1549-58.

Duncan, M., Mouihate, A., Mackie, K., Keenan, C. M., Buckley, N. E., Davison, J. S., Patel, K. D., Pittman, Q. J., Sharkey, K. A. 2008. Cannabinoid CB2 receptors in the enteric nervous system modulate gastrointestinal contractility in lipopolysaccharide-treated rats. *Am J Physiol Gastrointest Liver Physiol,* 295, G78-87.

Duricova, D., Burisch, J., Jess, T., Gower-Rousseau, C., Lakatos, P. L. 2014. Age-related differences in presentation and course of inflammatory bowel disease: An update on the population-based literature☆. *J Crohns Colitis,* 8, 1351-61.

Durnin, L., Sanders, K. M., Mutafova-Yambolieva, V. N. 2013. Differential release of β-NAD(+) and ATP upon activation of enteric motor neurons in primate and murine colons. *Neurogastroenterol Motil,* 25, e194-204.

Dvorak, A. M., Onderdonk, A. B., McLeod, R. S., Monahan-Earley, R. A., Cullen, J., Antonioli, D. A., Blair, J. E., Morgan, E. S., Cisneros, R. L., Estrella, P., et al. 1993. Axonal necrosis of enteric autonomic nerves in continent ileal pouches. Possible implications for pathogenesis of Crohn's disease. *Ann Surg,* 217, 260-71.

Dvorak, A. M., Osage, J. E., Monahan, R. A., Dickersin, G. R. 1980. Crohn's disease: transmission electron microscopic studies. III. Target tissues. Proliferation of and injury to smooth muscle and the autonomic nervous system. *Hum Pathol,* 11, 620-34.

Dvorak, A. M., Silen, W. 1985. Differentiation between Crohn's disease and other inflammatory conditions by electron microscopy. *Ann Surg,* 201, 53-63.

Dwyer, R. M., Potter-Beirne, S. M., Harrington, K. A., Lowery, A. J., Hennessy, E., Murphy, J. M., Barry, F. P., O'Brien, T., Kerin, M. J. 2007. Monocyte chemotactic protein-1 secreted by primary breast tumors stimulates migration of mesenchymal stem cells. *Clin Cancer Res,* 13, 5020-7.

Ebrahimi, B., Eirin, A., Li, Z., Zhu, X. Y., Zhang, X., Lerman, A., Textor, S. C., Lerman, L. O. 2013. Mesenchymal stem cells improve medullary inflammation and fibrosis after revascularization of swine atherosclerotic renal artery stenosis. *PLoS One,* 8, e67474.

Eckburg, P. B., Bik, E. M., Bernstein, C. N., Purdom, E., Dethlefsen, L., Sargent, M., Gill, S. R., Nelson, K. E., Relman, D. A. 2005. Diversity of the human intestinal microbial flora. *Science,* 308, 1635-8.

Eirin, A., Lerman, L. O. 2014. Mesenchymal stem cell treatment for chronic renal failure. *Stem Cell Res Ther,* 5, 83.

Eirin, A., Zhu, X. Y., Krier, J. D., Tang, H., Jordan, K. L., Grande, J. P., Lerman, A., Textor, S. C., Lerman, L. O. 2012. Adipose tissue-derived mesenchymal stem cells improve revascularization outcomes to restore renal function in swine atherosclerotic renal artery stenosis. *Stem cells,* 30, 1030-41.

El-Tantawy, W. H., Haleem, E. N. 2014. Therapeutic effects of stem cell on hyperglycemia, hyperlipidemia, and oxidative stress in alloxan-treated rats. *Mol Cell Biochem,* 391, 193-200.

Ellinghaus, D., Bethune, J., Petersen, B. S., Franke, A. 2015. The genetics of Crohn's disease and ulcerative colitis--status quo and beyond. *Scand J Gastroenterol,* 50, 13-23.

Elman, J. S., Li, M., Wang, F., Gimble, J. M., Parekkadan, B. 2014. A comparison of adipose and bone marrow-derived mesenchymal stromal cell secreted factors in the treatment of systemic inflammation. *J Inflamm (Lond),* 11, 1.

Elsden, S. R., Hilton, M. G., Waller, J. M. 1976. The end products of the metabolism of aromatic amino acids by *Clostridia*. *Arch Microbiol,* 107, 283-8.

Elson, C. O., Cong, Y., McCracken, V. J., Dimmitt, R. A., Lorenz, R. G., Weaver, C. T. 2005. Experimental models of inflammatory bowel disease reveal innate, adaptive, and regulatory mechanisms of host dialogue with the microbiota. *Immunol Rev,* 206, 260-76.

Elson, C. O., Sartor, R. B., Tennyson, G. S., Riddell, R. H. 1995. Experimental models of inflammatory bowel disease. *Gastroenterology,* 109, 1344-67.

Endo, A., Futagawa-Endo, Y., Dicks, L. M. 2009. Isolation and characterization of fructophilic lactic acid bacteria from fructose-rich niches. *Syst Appl Microbiol,* 32, 593-600.

English, K. 2013. Mechanisms of mesenchymal stromal cell immunomodulation. *Immunol Cell Biol,* 91, 19-26.

Eri, R. D., Adams, R. J., Tran, T. V., Tong, H., Das, I., Roche, D. K., Oancea, I., Png, C. W., Jeffery, P. L., Radford-Smith, G. L., Cook, M. C., Florin, T. H., McGuckin, M. A. 2011. An intestinal epithelial defect conferring ER stress results in inflammation involving both innate and adaptive immunity. *Mucosal Immunol,* 4, 354-64.

Everaert, B. R., Bergwerf, I., De Vocht, N., Ponsaerts, P., Van Der Linden, A., Timmermans, J. P., Vrints, C. J. 2012. Multimodal *in vivo* imaging reveals

limited allograft survival, intrapulmonary cell trapping and minimal evidence for ischemia-directed BMSC homing. *BMC Biotechnol,* 12, 93.
Eysselein, V. E., Reinshagen, M., Cominelli, F., Sternini, C., Davis, W., Patel, A., Nast, C. C., Bernstein, D., Anderson, K., Khan, H., Snape, W. J. 1991. Calcitonin gene-related peptide and substance P decrease in the rabbit colon during colitis. A time study. *Gastroenterology,* 101, 1211-9.
Eysselein, V. E., Reinshagen, M., Patel, A., Davis, W., Nast, C., Sternini, C. 1992. Calcitonin gene-related peptide in inflammatory bowel disease and experimentally induced colitis. *Ann N Y Acad Sci,* 657, 319-27.
Ezquer, F., Ezquer, M., Simon, V., Conget, P. 2011. The antidiabetic effect of MSCs is not impaired by insulin prophylaxis and is not improved by a second dose of cells. *PLoS One,* 6, e16566.
Ezquer, F. E., Ezquer, M. E., Parrau, D. B., Carpio, D., Yanez, A. J., Conget, P. A. 2008. Systemic administration of multipotent mesenchymal stromal cells reverts hyperglycemia and prevents nephropathy in type 1 diabetic mice. *Biol Blood Marrow Transplant,* 14, 631-40.
Fakhoury, M., Negrulj, R., Mooranian, A., Al-Salami, H. 2014. Inflammatory bowel disease: Clinical aspects and treatments. *J Inflamm Res,* 7, 113-20.
Farini, A., Sitzia, C., Erratico, S., Meregalli, M., Torrente, Y. 2014. Clinical applications of mesenchymal stem cells in chronic diseases. *Stem Cells Int,* 2014, 306573.
Farrell, D., Savage, E. 2012. Symptom burden: A forgotten area of measurement in inflammatory bowel disease. *Int J Nurs Pract,* 18, 497-500.
Favier, C., Neut, C., Mizon, C., Cortot, A., Colombel, J. F., Mizon, J. 1997. Fecal beta-D-galactosidase production and *Bifidobacteria* are decreased in Crohn's disease. *Dig Dis Sci,* 42, 817-22.
Fawzy, S. A., El-din Abo-Elnou, R. K., Abd-El-Maksoud El-Deeb, D. F., Yousry Abd-Elkader, M. M. 2013. The possible role of mesenchymal stem cells therapy in the repair of experimentally induced colitis in male albino rats. *Int J Stem Cells,* 6, 92-103.
Feldman, P. A., Wolfson, D., Barkin, J. S. 2007. Medical management of Crohn's disease. *Clin Colon Rectal Surg,* 20, 269-81.
Fernandez-Garcia, M., Yanez, R. M., Sanchez-Dominguez, R., Hernando-Rodriguez, M., Peces-Barba, M., Herrera, G., O'Connor, J. E., Segovia, J. C., Bueren, J. A., Lamana, M. L. 2015. Mesenchymal stromal cells enhance the engraftment of hematopoietic stem cells in an autologous mouse transplantation model. *Stem Cell Res Ther,* 6, 165.
Ferrante, M., de Hertogh, G., Hlavaty, T., D'Haens, G., Penninckx, F., D'Hoore, A., Vermeire, S., Rutgeerts, P., Geboes, K., van Assche, G. 2006. The value of myenteric plexitis to predict early postoperative Crohn's disease recurrence. *Gastroenterology,* 130, 1595-606.
Feuerstein, J. D., Cheifetz, A. S. 2017. Crohn disease: Epidemiology, diagnosis, and management. *Mayo Clin Proc,* 92, 1088-103.
Fichera, A., McCormack, R., Rubin, M. A., Hurst, R. D., Michelassi, F. 2005. Long-term outcome of surgically treated Crohn's colitis: A prospective study. *Dis Colon Rectum,* 48, 963-9.

Fida, R., Lyster, D. J. K., Bywater, R. A. R., Taylor, G. S. 1997. Colonic migrating motor complexes (CMMCs) in the isolated mouse colon. *Neurogastroenterol Motil,* 9, 99-107.

Fiedler, J., Roderer, G., Gunther, K. P., Brenner, R. E. 2002. BMP-2, BMP-4, and PDGF-bb stimulate chemotactic migration of primary human mesenchymal progenitor cells. *J Cell Biochem,* 87, 305-12.

Fierer, J., Okamoto, S., Banerjee, A., Guiney, D. G. 2012. Diarrhea and colitis in mice require the salmonella pathogenicity island 2-encoded secretion function but not *sifA* or *spv* effectors. *Infect Immun,* 80, 3360-70.

Finkelstone, L., Wolf, E. L., Stein, M. W. 2012. Etiology of small bowel thickening on computed tomography. *Can J Gastroenterol,* 26, 897-901.

Fiocchi, C. 2015. Inflammatory bowel disease pathogenesis: Where are we? *J Gastroenterol Hepatol,* 30 Suppl 1, 12-8.

Fischer, A. J., Schmidt, M., Omar, G., Reh, T. A. 2004. BMP4 and CNTF are neuroprotective and suppress damage-induced proliferation of Müller glia in the retina. *Mol Cell Neurosci,* 27, 531-42.

Fischer, M., Siva, S., Wo, J. M., Fadda, H. M. 2017. Assessment of small intestinal transit times in ulcerative colitis and Crohn's disease patients with different disease activity using video capsule endoscopy. *AAPS PharmSciTech,* 18, 404-9.

Fischer, U. M., Harting, M. T., Jimenez, F., Monzon-Posadas, W. O., Xue, H., Savitz, S. I., Laine, G. A., Cox, C. S. 2009. Pulmonary passage is a major obstacle for intravenous stem cell delivery: The pulmonary first-pass effect. *Stem Cells Dev,* 18, 683-91.

Fisher-Shoval, Y., Barhum, Y., Sadan, O., Yust-Katz, S., Ben-Zur, T., Lev, N., Benkler, C., Hod, M., Melamed, E., Offen, D. 2012. Transplantation of placenta-derived mesenchymal stem cells in the EAE mouse model of MS. *J Mol Neurosci,* 48, 176-84.

Floch, M. H., Hong-Curtiss, J. 2001. Probiotics and functional foods in gastrointestinal disorders. *Curr Gastroenterol Rep,* 3, 343-50.

Florea, V., Rieger, A. C., DiFede, D. L., El-Khorazaty, J., Natsumeda, M., Banerjee, M. N., Tompkins, B. A., Khan, A., Schulman, I. H., Landin, A. M., Mushtaq, M., Golpanian, S., Lowery, M. H., Byrnes, J. J., Hendel, R. C., Cohen, M. G., Valasaki, K., Pujol, M. V., Ghersin, E., Miki, R., Delgado, C., Abuzeid, F., Vidro-Casiano, M., Saltzman, R. G., DaFonseca, D., Caceres, L. V., Ramdas, K. N., Mendizabal, A., Heldman, A. W., Mitrani, R. D., Hare, J. M. 2017. Dose comparison study of allogeneic mesenchymal stem cells in patients with ischemic cardiomyopathy (the TRIDENT study). *Circ Res,* 121, 1279-90.

Fong, E. L. S., Chan, C. K., Goodman, S. B. 2011. Stem cell homing in musculoskeletal injury. *Biomaterials,* 32, 395-409.

Foong, J. P., Parry, L. J., Gwynne, R. M., Bornstein, J. C. 2010. 5-HT(1A), SST(1), and SST(2) receptors mediate inhibitory postsynaptic potentials in the submucous plexus of the guinea pig ileum. *Am J Physiol Gastrointest Liver Physiol,* 298, G384-94.

Forbes, G. M., Sturm, M. J., Leong, R. W., Sparrow, M. P., Segarajasingam, D., Cummins, A. G., Phillips, M., Herrmann, R. P. 2014. A phase 2 study of

allogeneic mesenchymal stromal cells for luminal Crohn's disease refractory to biologic therapy. *Clin Gastroenterol Hepatol,* 12, 64-71.

Forte, D., Ciciarello, M., Valerii, M. C., De Fazio, L., Cavazza, E., Giordano, R., Parazzi, V., Lazzari, L., Laureti, S., Rizzello, F., Cavo, M., Curti, A., Lemoli, R. M., Spisni, E., Catani, L. 2015. Human cord blood-derived platelet lysate enhances the therapeutic activity of adipose-derived mesenchymal stromal cells isolated from Crohn's disease patients in a mouse model of colitis. *Stem Cell Res Ther,* 6, 170.

Forte, G., Minieri, M., Cossa, P., Antenucci, D., Sala, M., Gnocchi, V., Fiaccavento, R., Carotenuto, F., De Vito, P., Baldini, P. M., Prat, M., Di Nardo, P. 2006. Hepatocyte growth factor effects on mesenchymal stem cells: Proliferation, migration, and differentiation. *Stem Cells,* 24, 23-33.

Foudah, D., Redaelli, S., Donzelli, E., Bentivegna, A., Miloso, M., Dalpra, L., Tredici, G. 2009. Monitoring the genomic stability of *in vitro* cultured rat bone-marrow-derived mesenchymal stem cells. *Chromosome Res,* 17, 1025-39.

Frank, D. N., St Amand, A. L., Feldman, R. A., Boedeker, E. C., Harpaz, N., Pace, N. R. 2007. Molecular-phylogenetic characterization of microbial community imbalances in human inflammatory bowel diseases. *Proc Natl Acad Sci U S A,* 104, 13780-5.

Franquesa, M., Herrero, E., Torras, J., Ripoll, E., Flaquer, M., Goma, M., Lloberas, N., Anegon, I., Cruzado, J. M., Grinyo, J. M., Herrero-Fresneda, I. 2012. Mesenchymal stem cell therapy prevents interstitial fibrosis and tubular atrophy in a rat kidney allograft model. *Stem Cells Dev,* 21, 3125-35.

Freedman, M. S., Bar-Or, A., Atkins, H. L., Karussis, D., Frassoni, F., Lazarus, H., Scolding, N., Slavin, S., Le Blanc, K., Uccelli, A. 2010. The therapeutic potential of mesenchymal stem cell transplantation as a treatment for multiple sclerosis: Consensus report of the International MSCT Study Group. *Mult Scler,* 16, 503-10.

Fu, Y., Karbaat, L., Wu, L., Leijten, J., Both, S. K., Karperien, M. 2017. Trophic effects of mesenchymal stem cells in tissue regeneration. *Tissue Eng Part B Rev,* 23, 515-28.

Fujimoto, N., Inoue, K., Ohgusu, Y., Hayashi, Y., Yuasa, H. 2007. Enhanced uptake of glycerol by butyrate treatment in HCT-15 human colon cancer cell line. *Drug Metab Pharmacokinet,* 22, 195-8.

Fung, C., Ellis, M., Bornstein, J. C. 2010. Luminal cholera toxin alters motility in isolated guinea-pig jejunum via a pathway independent of 5-HT(3) receptors. *Front Neurosci,* 4, 162.

Furness, J. B. 2000. Types of neurons in the enteric nervous system. *J Auton Nerv Syst,* 81, 87-96.

Furness, J. B. 2006. *The enteric nervous system,* Blackwell Publishing, Oxford.

Furness, J. B. 2012. The enteric nervous system and neurogastroenterology. *Nat Rev Gastroenterol Hepatol,* 9, 286-94.

Furness, J. B., Callaghan, B. P., Rivera, L. R., Cho, H. J. 2014. The enteric nervous system and gastrointestinal innervation: Integrated local and central control. *In:* LYTE, M. & CRYAN, J. F. (eds.) *Microbial*

Endocrinology: The Microbiota-Gut-Brain Axis in Health and Disease. New York, NY: Springer New York.
Furness, J. B., Robbins, H. L., Xiao, J., Stebbing, M. J., Nurgali, K. 2004. Projections and chemistry of Dogiel type II neurons in the mouse colon. *Cell Tissue Res,* 317, 1-12.
Galindo, L. T., Filippo, T. R. M., Semedo, P., Ariza, C. B., Moreira, C. M., Camara, N. O. S., Porcionatto, M. A. 2011. Mesenchymal stem cell therapy modulates the inflammatory response in experimental traumatic brain injury. *Neurol Res Int,* 2011, 564089.
Gallego, D., Gil, V., Martinez-Cutillas, M., Mane, N., Martin, M. T., Jimenez, M. 2012. Purinergic neuromuscular transmission is absent in the colon of P2Y(1) knocked out mice. *J Physiol,* 590, 1943-56.
Galligan, J. J. 2002. Ligand-gated ion channels in the enteric nervous system. *Neurogastroenterol Motil,* 14, 611-23.
Galligan, J. J. 2009. Na(V)-igating excitement in the enteric nervous system. *J Physiol,* 587, 1377.
Galligan, J. J., LePard, K. J., Schneider, D. A., Zhou, X. 2000. Multiple mechanisms of fast excitatory synaptic transmission in the enteric nervous system. *J Auton Nerv Syst,* 81, 97-103.
Galligan, J. J., North, R. A. 2004. Pharmacology and function of nicotinic acetylcholine and P2X receptors in the enteric nervous system. *Neurogastroenterol Motil,* 16 Suppl 1, 64-70.
Galligan, J. J., Pan, H., Messori, E. 2003. Signalling mechanism coupled to 5-hydroxytryptamine4 receptor-mediated facilitation of fast synaptic transmission in the guinea-pig ileum myenteric plexus. *Neurogastroenterol Motil,* 15, 523-9.
Gao, F., Chiu, S. M., Motan, D. A. L., Zhang, Z., Chen, L., Ji, H. L., Tse, H. F., Fu, Q. L., Lian, Q. 2016. Mesenchymal stem cells and immunomodulation: Current status and future prospects. *Cell Death Dis,* 7, e2062.
Garcia-Bosch, O., Ricart, E., Panes, J. 2010. Stem cell therapies for inflammatory bowel disease - efficacy and safety. *Aliment Pharmacol Ther,* 32, 939-52.
Garcia-Olmo, D., Garcia-Arranz, M., Herreros, D., Pascual, I., Peiro, C., Rodriguez-Montes, J. A. 2005. A phase I clinical trial of the treatment of Crohn's fistula by adipose mesenchymal stem cell transplantation. *Dis Colon Rectum,* 48, 1416-23.
Garcia-Olmo, D., Herreros, D., Pascual, I., Pascual, J. A., Del-Valle, E., Zorrilla, J., De-La-Quintana, P., Garcia-Arranz, M., Pascual, M. 2009. Expanded adipose-derived stem cells for the treatment of complex perianal fistula: A phase II clinical trial. *Dis Colon Rectum,* 52, 79-86.
Gardiner, K. R., Dasari, B. V. 2007. Operative management of small bowel Crohn's disease. *Surg Clin North Am,* 87, 587-610.
Gasparetto, M., Guariso, G. 2013. Highlights in IBD epidemiology and its natural history in the paediatric age. *Gastroenterol Res Pract,* 2013, 829040.
Gaughwin, P., Ciesla, M., Yang, H., Lim, B., Brundin, P. 2011. Stage-specific modulation of cortical neuronal development by Mmu-miR-134. *Cereb Cortex,* 21, 1857-69.

Gaya, D. R., Russell, R. K., Nimmo, E. R., Satsangi, J. 2006. New genes in inflammatory bowel disease: Lessons for complex diseases. *Lancet,* 367, 1271-84.

Ge, W., Jiang, J., Arp, J., Liu, W., Garcia, B., Wang, H. 2010. Regulatory T-cell generation and kidney allograft tolerance induced by mesenchymal stem cells associated with indoleamine 2,3-dioxygenase expression. *Transplantation,* 90.

Gearry, R. B., Barclay, M. L., Burt, M. J., Collett, J. A., Chapman, B. A. 2004. Thiopurine drug adverse effects in a population of New Zealand patients with inflammatory bowel disease. *Pharmacoepidemiol Drug Saf,* 13, 563-7.

Gearry, R. B., Richardson, A., Frampton, C. M., Collett, J. A., Burt, M. J., Chapman, B. A., Barclay, M. L. 2006. High incidence of Crohn's disease in Canterbury, New Zealand: Results of an epidemiologic study. *Inflamm Bowel Dis,* 12, 936-43.

Geboes, K., Collins, S. 1998. Structural abnormalities of the nervous system in Crohn's disease and ulcerative colitis. *Neurogastroenterol Motil,* 10, 189-202.

Geremia, A., Biancheri, P., Allan, P., Corazza, G. R., Di Sabatino, A. 2014. Innate and adaptive immunity in inflammatory bowel disease. *Autoimmun Rev,* 13, 3-10.

Ghannam, S., Pene, J., Torcy-Moquet, G., Jorgensen, C., Yssel, H. 2010. Mesenchymal stem cells inhibit human Th17 cell differentiation and function and induce a T regulatory cell phenotype. *J Immunol,* 185.

Ghia, J. E., Blennerhassett, P., Kumar-Ondiveeran, H., Verdu, E. F., Collins, S. M. 2006. The vagus nerve: A tonic inhibitory influence associated with inflammatory bowel disease in a murine model. *Gastroenterology,* 131, 1122-30.

Gibson, P. R., Shepherd, S. J. 2005. Personal view: Food for thought--western lifestyle and susceptibility to Crohn's disease. The FODMAP hypothesis. *Aliment Pharmacol Ther,* 21, 1399-409.

Gill, S. R., Pop, M., Deboy, R. T., Eckburg, P. B., Turnbaugh, P. J., Samuel, B. S., Gordon, J. I., Relman, D. A., Fraser-Liggett, C. M., Nelson, K. E. 2006. Metagenomic analysis of the human distal gut microbiome. *Science,* 312, 1355-9.

Gisbert, J. P., Chaparro, M., Gomollon, F. 2011. Common misconceptions about 5-aminosalicylates and thiopurines in inflammatory bowel disease. *World J Gastroenterol,* 17, 3467-78.

Glavaski-Joksimovic, A., Virag, T., Mangatu, T. A., McGrogan, M., Wang, X. S., Bohn, M. C. 2010. Glial cell line-derived neurotrophic factor-secreting genetically modified human bone marrow-derived mesenchymal stem cells promote recovery in a rat model of Parkinson's disease. *J Neurosci Res,* 88, 2669-81.

Glueckert, R., Bitsche, M., Miller, J. M., Zhu, Y., Prieskorn, D. M., Altschuler, R. A., Schrott-Fischer, A. 2008. Deafferentation-associated changes in afferent and efferent processes in the guinea pig cochlea and afferent regeneration with chronic intrascalar brain-derived neurotrophic factor and acidic fibroblast growth factor. *J Comp Neurol,* 507, 1602-21.

Golpanian, S., Schulman, I. H., Ebert, R. F., Heldman, A. W., DiFede, D. L., Yang, P. C., Wu, J. C., Bolli, R., Perin, E. C., Moyé, L., Simari, R. D., Wolf, A., Hare, J. M., for the Cardiovascular Cell Therapy Research, N. 2016. Review and perspective of cell dosage and routes of administration from preclinical and clinical studies of stem cell therapy for heart disease. *Stem Cells Transl Med,* 5, 186-91.

Goncalves, F. d. C., Schneider, N., Pinto, F. O., Meyer, F. S., Visioli, F., Pfaffenseller, B., Lopez, P. L. d. C., Passos, E. P., Cirne-Lima, E. O., Meurer, L., Paz, A. H. 2014. Intravenous vs intraperitoneal mesenchymal stem cells administration: What is the best route for treating experimental colitis? *World J Gastroenterol,* 20, 18228-39.

Gonzalez-Rey, E., Anderson, P., Gonzalez, M. A., Rico, L., Buscher, D., Delgado, M. 2009. Human adult stem cells derived from adipose tissue protect against experimental colitis and sepsis. *Gut,* 58, 929-39.

Gonzalez, A., Sarna, S. K. 2001. Different types of contractions in rat colon and their modulation by oxidative stress. *Am J Physiol Gastrointest Liver Physiol,* 280, G546-54.

Gonzalez, M. A., Gonzalez-Rey, E., Rico, L., Buscher, D., Delgado, M. 2009. Adipose-derived mesenchymal stem cells alleviate experimental colitis by inhibiting inflammatory and autoimmune responses. *Gastroenterology,* 136, 978-89.

Goodman, A. L., Kallstrom, G., Faith, J. J., Reyes, A., Moore, A., Dantas, G., Gordon, J. I. 2011. Extensive personal human gut microbiota culture collections characterized and manipulated in gnotobiotic mice. *Proc Natl Acad Sci U S A,* 108, 6252-7.

Gophna, U., Sommerfeld, K., Gophna, S., Doolittle, W. F., Veldhuyzen van Zanten, S. J. O. 2006. Differences between tissue-associated intestinal microfloras of patients with Crohn's disease and ulcerative colitis. *J Clin Microbiol,* 44, 4136-41.

Gordon, D., Pavlovska, G., Uney, J. B., Wraith, D. C., Scolding, N. J. 2010. Human mesenchymal stem cells infiltrate the spinal cord, reduce demyelination, and localize to white matter lesions in experimental autoimmune encephalomyelitis. *J Neuropathol Exp Neurol,* 69, 1087-95.

Gotsman, I., Shlomai, A., Alper, R., Rabbani, E., Engelhardt, D., Ilan, Y. 2001. Amelioration of immune-mediated experimental colitis: Tolerance induction in the presence of preexisting immunity and surrogate antigen bystander effect. *J Pharmacol Exp Ther,* 297, 926-32.

Goyal, N., Rana, A., Ahlawat, A., Bijjem, K. R., Kumar, P. 2014. Animal models of inflammatory bowel disease: A review. *Inflammopharmacology,* 22, 219-33.

Goyal, R. K., Chaudhury, A. 2013. Structure activity relationship of synaptic and junctional neurotransmission. *Auton Neurosci,* 176, 11-31.

Graff, L. A., Walker, J. R., Lix, L., Clara, I., Rawsthorne, P., Rogala, L., Miller, N., Jakul, L., McPhail, C., Ediger, J., Bernstein, C. N. 2006. The relationship of inflammatory bowel disease type and activity to psychological functioning and quality of life. *Clin Gastroenterol Hepatol,* 4, 1491-1501.e1.

Gray, W. N., Denson, L. A., Baldassano, R. N., Hommel, K. A. 2011. Disease activity, behavioral dysfunction, and health-related quality of life in adolescents with inflammatory bowel disease. *Inflamm Bowel Dis,* 17, 1581-6.

Grayson, W. L., Zhao, F., Izadpanah, R., Bunnell, B., Ma, T. 2006. Effects of hypoxia on human mesenchymal stem cell expansion and plasticity in 3D constructs. *J Cell Physiol,* 207, 331-9.

Grider, J. R. 2003. Neurotransmitters mediating the intestinal peristaltic reflex in the mouse. *J Pharmacol Exp Ther,* 307, 460-7.

Gross, M., Zollner, N. 1991. Serum levels of glucose, insulin, and C-peptide during long-term D-ribose administration in man. *Klin Wochenschr,* 69, 31-6.

Grossi, L., McHugh, K., Collins, S. M. 1993. On the specificity of altered muscle function in experimental colitis in rats. *Gastroenterology,* 104, 1049-56.

Grundy, D., Brookes, S. (eds.) 2012. *Neural control of gastrointestinal function,* Morgan & Claypool: San Rafael, CA.

Gulbransen, B. D., Bashashati, M., Hirota, S. A., Gui, X., Roberts, J. A., MacDonald, J. A., Muruve, D. A., McKay, D. M., Beck, P. L., Mawe, G. M., Thompson, R. J., Sharkey, K. A. 2012. Activation of neuronal P2X7 receptor-Pannexin-1 mediates death of enteric neurons during colitis. *Nat Med,* 18, 600-4.

Guo, Y., Wysoczynski, M., Nong, Y., Tomlin, A., Zhu, X., Gumpert, A. M., Nasr, M., Muthusamy, S., Li, H., Book, M., Khan, A., Hong, K. U., Li, Q., Bolli, R. 2017. Repeated doses of cardiac mesenchymal cells are therapeutically superior to a single dose in mice with old myocardial infarction. *Basic Res Cardiol,* 112, 18.

Gupta, N., Krasnodembskaya, A., Kapetanaki, M., Mouded, M., Tan, X., Serikov, V., Matthay, M. A. 2012. Mesenchymal stem cells enhance survival and bacterial clearance in murine Escherichia coli pneumonia. *Thorax,* 67.

Gustafsson, J. K., Hansson, G. C., Sjovall, H. 2012. Ulcerative colitis patients in remission have an altered secretory capacity in the proximal colon despite macroscopically normal mucosa. *Neurogastroenterol Motil,* 24, e381-91.

Gwynne, R. M., Bornstein, J. C. 2007a. Mechanisms underlying nutrient-induced segmentation in isolated guinea pig small intestine. *Am J Physiol Gastrointest Liver Physiol,* 292, G1162-72.

Gwynne, R. M., Bornstein, J. C. 2007b. Synaptic transmission at functionally identified synapses in the enteric nervous system: Roles for both ionotropic and metabotropic receptors. *Curr Neuropharmacol,* 5, 1-17.

Gwynne, R. M., Clarke, A. J., Furness, J. B., Bornstein, J. C. 2014. Both exogenous 5-HT and endogenous 5-HT, released by fluoxetine, enhance distension evoked propulsion in guinea-pig ileum *in vitro*. *Front Neurosci,* 8, 301.

Gwynne, R. M., Dombek, A., Chang, E., Tan, L. L., Bornstein, J. C. 2004a. Video mapping and extracellular recording studies of nutrient-induced segmentation in isolated guinea-pig small intestine. *Gastroenterology,* 126 Suppl 2, A-223.

Gwynne, R. M., Thomas, E. A., Goh, S. M., Sjovall, H., Bornstein, J. C. 2004b. Segmentation induced by intraluminal fatty acid in isolated guinea-pig duodenum and jejunum. *J Physiol,* 556, 557-69.

Habibi, F., Habibi, M. E., Gharavinia, A., Mahdavi, S. B., Akbarpour, M. J., Baghaei, A., Emami, M. H. 2017. Quality of life in inflammatory bowel disease patients: A cross-sectional study. *J Res Med Sci,* 22, 104.

Habiyakare, B., Alsaadon, H., Mathai, M. L., Hayes, A., Zulli, A. 2014. Reduction of angiotensin A and alamandine vasoactivity in the rabbit model of atherogenesis: Differential effects of alamandine and Ang(1-7). *Int J Exp Pathol,* 95, 290-5.

Haddad, R., Saldanha-Araujo, F. 2014. Mechanisms of T-cell immunosuppression by mesenchymal stromal cells: What do we know so far? *Biomed Res Int,* 2014, 216806.

Hale, L. P., Greer, P. K. 2012. A novel murine model of inflammatory bowel disease and inflammation-associated colon cancer with ulcerative colitis-like features. *PLoS One,* 7, e41797.

Hallert, C., Bjorck, I., Nyman, M., Pousette, A., Granno, C., Svensson, H. 2003. Increasing fecal butyrate in ulcerative colitis patients by diet: Controlled pilot study. *Inflamm Bowel Dis,* 9, 116-21.

Hamer, H. M., Jonkers, D., Venema, K., Vanhoutvin, S., Troost, F. J., Brummer, R. J. 2008. Review article: The role of butyrate on colonic function. *Aliment Pharmacol Ther,* 27, 104-19.

Han, S., Xiao, Z., Li, X., Zhao, H., Wang, B., Qiu, Z., Li, Z., Mei, X., Xu, B., Fan, C., Chen, B., Han, J., Gu, Y., Yang, H., Shi, Q., Dai, J. 2018. Human placenta-derived mesenchymal stem cells loaded on linear ordered collagen scaffold improves functional recovery after completely transected spinal cord injury in canine. *Sci China Life Sci,* 61, 2-13.

Han, Y. M., Park, J. M., Choi, Y. S., Jin, H., Lee, Y. S., Han, N. Y., Lee, H., Hahm, K. B. 2017. The efficacy of human placenta-derived mesenchymal stem cells on radiation enteropathy along with proteomic biomarkers predicting a favorable response. *Stem Cell Res Ther,* 8, 105.

Hang, H., Yu, Y., Wu, N., Huang, Q., Xia, Q., Bian, J. 2014. Induction of highly functional hepatocytes from human umbilical cord mesenchymal stem cells by HNF4α transduction. *PLoS One,* 9, e104133.

Hansen, M. B. 2003. The enteric nervous system I: Organisation and classification. *Pharmacol Toxicol,* 92, 105-13.

Hao, H., Liu, J., Shen, J., Zhao, Y., Liu, H., Hou, Q., Tong, C., Ti, D., Dong, L., Cheng, Y., Mu, Y., Liu, J., Fu, X., Han, W. 2013. Multiple intravenous infusions of bone marrow mesenchymal stem cells reverse hyperglycemia in experimental type 2 diabetes rats. *Biochem Biophys Res Commun,* 436, 418-23.

Hao, P., Liang, Z., Piao, H., Ji, X., Wang, Y., Liu, Y., Liu, R., Liu, J. 2014. Conditioned medium of human adipose-derived mesenchymal stem cells mediates protection in neurons following glutamate excitotoxicity by regulating energy metabolism and GAP-43 expression. *Metab Brain Dis,* 29, 193-205.

Harris, V. K., Yan, Q. J., Vyshkina, T., Sahabi, S., Liu, X., Sadiq, S. A. 2012. Clinical and pathological effects of intrathecal injection of mesenchymal

stem cell-derived neural progenitors in an experimental model of multiple sclerosis. *J Neurol Sci,* 313, 167-77.

Harting, M. T., Jimenez, F., Xue, H., Fischer, U. M., Baumgartner, J., Dash, P. K., Cox, C. S. 2009. Intravenous mesenchymal stem cell therapy for traumatic brain injury: Laboratory investigation. *J Neurosurg,* 110, 1189-97.

Hashemi, S. M., Ghods, S., Kolodgie, F. D., Parcham-Azad, K., Keane, M., Hamamdzic, D., Young, R., Rippy, M. K., Virmani, R., Litt, H., Wilensky, R. L. 2008. A placebo controlled, dose-ranging, safety study of allogenic mesenchymal stem cells injected by endomyocardial delivery after an acute myocardial infarction. *Eur Heart J,* 29, 251-9.

Hass, R., Kasper, C., Bohm, S., Jacobs, R. 2011. Different populations and sources of human mesenchymal stem cells (MSC): A comparison of adult and neonatal tissue-derived MSC. *Cell Commun Signal,* 9, 12.

Hayashi, Y., Tsuji, S., Tsujii, M., Nishida, T., Ishii, S., Iijima, H., Nakamura, T., Eguchi, H., Miyoshi, E., Hayashi, N., Kawano, S. 2008. Topical implantation of mesenchymal stem cells has beneficial effects on healing of experimental colitis in rats. *J Pharmacol Exp Ther,* 326, 523-31.

Hayes, P. A., Fraher, M. H., Quigley, E. M. M. 2014. Irritable bowel syndrome: the role of food in pathogenesis and management. *Gastroenterol Hepatol (N Y),* 10, 164-74.

He, Q., Li, X., Liu, C., Su, L., Xia, Z., Li, X., Li, Y., Li, L., Yan, T., Feng, Q., Xiao, L. 2016. Dysbiosis of the fecal microbiota in the TNBS-induced Crohn's disease mouse model. *Appl Microbiol Biotechnol,* 100, 4485-94.

He, X. W., He, X. S., Lian, L., Wu, X. J., Lan, P. 2012. Systemic infusion of bone marrow-derived mesenchymal stem cells for treatment of experimental colitis in mice. *Dig Dis Sci,* 57, 3136-44.

Heazlewood, C. K., Cook, M. C., Eri, R., Price, G. R., Tauro, S. B., Taupin, D., Thornton, D. J., Png, C. W., Crockford, T. L., Cornall, R. J., Adams, R., Kato, M., Nelms, K. A., Hong, N. A., Florin, T. H. J., Goodnow, C. C., McGuckin, M. A. 2008. Aberrant mucin assembly in mice causes endoplasmic reticulum stress and spontaneous inflammation resembling ulcerative colitis. *PLoS Med,* 5, e54.

Hebden, J. M., Blackshaw, P. E., Perkins, A. C., Wilson, C. G., Spiller, R. C. 2000. Limited exposure of the healthy distal colon to orally-dosed formulation is further exaggerated in active left-sided ulcerative colitis. *Aliment Pharmacol Ther,* 14, 155-61.

Hegyi, B., Sagi, B., Kovacs, J., Kiss, J., Urban, V. S., Meszaros, G., Monostori, E., Uher, F. 2010. Identical, similar or different? Learning about immunomodulatory function of mesenchymal stem cells isolated from various mouse tissues: bone marrow, spleen, thymus and aorta wall. *Int Immunol,* 22, 551-9.

Hendrickson, B. A., Gokhale, R., Cho, J. H. 2002. Clinical aspects and pathophysiology of inflammatory bowel disease. *Clin Microbiol Rev,* 15, 79-94.

Heredia, D. J., Dickson, E. J., Bayguinov, P. O., Hennig, G. W., Smith, T. K. 2010. Colonic elongation inhibits pellet propulsion and migrating motor complexes in the murine large bowel. *J Physiol,* 588, 2919-34.

Hicks, L. C., Huang, J., Kumar, S., Powles, S. T., Orchard, T. R., Hanna, G. B., Williams, H. R. 2015. Analysis of exhaled breath volatile organic compounds in inflammatory bowel disease: A pilot study. *J Crohns Colitis,* 9, 731-7.

Hilsden, R. 2002. Funding the new biologics--what can we learn from infliximab? The CCOHTA report: a gastroenterologist's viewpoint. *Can J Gastroenterol,* 16, 865-8.

Hirayama, A., Nakashima, E., Sugimoto, M., Akiyama, S., Sato, W., Maruyama, S., Matsuo, S., Tomita, M., Yuzawa, Y., Soga, T. 2012. Metabolic profiling reveals new serum biomarkers for differentiating diabetic nephropathy. *Anal Bioanal Chem,* 404, 3101-9.

Hofer, H. R., Tuan, R. S. 2016. Secreted trophic factors of mesenchymal stem cells support neurovascular and musculoskeletal therapies. *Stem Cell Res Ther,* 7, 131.

Hoff, S., Zeller, F., von Weyhern, C. W., Wegner, M., Schemann, M., Michel, K., Ruhl, A. 2008. Quantitative assessment of glial cells in the human and guinea pig enteric nervous system with an anti-Sox8/9/10 antibody. *J Comp Neurol,* 509, 356-71.

Hoffman, J. M., McKnight, N. D., Sharkey, K. A., Mawe, G. M. 2011. The relationship between inflammation-induced neuronal excitability and disrupted motor activity in the guinea pig distal colon. *Neurogastroenterol Motil,* 23, 673-e279.

Hoffmann, C., Hill, D. A., Minkah, N., Kirn, T., Troy, A., Artis, D., Bushman, F. 2009. Community-wide response of the gut microbiota to enteropathogenic *Citrobacter rodentium* infection revealed by deep sequencing. *Infect Immun,* 77, 4668-78.

Hofstetter, C. P., Schwarz, E. J., Hess, D., Widenfalk, J., El Manira, A., Prockop, D. J., Olson, L. 2002. Marrow stromal cells form guiding strands in the injured spinal cord and promote recovery. *Proc Natl Acad Sci U S A,* 99, 2199-204.

Hogaboam, C. M., Jacobson, K., Collins, S. M., Blennerhassett, M. G. 1995. The selective beneficial effects of nitric oxide inhibition in experimental colitis. *Am J Physiol* 268, G673-84.

Holko, P., Kawalec, P., Mossakowska, M., Pilc, A. 2016. Health-related quality of life impairment and indirect cost of Crohn's disease: A self-report study in Poland. *PLoS One,* 11, e0168586.

Holzer, P. 2007. Role of visceral afferent neurons in mucosal inflammation and defence. *Curr Opin Pharmacol,* 7, 563-9.

Hong, J., Jin, H., Han, J., Hu, H., Liu, J., Li, L., Huang, Y., Wang, D., Wu, M., Qiu, L., Qian, Q. 2014. Infusion of human umbilical cord-derived mesenchymal stem cells effectively relieves liver cirrhosis in DEN-induced rats. *Mol Med Rep,* 9, 1103-11.

Hong, Y. S., Ahn, Y. T., Park, J. C., Lee, J. H., Lee, H., Huh, C. S., Kim, D. H., Ryu, D. H., Hwang, G. S. 2010. 1H NMR-based metabonomic assessment of probiotic effects in a colitis mouse model. *Arch Pharm Res,* 33, 1091-101.

Hooper, L. V., Littman, D. R., Macpherson, A. J. 2012. Interactions between the microbiota and the immune system. *Science,* 336, 1268-73.

Hooper, L. V., Macpherson, A. J. 2010. Immune adaptations that maintain homeostasis with the intestinal microbiota. *Nat Rev Immunol,* 10, 159-69.
Hooper, L. V., Wong, M. H., Thelin, A., Hansson, L., Falk, P. G., Gordon, J. I. 2001. Molecular analysis of commensal host-microbial relationships in the intestine. *Science,* 291, 881-4.
Horne, S. M., Mattson, K. R., Pruss, B. M. 2009. An *Escherichia coli aer* mutant exhibits a reduced ability to colonize the streptomycin-treated mouse large intestine. *Antonie Van Leeuwenhoek,* 95, 149-58.
Hosseini, M., Yousefifard, M., Aziznejad, H., Nasirinezhad, F. 2015. The effect of bone marrow-derived mesenchymal stem cell transplantation on allodynia and hyperalgesia in neuropathic animals: A systematic review with meta-analysis. *Biol Blood Marrow Transplant,* 21, 1537-44.
Hsieh, S. C., Lu, C. C., Horng, Y. T., Soo, P. C., Chang, Y. L., Tsai, Y. H., Lin, C. S., Lai, H. C. 2007. The bacterial metabolite 2,3-butanediol ameliorates endotoxin-induced acute lung injury in rats. *Microbes Infect,* 9, 1402-9.
Hu, H. Z., Gao, N., Zhu, M. X., Liu, S., Ren, J., Gao, C., Xia, Y., Wood, J. D. 2003. Slow excitatory synaptic transmission mediated by P2Y1 receptors in the guinea-pig enteric nervous system. *J Physiol,* 550, 493-504.
Hu, J., Zhao, G., Zhang, L., Qiao, C., Di, A., Gao, H., Xu, H. 2016. Safety and therapeutic effect of mesenchymal stem cell infusion on moderate to severe ulcerative colitis. *Exp Ther Med,* 12, 2983-9.
Hu, S. L., Lu, P. G., Zhang, L. J., Li, F., Chen, Z., Wu, N., Meng, H., Lin, J. K., Feng, H. 2012. *In vivo* magnetic resonance imaging tracking of SPIO-labeled human umbilical cord mesenchymal stem cells. *J Cell Biochem,* 113, 1005-12.
Hu, X., Wang, J., Chen, J., Luo, R., He, A., Xie, X., Li, J. 2007. Optimal temporal delivery of bone marrow mesenchymal stem cells in rats with myocardial infarction. *Eur J Cardiothorac Surg,* 31, 438-43.
Huang, V., Mishra, R., Thanabalan, R., Nguyen, G. C. 2013. Patient awareness of extraintestinal manifestations of inflammatory bowel disease. *J Crohns Colitis,* 7, e318-24.
Huda-Faujan, N., Abdulamir, A. S., Fatimah, A. B., Anas, O. M., Shuhaimi, M., Yazid, A. M., Loong, Y. Y. 2010. The impact of the level of the intestinal short chain Fatty acids in inflammatory bowel disease patients versus healthy subjects. *Open Biochem J,* 4, 53-8.
Huizinga, J. D., Chen, J. H. 2014. The myogenic and neurogenic components of the rhythmic segmentation motor patterns of the intestine. *Front Neurosci,* 8, 78.
Huizinga, J. D., Chen, J. H., Zhu, Y. F., Pawelka, A., McGinn, R. J., Bardakjian, B. L., Parsons, S. P., Kunze, W. A., Wu, R. Y., Bercik, P., Khoshdel, A., Chen, S., Yin, S., Zhang, Q., Yu, Y., Gao, Q., Li, K., Hu, X., Zarate, N., Collins, P., Pistilli, M., Ma, J., Zhang, R., Chen, D. 2014. The origin of segmentation motor activity in the intestine. *Nat Commun,* 5, 3326.
Huizinga, J. D., Lammers, W. J. 2009. Gut peristalsis is governed by a multitude of cooperating mechanisms. *Am J Physiol Gastrointest Liver Physiol,* 296, G1-8.
Huppertz-Hauss, G., Hoivik, M. L., Langholz, E., Odes, S., Smastuen, M., Stockbrugger, R., Hoff, G., Moum, B., Bernklev, T. 2015. Health-related

quality of life in inflammatory bowel disease in a European-wide population-based cohort 10 years after diagnosis. *Inflamm Bowel Dis,* 21, 337-44.

Huttenhower, C., Kostic, A. D., Xavier, R. J. 2014. Inflammatory bowel disease as a model for translating the microbiome. *Immunity,* 40, 843-54.

Hwang, I., Park, Y. J., Kim, Y. R., Kim, Y. N., Ka, S., Lee, H. Y., Seong, J. K., Seok, Y. J., Kim, J. B. 2015. Alteration of gut microbiota by vancomycin and bacitracin improves insulin resistance via glucagon-like peptide 1 in diet-induced obesity. *FASEB J,* 29, 2397-411.

Hwang, J. M., Varma, M. G. 2008. Surgery for inflammatory bowel disease. *World J Gastroenterol,* 14, 2678-90.

Inan, M. S., Tolmacheva, V., Wang, Q. S., Rosenberg, D. W., Giardina, C. 2000. Transcription factor NF-kappaB participates in regulation of epithelial cell turnover in the colon. *Am J Physiol Gastrointest Liver Physiol,* 279, G1282-91.

Irving, P. M., Gearry, R. B., Sparrow, M. P., Gibson, P. R. 2007. Appropriate use of corticosteroids in Crohn's disease. *Aliment Pharmacol Ther,* 26, 313-29.

Isaacs, K. L., Sartor, R. B. 2004. Treatment of inflammatory bowel disease with antibiotics. *Gastroenterol Clin North Am,* 33, 335-45, x.

Isele, N. B., Lee, H. S., Landshamer, S., Straube, A., Padovan, C. S., Plesnila, N., Culmsee, C. 2007. Bone marrow stromal cells mediate protection through stimulation of PI3-K/Akt and MAPK signaling in neurons. *Neurochem Int,* 50, 243-50.

Izzo, A. A., Sharkey, K. A. 2010. Cannabinoids and the gut: New developments and emerging concepts. *Pharmacol Ther,* 126, 21-38.

Jackson, B., Con, D., Ma, R., Gorelik, A., Liew, D., De Cruz, P. 2017. Health care costs associated with Australian tertiary inflammatory bowel disease care. *Scand J Gastroenterol,* 52, 851-6.

Jacobs, S. A., Roobrouck, V. D., Verfaillie, C. M., Van Gool, S. W. 2013. Immunological characteristics of human mesenchymal stem cells and multipotent adult progenitor cells. *Immunol Cell Biol,* 91, 32-9.

Jakeman, L. B., Wei, P., Guan, Z., Stokes, B. T. 1998. Brain-derived neurotrophic factor stimulates hindlimb stepping and sprouting of cholinergic fibers after spinal cord injury. *Exp Neurol,* 154, 170-84.

Jandhyala, S. M., Talukdar, R., Subramanyam, C., Vuyyuru, H., Sasikala, M., Nageshwar Reddy, D. 2015. Role of the normal gut microbiota. *World J Gastroenterol,* 21, 8787-803.

Jang, S., Cho, H.-H., Cho, Y.-B., Park, J.-S., Jeong, H.-S. 2010. Functional neural differentiation of human adipose tissue-derived stem cells using bFGF and forskolin. *BMC Cell Biol,* 11, 25.

Jansson, J., Willing, B., Lucio, M., Fekete, A., Dicksved, J., Halfvarson, J., Tysk, C., Schmitt-Kopplin, P. 2009. Metabolomics reveals metabolic biomarkers of Crohn's disease. *PLoS One,* 4, e6386.

Jiang, W., Ma, A., Wang, T., Han, K., Liu, Y., Zhang, Y., Dong, A., Du, Y., Huang, X., Wang, J., Lei, X., Zheng, X. 2006. Homing and differentiation of mesenchymal stem cells delivered intravenously to ischemic myocardium *in vivo*: A time-series study. *Pflugers Arch,* 453, 43-52.

Jiang, X. X., Zhang, Y., Liu, B., Zhang, S. X., Wu, Y., Yu, X. D., Mao, N. 2005. Human mesenchymal stem cells inhibit differentiation and function of monocyte-derived dendritic cells. *Blood,* 105, 4120-6.

Jiminez, J. A., Uwiera, T. C., Douglas Inglis, G., Uwiera, R. R. 2015. Animal models to study acute and chronic intestinal inflammation in mammals. *Gut Pathog,* 7, 29.

Jin, D., Zhang, H., Sun, J. 2014. Manipulation of microbiome, a promising therapy for inflammatory bowel diseases. *J Clin Cell Immunol,* 5, 234.

Johnson, L. R., Said, H. M. (eds.) 2012. *Physiology of the Gastrointestinal Tract, Two Volume Set,* [5th ed]. Elsevier Science: London.

Johnson, P. J., Bornstein, J. C. 2004. Neurokinin-1 and -3 receptor blockade inhibits slow excitatory synaptic transmission in myenteric neurons and reveals slow inhibitory input. *Neuroscience,* 126, 137-47.

Johnson, T. V., DeKorver, N. W., Levasseur, V. A., Osborne, A., Tassoni, A., Lorber, B., Heller, J. P., Villasmil, R., Bull, N. D., Martin, K. R., Tomarev, S. I. 2014. Identification of retinal ganglion cell neuroprotection conferred by platelet-derived growth factor through analysis of the mesenchymal stem cell secretome. *Brain,* 137, 503-19.

Jones, E., McGonagle, D. 2008. Human bone marrow mesenchymal stem cells *in vivo*. *Rheumatology (Oxford),* 47, 126-31.

Jones, E., Schafer, R. 2015a. Biological differences between native and cultured mesenchymal stem cells: Implications for therapies. *Methods Mol Biol,* 1235, 105-20.

Jones, E., Schafer, R. 2015b. Where is the common ground between bone marrow mesenchymal stem/stromal cells from different donors and species? *Stem Cell Res Ther,* 6, 143.

Jonsson, M., Norrgard, O., Forsgren, S. 2007. Presence of a marked nonneuronal cholinergic system in human colon: Study of normal colon and colon in ulcerative colitis. *Inflamm Bowel Dis,* 13, 1347-56.

Joo, S. Y., Cho, K. A., Jung, Y. J., Kim, H. S., Park, S. Y., Choi, Y. B., Hong, K. M., Woo, S. Y., Seoh, J. Y., Cho, S. J., Ryu, K. H. 2010. Mesenchymal stromal cells inhibit graft-versus-host disease of mice in a dose-dependent manner. *Cytotherapy,* 12, 361-70.

Jostins, L., Ripke, S., Weersma, R. K., Duerr, R. H., McGovern, D. P., Hui, K. Y., Lee, J. C., Schumm, L. P., Sharma, Y., Anderson, C. A., Essers, J., Mitrovic, M., Ning, K., Cleynen, I., Theatre, E., Spain, S. L., Raychaudhuri, S., Goyette, P., Wei, Z., Abraham, C., Achkar, J.-P., Ahmad, T., Amininejad, L., Ananthakrishnan, A. N., Andersen, V., Andrews, J. M., Baidoo, L., Balschun, T., Bampton, P. A., Bitton, A., Boucher, G., Brand, S., Büning, C., Cohain, A., Cichon, S., D'Amato, M., De Jong, D., Devaney, K. L., Dubinsky, M., Edwards, C., Ellinghaus, D., Ferguson, L. R., Franchimont, D., Fransen, K., Gearry, R., Georges, M., Gieger, C., Glas, J., Haritunians, T., Hart, A., Hawkey, C., Hedl, M., Hu, X., Karlsen, T. H., Kupcinskas, L., Kugathasan, S., Latiano, A., Laukens, D., Lawrance, I. C., Lees, C. W., Louis, E., Mahy, G., Mansfield, J., Morgan, A. R., Mowat, C., Newman, W., Palmieri, O., Ponsioen, C. Y., Potocnik, U., Prescott, N. J., Regueiro, M., Rotter, J. I., Russell, R. K., Sanderson, J. D., Sans, M., Satsangi, J., Schreiber, S., Simms, L. A., Sventoraityte, J., Targan, S. R.,

Taylor, K. D., Tremelling, M., Verspaget, H. W., De Vos, M., Wijmenga, C., Wilson, D. C., Winkelmann, J., Xavier, R. J., Zeissig, S., Zhang, B., Zhang, C. K., Zhao, H., Silverberg, M. S., Annese, V., Hakonarson, H., Brant, S. R., Radford-Smith, G., Mathew, C. G., Rioux, J. D., Schadt, E. E., et al. 2012. Host-microbe interactions have shaped the genetic architecture of inflammatory bowel disease. *Nature,* 491, 119-24.

Joyce, N., Annett, G., Wirthlin, L., Olson, S., Bauer, G., Nolta, J. A. 2010. Mesenchymal stem cells for the treatment of neurodegenerative disease. *Regen Med,* 5, 933-46.

Jump, R. L., Polinkovsky, A., Hurless, K., Sitzlar, B., Eckart, K., Tomas, M., Deshpande, A., Nerandzic, M. M., Donskey, C. J. 2014. Metabolomics analysis identifies intestinal microbiota-derived biomarkers of colonization resistance in clindamycin-treated mice. *PLoS One,* 9, e101267.

Jung, J. E., Kim, G. S., Chan, P. H. 2011. Neuroprotection by interleukin-6 is mediated by signal transducer and activator of transcription 3 and antioxidative signaling in ischemic stroke. *Stroke,* 42, 3574-9.

Jung, S., Panchalingam, K. M., Rosenberg, L., Behie, L. A. 2012. *Ex vivo* expansion of human mesenchymal stem cells in defined serum-free media. *Stem Cells Int,* 2012, 123030.

Jung, W. Y., Kang, J. H., Kim, K. G., Kim, H. S., Jang, B. I., Park, Y. H., Song, I. H. 2015. Human adipose-derived stem cells attenuate inflammatory bowel disease in IL-10 knockout mice. *Tissue Cell,* 47, 86-93.

Juste, C., Kreil, D. P., Beauvallet, C., Guillot, A., Vaca, S., Carapito, C., Mondot, S., Sykacek, P., Sokol, H., Blon, F., Lepercq, P., Levenez, F., Valot, B., Carre, W., Loux, V., Pons, N., David, O., Schaeffer, B., Lepage, P., Martin, P., Monnet, V., Seksik, P., Beaugerie, L., Ehrlich, S. D., Gibrat, J. F., Van Dorsselaer, A., Dore, J. 2014. Bacterial protein signals are associated with Crohn's disease. *Gut,* 63, 1566-77.

Kalafateli, M., Triantos, C., Theocharis, G., Giannakopoulou, D., Koutroumpakis, E., Chronis, A., Sapountzis, A., Margaritis, V., Thomopoulos, K., Nikolopoulou, V. 2013. Health-related quality of life in patients with inflammatory bowel disease: A single-center experience. *Ann Gastroenterol,* 26, 243-8.

Kamada, T., Koda, M., Dezawa, M., Yoshinaga, K., Hashimoto, M., Koshizuka, S., Nishio, Y., Moriya, H., Yamazaki, M. 2005. Transplantation of bone marrow stromal cell-derived Schwann cells promotes axonal regeneration and functional recovery after complete transection of adult rat spinal cord. *J Neuropathol Exp Neurol,* 64, 37-45.

Kanbe, T., Murai, R., Mukoyama, T., Murawaki, Y., Hashiguchi, K., Yoshida, Y., Tsuchiya, H., Kurimasa, A., Harada, K., Yashima, K., Nishimuki, E., Shabana, N., Kishimoto, Y., Kojyo, H., Miura, K., Murawaki, Y., Kawasaki, H., Shiota, G. 2006. Naked gene therapy of hepatocyte growth factor for dextran sulfate sodium-induced colitis in mice. *Biochem Biophys Res Commun,* 345, 1517-25.

Kang, S. K., Shin, I. S., Ko, M. S., Jo, J. Y., Ra, J. C. 2012. Journey of mesenchymal stem cells for homing: Strategies to enhance efficacy and safety of stem cell therapy. *Stem Cells Int,* 2012, 342968.

Kaplan, G. G. 2015. The global burden of IBD: From 2015 to 2025. *Nat Rev Gastroenterol Hepatol,* 12, 720-7.
Kaplan, G. G., Ng, S. C. 2017. Understanding and preventing the global increase of inflammatory bowel disease. *Gastroenterology,* 152, 313-21.e2.
Kappelman, M. D., Moore, K. R., Allen, J. K., Cook, S. F. 2013. Recent trends in the prevalence of Crohn's disease and ulcerative colitis in a commercially insured US population. *Dig Dis Sci,* 58, 519-25.
Kariyawasam, V. C., Huang, T. D., Lunney, P. C., Middleton, K., Wang, R. R., Selinger, C. P., Katelaris, P., Andrews, J. M., Leong, R. W. 2013. Natural history of elderly onset inflammatory bowel disease - Sydney IBD cohort (1942–2012). *Gastroenterology,* 144, S634-5.
Karp, J. M., Teo, G. S. L. 2009. Mesenchymal stem cell homing: The devil is in the details. *Cell Stem Cell,* 4, 206-16.
Karussis, D., Kassis, I. 2008. The potential use of stem cells in multiple sclerosis: An overview of the preclinical experience. *Clin Neurol Neurosurg,* 110, 889-96.
Kaser, A., Zeissig, S., Blumberg, R. S. 2010. Inflammatory bowel disease. *Annu Rev Immunol,* 28, 573-621.
Kashyap, P. C., Marcobal, A., Ursell, L. K., Larauche, M., Duboc, H., Earle, K. A., Sonnenburg, E. D., Ferreyra, J. A., Higginbottom, S. K., Million, M., Tache, Y., Pasricha, P. J., Knight, R., Farrugia, G., Sonnenburg, J. l. 2013. Complex interactions among diet, gastrointestinal transit, and gut microbiota in humanized mice. *Gastroenterology,* 144, 967-77.
Kassis, I., Grigoriadis, N., Gowda-Kurkalli, B., Mizrachi-Kol, R., Ben-Hur, T., Slavin, S., Abramsky, O., Karussis, D. 2008. Neuroprotection and immunomodulation with mesenchymal stem cells in chronic experimental autoimmune encephalomyelitis. *Arch Neurol,* 65, 753-61.
Kato, T., Hayashi, Y., Inoue, K., Yuasa, H. 2005. Glycerol absorption by Na+-dependent carrier-mediated transport in the closed loop of the rat small intestine. *Biol Pharm Bull,* 28, 553-5.
Katsui, R., Kojima, Y., Kuniyasu, H., Shimizu, J., Koyama, F., Fujii, H., Nakajima, Y., Takaki, M. 2008. A new possibility for repairing the anal dysfunction by promoting regeneration of the reflex pathways in the enteric nervous system. *Am J Physiol Gastrointest Liver Physiol,* 294, G1084-93.
Katsuno, T., Ochi, M., Tominaga, K., Tanaka, F., Sogawa, M., Tanigawa, T., Yamagami, H., Shiba, M., Watanabe, K., Watanabe, T., Fujiwara, Y., Arakawa, T. 2013. Mesenchymal stem cells administered in the early phase of tumorigenesis inhibit colorectal tumor development in rats. *J Clin Biochem Nutr,* 53, 170-5.
Kean, T. J., Lin, P., Caplan, A. I., Dennis, J. E. 2013. MSCs: Delivery routes and engraftment, cell-targeting strategies, and immune modulation. *Stem Cells Int,* 2013, 732742.
Keeton, R. L., Mikocka-Walus, A., Andrews, J. M. 2015. Concerns and worries in people living with inflammatory bowel disease (IBD): A mixed methods study. *J Psychosom Res,* 78, 573-8.
Kemp, S. W., Walsh, S. K., Midha, R. 2008. Growth factor and stem cell enhanced conduits in peripheral nerve regeneration and repair. *Neurol Res,* 30, 1030-8.

Khan, K. J., Ullman, T. A., Ford, A. C., Abreu, M. T., Abadir, A., Marshall, J. K., Talley, N. J., Moayyedi, P. 2011. Antibiotic therapy in inflammatory bowel disease: A systematic review and meta-analysis. *Am J Gastroenterol,* 106, 661-73.

Khansari, N., Shakiba, Y., Mahmoudi, M. 2009. Chronic inflammation and oxidative stress as a major cause of age-related diseases and cancer. *Recent Pat Inflamm Allergy Drug Discov,* 3, 73-80.

Khor, B., Gardet, A., Xavier, R. J. 2011. Genetics and pathogenesis of inflammatory bowel disease. *Nature,* 474, 307-17.

Kiesler, P., Fuss, I. J., Strober, W. 2015. Experimental models of inflammatory bowel diseases. *Cell Mol Gastroenterol Hepatol,* 1, 154-70.

Kim, D. H., Cheon, J. H. 2017. Pathogenesis of inflammatory bowel disease and recent advances in biologic therapies. *Immune Network,* 17, 25-40.

Kim, E. R., Chang, D. K. 2014. Colorectal cancer in inflammatory bowel disease: The risk, pathogenesis, prevention and diagnosis. *World J Gastroenterol,* 20, 9872-81.

Kim, H., Kim, H. Y., Choi, M. R., Hwang, S., Nam, K. H., Kim, H. C., Han, J. S., Kim, K. S., Yoon, H. S., Kim, S. H. 2010a. Dose-dependent efficacy of ALS-human mesenchymal stem cells transplantation into cisterna magna in SOD1-G93A ALS mice. *Neurosci Lett,* 468, 190-4.

Kim, H. S., Shin, T. H., Lee, B. C., Yu, K. R., Seo, Y., Lee, S., Seo, M. S., Hong, I. S., Choi, S. W., Seo, K. W., Nunez, G., Park, J. H., Kang, K. S. 2013. Human umbilical cord blood mesenchymal stem cells reduce colitis in mice by activating NOD2 signaling to COX2. *Gastroenterology,* 145, 1392-1403.

Kim, I. W., Myung, S. J., Do, M. Y., Ryu, Y. M., Kim, M. J., Do, E. J., Park, S., Yoon, S. M., Ye, B. D., Byeon, J. S., Yang, S. K., Kim, J. H. 2010b. Western-style diets induce macrophage infiltration and contribute to colitis-associated carcinogenesis. *J Gastroenterol Hepatol,* 25, 1785-94.

Kim, J. Y., Kim, D. H., Kim, J. H., Lee, D., Jeon, H. B., Kwon, S. J., Kim, S. M., Yoo, Y. J., Lee, E. H., Choi, S. J., Seo, S. W., Lee, J. I., Na, D. L., Yang, Y. S., Oh, W., Chang, J. W. 2012. Soluble intracellular adhesion molecule-1 secreted by human umbilical cord blood-derived mesenchymal stem cell reduces amyloid-beta plaques. *Cell Death Differ,* 19, 680-91.

Kim, N., Cho, S. G. 2013. Clinical applications of mesenchymal stem cells. *Korean J Intern Med,* 28, 387-402.

Kim, N., Cho, S. G. 2015. New strategies for overcoming limitations of mesenchymal stem cell-based immune modulation. *Int J Stem Cells,* 8, 54-68.

Kim, S. S., Yoo, S. W., Park, T. S., Ahn, S. C., Jeong, H. S., Kim, J. W., Chang, D. Y., Cho, K. G., Kim, S. U., Huh, Y., Lee, J. E., Lee, S. Y., Lee, Y. D., Suh-Kim, H. 2008. Neural induction with neurogenin1 increases the therapeutic effects of mesenchymal stem cells in the ischemic brain. *Stem Cells,* 26, 2217-28.

Kim, Y.-S., Kim, J.-Y., Huh, J. W., Lee, S. W., Choi, S. J., Oh, Y.-M. 2015. The therapeutic effects of optimal dose of mesenchymal stem cells in a murine model of an elastase induced-emphysema. *Tuberc Respir Dis (Seoul),* 78, 239-45.

Kim, Y. J., Park, H. J., Lee, G., Bang, O. Y., Ahn, Y. H., Joe, E., Kim, H. O., Lee, P. H. 2009. Neuroprotective effects of human mesenchymal stem cells on dopaminergic neurons through anti-inflammatory action. *Glia,* 57, 13-23.

Kim, Y. S., Jung, S.-A., Lee, K.-M., Park, S. J., Kim, T. O., Choi, C. H., Kim, H. G., Moon, W., Moon, C. M., Song, H. K., Na, S.-Y., Yang, S.-K., Korean Association for the Study of Intestinal, D. 2017. Impact of inflammatory bowel disease on daily life: An online survey by the Korean Association for the Study of Intestinal Diseases. *Intest Res,* 15, 338-44.

Kinoshita, K., Hori, M., Fujisawa, M., Sato, K., Ohama, T., Momotani, E., Ozaki, H. 2006. Role of TNF-α in muscularis inflammation and motility disorder in a TNBS-induced colitis model: Clues from TNF-α-deficient mice. *Neurogastroenterol Motil,* 18, 578-88.

Kishino, S., Takeuchi, M., Park, S. B., Hirata, A., Kitamura, N., Kunisawa, J., Kiyono, H., Iwamoto, R., Isobe, Y., Arita, M., Arai, H., Ueda, K., Shima, J., Takahashi, S., Yokozeki, K., Shimizu, S., Ogawa, J. 2013. Polyunsaturated fatty acid saturation by gut lactic acid bacteria affecting host lipid composition. *Proc Natl Acad Sci U S A,* 110, 17808-13.

Kiyosue, M., Fujisawa, M., Kinoshita, K., Hori, M., Ozaki, H. 2006. Different susceptibilities of spontaneous rhythmicity and myogenic contractility to intestinal muscularis inflammation in the hapten-induced colitis. *Neurogastroenterol Motil,* 18, 1019-30.

Kjeldsen, L., Cowland, J. B., Borregaard, N. 2000. Human neutrophil gelatinase-associated lipocalin and homologous proteins in rat and mouse. *Biochim Biophys Acta,* 1482, 272-83.

Kleessen, B., Kroesen, A. J., Buhr, H. J., Blaut, M. 2002. Mucosal and invading bacteria in patients with inflammatory bowel disease compared with controls. *Scand J Gastroenterol,* 37, 1034-41.

Koch, T. R., Carney, J. A., Go, V. L. 1987. Distribution and quantitation of gut neuropeptides in normal intestine and inflammatory bowel diseases. *Dig Dis Sci,* 32, 369-76.

Koch, T. R., Carney, J. A., Go, V. L., Szurszewski, J. H. 1988. Spontaneous contractions and some electrophysiologic properties of circular muscle from normal sigmoid colon and ulcerative colitis. *Gastroenterology,* 95, 77-84.

Kondamudi, P. K., Malayandi, R., Eaga, C., Aggarwal, D. 2013. Drugs as causative agents and therapeutic agents in inflammatory bowel disease. *Acta Pharm Sin B,* 3, 289-96.

Kornbluth, A., Sachar, D. B. 2010. Ulcerative colitis practice guidelines in adults: American College Of Gastroenterology, Practice Parameters Committee. *Am J Gastroenterol,* 105, 501-23.

Koropatkin, N. M., Cameron, E. A., Martens, E. C. 2012. How glycan metabolism shapes the human gut microbiota. *Nat Rev Microbiol,* 10, 323-35.

Korpi, A., Jarnberg, J., Pasanen, A. L. 2009. Microbial volatile organic compounds. *Crit Rev Toxicol,* 39, 139-93.

Kostic, A. D., Howitt, M. R., Garrett, W. S. 2013. Exploring host-microbiota interactions in animal models and humans. *Genes Dev,* 27, 701-18.

Krakora, D., Mulcrone, P., Meyer, M., Lewis, C., Bernau, K., Gowing, G., Zimprich, C., Aebischer, P., Svendsen, C. N., Suzuki, M. 2013. Synergistic

effects of GDNF and VEGF on lifespan and disease progression in a familial ALS rat model. *Mol Ther,* 21, 1602-10.

Krampera, M., Cosmi, L., Angeli, R., Pasini, A., Liotta, F., Andreini, A., Santarlasci, V., Mazzinghi, B., Pizzolo, G., Vinante, F., Romagnani, P., Maggi, E., Romagnani, S., Annunziato, F. 2006. Role for interferon-gamma in the immunomodulatory activity of human bone marrow mesenchymal stem cells. *Stem Cells,* 24, 386-98.

Krauter, E. M., Linden, D. R., Sharkey, K. A., Mawe, G. M. 2007a. Synaptic plasticity in myenteric neurons of the guinea-pig distal colon: Presynaptic mechanisms of inflammation-induced synaptic facilitation. *J Physiol,* 581, 787-800.

Krauter, E. M., Strong, D. S., Brooks, E. M., Linden, D. R., Sharkey, K. A., Mawe, G. M. 2007b. Changes in colonic motility and the electrophysiological properties of myenteric neurons persist following recovery from trinitrobenzene sulfonic acid colitis in the guinea pig. *Neurogastroenterol Motil,* 19, 990-1000.

Kressel, M., Berthoud, H. R., Neuhuber, W. L. 1994. Vagal innervation of the rat pylorus: An anterograde tracing study using carbocyanine dyes and laser scanning confocal microscopy. *Cell Tissue Res,* 275, 109-23.

Krogius-Kurikka, L., Lyra, A., Malinen, E., Aarnikunnas, J., Tuimala, J., Paulin, L., Makivuokko, H., Kajander, K., Palva, A. 2009. Microbial community analysis reveals high level phylogenetic alterations in the overall gastrointestinal microbiota of diarrhoea-predominant irritable bowel syndrome sufferers. *BMC Gastroenterol,* 9, 95.

Kruis, W., Fric, P., Pokrotnieks, J., Lukas, M., Fixa, B., Kascak, M., Kamm, M. A., Weismueller, J., Beglinger, C., Stolte, M., Wolff, C., Schulze, J. 2004. Maintaining remission of ulcerative colitis with the probiotic *Escherichia coli* Nissle 1917 is as effective as with standard mesalazine. *Gut,* 53, 1617-23.

Kuihua, Z., Chunyang, W., Cunyi, F., Xiumei, M. 2014. Aligned SF/P(LLA-CL)-blended nanofibers encapsulating nerve growth factor for peripheral nerve regeneration. *J Biomed Mater Res A,* 102, 2680-91.

Kumar, R., Ghoshal, U. C., Singh, G., Mittal, R. D. 2004. Infrequency of colonization with Oxalobacter formigenes in inflammatory bowel disease: Possible role in renal stone formation. *J Gastroenterol Hepatol,* 19, 1403-9.

Kunze, W. A., Furness, J. B. 1999. The enteric nervous system and regulation of intestinal motility. *Annu Rev Physiol,* 61, 117-42.

Kuo, T. K., Hung, S. P., Chuang, C. H., Chen, C. T., Shih, Y. R., Fang, S. C., Yang, V. W., Lee, O. K. 2008. Stem cell therapy for liver disease: Parameters governing the success of using bone marrow mesenchymal stem cells. *Gastroenterology,* 134, 2111-21.e3.

Kupershmidt, L., Amit, T., Bar-Am, O., Youdim, M. B. H., Blumenfeld, Z. 2007. The neuroprotective effect of Activin A and B: Implication for neurodegenerative diseases. *J Neurochem,* 103, 962-71.

Kurada, S., Alkhouri, N., Fiocchi, C., Dweik, R., Rieder, F. 2015. Review article: Breath analysis in inflammatory bowel diseases. *Aliment Pharmacol Ther,* 41, 329-41.

Kurozumi, K., Nakamura, K., Tamiya, T., Kawano, Y., Ishii, K., Kobune, M., Hirai, S., Uchida, H., Sasaki, K., Ito, Y., Kato, K., Honmou, O., Houkin, K., Date, I., Hamada, H. 2005. Mesenchymal stem cells that produce neurotrophic factors reduce ischemic damage in the rat middle cerebral artery occlusion model. *Mol Ther,* 11, 96-104.

Kurtz, A. 2008. Mesenchymal stem cell delivery routes and fate. *Int J Stem Cells,* 1, 1-7.

Kuzmina, L. A., Petinati, N. A., Parovichnikova, E. N., Lubimova, L. S., Gribanova, E. O., Gaponova, T. V., Shipounova, I. N., Zhironkina, O. A., Bigildeev, A. E., Svinareva, D. A., Drize, N. J., Savchenko, V. G. 2012. Multipotent mesenchymal stromal cells for the prophylaxis of acute graft-versus-host disease - A phase II study. *Stem Cells Int,* 2012, 968213.

L'Episcopo, F., Serapide, M. F., Tirolo, C., Testa, N., Caniglia, S., Morale, M. C., Pluchino, S., Marchetti, B. 2011. A Wnt1 regulated Frizzled-1/beta-Catenin signaling pathway as a candidate regulatory circuit controlling mesencephalic dopaminergic neuron-astrocyte crosstalk: Therapeutical relevance for neuron survival and neuroprotection. *Mol Neurodegener,* 6, 49.

Labbe, A., Ganopolsky, J. G., Martoni, C. J., Prakash, S., Jones, M. L. 2014. Bacterial bile metabolising gene abundance in Crohn's, ulcerative colitis and type 2 diabetes metagenomes. *PLoS One,* 9, e115175.

Ladak, A., Olson, J., Tredget, E. E., Gordon, T. 2011. Differentiation of mesenchymal stem cells to support peripheral nerve regeneration in a rat model. *Exp Neurol,* 228, 242-52.

Lakatos, L., Kiss, L. S., David, G., Pandur, T., Erdelyi, Z., Mester, G., Balogh, M., Szipocs, I., Molnar, C., Komaromi, E., Lakatos, P. L. 2011. Incidence, disease phenotype at diagnosis, and early disease course in inflammatory bowel diseases in Western Hungary, 2002-2006. *Inflamm Bowel Dis,* 17, 2558-65.

Lakhan, S. E., Kirchgessner, A. 2010. Neuroinflammation in inflammatory bowel disease. *J Neuroinflammation,* 7, 37.

Lam, S. H., Chua, H. L., Gong, Z., Lam, T. J., Sin, Y. M. 2004. Development and maturation of the immune system in zebrafish, Danio rerio: a gene expression profiling, in situ hybridization and immunological study. *Dev Comp Immunol,* 28, 9-28.

Lanzoni, G., Roda, G., Belluzzi, A., Roda, E., Bagnara, G. P. 2008. Inflammatory bowel disease: Moving toward a stem cell-based therapy. *World J Gastroenterol,* 14, 4616-26.

Lara-Villoslada, F., de Haro, O., Camuesco, D., Comalada, M., Velasco, J., Zarzuelo, A., Xaus, J., Galvez, J. 2006. Short-chain fructooligosaccharides, in spite of being fermented in the upper part of the large intestine, have anti-inflammatory activity in the TNBS model of colitis. *Eur J Nutr,* 45, 418-25.

Laranjeira, C., Pachnis, V. 2009. Enteric nervous system development: Recent progress and future challenges. *Auton Neurosci,* 151, 61-9.

Laroni, A., Novi, G., Kerlero de Rosbo, N., Uccelli, A. 2013. Towards clinical application of mesenchymal stem cells for treatment of neurological

diseases of the central nervous system. *J Neuroimmune Pharmacol,* 8, 1062-76.

Lathrop, S. K., Bloom, S. M., Rao, S. M., Nutsch, K., Lio, C. W., Santacruz, N., Peterson, D. A., Stappenbeck, T. S., Hsieh, C. S. 2011. Peripheral education of the immune system by colonic commensal microbiota. *Nature,* 478, 250-4.

Lee, E., Schiller, L. R., Fordtran, J. S. 1988. Quantification of colonic lamina propria cells by means of a morphometric point-counting method. *Gastroenterology,* 94, 409-18.

Lee, H., Kim, K. C., Choi, S. J., Hong, Y. M. 2017. Optimal dose and timing of umbilical stem cells treatment in pulmonary arterial hypertensive rats. *Yonsei Med J,* 58, 570-80.

Lee, H. J., Lee, J. K., Lee, H., Carter, J. E., Chang, J. W., Oh, W., Yang, Y. S., Suh, J. G., Lee, B. H., Jin, H. K., Bae, J. S. 2012. Human umbilical cord blood-derived mesenchymal stem cells improve neuropathology and cognitive impairment in an Alzheimer's disease mouse model through modulation of neuroinflammation. *Neurobiol Aging,* 33, 588-602.

Lee, H. J., Lee, J. K., Lee, H., Shin, J. W., Carter, J. E., Sakamoto, T., Jin, H. K., Bae, J. S. 2010. The therapeutic potential of human umbilical cord blood-derived mesenchymal stem cells in Alzheimer's disease. *Neurosci Lett,* 481, 30-5.

Lee, H. J., Oh, S.-H., Jang, H. W., Kwon, J.-H., Lee, K. J., Kim, C. H., Park, S. J., Hong, S. P., Cheon, J. H., Kim, T. I., Kim, W. H. 2016. Long-term effects of bone marrow-derived mesenchymal stem cells in dextran sulfate sodium-induced murine chronic colitis. *Gut Liver,* 10, 412-9.

Lee, R. H., Seo, M. J., Reger, R. L., Spees, J. L., Pulin, A. A., Olson, S. D., Prockop, D. J. 2006. Multipotent stromal cells from human marrow home to and promote repair of pancreatic islets and renal glomeruli in diabetic NOD/scid mice. *Proc Natl Acad Sci U S A,* 103, 17438-43.

Lee, W. Y., Park, K. J., Cho, Y. B., Yoon, S. N., Song, K. H., Kim, D. S. 2013a. Autologous adipose tissue-derived stem cells treatment demonstrated favorable and sustainable therapeutic effect for Crohn’s fistula. *Stem Cells,* 31.

Lee, W. Y., Park, K. J., Cho, Y. B., Yoon, S. N., Song, K. H., Kim, D. S., Jung, S. H., Kim, M., Yoo, H. W., Kim, I., Ha, H., Yu, C. S. 2013b. Autologous adipose tissue-derived stem cells treatment demonstrated favorable and sustainable therapeutic effect for Crohn's fistula. *Stem Cells,* 31, 2575-81.

Lees, C. W., Maan, A. K., Hansoti, B., Satsangi, J., Arnott, I. D. 2008. Tolerability and safety of mercaptopurine in azathioprine-intolerant patients with inflammatory bowel disease. *Aliment Pharmacol Ther,* 27, 220-7.

Lepage, P., Hasler, R., Spehlmann, M. E., Rehman, A., Zvirbliene, A., Begun, A., Ott, S., Kupcinskas, L., Dore, J., Raedler, A., Schreiber, S. 2011. Twin study indicates loss of interaction between microbiota and mucosa of patients with ulcerative colitis. *Gastroenterology,* 141, 227-36.

Lepore, A. C., Maragakis, N. J. 2007. Targeted stem cell transplantation strategies in ALS. *Neurochem Int,* 50, 966-75.

Lewis, R. T., Maron, D. J. 2010. Efficacy and complications of surgery for Crohn's disease. *Gastroenterol Hepatol N Y,* 6, 587-96.

Ley, R. E., Hamady, M., Lozupone, C., Turnbaugh, P. J., Ramey, R. R., Bircher, J. S., Schlegel, M. L., Tucker, T. A., Schrenzel, M. D., Knight, R., Gordon, J. I. 2008. Evolution of mammals and their gut microbes. *Science,* 320, 1647-51.

Ley, R. E., Turnbaugh, P. J., Klein, S., Gordon, J. I. 2006. Microbial ecology: Human gut microbes associated with obesity. *Nature,* 444, 1022-3.

Li, J., Ezzelarab, M. B., Cooper, D. K. C. 2012. Do mesenchymal stem cells function across species barriers? Relevance for xenotransplantation. *Xenotransplantation,* 19, 273-85.

Li, L., Chen, X., Wang, W. E., Zeng, C. 2016a. How to improve the survival of transplanted mesenchymal stem cell in ischemic heart? *Stem Cells Int,* 2016, 9682757.

Li, L., Hui, H., Jia, X., Zhang, J., Liu, Y., Xu, Q., Zhu, D. 2016b. Infusion with human bone marrow-derived mesenchymal stem cells improves β-cell function in patients and non-obese mice with severe diabetes. *Sci Rep,* 6, 37894.

Li, L., Li, J., Rao, J. N., Li, M., Bass, B. L., Wang, J. Y. 1999. Inhibition of polyamine synthesis induces p53 gene expression but not apoptosis. *Am J Physiol,* 276, C946-54.

Li, L., Rao, J. N., Bass, B. L., Wang, J. Y. 2001. NF-kappaB activation and susceptibility to apoptosis after polyamine depletion in intestinal epithelial cells. *Am J Physiol Gastrointest Liver Physiol,* 280, G992-1004.

Li, M., Ikehara, S. 2013. Immunomodulatory properties and therapeutic application of bone marrow derived-mesenchymal stem cells. *J Bone Marrow Res,* 1, 131.

Li, M., Sun, X., Kuang, X., Liao, Y., Li, H., Luo, D. 2014. Mesenchymal stem cells suppress CD8(+) T cell-mediated activation by suppressing natural killer group 2, member D protein receptor expression and secretion of prostaglandin E(2), indoleamine 2, 3-dioxygenase and transforming growth factor-β. *Clin Exp Immunol,* 178, 516-24.

Li, X., Tamama, K., Xie, X., Guan, J. 2016c. Improving cell engraftment in cardiac stem cell therapy. *Stem Cells Int,* 2016, 7168797.

Li, Y., Chen, J., Chen, X. G., Wang, L., Gautam, S. C., Xu, Y. X., Katakowski, M., Zhang, L. J., Lu, M., Janakiraman, N., Chopp, M. 2002. Human marrow stromal cell therapy for stroke in rat: Neurotrophins and functional recovery. *Neurology,* 59, 514-23.

Li, Y. P., Paczesny, S., Lauret, E., Poirault, S., Bordigoni, P., Mekhloufi, F., Hequet, O., Bertrand, Y., Ou-Yang, J. P., Stoltz, J. F., Miossec, P., Eljaafari, A. 2008. Human mesenchymal stem cells license adult CD34+ hemopoietic progenitor cells to differentiate into regulatory dendritic cells through activation of the Notch pathway. *J Immunol,* 180, 1598-608.

Liang, L., Dong, C., Chen, X., Fang, Z., Xu, J., Liu, M., Zhang, X., Gu, D. S., Wang, D., Du, W., Zhu, D., Han, Z. C. 2011. Human umbilical cord mesenchymal stem cells ameliorate mice trinitrobenzene sulfonic acid (TNBS)-induced colitis. *Cell Transplant,* 20, 1395-408.

Lichtenstein, G. R., Hanauer, S. B., Sandborn, W. J. 2009. Management of Crohn's disease in adults. *Am J Gastroenterol,* 104, 465-83.

Lim, W. C., Hanauer, S. 2010. Aminosalicylates for induction of remission or response in Crohn's disease. *Cochrane Database Syst Rev*, CD008870.
Lin, A., Lourenssen, S., Stanzel, R. D. P., Blennerhassett, M. G. 2005. Selective loss of NGF-sensitive neurons following experimental colitis. *Exp Neurol,* 191, 337-43.
Lin, J., Hackam, D. J. 2011. Worms, flies and four-legged friends: the applicability of biological models to the understanding of intestinal inflammatory diseases. *Dis Model Mech,* 4, 447-56.
Lin, Q. M., Zhao, S., Zhou, L. L., Fang, X. S., Fu, Y., Huang, Z. T. 2013. Mesenchymal stem cells transplantation suppresses inflammatory responses in global cerebral ischemia: Contribution of TNF-α-induced protein 6. *Acta Pharmacol Sin,* 34, 784-92.
Linares, D. M., del Rio, B., Redruello, B., Ladero, V., Martin, M. C., Fernandez, M., Ruas-Madiedo, P., Alvarez, M. A. 2016. Comparative analysis of the *in vitro* cytotoxicity of the dietary biogenic amines tyramine and histamine. *Food Chem,* 197, 658-63.
Linden, D. R., Couvrette, J. M., Ciolino, A., McQuoid, C., Blaszyk, H., Sharkey, K. A., Mawe, G. M. 2005. Indiscriminate loss of myenteric neurones in the TNBS-inflamed guinea-pig distal colon. *Neurogastroenterol Motil,* 17, 751-60.
Linden, D. R., Sharkey, K. A., Ho, W., Mawe, G. M. 2004. Cyclooxygenase-2 contributes to dysmotility and enhanced excitability of myenteric AH neurones in the inflamed guinea pig distal colon. *J Physiol,* 557, 191-205.
Linden, D. R., Sharkey, K. A., Mawe, G. M. 2003. Enhanced excitability of myenteric AH neurones in the inflamed guinea-pig distal colon. *J Physiol,* 547, 589-601.
Lissner, D., Siegmund, B. 2013. Ulcerative colitis: Current and future treatment strategies. *Dig Dis,* 31, 91-4.
Liu, J. Z., van Sommeren, S., Huang, H., Ng, S. C., Alberts, R., Takahashi, A., Ripke, S., Lee, J. C., Jostins, L., Shah, T., Abedian, S., Cheon, J. H., Cho, J., Dayani, N. E., Franke, L., Fuyuno, Y., Hart, A., Juyal, R. C., Juyal, G., Kim, W. H., Morris, A. P., Poustchi, H., Newman, W. G., Midha, V., Orchard, T. R., Vahedi, H., Sood, A., Sung, J. Y., Malekzadeh, R., Westra, H.-J., Yamazaki, K., Yang, S.-K., Barrett, J. C., Alizadeh, B. Z., Parkes, M., Bk, T., Daly, M. J., Kubo, M., Anderson, C. A., Weersma, R. K. 2015a. Association analyses identify 38 susceptibility loci for inflammatory bowel disease and highlight shared genetic risk across populations. *Nat Genet,* 47, 979-986.
Liu, S., Zhou, J., Zhang, X., Liu, Y., Chen, J., Hu, B., Song, J., Zhang, Y. 2016a. Strategies to optimize adult stem cell therapy for tissue regeneration. *Int J Mol Sci,* 17, 982.
Liu, W., Zhang, S., Gu, S., Sang, L., Dai, C. 2015b. Mesenchymal stem cells recruit macrophages to alleviate experimental colitis through TGFβ1. *Cell Physiol Biochem,* 35, 858-65.
Liu, X., Zuo, D., Fan, H., Tang, Q., Shou, Z., Cao, D., Zou, Z. 2014. Over-expression of CXCR4 on mesenchymal stem cells protect against experimental colitis via immunomodulatory functions in impaired tissue. *J Mol Histol,* 45, 181-93.

Liu, Y., Li, T. R., Xu, C., Xu, T. 2016b. Ribose accelerates gut motility and suppresses mouse body weight gaining. *Int J Biol Sci,* 12, 701-9.
Liu, Y., Yan, X., Sun, Z., Chen, B., Han, Q., Li, J., Zhao, R. C. 2007. Flk-1+ adipose-derived mesenchymal stem cells differentiate into skeletal muscle satellite cells and ameliorate muscular dystrophy in mdx mice. *Stem Cells Dev,* 16, 695-706.
Liu, Z., Cao, A. T., Cong, Y. 2013. Microbiota regulation of inflammatory bowel disease and colorectal cancer. *Semin Cancer Biol,* 23, 543-52.
Liu, Z., Feng, B.-S., Yang, S.-B., Chen, X., Su, J., Yang, P.-C. 2012. Interleukin (IL)-23 suppresses IL-10 in inflammatory bowel disease. *J Biol Chem,* 287, 3591-7.
Liu, Z., Yadav, P. K., Xu, X., Su, J., Chen, C., Tang, M., Lin, H., Yu, J., Qian, J., Yang, P. C., Wang, X. 2011. The increased expression of IL-23 in inflammatory bowel disease promotes intraepithelial and lamina propria lymphocyte inflammatory responses and cytotoxicity. *J Leukoc Biol,* 89, 597-606.
Liu, Z., Yang, L., Cui, Y., Wang, X., Guo, C., Huang, Z., Kan, Q., Liu, Z., Liu, Y. 2009a. IL-21 enhances NK cell activation and cytolytic activity and induces Th17 cell differentiation in inflammatory bowel disease. *Inflamm Bowel Dis,* 15, 1133-44.
Liu, Z. J., Zhuge, Y., Velazquez, O. C. 2009b. Trafficking and differentiation of mesenchymal stem cells. *J Cell Biochem,* 106, 984-91.
Lo Furno, D., Mannino, G., Giuffrida, R. 2018. Functional role of mesenchymal stem cells in the treatment of chronic neurodegenerative diseases. *J Cell Physiol,* 233, 3982-99.
Loftus, C. G., Loftus, E. V., Jr., Harmsen, W. S., Zinsmeister, A. R., Tremaine, W. J., Melton, L. J., 3rd, Sandborn, W. J. 2007. Update on the incidence and prevalence of Crohn's disease and ulcerative colitis in Olmsted County, Minnesota, 1940-2000. *Inflamm Bowel Dis,* 13, 254-61.
Loftus, E. V. 2011. Progress in the diagnosis and treatment of inflammatory bowel disease. *Gastroenterol Hepatol (N Y),* 7, 3-16.
Lomax, A. E., Linden, D. R., Mawe, G. M., Sharkey, K. A. 2006. Effects of gastrointestinal inflammation on enteroendocrine cells and enteric neural reflex circuits. *Auton Neurosci,* 126-127, 250-7.
Lomax, A. E., Mawe, G. M., Sharkey, K. A. 2005. Synaptic facilitation and enhanced neuronal excitability in the submucosal plexus during experimental colitis in guinea-pig. *J Physiol,* 564, 863-75.
Lomax, A. E., O'Hara, J. R., Hyland, N. P., Mawe, G. M., Sharkey, K. A. 2007a. Persistent alterations to enteric neural signaling in the guinea pig colon following the resolution of colitis. *Am J Physiol Gastrointest Liver Physiol,* 292, G482-91.
Lomax, A. E., O'Reilly, M., Neshat, S., Vanner, S. J. 2007b. Sympathetic vasoconstrictor regulation of mouse colonic submucosal arterioles is altered in experimental colitis. *J Physiol,* 583, 719-30.
Lomax, A. E., Sharkey, K. A., Furness, J. B. 2010. The participation of the sympathetic innervation of the gastrointestinal tract in disease states. *Neurogastroenterol Motil,* 22, 7-18.

Lonnfors, S., Vermeire, S., Greco, M., Hommes, D., Bell, C., Avedano, L. 2014. IBD and health-related quality of life -- discovering the true impact. *J Crohns Colitis,* 8, 1281-6.

Lopatina, T., Kalinina, N., Karagyaur, M., Stambolsky, D., Rubina, K., Revischin, A., Pavlova, G., Parfyonova, Y., Tkachuk, V. 2011. Adipose-derived stem cells stimulate regeneration of peripheral nerves: BDNF secreted by these cells promotes nerve healing and axon growth *de novo*. *PLoS One,* 6, e17899.

Louis, P., Flint, H. J. 2009. Diversity, metabolism and microbial ecology of butyrate-producing bacteria from the human large intestine. *FEMS Microbiol Lett,* 294, 1-8.

Lourenssen, S., Wells, R. W., Blennerhassett, M. G. 2005. Differential responses of intrinsic and extrinsic innervation of smooth muscle cells in rat colitis. *Exp Neurol,* 195, 497-507.

Lucchini, G., Introna, M., Dander, E., Rovelli, A., Balduzzi, A., Bonanomi, S., Salvade, A., Capelli, C., Belotti, D., Gaipa, G., Perseghin, P., Vinci, P., Lanino, E., Chiusolo, P., Orofino, M. G., Marktel, S., Golay, J., Rambaldi, A., Biondi, A., D'Amico, G., Biagi, E. 2010. Platelet-lysate-expanded mesenchymal stromal cells as a salvage therapy for severe resistant graft-versus-host disease in a pediatric population. *Biol Blood Marrow Transplant,* 16, 1293-301.

Lucke, K., Miehlke, S., Jacobs, E., Schuppler, M. 2006. Prevalence of *Bacteroides* and *Prevotella spp.* in ulcerative colitis. *J Med Microbiol,* 55, 617-24.

Lukas, M. 2008. What is the time for surgery in severe Crohn's disease? *Inflamm Bowel Dis,* 14, S271-2.

Lupp, C., Robertson, M. L., Wickham, M. E., Sekirov, I., Champion, O. L., Gaynor, E. C., Finlay, B. B. 2007. Host-mediated inflammation disrupts the intestinal microbiota and promotes the overgrowth of *Enterobacteriaceae*. *Cell Host Microbe,* 2, 119-29.

M'Koma, A. E. 2013. Inflammatory bowel disease: An expanding global health problem. *Clin Med Insights Gastroenterol,* 6, 33-47.

Machado, C. V., Telles, P. D. S., Nascimento, I. L. O. 2013. Immunological characteristics of mesenchymal stem cells. *Rev Bras Hematol Hemoter,* 35, 62-7.

Machida, S., Tanaka, M., Ishii, T., Ohtaka, K., Takahashi, T., Tazawa, Y. 2004. Neuroprotective effect of hepatocyte growth factor against photoreceptor degeneration in rats. *Invest Ophthalmol Vis Sci,* 45, 4174-82.

Maggi, C. A., Giuliani, S., Zagorodnyuk, V. 1997. Sequential activation of the triple excitatory transmission to the circular muscle of guinea-pig colon. *Neuroscience,* 79, 263-74.

Magro, F., Vieira-Coelho, M. A., Fraga, S., Serrao, M. P., Veloso, F. T., Ribeiro, T., Soares-da-Silva, P. 2002. Impaired synthesis or cellular storage of norepinephrine, dopamine, and 5-hydroxytryptamine in human inflammatory bowel disease. *Dig Dis Sci,* 47, 216-24.

Maguire, G. 2013. Stem cell therapy without the cells. *Commun Integr Biol,* 6, e26631.

Manabe, N., Wong, B. S., Camilleri, M., Burton, D., McKinzie, S., Zinsmeister, A. R. 2010. Lower functional gastrointestinal disorders: Evidence of abnormal colonic transit in a 287 patient cohort. *Neurogastroenterol Motil,* 22, 293-e82.

Mandel, M. D., Miheller, P., Mullner, K., Golovics, P. A., Lakatos, P. L. 2014. Have biologics changed the natural history of Crohn's disease? *Dig Dis,* 32, 351-9.

Manichanh, C., Borruel, N., Casellas, F., Guarner, F. 2012. The gut microbiota in IBD. *Nat Rev Gastroenterol Hepatol,* 9, 599-608.

Manichanh, C., Rigottier-Gois, L., Bonnaud, E., Gloux, K., Pelletier, E., Frangeul, L., Nalin, R., Jarrin, C., Chardon, P., Marteau, P., Roca, J., Dore, J. 2006. Reduced diversity of faecal microbiota in Crohn's disease revealed by a metagenomic approach. *Gut,* 55, 205-11.

Manieri, N. A., Stappenbeck, T. S. 2011. Mesenchymal stem cell therapy of intestinal disease: Are their effects systemic or localized? *Curr Opin Gastroenterol,* 27, 119-24.

Marchesi, J. R., Holmes, E., Khan, F., Kochhar, S., Scanlan, P., Shanahan, F., Wilson, I. D., Wang, Y. 2007. Rapid and noninvasive metabonomic characterization of inflammatory bowel disease. *J Proteome Res,* 6, 546-51.

Marconi, S., Bonaconsa, M., Scambi, I., Squintani, G. M., Rui, W., Turano, E., Ungaro, D., D'Agostino, S., Barbieri, F., Angiari, S., Farinazzo, A., Constantin, G., Del Carro, U., Bonetti, B., Mariotti, R. 2013. Systemic treatment with adipose-derived mesenchymal stem cells ameliorates clinical and pathological features in the amyotrophic lateral sclerosis murine model. *Neuroscience,* 248, 333-43.

Marconi, S., Castiglione, G., Turano, E., Bissolotti, G., Angiari, S., Farinazzo, A., Constantin, G., Bedogni, G., Bedogni, A., Bonetti, B. 2012. Human adipose-derived mesenchymal stem cells systemically injected promote peripheral nerve regeneration in the mouse model of sciatic crush. *Tissue Eng Part A,* 18, 1264-72.

Marino, R., Martinez, C., Boyd, K., Dominici, M., Hofmann, T. J., Horwitz, E. M. 2008. Transplantable marrow osteoprogenitors engraft in discrete saturable sites in the marrow microenvironment. *Exp Hematol,* 36, 360-8.

Marquardt, L. M., Heilshorn, S. C. 2016. Design of injectable materials to improve stem cell transplantation. *Curr Stem Cell Rep,* 2, 207-20.

Marquez-Curtis, L. A., Janowska-Wieczorek, A. 2013. Enhancing the migration ability of mesenchymal stromal cells by targeting the SDF-1/CXCR4 axis. *Biomed Res Int,* 2013, 561098.

Martinez-Lorenzo, M. J., Royo-Canas, M., Alegre-Aguaron, E., Desportes, P., Castiella, T., Garcia-Alvarez, F., Larrad, L. 2009. Phenotype and chondrogenic differentiation of mesenchymal cells from adipose tissue of different species. *J Orthop Res,* 27, 1499-507.

Martinez-Montiel, M. P., Casis-Herce, B., Gomez-Gomez, G. J., Masedo-Gonzalez, A., Yela-San Bernardino, C., Piedracoba, C., Castellano-Tortajada, G. 2015. Pharmacologic therapy for inflammatory bowel disease refractory to steroids. *Clin Exp Gastroenterol,* 8, 257-69.

Martinolle, J. P., Garcia-Villar, R., Fioramonti, J., Bueno, L. 1997. Altered contractility of circular and longitudinal muscle in TNBS-inflamed guinea pig ileum. *Am J Physiol,* 272, G1258-67.

Mason, R. P., Casu, M., Butler, N., Breda, C., Campesan, S., Clapp, J., Green, E. W., Dhulkhed, D., Kyriacou, C. P., Giorgini, F. 2013. Glutathione peroxidase activity is neuroprotective in models of Huntington's disease. *Nat Genet,* 45, 1249-54.

Mathison, R., Ho, W., Pittman, Q. J., Davison, J. S., Sharkey, K. A. 2004. Effects of cannabinoid receptor-2 activation on accelerated gastrointestinal transit in lipopolysaccharide-treated rats. *Br J Pharmacol,* 142, 1247-54.

Matricon, J., Barnich, N., Ardid, D. 2010. Immunopathogenesis of inflammatory bowel disease. *Self Nonself,* 1, 299-309.

Matsumoto, M., Benno, Y. 2007. The relationship between microbiota and polyamine concentration in the human intestine: A pilot study. *Microbiol Immunol,* 51, 25-35.

Matsumoto, M., Kibe, R., Ooga, T., Aiba, Y., Kurihara, S., Sawaki, E., Koga, Y., Benno, Y. 2012. Impact of intestinal microbiota on intestinal luminal metabolome. *Sci Rep,* 2, 233.

Matthay, M. A., Thompson, B. T., Read, E. J., McKenna, D. H., Liu, K. D., Calfee, C. S., Lee, J. W. 2010. Therapeutic potential of mesenchymal stem cells for severe acute lung injury. *Chest,* 138, 965-72.

Mawe, G. M. 2015. Colitis-induced neuroplasticity disrupts motility in the inflamed and post-inflamed colon. *J Clin Invest,* 125, 949-55.

Mawe, G. M., Strong, D. S., Sharkey, K. A. 2009. Plasticity of enteric nerve functions in the inflamed and post-inflamed gut. *Neurogastroenterol Motil,* 21, 481-91.

Mazmanian, S. K., Liu, C. H., Tzianabos, A. O., Kasper, D. L. 2005. An immunomodulatory molecule of symbiotic bacteria directs maturation of the host immune system. *Cell,* 122, 107-18.

McGovern, D. P., Jones, M. R., Taylor, K. D., Marciante, K., Yan, X., Dubinsky, M., Ippoliti, A., Vasiliauskas, E., Berel, D., Derkowski, C., Dutridge, D., Fleshner, P., Shih, D. Q., Melmed, G., Mengesha, E., King, L., Pressman, S., Haritunians, T., Guo, X., Targan, S. R., Rotter, J. I. 2010. Fucosyltransferase 2 (FUT2) non-secretor status is associated with Crohn's disease. *Hum Mol Genet,* 19, 3468-76.

McGuckin, M. A., Eri, R. D., Das, I., Lourie, R., Florin, T. H. 2011. Intestinal secretory cell ER stress and inflammation. *Biochem Soc Trans,* 39, 1081-5.

Medina, M., Izquierdo, E., Ennahar, S., Sanz, Y. 2007. Differential immunomodulatory properties of *Bifidobacterium logum* strains: Relevance to probiotic selection and clinical applications. *Clin Exp Immunol,* 150, 531-8.

Melief, S. M., Zwaginga, J. J., Fibbe, W. E., Roelofs, H. 2013. Adipose tissue-derived multipotent stromal cells have a higher immunomodulatory capacity than their bone marrow-derived counterparts. *Stem Cells Transl Med.,* 2.

Melo, F. R., Bressan, R. B., Forner, S., Martini, A. C., Rode, M., Delben, P. B., Rae, G. A., Figueiredo, C. P., Trentin, A. G. 2017. Transplantation of

human skin-derived mesenchymal stromal cells improves locomotor recovery after spinal cord injury in rats. *Cell Mol Neurobiol,* 37, 941-7.
Mendicino, M., Bailey, A. M., Wonnacott, K., Puri, R. K., Bauer, S. R. 2014. MSC-based product characterization for clinical trials: An FDA perspective. *Cell Stem Cell,* 14, 141-5.
Mercier, S., Breuille, D., Mosoni, L., Obled, C., Patureau Mirand, P. 2002. Chronic inflammation alters protein metabolism in several organs of adult rats. *J Nutr,* 132, 1921-8.
Mesentier-Louro, L. A., Zaverucha-do-Valle, C., da Silva-Junior, A. J., Nascimento-dos-Santos, G., Gubert, F., de Figueiredo, A. B. P., Torres, A. L., Paredes, B. D., Teixeira, C., Tovar-Moll, F., Mendez-Otero, R., Santiago, M. F. 2014. Distribution of mesenchymal stem cells and effects on neuronal survival and axon regeneration after optic nerve crush and cell therapy. *PLoS One,* 9, e110722.
Meyer, G. P., Wollert, K. C., Lotz, J., Steffens, J., Lippolt, P., Fichtner, S., Hecker, H., Schaefer, A., Arseniev, L., Hertenstein, B., Ganser, A., Drexler, H. 2006. Intracoronary bone marrow cell transfer after myocardial infarction: Eighteen months' follow-up data from the randomized, controlled BOOST (BOne marrOw transfer to enhance ST-elevation infarct regeneration) trial. *Circulation,* 113, 1287-94.
Miampamba, M., Chery-Croze, S., Chayvialle, J. A. 1992. Spinal and intestinal levels of substance P, calcitonin gene-related peptide and vasoactive intestinal polypeptide following perendoscopic injection of formalin in rat colonic wall. *Neuropeptides,* 22, 73-80.
Miampamba, M., Sharkey, K. A. 1998. Distribution of calcitonin gene-related peptide, somatostatin, substance P and vasoactive intestinal polypeptide in experimental colitis in rats. *Neurogastroenterol Motil,* 10, 315-29.
Miceli, P. C., Jacobson, K. 2003. Cholinergic pathways modulate experimental dinitrobenzene sulfonic acid colitis in rats. *Auton Neurosci,* 105, 16-24.
Michail, S., Lin, M., Frey, M. R., Fanter, R., Paliy, O., Hilbush, B., Reo, N. V. 2015. Altered gut microbial energy and metabolism in children with non-alcoholic fatty liver disease. *FEMS Microbiol Ecol,* 91, 1-9.
Michielan, A., D'Inca, R. 2015. Intestinal permeability in inflammatory bowel disease: Pathogenesis, clinical evaluation, and therapy of leaky gut. *Mediators Inflamm,* 2015, 628157.
Middleton, S. J., Shorthouse, M., Hunter, J. O. 1993. Increased nitric oxide synthesis in ulcerative colitis. *Lancet,* 341, 465-6.
Miller, A. W., Dearing, D. 2013. The metabolic and ecological interactions of oxalate-degrading bacteria in the mammalian gut. *Pathogens,* 2, 636-52.
Minamoto, Y., Otoni, C. C., Steelman, S. M., Buyukleblebici, O., Steiner, J. M., Jergens, A. E., Suchodolski, J. S. 2015. Alteration of the fecal microbiota and serum metabolite profiles in dogs with idiopathic inflammatory bowel disease. *Gut Microbes,* 6, 33-47.
Mirsaidi, A., Kleinhans, K. N., Rimann, M., Tiaden, A. N., Stauber, M., Rudolph, K. L., Richards, P. J. 2012. Telomere length, telomerase activity and osteogenic differentiation are maintained in adipose-derived stromal cells from senile osteoporotic SAMP6 mice. *J Tissue Eng Regen Med,* 6, 378-90.

Miyoshi, J., Yajima, T., Okamoto, S., Matsuoka, K., Inoue, N., Hisamatsu, T., Shimamura, K., Nakazawa, A., Kanai, T., Ogata, H., Iwao, Y., Mukai, M., Hibi, T. 2011. Ectopic expression of blood type antigens in inflamed mucosa with higher incidence of FUT2 secretor status in colonic Crohn's disease. *J Gastroenterol,* 46, 1056-63.

Mizoguchi, A. 2012. Animal models of inflammatory bowel disease. *Prog Mol Biol Transl Sci,* 105, 263-320.

Mizoguchi, A., Mizoguchi, E. 2010. Animal models of IBD: Linkage to human disease. *Curr Opin Pharmacol,* 10, 578-87.

Mohammadi, R., Ahsan, S., Masoumi, M., Amini, K. 2013. Vascular endothelial growth factor promotes peripheral nerve regeneration after sciatic nerve transection in rat. *Chin J Traumatol,* 16, 323-9.

Molendijk, I., Bonsing, B. A., Roelofs, H., Peeters, K. C. M. J., Wasser, M. N. J. M., Dijkstra, G., van der Woude, C. J., Duijvestein, M., Veenendaal, R. A., Zwaginga, J. J., Verspaget, H. W., Fibbe, W. E., van der Meulen-de Jong, A. E., Hommes, D. W. 2015. Allogeneic bone marrow-derived mesenchymal stromal cells promote healing of refractory perianal fistulas in patients with Crohn's disease. *Gastroenterology,* 149, 918-27.

Molendijk, I., Duijvestein, M., van der Meulen-de Jong, A. E., van Deen, W. K., Swets, M., Hommes, D. W., Verspaget, H. W. 2012. Immunomodulatory effects of mesenchymal stromal cells in Crohn's disease. *J Allergy (Cairo),* 2012, 187408.

Molodecky, N. A., Kaplan, G. G. 2010. Environmental risk factors for inflammatory bowel disease. *Gastroenterol Hepatol (N Y),* 6, 339-46.

Molodecky, N. A., Soon, I. S., Rabi, D. M., Ghali, W. A., Ferris, M., Chernoff, G., Benchimol, E. I., Panaccione, R., Ghosh, S., Barkema, H. W., Kaplan, G. G. 2012. Increasing incidence and prevalence of the inflammatory bowel diseases with time, based on systematic review. *Gastroenterology,* 142, 46-54.e42.

Monro, R. L., Bertrand, P. P., Bornstein, J. C. 2004. ATP participates in three excitatory postsynaptic potentials in the submucous plexus of the guinea pig ileum. *J Physiol,* 556, 571-84.

Monro, R. L., Bornstein, J. C., Bertrand, P. P. 2005. Slow excitatory post-synaptic potentials in myenteric AH neurons of the guinea-pig ileum are reduced by the 5-hydroxytryptamine7 receptor antagonist SB 269970. *Neuroscience,* 134, 975-86.

Monro, R. L., Bornstein, J. C., Bertrand, P. P. 2008. Synaptic transmission from the submucosal plexus to the myenteric plexus in Guinea-pig ileum. *Neurogastroenterol Motil,* 20, 1165-73.

Moran, J. P., Walter, J., Tannock, G. W., Tonkonogy, S. L., Sartor, R. B. 2009. *Bifidobacterium animalis* causes extensive duodenitis and mild colonic inflammation in monoassociated interleukin-10 deficient mice. *Inflamm bowel dis,* 15, 1022-31.

Morcuende, S., Munoz-Hernandez, R., Benitez-Temino, B., Pastor, A. M., de la Cruz, R. R. 2013. Neuroprotective effects of NGF, BDNF, NT-3 and GDNF on axotomized extraocular motoneurons in neonatal rats. *Neuroscience,* 250, 31-48.

Morgan, X. C., Tickle, T. L., Sokol, H., Gevers, D., Devaney, K. L., Ward, D. V., Reyes, J. A., Shah, S. A., LeLeiko, N., Snapper, S. B., Bousvaros, A., Korzenik, J., Sands, B. E., Xavier, R. J., Huttenhower, C. 2012. Dysfunction of the intestinal microbiome in inflammatory bowel disease and treatment. *Genome Biol,* 13, R79.

Motavallian-Naeini, A., Andalib, S., Rabbani, M., Mahzouni, P., Afsharipour, M., Minaiyan, M. 2012. Validation and optimization of experimental colitis induction in rats using 2, 4, 6-trinitrobenzene sulfonic acid. *Res Pharm Sci,* 7, 159-69.

Moussa, L., Pattappa, G., Doix, B., Benselama, S. L., Demarquay, C., Benderitter, M., Semont, A., Tamarat, R., Guicheux, J., Weiss, P., Rethore, G., Mathieu, N. 2017. A biomaterial-assisted mesenchymal stromal cell therapy alleviates colonic radiation-induced damage. *Biomaterials,* 115, 40-52.

Moynes, D. M., Lucas, G. H., Beyak, M. J., Lomax, A. E. 2014. Effects of inflammation on the innervation of the colon. *Toxicol Pathol,* 42, 111-7.

Muguruma, Y., Yahata, T., Miyatake, H., Sato, T., Uno, T., Itoh, J., Kato, S., Ito, M., Hotta, T., Ando, K. 2006. Reconstitution of the functional human hematopoietic microenvironment derived from human mesenchymal stem cells in the murine bone marrow compartment. *Blood,* 107, 1878-87.

Mukhopadhya, I., Hansen, R., El-Omar, E. M., Hold, G. L. 2012. IBD-what role do *Proteobacteria* play? *Nat Rev Gastroenterol Hepatol,* 9, 219-30.

Mulder, D. J., Noble, A. J., Justinich, C. J., Duffin, J. M. 2014. A tale of two diseases: The history of inflammatory bowel disease. *Journal of Crohn's and Colitis,* 8, 341-348.

Muller-Ehmsen, J., Krausgrill, B., Burst, V., Schenk, K., Neisen, U. C., Fries, J. W. U., Fleischmann, B. K., Hescheler, J., Schwinger, R. H. G. 2006. Effective engraftment but poor mid-term persistence of mononuclear and mesenchymal bone marrow cells in acute and chronic rat myocardial infarction. *J Mol Cell Cardiol,* 41, 876-84.

Muller, I., Kordowich, S., Holzwarth, C., Isensee, G., Lang, P., Neunhoeffer, F., Dominici, M., Greil, J., Handgretinger, R. 2008. Application of multipotent mesenchymal stromal cells in pediatric patients following allogeneic stem cell transplantation. *Blood Cells Mol Dis,* 40, 25-32.

Murphy, S. J., Wang, L., Anderson, L. A., Steinlauf, A., Present, D. H., Mechanick, J. I. 2009. Withdrawal of corticosteroids in inflammatory bowel disease patients after dependency periods ranging from 2 to 45 years: A proposed method. *Aliment Pharmacol Ther,* 30, 1078-86.

Mutafova-Yambolieva, V. N., Hwang, S. J., Hao, X., Chen, H., Zhu, M. X., Wood, J. D., Ward, S. M., Sanders, K. M. 2007. β-Nicotinamide adenine dinucleotide is an inhibitory neurotransmitter in visceral smooth muscle. *Proc Natl Acad Sci U S A,* 104, 16359-64.

Myagmarjalbuu, B., Moon, M. J., Heo, S. H., Jeong, S. I., Park, J. S., Jun, J. Y., Jeong, Y. Y., Kang, H. K. 2013. Establishment of a protocol for determining gastrointestinal transit time in mice using barium and radiopaque markers. *Korean J Radiol,* 14, 45-50.

Nacif, L. S., Ferreira, A. O., Maria, D. A., Kubrusly, M. S., Molan, N., Chaib, E., D'Albuquerque, L. C., Andraus, W. 2015. Which is the best route of

administration for cell therapy in experimental model of small-for size syndrome in rats? *Acta Cir Bras,* 30, 100-6.

Nagalingam, N. A., Kao, J. Y., Young, V. B. 2011. Microbial ecology of the murine gut associated with the development of dextran sodium sulfate-induced colitis. *Inflamm bowel dis,* 17, 917-26.

Nagaya, N., Fujii, T., Iwase, T., Ohgushi, H., Itoh, T., Uematsu, M., Yamagishi, M., Mori, H., Kangawa, K., Kitamura, S. 2004. Intravenous administration of mesenchymal stem cells improves cardiac function in rats with acute myocardial infarction through angiogenesis and myogenesis. *Am J Physiol Heart Circ Physiol,* 287, H2670-6.

Naghdi, M., Tiraihi, T., Namin, S. A., Arabkheradmand, J. 2009. Transdifferentiation of bone marrow stromal cells into cholinergic neuronal phenotype: a potential source for cell therapy in spinal cord injury. *Cytotherapy,* 11, 137-52.

Nair, D. G., Miller, K. G., Lourenssen, S. R., Blennerhassett, M. G. 2014. Inflammatory cytokines promote growth of intestinal smooth muscle cells by induced expression of PDGF-Rβ. *J Cell Mol Med,* 18, 444-54.

Nakamizo, A., Marini, F., Amano, T., Khan, A., Studeny, M., Gumin, J., Chen, J., Hentschel, S., Vecil, G., Dembinski, J., Andreeff, M., Lang, F. F. 2005. Human bone marrow-derived mesenchymal stem cells in the treatment of gliomas. *Cancer Res,* 65, 3307-18.

Nam, S. Y., Ricles, L. M., Suggs, L. J., Emelianov, S. Y. 2012. *In vivo* ultrasound and photoacoustic monitoring of mesenchymal stem cells labeled with gold nanotracers. *PLoS One,* 7, e37267.

Nam, Y. S., Kim, N., Im, K. I., Lim, J. Y., Lee, E. S., Cho, S. G. 2015. Negative impact of bone-marrow-derived mesenchymal stem cells on dextran sulfate sodium-induced colitis. *World J Gastroenterol,* 21, 2030-9.

Neis, E. P., Dejong, C. H., Rensen, S. S. 2015. The role of microbial amino acid metabolism in host metabolism. *Nutrients,* 7, 2930-46.

Nell, S., Suerbaum, S., Josenhans, C. 2010. The impact of the microbiota on the pathogenesis of IBD: lessons from mouse infection models. *Nat Rev Microbiol,* 8, 564-77.

Nemeth, K., Leelahavanichkul, A., Yuen, P. S., Mayer, B., Parmelee, A., Doi, K., Robey, P. G., Leelahavanichkul, K., Koller, B. H., Brown, J. M., Hu, X., Jelinek, I., Star, R. A., Mezey, E. 2009. Bone marrow stromal cells attenuate sepsis via prostaglandin E(2)-dependent reprogramming of host macrophages to increase their interleukin-10 production. *Nat Med,* 15, 42-9.

Nemoto, H., Kataoka, K., Ishikawa, H., Ikata, K., Arimochi, H., Iwasaki, T., Ohnishi, Y., Kuwahara, T., Yasutomo, K. 2012. Reduced diversity and imbalance of fecal microbiota in patients with ulcerative colitis. *Dig Dis Sci,* 57, 2955-64.

Neuhuber, B., Timothy Himes, B., Shumsky, J. S., Gallo, G., Fischer, I. 2005. Axon growth and recovery of function supported by human bone marrow stromal cells in the injured spinal cord exhibit donor variations. *Brain Res,* 1035.

Neunlist, M., Aubert, P., Toquet, C., Oreshkova, T., Barouk, J., Lehur, P. A., Schemann, M., Galmiche, J. P. 2003. Changes in chemical coding of myenteric neurones in ulcerative colitis. *Gut,* 52, 84-90.

Neurath, M. F. 2017. Current and emerging therapeutic targets for IBD. *Nat Rev Gastroenterol Hepatol,* 14, 269-78.

Neut, C., Bulois, P., Desreumaux, P., Membre, J. M., Lederman, E., Gambiez, L., Cortot, A., Quandalle, P., van Kruiningen, H., Colombel, J. F. 2002. Changes in the bacterial flora of the neoterminal ileum after ileocolonic resection for Crohn's disease. *Am J Gastroenterol,* 97, 939-46.

Newman, R. E., Yoo, D., LeRoux, M. A., Danilkovitch-Miagkova, A. 2009. Treatment of inflammatory diseases with mesenchymal stem cells. *Inflamm Allergy Drug Targets,* 8, 110-23.

Ng, J. S. Y., Ryan, U., Trengove, R. D., Maker, G. L. 2012. Development of an untargeted metabolomics method for the analysis of human faecal samples using *Cryptosporidium*-infected samples. *Mol Biochem Parasitol,* 185, 145-50.

Ng, S. C., Bernstein, C. N., Vatn, M. H., Lakatos, P. L., Loftus, E. V., Jr., Tysk, C., O'Morain, C., Moum, B., Colombel, J. F. 2013. Geographical variability and environmental risk factors in inflammatory bowel disease. *Gut,* 62, 630-49.

Ng, S. C., Lied, G. A., Kamm, M. A., Sandhu, F., Guenther, T., Arebi, N. 2009. Predictive value and clinical significance of myenteric plexitis in Crohn's disease. *Inflamm Bowel Dis,* 15, 1499-507.

Ng, S. C., Shi, H. Y., Hamidi, N., Underwood, F. E., Tang, W., Benchimol, E. I., Panaccione, R., Ghosh, S., Wu, J. C. Y., Chan, F. K. L., Sung, J. J. Y., Kaplan, G. G. 2017. Worldwide incidence and prevalence of inflammatory bowel disease in the 21st century: A systematic review of population-based studies. *Lancet,* 390, 2769-78.

Nguyen, M. T., Favelyukis, S., Nguyen, A. K., Reichart, D., Scott, P. A., Jenn, A., Liu-Bryan, R., Glass, C. K., Neels, J. G., Olefsky, J. M. 2007. A subpopulation of macrophages infiltrates hypertrophic adipose tissue and is activated by free fatty acids via Toll-like receptors 2 and 4 and JNK-dependent pathways. *J Biol Chem,* 282, 35279-92.

Nichols, J. E., Niles, J. A., DeWitt, D., Prough, D., Parsley, M., Vega, S., Cantu, A., Lee, E., Cortiella, J. 2013. Neurogenic and neuro-protective potential of a novel subpopulation of peripheral blood-derived CD133+ ABCG2+CXCR4+ mesenchymal stem cells: Development of autologous cell-based therapeutics for traumatic brain injury. *Stem Cell Res Ther,* 4, 3.

Nicholson, J. K., Holmes, E., Kinross, J., Burcelin, R., Gibson, G., Jia, W., Pettersson, S. 2012. Host-gut microbiota metabolic interactions. *Science,* 336, 1262-7.

Nicoletti, J. N., Shah, S. K., McCloskey, D. P., Goodman, J. H., Elkady, A., Atassi, H., Hylton, D., Rudge, J. S., Scharfman, H. E., Croll, S. D. 2008. Vascular endothelial growth factor is up-regulated after status epilepticus and protects against seizure-induced neuronal loss in hippocampus. *Neuroscience,* 151, 232-41.

Nieto, N., Giron, M. D., Suarez, M. D., Gil, A. 1998. Changes in plasma and colonic mucosa fatty acid profiles in rats with ulcerative colitis induced by trinitrobenzene sulfonic acid. *Dig Dis Sci,* 43, 2688-95.

Nikolic, A., Simovic Markovic, B., Gazdic, M., Randall Harrell, C., Fellabaum, C., Jovicic, N., Djonov, V., Arsenijevic, N., M, L. L., Stojkovic, M., Volarevic, V. 2018. Intraperitoneal administration of mesenchymal stem cells ameliorates acute dextran sulfate sodium-induced colitis by suppressing dendritic cells. *Biomed Pharmacother,* 100, 426-32.

Nishida, T., Miwa, H., Shigematsu, A., Yamamoto, M., Iida, M., Fujishima, M. 1987. Increased arachidonic acid composition of phospholipids in colonic mucosa from patients with active ulcerative colitis. *Gut,* 28, 1002-7.

Nishihara, T., Matsuda, M., Araki, H., Oshima, K., Kihara, S., Funahashi, T., Shimomura, I. 2006. Effect of adiponectin on murine colitis induced by dextran sulfate sodium. *Gastroenterology,* 131, 853-61.

Nitkin, C. R., Bonfield, T. L. 2016. Mesenchymal stem cell therapy for pediatric disease: Perspectives on success and potential improvements. *Stem Cells Transl Med,* 6, 539-65.

Nitzan, O., Elias, M., Chazan, B., Raz, R., Saliba, W. 2013. *Clostridium difficile* and inflammatory bowel disease: role in pathogenesis and implications in treatment. *World J Gastroenterol,* 19, 7577-85.

Nitzan, O., Elias, M., Peretz, A., Saliba, W. 2016. Role of antibiotics for treatment of inflammatory bowel disease. *World J Gastroenterol,* 22, 1078-87.

Niv, E., Fishman, S., Kachman, H., Arnon, R., Dotan, I. 2014. Sequential capsule endoscopy of the small bowel for follow-up of patients with known Crohn's disease. *J Crohns Colitis,* 8, 1616-23.

Noack, J., Dongowski, G., Hartmann, L., Blaut, M. 2000. The human gut bacteria *Bacteroides thetaiotaomicron* and *Fusobacterium varium* produce putrescine and spermidine in cecum of pectin-fed gnotobiotic rats. *J Nutr,* 130, 1225-31.

Noiseux, N., Gnecchi, M., Lopez-Ilasaca, M., Zhang, L., Solomon, S. D., Deb, A., Dzau, V. J., Pratt, R. E. 2006. Mesenchymal stem cells overexpressing Akt dramatically repair infarcted myocardium and improve cardiac function despite infrequent cellular fusion or differentiation. *Mol Ther,* 14, 840-50.

North, R. A., Slack, B. E., Surprenant, A. 1985. Muscarinic M1 and M2 receptors mediate depolarization and presynaptic inhibition in guinea-pig enteric nervous system. *J Physiol,* 368, 435-52.

North, R. A., Surprenant, A. 1985. Inhibitory synaptic potentials resulting from alpha 2-adrenoceptor activation in guinea-pig submucous plexus neurones. *J Physiol,* 358, 17-33.

North, R. A., Tokimasa, T. 1982. Muscarinic synaptic potentials in guinea-pig myenteric plexus neurones. *J Physiol,* 333, 151-6.

Novikova, L. N., Kolar, M. K., Kingham, P. J., Ullrich, A., Oberhoffner, S., Renardy, M., Doser, M., Muller, E., Wiberg, M., Novikov, L. N. 2018. Trimethylene carbonate-caprolactone conduit with poly-p-dioxanone microfilaments to promote regeneration after spinal cord injury. *Acta Biomater,* 66, 177-91.

Nurgali, K., Nguyen, T. V., Matsuyama, H., Thacker, M., Robbins, H. L., Furness, J. B. 2007. Phenotypic changes of morphologically identified guinea-pig

myenteric neurons following intestinal inflammation. *J Physiol,* 583, 593-609.
Nurgali, K., Nguyen, T. V., Thacker, M., Pontell, L., Furness, J. B. 2009. Slow synaptic transmission in myenteric AH neurons from the inflamed guinea pig ileum. *Am J Physiol Gastrointest Liver Physiol,* 297, G582-93.
Nurgali, K., Qu, Z., Hunne, B., Thacker, M., Pontell, L., Furness, J. B. 2011. Morphological and functional changes in guinea-pig neurons projecting to the ileal mucosa at early stages after inflammatory damage. *J Physiol,* 589, 325-39.
Nurgali, K., Stebbing, M. J., Furness, J. B. 2004. Correlation of electrophysiological and morphological characteristics of enteric neurons in the mouse colon. *J Comp Neurol,* 468, 112-24.
O'Brien, M. D., Phillips, S. F. 1996. Colonic motility in health and disease. *Gastroenterol Clin North Am,* 25, 147-62.
O'Connor, M., Patil, R., Yu, J., Hickey, R., Premanand, K., Kajdacsy-Balla, A., Benedetti, E., Bartholomew, A. 2016. Mesenchymal stem cells synergize with 635, 532, and 405 nm laser wavelengths in renal fibrosis: A pilot study. *Photomed Laser Surg,* 34, 556-63.
Oh, K., Iimuro, Y., Takeuchi, M., Kaneda, Y., Iwasaki, T., Terada, N., Matsumoto, T., Nakanishi, K., Fujimoto, J. 2005. Ameliorating effect of hepatocyte growth factor on inflammatory bowel disease in a murine model. *Am J Physiol Gastrointest Liver Physiol,* 288, G729-35.
Oh, S. H., Kim, H. N., Park, H. J., Shin, J. Y., Lee, P. H. 2015. Mesenchymal stem cells increase hippocampal neurogenesis and neuronal differentiation by enhancing the Wnt signaling pathway in an Alzheimer's disease model. *Cell Transplant,* 24, 1097-109.
Ohama, T., Hori, M., Ozaki, H. 2007. Mechanism of abnormal intestinal motility in inflammatory bowel disease: How smooth muscle contraction is reduced? *J Smooth Muscle Res,* 43, 43-54.
Ohlsson, B., Veress, B., Lindgren, S., Sundkvist, G. 2007. Enteric ganglioneuritis and abnormal interstitial cells of Cajal: Features of inflammatory bowel disease. *Inflamm Bowel Dis,* 13, 721-6.
Ohtaki, H., Ylostalo, J. H., Foraker, J. E., Robinson, A. P., Reger, R. L., Shioda, S., Prockop, D. J. 2008. Stem/progenitor cells from bone marrow decrease neuronal death in global ischemia by modulation of inflammatory/immune responses. *Proc Natl Acad Sci U S A,* 105, 14638-43.
Oliveira, S. L., Pillat, M. M., Cheffer, A., Lameu, C., Schwindt, T. T., Ulrich, H. 2013. Functions of neurotrophins and growth factors in neurogenesis and brain repair. *Cytometry A,* 83, 76-89.
Onda, T., Honmou, O., Harada, K., Houkin, K., Hamada, H., Kocsis, J. D. 2008. Therapeutic benefits by human mesenchymal stem cells (hMSCs) and Ang-1 gene-modified hMSCs after cerebral ischemia. *J Cereb Blood Flow Metab,* 28, 329-40.
Onishi, R., Ohnishi, S., Higashi, R., Watari, M., Yamahara, K., Okubo, N., Nakagawa, K., Katsurada, T., Suda, G., Natsuizaka, M., Takeda, H., Sakamoto, N. 2015. Human amnion-derived mesenchymal stem cell transplantation ameliorates dextran sulfate sodium-induced severe colitis in rats. *Cell Transplant,* 24, 2601-14.

Onrust, L., Ducatelle, R., Van Driessche, K., De Maesschalck, C., Vermeulen, K., Haesebrouck, F., Eeckhaut, V., Van Immerseel, F. 2015. Steering endogenous butyrate production in the intestinal tract of broilers as a tool to improve gut health. *Front Vet Sci,* 2, 75.

Onuma-Ukegawa, M., Bhatt, K., Hirai, T., Kaburagi, H., Sotome, S., Wakabayashi, Y., Ichinose, S., Shinomiya, K., Okawa, A., Enomoto, M. 2015. Bone marrow stromal cells combined with a honeycomb collagen sponge facilitate neurite elongation *in vitro* and neural restoration in the hemisected rat spinal cord. *Cell Transplant,* 24, 1283-97.

Ooi, M., Nishiumi, S., Yoshie, T., Shiomi, Y., Kohashi, M., Fukunaga, K., Nakamura, S., Matsumoto, T., Hatano, N., Shinohara, M., Irino, Y., Takenawa, T., Azuma, T., Yoshida, M. 2011. GC/MS-based profiling of amino acids and TCA cycle-related molecules in ulcerative colitis. *Inflamm Res,* 60, 831-40.

Ordas, I., Eckmann, L., Talamini, M., Baumgart, D. C., Sandborn, W. J. 2012. Ulcerative colitis. *Lancet,* 380, 1606-19.

Ortiz, L. A., Gambelli, F., McBride, C., Gaupp, D., Baddoo, M., Kaminski, N., Phinney, D. G. 2003. Mesenchymal stem cell engraftment in lung is enhanced in response to bleomycin exposure and ameliorates its fibrotic effects. *Proc Natl Acad Sci U S A,* 100, 8407-11.

Ostanin, D. V., Bao, J., Koboziev, I., Gray, L., Robinson-Jackson, S. A., Kosloski-Davidson, M., Price, V. H., Grisham, M. B. 2009. T cell transfer model of chronic colitis: Concepts, considerations, and tricks of the trade. *Am J Physiol Gastrointest Liver Physiol,* 296, G135-46.

Ott, S. J., Musfeldt, M., Wenderoth, D. F., Hampe, J., Brant, O., Folsch, U. R., Timmis, K. N., Schreiber, S. 2004. Reduction in diversity of the colonic mucosa associated bacterial microflora in patients with active inflammatory bowel disease. *Gut,* 53, 685-93.

Ouchi, N., Walsh, K. 2007. Adiponectin as an anti-inflammatory factor. *Clin Chim Acta,* 380, 24-30.

Ozeki, N., Muneta, T., Koga, H., Nakagawa, Y., Mizuno, M., Tsuji, K., Mabuchi, Y., Akazawa, C., Kobayashi, E., Matsumoto, K., Futamura, K., Saito, T., Sekiya, I. 2016. Not single but periodic injections of synovial mesenchymal stem cells maintain viable cells in knees and inhibit osteoarthritis progression in rats. *Osteoarthritis Cartilage,* 24, 1061-70.

Panaccione, R. 2013. Mechanisms of Inflammatory Bowel Disease. *Gastroenterol Hepatol (N Y),* 9, 529-32.

Panaccione, R., Ghosh, S. 2010. Optimal use of biologics in the management of Crohn's disease. *Therap Adv Gastroenterol,* 3, 179-89.

Parcell, S. 2002. Sulfur in human nutrition and applications in medicine. *Altern Med Rev,* 7, 22-44.

Parekkadan, B., Milwid, J. M. 2010. Mesenchymal stem cells as therapeutics. *Annu Rev Biomed Eng,* 12, 87-117.

Parekkadan, B., Upadhyay, R., Dunham, J., Iwamoto, Y., Mizoguchi, E., Mizoguchi, A., Weissleder, R., Yarmush, M. L. 2011. Bone marrow stromal cell transplants prevent experimental enterocolitis and require host CD11b+ splenocytes. *Gastroenterology,* 140, 966-75.

Park, H. J., Lee, P. H., Bang, O. Y., Lee, G., Ahn, Y. H. 2008. Mesenchymal stem cells therapy exerts neuroprotection in a progressive animal model of Parkinson's disease. *J Neurochem,* 107, 141-51.

Park, H. J., Oh, S. H., Kim, H. N., Jung, Y. J., Lee, P. H. 2016. Mesenchymal stem cells enhance alpha-synuclein clearance via M2 microglia polarization in experimental and human parkinsonian disorder. *Acta Neuropathol,* 132, 685-701.

Park, H. J., Shin, J. Y., Kim, H. N., Oh, S. H., Lee, P. H. 2014a. Neuroprotective effects of mesenchymal stem cells through autophagy modulation in a parkinsonian model. *Neurobiol Aging,* 35, 1920-8.

Park, H. J., Shin, J. Y., Lee, B. R., Kim, H. O., Lee, P. H. 2012. Mesenchymal stem cells augment neurogenesis in the subventricular zone and enhance differentiation of neural precursor cells into dopaminergic neurons in the substantia nigra of a parkinsonian model. *Cell Transplant,* 21, 1629-40.

Park, J. H., Kwon, J. G., Kim, S. J., Song, D. K., Lee, S. G., Kim, E. S., Cho, K. B., Jang, B. I., Kim, D. H., Sin, J. I., Kim, T. W., Song, I. H., Park, K. S. 2015. Alterations of colonic contractility in an interleukin-10 knockout mouse model of inflammatory bowel disease. *J Neurogastroenterol Motil,* 21, 51-61.

Park, K. T., Bass, D. 2011. Inflammatory bowel disease-attributable costs and cost-effective strategies in the United States: A review. *Inflamm Bowel Dis,* 17, 1603-9.

Park, S. C., Jeen, Y. T. 2015. Current and emerging biologics for ulcerative colitis. *Gut Liver,* 9, 18-27.

Park, S. J., Kim, W. H., Cheon, J. H. 2014b. Clinical characteristics and treatment of inflammatory bowel disease: A comparison of Eastern and Western perspectives. *World J Gastroenterol,* 20, 11525-37.

Patel, D. M., Shah, J., Srivastava, A. S. 2013. Therapeutic potential of mesenchymal stem cells in regenerative medicine. *Stem Cells Int,* 2013, 496218.

Paul, G., Anisimov, S. V. 2013. The secretome of mesenchymal stem cells: Potential implications for neuroregeneration. *Biochimie,* 95, 2246-56.

Payne, A. N., Chassard, C., Lacroix, C. 2012a. Gut microbial adaptation to dietary consumption of fructose, artificial sweeteners and sugar alcohols: implications for host-microbe interactions contributing to obesity. *Obes Rev,* 13, 799-809.

Payne, N. L., Dantanarayana, A., Sun, G., Moussa, L., Caine, S., McDonald, C., Herszfeld, D., Bernard, C. C., Siatskas, C. 2012b. Early intervention with gene-modified mesenchymal stem cells overexpressing interleukin-4 enhances anti-inflammatory responses and functional recovery in experimental autoimmune demyelination. *Cell Adh Migr,* 6, 179-89.

Payne, N. L., Sun, G., McDonald, C., Layton, D., Moussa, L., Emerson-Webber, A., Veron, N., Siatskas, C., Herszfeld, D., Price, J., Bernard, C. C. 2013a. Distinct immunomodulatory and migratory mechanisms underpin the therapeutic potential of human mesenchymal stem cells in autoimmune demyelination. *Cell Transplant,* 22, 1409-25.

Payne, N. L., Sun, G., McDonald, C., Moussa, L., Emerson-Webber, A., Loisel-Meyer, S., Medin, J. A., Siatskas, C., Bernard, C. C. A. 2013b. Human

adipose-derived mesenchymal stem cells engineered to secrete IL-10 inhibit APC function and limit CNS autoimmunity. *Brain Behav Immun,* 30, 103-14.

Pegg, A. E. 2009. Mammalian polyamine metabolism and function. *IUBMB Life,* 61, 880-94.

Pelli, M. A., Trovarelli, G., Capodicasa, E., De Medio, G. E., Bassotti, G. 1999. Breath alkanes determination in ulcerative colitis and Crohn's disease. *Dis Colon Rectum,* 42, 71-6.

Perencevich, M., Burakoff, R. 2006. Use of antibiotics in the treatment of inflammatory bowel disease. *Inflamm Bowel Dis,* 12, 651-64.

Perez-Merino, E. M., Uson-Casaus, J. M., Zaragoza-Bayle, C., Duque-Carrasco, J., Marinas-Pardo, L., Hermida-Prieto, M., Barrera-Chacon, R., Gualtieri, M. 2015. Safety and efficacy of allogeneic adipose tissue-derived mesenchymal stem cells for treatment of dogs with inflammatory bowel disease: Clinical and laboratory outcomes. *Vet J,* 206, 385-90.

Perse, M., Cerar, A. 2012. Dextran sodium sulphate colitis mouse model: Traps and tricks. *J Biomed Biotechnol,* 2012, 718617.

Petersen, C., Round, J. L. 2014. Defining dysbiosis and its influence on host immunity and disease. *Cell Microbiol,* 16, 1024-33.

Peterson, D. A., Frank, D. N., Pace, N. R., Gordon, J. I. 2008. Metagenomic approaches for defining the pathogenesis of inflammatory bowel diseases. *Cell Host Microbe,* 3, 417-27.

Petritsch, W., Fuchs, S., Berghold, A., Bachmaier, G., Hogenauer, C., Hauer, A. C., Weiglhofer, U., Wenzl, H. H. 2013. Incidence of inflammatory bowel disease in the province of Styria, Austria, from 1997 to 2007: A population-based study. *J Crohns Colitis,* 7, 58-69.

Petrova, E. S. 2015. Injured nerve regeneration using cell-based therapies: Current challenges. *Acta Naturae,* 7, 38-47.

Petryszyn, P. W., Witczak, I. 2016. Costs in inflammatory bowel diseases. *Prz Gastroenterol,* 11, 6-13.

Peyrin-Biroulet, L., Lemann, M. 2011. Remission rates achievable by current therapies for inflammatory bowel disease. *Aliment Pharmacol Ther,* 33, 870-9.

Pfeffer, L. M., Yang, C. H., Murti, A., McCormack, S. A., Viar, M. J., Ray, R. M., Johnson, L. R. 2001. Polyamine Depletion Induces Rapid NF-κB Activation in IEC-6 Cells. *J Biol Chem,* 276, 45909-13.

Phani, S., Jablonski, M., Pelta-Heller, J., Cai, J., Iacovitti, L. 2013. Gremlin is a novel VTA derived neuroprotective factor for dopamine neurons. *Brain Res,* 1500, 88-98.

Phillips, R. J., Powley, T. L. 2007. Innervation of the gastrointestinal tract: Patterns of aging. *Auton Neurosci,* 136, 1-19.

Phinney, D. G., Prockop, D. J. 2007. Mesenchymal stem/multipotent stromal cells: The state of transdifferentiation and modes of tissue repair--current views. *Stem Cells,* 25, 2896-902.

Piatti, V. C., Davies-Sala, M. G., Esposito, M. S., Mongiat, L. A., Trinchero, M. F., Schinder, A. F. 2011. The timing for neuronal maturation in the adult hippocampus is modulated by local network activity. *J Neurosci,* 31, 7715-28.

Pitcher, M. C., Cummings, J. H. 1996. Hydrogen sulphide: A bacterial toxin in ulcerative colitis? *Gut,* 39, 1-4.

Pithadia, A. B., Jain, S. 2011. Treatment of inflammatory bowel disease (IBD). *Pharmacol Rep,* 63, 629-42.

Pittenger, M. F., Mackay, A. M., Beck, S. C., Jaiswal, R. K., Douglas, R., Mosca, J. D., Moorman, M. A., Simonetti, D. W., Craig, S., Marshak, D. R. 1999. Multilineage potential of adult human mesenchymal stem cells. *Science,* 284, 143-7.

Poli, E., Lazzaretti, M., Grandi, D., Pozzoli, C., Coruzzi, G. 2001. Morphological and functional alterations of the myenteric plexus in rats with TNBS-induced colitis. *Neurochem Res,* 26, 1085-93.

Pollock, K., Dahlenburg, H., Nelson, H., Fink, K. D., Cary, W., Hendrix, K., Annett, G., Torrest, A., Deng, P., Gutierrez, J., Nacey, C., Pepper, K., Kalomoiris, S., J, D. A., McGee, J., Gruenloh, W., Fury, B., Bauer, G., Duffy, A., Tempkin, T., Wheelock, V., Nolta, J. A. 2016. Human mesenchymal stem cells genetically engineered to overexpress brain-derived neurotrophic factor improve outcomes in Huntington's disease mouse models. *Mol Ther,* 24, 965-77.

Pontell, L., Castelucci, P., Bagyanszki, M., Jovic, T., Thacker, M., Nurgali, K., Bron, R., Furness, J. B. 2009. Structural changes in the epithelium of the small intestine and immune cell infiltration of enteric ganglia following acute mucosal damage and local inflammation. *Virchows Archiv,* 455, 55-65.

Powrie, F. 1995. T cells in inflammatory bowel disease: Protective and pathogenic roles. *Immunity,* 3, 171-4.

Pradhan, A. D., Cook, N. R., Buring, J. E., Manson, J. E., Ridker, P. M. 2003. C-reactive protein is independently associated with fasting insulin in nondiabetic women. *Arterioscler Thromb Vasc Biol,* 23, 650-5.

Prantera, C., Lochs, H., Grimaldi, M., Danese, S., Scribano, M. L., Gionchetti, P. 2012. Rifaximin-extended intestinal release induces remission in patients with moderately active Crohn's disease. *Gastroenterology,* 142, 473-81.e4.

Preising, J., Philippe, D., Gleinser, M., Wei, H., Blum, S., Eikmanns, B. J., Niess, J. H., Riedel, C. U. 2010. Selection of *Bifidobacteria* based on adhesion and anti-inflammatory capacity *in vitro* for amelioration of murine colitis. *Appl Environ Microbiol,* 76, 3048-51.

Prockop, D. J. 2009. Repair of tissues by adult stem/progenitor cells (MSCs): Controversies, myths, and changing paradigms. *Mol Ther,* 17, 939-46.

Qin, J., Li, R., Raes, J., Arumugam, M., Burgdorf, K. S., Manichanh, C., Nielsen, T., Pons, N., Levenez, F., Yamada, T., Mende, D. R., Li, J., Xu, J., Li, S., Li, D., Cao, J., Wang, B., Liang, H., Zheng, H., Xie, Y., Tap, J., Lepage, P., Bertalan, M., Batto, J. M., Hansen, T., Le Paslier, D., Linneberg, A., Nielsen, H. B., Pelletier, E., Renault, P., Sicheritz-Ponten, T., Turner, K., Zhu, H., Yu, C., Li, S., Jian, M., Zhou, Y., Li, Y., Zhang, X., Li, S., Qin, N., Yang, H., Wang, J., Brunak, S., Dore, J., Guarner, F., Kristiansen, K., Pedersen, O., Parkhill, J., Weissenbach, J., Bork, P., Ehrlich, S. D., Wang, J. 2010. A human gut microbial gene catalog established by metagenomic sequencing. *Nature,* 464, 59-65.

Qiu, W. C., Wang, Z. G., Lv, R., Wang, W. G., Han, X. D., Yan, J., Wang, Y., Zheng, Q., Ai, K. X. 2008. Ghrelin improves delayed gastrointestinal transit in alloxan-induced diabetic mice. *World J Gastroenterol,* 14, 2572-7.

Qiu, X. C., Jin, H., Zhang, R. Y., Ding, Y., Zeng, X., Lai, B. Q., Ling, E. A., Wu, J. L., Zeng, Y. S. 2015. Donor mesenchymal stem cell-derived neural-like cells transdifferentiate into myelin-forming cells and promote axon regeneration in rat spinal cord transection. *Stem Cell Res Ther,* 6, 105.

Qu, Z. D., Thacker, M., Castelucci, P., Bagyanszki, M., Epstein, M. L., Furness, J. B. 2008. Immunohistochemical analysis of neuron types in the mouse small intestine. *Cell Tissue Res,* 334, 147-61.

Qureshi, S., Song, J., Lee, H. T., Koh, S. D., Hennig, G. W., Perrino, B. A. 2010. CaM kinase II in colonic smooth muscle contributes to dysmotility in murine DSS-colitis. *Neurogastroenterol Motil,* 22, 186-95, e64.

Raad, M. A., Chams, N. H., Sharara, A. I. 2016. New and evolving immunotherapy in inflammatory bowel disease. *Inflamm Intest Dis,* 1, 85-95.

Rachmilewitz, D., Stamler, J. S., Bachwich, D., Karmeli, F., Ackerman, Z., Podolsky, D. K. 1995. Enhanced colonic nitric oxide generation and nitric oxide synthase activity in ulcerative colitis and Crohn's disease. *Gut,* 36, 718-23.

Rahman, A. A., Robinson, A. M., Brookes, S. J. H., Eri, R., Nurgali, K. 2016. Rectal prolapse in *Winnie* mice with spontaneous chronic colitis: Changes in intrinsic and extrinsic innervation of the rectum. *Cell Tissue Res,* 366, 285-99.

Rahman, A. A., Robinson, A. M., Jovanovska, V., Eri, R., Nurgali, K. 2015. Alterations in the distal colon innervation in *Winnie* mouse model of spontaneous chronic colitis. *Cell Tissue Res,* 362, 497-512.

Rajagopal, S., Nalli, A. D., Kumar, D. P., Bhattacharya, S., Hu, W., Mahavadi, S., Grider, J. R., Murthy, K. S. 2015. Cytokine-induced S-nitrosylation of soluble guanylyl cyclase and expression of phosphodiesterase 1A contribute to dysfunction of longitudinal smooth muscle relaxation. *J Pharmacol Exp Ther,* 352, 509-18.

Ramasamy, R., Fazekasova, H., Lam, E. W., Soeiro, I., Lombardi, G., Dazzi, F. 2007. Mesenchymal stem cells inhibit dendritic cell differentiation and function by preventing entry into the cell cycle. *Transplantation,* 83, 71-6.

Randhawa, P. K., Singh, K., Singh, N., Jaggi, A. S. 2014. A review on chemical-induced inflammatory bowel disease models in rodents. *Korean J Physiol Pharmacol,* 18, 279-88.

Ranganath, S. H., Levy, O., Inamdar, M. S., Karp, J. M. 2012. Harnessing the mesenchymal stem cell secretome for the treatment of cardiovascular disease. *Cell Stem Cell,* 10, 244-58.

Rao, J. N., Wang, J. Y. 2011. *Regulation of gastrointestinal mucosal growth,* Morgan & Claypool, San Rafael, CA.

Rastall, R. A., Gibson, G. R., Gill, H. S., Guarner, F., Klaenhammer, T. R., Pot, B., Reid, G., Rowland, I. R., Sanders, M. E. 2005. Modulation of the microbial ecology of the human colon by probiotics, prebiotics and synbiotics to enhance human health: An overview of enabling science and potential applications. *FEMS Microbiol Ecol,* 52, 145-52.

Rath, H. C. 2002. Role of commensal bacteria in chronic experimental colitis: Lessons from the HLA-B27 transgenic rat. *Pathobiology,* 70, 131-8.

Redaelli, S., Bentivegna, A., Foudah, D., Miloso, M., Redondo, J., Riva, G., Baronchelli, S., Dalpra, L., Tredici, G. 2012. From cytogenomic to epigenomic profiles: monitoring the biologic behavior of *in vitro* cultured human bone marrow mesenchymal stem cells. *Stem Cell Res Ther,* 3, 47.

Reddy, P. M. K. 2010. Effects of the autonomic nervous system, central nervous system and enteric nervous system on gastrointestinal motility. *East Cent Afr J Pharm Sci,* 13, 50-7.

Reddy, S. N., Bazzocchi, G., Chan, S., Akashi, K., Villanueva-Meyer, J., Yanni, G., Mena, I., Snape, W. J. 1991. Colonic motility and transit in health and ulcerative colitis. *Gastroenterology,* 101, 1289-97.

Regueiro, M. D., Greer, J. B., Hanauer, S. B. 2016. Established management paradigms in IBD: Treatment targets and therapeutic tools. *Am J Gastroenterol Suppl,* 3, 8-16.

Rehman, J., Traktuev, D., Li, J., Merfeld-Clauss, S., Temm-Grove, C. J., Bovenkerk, J. E., Pell, C. L., Johnstone, B. H., Considine, R. V., March, K. L. 2004. Secretion of angiogenic and antiapoptotic factors by human adipose stromal cells. *Circulation,* 109, 1292-8.

Reich, H., Tseliou, E., de Couto, G., Angert, D., Valle, J., Kubota, Y., Luthringer, D., Mirocha, J., Sun, B., Smith, R. R., Marban, L., Marban, E. 2016. Repeated transplantation of allogeneic cardiosphere-derived cells boosts therapeutic benefits without immune sensitization in a rat model of myocardial infarction. *J Heart Lung Transplant,* 35, 1348-57.

Ren, G., Chen, X., Dong, F., Li, W., Ren, X., Zhang, Y., Shi, Y. 2012a. Mesenchymal stem cells and translational medicine: Emerging issues. *Stem Cells Transl Med,* 1, 51-8.

Ren, G., Roberts, A. I., Shi, Y. 2011. Adhesion molecules: Key players in mesenchymal stem cell-mediated immunosuppression. *Cell Adh Migr,* 5, 20-2.

Ren, G., Su, J., Zhang, L., Zhao, X., Ling, W., L'Huillie, A., Zhang, J., Lu, Y., Roberts, A. I., Ji, W., Zhang, H., Rabson, A. B., Shi, Y. 2009. Species variation in the mechanisms of mesenchymal stem cell-mediated immunosuppression. *Stem Cells,* 27, 1954-62.

Ren, G., Zhang, L., Zhao, X., Xu, G., Zhang, Y., Roberts, A. I., Zhao, R. C., Shi, Y. 2008. Mesenchymal stem cell-mediated immunosuppression occurs via concerted action of chemokines and nitric oxide. *Cell Stem Cell,* 2, 141-50.

Ren, J., Bertrand, P. P. 2008. Purinergic receptors and synaptic transmission in enteric neurons. *Purinergic Signal,* 4, 255-66.

Ren, J., Stroncek, D. F., Zhao, Y., Jin, P., Castiello, L., Civini, S., Wang, H., Feng, J., Tran, K., Kuznetsov, S. A., Robey, P. G., Sabatino, M. 2013. Intra-subject variability in human bone marrow stromal cell (BMSC) replicative senescence: Molecular changes associated with BMSC senescence. *Stem Cell Res,* 11, 1060-73.

Ren, J., Yan, X., Ai, H., Zhang, Z., Huang, X., Ouyang, J., Yang, M., Yang, H., Han, P., Zeng, W., Chen, Y., Guo, Y., Xiao, S., Ding, N., Huang, L. 2012b.

Susceptibility towards enterotoxigenic *Escherichia coli F4ac* diarrhea is governed by the *Muc13* gene in pigs. *PLoS One,* 7, e44573.
Ren, N., Xing, D., Rittmann, B. E., Zhao, L., Xie, T., Zhao, X. 2007. Microbial community structure of ethanol type fermentation in bio-hydrogen production. *Environ Microbiol,* 9, 1112-25.
Rennert, R. C., Sorkin, M., Garg, R. K., Gurtner, G. C. 2012. Stem cell recruitment after injury: Lessons for regenerative medicine. *Regen Med,* 7, 833-50.
Rezaie, A., Parker, R. D., Abdollahi, M. 2007. Oxidative stress and pathogenesis of inflammatory bowel disease: An epiphenomenon or the cause? *Dig Dis Sci,* 52, 2015-21.
Ribeiro-Paes, J. T., Bilaqui, A., Greco, O. T., Ruiz, M. A., Marcelino, M. Y., Stessuk, T., de Faria, C. A., Lago, M. R. 2011. Unicentric study of cell therapy in chronic obstructive pulmonary disease/pulmonary emphysema. *Int J Chron Obstruct Pulmon Dis,* 6, 63-71.
Ribeiro-Resende, V. T., Pimentel-Coelho, P. M., Mesentier-Louro, L. A., Mendez, R. M. B., Mello-Silva, J. P. C., Cabral-da-Silva, M. C., de Mello, F. G., de Melo Reis, R. A., Mendez-Otero, R. 2009. Trophic activity derived from bone marrow mononuclear cells increases peripheral nerve regeneration by acting on both neuronal and glial cell populations. *Neuroscience,* 159, 540-49.
Ribeiro, C. A., Salgado, A. J., Fraga, J. S., Silva, N. A., Reis, R. L., Sousa, N. 2011. The secretome of bone marrow mesenchymal stem cells-conditioned media varies with time and drives a distinct effect on mature neurons and glial cells (primary cultures). *J Tissue Eng Regen Med,* 5, 668-72.
Ribeiro, T. B., Duarte, A. S., Longhini, A. L., Pradella, F., Farias, A. S., Luzo, A. C., Oliveira, A. L., Olalla Saad, S. T. 2015. Neuroprotection and immunomodulation by xenografted human mesenchymal stem cells following spinal cord ventral root avulsion. *Sci Rep,* 5, 16167.
Richardson, J. D., Bertaso, A. G., Psaltis, P. J., Frost, L., Carbone, A., Paton, S., Nelson, A. J., Wong, D. T., Worthley, M. I., Gronthos, S., Zannettino, A. C., Worthley, S. G. 2013. Impact of timing and dose of mesenchymal stromal cell therapy in a preclinical model of acute myocardial infarction. *J Card Fail,* 19, 342-53.
Rivera-Nieves, J., Bamias, G., Vidrich, A., Marini, M., Pizarro, T. T., McDuffie, M. J., Moskaluk, C. A., Cohn, S. M., Cominelli, F. 2003. Emergence of perianal fistulizing disease in the SAMP1/YitFc mouse, a spontaneous model of chronic ileitis. *Gastroenterology,* 124, 972-82.
Rivera, L. R., Poole, D. P., Thacker, M., Furness, J. B. 2011. The involvement of nitric oxide synthase neurons in enteric neuropathies. *Neurogastroenterol Motil,* 23, 980-8.
Roberts, J. A., Durnin, L., Sharkey, K. A., Mutafova-Yambolieva, V. N., Mawe, G. M. 2013. Oxidative stress disrupts purinergic neuromuscular transmission in the inflamed colon. *J Physiol,* 591, 3725-37.
Roberts, R. R., Bornstein, J. C., Bergner, A. J., Young, H. M. 2008a. Disturbances of colonic motility in mouse models of Hirschsprung's disease. *Am J Physiol Gastrointest Liver Physiol,* 294, G996-1008.

Roberts, R. R., Bornstein, J. C., Bergner, A. J., Young, H. M. 2008b. Disturbances of colonic motility in mouse models of Hirschsprung's disease. *Am J Physiol Gastrointest Liver Physiol,* 294, G996-1008.

Roberts, R. R., Murphy, J. F., Young, H. M., Bornstein, J. C. 2007. Development of colonic motility in the neonatal mouse-studies using spatiotemporal maps. *Am J Physiol Gastrointest Liver Physiol,* 292, G930-8.

Robey, T. E., Saiget, M. K., Reinecke, H., Murry, C. E. 2008. Systems approaches to preventing transplanted cell death in cardiac repair. *J Mol Cell Cardiol,* 45, 567-81.

Robinson, A. M., Gondalia, S. V., Karpe, A. V., Eri, R., Beale, D. J., Morrison, P. D., Palombo, E. A., Nurgali, K. 2016. Fecal microbiota and metabolome in a mouse model of spontaneous chronic colitis: Relevance to human inflammatory bowel disease. *Inflamm Bowel Dis,* 22, 2767-87.

Robinson, A. M., Miller, S., Payne, N., Boyd, R., Sakkal, S., Nurgali, K. 2015. Neuroprotective potential of mesenchymal stem cell-based therapy in acute stages of TNBS-induced colitis in guinea-pigs. *PLoS One,* 10, e0139023.

Robinson, A. M., Rahman, A. A., Carbone, S. E., Randall-Demllo, S., Filippone, R., Bornstein, J. C., Eri, R., Nurgali, K. 2017a. Alterations of colonic function in the *Winnie* mouse model of spontaneous chronic colitis. *Am J Physiol Gastrointest Liver Physiol,* 312, G85-102.

Robinson, A. M., Rahman, A. A., Miller, S., Stavely, R., Sakkal, S., Nurgali, K. 2017b. The neuroprotective effects of human bone marrow mesenchymal stem cells are dose-dependent in TNBS colitis. *Stem Cell Res Ther,* 8, 87.

Robinson, A. M., Sakkal, S., Park, A., Jovanovska, V., Payne, N., Carbone, S. E., Miller, S., Bornstein, J. C., Bernard, C., Boyd, R., Nurgali, K. 2014. Mesenchymal stem cells and conditioned medium avert enteric neuropathy and colon dysfunction in guinea pig TNBS-induced colitis. *Am J Physiol Gasrointest Liver Physiol,* 307, G1115-29.

Rocchi, A., Benchimol, E. I., Bernstein, C. N., Bitton, A., Feagan, B., Panaccione, R., Glasgow, K. W., Fernandes, A., Ghosh, S. 2012. Inflammatory bowel disease: A Canadian burden of illness review. *Can J Gastroenterol,* 26, 811-7.

Rodrigues Hell, R. C., Silva Costa, M. M., Goes, A. M., Oliveira, A. L. 2009. Local injection of BDNF producing mesenchymal stem cells increases neuronal survival and synaptic stability following ventral root avulsion. *Neurobiol Dis,* 33, 290-300.

Roediger, W. E. 1998. Decreased sulphur aminoacid intake in ulcerative colitis. *Lancet,* 351, 1555.

Roediger, W. E., Moore, J., Babidge, W. 1997. Colonic sulfide in pathogenesis and treatment of ulcerative colitis. *Dig Dis Sci,* 42, 1571-9.

Roediger, W. E. W., Macfarlane, G. T. 2002. A role for intestinal mycoplasmas in the aetiology of Crohn's disease? *J Appl Microbiol,* 92, 377-81.

Roemeling-van Rhijn, M., Khairoun, M., Korevaar, S. S., Lievers, E., Leuning, D. G., Ijzermans, J. N. M., Betjes, M. G. H., Genever, P. G., van Kooten, C., de Fijter, H. J. W., Rabelink, T. J., Baan, C. C., Weimar, W., Roelofs, H., Hoogduijn, M. J., Reinders, M. E. 2013. Human bone marrow and adipose tissue-derived mesenchymal stromal cells are immunosuppressive *in vitro*

and in a humanized allograft rejection model. *J Stem Cell Res Ther,* 6, 20780.

Rogler, G., Biedermann, L., Scharl, M. 2018. New insights into the pathophysiology of inflammatory bowel disease: Microbiota, epigenetics and common signalling pathways. *Swiss Med Wkly,* 148, w14599.

Rogler, G., Zeitz, J., Biedermann, L. 2016. The search for causative environmental factors in inflammatory bowel disease. *Dig Dis,* 34 Suppl 1, 48-55.

Romanato, G., Scarpa, M., Angriman, I., Faggian, D., Ruffolo, C., Marin, R., Zambon, S., Basato, S., Zanoni, S., Filosa, T., Pilon, F., Manzato, E. 2009. Plasma lipids and inflammation in active inflammatory bowel diseases. *Aliment Pharmacol Ther,* 29, 298-307.

Romberg-Camps, M. J. L., Bol, Y., Dagnelie, P. C., Hesselink-van de Kruijs, M. A. M., Kester, A. D. M., Engels, L. G. J. B., van Deursen, C., Hameeteman, W. H. A., Pierik, M., Wolters, F., Russel, M. G. V. M., Stockbrügger, R. W. 2010. Fatigue and health-related quality of life in inflammatory bowel disease: Results from a population-based study in the Netherlands: The IBD-South Limburg cohort. *Inflamm Bowel Dis,* 16, 2137-47.

Rooks, M. G., Veiga, P., Wardwell-Scott, L. H., Tickle, T., Segata, N., Michaud, M., Gallini, C. A., Beal, C., van Hylckama-Vlieg, J. E. T., Ballal, S. A., Morgan, X. C., Glickman, J. N., Gevers, D., Huttenhower, C., Garrett, W. S. 2014. Gut microbiome composition and function in experimental colitis during active disease and treatment-induced remission. *ISME J,* 8, 1403-17.

Rubin, D. C., Shaker, A., Levin, M. S. 2012. Chronic intestinal inflammation: Inflammatory bowel disease and colitis-associated colon cancer. *Front Immunol,* 3, 107.

Ruel, J., Ruane, D., Mehandru, S., Gower-Rousseau, C., Colombel, J.-F. 2014. IBD across the age spectrum - is it the same disease? *Nat Rev Gastroenterol Hepatol,* 11, 88-98.

Ruhl, A. 2005. Glial cells in the gut. *Neurogastroenterol Motil,* 17, 777-90.

Ryan, J. M., Barry, F. P., Murphy, J. M., Mahon, B. P. 2005. Mesenchymal stem cells avoid allogeneic rejection. *J Inflamm (Lond),* 2, 8.

Rychter, J., Espin, F., Gallego, D., Vergara, P., Jimenez, M., Clave, P. 2014. Colonic smooth muscle cells and colonic motility patterns as a target for irritable bowel syndrome therapy: mechanisms of action of otilonium bromide. *Therap Adv Gastroenterol,* 7, 156-66.

Sadan, O., Bahat-Stromza, M., Barhum, Y., Levy, Y. S., Pisnevsky, A., Peretz, H., Ilan, A. B., Bulvik, S., Shemesh, N., Krepel, D., Cohen, Y., Melamed, E., Offen, D. 2009. Protective effects of neurotrophic factor-secreting cells in a 6-OHDA rat model of Parkinson disease. *Stem Cells Dev,* 18, 1179-90.

Sadan, O., Shemesh, N., Barzilay, R., Dadon-Nahum, M., Blumenfeld-Katzir, T., Assaf, Y., Yeshurun, M., Djaldetti, R., Cohen, Y., Melamed, E., Offen, D. 2012. Mesenchymal stem cells induced to secrete neurotrophic factors attenuate quinolinic acid toxicity: A potential therapy for Huntington's disease. *Exp Neurol,* 234, 417-27.

Sadik, R., Stotzer, P. O., Simren, M., Abrahamsson, H. 2008. Gastrointestinal transit abnormalities are frequently detected in patients with unexplained GI symptoms at a tertiary centre. *Neurogastroenterol Motil,* 20, 197-205.

Saether, E. E., Chamberlain, C. S., Leiferman, E. M., Kondratko-Mittnacht, J. R., Li, W. J., Brickson, S. L., Vanderby, R. 2014. Enhanced medial collateral ligament healing using mesenchymal stem cells: Dosage effects on cellular response and cytokine profile. *Stem cell Rev,* 10, 86-96.

Sajadinejad, M. S., Asgari, K., Molavi, H., Kalantari, M., Adibi, P. 2012. Psychological issues in inflammatory bowel disease: An overview. *Gastroenterol Res Pract,* 2012, 106502.

Sala, E., Genua, M., Petti, L., Anselmo, A., Arena, V., Cibella, J., Zanotti, L., D'Alessio, S., Scaldaferri, F., Luca, G., Arato, I., Calafiore, R., Sgambato, A., Rutella, S., Locati, M., Danese, S., Vetrano, S. 2015. Mesenchymal stem cells reduce colitis in mice via release of TSG6, independently of their localization to the intestine. *Gastroenterology,* 149, 163-76.e20.

Salgado, A. J., Fraga, J. S., Mesquita, A. R., Neves, N. M., Reis, R. L., Sousa, N. 2010a. Role of human umbilical cord mesenchymal progenitors conditioned media in neuronal/glial cell densities, viability, and proliferation. *Stem Cells Dev,* 19, 1067-74.

Salgado, A. J., Reis, R. L., Sousa, N. J., Gimble, J. M. 2010b. Adipose tissue derived stem cells secretome: soluble factors and their roles in regenerative medicine. *Curr Stem Cell Res Ther,* 5, 103-10.

Sandborn, W. J., Hanauer, S., Van Assche, G., Panes, J., Wilson, S., Petersson, J., Panaccione, R. 2014. Treating beyond symptoms with a view to improving patient outcomes in inflammatory bowel diseases. *J Crohns Colitis,* 8, 927-35.

Sandborn, W. J., Rutgeerts, P., Feagan, B. G., Reinisch, W., Olson, A., Johanns, J., Lu, J., Horgan, K., Rachmilewitz, D., Hanauer, S. B., Lichtenstein, G. R., de Villiers, W. J., Present, D., Sands, B. E., Colombel, J. F. 2009. Colectomy rate comparison after treatment of ulcerative colitis with placebo or infliximab. *Gastroenterology,* 137, 1250-60.

Sanders, K. M. 2008. Regulation of smooth muscle excitation and contraction. *Neurogastroenterol Motil,* 20 Suppl 1, 39-53.

Sands, B. E. 2007. Inflammatory bowel disease: Past, present, and future. *J Gastroenterol,* 42, 16-25.

Sang, Q., Young, H. M. 1998. The identification and chemical coding of cholinergic neurons in the small and large intestine of the mouse. *Anat Rec,* 251, 185-99.

Sanovic, S., Lamb, D. P., Blennerhassett, M. G. 1999. Damage to the enteric nervous system in experimental colitis. *Am J Pathol,* 155, 1051-7.

Sargent, A., Miller, R. H. 2016. MSC therapeutics in chronic inflammation. *Curr Stem Cell Rep,* 2, 168-73.

Sarna, J. R., Furtado, S., Brownell, A. K. 2013. Neurologic complications of metronidazole. *Can J Neurol Sci,* 40, 768-76.

Sarna, S. K. 2010. *Colonic motility: From bench side to bedside,* Morgan & Claypool Life Sciences, San Rafael, CA.

Sarnelli, G., De Giorgio, R., Gentile, F., Cali, G., Grandone, I., Rocco, A., Cosenza, V., Cuomo, R., D'Argenio, G. 2009. Myenteric neuronal loss in

rats with experimental colitis: role of tissue transglutaminase-induced apoptosis. *Dig Liver Dis,* 41, 185-93.
Sarosiek, I., Schicho, R., Blandon, P., Bashashati, M. 2016. Urinary metabolites as noninvasive biomarkers of gastrointestinal diseases: A clinical review. *World J Gastrointest Oncol,* 8, 459-65.
Sartor, R. B. 2004. Therapeutic manipulation of the enteric microflora in inflammatory bowel diseases: Antibiotics, probiotics, and prebiotics. *Gastroenterology,* 126, 1620-33.
Sartor, R. B. 2008. Microbial influences in inflammatory bowel diseases. *Gastroenterology,* 134, 577-94.
Sartor, R. B., Mazmanian, S. K. 2012. Intestinal microbes in inflammatory bowel diseases. *Am J Gastroenterol Suppl,* 1, 15-21.
Sarugaser, R., Hanoun, L., Keating, A., Stanford, W. L., Davies, J. E. 2009. Human mesenchymal stem cells self-renew and differentiate according to a deterministic hierarchy. *PLoS One,* 4, e6498.
Sato, K., Ohkura, S., Kitahara, Y., Ohama, T., Hori, M., Sato, M., Kobayashi, S., Sasaki, Y., Hayashi, T., Nasu, T., Ozaki, H. 2007. Involvement of CPI-17 downregulation in the dysmotility of the colon from dextran sodium sulphate-induced experimental colitis in a mouse model. *Neurogastroenterol Motil,* 19, 504-14.
Sayegh, A. I., Washington, M. C. 2012. Back to basics: Regulation of the gastrointestinal functions. *J Gastroint Dig Syst,* 2, 1-4.
Scanlan, P. D., Shanahan, F., Marchesi, J. R. 2009. Culture-independent analysis of desulfovibrios in the human distal colon of healthy, colorectal cancer and polypectomized individuals. *FEMS Microbiol Ecol,* 69, 213-21.
Scanlan, P. D., Shanahan, F., O'Mahony, C., Marchesi, J. R. 2006. Culture-independent analyses of temporal variation of the dominant fecal microbiota and targeted bacterial subgroups in Crohn's disease. *J Clin Microbiol,* 44, 3980-8.
Schaible, U. E., Kaufmann, S. H. 2005. A nutritive view on the host-pathogen interplay. *Trends Microbiol,* 13, 373-80.
Schaubeck, M., Clavel, T., Calasan, J., Lagkouvardos, I., Haange, S. B., Jehmlich, N., Basic, M., Dupont, A., Hornef, M., von Bergen, M., Bleich, A., Haller, D. 2016. Dysbiotic gut microbiota causes transmissible Crohn's disease-like ileitis independent of failure in antimicrobial defence. *Gut,* 65, 225-37.
Scheibe, F., Klein, O., Klose, J., Priller, J. 2012. Mesenchymal stromal cells rescue cortical neurons from apoptotic cell death in an *in vitro* model of cerebral ischemia. *Cell Mol Neurobiol,* 32, 567-76.
Schloss, P. D., Handelsman, J. 2005. Metagenomics for studying unculturable microorganisms: Cutting the Gordian knot. *Genome Biol,* 6, 229.
Schneider, D. A., Galligan, J. J. 2000. Presynaptic nicotinic acetylcholine receptors in the myenteric plexus of guinea pig intestine. *Am J Physiol Gastrointest Liver Physiol,* 279, G528-35.
Scholz, T., Rogers, J. M., Krichevsky, A., Dhar, S., Evans, G. R. 2010. Inducible nerve growth factor delivery for peripheral nerve regeneration *in vivo*. *Plast Reconstr Surg,* 126, 1874-89.

Schreiber, S. 2011. Certolizumab pegol for the treatment of Crohn's disease. *Therap Adv Gastroenterol,* 4, 375-89.
Schrepfer, S., Deuse, T., Reichenspurner, H., Fischbein, M. P., Robbins, R. C., Pelletier, M. P. 2007. Stem cell transplantation: The lung barrier. *Transplant Proc,* 39, 573-6.
Schuleri, K. H., Feigenbaum, G. S., Centola, M., Weiss, E. S., Zimmet, J. M., Turney, J., Kellner, J., Zviman, M. M., Hatzistergos, K. E., Detrick, B., Conte, J. V., McNiece, I., Steenbergen, C., Lardo, A. C., Hare, J. M. 2009. Autologous mesenchymal stem cells produce reverse remodelling in chronic ischaemic cardiomyopathy. *Eur Heart J,* 30, 2722-32.
Schwab, C., Berry, D., Rauch, I., Rennisch, I., Ramesmayer, J., Hainzl, E., Heider, S., Decker, T., Kenner, L., Muller, M., Strobl, B., Wagner, M., Schleper, C., Loy, A., Urich, T. 2014. Longitudinal study of murine microbiota activity and interactions with the host during acute inflammation and recovery. *ISME J,* 8, 1101-14.
Scribano, M. L. 2008. Adverse events of IBD therapies. *Inflamm Bowel Dis,* 14, S210-1.
Scribano, M. L., Prantera, C. 2013. Antibiotics and inflammatory bowel diseases. *Dig Dis,* 31, 379-84.
Scuteri, A., Donzelli, E., Foudah, D., Caldara, C., Redondo, J., D'Amico, G., Tredici, G., Miloso, M. 2014. Mesengenic differentiation: Comparison of human and rat bone marrow mesenchymal stem cells. *Int J Stem Cells,* 7, 127-34.
Sebben, A. D., Lichtenfels, M., da Silva, J. L. B. 2011. Peripheral nerve regeneration: Cell therapy and neurotrophic factors. *Rev Bras Ortop,* 46, 643-9.
Segain, J. P., Raingeard de la Bletiere, D., Bourreille, A., Leray, V., Gervois, N., Rosales, C., Ferrier, L., Bonnet, C., Blottiere, H. M., Galmiche, J. P. 2000. Butyrate inhibits inflammatory responses through NFkappaB inhibition: implications for Crohn's disease. *Gut,* 47, 397-403.
Sekiya, I., Larson, B. L., Smith, J. R., Pochampally, R., Cui, J. G., Prockop, D. J. 2002. Expansion of human adult stem cells from bone marrow stroma: Conditions that maximize the yields of early progenitors and evaluate their quality. *Stem Cells,* 20, 530-41.
Seksik, P., Rigottier-Gois, L., Gramet, G., Sutren, M., Pochart, P., Marteau, P., Jian, R., Dore, J. 2003. Alterations of the dominant faecal bacterial groups in patients with Crohn's disease of the colon. *Gut,* 52, 237-42.
Sellon, R. K., Tonkonogy, S., Schultz, M., Dieleman, L. A., Grenther, W., Balish, E., Rennick, D. M., Sartor, R. B. 1998. Resident enteric bacteria are necessary for development of spontaneous colitis and immune system activation in interleukin-10-deficient Mice. *Infect Immun,* 66, 5224-31.
Selmani, Z., Naji, A., Zidi, I., Favier, B., Gaiffe, E., Obert, L., Borg, C., Saas, P., Tiberghien, P., Rouas-Freiss, N., Carosella, E. D., Deschaseaux, F. 2008. Human leukocyte antigen-G5 secretion by human mesenchymal stem cells is required to suppress T lymphocyte and natural killer function and to induce CD4+CD25highFOXP3+ regulatory T cells. *Stem Cells,* 26, 212-22.

Semedo, P., Palasio, C. G., Oliveira, C. D., Feitoza, C. Q., Goncalves, G. M., Cenedeze, M. A., Wang, P. M. H., Teixeira, V. P. A., Reis, M. A., Pacheco-Silva, A., Camara, N. O. S. 2009. Early modulation of inflammation by mesenchymal stem cell after acute kidney injury. *Int Immunopharmacol,* 9, 677-82.

Semont, A., Demarquay, C., Bessout, R., Durand, C., Benderitter, M., Mathieu, N. 2013. Mesenchymal stem cell therapy stimulates endogenous host progenitor cells to improve colonic epithelial regeneration. *PLoS One,* 8, e70170.

Semont, A., Mouiseddine, M., Francois, A., Demarquay, C., Mathieu, N., Chapel, A., Sache, A., Thierry, D., Laloi, P., Gourmelon, P. 2010. Mesenchymal stem cells improve small intestinal integrity through regulation of endogenous epithelial cell homeostasis. *Cell Death Differ,* 17, 952-61.

Senn, J. J. 2006. Toll-like receptor-2 is essential for the development of palmitate-induced insulin resistance in myotubes. *J Biol Chem,* 281, 26865-75.

Serio, R., Zizzo, M. G., Mastropaolo, M. 2011. The enteric nervous system: New developments and emerging concepts *Malta Med J,* 23, 1-4.

Sha, S., Xu, B., Wang, X., Zhang, Y., Wang, H., Kong, X., Zhu, H., Wu, K. 2013. The biodiversity and composition of the dominant fecal microbiota in patients with inflammatory bowel disease. *Diagn Microbiol Infect Dis,* 75, 245-51.

Shabala, L., Walker, E. J., Eklund, A., Randall-Demllo, S., Shabala, S., Guven, N., Cook, A. L., Eri, R. D. 2013. Exposure of colonic epithelial cells to oxidative and endoplasmic reticulum stress causes rapid potassium efflux and calcium influx. *Cell Biochem Funct,* 31, 603-11.

Shalaby, S. M., Sabbah, N. A., Saber, T., Abdel Hamid, R. A. 2016. Adipose-derived mesenchymal stem cells modulate the immune response in chronic experimental autoimmune encephalomyelitis model. *IUBMB Life,* 68, 106-15.

Sharkey, K. A., Kroese, A. B. 2001. Consequences of intestinal inflammation on the enteric nervous system: Neuronal activation induced by inflammatory mediators. *Anat Rec,* 262, 79-90.

Sharkey, K. A., Savidge, T. C. 2014. Role of enteric neurotransmission in host defense and protection of the gastrointestinal tract. *Autonomic Neurosci,* 181, 94-106.

Sharma, R. R., Pollock, K., Hubel, A., McKenna, D. 2014. Mesenchymal stem or stromal cells: A review of clinical applications and manufacturing practices. *Transfusion,* 54, 1418-37.

Shen, K. Z., Surprenant, A. 1993. Somatostatin-mediated inhibitory postsynaptic potential in sympathetically denervated guinea-pig submucosal neurones. *J Physiol,* 470, 619-35.

Shen, L. H., Li, Y., Chen, J., Zhang, J., Vanguri, P., Borneman, J., Chopp, M. 2006. Intracarotid transplantation of bone marrow stromal cells increases axon-myelin remodeling after stroke. *Neuroscience,* 137, 393-9.

Shepela, C. 2008. The safety of biologic agents in the treatment of inflammatory bowel disease. *Minn Med,* 91, 42-5.

Shi, H., Kokoeva, M. V., Inouye, K., Tzameli, I., Yin, H., Flier, J. S. 2006. TLR4 links innate immunity and fatty acid-induced insulin resistance. *J Clin Invest,* 116, 3015-25.

Shi, X. Z., Sarna, S. K. 1999. Differential inflammatory modulation of canine ileal longitudinal and circular muscle cells. *Am J Physiol,* 277, G341-50.

Shi, Y., Su, J., Roberts, A. I., Shou, P., Rabson, A. B., Ren, G. 2012. How mesenchymal stem cells interact with tissue immune responses. *Trends Immunol,* 33, 136-43.

Shin, J. Y., Park, H. J., Kim, H. N., Oh, S. H., Bae, J. S., Ha, H. J., Lee, P. H. 2014. Mesenchymal stem cells enhance autophagy and increase beta-amyloid clearance in Alzheimer disease models. *Autophagy,* 10, 32-44.

Shiomi, Y., Nishiumi, S., Ooi, M., Hatano, N., Shinohara, M., Yoshie, T., Kondo, Y., Furumatsu, K., Shiomi, H., Kutsumi, H., Azuma, T., Yoshida, M. 2011. GCMS-based metabolomic study in mice with colitis induced by dextran sulfate sodium. *Inflamm Bowel Dis,* 17, 2261-74.

Shomer, N. H., Dangler, C. A., Marini, R. P., Fox, J. G. 1998. *Helicobacter bilis*/*Helicobacter rodentium* co-infection associated with diarrhea in a colony of scid mice. *Lab Anim Sci,* 48, 455-9.

Shouval, D. S., Rufo, P. A. 2017. The role of environmental factors in the pathogenesis of inflammatory bowel diseases: A review. *JAMA Pediatr,* 171, 999-1005.

Singer, N. G., Caplan, A. I. 2011. Mesenchymal stem cells: Mechanisms of inflammation. *Annu Rev Pathol,* 6, 457-78.

Skalnikova, H., Motlik, J., Gadher, S. J., Kovarova, H. 2011. Mapping of the secretome of primary isolates of mammalian cells, stem cells and derived cell lines. *Proteomics,* 11, 691-708.

Slater, P. G., Ramirez, V. T., Gonzalez-Billault, C., Varela-Nallar, L., Inestrosa, N. C. 2013. Frizzled-5 receptor is involved in neuronal polarity and morphogenesis of hippocampal neurons. *PLoS One,* 8, e78892.

Slavin, S., Kurkalli, B. G. S., Karussis, D. 2008. The potential use of adult stem cells for the treatment of multiple sclerosis and other neurodegenerative disorders. *Clin Neurol Neurosurg,* 110, 943-6.

Smith, A. S., Smid, S. D. 2005. Impaired capsaicin and neurokinin-evoked colonic motility in inflammatory bowel disease. *J Gastroenterol Hepatol,* 20, 697-704.

Smith, E. A., Macfarlane, G. T. 1996. Enumeration of human colonic bacteria producing phenolic and indolic compounds: Effects of pH, carbohydrate availability and retention time on dissimilatory aromatic amino acid metabolism. *J Appl Bacteriol,* 81, 288-302.

Smith, E. A., Macfarlane, G. T. 1997. Formation of phenolic and indolic compounds by anaerobic bacteria in the human large intestine. *Microb Ecol,* 33, 180-8.

Soeda, S., Koyanagi, S., Kuramoto, Y., Kimura, M., Oda, M., Kozako, T., Hayashida, S., Shimeno, H. 2008. Anti-apoptotic roles of plasminogen activator inhibitor-1 as a neurotrophic factor in the central nervous system. *Thromb Haemost,* 100, 1014-20.

Sokol, H., Polin, V., Lavergne-Slove, A., Panis, Y., Treton, X., Dray, X., Bouhnik, Y., Valleur, P., Marteau, P. 2009. Plexitis as a predictive factor of early postoperative clinical recurrence in Crohn's disease. *Gut,* 58, 1218-25.

Sokol, H., Seksik, P., Rigottier-Gois, L., Lay, C., Lepage, P., Podglajen, I., Marteau, P., Dore, J. 2006. Specificities of the fecal microbiota in inflammatory bowel disease. *Inflamm Bowel Dis,* 12, 106-11.

Sola, A., Peng, H., Rogido, M., Wen, T. C. 2008. Animal models of neonatal stroke and response to erythropoietin and cardiotrophin-1. *Int J Dev Neurosci,* 26, 27-35.

Son, B. R., Marquez-Curtis, L. A., Kucia, M., Wysoczynski, M., Turner, A. R., Ratajczak, J., Ratajczak, M. Z., Janowska-Wieczorek, A. 2006. Migration of bone marrow and cord blood mesenchymal stem cells in vitro is regulated by stromal-derived factor-1-CXCR4 and hepatocyte growth factor-c-met axes and involves matrix metalloproteinases. *Stem Cells,* 24, 1254-64.

Song-Zhao, G. X., Maloy, K. J. 2014. Experimental Mouse Models of T Cell-Dependent Inflammatory Bowel Disease. *In:* WAISMAN, A. & BECHER, B. (eds.) *T-Helper Cells: Methods and Protocols.* New York, NY: Springer New York.

Song, C. H., Honmou, O., Furuoka, H., Horiuchi, M. 2011. Identification of chemoattractive factors involved in the migration of bone marrow-derived mesenchymal stem cells to brain lesions caused by prions. *J Virol,* 85, 11069-78.

Song, E. M., Jung, S. A., Lee, K. E., Jang, J. Y., Lee, K. H., Tae, C. H., Moon, C. M., Joo, Y. H., Kim, S. E., Jung, H. K., Shim, K. N. 2017. The therapeutic efficacy of tonsil-derived mesenchymal stem cells in dextran sulfate sodium-induced acute murine colitis model. *Korean J Gastroenterol,* 69, 119-28.

Song, H., Cha, M. J., Song, B. W., Kim, I. K., Chang, W., Lim, S., Choi, E. J., Ham, O., Lee, S. Y., Chung, N., Jang, Y., Hwang, K. C. 2010. Reactive oxygen species inhibit adhesion of mesenchymal stem cells implanted into ischemic myocardium via interference of focal adhesion complex. *Stem Cells,* 28, 555-63.

Song, M., Mohamad, O., Gu, X., Wei, L., Yu, S. P. 2013. Restoration of intracortical and thalamocortical circuits after transplantation of bone marrow mesenchymal stem cells into the ischemic brain of mice. *Cell Transplant,* 22, 2001-15.

Sotiropoulou, P. A., Perez, S. A., Salagianni, M., Baxevanis, C. N., Papamichail, M. 2006. Characterization of the optimal culture conditions for clinical scale production of human mesenchymal stem cells. *Stem Cells,* 24, 462-71.

Spaeth, E., Klopp, A., Dembinski, J., Andreeff, M., Marini, F. 2008. Inflammation and tumor microenvironments: Defining the migratory itinerary of mesenchymal stem cells. *Gene Ther,* 15, 730-8.

Spaggiari, G. M., Capobianco, A., Becchetti, S., Mingari, M. C., Moretta, L. 2006. Mesenchymal stem cell-natural killer cell interactions: Evidence that activated NK cells are capable of killing MSCs, whereas MSCs can inhibit IL-2-induced NK-cell proliferation. *Blood,* 107, 1484-90.

Spehlmann, M. E., Dann, S. M., Hruz, P., Hanson, E., McCole, D. F., Eckmann, L. 2009. CXCR2-dependent mucosal neutrophil influx protects against colitis-associated diarrhea caused by an attaching/effacing lesion-forming bacterial pathogen. *J Immunol,* 183, 3332-43.

Spencer, N., Walsh, M., Smith, T. K. 1999. Does the guinea-pig ileum obey the 'law of the intestine'? *J Physiol,* 517, 889-98.

Spencer, N. J., Bayguinov, P., Hennig, G. W., Park, K. J., Lee, H. T., Sanders, K. M., Smith, T. K. 2007. Activation of neural circuitry and Ca2+ waves in longitudinal and circular muscle during CMMCs and the consequences of rectal aganglionosis in mice. *Am J Physiol Gastrointest Liver Physiol,* 292, G546-55.

Spencer, N. J., Bywater, R. A. 2002. Enteric nerve stimulation evokes a premature colonic migrating motor complex in mouse. *Neurogastroenterol Motil,* 14, 657-65.

Spencer, N. J., Bywater, R. A. R., Taylor, G. S. 1998. Disinhibition during myoelectric complexes in the mouse colon. *J Auton Nerv Syst,* 71, 37-47.

Spencer, N. J., Hennig, G. W., Dickson, E., Smith, T. K. 2005. Synchronization of enteric neuronal firing during the murine colonic MMC. *J Physiol,* 564, 829-47.

Spencer, N. J., Nicholas, S. J., Sia, T. C., Staikopoulos, V., Kyloh, M., Beckett, E. A. 2013. By what mechanism does ondansetron inhibit colonic migrating motor complexes: Does it require endogenous serotonin in the gut wall? *Neurogastroenterol Motil,* 25, 677-85.

Spencer, N. J., Sanders, K. M., Smith, T. K. 2003. Migrating motor complexes do not require electrical slow waves in the mouse small intestine. *J Physiol,* 553, 881-893.

Spencer, N. J., Smith, T. K. 2001. Simultaneous intracellular recordings from longitudinal and circular muscle during the peristaltic reflex in guinea-pig distal colon. *J Physiol,* 533, 787-99.

Stahl, M., Friis, L. M., Nothaft, H., Liu, X., Li, J., Szymanski, C. M., Stintzi, A. 2011. L-fucose utilization provides *Campylobacter jejuni* with a competitive advantage. *Proc Natl Acad Sci U S A,* 108, 7194-9.

Stallmach, A., Hagel, S., Bruns, T. 2010. Adverse effects of biologics used for treating IBD. *Best Pract Res Clin Gastroenterol,* 24, 167-82.

Stavely, R., Robinson, A. M., Miller, S., Boyd, R., Sakkal, S., Nurgali, K. 2015a. Allogeneic guinea pig mesenchymal stem cells ameliorate neurological changes in experimental colitis. *Stem Cell Res Ther,* 6, 263.

Stavely, R., Robinson, A. M., Miller, S., Boyd, R., Sakkal, S., Nurgali, K. 2015b. Human adult stem cells derived from adipose tissue and bone marrow attenuate enteric neuropathy in the guinea-pig model of acute colitis. *Stem Cell Res Ther,* 6, 244.

Stavely, R., Sakkal, S., Stojanovska, V., Nurgali, K. 2014. Mesenchymal stem cells for the treatment of inflammatory bowel disease: From experimental models to clinical application. *Inflamm Regen,* 34, 184-97.

Steinkamp, M., Gundel, H., Schulte, N., Spaniol, U., Pflueger, C., Zizer, E., von Boyen, G. B. T. 2012. GDNF protects enteric glia from apoptosis: Evidence for an autocrine loop. *BMC Gastroenterol,* 12, 6.

Stessuk, T., Ruiz, M. A., Greco, O. T., Bilaqui, A., Ribeiro-Paes, M. J. O., Ribeiro-Paes, J. T. 2013. Phase I clinical trial of cell therapy in patients with advanced chronic obstructive pulmonary disease: Follow-up of up to 3 years. *Rev Bras Hematol Hemoter,* 35, 352-7.

Storr, M. A., Yuce, B., Andrews, C. N., Sharkey, K. A. 2008. The role of the endocannabinoid system in the pathophysiology and treatment of irritable bowel syndrome. *Neurogastroenterol Motil,* 20, 857-68.

Storsteen, K. A., Kernohan, J. W., Bargen, J. A. 1953. The myenteric plexus in chronic ulcerative colitis. *Surg Gynecol Obstet,* 97, 335-43.

Straub, R. H., Grum, F., Strauch, U., Capellino, S., Bataille, F., Bleich, A., Falk, W., Scholmerich, J., Obermeier, F. 2008. Anti-inflammatory role of sympathetic nerves in chronic intestinal inflammation. *Gut,* 57, 911-21.

Straub, R. H., Stebner, K., Harle, P., Kees, F., Falk, W., Scholmerich, J. 2005. Key role of the sympathetic microenvironment for the interplay of tumour necrosis factor and interleukin 6 in normal but not in inflamed mouse colon mucosa. *Gut,* 54, 1098-106.

Stringer, A. M., Gibson, R. J., Logan, R. M., Bowen, J. M., Yeoh, A. S. J., Laurence, J., Keefe, D. M. K. 2009. Irinotecan-induced mucositis is associated with changes in intestinal mucins. *Cancer Chemother Pharmacol,* 64, 123-32.

Strong, D. S., Cornbrooks, C. F., Roberts, J. A., Hoffman, J. M., Sharkey, K. A., Mawe, G. M. 2010. Purinergic neuromuscular transmission is selectively attenuated in ulcerated regions of inflamed guinea pig distal colon. *J Physiol,* 588, 847-59.

Su, J. W., Ma, J. J., Zhang, H. J. 2015. Use of antibiotics in patients with Crohn's disease: A systematic review and meta-analysis. *J Dig Dis,* 16, 58-66.

Suau, A., Bonnet, R., Sutren, M., Godon, J. J., Gibson, G. R., Collins, M. D., Dore, J. 1999. Direct analysis of genes encoding 16S rRNA from complex communities reveals many novel molecular species within the human gut. *Appl Environ Microbiol,* 65, 4799-807.

Sudres, M., Norol, F., Trenado, A., Gregoire, S., Charlotte, F., Levacher, B., Lataillade, J. J., Bourin, P., Holy, X., Vernant, J. P., Klatzmann, D., Cohen, J. L. 2006. Bone marrow mesenchymal stem cells suppress lymphocyte proliferation *in vitro* but fail to prevent graft-versus-host disease in mice. *J Immunol,* 176, 7761-7.

Sumner, L. W., Amberg, A., Barrett, D., Beale, M. H., Beger, R., Daykin, C. A., Fan, T. W. M., Fiehn, O., Goodacre, R., Griffin, J. L., Hankemeier, T., Hardy, N., Harnly, J., Higashi, R., Kopka, J., Lane, A. N., Lindon, J. C., Marriott, P., Nicholls, A. W., Reily, M. D., Thaden, J. J., Viant, M. R. 2007. Proposed minimum reporting standards for chemical analysis. *Metabolomics,* 3, 211-21.

Sussman, D. A., Santaolalla, R., Strobel, S., Dheer, R., Abreu, M. T. 2012. Cancer in inflammatory bowel disease: Lessons from animal models. *Curr Opin Gastroenterol,* 28, 327-33.

Suzuki, M., McHugh, J., Tork, C., Shelley, B., Hayes, A., Bellantuono, I., Aebischer, P., Svendsen, C. N. 2008. Direct muscle delivery of GDNF with human mesenchymal stem cells improves motor neuron survival and function in a rat model of familial ALS. *Mol Ther,* 16, 2002-10.

Suzuki, M., Svendsen, C. N. 2008. Combining growth factor and stem cell therapy for amyotrophic lateral sclerosis. *Trends Neurosci,* 31, 192-8.

Swain, M. G., Blennerhassett, P. A., Collins, S. M. 1991. Impaired sympathetic nerve function in the inflamed rat intestine. *Gastroenterology,* 100, 675-82.

Swenson, E. S., Theise, N. D. 2010. Stem cell therapeutics: Potential in the treatment of inflammatory bowel disease. *Clin Exp Gastroenterol,* 3, 1-10.

Takahashi, H., Matsui, T., Hisabe, T., Hirai, F., Takatsu, N., Tsurumi, K., Kanemitsu, T., Sato, Y., Kinjyo, K., Yano, Y., Takaki, Y., Nagahama, T., Yao, K., Washio, M. 2014. Second peak in the distribution of age at onset of ulcerative colitis in relation to smoking cessation. *J Gastroenterol Hepatol,* 29, 1603-8.

Takaishi, H., Matsuki, T., Nakazawa, A., Takada, T., Kado, S., Asahara, T., Kamada, N., Sakuraba, A., Yajima, T., Higuchi, H., Inoue, N., Ogata, H., Iwao, Y., Nomoto, K., Tanaka, R., Hibi, T. 2008. Imbalance in intestinal microflora constitution could be involved in the pathogenesis of inflammatory bowel disease. *Int J Med Microbiol,* 298, 463-72.

Takatsu, N., Matsui, T., Murakami, Y., Ishihara, H., Hisabe, T., Nagahama, T., Maki, S., Beppu, T., Takaki, Y., Hirai, F., Yao, K. 2009. Adverse reactions to azathioprine cannot be predicted by thiopurine S-methyltransferase genotype in Japanese patients with inflammatory bowel disease. *J Gastroenterol Hepatol,* 24, 1258-64.

Tanaka, F., Tominaga, K., Ochi, M., Tanigawa, T., Watanabe, T., Fujiwara, Y., Ohta, K., Oshitani, N., Higuchi, K., Arakawa, T. 2008. Exogenous administration of mesenchymal stem cells ameliorates dextran sulfate sodium-induced colitis via anti-inflammatory action in damaged tissue in rats. *Life Sci,* 83, 771-9.

Tanaka, H., Arimura, Y., Yabana, T., Goto, A., Hosokawa, M., Nagaishi, K., Yamashita, K., Yamamoto, H., Sasaki, Y., Fujimiya, M., Imai, K., Shinomura, Y. 2011. Myogenic lineage differentiated mesenchymal stem cells enhance recovery from dextran sulfate sodium-induced colitis in the rat. *J Gastroenterol,* 46, 143-52.

Tang, L., Lu, X., Zhu, R., Qian, T., Tao, Y., Li, K., Zheng, J., Zhao, P., Li, S., Wang, X., Li, L. 2016. Adipose-derived stem cells expressing the neurogenin-2 promote functional recovery after spinal cord injury in rat. *Cell Mol Neurobiol,* 36, 657-67.

Tang, R. J., Shen, S. N., Zhao, X. Y., Nie, Y. Z., Xu, Y. J., Ren, J., Lv, M. M., Hou, Y. Y., Wang, T. T. 2015. Mesenchymal stem cells-regulated Treg cells suppress colitis-associated colorectal cancer. *Stem Cell Res Ther,* 6, 71.

Tang, S., Zhu, J., Xu, Y., Xiang, A. P., Jiang, M. H., Quan, D. 2013. The effects of gradients of nerve growth factor immobilized PCLA scaffolds on neurite outgrowth in vitro and peripheral nerve regeneration in rats. *Biomaterials,* 34, 7086-96.

Tanna, T., Sachan, V. 2014. Mesenchymal stem cells: Potential in treatment of neurodegenerative diseases. *Curr Stem Cell Res Ther,* 9, 513-21.

Tattoli, I., Sorbara, M. T., Vuckovic, D., Ling, A., Soares, F., Carneiro, L. A. M., Yang, C., Emili, A., Philpott, D. J., Girardin, S. E. 2012. Amino acid

starvation induced by invasive bacterial pathogens triggers an innate host defense program. *Cell Host Microbe,* 11, 563-75.

Tejima, E., Guo, S., Murata, Y., Arai, K., Lok, J., van Leyen, K., Rosell, A., Wang, X., Lo, E. H. 2009. Neuroprotective effects of overexpressing tissue inhibitor of metalloproteinase TIMP-1. *J Neurotrauma,* 26, 1935-41.

Tepperman, B. L., Brown, J. F., Whittle, B. J. 1993. Nitric oxide synthase induction and intestinal epithelial cell viability in rats. *Am J Physiol,* 265, G214-8.

Theodoratou, E., Campbell, H., Ventham, N. T., Kolarich, D., Pucic-Bakovic, M., Zoldos, V., Fernandes, D., Pemberton, I. K., Rudan, I., Kennedy, N. A., Wuhrer, M., Nimmo, E., Annese, V., McGovern, D. P. B., Satsangi, J., Lauc, G. 2014. The role of glycosylation in IBD. *Nat Rev Gastroenterol Hepatol,* 11, 588-600.

Thibault, R., Blachier, F., Darcy-Vrillon, B., de Coppet, P., Bourreille, A., Segain, J. 2010. Butyrate utilization by the colonic mucosa in inflammatory bowel diseases: A transport deficiency. *Inflamm Bowel Dis,* 16, 684-95.

Thomas, A., Lodhia, N. 2014. Advanced therapy for inflammatory bowel disease: A guide for the primary care physician. *J Am Board Fam Med,* 27, 411-20.

Thomson, J. M., Hansen, R., Berry, S. H., Hope, M. E., Murray, G. I., Mukhopadhya, I., McLean, M. H., Shen, Z., Fox, J. G., El-Omar, E., Hold, G. L. 2011. Enterohepatic *helicobacter* in ulcerative colitis: Potential pathogenic entities? *PLoS One,* 6, e17184.

Thway, K., Selfe, J., Shipley, J. 2012. Immunohistochemical detection of glypican-5 in paraffin-embedded material: An optimized method for a novel research antibody. *Appl Immunohistochem Mol Morphol,* 20, 189-95.

Timmermans, J. P., Adriaensen, D., Cornelissen, W., Scheuermann, D. W. 1997. Structural organization and neuropeptide distribution in the mammalian enteric nervous system, with special attention to those components involved in mucosal reflexes. *Comp Biochem Physiol A Physiol,* 118, 331-40.

Tokita, Y., Tang, X. L., Li, Q., Wysoczynski, M., Hong, K. U., Nakamura, S., Wu, W. J., Xie, W., Li, D., Hunt, G., Ou, Q., Stowers, H., Bolli, R. 2016. Repeated administrations of cardiac progenitor cells are markedly more effective than a single administration: A new paradigm in cell therapy. *Circ Res,* 119, 635-51.

Tontini, G. E., Vecchi, M., Pastorelli, L., Neurath, M. F., Neumann, H. 2015. Differential diagnosis in inflammatory bowel disease colitis: State of the art and future perspectives. *World J Gastroenterol,* 21, 21-46.

Torres-Espin, A., Corona-Quintanilla, D. L., Fores, J., Allodi, I., Gonzalez, F., Udina, E., Navarro, X. 2013a. Neuroprotection and axonal regeneration after lumbar ventral root avulsion by re-implantation and mesenchymal stem cells transplant combined therapy. *Neurotherapeutics,* 10, 354-68.

Torres-Espin, A., Hernandez, J., Navarro, X. 2013b. Gene expression changes in the injured spinal cord following transplantation of mesenchymal stem cells or olfactory ensheathing cells. *PLoS One,* 8, e76141.

Triantafillidis, J. K., Merikas, E., Georgopoulos, F. 2011. Current and emerging drugs for the treatment of inflammatory bowel disease. *Drug Des Devel Ther,* 5, 185-210.

Trounson, A., McDonald, C. 2015. Stem cell therapies in clinical trials: Progress and challenges. *Cell Stem Cell,* 17, 11-22.

Tsai, H. H., Dwarakanath, A. D., Hart, C. A., Milton, J. D., Rhodes, J. M. 1995. Increased faecal mucin sulphatase activity in ulcerative colitis: A potential target for treatment. *Gut,* 36, 570-76.

Tsai, M. J., Tsai, S. K., Hu, B. R., Liou, D. Y., Huang, S. L., Huang, M. C., Huang, W. C., Cheng, H., Huang, S. S. 2014. Recovery of neurological function of ischemic stroke by application of conditioned medium of bone marrow mesenchymal stem cells derived from normal and cerebral ischemia rats. *J Biomed Sci,* 21, 5.

Tse, W. T., Pendleton, J. D., Beyer, W. M., Egalka, M. C., Guinan, E. C. 2003. Suppression of allogeneic T-cell proliferation by human marrow stromal cells: Implications in transplantation. *Transplantation,* 75, 389-97.

Tsune, I., Ikejima, K., Hirose, M., Yoshikawa, M., Enomoto, N., Takei, Y., Sato, N. 2003. Dietary glycine prevents chemical-induced experimental colitis in the rat. *Gastroenterology,* 125, 775-85.

Tytgat, K. M. A. J., van der Wal, J. W. G., Einerhand, A. W. C., Buller, H. A., Dekker, J. 1996. Quantitative Analysis of *Muc2* synthesis in ulcerative colitis. *Biochem Biophys Res Commun,* 224, 397-405.

Uccelli, A., Benvenuto, F., Laroni, A., Giunti, D. 2011. Neuroprotective features of mesenchymal stem cells. *Best Pract Res Clin Haematol,* 24, 59-64.

Uccelli, A., Moretta, L., Pistoia, V. 2008. Mesenchymal stem cells in health and disease. *Nat Rev Immunol,* 8, 726-36.

Uccelli, A., Prockop, D. J. 2010. Why should mesenchymal stem cells (MSCs) cure autoimmune diseases? *Curr Opin Immunol,* 22, 768-74.

Uhlig, H. H. 2013. Monogenic diseases associated with intestinal inflammation: implications for the understanding of inflammatory bowel disease. *Gut,* 62, 1795-805.

Uhlig, H. H., Powrie, F. 2009. Mouse models of intestinal inflammation as tools to understand the pathogenesis of inflammatory bowel disease. *Eur J Immunol,* 39, 2021-6.

Ullah, I., Subbarao, R. B., Rho, G. J. 2015. Human mesenchymal stem cells - Current trends and future prospective. *Biosci Rep,* 35, e00191.

Ulloa, L. 2005. The vagus nerve and the nicotinic anti-inflammatory pathway. *Nat Rev Drug Discov,* 4, 673-84.

Umanskiy, K., Fichera, A. 2010. Health related quality of life in inflammatory bowel disease: The impact of surgical therapy. *World J Gastroenterol,* 16, 5024-34.

Uyttebroek, L., Shepherd, I. T., Harrisson, F., Hubens, G., Blust, R., Timmermans, J.-P., Van Nassauw, L. 2010. Neurochemical coding of enteric neurons in adult and embryonic zebrafish (*Danio rerio*). *J Comp Neurol,* 518, 4419-4438.

Valatas, V., Vakas, M., Kolios, G. 2013. The value of experimental models of colitis in predicting efficacy of biological therapies for inflammatory bowel diseases. *Am J Physiol Gastrointest Liver Physiol,* 305, G763-85.

van Bergeijk, J. D., van Westreenen, H., Adhien, P., Zijlstra, F. J. 1998. Diminished nitroprusside-induced relaxation of inflamed colonic smooth muscle in mice. *Mediators Inflamm,* 7, 283-87.

van der Burg, J. M., Winqvist, A., Aziz, N. A., Maat-Schieman, M. L., Roos, R. A., Bates, G. P., Brundin, P., Bjorkqvist, M., Wierup, N. 2011. Gastrointestinal dysfunction contributes to weight loss in Huntington's disease mice. *Neurobiol Dis,* 44, 1-8.

Van Dieren, J. M., Hansen, B. E., Kuipers, E. J., Nieuwenhuis, E. E., Van der Woude, C. J. 2007. Meta-analysis: Inosine triphosphate pyrophosphatase polymorphisms and thiopurine toxicity in the treatment of inflammatory bowel disease. *Aliment Pharmacol Ther,* 26, 643-52.

Van Geldre, L. A., Lefebvre, R. A. 2004. Interaction of NO and VIP in gastrointestinal smooth muscle relaxation. *Curr Pharm Des,* 10, 2483-97.

Van Klinken, B. J. W., Van der Wal, J. W. G., Einerhand, A. W., Buller, H. A., Dekker, J. 1999. Sulphation and secretion of the predominant secretory human colonic mucin *Muc2* in ulcerative colitis. *Gut,* 44, 387-93.

Van Landeghem, L., Mahe, M. M., Teusan, R., Leger, J., Guisle, I., Houlgatte, R., Neunlist, M. 2009. Regulation of intestinal epithelial cells transcriptome by enteric glial cells: impact on intestinal epithelial barrier functions. *BMC Genomics,* 10, 507.

Van Limbergen, J., Russell, R. K., Drummond, H. E., Aldhous, M. C., Round, N. K., Nimmo, E. R., Smith, L., Gillett, P. M., McGrogan, P., Weaver, L. T., Bisset, W. M., Mahdi, G., Arnott, I. D., Satsangi, J., Wilson, D. C. 2008. Definition of phenotypic characteristics of childhood-onset inflammatory bowel disease. *Gastroenterology,* 135, 1114-22.

Varma, S., Bird, R., Eskin, M., Dolenko, B., Raju, J., Bezabeh, T. 2007. Detection of inflammatory bowel disease by proton magnetic resonance spectroscopy (1H MRS) using an animal model. *J Inflamm (Lond),* 4, 24.

Vasina, V., Abu-Gharbieh, E., Barbara, G., De Giorgio, R., Colucci, R., Blandizzi, C., Bernardini, N., Croci, T., Del Tacca, M., De Ponti, F. 2008. The β3-adrenoceptor agonist SR58611A ameliorates experimental colitis in rats. *Neurogastroenterol Motil,* 20, 1030-41.

Vasina, V., Barbara, G., Talamonti, L., Stanghellini, V., Corinaldesi, R., Tonini, M., De Ponti, F., De Giorgio, R. 2006. Enteric neuroplasticity evoked by inflammation. *Auton Neurosci,* 126-127, 264-72.

Vatn, M. H. 2009. Natural history and complications of IBD. *Curr Gastroenterol Rep,* 11, 481-7.

Vavricka, S. R., Schoepfer, A., Scharl, M., Lakatos, P. L., Navarini, A., Rogler, G. 2015. Extraintestinal manifestations of inflammatory bowel disease. *Inflamm Bowel Dis,* 21, 1982-92.

Vecchi Brumatti, L., Marcuzzi, A., Tricarico, M. P., Zanin, V., Girardelli, M., Bianco, M. A. 2014. Curcumin and inflammatory bowel disease: Potential and limits of innovative treatments. *Molecules,* 19, 21127-53.

Vercelli, A., Mereuta, O. M., Garbossa, D., Muraca, G., Mareschi, K., Rustichelli, D., Ferrero, I., Mazzini, L., Madon, E., Fagioli, F. 2008. Human mesenchymal stem cell transplantation extends survival, improves motor performance and decreases neuroinflammation in mouse model of amyotrophic lateral sclerosis. *Neurobiol Dis,* 31, 395-405.

Vermeire, S., Ferrante, M., Rutgeerts, P. 2013. Recent advances: Personalised use of current Crohn's disease therapeutic options. *Gut,* 62, 1511-5.

Vermeire, S., Van Assche, G., Rutgeerts, P. 2012. Classification of inflammatory bowel disease: The old and the new. *Curr Opin Gastroenterol,* 28, 321-6.
Vernia, P., Gnaedinger, A., Hauck, W., Breuer, R. I. 1988. Organic anions and the diarrhea of inflammatory bowel disease. *Dig Dis Sci,* 33, 1353-8.
Viana, M. L., Pontes, R. M., Garcia, W. E., Favero, M. E., Prete, D. C., Matsuo, T. 2007. [Crohn's disease and kidney stones: much more than coincidence?]. *Arq Gastroenterol,* 44, 210-4.
Vigsnaes, L. K., van den Abbeele, P., Sulek, K., Frandsen, H. L., Steenholdt, C., Brynskov, J., Vermeiren, J., van de Wiele, T., Licht, T. R. 2013. Microbiotas from UC patients display altered metabolism and reduced ability of LAB to colonize mucus. *Sci Rep,* 3, 1110.
Villanacci, V., Bassotti, G., Nascimbeni, R., Antonelli, E., Cadei, M., Fisogni, S., Salerni, B., Geboes, K. 2008. Enteric nervous system abnormalities in inflammatory bowel diseases. *Neurogastroenterol Motil,* 20, 1009-16.
Villanacci, V., Falchetti, D., Liserre, B., Soresina, A. R., Plebani, A., Ekema, G., Bassotti, G. 2007. Diversion of the fecal stream resolves ulcerative colitis complicating chronic granulomatous disease in an adult patient. *J Clin Gastroenterol,* 41, 491-3.
Vind, I., Riis, L., Jess, T., Knudsen, E., Pedersen, N., Elkjaer, M., Bak Andersen, I., Wewer, V., Norregaard, P., Moesgaard, F., Bendtsen, F., Munkholm, P. 2006. Increasing incidences of inflammatory bowel disease and decreasing surgery rates in Copenhagen City and County, 2003-2005: A population-based study from the Danish Crohn colitis database. *Am J Gastroenterol,* 101, 1274-82.
Viswanathan, S., Benatar, T., Rose-John, S., Lauffenburger, D. A., Zandstra, P. W. 2002. Ligand/receptor signaling threshold (LIST) model accounts for gp130-mediated embryonic stem cell self-renewal responses to LIF and HIL-6. *Stem Cells,* 20, 119-38.
Volkman, R., Offen, D. 2017. Mesenchymal stem cells in neurodegenerative diseases. *Stem Cells,* 35, 1867-80.
von Bahr, L., Batsis, I., Moll, G., Hagg, M., Szakos, A., Sundberg, B., Uzunel, M., Ringden, O., Le Blanc, K. 2012. Analysis of tissues following mesenchymal stromal cell therapy in humans indicates limited long-term engraftment and no ectopic tissue formation. *Stem Cells,* 30, 1575-8.
von Boyen, G. B. T., Reinshagen, M., Steinkamp, M., Adler, G., Kirsch, J. 2002. Enteric nervous plasticity and development: Dependence on neurotrophic factors. *J Gastroenterol,* 37, 583-8.
von Boyen, G. B. T., Steinkamp, M., Geerling, I., Reinshagen, M., Adler, G., Schafer, K. H., Kirsch, J. 2006. Proinflammatory cytokines induce neurotrophic factor expression in enteric glia: A key to the regulation of epithelial apoptosis in Crohn's disease. *Inflamm Bowel Dis,* 12, 346-54.
Voulgari-Kokota, A., Fairless, R., Karamita, M., Kyrargyri, V., Tseveleki, V., Evangelidou, M., Delorme, B., Charbord, P., Diem, R., Probert, L. 2012. Mesenchymal stem cells protect CNS neurons against glutamate excitotoxicity by inhibiting glutamate receptor expression and function. *Exp Neurol,* 236, 161-170.

Vrees, M. D., Pricolo, V. E., Potenti, F. M., Cao, W. 2002. Abnormal motility in patients with ulcerative colitis: The role of inflammatory cytokines. *Arch Surg,* 137, 439-46.

Wadie, W., Abdel-Aziz, H., Zaki, H. F., Kelber, O., Weiser, D., Khayyal, M. T. 2012. STW 5 is effective in dextran sulfate sodium-induced colitis in rats. *Int J Colorectal Dis,* 27, 1445-53.

Waljee, A. K., Joyce, J. C., Wren, P. A., Khan, T., Higgins, P. D. R. 2009. Patient reported symptoms during an ulcerative colitis flare: A qualitative focus group study. *Eur J Gastroenterol Hepatol,* 21, 558-64.

Waljee, A. K., Wiitala, W. L., Govani, S., Stidham, R., Saini, S., Hou, J., Feagins, L. A., Khan, N., Good, C. B., Vijan, S., Higgins, P. D. R. 2016. Corticosteroid use and complications in a US inflammatory bowel disease cohort. *PLoS One,* 11, e0158017.

Walker, A. W., Sanderson, J. D., Churcher, C., Parkes, G. C., Hudspith, B. N., Rayment, N., Brostoff, J., Parkhill, J., Dougan, G., Petrovska, L. 2011. High-throughput clone library analysis of the mucosa-associated microbiota reveals dysbiosis and differences between inflamed and non-inflamed regions of the intestine in inflammatory bowel disease. *BMC Microbiol,* 11, 7.

Wallace, K. L., Zheng, L.-B., Kanazawa, Y., Shih, D. Q. 2014. Immunopathology of inflammatory bowel disease. *World J Gastroenterol,* 20, 6-21.

Walters, E. M., Wolf, E., Whyte, J. J., Mao, J., Renner, S., Nagashima, H., Kobayashi, E., Zhao, J., Wells, K. D., Critser, J. K., Riley, L. K., Prather, R. S. 2012. Completion of the swine genome will simplify the production of swine as a large animal biomedical model. *BMC Med Genomics,* 5, 55.

Wang, C., Chen, J., Sun, L., Liu, Y. 2014a. TGF-beta signaling-dependent alleviation of dextran sulfate sodium-induced colitis by mesenchymal stem cell transplantation. *Mol Biol Rep,* 41, 4977-83.

Wang, H., Nagai, A., Sheikh, A. M., Liang, X. Y., Yano, S., Mitaki, S., Ishibashi, Y., Kobayashi, S., Kim, S. U., Yamaguchi, S. 2013a. Human mesenchymal stem cell transplantation changes proinflammatory gene expression through a nuclear factor-kappaB-dependent pathway in a rat focal cerebral ischemic model. *J Neurosci Res,* 91, 1440-9.

Wang, J., Yin, L., Chen, Z. 2013b. Neuroprotective role of fibronectin in neuron-glial extrasynaptic transmission. *Neural Regen Res,* 8, 376-82.

Wang, M. H., Fiocchi, C., Duerr, R. H., Zhu, X., Ripke, S., Achkar, J. P. 2013c. A novel approach to detect cumulative genetic effects and genetic interactions in Crohn's disease. *Inflamm Bowel Dis,* 19, 1799-1808.

Wang, S., Qu, X., Zhao, R. C. 2012a. Clinical applications of mesenchymal stem cells. *J Hematol Oncol,* 5, 19.

Wang, S. L., Wang, Z. R., Yang, C. Q. 2012b. Meta-analysis of broad-spectrum antibiotic therapy in patients with active inflammatory bowel disease. *Exp Ther Med,* 4, 1051-6.

Wang, W., Chen, L., Zhou, R., Wang, X., Song, L., Huang, S., Wang, G., Xia, B. 2014b. Increased proportions of *Bifidobacterium* and the *Lactobacillus* group and loss of butyrate-producing bacteria in inflammatory bowel disease. *J Clin Microbiol,* 52, 398-406.

Wang, X. Y., Alberti, E., White, E. J., Mikkelsen, H. B., Larsen, J. O., Jimenez, M., Huizinga, J. D. 2009a. Igf1r+/CD34+ immature ICC are putative adult progenitor cells, identified ultrastructurally as fibroblast-like ICC in Ws/Ws rat colon. *J Cell Mol Med,* 13, 3528-40.

Wang, Y., Chen, X., Cao, W., Shi, Y. 2014c. Plasticity of mesenchymal stem cells in immunomodulation: Pathological and therapeutic implications. *Nat Immunol,* 15, 1009-16.

Wang, Y., Tu, W., Lou, Y., Xie, A., Lai, X., Guo, F., Deng, Z. 2009b. Mesenchymal stem cells regulate the proliferation and differentiation of neural stem cells through Notch signaling. *Cell Biol Int,* 33, 1173-9.

Watanabe, S., Arimura, Y., Nagaishi, K., Isshiki, H., Onodera, K., Nasuno, M., Yamashita, K., Idogawa, M., Naishiro, Y., Murata, M., Adachi, Y., Fujimiya, M., Imai, K., Shinomura, Y. 2014. Conditioned mesenchymal stem cells produce pleiotropic gut trophic factors. *J Gastroenterol,* 49, 270-82.

Waterman, M., Xu, W., Stempak, J. M., Milgrom, R., Bernstein, C. N., Griffiths, A. M., Greenberg, G. R., Steinhart, A. H., Silverberg, M. S. 2011. Distinct and overlapping genetic loci in Crohn's disease and ulcerative colitis: Correlations with pathogenesis. *Inflamm Bowel Dis,* 17, 1936-42.

Waterston, R. H., Lindblad-Toh, K., Birney, E., Rogers, J., Abril, J. F., Agarwal, P., Agarwala, R., Ainscough, R., Alexandersson, M., An, P., Antonarakis, S. E., Attwood, J., Baertsch, R., Bailey, J., Barlow, K., Beck, S., Berry, E., Birren, B., Bloom, T., Bork, P., Botcherby, M., Bray, N., Brent, M. R., Brown, D. G., Brown, S. D., Bult, C., Burton, J., Butler, J., Campbell, R. D., Carninci, P., Cawley, S., Chiaromonte, F., Chinwalla, A. T., Church, D. M., Clamp, M., Clee, C., Collins, F. S., Cook, L. L., Copley, R. R., Coulson, A., Couronne, O., Cuff, J., Curwen, V., Cutts, T., Daly, M., David, R., Davies, J., Delehaunty, K. D., Deri, J., Dermitzakis, E. T., Dewey, C., Dickens, N. J., Diekhans, M., Dodge, S., Dubchak, I., Dunn, D. M., Eddy, S. R., Elnitski, L., Emes, R. D., Eswara, P., Eyras, E., Felsenfeld, A., Fewell, G. A., Flicek, P., Foley, K., Frankel, W. N., Fulton, L. A., Fulton, R. S., Furey, T. S., Gage, D., Gibbs, R. A., Glusman, G., Gnerre, S., Goldman, N., Goodstadt, L., Grafham, D., Graves, T. A., Green, E. D., Gregory, S., Guigo, R., Guyer, M., Hardison, R. C., Haussler, D., Hayashizaki, Y., Hillier, L. W., Hinrichs, A., Hlavina, W., Holzer, T., Hsu, F., Hua, A., Hubbard, T., Hunt, A., Jackson, I., Jaffe, D. B., Johnson, L. S., Jones, M., Jones, T. A., Joy, A., Kamal, M., Karlsson, E. K., et al. 2002. Initial sequencing and comparative analysis of the mouse genome. *Nature,* 420, 520-62.

Wattchow, D. A., Brookes, S. J., Costa, M. 1995. The morphology and projections of retrogradely labeled myenteric neurons in the human intestine. *Gastroenterology,* 109, 866-75.

Wei, X., Yang, X., Han, Z. P., Qu, F. F., Shao, L., Shi, Y. F. 2013. Mesenchymal stem cells: A new trend for cell therapy. *Acta Pharmacol Sin,* 34, 747-54.

Wei, X., Zhao, L., Zhong, J., Gu, H., Feng, D., Johnstone, B. H., March, K. L., Farlow, M. R., Du, Y. 2009. Adipose stromal cells-secreted neuroprotective media against neuronal apoptosis. *Neurosci Lett,* 462, 76-9.

Weinger, J. G., Brosnan, C. F., Loudig, O., Goldberg, M. F., Macian, F., Arnett, H. A., Prieto, A. L., Tsiperson, V., Shafit-Zagardo, B. 2011. Loss of the

receptor tyrosine kinase Axl leads to enhanced inflammation in the CNS and delayed removal of myelin debris during experimental autoimmune encephalomyelitis. *J Neuroinflammation,* 8, 49.

Weng, J. Y., Du, X., Geng, S. X., Peng, Y. W., Wang, Z., Lu, Z. S., Wu, S. J., Luo, C. W., Guo, R., Ling, W., Deng, C. X., Liao, P. J., Xiang, A. P. 2010. Mesenchymal stem cell as salvage treatment for refractory chronic GVHD. *Bone Marrow Transplant,* 45, 1732-40.

Whitehead, K. J., Schmitz, J. M., Carroll, I. M., Arthur, J. C., Jobin, C., Sartor, R. B. 2011. Ingestion of dietary carbohydrates influences the aggressiveness of colitis and intestinal microbial composition in IL-10-/- mice. *Gastroenterology,* 140, S-47.

Wieczorek, G., Steinhoff, C., Schulz, R., Scheller, M., Vingron, M., Ropers, H. H., Nuber, U. A. 2003. Gene expression profile of mouse bone marrow stromal cells determined by cDNA microarray analysis. *Cell Tissue Res,* 311, 227-37.

Williams, C., Panaccione, R., Ghosh, S., Rioux, K. 2011. Optimizing clinical use of mesalazine (5-aminosalicylic acid) in inflammatory bowel disease. *Therap Adv Gastroenterol,* 4, 237-48.

Willing, B. P., Dicksved, J., Halfvarson, J., Andersson, A. F., Lucio, M., Zheng, Z., Jarnerot, G., Tysk, C., Jansson, J. K., Engstrand, L. 2010. A pyrosequencing study in twins shows that gastrointestinal microbial profiles vary with inflammatory bowel disease phenotypes. *Gastroenterology,* 139, 1844-54.e1.

Wilson, J., Hair, C., Knight, R., Catto-Smith, A., Bell, S., Kamm, M., Desmond, P., McNeil, J., Connell, W. 2010. High incidence of inflammatory bowel disease in Australia: A prospective population-based Australian incidence study. *Inflamm Bowel Dis,* 16, 1550-6.

Winston, J. H., Li, Q., Sarna, S. K. 2013. Paradoxical regulation of ChAT and nNOS expression in animal models of Crohn's colitis and ulcerative colitis. *Am J Physiol Gastrointest Liver Physiol,* 305, G295-302.

Wirtz, S., Neufert, C., Weigmann, B., Neurath, M. F. 2007. Chemically induced mouse models of intestinal inflammation. *Nat Protoc,* 2, 541-6.

Wirtz, S., Neurath, M. F. 2000. Animal models of intestinal inflammation: New insights into the molecular pathogenesis and immunotherapy of inflammatory bowel disease. *Int J Colorectal Dis,* 15, 144-60.

Wirtz, S., Neurath, M. F. 2007. Mouse models of inflammatory bowel disease. *Adv Drug Deliv Rev,* 59, 1073-83.

Wold, S., Sjostrom, M., Eriksson, L. 2001. PLS-regression: a basic tool of chemometrics. *Chemometr Intell Lab Syst,* 58, 109-30.

Wolever, T. M. S., Piekarz, A., Hollands, M., Younker, K. 2002. Sugar alcohols and diabetes: A review. *Can J Diabetes,* 26, 356-62.

Wong, J. M., de Souza, R., Kendall, C. W., Emam, A., Jenkins, D. J. 2006. Colonic health: Fermentation and short chain fatty acids. *J Clin Gastroenterol,* 40, 235-43.

Wood, J. D. 2011. *Enteric nervous system: The brain-in-the-gut,* Morgan & Claypool, San Rafael, CA.

Wood, J. D., Alpers, D. H., Andrews, P. L. 1999. Fundamentals of neurogastroenterology. *Gut,* 45 Suppl 2, Ii6-ii16.

Wood, J. D., Kirchgessner, A. 2004. Slow excitatory metabotropic signal transmission in the enteric nervous system. *Neurogastroenterol Motil,* 16 Suppl 1, 71-80.

Xavier, R. J., Podolsky, D. K. 2007. Unravelling the pathogenesis of inflammatory bowel disease. *Nature,* 448, 427-34.

Xu, X. R., Liu, C. Q., Feng, B. S., Liu, Z. J. 2014. Dysregulation of mucosal immune response in pathogenesis of inflammatory bowel disease. *World J Gastroenterol,* 20, 3255-64.

Yabana, T., Arimura, Y., Tanaka, H., Goto, A., Hosokawa, M., Nagaishi, K., Yamashita, K., Yamamoto, H., Adachi, Y., Sasaki, Y., Isobe, M., Fujimiya, M., Imai, K., Shinomura, Y. 2009. Enhancing epithelial engraftment of rat mesenchymal stem cells restores epithelial barrier integrity. *J Pathol,* 218, 350-9.

Yamamoto, K., Kiyohara, T., Murayama, Y., Kihara, S., Okamoto, Y., Funahashi, T., Ito, T., Nezu, R., Tsutsui, S., Miyagawa, J. I., Tamura, S., Matsuzawa, Y., Shimomura, I., Shinomura, Y. 2005. Production of adiponectin, an anti-inflammatory protein, in mesenteric adipose tissue in Crohn's disease. *Gut,* 54, 789-96.

Yanai, H., Hanauer, S. B. 2011. Assessing response and loss of response to biological therapies in IBD. *Am J Gastroenterol,* 106, 685-98.

Yang, J., Liu, X. X., Fan, H., Tang, Q., Shou, Z. X., Zuo, D. M., Zou, Z., Xu, M., Chen, Q. Y., Peng, Y., Deng, S. J., Liu, Y. J. 2015. Extracellular vesicles derived from bone marrow mesenchymal stem cells protect against experimental colitis via attenuating colon inflammation, oxidative stress and apoptosis. *PLoS ONE,* 10, e0140551.

Yang, J., Wu, H., Hu, N., Gu, X., Ding, F. 2009. Effects of bone marrow stromal cell-conditioned medium on primary cultures of peripheral nerve tissues and cells. *Neurochem Res,* 34, 1685-94.

Yoo, B. B., Mazmanian, S. K. 2017. The enteric network: Interactions between the immune and nervous systems of the gut. *Immunity,* 46, 910-26.

Yoon, S. S., Mekalanos, J. J. 2006. 2,3-butanediol synthesis and the emergence of the *Vibrio cholerae El Tor* biotype. *Infect Immun,* 74, 6547-56.

Yoshida, M., Watanabe, T., Usui, T., Matsunaga, Y., Shirai, Y., Yamori, M., Itoh, T., Habu, S., Chiba, T., Kita, T., Wakatsuki, Y. 2001. CD4 T cells monospecific to ovalbumin produced by *Escherichia coli* can induce colitis upon transfer to BALB/c and SCID mice. *Int Immunol,* 13, 1561-70.

Yousefifard, M., Nasirinezhad, F., Shardi Manaheji, H., Janzadeh, A., Hosseini, M., Keshavarz, M. 2016. Human bone marrow-derived and umbilical cord-derived mesenchymal stem cells for alleviating neuropathic pain in a spinal cord injury model. *Stem Cell Res Ther,* 7, 36.

Yu, H., Liu, J., Ma, J., Xiang, L. 2014. Local delivery of controlled released nerve growth factor promotes sciatic nerve regeneration after crush injury. *Neurosci Lett,* 566, 177-81.

Yu, Q., Zhang, S., Li, L., Xiong, L., Chao, K., Zhong, B., Li, Y., Wang, H., Chen, M. 2015. Enterohepatic *Helicobacter* species as a potential causative factor in inflammatory bowel disease: A meta-analysis. *Medicine (Baltimore),* 94, e1773.

Yu, Y., Song, E. M., Lee, K. E., Joo, Y. H., Kim, S. E., Moon, C. M., Kim, H. Y., Jung, S. A., Jo, I. 2017. Therapeutic potential of tonsil-derived mesenchymal stem cells in dextran sulfate sodium-induced experimental murine colitis. *PLoS One,* 12, e0183141.

Zachar, L., Bacenkova, D., Rosocha, J. 2016. Activation, homing, and role of the mesenchymal stem cells in the inflammatory environment. *J Inflamm Res,* 9, 231-240.

Zappia, E., Casazza, S., Pedemonte, E., Benvenuto, F., Bonanni, I., Gerdoni, E., Giunti, D., Ceravolo, A., Cazzanti, F., Frassoni, F., Mancardi, G., Uccelli, A. 2005. Mesenchymal stem cells ameliorate experimental autoimmune encephalomyelitis inducing T-cell anergy. *Blood,* 106, 1755-61.

Zavan, B., Giorgi, C., Bagnara, G. P., Vindigni, V., Abatangelo, G., Cortivo, R. 2007. Osteogenic and chondrogenic differentiation: Comparison of human and rat bone marrow mesenchymal stem cells cultured into polymeric scaffolds. *Eur J Histochem,* 51, 1-8.

Zeng, R., Wang, L. W., Hu, Z. B., Guo, W. T., Wei, J. S., Lin, H., Sun, X., Chen, L. X., Yang, L. J. 2011. Differentiation of human bone marrow mesenchymal stem cells into neuron-like cells *in vitro*. *Spine* 36, 997-1005.

Zhang, C., Zhou, C., Teng, J. J., Zhao, R. L., Song, Y. Q., Zhang, C. 2009a. Multiple administrations of human marrow stromal cells through cerebrospinal fluid prolong survival in a transgenic mouse model of amyotrophic lateral sclerosis. *Cytotherapy,* 11, 299-306.

Zhang, D., Kilian, K. A. 2013. The effect of mesenchymal stem cell shape on the maintenance of multipotency. *Biomaterials,* 34, 3962-9.

Zhang, J., Huang, X., Wang, H., Liu, X., Zhang, T., Wang, Y., Hu, D. 2015. The challenges and promises of allogeneic mesenchymal stem cells for use as a cell-based therapy. *Stem Cell Res Ther,* 6, 234.

Zhang, J., Li, Y., Chen, J., Cui, Y., Lu, M., Elias, S. B., Mitchell, J. B., Hammill, L., Vanguri, P., Chopp, M. 2005. Human bone marrow stromal cell treatment improves neurological functional recovery in EAE mice. *Exp Neurol,* 195, 16-26.

Zhang, J., Li, Y., Lu, M., Cui, Y., Chen, J., Noffsinger, L., Elias, S. B., Chopp, M. 2006. Bone marrow stromal cells reduce axonal loss in experimental autoimmune encephalomyelitis mice. *J Neurosci Res,* 84, 587-95.

Zhang, J., Shi, Q., Yang, P., Xu, X., Chen, X., Qi, C., Zhang, J., Lu, H., Zhao, B., Zheng, P., Zhang, P., Liu, Y. 2012. Neuroprotection of neurotrophin-3 against focal cerebral ischemia/reperfusion injury is regulated by hypoxia-responsive element in rats. *Neuroscience,* 222, 1-9.

Zhang, L., Li, Y., Guan, C.-Y., Tian, S., Lv, X.-D., Li, J.-H., Ma, X., Xia, H.-F. 2018. Therapeutic effect of human umbilical cord-derived mesenchymal stem cells on injured rat endometrium during its chronic phase. *Stem Cell Res Ther,* 9, 36.

Zhang, Q., Shi, S., Liu, Y., Uyanne, J., Shi, Y., Shi, S., Le, A. D. 2009b. Mesenchymal stem cells derived from human gingiva are capable of immunomodulatory functions and ameliorate inflammation-related tissue destruction in experimental colitis. *J Immunol,* 183, 7787-98.

Zhang, Y.-Z., Li, Y.-Y. 2014. Inflammatory bowel disease: Pathogenesis. *World J Gastroenterol,* 20, 91-9.

Zhang, Y., Paterson, W. G. 2005. Excitatory purinergic neurotransmission in smooth muscle of guniea-pig taenia caeci. *J Physiol,* 563, 855-65.
Zhao, C. P., Zhang, C., Zhou, S. N., Xie, Y. M., Wang, Y. H., Huang, H., Shang, Y. C., Li, W. Y., Zhou, C., Yu, M. J., Feng, S. W. 2007. Human mesenchymal stromal cells ameliorate the phenotype of SOD1-G93A ALS mice. *Cytotherapy,* 9, 414-26.
Zhao, J., Chen, N., Shen, N., Zhao, H., Wang, D., Shi, J., Wang, Y., Cui, X., Yan, Z., Xue, H. 2012. Transplantation of human umbilical cord blood mesenchymal stem cells to treat a rat model of traumatic brain injury. *Neural Regen Res,* 7, 741-8.
Zhao, Q., Ren, H., Han, Z. 2016. Mesenchymal stem cells: Immunomodulatory capability and clinical potential in immune diseases. *J Cell Immunother,* 2, 3-20.
Zheng, W. H., Kar, S., Dore, S., Quirion, R. 2000. Insulin-like growth factor-1 (IGF-1): A neuroprotective trophic factor acting via the Akt kinase pathway. *J Neural Transm Suppl*, 261-72.
Zheng, Z. H., Li, X. Y., Ding, J., Jia, J. F., Zhu, P. 2008. Allogeneic mesenchymal stem cell and mesenchymal stem cell-differentiated chondrocyte suppress the responses of type II collagen-reactive T cells in rheumatoid arthritis. *Rheumatology (Oxford),* 47, 22-30.
Zhou, C. H., Li, M. L., Qin, A. L., Lv, S. X., Wen, T., Zhu, X. Y., Li, L. Y., Dong, Y., Hu, C. Y., Hu, D. M., Wang, S. F. 2013. Reduction of fibrosis in dibutyltin dichloride-induced chronic pancreatitis using rat umbilical mesenchymal stem cells from Wharton's jelly. *Pancreas,* 42, 1291-302.
Zhu, X. Y., Urbieta-Caceres, V., Krier, J. D., Textor, S. C., Lerman, A., Lerman, L. O. 2013. Mesenchymal stem cells and endothelial progenitor cells decrease renal injury in experimental swine renal artery stenosis through different mechanisms. *Stem cells,* 31, 117-25.
Ziambaras, T., Rubin, D. C., Perlmutter, D. H. 1996. Regulation of sucrase-isomaltase gene expression in human intestinal epithelial cells by inflammatory cytokines. *J Biol Chem,* 271, 1237-42.
Zitomersky, N. L., Atkinson, B. J., Franklin, S. W., Mitchell, P. D., Snapper, S. B., Comstock, L. E., Bousvaros, A. 2013. Characterization of adherent *Bacteroidales* from intestinal biopsies of children and young adults with inflammatory bowel disease. *PLoS One,* 8, e63686.
Zuo, D., Tang, Q., Fan, H., Shou, Z., Liu, X., Cao, D., Zou, Z. 2015. Modulation of nuclear factor-kappaB-mediated pro-inflammatory response is associated with exogenous administration of bone marrow-derived mesenchymal stem cells for treatment of experimental colitis. *Mol Med Rep,* 11, 2741-8.
Zurita, M., Vaquero, J., Bonilla, C., Santos, M., De Haro, J., Oya, S., Aguayo, C. 2008. Functional recovery of chronic paraplegic pigs after autologous transplantation of bone marrow stromal cells. *Transplantation,* 86, 845-53.
Zvonic, S., Lefevre, M., Kilroy, G., Floyd, Z. E., DeLany, J. P., Kheterpal, I., Gravois, A., Dow, R., White, A., Wu, X., Gimble, J. M. 2007. Secretome of primary cultures of human adipose-derived stem cells: modulation of serpins by adipogenesis. *Mol Cell Proteomics,* 6, 18-28.

Zwi, A. B., Mills, A. 1995. Health policy in less developed countries: Past trends and future directions. *J Int Dev,* 7, 299-328.

APPENDICES

Appendix A: Microbial diversity and richness, PCA score and PLS-DA loading scatter plots of fecal samples from Winnie vs C57BL/6 mice

Table S1. Sample diversity and richness

Sample ID	16S rRNA amplicon sequences	Simpson Diversity	Shannon Diversity	Good's Coverage	Chao Richness
C57BL/6_1	48907	0.990	9.09	0.94	8900
C57BL/6_2	36613	0.980	8.72	0.94	6410
C57BL/6_3	20158	0.970	8.18	0.92	5096
C57BL/6_4	15323	0.980	8.66	0.88	5501
C57BL/6_5	20724	0.970	8.53	0.90	6676
C57BL/6_6	33436	0.980	8.57	0.92	7838
C57BL/6_7	11551	0.970	7.81	0.89	3793
C57BL/6_8	14494	0.990	8.82	0.88	5173
C57BL/6_9	26462	0.990	9.07	0.90	8005
C57BL/6_10	14749	0.980	8.30	0.91	3932
C57BL/6 Mean	**24241.7**	**0.980**	**8.58**	**0.91**	**6132.4**
C57BL/6 SD	**12044.7**	**0.008**	**0.40**	**0.02**	**1737.0**
C57BL/6 SEM	**3808.9**	**0.003**	**0.13**	**0.01**	**549.3**
C57BL/6 Min	**11551**	**0.970**	**7.81**	**0.88**	**3793**
C57BL/6 Max	**48907**	**0.990**	**9.09**	**0.94**	**8900**
C57BL/6 Med	**20441**	**0.980**	**8.62**	**0.91**	**5955.5**
*Winnie*_1	26615	0.990	8.99	0.92	6476
*Winnie*_2	53756	0.980	8.17	0.97	5697
*Winnie*_3	22280	0.970	8.20	0.92	5339
*Winnie*_4	21330	0.990	8.62	0.90	6633
*Winnie*_5	45834	0.990	8.97	0.93	10285
*Winnie*_6	45999	0.990	9.27	0.93	9633
*Winnie*_7	51534	0.990	9.16	0.95	8222
*Winnie*_8	25953	0.980	8.15	0.93	5878

Sample ID	16S rRNA amplicon sequences	Simpson Diversity	Shannon Diversity	Good's Coverage	Chao Richness
*Winnie*_9	33686	0.970	8.36	0.92	8584
*Winnie*_10	23730	0.980	8.53	0.93	5468
***Winnie* Mean**	**35071.7**	**0.983**	**8.64**	**0.93**	**7221.5**
***Winnie* SD**	**12879.9**	**0.008**	**0.43**	**0.02**	**1816.8**
***Winnie* SEM**	**4073.0**	**0.003**	**0.14**	**0.01**	**574.5**
***Winnie* Min**	**21330**	**0.970**	**8.15**	**0.90**	**5339**
***Winnie* Max**	**53756**	**0.990**	**9.27**	**0.97**	**10285**
***Winnie* Med**	**30150.5**	**0.985**	**8.58**	**0.93**	**6554.5**

Figure S1. Principal component analysis. Principal component analysis (PCA) score scatter plot of fecal samples from *Winnie* vs C57BL/6. The $R^2X(cum)=88\%$ and $Q^2(cum)=63.9\%$. The Eclipse represents Hoteling's T^2 value of 95% confidence level.

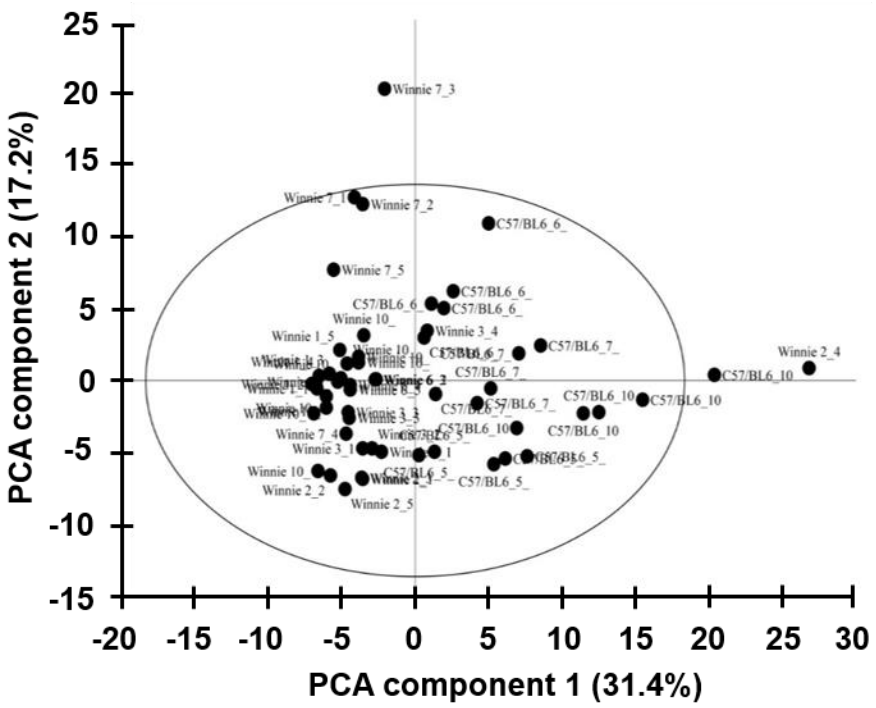
PCA component 2 (17.2%)
PCA component 1 (31.4%)
25
20
15
10
5
0
-5
-10
-15
-20
-15
-10
-5
0
5
10
15
20
25
30
Winnie 7_3
Winnie 7_2
C57/BL6_6_
Winnie 7_5
C57/BL6_6_
C57/BL6_6_
C57/BL6_6_
Winnie 10_
Winnie 3_4
Winnie 1_5
C57/BL6_7_
Winnie 2_4
C57/BL6_10
C57/BL6_7_
C57/BL6_10
C57/BL6_10
C57/BL6_7_
C57/BL6_10
C57/BL6_10
Winnie 7_4
C57/BL6_5_
Winnie 3_1
C57/BL6_5_
Winnie 10_
C57/BL6_5_
Winnie 2_2
Winnie 2_5
C57/BL6_5_

Figure S2. Partial least squares-discriminant analysis components. Partial least squares-discriminant analysis (PLS-DA) loading scatter plots among samples from C57BL/6 and *Winnie* mice **(A-B)**. Distance between X modal plane **(**DModX) plot for PLS-DA **(C)**. The Dcrit value is marked with black dotted line. The samples outside this line are considered as moderate outliers. Note: The Dcrit value is calculated by the equations: $1–R^2X(cum)=0.3657$; M4-Dcrit=1.227. The samples from 1-35 were from *Winnie* mice, while 36-55 were from C57BL/6 mice.

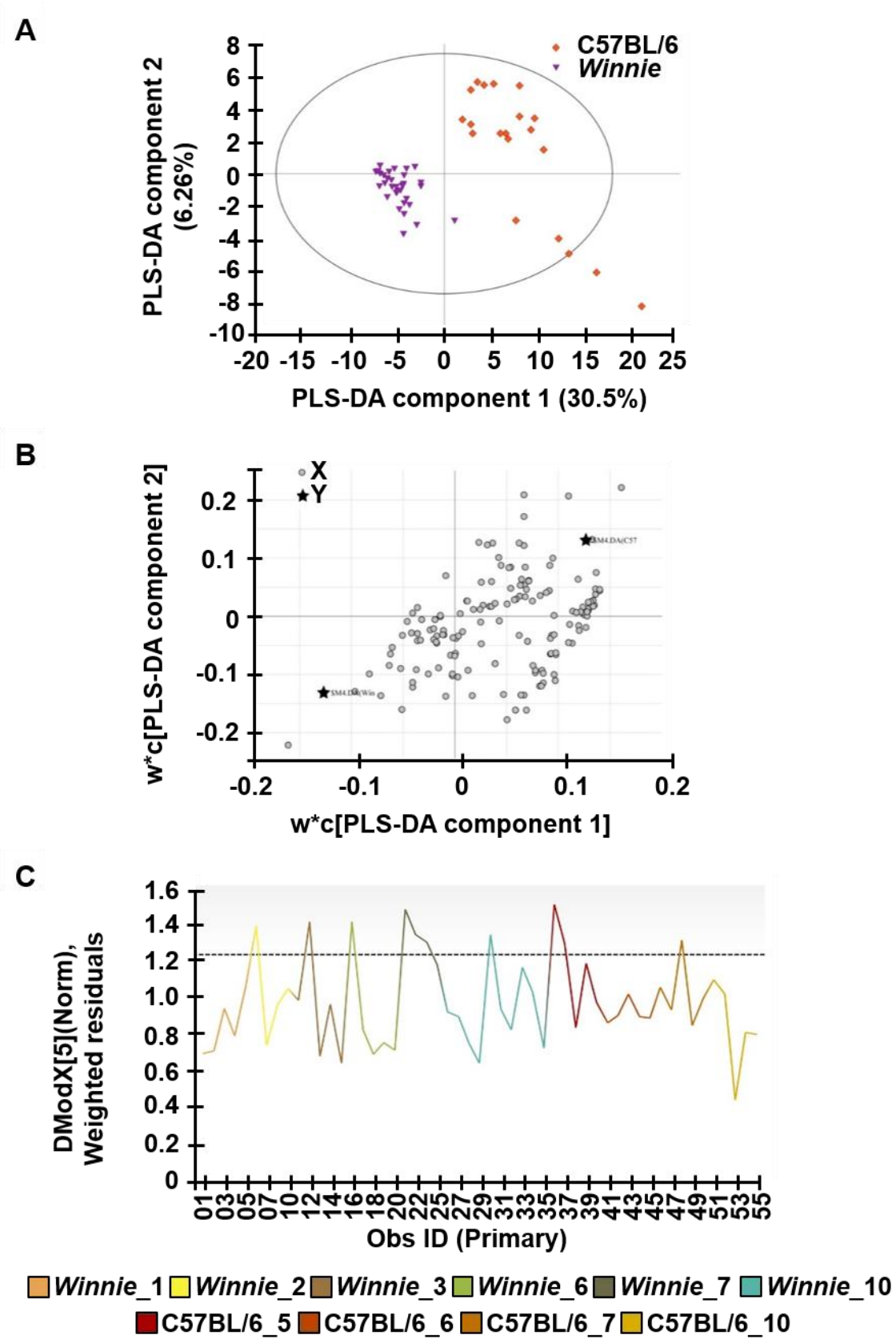
A
C57BL/6
Winnie
PLS-DA component 2 (6.26%)
PLS-DA component 1 (30.5%)
B
X
Y
w*c[PLS-DA component 2]
w*c[PLS-DA component 1]
C
DModX[5](Norm), Weighted residuals
Obs ID (Primary)
Winnie_1 Winnie_2 Winnie_3 Winnie_6 Winnie_7 Winnie_10
C57BL/6_5 C57BL/6_6 C57BL/6_7 C57BL/6_10

Appendix B: Effects of a single MSC treatment on fecal lipocalin-2 levels

Table S2. Average fecal lipocalin-2 levels (pg/mL) in sham-treated and MSC-treated *Winnie* mice over 60 days

Day	C57BL/6+sham	*Winnie*+sham	*Winnie*+MSC
BT	0.7±0.2	4.5±0.7***	4.4±0.4***
3	0.7±0.1	4.2±0.2***	4.1±0.1***
7	0.7±0.05	4.6±0.6***	4.3±0.2***
10	0.7±0.05	4.4±0.3***	3.9±0.4***
14	0.9±0.1	4.2±0.3***	4.2±0.2***
17	0.9±0.03	4.1±0.2***	4.1±0.2***
21	0.9±0.1	4.4±0.2***	4.5±0.5***
24	1.0±0.1	4.5±0.3***	4.4±0.3***
28	0.9±0.1	4.1±0.3***	4.6±0.3***
31	0.7±0.1	4.2±0.2***	4.2±0.2***
35	0.7±0.05	4.9±0.2***	4.6±0.3***
38	0.8±0.1	3.9±0.4***	4.2±0.2***
42	0.5±0.1	4.5±0.4***	4.5±0.3***
45	0.8±0.1	4.4±0.4***	4.4±0.3***
49	0.8±0.04	3.8±0.1***	4.0±0.3***
53	0.9±0.1	4.3±0.2***	4.6±0.6***
56	0.9±0.1	4.6±0.3***	4.8±0.1***
60	0.8±0.1	4.2±0.4***	4.4±0.5***

****P*<0.001 when compared to C57BL/6+sham-treated mice.

Appendix C: Effects of multiple low dose and high dose MSC treatments on fecal lipocalin-2 levels

Table S3. Average fecal lipocalin-2 levels (pg/mL) in sham-treated, low dose (LD) MSC-treated, and high dose (HD) MSC-treated mice over 60 days

Day	C57BL/6+sham	*Winnie*+sham	*Winnie*+LD MSC	*Winnie*+HD MSC
BT	0.8±0.1	4.1±0.4***^^^	4.3±0.3***^^^	4.7±0.1
3	0.8±0.1	4.3±0.3***^^^	4.1±0.1***^^^	1.2±0.1
7	0.8±0.1	4.6±0.4***^^^	4.4±0.4***^^^	1.0±0.1
10	1.0±0.1	4.5±0.2***^^^	4.3±0.3***^^^	1.1±0.1
14	0.8±0.1	4.1±0.3***^^^	4.2±0.2***^^^	1.1±0.1
17	0.7±0.04	4.0±0.2***^^^	4.2±0.1***^^^	1.3±0.1
21	0.7±0.1	4.4±0.2***^^^	4.6±0.3***^^^	1.1±0.1
24	0.8±0.1	4.6±0.2***^^^	4.2±0.2***^^^	1.4±0.2
28	0.9±0.1	4.2±0.2***^^^	4.7±0.3***^^^	1.3±0.2
31	0.8±0.1	4.6±0.2***^^^	4.3±0.2***^^^	1.5±0.2
35	0.7±0.04	4.5±0.3***^^^	4.6±0.2***^^^	1.6±0.2*
38	0.8±0.1	4.2±0.3***^^^	4.6±0.5***^^^	1.5±0.3
42	0.7±0.1	4.6±0.3***^^^	4.7±0.3***^^^	1.8±0.3**
45	0.8±0.1	4.2±0.3***^^^	4.5±0.2***^^^	1.7±0.4*
49	0.8±0.1	3.9±0.2***^^^	4.2±0.3***^^^	1.6±0.3
53	1.0±0.1	4.4±0.2***^^^	4.5±0.5***^^^	1.7±0.4
56	0.8±0.1	4.2±0.3***^^^	4.7±0.1***^^^	1.7±0.5*
60	0.8±0.02	4.2±0.2***^^^	4.4±0.1***^^^	1.6±0.1**

BT = before treatment. *P<0.05, **P<0.01, ***P<0.001 when compared to C57BL/6+sham-treated mice. ^^^P<0.001 when compared to *Winnie*+HD MSC-treated mice.